'Aha Huliko'a

THE ROLE OF EDDIES IN THE GENERAL OCEAN CIRCULATION

JAN 2 3 1984

A

Proceedings
Hawaiian Winter Workshop
University of Hawaii at Manoa
January 5-7, 1983

84 01 23 063

DISCLAIMER NOTICE
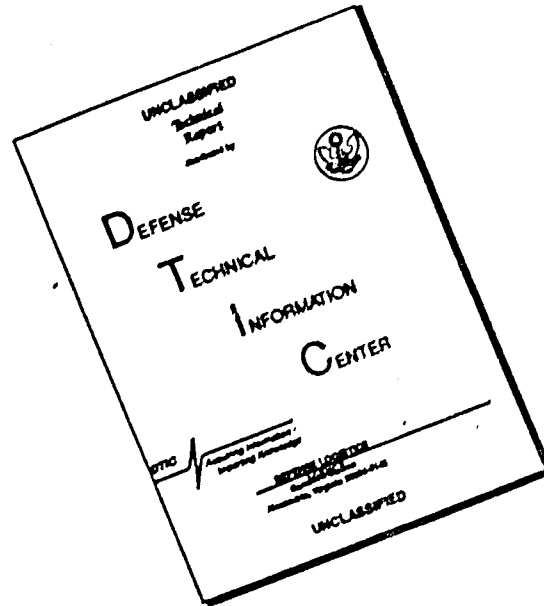
THIS DOCUMENT IS BEST QUALITY AVAILABLE. THE COPY FURNISHED TO DTIC CONTAINED A SIGNIFICANT NUMBER OF PAGES WHICH DO NOT REPRODUCE LEGIBLY.

COMPONENT PART NOTICE

THIS PAPER IS A COMPONENT PART OF THE FOLLOWING COMPILATION REPORT:

(TITLE): The Role of Eddies in the General Ocean Circulation: Proceedings of

'Aha Huliko'a Hawaiian Winter Workshop Held at Manoa on January 5-7, 1983.

(SOURCE): Hawaii Inst. of Geophysics, Honolulu.

To ORDER THE COMPLETE COMPILATION REPORT USE __AD-A137 212__ .

THE COMPONENT PART IS PROVIDED HERE TO ALLOW USERS ACCESS TO INDIVIDUALLY AUTHORED SECTIONS OF PROCEEDINGS, ANNALS, SYMPOSIA, ETC. HOWEVER, THE COMPONENT SHOULD BE CONSIDERED WITHIN THE CONTEXT OF THE OVERALL COMPILATION REPORT AND NOT AS A STAND-ALONE TECHNICAL REPORT.

THE FOLLOWING COMPONENT PART NUMBERS COMPRISE THE COMPILATION REPORT:

DTIC
SELEC
JAN 26 1984
A

By_____
Distribution/
Availability Codes
Dist | Avail and/or Special
A-1

AD#:   TITLE:

The Role of Eddies in the
General Ocean Circulation

LORENZ MAGAARD
PETER MULLER
RITA PUJALET

editors

PROCEEDINGS

'Aha Huliko'a
Hawaiian Winter Workshop
University of Hawaii at Manoa
January 5–7, 1983
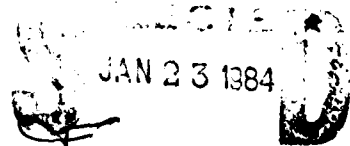
FOREWORD

In the Hawaiian language 'Aha Huliko'a means an assembly to seek into the depth of a matter and to describe it fully. We felt that this was an appropriate description of a scientific workshop to be held in Hawaii. Thus our 'Aha Huliko'a, entitled "The Role of Eddies in the General Ocean Circulation" was held in Honolulu from January 5 to 7, 1983.

The intent of this workshop was to bring together a limited number of scientists who have played a leading role in the studies of eddies in the general ocean circulation, in order to determine the state of the art and to discuss plans for future directions of research. Because of similarities in the methodological approach and because of the great relevance for oceanography, eddies in the general circulation of the atmosphere were also a topic of this workshop and, accordingly, meteorologists were invited.

Fifteen colleagues from the U. S. mainland and two foreign countries accepted our invitation to attend this workshop. Their lectures, together with those of the first two editors, are published in these proceedings, for the most part, as submitted in camera-ready form. In line with the general informality of the meeting we did not rigidly enforce our guidelines for the preparation of the manuscripts; some degree of inhomogeneity in format is the consequence.

During the workshop, time was devoted to both formal and informal discussions. Two sessions of round-table discussions concluded the workshop. These discussions are published almost verbatim. Trivial phrases were omitted, and, in a few cases, standard English was substituted for colloquial expressions. Before publication the participants were given an opportunity to read the transcript of their contributions to the discussions and to make changes, especially in cases where the tape recordings were unintelligible.

It is our pleasure to extend our warmest thanks to the U. S. Office of Naval Research for sponsoring this workshop. Their support covered more than 95% of its cost. Further support came from the Hawaii Institute of Geophysics and the Department of Oceanography of the University of Hawaii. The excellent facilities at the East-West Center and the capable staff directed by James McMahon contributed greatly to the success of the workshop. The local organization and logistical management of the workshop was done by Irene E. Vasey. Without her invaluable help this workshop would not have been possible. Graphic design for the Workshop and the cover of this volume was by April Kam. We appreciate the competent assistance of Vicki Gaynor during the preparation of this volume.

Lorenz Magaard
Peter Muller
Rita Pujalet
  editors

iii
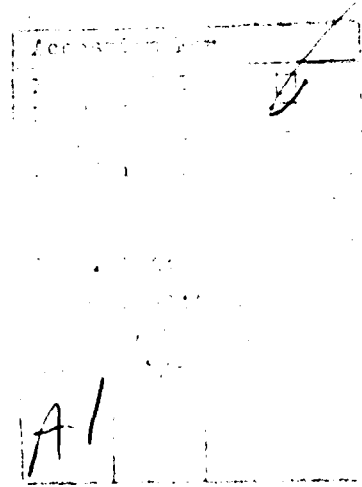
Standing, left to right: N. Hogg, T. Spence, A. Robinson, G. Flierl,
P. Rhines, L. Magaard, A. Bennett, W. Krauss, I. S. Oh, K. Wyrtki,
W. White, P. Muller, and J. Huang.

Seated, left to right: W. Holland, J. Holton, T. Rossby, R. Salmon,
W. Young, and L. Fu.

Not present for photograph: D. E. Harrison and J. McWilliams.

CONTENTS

WAVES AND CIRCULATION DRIVEN BY OSCILLATORY WINDS IN AN IDEALIZED OCEAN BASIN

Dale Haidvogel and Peter Rhines

Woods Hole Oceanographic Institution
Woods Hole, Massachusetts   02543

We have examined, via direct numerical integration, the transient and rectified response of a flat-bottomed barotropic ocean to a spatially localized oscillatory wind-stress pattern. These experiments exemplify in many respects the dynamics which drive the deep motion in recent eddy-resolving ocean circulation studies (e.g., Holland and Rhines, 1980), and may be contrasted with the results of Pedlosky (1965) and Veronis (1966) for spatially broad, time-dependent forcing.

By considering doubly re-entrant (periodic) and closed basin geometries, the structure and magnitude of the induced circulation is shown to depend most critically on the form of the mean quasi-geostrophic contours (which are free in the periodic geometry yet blocked in the closed basin). In both situations, however, the forced primary wave field may usefully be understood by appeal to the radiation pattern of a time-periodic Greens function and its image in the western boundary.

The dynamics of the prograde and retrograde rectified circulation is seen to relate most directly to the eddy potential vorticity flux $\overline{v' q'}$ (and not to the Reynolds stress $\overline{u'v'}$). Here q is potential vorticity and u,v are east and north velocity, respectively. In particular, Eulerian vorticity budgets indicate the dominance of the 'turbulent Sverdrup balance', $\beta v = -\nabla * \overline{v' q'}$ in nearly all parts of the flow. Lagrangian (particle-wise) balances clearly emphasize the regions of counter-gradient q-fluxes in providing the propulsion necessary for fluid particles to cross the mean quasi-geostrophic contours. Although these flows do not strictly comply with the assumptions of recent q-transport theories, nonetheless all the qualitative (and some of the quantitative) features predicted by these theories are confirmed in the simulations.

In Figure 1 are plotted the early development of the streamfunction, ψ, and vorticity, ζ for the case of open (periodic geometry). The basin is 2000 km wide, with a 200-km-wide wavemaker in the center, essentially a Gaussian distribution of w (vertical velocity) sinusoidal in time, with
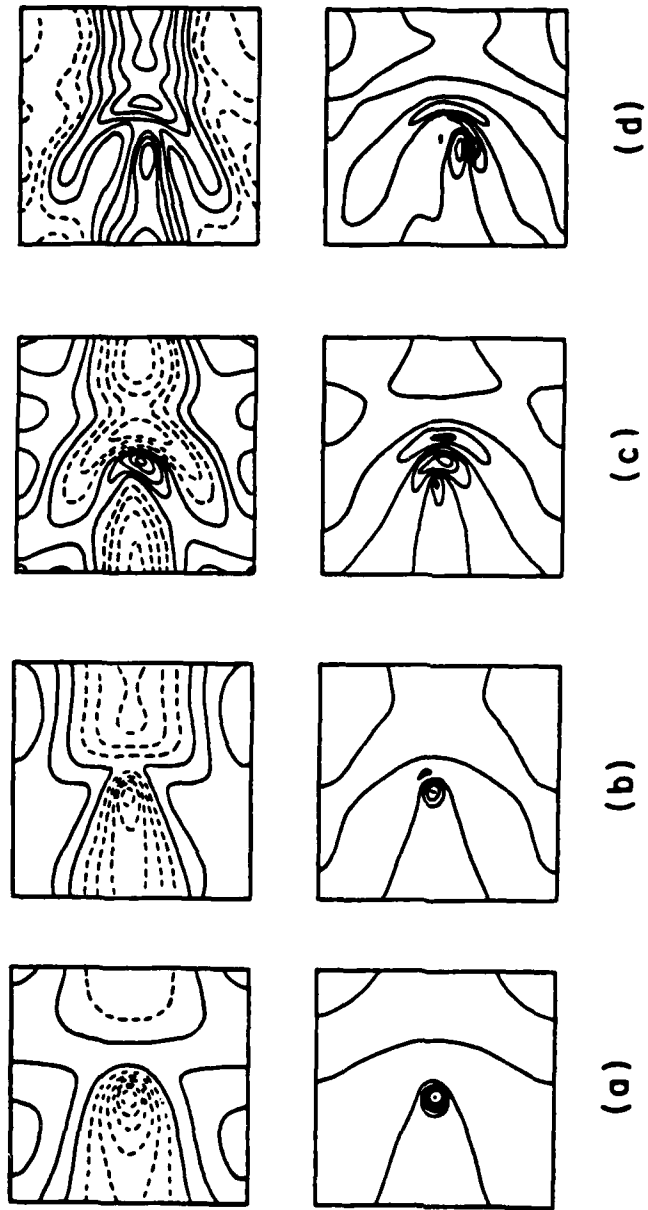
Fig. 1. Contour maps showing the early development of ψ (upper) and ζ (lower) fields with periodic geometry. Times are 10 days, 20, 40, and 80, respectively. Contour interval is not fixed.

(a)   (b)   (c)   (d)

period 100 days. To be consistent with mass conservation, we have a weak, vertical velocity uniform across the basin such that the spatial integral of w vanishes. Figure 2 shows a similar sequence, but with closed-basin geometry. In Figure 1 the primarily westward setup of the Rossby wave field is evident, as is the increasingly strong zonally averaged circulation. In Figure 2 the reflected short Rossby waves are evident. Both fields have similar eddy potential vorticity flux near the wavemaker, yet the induced mean circulation differs greatly in the two respective cases (Figs. 3 and 4). With open geometry the mean flow is itself a low-frequency Rossby wave that progresses westward from the wavemaker, strengthening with each pass through the periodic domain. With closed basin geometry (Fig. 4) this induced flow must itself accommodate to the western boundary. The mean velocity is typically ?) 4 times stronger with open geometry, and this contrast would be great if the friction were weaker (the ratio of mean induced velocities in two experiments should be $\beta L^2/RL_0$, where L_0 is the width of the domain, R the bottom friction, and L the meridional scale, here about ' km).

The time-averaged potential vorticity flux (Figs. 5 and 6) shows several 'signatures' predicted by the theory (Rhines and Holland, 1979). Outside of the region of the wavemaker the vorticity-mixing theory leads us to expect a down-gradient (southward) component of $\underline{v}' q'$. But in the presence of strong orbital particle motions due to the primary wave field, the largest signal is a cross-gradient flux (east and west). Such is the nature of Figures 5b, 5c, and 6c. In a strong dissipation region like the western boundary, the theory suggests strong southward (downgradient) flux. This is clearly evident in Figure 6b. In a region of direct external forcing (that is, beneath the wavemaker), fluid particles are continually being 'kicked' and subsequently falling back toward their 'rest latitude' (the latitude at which their relative vorticity would vanish). The signature of particles 'falling back to rest' is a counter-gradient flux, which is clear in Figures 5a and 6a.

A Lagrangian (particle-following) analysis of these same events is described in Haidvogel and Rhines (1983). There we see particles travelling essentially freely along geostrophic contours (latitude lines) between the wavemaker and the western boundary. At those two special sites the particle's potential vorticity is rapidly altered by (respectively) external force and friction, allowing the particle to alter its latitude in preparation for the next leg of free travel. With periodic geometry the impulsive western boundary dissipation is replaced by a gradual distributed dissipation by which a particle drifts slowly across latitude lines.

4
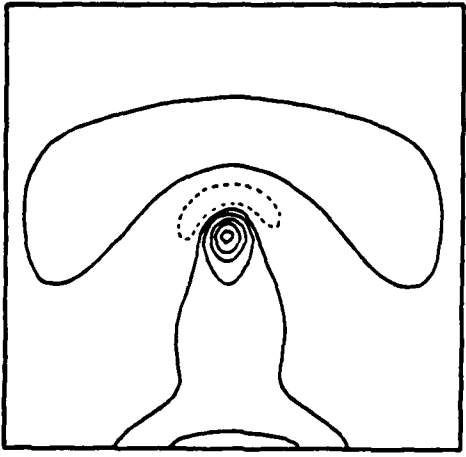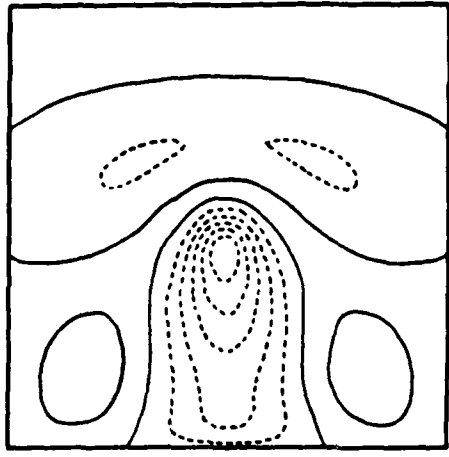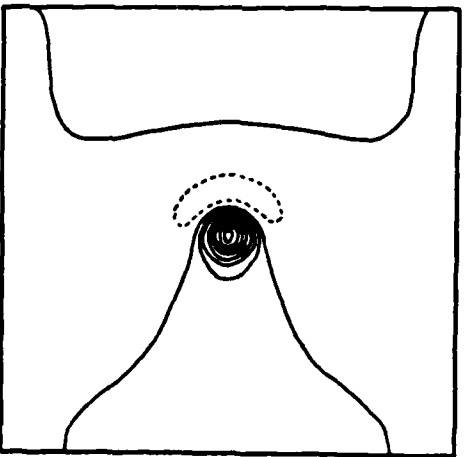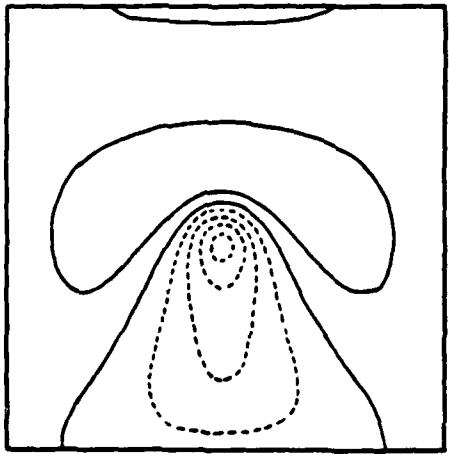
Fig. 2. As in Fig. 1, but with closed basin geometry.

5
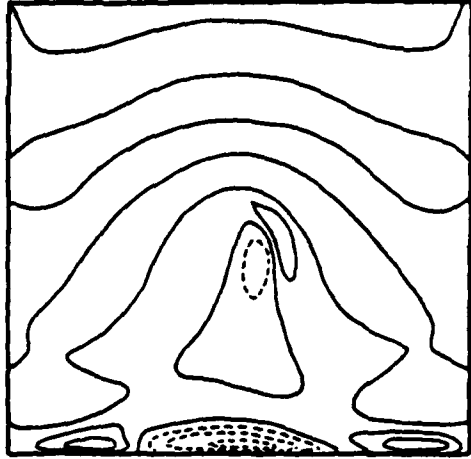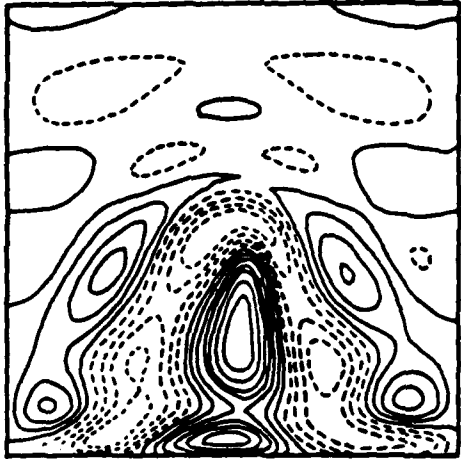
(d)
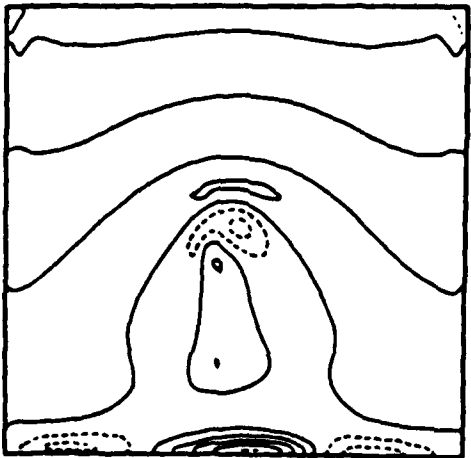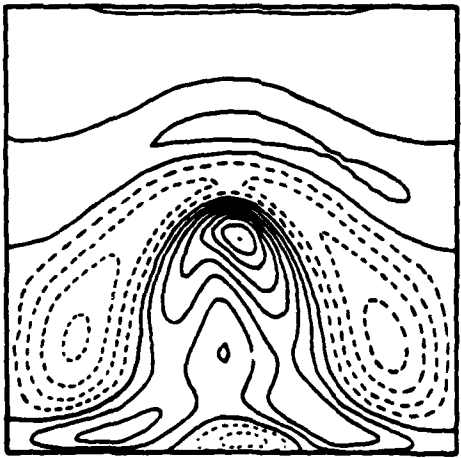
(c)

Fig. 2. (continued)
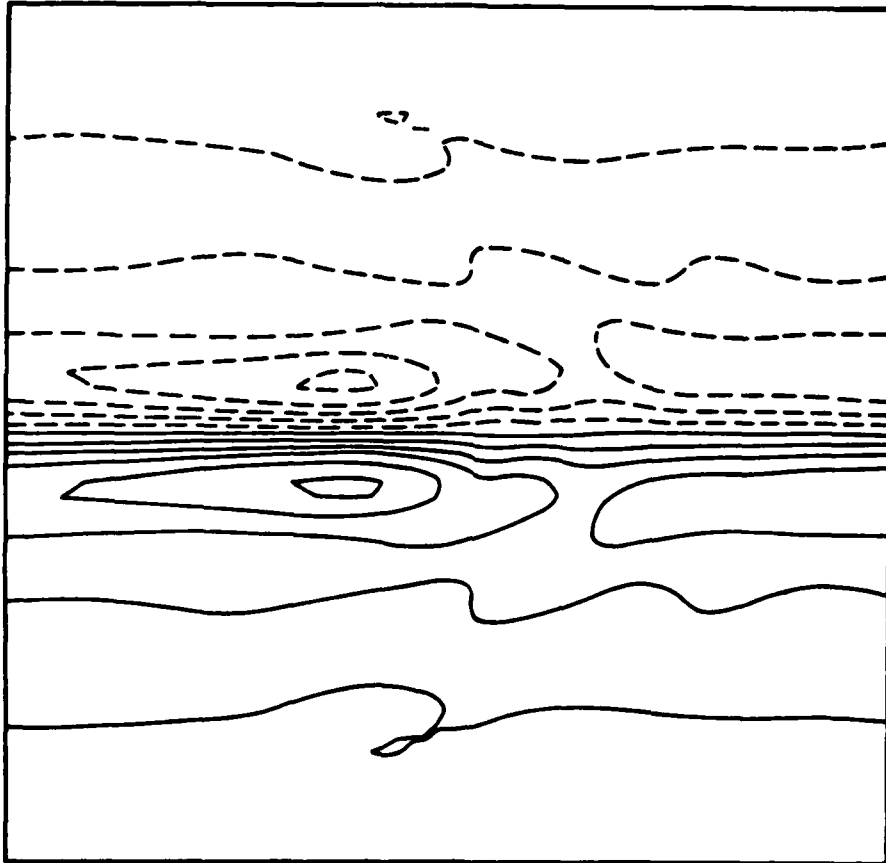
(a)

Fig. 3. Time-mean induced circulation for periodic geometry;
ψ contour interval 1.3×10^7 cm^2 sec^{-1}.
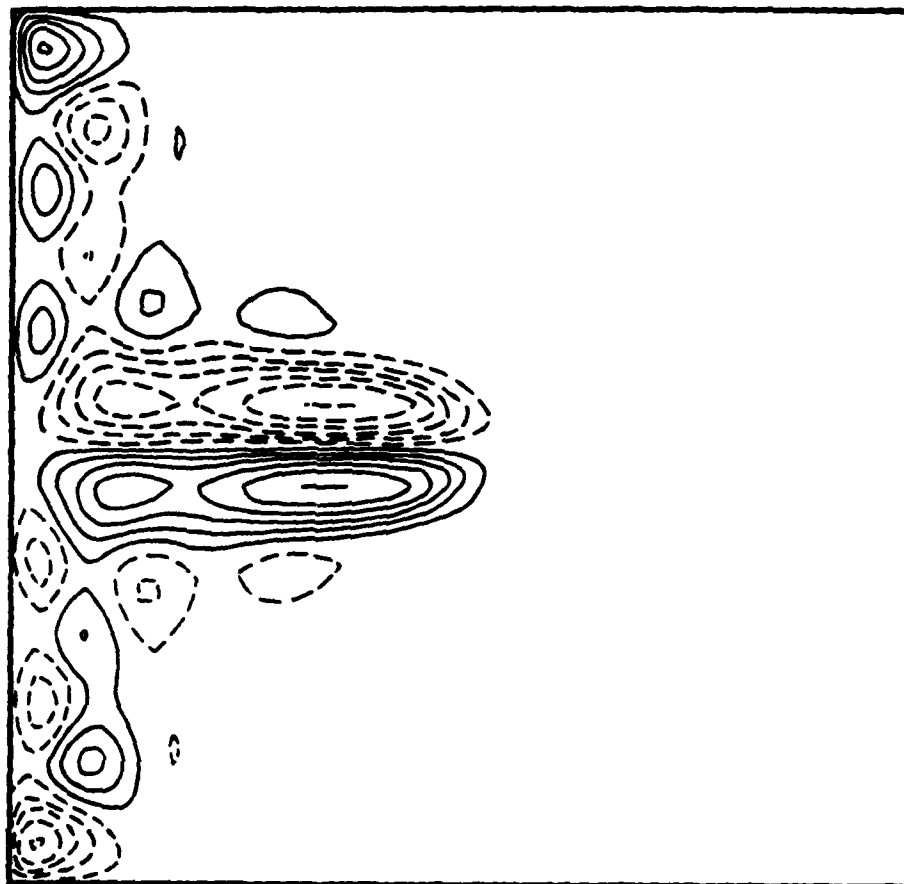
(a)

Fig. 4. As above, but for closed-basin geometry. Note contour
interval is now 4×10^7 cm^2 sec^{-1}.
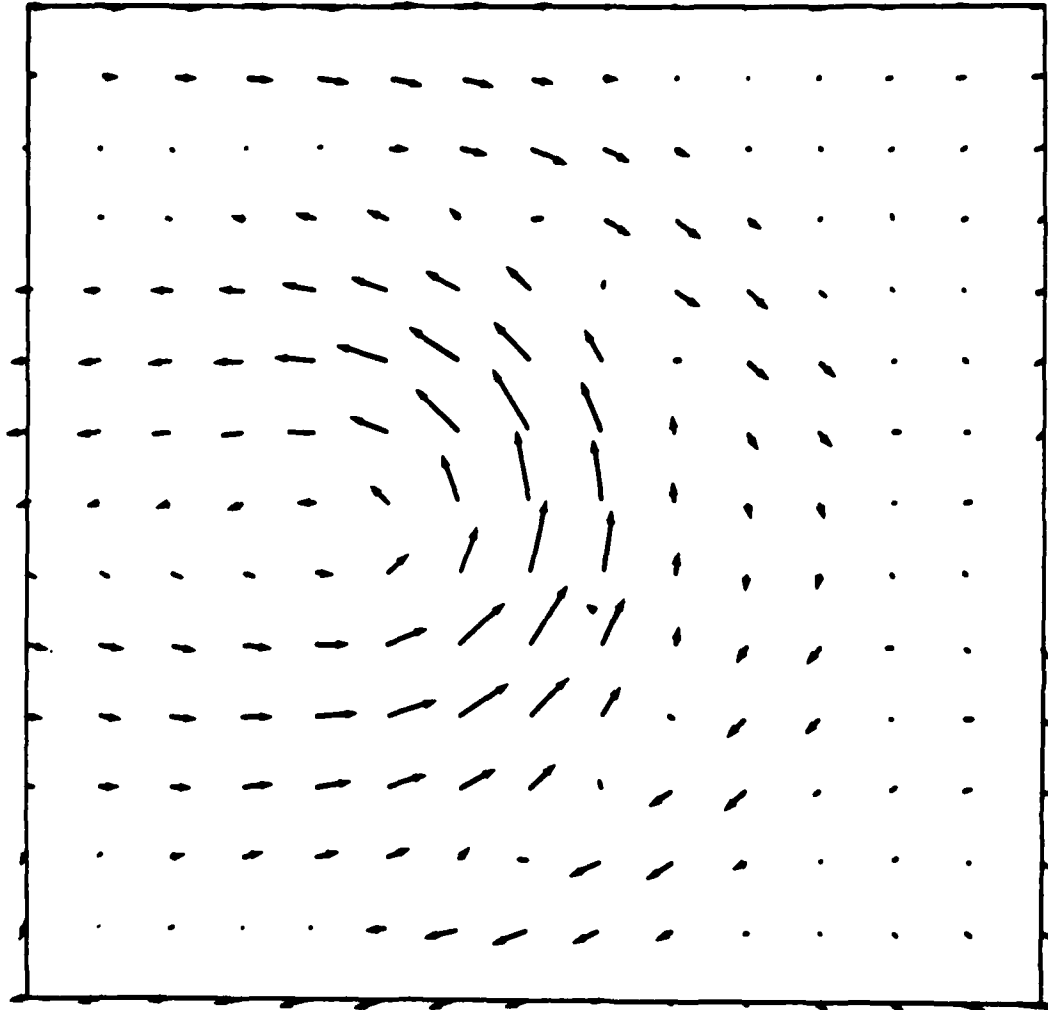
(a)

Fig. 5. Vector plot of time-averaged potential vorticity flux, $\overline{v'\,q'}$, for periodic geometry. The patterns are characteristic of those found in the theory, even though that theory is based on there being a scale separation between eddies and mean flow.

(a) forcing region $780 < x,y < 1220$ km.

9
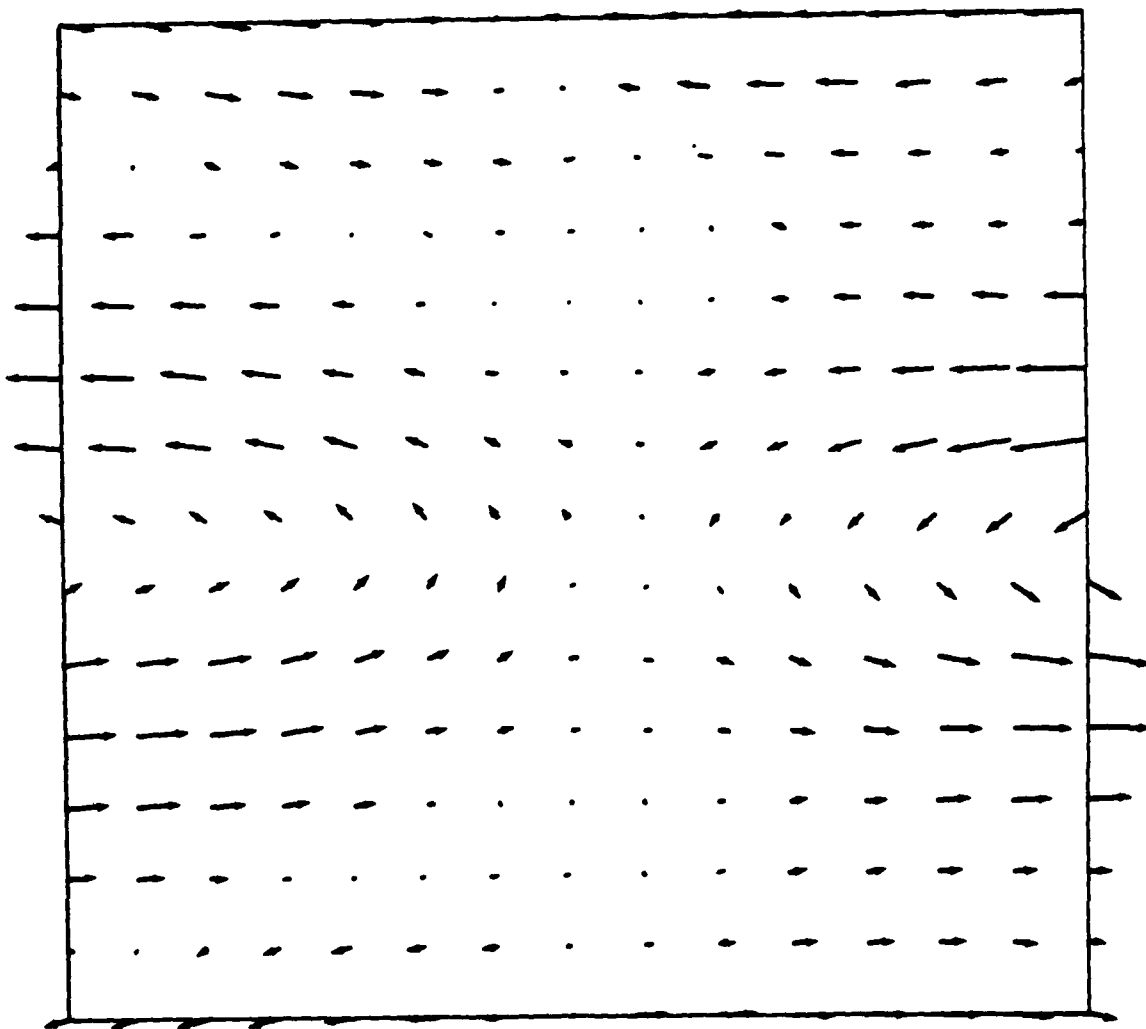
(b)

Fig. 5. (b) boundary region, $0 < x < 440$ km, $780 < y < 1220$ km.
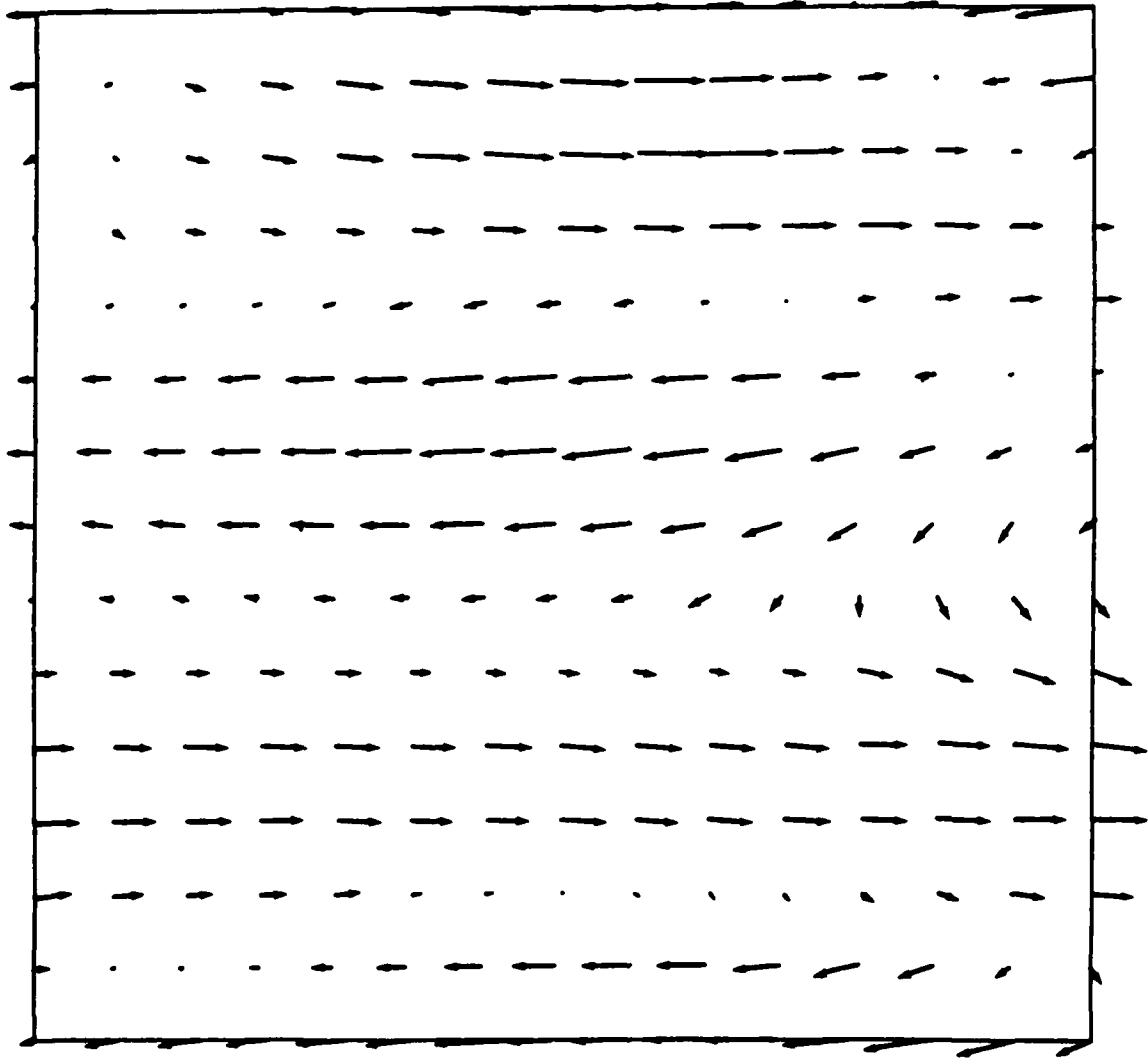
(c)

Fig. 5. (c) unforced latitudes 780 < x < 1220 km, 1780 > y > 1340 km.
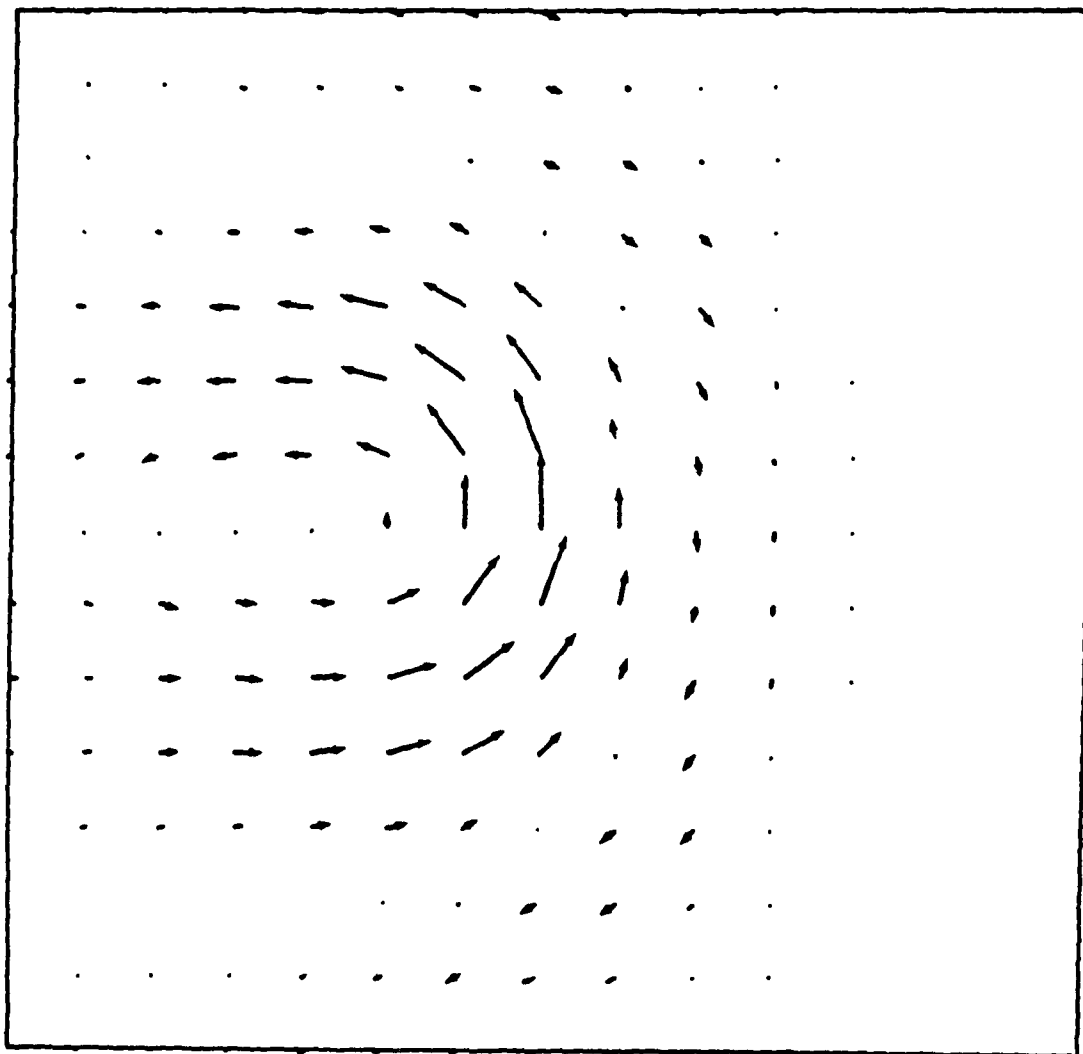
(a)

Fig. 6. As above, but with closed basin. The down-gradient flux is
concentrated near the western boundary, in an oscillating boundary layer.

12
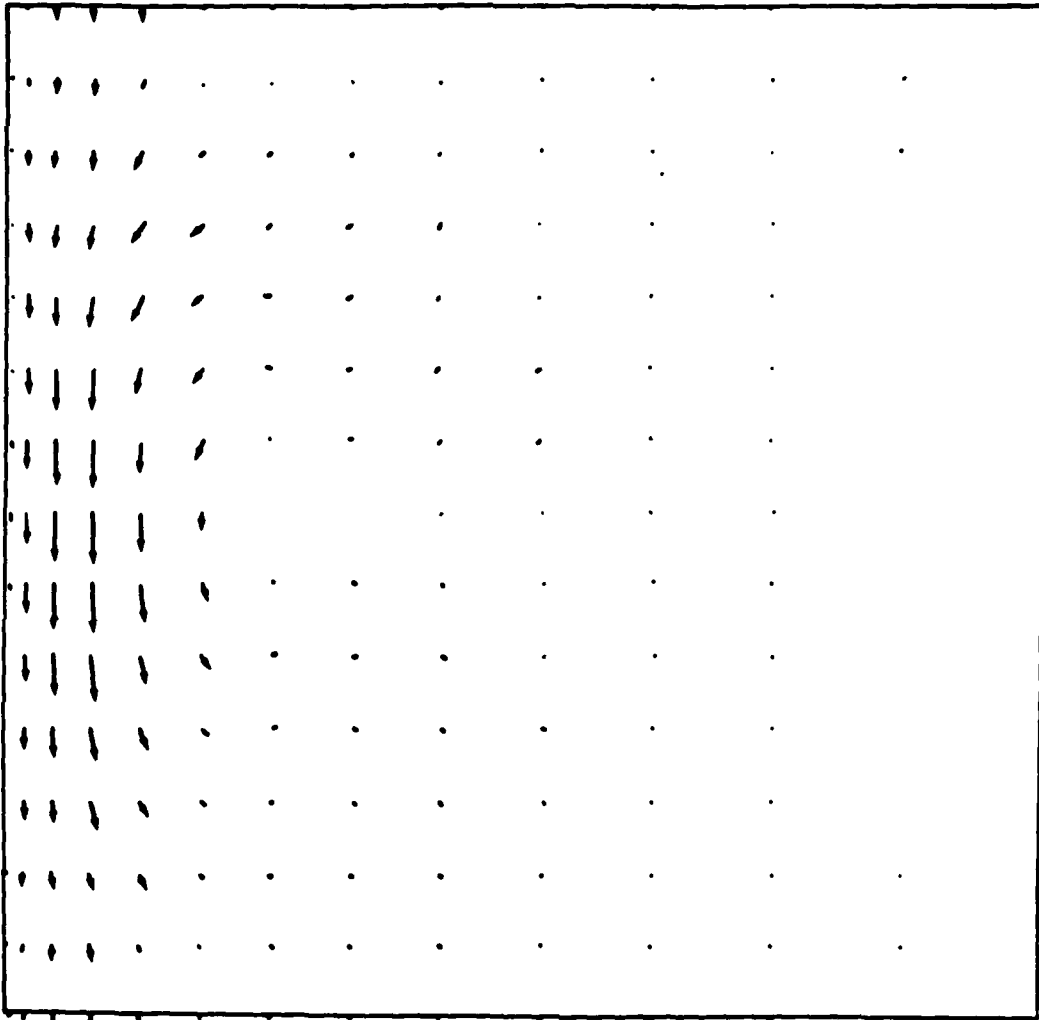
(b)
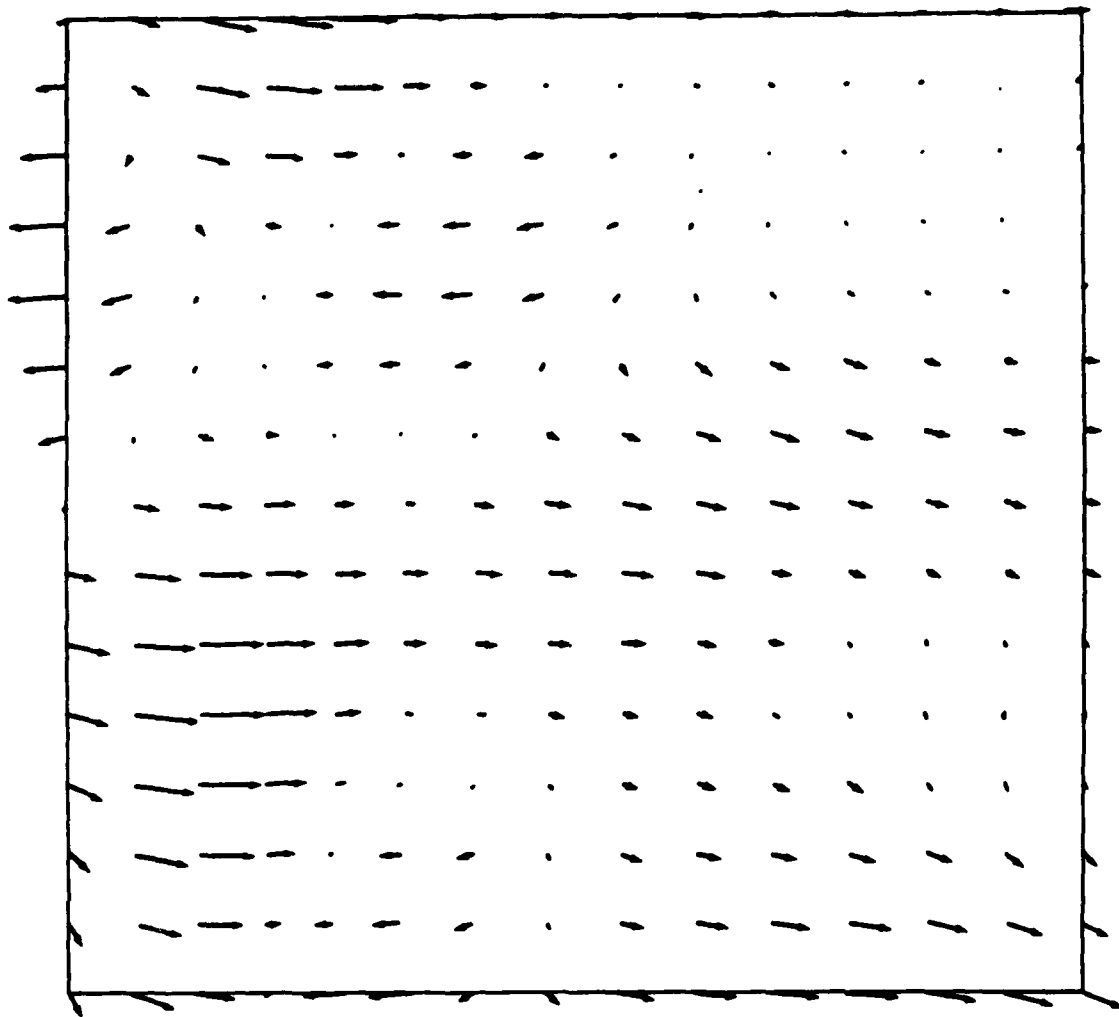
Fig. 6. (continued)

(c)

Fig. 6. (continued)
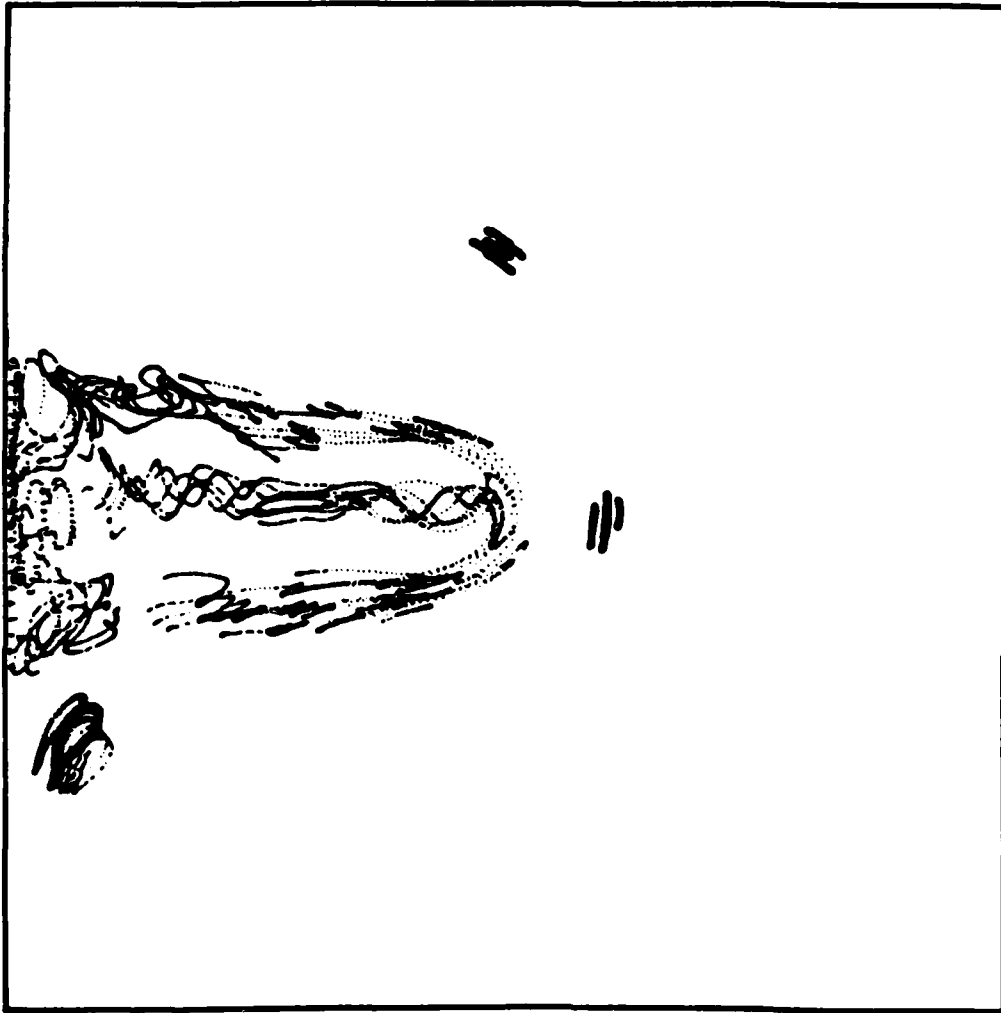
Fig. 7.   300-day float tracks showing the combination of primary
wave field oscillations and rectified mean translation.   Despite
the dominance of the primary wave field instantaneously (Fig. 2),
the rectified circulation is the dominant feature of the Langrangian
frame.

References

Haidvogel, D. and P.B. Rhines, 1983. Waves and circulation driven by
oscillatory winds and idealized ocean basins. Geophysical and
Astrophysical Fluid Dynamics, 25,   1-63.

Holland, W.R. and P.B. Rhines, 1980. An example of eddy-induced ocean
circulation. Journal of Physical Oceanography, 10, 1010-1031.

Pedlosky, J. 1965. A study of the time-dependent ocean circulation.
Journal of Atmospheric Sciences, 22, 267-272.

Rhines, P.B. and W.R. Holland, 1979. A theoretical discussion of
eddy-driven mean flows. Dynamic Atmosphere and Oceans, 3, 289-325.

Veronis, G., 1966. Generation of mean ocean circulation by fluctuating
winds. Tellus, 18 , 67-76.
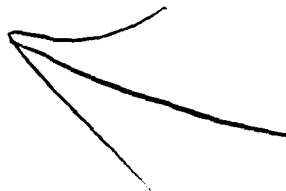
RECENT WORK AND THOUGHTS ON EDDY-MEAN FLOW INTERACTION

D. E. Harrison

Department of Meteorology and Physical Oceanography
Massachusetts Institute of Technology
Cambridge, Massachusetts 02139

In order to address the question of the roles of mesoscale eddies in the ocean general circulation it is necessary first to determine the ocean general circulation. Unless this circulation is known well enough to estimate the dominant terms in the mean heat, momentum and vorticity equations, it is not possible to evaluate the "eddy turbulence" terms-- divergence of the eddy heat flux, divergence of the Reynolds stress tensor and curl of the divergence of the Reynolds stress tensor--and one can at best speculate on the basis of fragmentary data or theoretical concepts. Even if the detailed balances of the mean equations are known, it may not be simple to establish the roles of the eddies (viz. the meteorological experience), but the task is almost exclusively inferential if the data are unavailable. As it is now clear that there is substantial low-frequency variability over most of the ocean, determining the general circulation will be an enormous task.

In those few mid-latitude areas where multi-year current meter deployments have taken place, the available data suggest that 5-to 10-year records may be required to obtain stable means and second-order moments (e.g., $\overline{u'v'}$, $\overline{u'T'}$, etc.). Such long records appear necessary in these areas both because the variability is much more energetic than the mean and because the most energetic variability is often very intermittent. At present we do not have adequate statistics on the intermittency, so even the 5-to 10-year duration estimate offered above may prove to be too short. Stable statistics are required because the mean field equations require that we be able to differentiate at least once the means and eddy fluxes, in order to estimate the mean balances.

Since the ocean general circulation will not soon be known on the large scale to the accuracy required for direct dynamical study, it is necessary to work with the available data and concepts obtained from theory and/or numerical model results to investigate the roles of the mesoscale in this circulation. My purpose here is to offer a personal perspective on some of the problems of trying to determine the kinematics of the ocean eddy field and the roles of the mesoscale in the general circulation, based on my recent work and work that is closely related to mine in interest. Much of what follows is very much work in progress and should be accorded the skepticism such results deserve.

The first general area of interest here concerns the kinematics of the ocean mesoscale variability field. In different words, how much do we know about what the eddies look like from the instantaneous and statistical perspectives? As mentioned above, to characterize the variability one must first know the mean. For good pragmatic reasons it has been common to assume that a satisfactory approximation of the mean field can be obtained by plausible manipulations of the data set just obtained (whether XBT section, current meter array or whatever). This "local" mean (as opposed to a true climatological mean) becomes the referent for all subsequent eddy calculations.

Now consider some recent upper-ocean thermal data. First we shall look at some long (several thousand km) zonal sections of XBT data (Harrison et al., 1983) from the North Atlantic and North Pacific. Figure 1 shows the areas sampled in each multi-ship survey. Data are available from true mid-gyre areas as well as adjacent to strong western boundary currents. Data for 450-m temperatures from the first "swath" (N. Pac.) are shown in Figure 2. This is a "nice" swath, in that the climatological mean (computed from an independent historical XBT archive from NODC) and the linear trend (or "local" mean) through the swath data differ by amounts that are small relative to the mesoscale features in the data; statistics computed relative either to the climatology or the trend are quite similar. Figure 3 shows a N. Atlantic swath for which there are very large differences between climatology and trend. For these data the mesoscale is very different, depending on the chosen "mean."

One of the more interesting differences is that cold features tend to have quite different scales and amplitudes from warm features. This tendency is observed in a number of swaths, relative to climatology, and in some even relative to trend. Chi-squared tests for the Gaussianity of the data confirm the impression that the variability (sub-sampled every 150 km to reduce problems of data dependence) often is not Gaussian at the 95% level. A simple illustration of the statistical differences introduced by defining the variability properties relative to different means is given in the zonal autocorrelation functions of T_{450} shown in Figure 4. Relative to climatology, the North Atlantic scales tend to be very much larger than relative to trend; in fact, the scales for swaths 4, 5 and 6 are long enough that calling them "mesoscale" begins to be marginal.

The climatological T_{450} field used above is based on cubic spline fits to averages over 2° (latitude) by 10° (longitude) areas, and has various shortcomings of its own. In particular, a number of areas do not have data even approximately uniformly distributed by month and also have only a few 0(50) observations. In these areas the mean may not fairly represent the climatological mean. In other areas the data may be aliased by very large numbers of observations from anomalous features (e.g., Gulf Stream rings) as Ebbesmeyer and Taft (1979) have shown.
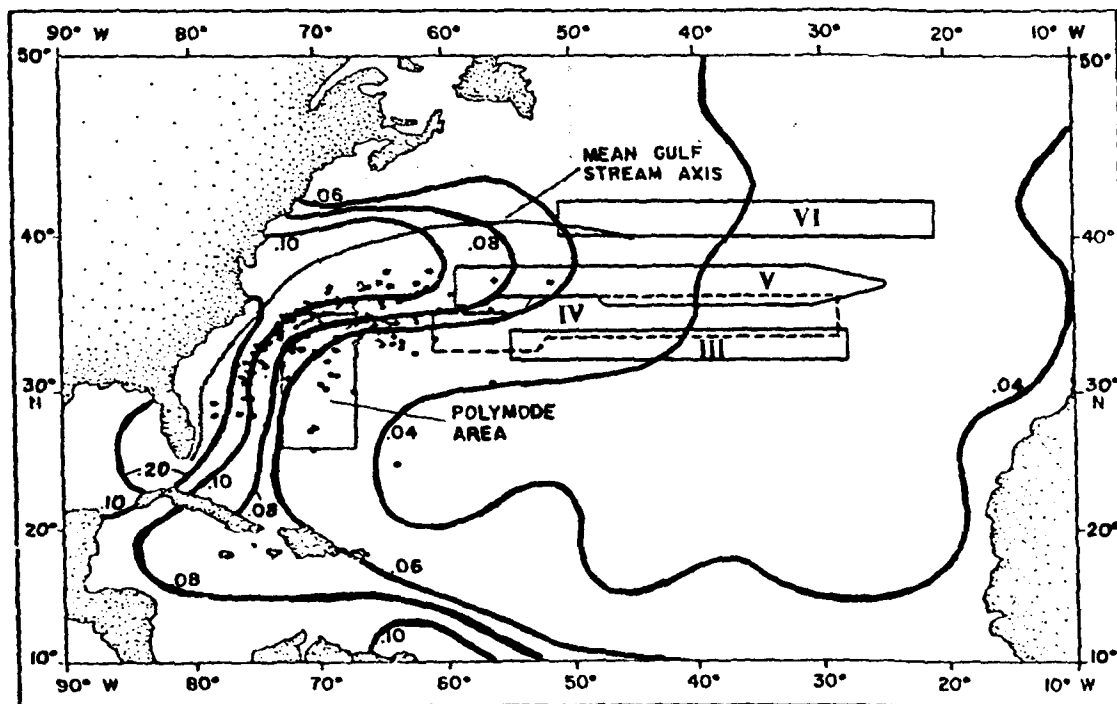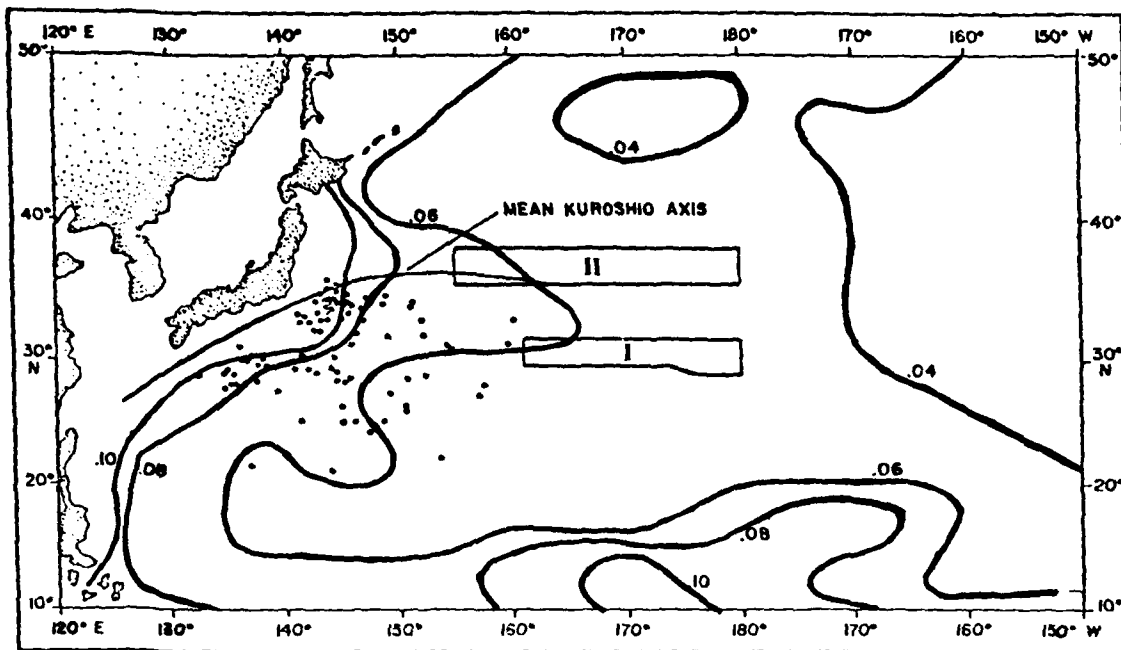
Fig. 1. Schematic description of the areas sampled in six multi-ship
XBT surveys (from Harrison et al., 1983).
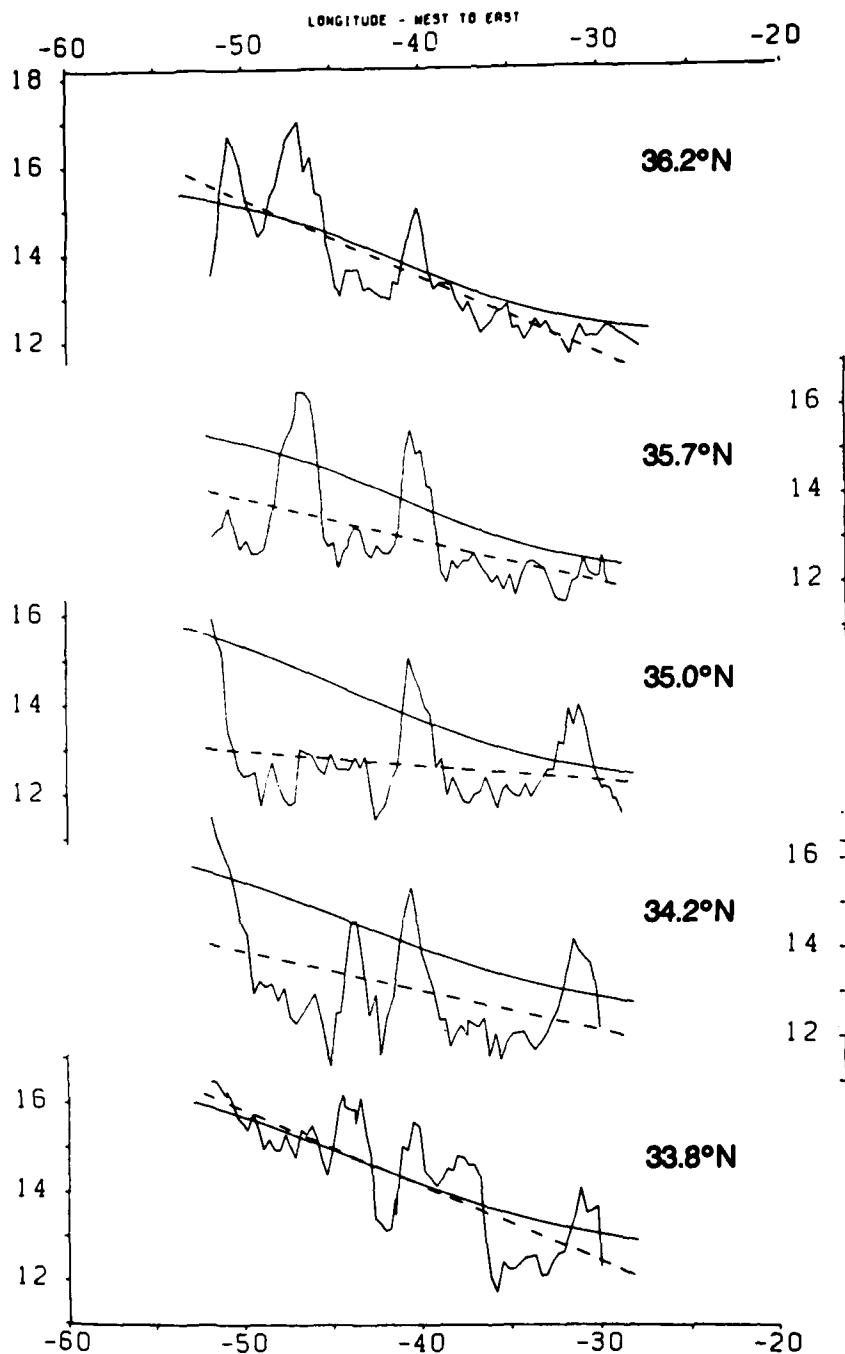
Fig. 2. Temperature (450 m) sections from a North Pacific
multi-ship survey. Climatology is indicated by a solid
line; least squares straight line through data is indi-
cated. Stastics are quite similar, relative to either
climatology or trend (see text).
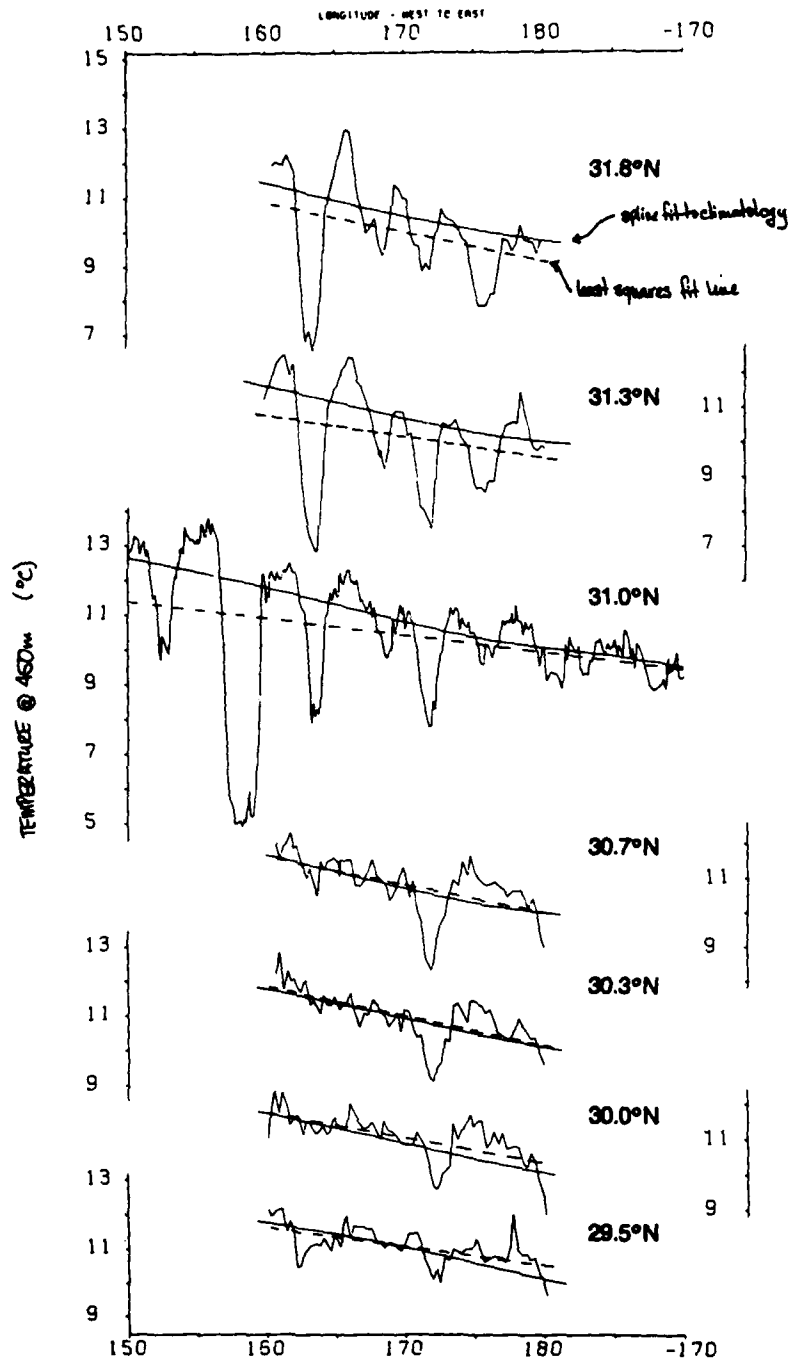
Fig. 3. As in Fig. 2 for a North Atlantic multi-ship
survey. Climatology and trend are different enough
that stastics of the mesoscale are very different
relative to trend than they are relative to climatology.
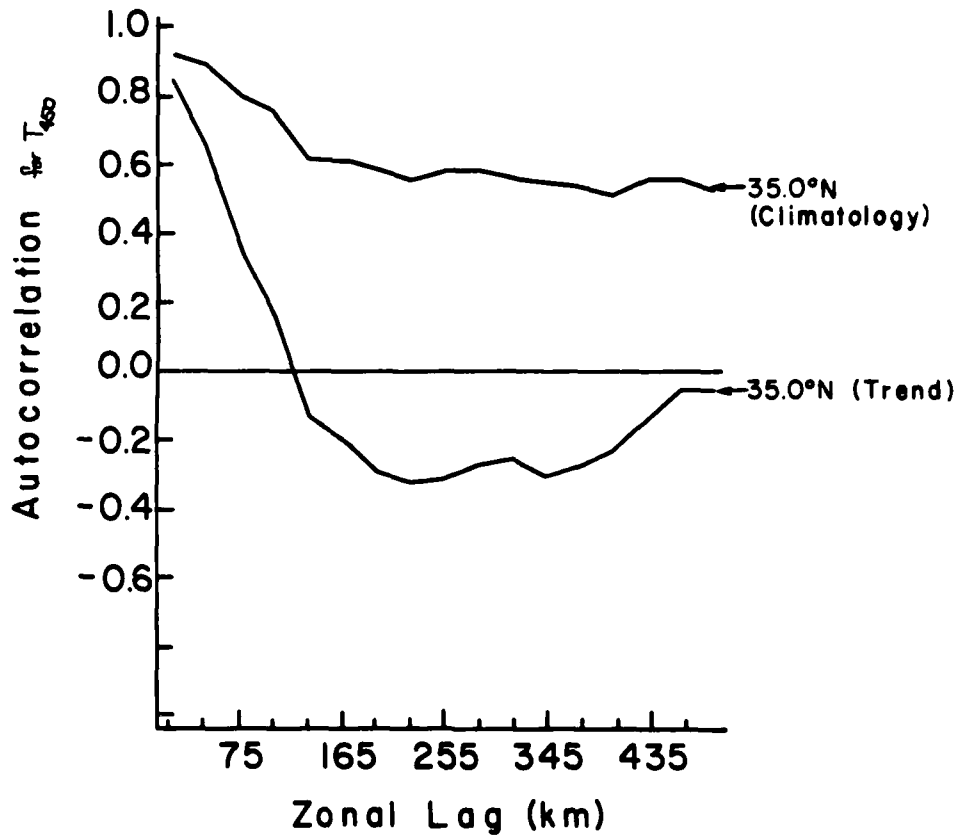
Fig. 4. Zonal autocorrelation functions for T_{450} data from Fig. 3, relative to trend and climatology.

That the upper ocean temperature field is not well know climatologically
on the these scales is something of a surprise, since it is (after SST)
the best observed oceanic quantity.

Of course the climatological mean is much less well known on shorter
space scales than it is on the $2° \times 10°$ scale, so we do not know if the
cubic spline fit properly represents the space scales of the climatologi-
cal mean. In the numerical ocean models there is often mesoscale structure
in areas of the mean fields adjacent to the model "Gulf Streams", and
there are plausible (i.e., topographic) reasons to anticipate mesoscale
mean features in the ocean, but the oceanic data base is not adequate to
examine these scales.

The issue of mean field variations on the mesoscale recently arose in
efforts to analyze the XBT data set from the POLYMODE Synoptic Experiment
(Harrison and Heinmiller, 1983). Figure 5 shows the mean depth of the
15°C isotherm and its standard deviation, based on this data set. Over
the main Synoptic Experiment region (67 to 73°W by 26 to 32°N) the
standard deviation is less than 50 m, and the mean field variations are
of the same magnitude. Such variations in the mean field are statistic-
ally significant at the 95% level (relative to standard hypotheses) if
there are roughly ten degrees of freedom in the data set and are
marginally significant if there are only five degrees of freedom.

The reliability of the existence of mesoscale structure in the mean is
of consequence because it can strongly affect even simple statistics
of the variability. Figure 6 shows the autocorrelation functions for
temperature at 600 m (roughly the depth of the z_{15} surface) based on
assuming that the mean is a constant, a linear function of latitude and
as represented in Figure 5. Statistically significantly different cor-
relations can result, as Figure 6 makes clear.

As correlation functions like all of those shown above increasingly
serve as the basis for both analysis of data sets and design of future
field programs, it is very important to know them well. Proceeding with
"objective analysis" techniques on the basis of marginal or inadequate
statistics at a minimum violates the underlying assumptions of ob-
jective analysis and can lead to seriously flawed analysis and design
results. These two examples suggest that considerable caution must be
exercised with these techniques at the present.

Consider next a few items concerning the characteristics of the mesoscale
variability in numerical model systems. Early EGCM studies (Holland and
Lin, 1975; Robinson et al., 1977; Holland, 1978) devoted some attention
to the detailed characteristics of the model variability as well as
statistics. These early studies tended to produce a variability field
with most of its energy in forced, quasi-basin modes (Harrison and Robinson,

24
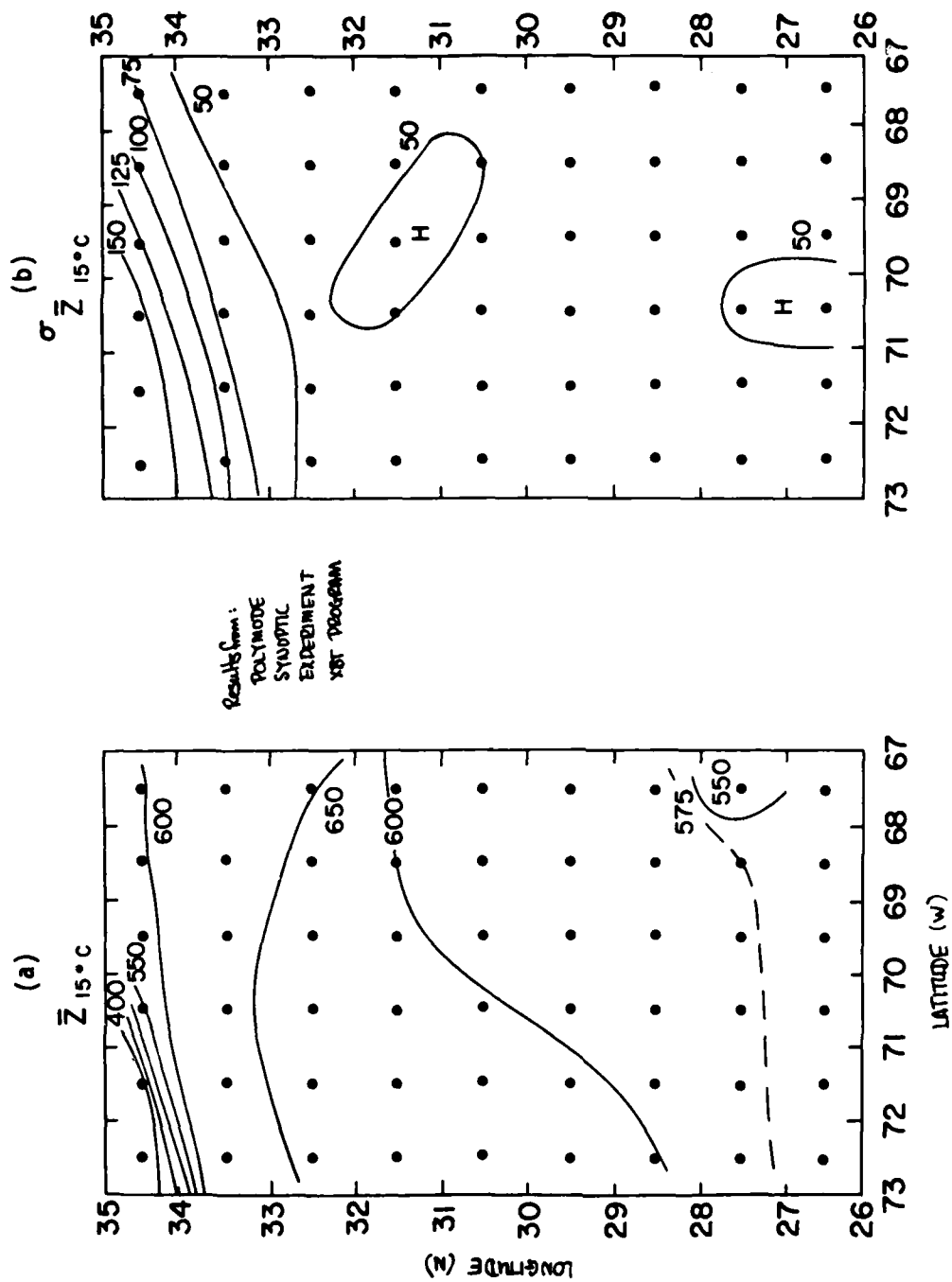
Fig. 5. (a) Mean depth of 15° isotherm (Z_{15}) during the POLYMODE Synoptic Experiment, as measured by XBTs. (b) Standard deviation of Z_{15}. Note that there is mean field structure on "meso" scales.

Autocorrelation Function for T_{600}

26-32 N, 68-72 W   July 1977-July 1978
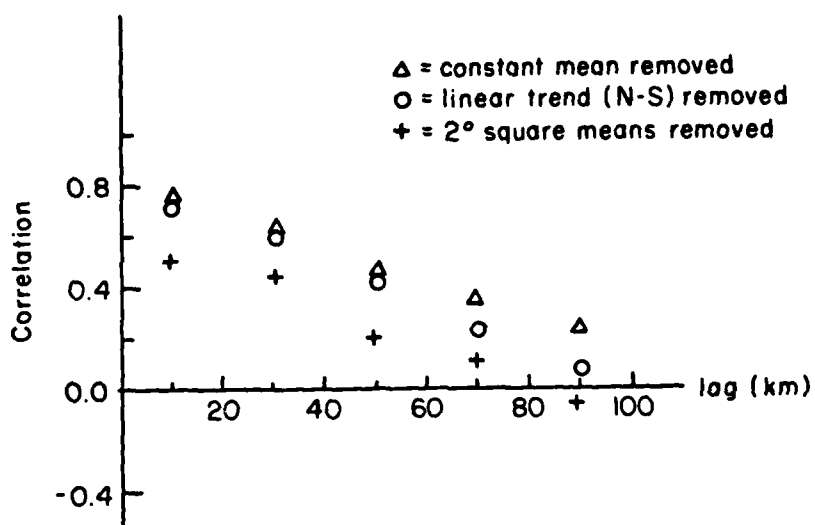
Fig. 6. Autocorrelation function for temperature at 600 m from the POLYMODE Synoptic Experiment, with mean removed three different ways.

1979). They thus have a rather different sort of variability than seems to be found in the energetic areas of the ocean, where intermittency of strong "events" seems to be common (e.g., POLYMODE array 2 results).

Recent model/data studies have tended to emphasize the patterns of eddy kinetic energy and very broad-band power spectral results. A feature-characteristic perspective has not been used. I believe that additional efforts to characterize the temporal and spatial properties of the variability of both the ocean and the models could help us understand the utility of our present models.

For example, in those EGCM experiments with which I am familiar, the eddy fluxes like $\overline{u'T'}$, $\overline{u'v'}$, etc. tend to have quite small space scales (perhaps 100 km) in those regions where the eddy fluxes are large. Although one cannot speak with confidence about such scales in the ocean, it appears at present that oceanic scales are quite a lot larger. I have suggested (Harrision, 1980) that the smaller model scales quite plausibly result from the special character of the forced, quasi-basin modes of the model variability in the early experiments. Because it is the divergence of the eddy fluxes that appears in the mean dynamical equations, the models must produce fluxes with scales comparable to those in the ocean if the model eddy term importance is to be realistic. We shall return to this below.

Consider now the question of the roles of the mesoscale in the mean ocean circulation. My personal belief is that we do not yet have enough ocean information to address this issue directly, although McWilliams will present some tantalizing new results from the POLYMODE Local Dynamics Experiment later in this meeting. Based on the available POLYMODE Array 1 and 2 data (then the only suitable ocean data set for such studies) Harrison (1980) suggested that: (a) Eddy terms are not dominant in the mean heat, momentum or relative vorticity equations, (b) the eddy term most likely to be important is the eddy heat flux divergence and it might be 0(1) in some locations, (c) a consistent balance could not be found if quasi-geostrophic dynamics were assumed for the mean flow. These results remain quite tentative, because a number of assumptions had to be made in order to use the available data, but no contradictions have surfaced to date.

Another way of looking for eddy-mean flow interaction is through SOFAR float dispersion (e.g., Freeland et al., 1975). These data suggest, after making a number of assumptions in order to relate float dispersion to a sort of Lagrangian eddy diffusivity amplitude, that the eddies may be important in mean vorticity dynamics. Several factors may limit this inference, beyond the basic assumptions that have to be made to relate short-time dispersion to some sort of "effective eddy diffusivity," and they relate to sampling problems.

The first issue is that an ensemble of floats tracked for a time short compared to the low-frequency scales of the variability can appear to disperse, even if there is not true dispersion at all. This can be observed by examining the behavior of floats in a simple Rossby wave field and is a problem for all MODE and LDE duration experiments. Another problem arises out of the apparent intermittency of strong variability, because one needs to have enough realizations of float dispersion to get an average value that reflects the average behavior of the ocean in that region. It thus may be useful to regard LDE-type events as plausible upper bounds on eddy importance rather than as typical measures of it.

A number of interesting ideas concerning eddy/mean flow interaction have been proposed from a theoretical perspective, sometimes motivated by numerical model results. In particular it has been suggested that eddies may mix potential vorticity downgradient, may homogenize potential vorticity in particular regions, may help equilibrate the ocean subtropical gyres through lateral transport of relative vorticity across gyre boundaries, and may drive deep mean flows. Our observational knowledge makes it very difficult to determine if any of these processes is actually important in the ocean. Obviously it would be of great interest to be able to design experiments able to look for these sorts of behavior.

The last topic I shall touch on concerns the roles of mesoscale variability in the mean circulation of the eddy-resolving general circulation model (EGCM) experiments that have been done. Some EGCM results were described above. I emphasize that EGCM research is *ongoing*, and that I am not conversant with all the results of my colleagues; again only certain topics can be touched on here.

The most basic result from EGCMs is that, in certain parameter ranges defined by model physical assumptions as well as forcing and dissipation types and amplitudes, mean flows can be produced with roughly oceanic scales in which eddy terms (usually, but not always, eddy heat flux divergence) are order unity in the mean balances. As these are forced and dissipative systems to which the wave-mean flow noninteraction theorems do not apply, it seems reasonable to infer that, where eddy terms are $O(1)$, the eddies are playing a significant role in the mean flow. However, as mentioned above, the eddy terms tend to be very spatially variable in the regions where they are large--with areas of large positive and negative values adjacent to each other. The result of this is that the eddy term importance often drops drastically when area average values are compared rather than point values (e.g., Harrison and Holland, 1981). When this type of behavior is found it is not clear that the eddies contribute in a fundamental way to the general character of the general circulation, even though they are locally important.

Two important exceptions to this type of small-scale structure have been discussed in the literature. In the first case, a broad area of systematic eddy heat flux convergence is found to be important in the lower layer in the area of westward-flowing upper-layer recirculation (adjacent to the eastward-flowing "Gulf Stream") of Holland (1978) experiment 5. In the second instance, involving this same experiment, there is a small region of very intense upper-layer lateral eddy transport of relative vorticity. Here the eddy term is so large that it represents a dynamically crucial amount of vorticity transport even though the region is quite small. The first instance has been discussed from different perspectives by Holland and Rhines (1980) and Harrison and Holland (1981), and the second instance principally by Harrison and Holland (1981).

The most prominent aspects of the mean EGCM flows which differ from the simple steady, linear and viscous circulations of classical wind-driven ocean circulation theories are the recirculating upper layer "Gulf Stream" gyres (near the northern boundary of the model subtropical gyre) and the deep flow gyre(s) that underlie or are adjacent to the upper layer re-circulation. The upper layer recirculation is fundamentally a mean non-linear effect; instability of this flow (in either its eastward or west-ward flowing part) can alter the flow in detail, but the existence of the recirculation fundamentally arises out of the inability of the western boundary current to rid the flow of all the vorticity put in over the gyre by the wind stress curl field. Harrison and Stalos (1982) have discussed this issue at length for the barotropic vorticity equation with a linear frictional mechanism, although the existence of recircu-lations in the absence of eddies has been clear at least since Veronis (1966). Recent work by Holland (personal communication) also indicates that the character of the upper layer recirculations in his QG experiments results largely from factors that do not explicitly involve the model eddies. It is quite clear, however, that the eddy terms do enter the mean equation balances at $O(1)$ in many EGCM experiments in this recircu-lation. Locally, the eddy effects thus may be quite important. But the available evidence from watching these flows spin up from rest suggests strongly that a fundamentally similar recirculation exists prior to the onset of eddy activity.

It is more difficult to discuss the dynamics of the deep flow recirculat-ing gyres, since a variety of flows have been observed (Harrison, 1982). The published QG adiabatic experiments all have a pair of "counter-rotating" gyres underlying the upper-layer recirculation; other experiments have a single deep "corotating" gyre in which the flow has the same clockwise sense of circulation as the upper-layer flow. Still other experiments, using bottom topography and altered basin geometry (e.g., Semtner and Holland, 1978) produce flows that do not fit conveniently into either the "corotating" or "counterrotating" classification. Since the adiabatic QG system is constrained by its basic assumptions to have no lower layer mean flow unless eddies are present, it has been conventional to assert that the presence of both deep gyres is an eddy result. Strictly taken this is correct, but Holland and Lin (1975) experiment 5 shows a 2-layer adiabatic primitive equation case without eddies in which there clearly

is a corotating deep gyre. Also, the adiabatic QG flows often show a co-rotating deep gyre as they spin up from rest. Thus the connection between eddies and the corotating deep gyre seems to deserve more attention, in systems somewhat less restrictive than those of adiabatic QG physics.

The evidence that the counterrotating deep gyre, which seems always to underlie the westward-flowing part of the upper layer recirculation, is an eddy effect seems more persuasive. Its existence, as a plausible result of baroclinic instability in the region of westward flow in the upper-layer recirculation, has been discussed in very simple terms by Harrison (1982). Holland and Rhines (1980) have discussed it in terms of eddy potential vorticity diffusion. From either perspective, it is clear that the eddy heat flux divergence, acting through the model heat equation to determine the mean vertical velocity, which in turn is the only vorticity source for the lower layer, is $O(1)$ in the lower layer mean vorticity equation in this region.

It is somewhat puzzling that the pair of counterrotating deep gyres is only found in the adiabatic QG experiments. As Harrison (1982) noted, this might result from the general character of the flow coupled with the QG adiabatic constraints, and/or might be a result peculiar to the parameter range of Holland (1978), and/or might result from a combination of QG con-straints and the choice of linear bottom friction as the dominant vorticity sink. Semtner and I have been exploring these questions and it definitely appears that the choice of lower-layer frictional form can have a major impact on the lower-layer flow character, in adiabatic QG experiments like those of Holland (1978) and of Holland and Lin (1975). We have found that using the parameters of Holland and Lin (1975) experiment 3, but changing the lower-layer friction from eddy viscosity (which gave a single deep co-rotating gyre in the mean flow) to linear bottom drag results in a pair of deep counterrotating gyres.

The physics of deep flow generation is delicate, because a small amount of vorticity can result in substantial deep flows. In fact, the vorticity balance of the upper-layer mean flow would be substantially unaltered in many EGCM cases if there were no vorticity input into the lower layer, yet this almost dynamically insignificant amount of vorticity is responsible for the deep flow. Much work remains to be done on the problems surrounding deep mean flow generation in the EGCMs; at present the connection to oceanic deep mean flow generation is unclear.

As an effort to summarize about the roles of eddies in EGCM mean flows, I think it is most prudent to say that they can be important, particularly near strong mean currents, but that questions concerning the extent to which they result in qualitative changes in the mean flows remains an un-clear function of assumed model physics and other parameter choices. Few general results have been established thus far; local effects are clear, but systemic effects are much less so.

The main topic of this conference will remain an active research area for many more years. Because the oceanic mesoscale is so demanding to sample for stable statistics, much more data must be collected before we shall have ocean dynamical statistics even roughly comparable to those now available from EGCMs. Without better ocean statistics it will remain difficult to carry out ocean-model intercomparisons on other than a gross kinematic level. Of course EGCM studies will continue to be made, and one hopes that new results will become established that are not sensitive to choices about model frictions and other aspects of model physics. Seeking relatively model-insensitive results appears to be the most fruitful path for future EGCM research, the one most likely to provide points of contact with observational data.

REFERENCES

Ebbesmeyer, C. C. and B. A. Taft, 1979. Variability of potential energy, dynamic height and salinity in the main pycnocline of the western North Atlantic. J. Phys. Oceanogr., 9, 1073-1089.

Freeland, H. J., P. B. Rhines and H. T. Rossby, 1975. Statistical observations of the trajectories of neutrally buoyant floats in the North Atlantic. J. Marine Res., 33, 383-404.

Harrison, D. E., 1980. Some Eulerian scale analysis results: eddy terms the mean heat, momentum and vorticity equations. J. Phys. Oceanogr., 10, 1221-1227.

Harrison, D. E., 1981. Eddy lateral vorticity transport and the equilibrium of the North Atlantic subtropical gyre. J. Phys. Oceanogr., 11, 1154-1159.

Harrison, D. E., 1982. On deep mean flow generation mechanisms and the abyssal circulation of numerical model gyres. Dynamics of Atmospheres and Oceans, 6, 135-152.

Harrison, D. E. and A. R. Robinson, 1979. Boundary-forced planetary waves: a simple mid-ocean response to strong current variability. J. Phys. Oceanogr., 9, 919-929.

Harrison, D. E. and W. R. Holland 1981. Regional eddy vorticity transport and the equilibrium vorticity budgets of a numerical model ocean circulation. J. Phys. Oceanogr., 11, 190-208.

Harrison, D. E. and S. Stalos, 1982. On the wind-driven ocean circulation. J. Marine Res., 40, 773-791.

Harrison, D. E. and R. H. Heinmiller, 1983. Upper ocean thermal variability in the Sargasso Sea July 1977-July 1978; the POLYMODE XBT Program. J. Phys. Oceanogr., 13, 859-872.

Harrison, D. E., W. J. Emery, J. P. Dugan and Li, B.-C., 1983. Mid-latitude mesoscale temperature variability in six multi-ship XBT surveys. J. Phys. Oceanogr., 648-662.

Holland, W. R. and L. B. Lin, 1975. On the generation of mesoscale eddies and their contribution to the oceanic general circulation. Parts I & II. Journal of Physical Oceanogr., 5, 642-669.

Holland, W. R., 1978. The role of mesoscale eddies in the general circulation of the ocean--numerical experiments using a wind-driven quasi-geostrophic model. J. Phys. Oceanogr., 8, 363-392.

Holland, W. R. and P. B. Rhines, 1980. An example of eddy-induced ocean circulation. J. Phys. Oceanogr., 10, 1010-1031.

Robinson, A. R., D. E. Harrison, Y. Mintz and A. J. Semtner, Jr., 1977. Eddies and the general circulation of an idealized oceanic gyre: a wind and thermally driven primitive equation numerical experiment. J. Phys. Oceanogr., 7, 182-207.

Semtner, A. J., Jr. and W. R. Holland, 1978. Intercomparison of quasi-geostrophic simulations of the western North Atlantic circulation with primitive-equation results. J. Phys. Oceanogr., 8, 735-754.

Veronis, G., 1966. Wind driven ocean circulation: Part II. Numerical solutions of the non-linear problem. Deep-Sea Res., 13, 31-55.

ESTIMATION AND PREDICTION OF OCEANIC EDDY FIELDS*

Allan R. Robinson and Wayne G. Leslie

Division of Applied Sciences, Harvard University
Cambridge, Massachusetts 02138

ABSTRACT

`A system for the optimal estimation and forecasting synoptic/mesocale
ocean currents is presented consisting of an observational system, a
statistical model and a dynamical model. The methodology is developed for
the case when the dynamical model is a baroclinic, quasigeostrophic
open-ocean model. Issues involved include the synoptic and regular gridding
of asynoptic non-uniform data, the construction of composite fields from
several data types, and the initialization and verification of the dynamical
model. Models for the error fields required for weighted combinations of
independent field estimates are obtained from the analysis of an
observational system simulation carried out with a large numerical data set
generated by the dynamical model; a barotropic example is presented. The
statistical model is applied to the POLYMODE Synoptic-Dynamic Experiment
(SDE) XBT and current meter data which is successfuly assimilated in the
dynamical model. Dynamical forecasting experiments are carried out and the
difference fields between analysis fields and forecast fields are studied
and attributed to: error sources in the analysis, in intitial and boundary
condition data, and to the dynamical adjustment of those fields by the
model. Quantitative results indicate that useful accuracies can be
efficiently obtained.

1. INTRODUCTION

Physical fields of interest in the ocean are energetically variable in
the mesoscale range (tens to hundreds of kilometers and weeks to months.)
These scales are the dynamical analogue in the ocean of the atmospheric
synoptic scale, i.e. weather. Thus it is often necessary to describe and
predict the fields of ocean current, temperature, density, etc. with
resolution adequate for the mesoscale variability over large-scale regions
for scientific studies or for practical purposes. Scientifically accurate

---

* This report is a preprint of a paper submitted to "Progress in
Oceanography". It constitutes an updated version of the material presented
at the Hawaiian meeting in January, 1983.

knowledge of the fields is required in order to infer local mesoscale dynamical processes via balance of terms in energy, vorticity and heat equations. Since mesoscale processes can influence the mean fields and their very low frequency fluctuations, accurate field descriptions with mesoscale resolution are also essential now for general ocean circulation and climate oriented research. Nowcasts and forecasts for commercial and military operations have their own accuracy requirements.

To obtain mesoscale resolution over large scale regions presents a formidable task to oceanographers. Intensive dynamical experiments are necessarily limited in areal extent and the capability of forecasting in open regions must be developed. The large resources required to obtain information and the sparseness of the existing and potential data sets relative to the amount of data actually required to answer questions of interest make efficient utilization and exploitation of data sets important. Remotely sensed oceanic data sets present their own special problems for management and utilization. Sea surface heights and temperatures obtained by radar altimetric and infrared measurements from satellites are voluminous data sets, the value of which can be very much enhanced by combination with related in situ observations. Interpreted in conjunction with relevant oceanic models, remotely sensed surface observations can powerfully contribute to four-dimensional sub-surface field descriptions.

Here we present a method for the efficient and accurate description and prediction of fields in arbitrary open ocean regions. The approach is a combined statistical and dynamical method. It is based upon optimal estimation techniques used in electrical engineering and orbit analysis (Liebelt, 1967) and four-dimensional data assimilation techniques of modern meterology (Bengtson, Ghil and Kallen, 1981). The method is a systematic one which allows for the efficient pooling of information from all available sources. It deals with such issues as (1) the estimation of physical fields (velocity, temperature, density, pressure, etc.) by combining measurements from a variety of instruments (current meters, floats, hydrography, XBT's, remote sensors, etc.), (2) the construction of regular time series of synoptic maps from data sets which have gaps in time and space, and (3) the design of observational networks and experimental sampling strategies. The method blends and interpolates contemporary measurements subject to constraints based upon both the general dynamics and the past statistics of similar flows.

The general procedure of the optimal estimation method is the minimization of the expectation value of a pre-selected error norm. A norm often chosen is the mean square difference between the estimate and the true value of the field. The procedure is thus optimal in a statistical sense and depends crucially on a knowledge of the statistics. The quantities needed relate to the noise and error characteristics of the observational network, the analysis scheme for treating the instrumental records, and the dynamical model. These quantities determine the error statistics of the particular estimation procedure. A central principle is that two or more a priori independent estimates for a quantity of interest may be combined in a

manner such that the combined estimate has a lower expected error than any
of the expected errors of the elements of the combination. The combined
optimal estimate weights the elements inversely to the strength of their
individual error variances. The formalism is a generalization of the method
used to weight the influence of the data points on an analysis point in an
objective analysis scheme.

A schematic of the descriptive-predictive system we have developed for
the optimal estimation of oceanic fields is shown in Figure 1. The
"statistical model" is a multivariate space-time objective analysis scheme.
It is used to produce regularly gridded fields in time and space (analyses)
from the irregularly distributed composite data of the observational network
and to make statistical forecasts (forward interpolation in time). The
dynamical model is a baroclinic, quasigeostrophic, open ocean model. It is
initialized with analyzed data from the observational data for the requisite
boundary conditions around the edge of the domain, the model"nowcasts" the
fields in the interior. If the boundary conditions are forecast by some
scheme, the model can be used to make dynamical forecasts for the region.
The dynamical model can also be fed partial or sparse data in the interior
domain in the course of a nowcast or forecast, i.e., "up-dated". Utilized
in this manner, the dynamical model may be regarded as an interpolation
scheme for the data. If the general dynamics of the model are a valid
representation of the regional dynamics, dynamical interpolation can reduce
data requirements or extend the domain of influence (e.g. of satellite
data). Consider now the outputs of the statistical model and the dynamical
model as independent field estimates which serve as the basis for a combined
optimal field estimate. An optimal estimate will agree with the observation
within the noise level where data exists and will be dynamically adjusted
across sparse data regions. Such fields provide a consistent and relatively
accurate basis for regional physical process studies.

Error sources for the analyzed fields arise not only from instrumental
and environmental noise and data sampling schemes but also from the
statistical model adopted and from an imperfect knowledge of the statistical
quantities. The dynamical model may have errors on explicitly resolved
physical scales and/or in the parameterization of sub-grid scale physical
processes. Dynamical forecast errors occur because of inaccurate initial
and boundary conditions and can occur also from an inadequate choice of
computational parameters such as grid spacing or time-step. The models
should be carefully calibrated computationally and verified physically by
comparison with densely sampled accurate data sets. Such data is generally
not available in the ocean, so that the development of the methodology and
the verification of the models must occur gradually and side-by-side. In
such circumstances the difference field between a dynamical forecast and
analyzed observations needs to be studied carefully for attribution of error
sources. Such attribution is essential for the proper blending of the
fields into a combined optimal estimate. The practical implementation of
the method also involves numerous detailed technical problems including the
choice of efficient and stable computational schemes.
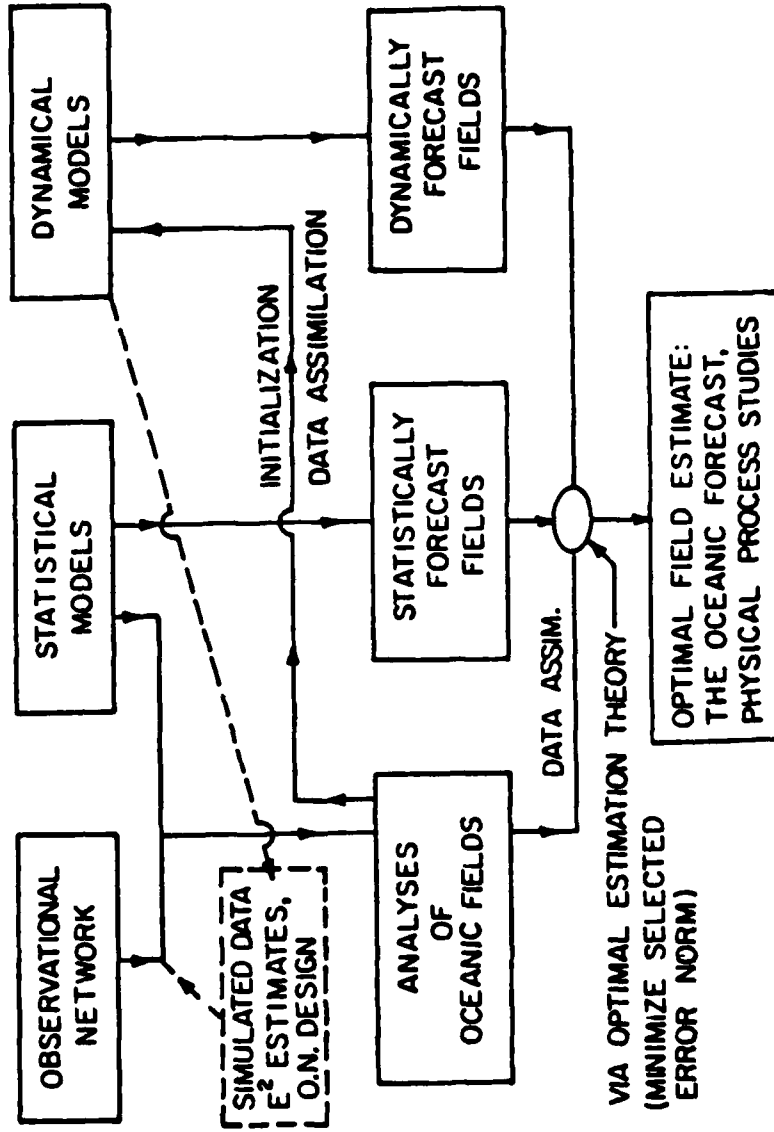
Fig. 1. Schematic of the oceanic descriptive/predictive system.

Since oceanic data is not adequate at this time to provide the required statistical quantities, the approach adopted involves computer simulated data sets generated using the dynamical model. The procedure is to use available statistical and/or synoptic data for a region to initialize and drive the model and to vary parameters so as to tune the simulation to the known data. The observational network and the estimation scheme can then be run through an ensemble of independent realizations to produce the required statistics. The statistics are then used in real ocean situations and iterated as experience is gained and more real data is accumulated.

This paper presents the methodology of the optimal estimation and illustrates some of the issues involved in the context of analysis in progress of the POLYMODE Synoptic/Dynamic Experiment (Robinson,1982; Heinmiller,1977; Grachev et al.,1978) by the Harvard physical oceanography group. The data set includes measurements of temperature and current at several levels for over a year over a several-hundred-kilometer-square domain. The formalism is briefly presented, the data set is exemplified, and the optimal combination procedure illustrated via a barotropic prototype calculation based on the MODE-1 current meter and float network at 1500 m. The baroclinic model is initialized with the POLYMODE data and the results of hindcasting experiments are interpreted.

2. MODELS AND METHODOLOGY

2.1 Formulation

Consider two a priori independent estimates, $(\psi_{1,2})$ of a field ψ. The mean value of ψ is zero, but the estimates may be biased $(B_{1,2})$. Then the error fields may be biased and are possibly correlated. Thus,

$$\overline{\psi_1 - \psi} = B_1 \qquad\qquad \overline{\psi_2 - \psi} = B_2$$

$$\overline{(\psi_1 - \psi)^2} = E^2_1 + B^2_1 \qquad\qquad \overline{(\psi_2 - \psi)^2} = E^2_2 + B^2_2$$

$$\overline{(\psi_1 - \psi)(\psi_2 - \psi)} = \gamma E_1 E_2 + B_1 B_2$$

where an overbar denotes an expectation value, and γ is the correlation coefficient (normalized covariance) of the estimates errors. We seek an optimal estimate (ψ_0) which is a convex linear combination of $\psi_{1,2}$, and which minimizes the mean square error $E^2 = \overline{(\psi_0 - \psi)^2}$.

$$\psi_0 = \alpha\,(\psi_1 - B_1) + (1-\alpha)(\psi_2 - B_2) \qquad 0 \le \alpha \le 1$$

38

it is readily shown (Tu,1981, Ghil,et al. 1981) that the minimization procedure yields

$$\alpha = \frac{E_2^2 - \gamma E_1 E_2}{E_1^2 + E_2^2 - 2\gamma E_1 E_2} \qquad (1-\alpha) = \frac{E_1^2 - \gamma E_1 E_2}{E_1^2 + E_2^2 - 2\gamma E_1 E_2}$$

with the expected error in ψ_0 given by

$$E^2 = \frac{E_1^2 E_2^2 (1-\gamma)}{E_1^2 + E_2^2 - 2\gamma E_1 E_2}$$

For the case of unbiased estimates and uncorrelated errors ($\gamma = 0$), the result is

$$\psi_0 = \frac{E_2^2}{E_1^2 + E_2^2} \psi_1 + \frac{E_1^2}{E_1^2 + E_2^2} \psi_2 \ , \qquad E^2 = \frac{E_1^2 E_2^2}{E_2^2 + E_2^2}$$

The estimates are seen to be weighted proportionately to their relative accuracies and the expected error to be less than either E_1^2 or E_2^2.

The Harvard statistical model (Carter, 1983) is based on standard objective analysis techniques (Gandin,1965, Bretherton, Davis and Fandry 1976). A set of n measurements ϕ_r, $r=1\cdots n$ taken at space-time points, $\underline{x}_r$: (x_r, y_r, z_r, t_r) with noise level ϵ_r optimally linearly interpolate (in a least squares sense) to the point $\underline{x}$ by the formula

$$\psi = \sum_{r=1}^{n} B_{xr} \sum_{s=1}^{n} \left(A_{rs}^{-1} \phi_s \right)$$

with expected error variance

$$\overline{(\psi - \psi)^2} = B_{xx} - \sum_{r,s=1}^{n} B_{xr} B_{xs} A_{rs}^{-1}$$

where

$$A_{rs} = \overline{\phi_r \phi_s} = C(\underline{x} - \underline{x}_r) + \epsilon \delta_{rs}$$

$$B_{sr} = C(\underline{x} - \underline{x}_r)$$

if the noise in the measurements is uncorrelated with itself and the true field, i.e.

$$\overline{\epsilon_r \phi_s} = 0 \qquad \text{and} \qquad \overline{\epsilon_r \epsilon_s} = \epsilon \delta_{rs}$$

Here C is the correlation function. In the version of the model used to
analyze the data of this study, the correlation fuction is taken to depend
upon two horizontal variables and time as a function of depth in the ocean
but otherwise assumed homogeneous and stationary over the observational
domain.

Thus, schematically

$$C_z^{nm}(\Delta x, \Delta y, \Delta t) \approx \overline{\phi_n(x,y,z,t)\phi_m(x+\Delta x, y+\Delta y, z, t+\Delta t)}$$

is our anisotropic space-time correlation model as a function of east-west,
north-south and temporal lags (Δx, Δy, Δt) for the correlation between two
scalar measurements $\phi_{n,m}$. In the XBT analyses referred to below $n=m$ and ϕ
is the depth of the $15^{\circ}C$ isotherm; in the current meter analyses $\phi_1 = u$, $\phi_2 \approx v$
or alternatively, $\phi_1 =$ speed, $\phi_2 =$ direction. The parameters of the
statistical model which must be specified to carry out an analysis are: the
maximum region of influence (in space-time domain) of a data point, the
number of influential data points per analysis point, the maximum
correlation allowed among the influential data points, and the noise level.

The Harvard Open Ocean Dynamical Model integrates forward in time for
the class of initial-boundary value problems defined by the specification
of: (1) an initial volume distribution of quasigeostrophic stream-function
(and vorticity) and (2) the inflow everywhere on the vertical water-water
boundaries at the horizontal edges of the domain, and the vorticity on the
inflow everywhere on the vertical water-water boundaries at the horizontal
edges of the domain, and the vorticity on the inflow (Charney et al. 1950)
and (3) the normal velocity at the top and bottom boundaries. The latter
condition is simply w=o if the boundaries are flat and there is no Ekman
pumping, which are the only cases treated here. Bottom slopes on the order
of the basic flow Rossby number are, however, allowed and have been
studied. The vorticity is related to the nondimensional quasigeostrophic
stream function by a Poisson-like equation

$$\zeta = \nabla^2 \psi + \Gamma^2 (\sigma \psi_z)_z$$

where

$$\sigma(z) = N_0^2/N^2(z) \qquad\qquad N^2 = (-g/\rho_0)\left(\frac{d\bar{\rho}}{dz}\right)$$

and evolves in time under the conservation of potential vorticity.

$$\frac{\partial \zeta}{\partial t} + \epsilon J(\psi, \zeta) + \psi_x = F$$

where ∇^2 and J are horizontal two-dimensional operators. F represents sub-grid scale dissipative processes which are taken to be a weak bottom friction for long runs and more importantly, an "ideal" filtering operation (Shapiro, 1971) on the vorticity of arbitrary order and frequency, which is intended to wipe-up the enstrophy cascade to small scales with negligible effect on the energy flow. The physical parameters that enter are

$$\varepsilon = \frac{V_0}{\beta d^2} \qquad\qquad \Gamma^2 = \frac{f_0 d^2}{N_0^2 h_t^2}$$

a β-Rossby number and stratification parameter, respectively. N is the Brunt-Väisälä frequency, h_t is the depth of the main thermocline, d is a horizontal (meso)-scale length and V_0 the particle speed. The rest of the notation is standard.

The quasigeostrophic stream function is essential for the geostrophic-hydrostatic pressure field, $p = f_0 \rho_0 \psi$ (dimensionally), from which the velocity components and associated density fluctuations ($\rho = \bar{\rho}(z) + \rho'$) can be derived

$$u = \psi_y, \qquad v = \psi_x, \qquad \rho' = -\frac{\rho_0 f_0}{g} \psi_z$$

and

$$w = \frac{\rho_0 f_0}{g \frac{d\bar{\rho}}{dz}} \left[\psi_{zt} + J(\psi, \psi_z) \right]$$

Computationally, the model time steps forward via an Adams-Bashforth scheme, is finite-element in the horizontal and in the vertical utilizes either an arbitrary number of finite-difference levels or a collocation scheme. Details of the model have been documented and its computational errors calibrated (Haidvogel, Robinson and Schulman, 1980; Miller, Robinson and Haidvogel, 1983). The parameters which must be specified in order to carry out a regional dynamical forecast calculation are: the area average mean stratification ($\bar{\rho}(z)$), the bottom topography, initial conditions, boundary conditions, bottom friction coefficient, filter shape, strength, and frequency of application, horizontal resolution, number and location of vertical levels, and time-step length.

2.2 A baroclinic simulation

Simulations for the MODE-POLYMODE region have been carried out based upon the MODE-1 experimental data. The technique was a baroclinic extension of the method used in the barotropic prototype study by Robinson and Haidvogel (1980) for the MODE-1 1500 float and current meter data. In order to impose regionally dominant scales, amplitudes and phases, the best four Rossby wave set (two baroclinic and two barotropic) to the composite data set (McWilliams and Flierl, 1976) were used (Miller, Robinson and Haidvogel, 1983) to initialize and to provide boundary conditions throughout the duration of a

several-year-long simulation in a thousand kilometer square domain. The
linear superposition of the four waves is not a solution to the nonlinear
potential vorticity equation and the fields rapidly evolve to a statistical
equilibrium with a continuous spectrum and oceanic-like eddies (Fig. 2a,b).
In order to stay well away from the forcing wave fields, the initial time
period and the outer few hundred kilometer rim are then discarded and
simulated data for the interior region stored at six levels in the vertical,
daily over a 15-km grid. This "true" simulated data set is dubbed "Veritas"
and is used directly or with various imposed errors and gaps for a number of
studies. In order to establish the ability of the baroclinic open ocean model
to perform in a realistic nonlinear flow regime, and to quantify the model's
computational error characteristics for these parameters, a "benchmark"
forecast is made for the interior region. A benchmark experiment consists of
providing Veritas initial and boundary condition data to the model,
recalculating the interior fields and verifying the interior nowcast fields
against Veritas. Figure 2c,d shows such a comparison of main thermocline
streamfunction two months after the initialization of a benchmark. The eye
can detect no difference; the normalized root mean square (nrms) error is
seven percent. Miller and Robinson (1983) analyze this simulation further.

2.3 Dynamical adjustment and optimal estimation: A barotropic prototype example

We present next a prototype barotropic hindcasting study based on MODE-1
1500 m Sofar float and current meter data. The purposes are to demonstrate
the process of "dynamical adjustment" of data fields by a dynamical model and
to provide a concrete example of our method of optimal field estimation. An
optimal combination of the analysis and forecast field minimizes the
difference field and provides an estimate which agrees with the data within
the noise level where data is available and which is dynamically adjusted
between data points consistently with the expected accuracy of the forecast
procedure.

We have performed several numerical experiments based upon a month-long
period during which the floats moved about and current meters failed or were
restarted, but during which the expected error of the analysis for the 1500 m
stream function was relatively low. The simulated data for these 1500-m
fields is that used previously in the barotropic dynamical forecasting studies
by Robinson and Haidvogel (1980), who showed its frequency spectrum and
correlation function to be reasonably similar to observations. A sample
analysis stream function map over a 500-km-square domain is shown in Figure
3a. In Figure 4a the float and current meter observational network on a
typical day is displayed on its associated map of expected error of objective
analysis. Obviously only the central region of the map is defined credibly by
the data. The result of a one-week-long benchmark forecast is shown in Figure
3b. Compared to the analysis, the forecast high has strengthened and the low
is slightly weaker with its center displaced. Figure 5a shows the difference
field between Figure 3a and 3b, normalized by the rms of the analysis field.
The area averaged nrms difference field is 69% which clearly stands out above
the 33% value of the nrms expected error field derived from the central field
of Figure 4a.

42

MIN=-22.5110 MAX=13.95870 CI=4.000

MIN=-26.11740 MAX=14.75940 CI=5.000

MIN=-23.86300 MAX=10.43450 CI=4.000

MIN=-2.36E+01 MIN=1.04E+01 CI=4.000
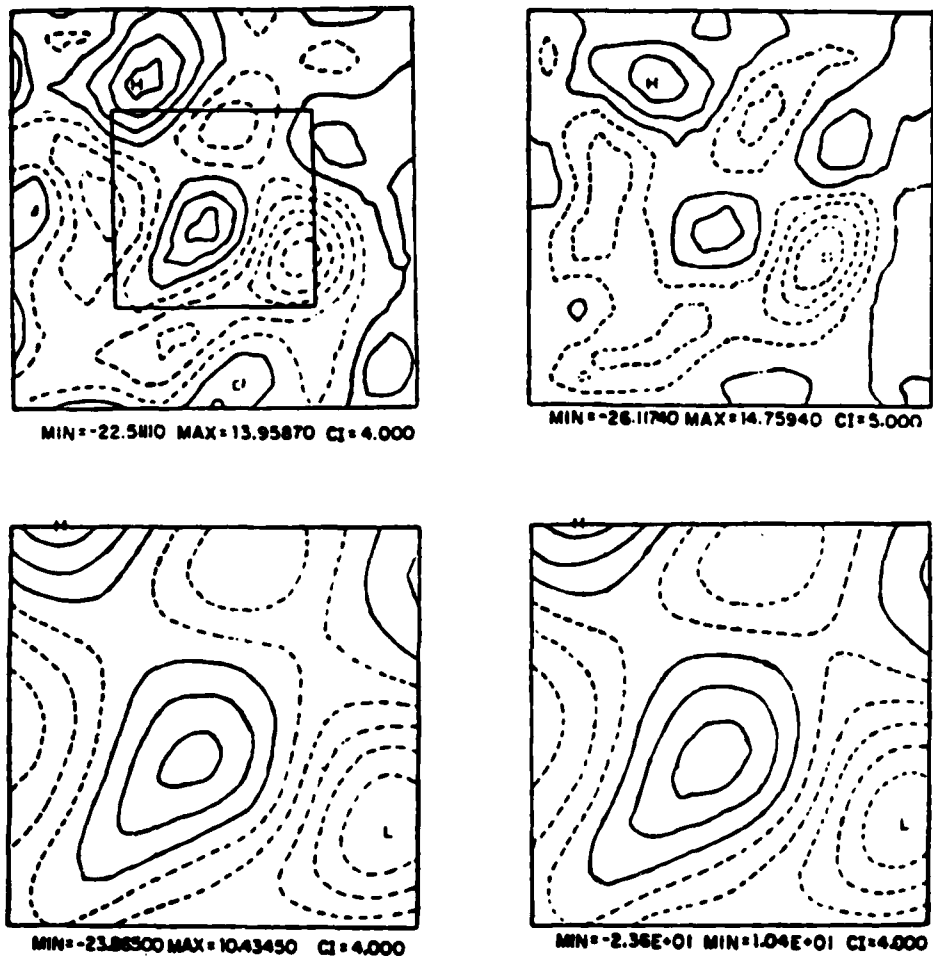
Fig. 2. (a) Baroclinic simulated streamfunction field at 750 m
generated by nonlinear evolution from initial condition of
best-fit Rossby wave field to the MODE-1 data. Field is
1000 km square. Small box represents the central 500-km-
square domain.
(b) Deviation from linearity of above field.
(c) Central domain streamfunction at 750 m (corresponds to
the inner box in (a)).
(d) Forecast streamfunction field (after Miller et al., 1983,
Figs. 15 and 16).
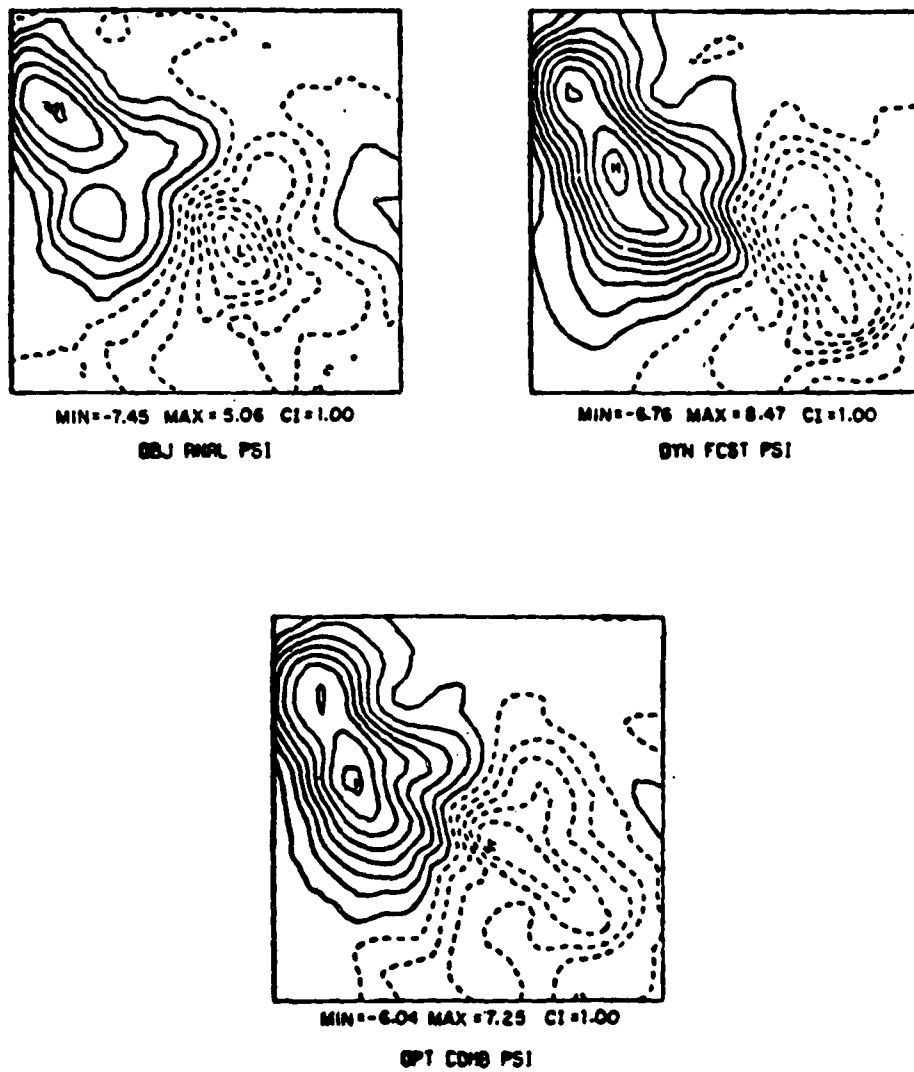
Fig. 3. An example of the optimal combination procedure.
(a) The objectively analyzed streamfunction.
(b) The dynamically forecast streamfunction.
(c) The optimal combination of (a) and (b).

44

MIN=0.01 MAX=1.00 CI=0.10
EXPECTED ERROR OA
(a)

MIN=0.01 MAX=0.70 CI=0.06
EXP ERROR OPT COMB
(b)

OA

PF

MIN=0.00 MAX=3.32 CI=0.25
AVERAGE ABSOL ERR SQRD
(c)

MIN=0.02 MAX=2.78 CI=0.25
AVERAGE ABSOL ERR SQRD
(d)
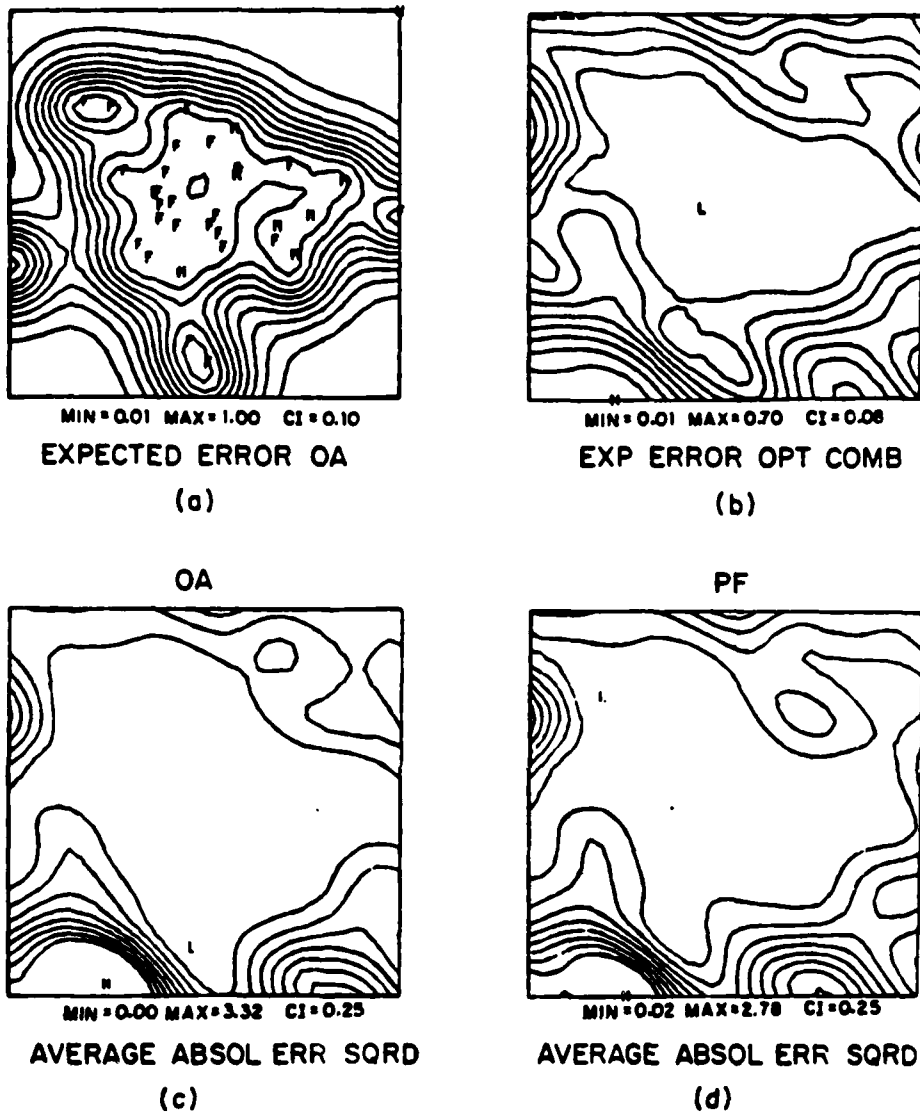
Fig. 4. The error fields which are used in the optimal
combination procedure.
(a) The expected error of the objective analysis. The
observational network is superimposed. An "F" represents
a float; an "M" represents a mooring.
(b) The expected error of the optimal combination.
(c) The average (over 10 realizations) of the difference
(squared) between simulated data and simulated data sampled
with the observational network and objectively analyzed.
(d) The average (over 10 realizations) of the difference
(squared) between simulated data and fields from a persis-
tence forecast initialized with simulated data sampled with
the observational network and objectively analyzed.

BENCHMARK

PERSISTENCE

MIN=-1.48 MAX= 2.63 CI=0.50
NORM = 2.183

MIN=-1.58 MAX= 3.09 CI = 0.50
NORM = 2.183

BENCHMARK

INTERIOR BENCHMARK

MIN=-1.48 MAX= 2.63 CI = 0.50
NORM = 2.183

MIN=-0.50 MAX= 2.03 CI = 0.30
NORM = 2.036
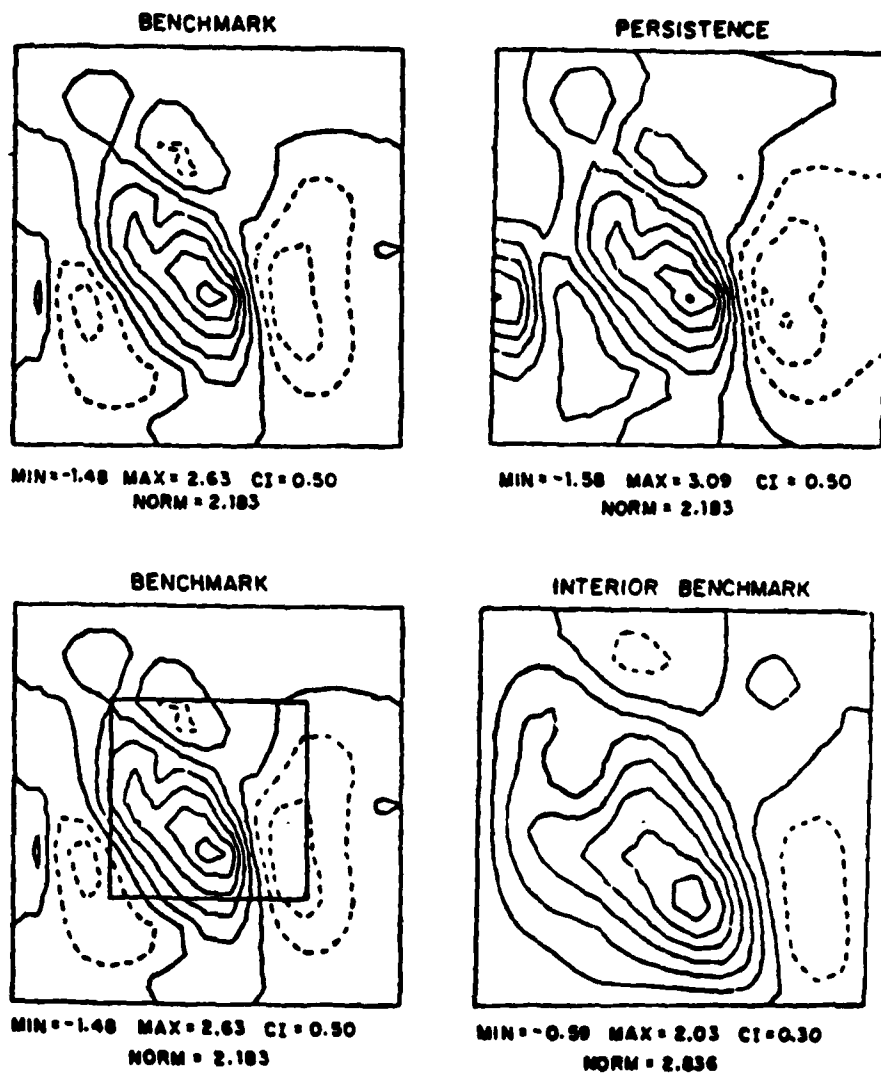
Fig. 5. The difference fields between forecast and verification
streamfunction for barotropic forecasts.
(a) 33 x 33 benchmark forecast.
(b) 33 x 33 persistence forecast.
(c) 33 x 33 benchmark forecast with 17 x 17 interior region
outlined
(d) 17 x 17 benchmark forecast.

In order to interpret the difference field, the results of three
additional hindcast experiments are shown in Figure 5b,c,d. Initializing the
model and running a dynamical forecast forward in time maintaining the initial
boundary conditions as the boundary conditions throughout the duration of the
computation is called a "persistence" forecast. The four experiments of
Figure 5 are benchmark and persistence forecasts both over the full domain and
also over the interior half domain (250 km square). The smaller domain
calculations provide boundary condition information where the analysis field
is relatively good and also explores the dependence of boundary condition
influence upon domain size. The remarkable aspect of Figure 5 is the
robustness of the appearance of the major features of the difference fields
which are essentially independent of the particular experiment, which is most
strikingly evident in the small domain persistence. This robustness
identifies the difference field as the dynamical adjustment of the fields to
the dynamics of the model. Running the barotropic model with real ocean data
exhibits the dynamical adjustment phenomenon well because the ocean really is
not governed by barotropic dynamics (even at the zero crossing level of the
first linear baroclinic mode).

To carry out the optimal estimation procedure, the observational network
is applied to an ensemble (ten) of independent synoptic realizations of the
simulated data. The sampled data is then objectively analyzed (gridded into a
full field by the statistical model) and used for dynamical model
initialization, boundary condition and comparison data. The Veritas
barotropic data is available for verification at any step of the procedure.
It is needed so that absolute forecast error fields and their statistics can
be generated. Figure 6a shows the observational network superimposed on a
simulated eddy field. The objective analysis expected error field, which has
been constructed from the 10 realizations, is shown in Figure 4c. Figure 4d
is the expected error after about a week of persistence dynamical forecast
initialized by an analysis generated by the observational network.
Persistence was chosen because it differs little from benchmark in this case
and also because it simulates a situation in which only one synoptic
realization is required. An optimal combination procedure is now carried out,
as before, where the analysis streamfuction and the dynamically forecast
streamfunction are the independent estimates (ψ_1, ψ_2) of Section 2.1. The
expected error of the analysis (Fig. 4c) is ε_1^2, and the dynamical forecast
error (Fig. 4d) is ε_2^2. The expected error of the combination ε_0^2 is shown in
Figure 4b and the sample optimal field estimate is displayed in Figure 3c.

The combined statistical and dynamical approach has been applied to a
number of sample problems using the barotropic version of the model and
simulated data (Robinson and Tu, 1981; Tu, 1981). These include studies of
the sensitivity of the model to initial and boundary condition analysis
errors, and boundary condition and patch updating schemes. Since the model is
non-linear and the system is complex, the statistical and dynamical models may
be related in a number of ways and the optimal combination procedure invoked
variously.

MIN = -4.40 MAX = 6.33 CI = 1.00
VERITAS PSI

MIN = -3.84 MAX = 5.02 CI = 1.00
OBJ ANAL PSI

MIN = -2.10 MAX = 2.65 CI = 0.50
NORM = 1.903

NORMAL ABSOL ERROR PSI
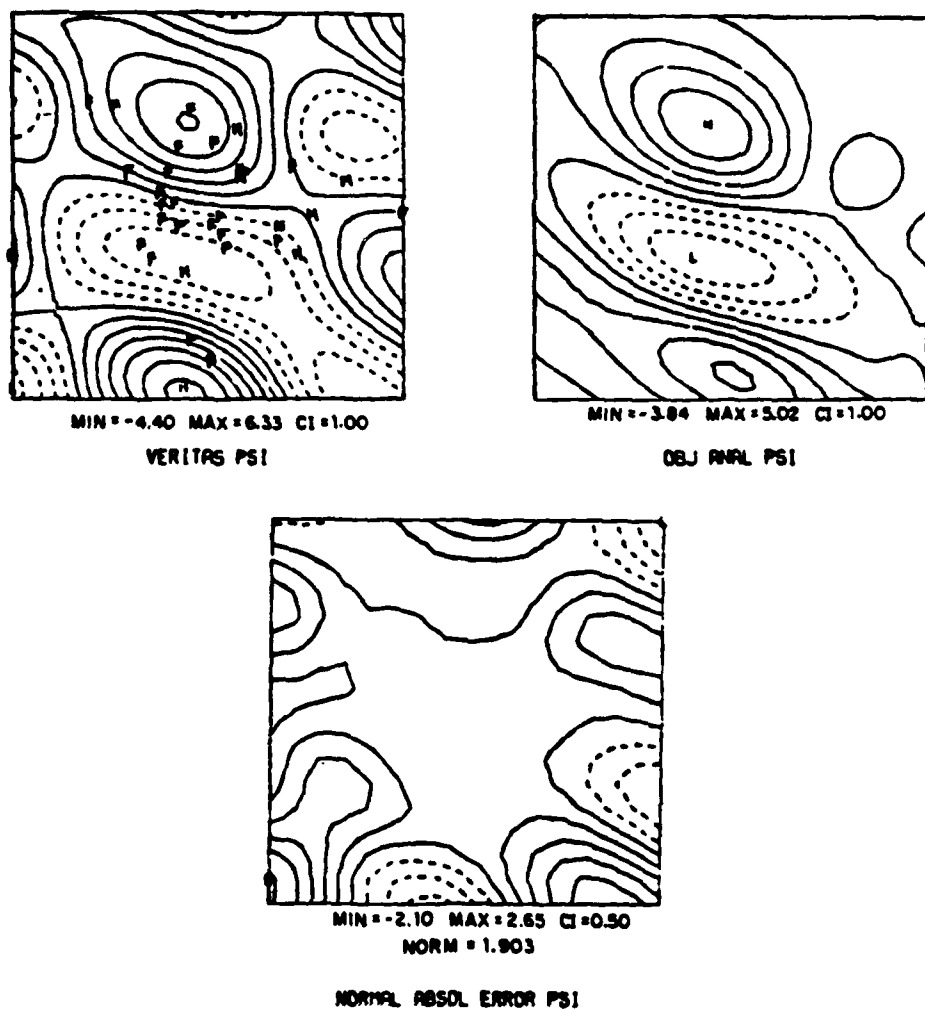
Fig. 6. (a) Simulated barotropic streamfunction field with an
observational network superimposed.
(b) The objectively analyzed streamfunction field from the
sampled simulated data.
(c) The difference between the simulated (veritas) data and
the objectively analyzed streamfunction.

3. ANALYSIS AND FORECAST MODELING OF THE POLYMODE SDE DATA

The statistical model has been used to produce regular time series of synoptic maps from the more than year-long US-USSR POLYMODE Synoptic/Dynamic Experiment (P-SDE). The data set analyzed consists of approximately 6000 XBTs taken asynoptically over a region about 600 km square, and current meter records from 19 USSR moorings in the center 300-km-square region at 700-m and 1400-m depths. Additional current meter records exist at 100 and 400 m as well as Sofar float data and CTD casts. The ten-day time series of 15°C isotherm depth (Fig. 7) analyzed by Carter and Robinson (1983) spans four or five independent synoptic realizations containing typically three eddies each. The XBT sampling (Carter and Robinson, 1981) was usually nonuniform and contained several time gaps (Fig. 8). Subjective mapping (Taft, Baranov, et al. 1978) showed little continuity of features. The objective analysis typically used 8 data points for an analysis point, usually chosen within 100 km and 20 days. However, to span gaps, the domain of influence was extended to 360 km and 60 days and both future and past data were used to bracket the gaps. In addition as an illustration of the statistical model used in the forecast mode we show a sample statistical hindcast, i.e. forward interpolation in time from a single synoptic realization (Fig. 9). The ten-day forecast is excellent; by 20 days it is deteriorating, especially in the east. The USSR type of surface mooring system is well known to rectify high-frequency environmental noise into apparent low-frequency signal. The system yields accurate directions for the horizontal current vectors, but inaccurate speeds. The speed correction model used in the Harvard objective analysis was obtained from a least squares fit to an in situ intercomparison between sofar float measurements and the current meter measurements (Polloni, Mariano and Rossby, 1981) (Fig. 10). Stream function maps have been prepared with a 23% error variance in speed derived from the scatter of data points in Figure 10 and have been shown not to be sensitive to the noise level chosen (Carter and Robinson, 1983). The maps are similar to those from an earlier analysis using velocity components, but the expected error maps from the speed and direction analysis are more useful. These statistical analysis methods have now been successful in providing credible, quantitative and continuous estimates of physical fields throughout the extensive domain of the POLYMODE Synoptic/Dynamics Experiment.

An interesting sample set of current flow and thermocline displacement fields are shown in Figure 11 for 5 June 1978 (Julian Day 3665) which is during the intensive period of the POLYMODE Local Dynamics Experiment (P-LDE) (McWilliams and Heinmiller, 1978; McWilliams et al., 1983). Our intention is to make composite quasigeostrophic stream functions from the POLYMODE data set, but the data maps of Figure 11 are each from independent data. The LDE data has been purposefully omitted in order to provide a spatial "gap" to test our methodology. Three points are noteworthy: (1) the good agreement between general features of the flow in the thermocline from the P-SDE XBT and current meter data; (2) the reconstruction of the P-LDE features from the P-SDE data and (3) the larger scale synoptic context for the very accurate P-LDE data set provided by the analyzed P-SDE data set. By JD 3665, the intense "thermocline jet", one of the major phenomenological features studied in the LDE (Owens, Luyten and Bryden, 1982) was well established in the LDE
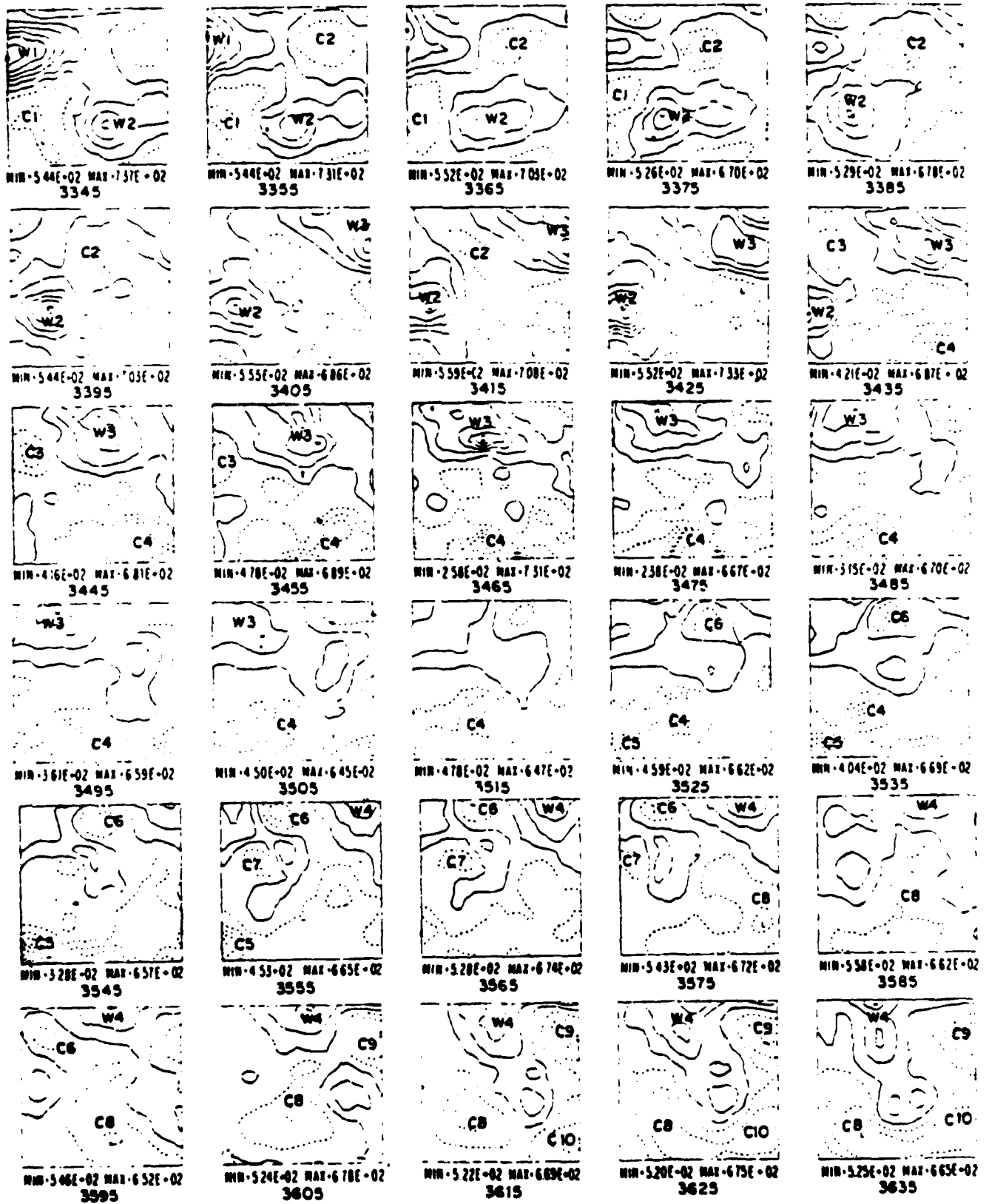
Fig. 7. The time series of objective maps at 10-day intervals showing the depth of the 15°C isotherm. The series spans the dates 3345 to 3635 (20 July 1977 to 6 May 1978) and covers the 6° square centered at 70°W 29°N. The contour interval is 25 m; the first solid contour is the 600-m level. (After Carter and Robinson, 1983, Fig. 4.)
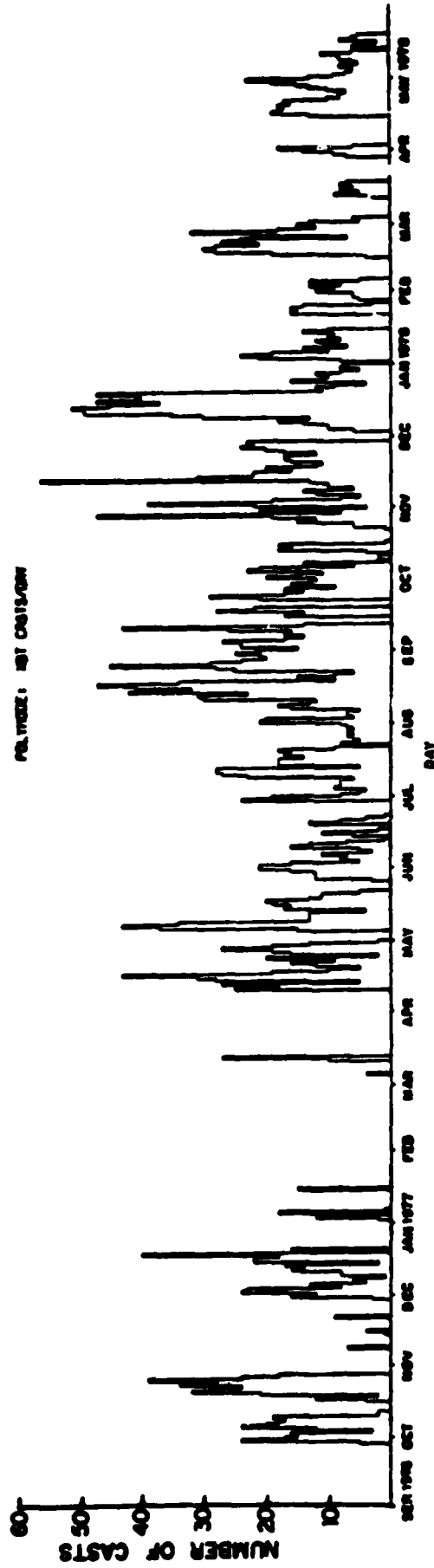
Fig. 8. The daily XBT count in the POLYMODE region throughout the major portion of the synoptic experiment. (After Carter and Robinson, 1983, Fig. 1).

MIN=5.41E+02 MAX=7.37E+02 CI=2.50E+01   MIN=5.41E+02 MAX=7.37E+02 CI=2.50E+01

MIN=5.37E+02 MAX=7.36E+02 CI=2.50E+01   MIN=5.32E+02 MAX=7.43E 02 CI=2.50E+01

MIN=5.36E+02 MAX=7.24E+02 CI=2.50E+01   MIN=5.25E 02 MAX=7.35E+02 CI=2.50E+01
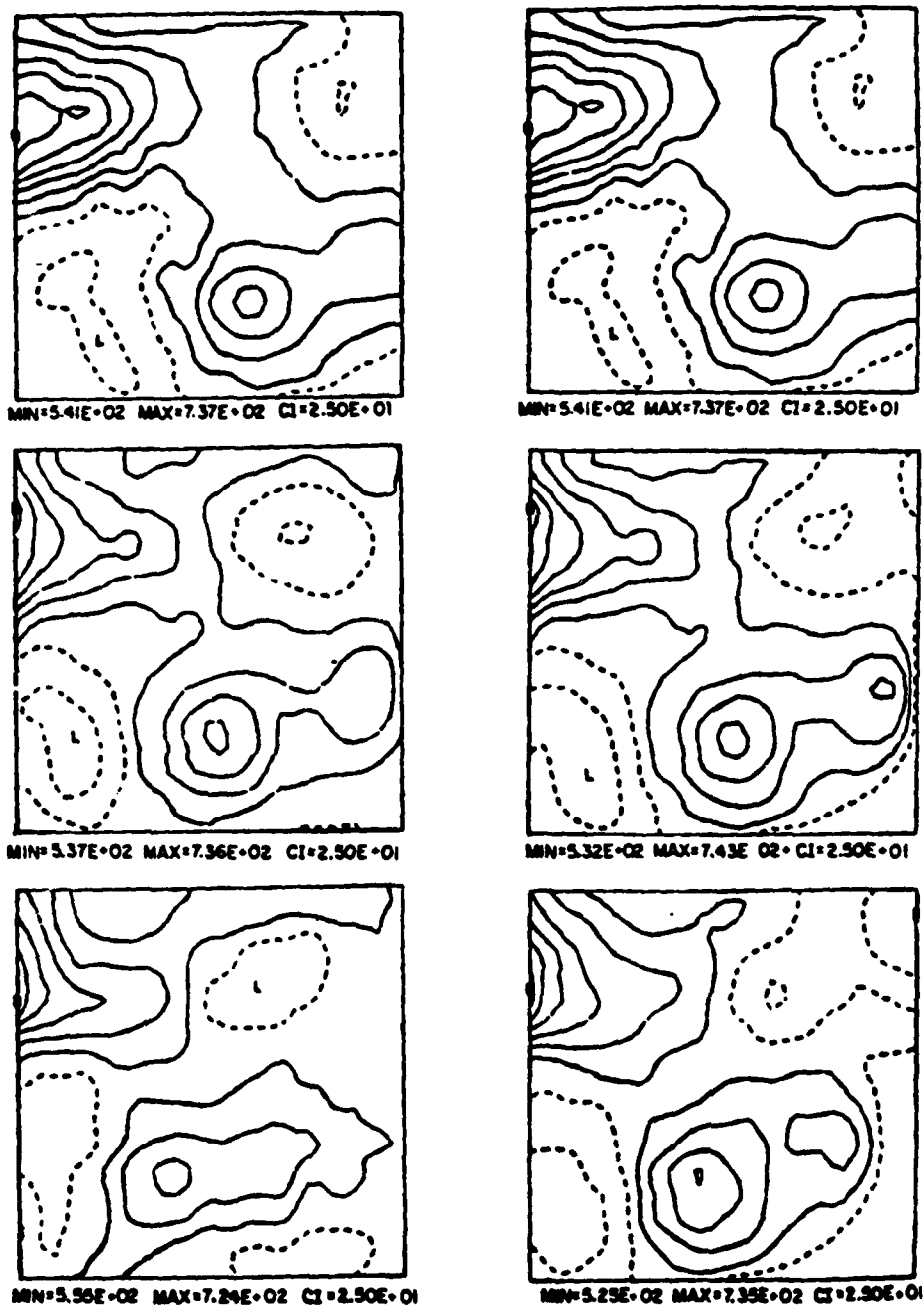
Fig. 9. An example of a statistical forecast (on the right)
compared to the objective analysis of the same data (on the
left). The initial date is day 3346. This data is used to
estimate on the dates 3346, 3356, 3366, from top to bottom
for the forecast field which can be directly compared to the
objective analysis of those dates (Carter and Robinson, 1983,
Fig. 10).
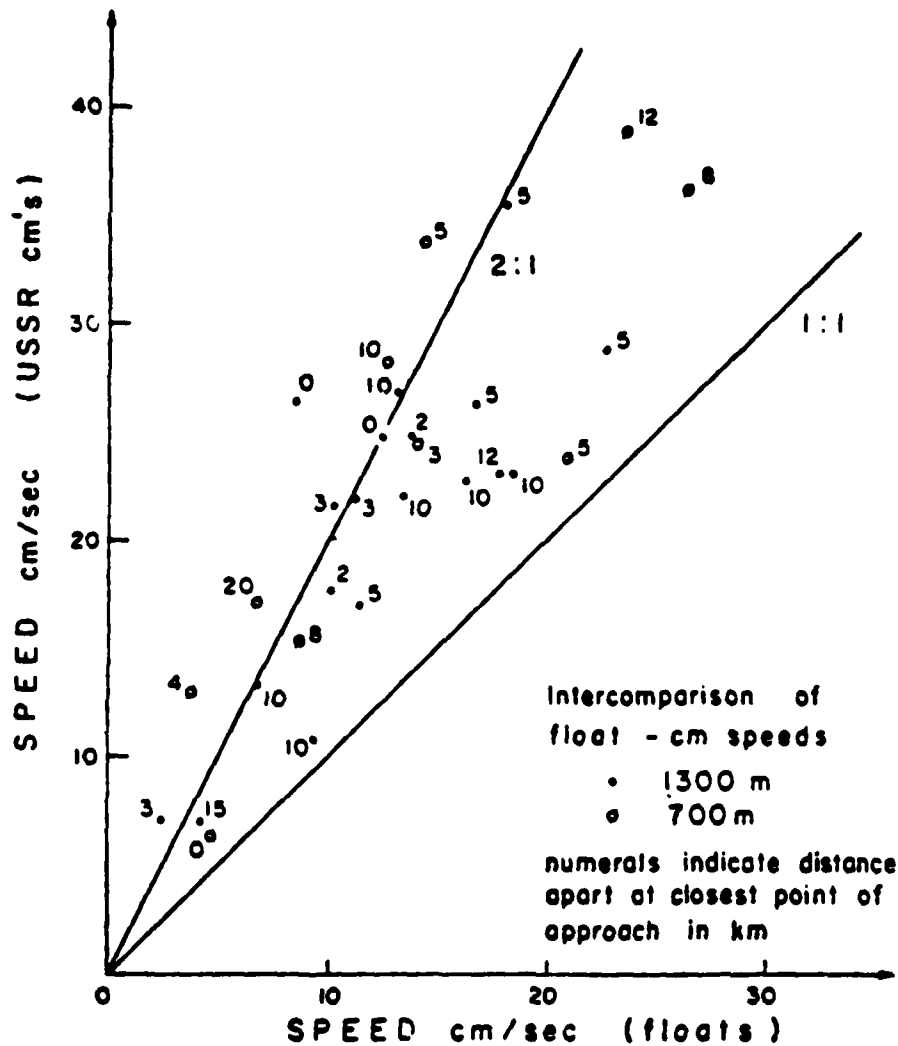
Fig. 10. An intercomparison of USSR POLYMODE current meter and U.S. SOFAR Float speeds. The number on the data point is the distance between measurements in km. The 1:1 and 2:1 lines are for reference. See text for fits (Polloni et al., 1981, Fig. Z).

region. Figure 11 shows the jet originating in the north and flowing through the SDE region for over 700 km, executing a deep V-shaped meander in the southwest and exiting to the west.

We next present the results of a benchmark dynamical forecast experiment carried out with real data fields from the POLYMODE SDE. The data utilized were USSR current meter records of about one-month duration at all four levels. An absolute (quasigeostrophic) streamfunction was constructed (P-SDE "Mark I" analysis) by compositing this data with 30 hydrocasts, a single cast for each day (Kamenkovich, Larichev and Nikitin, 1980). The hydrographic data is necessary in order to relate ψ at one level to another via the relationship $\psi_z = -(g\rho')/(\rho_0 f_0)$. What is really required is a horizontal average of this relationship over tne domain of interest utilizing all the T,S,ρ information available. The four levels of streamfunction data from the current meters have been extended to deeper layers using a successive least squares fit to the normal modes. This method determines the barotropic and first and second baroclinic modes from the data and applies them to extend the data to the bottom. This extension is necessary for computational accuracy and the resolution of possible topographic effects. This approach is being continued with the data typified in Figure 11 for the more complete data set (Harvard P-SDE Mark II Analysis). Further analyses will be carried out until all the available data has been combined using adequate noise and error models. The Mark II analysis was carried out to provide a basis for the development of model initialization and verification techniques and the preliminary intercomparison between the Harvard model and the open ocean dynamical model developed by Professor Kamenkovich's group at the PP Shirshov Institute of Oceanology in Moscow.

Figure 12a and 13a,c illustrate the result of a 6-level 17 day benchmark forecast in which new boundary conditions were continually provided from data around the edge of a 270-km domain resolved by 31 x 31 grid points (9 km resolution). The normalized root mean square difference field between the nowcast and the analysis in the upper levels are maintained at about 20% for the first 8 days and then grow linearly for the remaining 9 days of the experiment to about 100%. Magnitude at the lower levels is less; all levels demonstrate a spikiness in the nrms difference field. The order one difference between the fields is pictorially evident in the upper thermocline maps of Figure 13a,c. The forecast has strengthened the low, moved the high to the west and distorted the jet as compared to the analysis; the benchmark boundary conditions, of course, maintain on the boundaries a forecast field identical to the analysis.

The term "difference" field was purposefully introduced in the preceding paragraph rather than "error" field in order to emphasize the importance of interpreting the source of the difference and attributing it to one or several of the source(s) of both accuracy and error in both the analysis and the dynamical forecast. Possible important error sources in the Mark I fields include: (1) (residual) speed errors in the current meter data, (2) gaps in the cm records, (3) the sparseness of the hydrocast data, (4) the quality of the hydrocast chosen, (5) the Shirshov statistical model (objective analysis scheme) assumptions and statistics, (6) inadequacy of the data extension

JULIAN DATE: 3665
15 DEGREE ISOTHERM
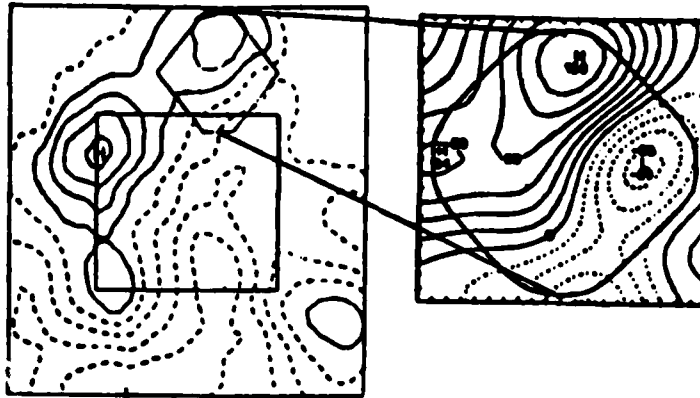
MIN=5.31E+02 MAX=6.69E+02 CI=1.70E+01

700 M STREAMFUNCTION

MIN=-4.76E+01 MAX=1.45E+02 CI=2.40E+01

1400 M STREAMFUNCTION

MIN=-2.42E+01 MAX=5.94E+01 CI=1.00E+01

Fig. 11. An analysis of the POLYMODE data at Julian day 3665.
The top figure shows the depth of the 15° isotherm objectively
analyzed from POLYMODE XBT's. The first solid contour is the
600-m level. Enclosed areas indicate the LDE region (six-sided
area) and the region of the Soviet current meter array. The
lower two figures show the streamfunction fields at 700 and
1400 m objectively analyzed from Soviet current meter data.
The first solid contour is the zero contour. Dots indicate
current meter locations; arrows indicate current meter
speeds (from Carter and Robinson, 1983).

RMS(DIFF(STFN))
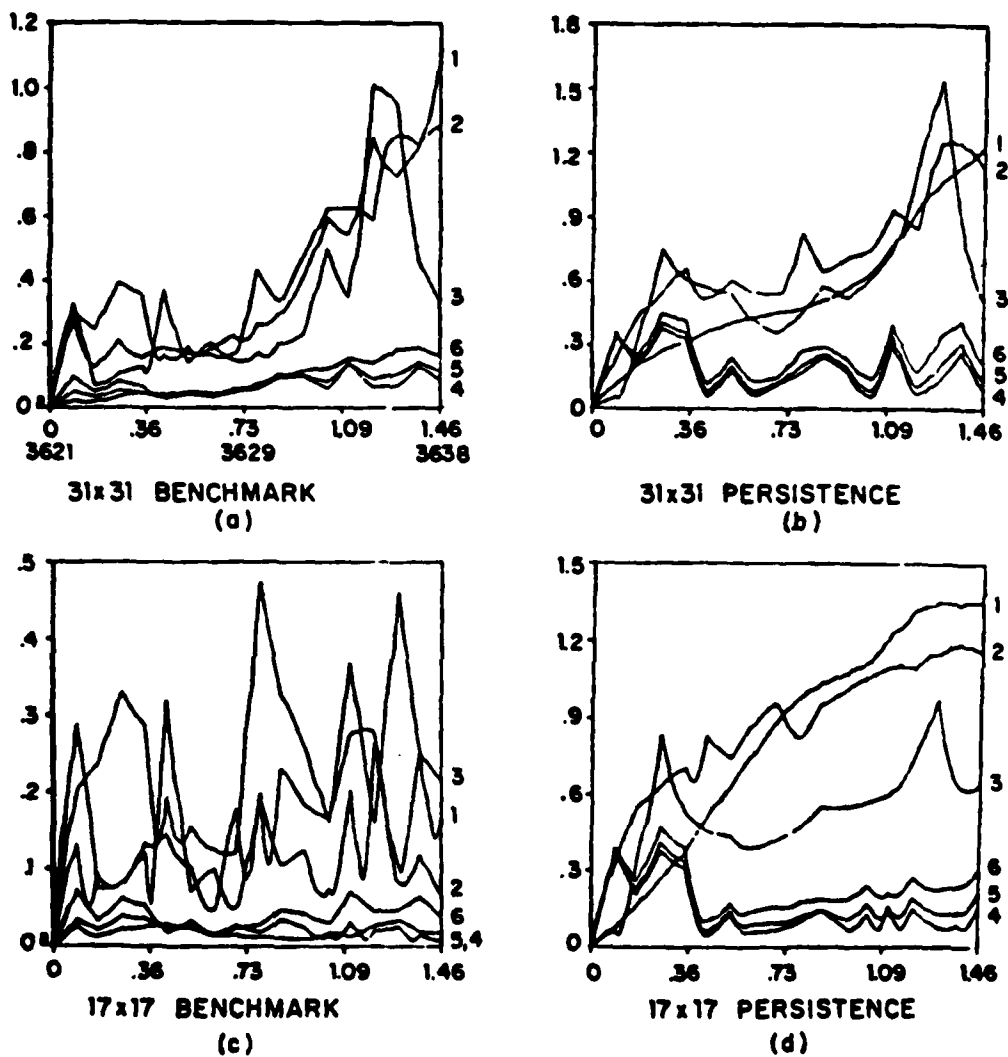
Fig. 12. RMS values of the normalized root mean square difference
field between forecast and verification streamfunction for four
baroclinic forecasts using real data. Levels are 100, 400, 700,
1400, 2400, and 3950 m.
(a) 31 x 31 (grid size) benchmark forecast.
(b) 31 x 31 persistence forecast.
(c) 17 x 17 benchmark forecast.
(d) 17 x 17 persistence forecast.

procedure. Possible important error sources in the dynamical forecast
include: (1) the quasigeostrophic dynamics of the Harvard model (here run
over a flat bottom), (2) the filtering assumptions, (3) the quality of the
initial and boundary condition data, (4) computational error (but this should
be only a few percent). The most important source of accuracy in the analysis
is the continual accessing of new observations and the most important source
of accuracy in the dynamical forecast is baroclinic quasigeostrophic dynamics.

In addition to the 17-day benchmark forecast in the full 270-km domain
(Fig. 12a, 13c and 14) we show the results of: a 270 km domain persistence
forecast (Fig. 12b, 13d, and 14b), a smaller interior 144-km domain (17 x 17
grid points, 9-km resolution) benchmark forecast (Fig. 12d and 14a). By
intercomparing the character of these four experimental difference fields we
can reasonably attribute their features to the various error sources and the
dynamical adjustment process. Figure 12 shows that records are spikey; the
spikiness is most pronounced in the best forecast. From these experiments and
by comparison with other experiments started at other initial times, the
spikes appear to be due to a bad or unrepresentative hydrocast. This affects
the difference field through the analysis field in all four cases and also
through the boundary conditions in the benchmarks.

The dominant influence of boundary condition control in the small domain
is evident. Except for the spikes, the small domain benchmark maintains an
rms error level below 20% throughout the 17-day duration of the experiment.
The dynamical model is serving as a good interpolation scheme for the boundary
conditions. Research directed along these lines could yield interesting
results related to the design of sampling schemes consisting of coarsely
spaced lines of finely sampled data points for real time field description
observational networks. In contrast, the small persistence experiment rms
error grows most rapidly, reaching 100% in less than a week. This difference
field is error growth due to the incorrect persistent boundary condition. The
full domain benchmark nrms error is maintained for about a week around the 20%
level comparable to the small benchmark and then grows to about 100% in the
upper levels by the end of 17 days. The difference field we attribute to the
dynamical adjustment process. For the integrated nrms diagnostic quantity of
Figure 12, the persistent boundary condition in the large domain is clearly
not as bad as in the small domain. Comparing the curves of Figure 12b with
those of Figure 12a and 12c indicates a mixture of persistent boundary
condition error and dynamical adjustment to be occurring in this case. It is
interesting to examine the difference field maps after 17 days in the light of
these interpretations. Figure 14a shows the form of the dynamical adjustment,
which is reflected also in Figure 14b where it appears contaminated by
boundary condition error. The small domain persistence field resembles the
inverse of the analysis field (Fig. 13a) but does have flow feature relatable
to Figure 14a and b. The small amplitude structure of the small domain
benchmark is very different. It could be the form of the dynamical adjustment
in the presence of boundary condition dominance but could conceivably contain
computational error.

A sequence of forecasts has been run testing the ability of the dynamical
model to interpolate the data for the entire field using only boundary data.

STREAMFUNCTION
JULIAN DAY 3645

LEVEL = 3
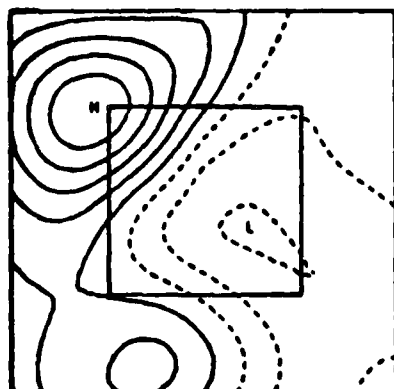
MIN = -1.87 MAX = 2.94 CI = 0.60
REAL DATA
(a)
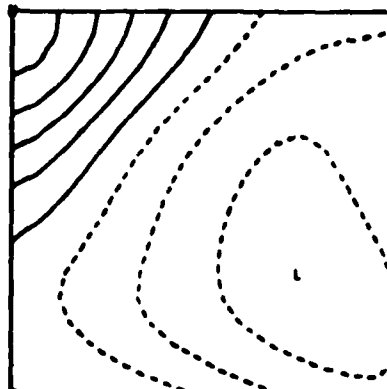
MIN = -2.19 MAX = 2.86 CI = 0.60
17 x 17 BENCHMARK
(b)
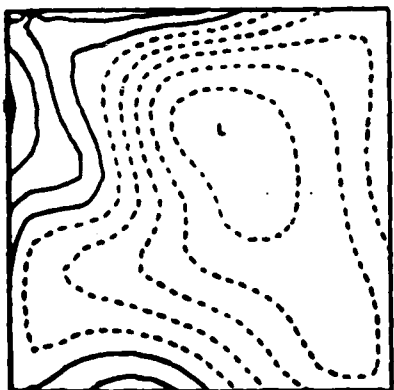
MIN = -2.87 MAX = 1.63 CI = 0.50
31 x 31 BENCHMARK
(c)
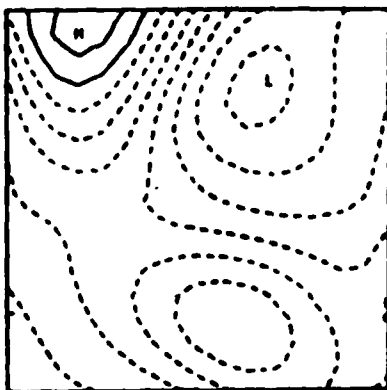
MIN = -3.66 MAX = 0.75 CI = 0.50
31 x 31 PERSISTENCE
(d)

Fig. 13. A comparison of verification streamfunction at 700 m with
the equivalent forecast field after 15 days from a 17 x 17 bench-
mark forecast (b); a 31 x 31 benchmark forecast (c); and a
31 x 31 persostence forecast (d).

58
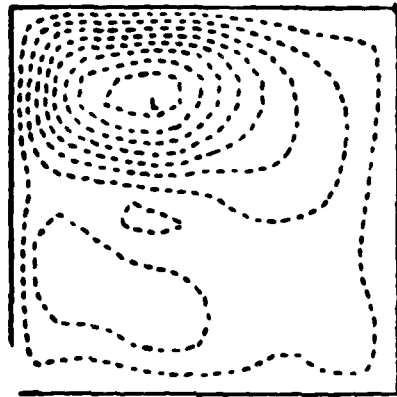
MIN=-3.47 MAX= 0.00 CI=0.40
31x31 BENCHMARK
(a)
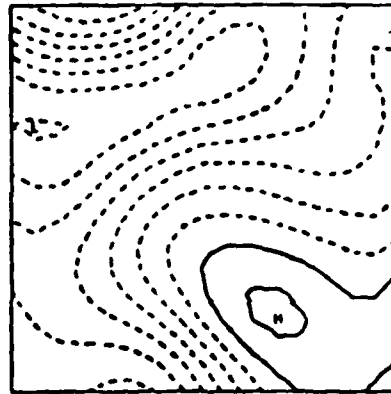
MIN=-3.56 MAX=0.62 CI=0.50
31x31 PERSISTENCE
(b)
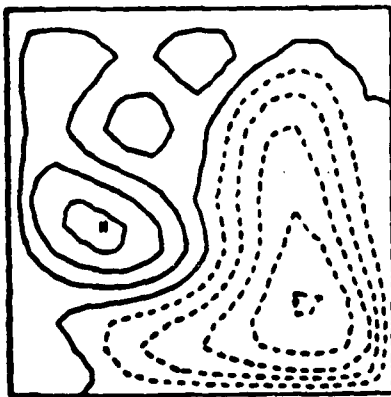
MIN=-0.35 MAX=0.23 CI=0.07
17x17 BENCHMARK
(c)
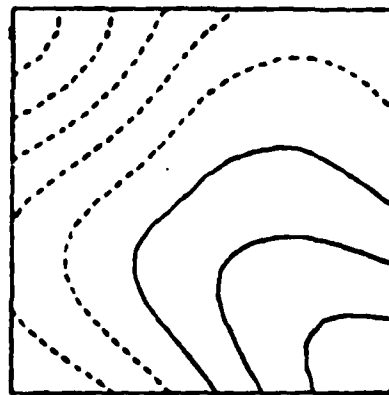
MIN=-3.88 MAX=1.89 CI=0.70
17x17 PERSISTENCE
(d)

Fig. 14. Baroclinic dynamical forecast experiments with the MK-1
P-SDE data. The difference fields between forecast and verifi-
cation streamfunction at 700 m after 15 days
(a) 31 x 31 benchmark forecast.
(b) 31 x 31 persistence forecast.
(c) 17 x 17 benchmark forecast.
(d) 17 x 17 persistence forecast.

This is done by specifying the intial fields except for the initial boundary
conditions and the boundary conditions at every time step as well as possible
from the data, i.e. "benchmark boundary conditions". The results for three
different domain sizes are shown in Figure 15. The large domain (270 km, 31 x
31 grid points) is unable to interpolate across the entire field very
effectively but the two smaller domains (144 km, 17 x 17 grid points; 81 km,
10 x 10 grid points) are able to recreate the field quite well from only
boundary condition data. The ability of the dynamical model to interpolate
across the entire domain suggests that for such size regions only boundary
data might need be collected. It is interesting to note that each side of the
144-km domain is three times the length of the first zero crossing of the zero
time-lag correlation function.

Forecasts using real data have been made over real bottom topography for
the POLYMODE region. Preliminary results (Fig. 16) show that the addition of
topographic effects to the dynamical model slows somewhat the too rapid
westward feature propagation of the flat bottom forecasts. Further studies
including improvements in the data analysis and extension techniques appear to
enhance these effects of topography.

4. SUMMARY

We introduce and discuss a method for the analysis, optimal estimation and
dynamic forecasting of synoptic/mesoscale ocean currents over large-scale open
regions. The method involves a multivariate space-time objective analysis
scheme and a baroclinic quasigeostrophic open ocean model. Error sources in
the analysis field and the dynamical model are identified and located.
Requisite error models are constructed from simulated data. A barotropic
prototype example illustrates the dynamical adjustment of fields to the
dynamics of the model. An analysis of the POLYMODE Synoptic/Dynamic
Experiment data successfully achieves a continuous time series field
description including the period of the POLYMODE Local Dynamics Experiment.
Dynamical studies via boundary condition and domain size comparisons using the
P-SDE data are used to attribute features of the difference fields to the
various error sources and dynamical adjustment. Zero initial condition
forecasts suggest the ability of the dynamical model to interpolate
effectively from boundary data. The Harvard quasigeostrophic open ocean
dynamical model has been initialized with Rossby waves, simulated data and
real data. It has been run over flat bottoms and real topography. Current
research efforts involve the use of data from other regions of the world's
oceans, including the Mediterranean Sea, Caribbean Sea, near Hawaii, and the
California Current Regime. This model is proving to be an efficient and
accurate component in the prediction and description of fields in open ocean
regions of various internal dynamics.

The successful initialization of the dynamical model with the analysis
fields has been an important achievement. Runs have been carried out with
"errors" of difference between forecasts and verification analyses maintained
at about 20 percent for weeks. Thus the prospects for data assimilation in
dynamical oceanography are excellent.

ZERO INITIAL CONDITION
STREAMFUNCTION
JULIAN DAY 3645
LEVEL=2

MIN=-1.28 MAX=4.11 CI=0.60
REAL DATA
(a)

MIN=-3.73 MAX=2.84 CI=0.80
31x31 BENCHMARK
(b)

MIN=-1.30 MAX=3.90 CI=0.60
17x17 BENCHMARK
(c)

MIN=-1.39 MAX=2.13 CI=0.40
10x10 BENCHMARK
(d)
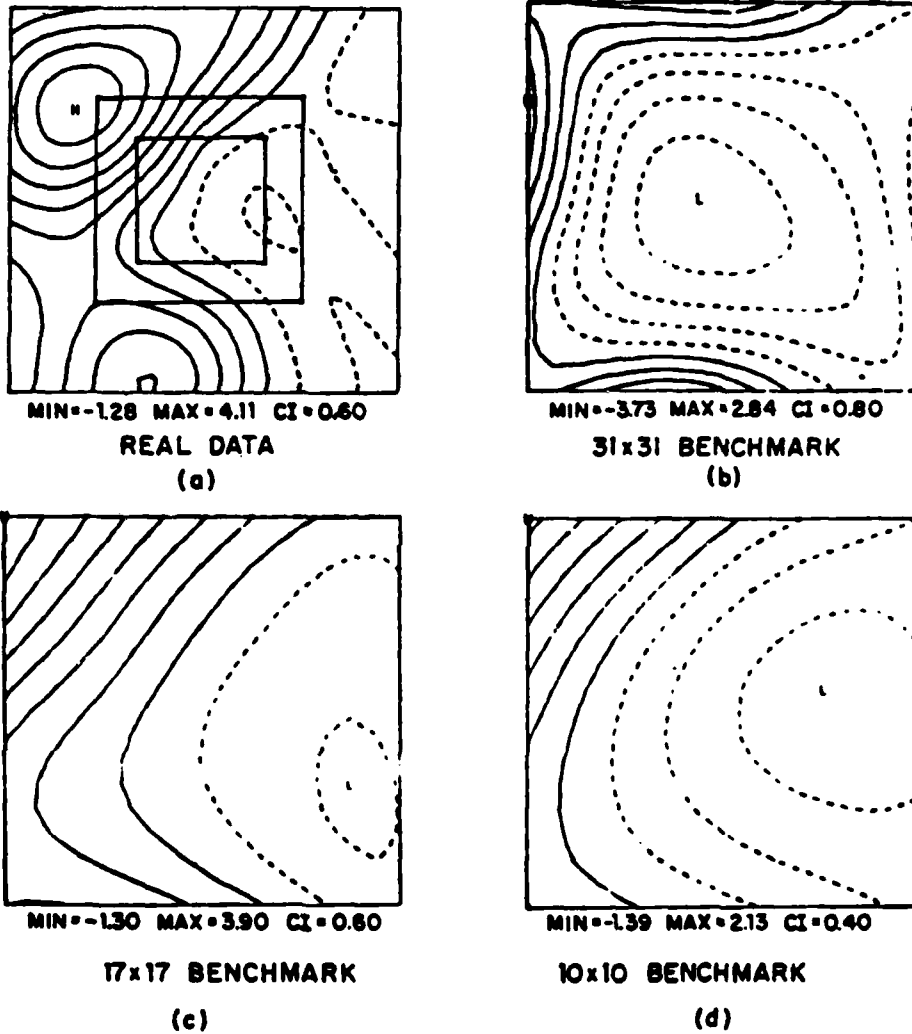
Fig. 15. A comparison of verification streamfunction at 400 m
with equivalent zero initial condition forecast field.
(a) 31 x 31 streamfunction. Smaller boxes define inner
17 x 17 and 10 x 10 domains.
(b) 31 x 31 benchmark forecast.
(c) 17 x 17 benchmark forecast.
(d) 10 x 10 benchmark forecast.

STREAMFUNCTION
JULIAN DAY 3645
LEVEL=6
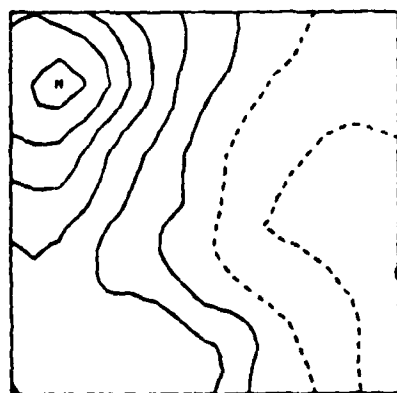
MIN=-1.15 MAX=2.13 CI=0.40
REAL DATA
(a)
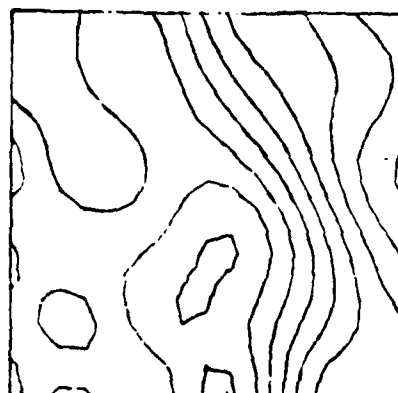
MIN=5135 MAX=5575 CI=50.0
BOTTOM TOPOGRAPHY
(b)
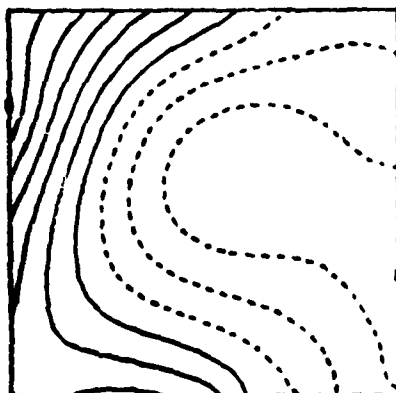
MIN=-1.16 MAX=1.81 CI=0.30
FLAT BOTTOM FCST
(c)
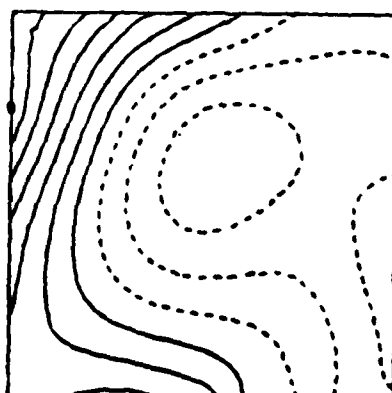
MIN=-1.15 MAX=1.79 CI=0.30
ROUGH BOTTOM FCST
(d)

Fig. 16.   (a) 3950 streamfunction field.
     (b) Bottom topography.
     (c) 31 x 31 flat bottom benchmark forecast.
     (d) 31 x 31 rough bottom benchmark forecast.

61

ACKNOWLEDGMENTS

REFERENCES

Bengston, L., M. Ghil and E. Kallen, Editors, 1981. Dynamic Meteorology: Data Assimilation Methods.

Bretherton, F.P., R.E. Davis and C.B. Fandry, 1976. A Technique for Objective Analysis and Design of Oceanographic Experiments Applied To Mode-73. DSR 23. 559-582.

Carter, E.F., 1983. The Statistics and Dynamics of Ocean Eddies. Ph.D. Thesis, Harvard University.

Carter, E.F. and A.R. Robinson, 1981. Time Series of Synoptic Maps of the Western North Atlantic: A Space-Time Objective Analysis of POLYMODE XBTs. Reports in Meteorology and Oceanography, Number 15, Division of Applied Sciences, Harvard University.

Carter, E.F. and A.R. Robinson, 1983. Time Series of Synoptic Maps from the POLYMODE Synoptic/Dynamic Experiment. Harvard Analysis Mark II Reports in Meteorology and Oceanography, Number 17, Division of Applied Sciences, Harvard University. (In preparation).

Charney, J.G., R. Fjortoft and J. von Neumann, 1950. Numerical Integration of the barotropic vorticity equation. Tellus, 2, 237-254.

Gandin, L.S. (1965) Objective Analysis of Meteorological Fields. Israel Program for Scientific Translations, Jerusalem, 242 pages.

Ghil, M., S. Cohn, J. Tavantzis, K. Bube and E. Issacson, 1981. Application of Estimation Theory to Numerical Weather Prediction in Dynamic Meteorology. Data Assimilation Methods, L. Bengtsson, M. Ghil and E. Kallen, editors, Springer-Verlag, New York.

Grachev, Y., M. Koshlyakov, T. Tikhomirova and Y. Yenikeyev, Doklady Akademii Nauk USSR, 1978. Vol. 243, No. 4, pp. 1039-1044. Also published as (1979) Synoptic Eddy Field in the POLYMODE Area, September 1977 to May 1978: POLYMODE news No. 69.

Haidvogel, D.B., A.R. Robinson and E.E. Schulman, 1980. The Accuracy, Efficiency and Stability of the Numerical Modes with Application to Open Ocean Problems. Journal of Computational Physics, 34, 1-53.

Heinmiller, R.M., 1977. POLYMODE Overview. POLYMODE News #27 (unpublished ms.)

Kamenkovich, Larichev and Nikitin, 1980. Private communication.

Liebelt, P.B., 1967. An Introduction to Optimal Estimation, Addison-Wesley, Reading, MA.

McWilliams, J.C. and G.R. Flierl, 1976. Optimal Quasigeostrophic Wave Analysis of MODE Array Data. Deep-Sea Research 23, 285-300.

64

McWilliams, J.C. and R.M. Heinmiller, 1978. The POLYMODE Local Dynamic
    Experiment. Objectives, location and plan. POLYMODE Report.

McWilliams, J.C. et al, 1983. The Local Dynamics of Eddies in the Western
    North Atlantic. Eddies in Marine Science, A.R. Robinson, editor, Springer-
    Verlag, New York.

Miller, R.N. and A.R. Robinson, 1983. Dynamical Forecast Experiments with a
    Baroclinic Quasigeostrophic Open Ocean Model. Proceedings of Conference
    on Predictability of Fluid Motion, La Jolla, CA., G. Holloway, Editor
    (in press).

Miller, R.N., A.R. Robinson and D.B. Haidvogel, 1983. A Baroclinic
    Quasigeostrophic Open Ocean Model. Journal of Computational Physics 5, 50,
    38-70.

Owens, W.B., J.R. Luyten and H.L. Bryden, 1982. Moored Velocity Measurements
    on the edge of the Gulf Stream recirculation. Journal of Marine Research
    40, 509-524.

Polloni, C.A., A. Mariano and T. Rossby, 1981. Streamfunction Maps of the
    POLYMODE Current Meter Array. U.R.I. Technical Report No. 81-1, MODE
    Contribution No. 36-T.

Robinson, A.R., 1982. Dynamics of Ocean Currents and Circulation: Results of
    POLYMODE and related investigations. in Topics in Ocean Physics, Proc.
    Summer Sch 1980 A. Osborne and P.M. Rizzoli, eds, Soc. Italiana di Fisica,
    Bologna (Elsevier, NY). Also available as POLYMODE (MODE) Report TR335-7
    (1980).

Robinson, A.R. and D.B. Haidvogel, 1980. Dynamical Forecast Experiments with
    a Barotropic Open Ocean Model. Journal of Physical Oceanography 10, 1909-
    1928.

Robinson, A.R. and K. Tu, 1981. A Combined Statistical/Dynamical Approach to
    Regional Forecast Modeling of Open Ocean Currents. in Ocean Prediction:
    The Scientific Basis and the Navy's Needs, Proceedings of the Ocean
    Prediction Workshop, Monterey, CA.

Shapiro, R., 1971. The use of Linear Filtering as a Parameterization of
    Atmospheric Diffusion. Journal of Atmospheric Science, 28, 523-531.

Taft, B. and E. Barnov et al., 1978. Preliminary Interpretation of POLYMODE
    Synoptic XBT Data. POLYMODE News No. 47.

Tu, K., 1981. A Combined Statistical and Dynamical Approach to Regional
    Forecast Modeling of Open Ocean Currents. Ph.D. Thesis, Harvard
    University, also available as Harvard Open Ocean Model Report #3, Reports
    in Meteorology and Oceanography, Number 13, Division of Applied Sciences,
    Harvard University.

ADP002653

OCEANIC MESOSCALE VARIABILITY AND GENERAL CIRCULATION FROM SATELLITE ALTIMETRY: A STATUS REPORT

Lee-Lueng Fu

Jet Propulsion Laboratory, California Institute of Technology, Pasadena, CA 91109

ABSTRACT

Progress on the applications of satellite altimetry from Seasat and Geos-3 to the study of oceanic mesoscale variability and general circulation is reviewed. The major conclusion for the applications to mesoscale variability is that an optimally designed altimetric mission with a lifetime of several years will improve our knowledge of the global mesoscale variability to an extent unattainable by any other practical means. The proposed Topex mission will allow one to view the global oceanic variability in such a wide range of periods and wavelengths: from 20 days to 3-5 years; from 50 to 10,000 km. However, the goal of determining the general circulation cannot be achieved by a single altimetric mission, because a highly accurate geoid needs to be determined independently. The scenario of the combination of Topex with Gravsat, a gravity mission that will give accurate geoid information, will allow the global general circulation to be determined at scales as small as 100 km. Areas of research needingto be performed with existing altimeter data are also discussed.

INTRODUCTION

To understand the role of eddies in ocean general circulation, one needs a statistical description of the oceanic variability on a wide range of space and time scales: from tens to thousands of kilometers and from days to years. It is obvious that observations made by conventional methods, i.e., ship-borne measurements, will never meet this need. Satellite altimetry (for a general review, see Stewart, 1983), however, holds the promise to provide the required surface observations. When it is coupled with acoustic tomography which provides information on the density structure at depths, a global, three-dimensional description of the oceanic variability will begin to emerge (see Munk and Wunsch, 1982). The purpose of this paper is to present a brief review

on the application of satellite altimetry to the study of the mesoscale variability and general circulation of the oceans, with emphasis placed on the most recent progress.

A satellite altimeter measures the altitude of the satellite above the sea surface through radio-pulse ranging. With the height of the satellite (orbit height) above a reference surface determined independently by tracking and modeling, sea-surface height above the same reference surface is obtained by subtracting the satellite altitude from the orbit height. Horizontal gradient of the difference between the resulting sea-surface height and the geoid (equi-geopotential surface) is thus a measure of surface geostrophic current. Such measurement is inevitably contaminated by a large number of errors: those of orbit, altitude (due to instrument errors, ionospheric and atmospheric effects, ocean and earth tides, sea-state bias, etc.) and the geoid (e.g., Wunsch and Gaposchkin, 1980; Stewart, 1983). To obtain useful measurements of ocean currents, these errors have to be reduced to certain acceptable levels.

There have been three satellites carrying an altimeter for earth observations: Skylab (1973), Geos-3 (1975), and Seasat (1978). The noise level of the altimeter on board Skylab was so high (60 cm for one-second average) that even the Gulf Stream boundary could not be unambiguously detected in the data (Leitao et al., 1974). With much improved precision (25 cm for one-second average), the Geos-3 altimeter data began to reveal surprisingly detailed information on the Gulf Stream meanders and rings (e.g., Huang et al., 1978), among other features. The disadvantage of the Geos-3 data is the lack of corrections of errors due to the effects of ionospheric free electrons, atmospheric water vapor and pressure loading (the inverse barometer effect), resulting in unknown errors at all scales. Nevertheless, the 3.5 years of Geos-3 data have generated numerous interesting studies to be discussed later in the paper. With further improved precision (5 cm for one-second average) and correction algorithms, the accuracy of the Seasat altimeter data (altitude) has reached the 10-cm level required for oceanographic applications (Tapley et al., 1982). Despite the fact that only three months of data were collected, a large number of studies have demonstrated the potential value of a well-designed altimeter in improving our knowledge of the global mesoscale variability and general circulation.

In the following I will discuss the progress to date on the application of Geos-3 and Seasat data to ocean circulation problems. I will first discuss the problem of mesoscale variability and then the more difficult problem of general circulation.

MESOSCALE VARIABILITY

The major difficulty in applying satellite altimetry to ocean circulation problems lies in the fact that the variability of sea-surface

height is dominated by that of the geoid. The amplitude of the geoid variability is on the order of tens of me.·?s, whereas that of the oceanic variability is on the order of only one meter. Since geoid models with sufficient accuracy at mesoscales do not exist, most oceanographic applications of satellite altimetry to date are thus confined to the study of the time-varying mesoscale variability using differences between altimetric measurements taken at the same earth location at different times, whereby the time-invariant geoid is removed. There are three methods frequently being used in this kind of study. One of them is the "repeat-track method" in which the differences between altimetric measurements taken along nearly repeat tracks are used. Another method is the "mean sea surface method" in which the differences between altimetric measurements and an altimetrically constructed mean sea surface are used. The third method is the "cross-over differences method" in which the differences between altimetric measurements taken at the intersections of altimeter tracks are used. In these methods, a tilt and a bias are usually removed by one way or another over a distance of several thousand kilometers along each track to minimize the long-wavelength orbital and tidal errors; however, these procedures minimize also the long-wavelength oceanic variability, making the results applicable only for studying the mesoscale variability. Most of the studies to be discussed below are based on these three methods.

To make the following discussion in some order, results from Geos-3 and Seasat are discussed in separate sections.

Geos-3 Results

Due to the lack of recording capability on board Geos-3, continuous data coverage is limited to the western North Atlantic Ocean, and so have been most of the studies using Geos-3 data. For a mission overview, the reader is referred to Stanley (1979). The first attempt at using Geos-3 data for mesoscale variability study was made by Huang et al (1978) in the Gulf Stream area. After minimizing the radial orbital error by a linear adjustment (through a bias and a tilt) of each pass such that the cross-over differences in the study area are minimized, they computed maps of monthly mean sea surface using data at the cross-over points and studied the monthly variations of the Gulf Stream and eddies by differencing the monthly map with a six-month mean map. Their results showed surprisingly good agreement with concurrent IR images. The same method was applied to a longer data set in the same area by Mather et al. (1979, 1980) with similar results. Robinson et al. (1983) extended the method to include all the data (not exclusive to cross-over points) in the computation of mean sea surface and applied it to three years of data, resulting in a three-year time series of sea-surface topography maps. Their results also showed qualitative agreement with in situ and IR observations. A disadvantage of these methods is that significant geoid errors are introduced to the monthly variability maps as a result of the much sparser data coverage for the monthly maps than for the mean map with which the differencing is made.

More accurate information on the variability can be obtained by
studying individual tracks of data; however, instead of maps, only one-
dimensional profiles are obtained. Douglas and Gaborski (1979) and
Mather et al. (1980) are among the early demonstrations of the utility of
repeat-track data to detect individual mesoscale features. They demon-
strated also that the Gulf Stream boundaries and rings could even be
detected by differencing the altimeter data with the high-resolution
geoid models of Marsh and Chang (1978).

In addition to individual features, geographic distributions of
mesoscale variability can be obtained from a dense net of repeat tracks.
Using data in the western North Atlantic, Douglas and Cheney (1981) made
the first of such attempts. To maximize the number of tracks in each
repeat group, they included all the tracks lying within 20 km of each
other in the computation of sea-surface height variability and used the
geoid model of Mader (1979) to compensate the geoid variability result-
ing from the track spacings. Their result showed qualitative agreement
with the eddy potential energy map of Dantzler (1977) based on ship
measurements; however, their maximum r.m.s. variability of 48 cm in the
Gulf Stream was somewhat higher than the eddy-potential-energy map
implied, partly due to the errors of the geoid model used.

Using only pairs of tracks lying within a few kilometers of each
other, Douglas et al. (1983) recomputed the mesoscale variability in the
western North Atlantic and extended the computation to cover the Gulf of
Mexico. These results should be less contaminated by geoid noise. Two
of the figures summarizing their results are reproduced here in Figures
1a and 1b showing sea-surface height variability and eddy kinetic
energy, respectively. The kinetic energy was computed from the slope of
sea-surface height using the geostrophic relation. Note that the maxima
of both sea-surface height variability and kinetic energy correspond to
the meandering of the Gulf Stream and the Loop Current. Detailed quan-
titative comparisons were made of both maps with results based on vari-
ous ship measurements: XBTs, inverted echo sounders, and drifters.
Significant differences in sea-surface height variability were found
between the results of altimeter and XBT; it was argued, however, that
the altimeter results were more reliable. In addition, good agreement
in sea-surface height variability was found between the results of
altimeter and inverted echo sounder, providing a solid piece of evidence
for the credibility of altimetric measurements. Comparisons of the
kinetic energy map with results from surface drifters showed that the
drifter-derived energies were consistently higher in the vicinity of the
Gulf Stream, especially along the coast. Both results are problematic
at present; it is not clear which one is better.

Maps of mesoscale variability can be obtained from the cross-over
differences method as well. After a linear adjustment which minimizes
the cross-over differences, the magnitude of the residual cross-over
differences is thus a measure of the mesoscale variability. Using six
months of data, Huang et al. (1978) presented the first variability map
thus obtained of the western North Atlantic with encouraging results.
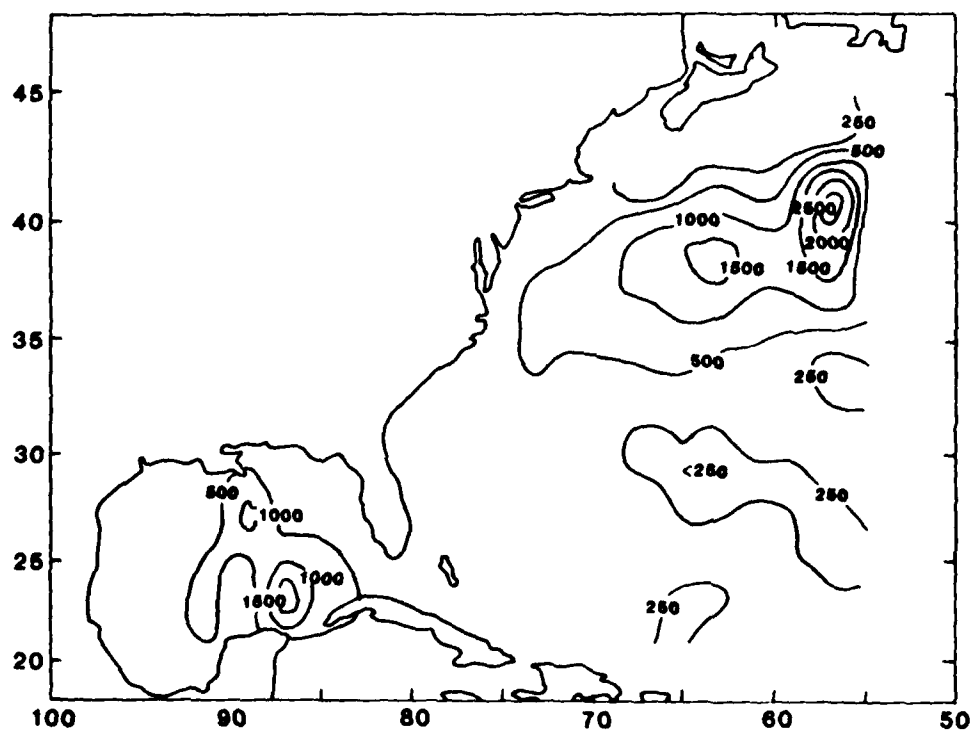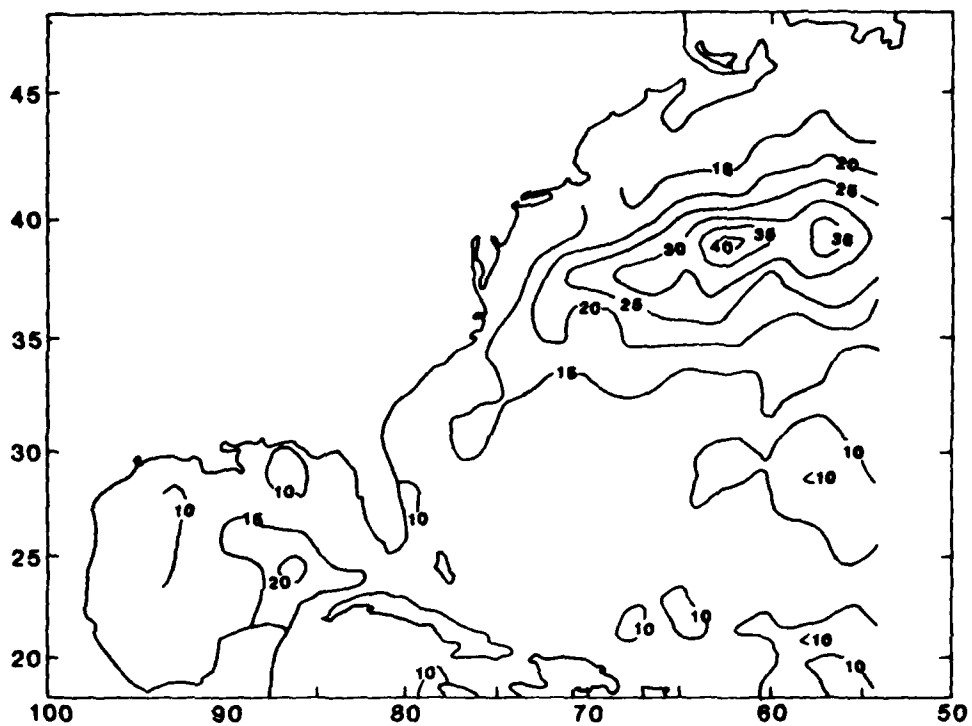
Fig. 1. (a) Sea-surface height variability in cm and (b) eddy kinetic energy in cm^2/s^2, from Geos-3 altimeter repeat pairs (from Douglas et al., 1983).

Cheney and Marsh (1981a) applied the same method to a longer data set (1.5 years) in the same area, resulting in a variability map not dissimilar to the one shown in Figure 1a but with consistently higher values. The reason for the discrepancy is not clear at present; it is probably due to the differences in the data sampling schemes of these two methods. Investigation of this problem, perhaps with simulated data, is in order. Gordon et al. (1983) applied the method to the data in the southern hemisphere and produced variability maps of major currents with details undiscovered before.

The fast along-track sampling ability of an altimeter (a few thousand kilometers in ten minutes) provides nearly synoptic measurements of sea-surface height for the estimation of wavenumber spectrum of mesoscale variability, a quantity having been difficult to measure due to the lack of synoptic measurements with sufficient spatial resolutions. Gordon and Baker (1980), using a number of repeat tracks in the western North Atlantic, demonstrated the utility of altimetry in providing the along-track component of the wavenumber spectrum of mesoscale variability. At wavelengths shorter than 200 km, their spectrum was dominated by instrument noise; at longer wavelengths, the spectral energy increased with decreasing wavenumber following a -2 power dependence until the spectrum leveled off at a wavelength of about 500 km. Because their results were based on a small set of data, geographic variability of the spectrum could not be examined.

Seasat Results

The advantages of the Seasat altimeter over the Geos-3 altimeter are its high precision (5 cm vs 25 cm) and global repeat-track coverage (see Born et al. 1979, for a mission overview), whereas these advantages are frequently overshadowed by the unfortunate fact that Seasat lasted only 3.5 months, in contrast to 3.5 years for Geos-3. Therefore, one cannot obtain from the Seasat data long-term statistics of the oceans; most studies using Seasat data are of a demonstrative nature, showing the kind of information one could obtain from a well-designed altimetric mission.

Subtracting the 5' x 5' gravimetric geoid of Marsh and Chang (1978) from the Seasat altimeter data, Cheney and Marsh (1981b) demonstrated how well individual oceanic features (Gulf Stream boundaries and eddies) were detected by the Seasat altimeter. They showed excellent agreement between altimetric measurements and concurrent observations from IR imagery, XBTs, and surface drifters. In addition, Cheney (1982) assembled a comprehensive data set taken in the western North Atlantic during the Seasat mission, providing a valuable data set for comparisons with altimetric measurements. Other examples of similar studies demonstrating the utility of the Seasat altimeter data include Wunsch and Gaposchin (1980) and Byrne and Pullen (1981).

Bernstein et al. (1982) conducted an experiment in the Kuroshio east of Japan to verify the sea-surface height measurements by the Seasat

altimeter. They dropped AXBTs along the satellite's ground tracks and used the data to compute the dynamic height of sea surface relative to 1000 db. It was found that the variations of dynamic height agreed with those of the altimeter-measured sea-surface height within 10 cm. Part of the discrepancy was due to the fact that only a portion of the baroclinic component of the variability was reflected in the 0/1000 db dynamic height measurement, whereas the altimeter-measured variability contains both the baroclinic and the barotropic components.

Using data taken in repeat tracks during the last 24 days of the mission, Cheney et al. (1983) made the first map of global mesoscale variability based on altimetry. Their map is reproduced here in Figure 2. The repeat tracks from which the data were taken are displayed in Figure 3. Each track represents eight to ten closely spaced (within a band of 2.5 km) tracks with a repeat cycle of three days. The analysis techniques are similar to those used in Douglas and Cheney (1981). For each group of repeat tracks, a mean sea-surface height profile was first formed and then subtracted from each individual profile. After the removal of a linear trend from the residual profiles, root-mean-squares of the residuals are computed, interpolated, and gridded in 2° x 2° to produce the map shown in Figure 2.

As one would expect, a local maximum of variability is associated with each of the major western boundary currents. The maximum value of 12 cm occurs in the Gulf Stream area. A series of local maxima are found in the Antarctic Circumpolar Current; most of them are located downstream of prominent topographic features. Colton and Chase (1983) studied in some detail the interaction of current with topography in these regions from the Seasat altimetry. Another notable feature on the map is the secondary maxima in the North Equatorial Currents of the Pacific and the Atlantic Oceans. No prominent variability is found in the South Equatorial Currents. Also notable on the map is the absence of significant variability along the equator, whereas a narrow zone of maximum variability is found along the equator on the eddy kinetic-energy map of Wyrtki et al. (1976). Perhaps this is due to the fact that the Coriolis parameter diminishes on the equator so that less sea-surface height variations are associated with equatorial waves than with mid-latitude eddies.

Because the variability map is based on the standard deviations from a 24-day mean, only the energies at periods shorter than 24 days are sampled adequately. The energy (square the values on the map) can be expressed by the following integral:

$$E = \int_0^\infty F(f)R(f)df \qquad (1)$$

where $F(f)$ is the frequency spectrum of sea-surface height, f is frequency in cycles/day, and

$$R(f) = (1 - \frac{\sin 24\pi f}{24\pi f})^2 \qquad (2)$$
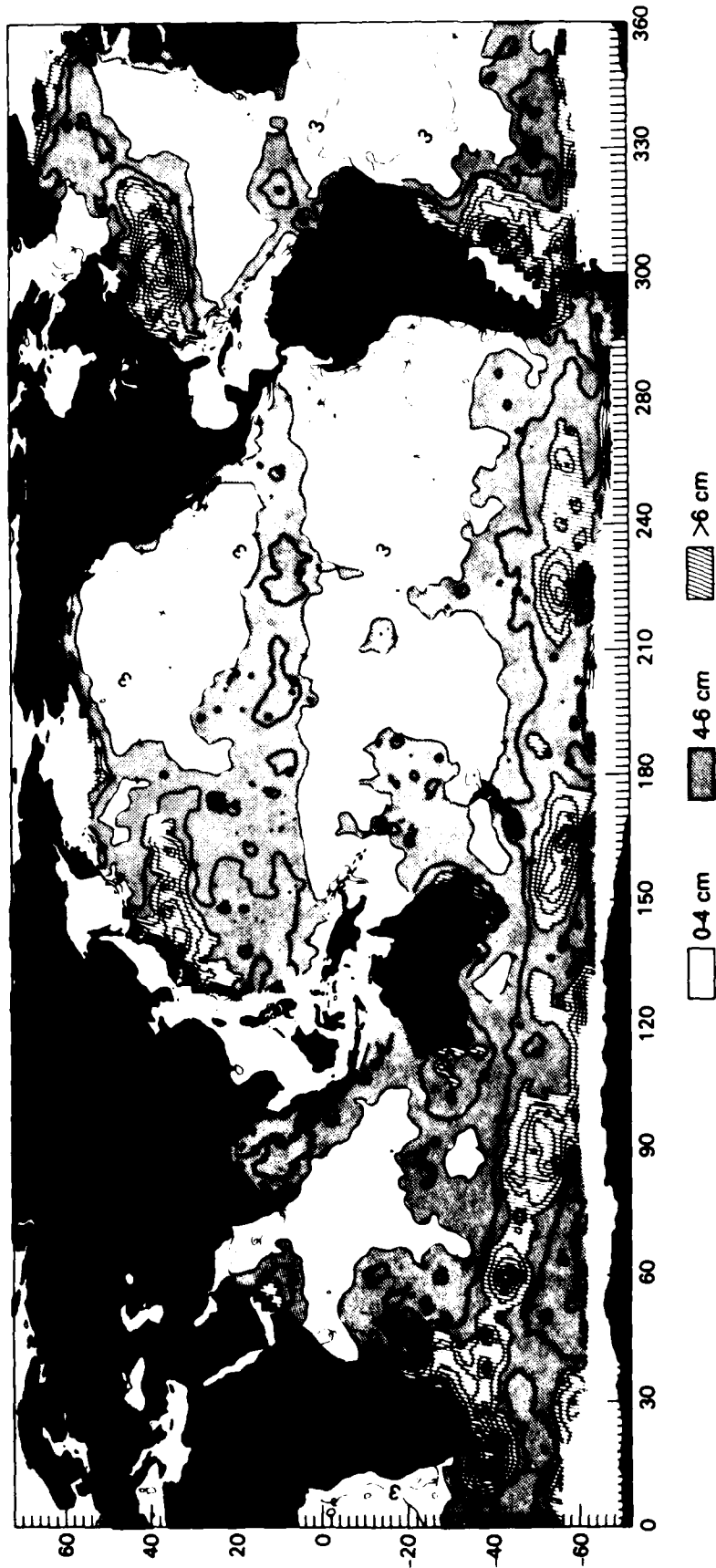
Fig. 2. Sea-surface height variability from Seasat altimetry in repeat tracks (from Cheney et al., 1983). Contour interval is 1 cm.

0-4 cm   4-6 cm   >6 cm
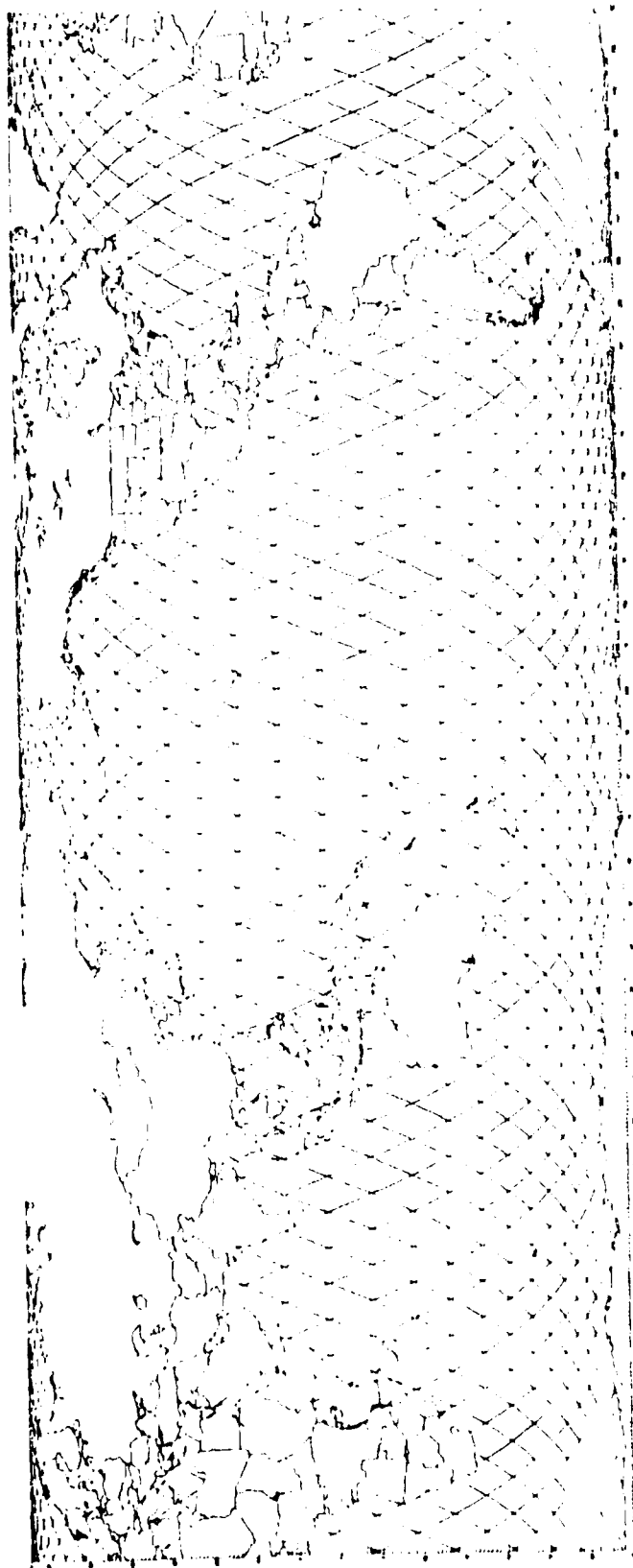
Fig. 3. Seasat ground tracks during the three-day repeat cycle (from Cheney et al., 1983).

is the transfer function of the 24-day filter. This transfer function is plotted in Figure 4. Note that the bulk of the mesoscale energy at periods from 50 to 150 days is suppressed severely. However, the low-frequency tail of the transfer function does pick up some of the mesoscale energy. The maximum variability of 12 cm in the Gulf Stream is about one third of the value shown in Figure 1a, which is based on 3.5 years of data. This implies that the energy sampled by the 24-day data is about one tenth of the total energy. This fraction is consistent with what one would expect from the known frequency spectra of mesoscale motions (e.g., see Wunsch, 1981).

Using the cross-over differences technique, Parke and Stavert (1983) also computed the global mesoscale variability from the Seasat altimetry. Their variability map is displayed in Figure 5. Only those cross-over points resulting from tracks more than 30 days apart were retained in the map. Consequently, the overall variability shown here is slightly higher than those shown in Figure 2. These two maps agree with each other in most of the main features. However, significant differences do exist. For example, in Figure 5 there is not a well-defined belt of high variability along the Pacific North Equatorial Current as the one in Figure 2; the maximum at 50°S, 90°E in Figure 2 is absent in Figure 5. These differences reflect basically that the duration of the Seasat data is too short to yield statistical significance.

Menard (1983) used the repeat-track data to compute eddy kinetic energy in the regions of the Gulf Stream and Kuroshio. His results agree with the map of Wyrtki et al.(1976) within a factor of two. This close agreement is puzzling because the energy resulting from the 24-day data used by Menard (1983) represents presumably only a small fraction (about one tenth) of the total energy represented by the map of Wyrtki et al.(1976).

Fu (1983) computed the wavenumber spectra of the variability shown in Figure 2, using the same repeat-track data. He divided the area of the oceans into two categories according to mesoscale energy level for separate spectral computations: the "high-energy areas" close to major currents and the "low-energy areas" remote from major currents. The resulting spectra are displayed in Figures 6a and 6b for the high-energy and the low-energy areas, respectively. Note that the spectra in each category overlap one another within error bars, exhibiting two distinctly different spectral characteristics.

In the high-energy areas, the spectra follow basically a -5 power dependence at wavelengths shorter than 250 km. This power-law regime was not detected by Gordon and Baker (1980) due to the high noise level of the Geos-3 altimeter. The -5 power law for the sea-surface height spectrum implies a -3 power law for the kinetic energy spectrum, which is the prediction of geostrophic turbulence theory (Charney, 1971) and numerical models (McWilliams and Chow, 1981). At wavelengths longer than 250 km, the spectra begin to level off, indicating that the energy-containing eddies have wavelengths longer than 250 km.
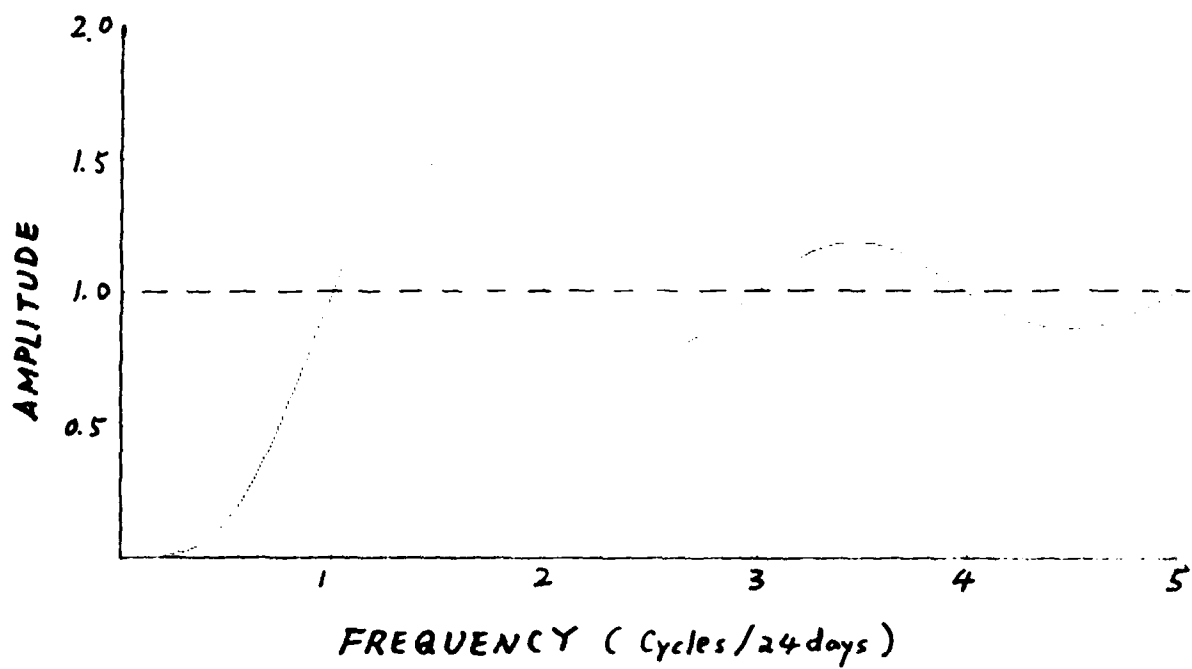
Fig. 4. The transfer function of the 24-day repeat-track, high-pass filter.

76
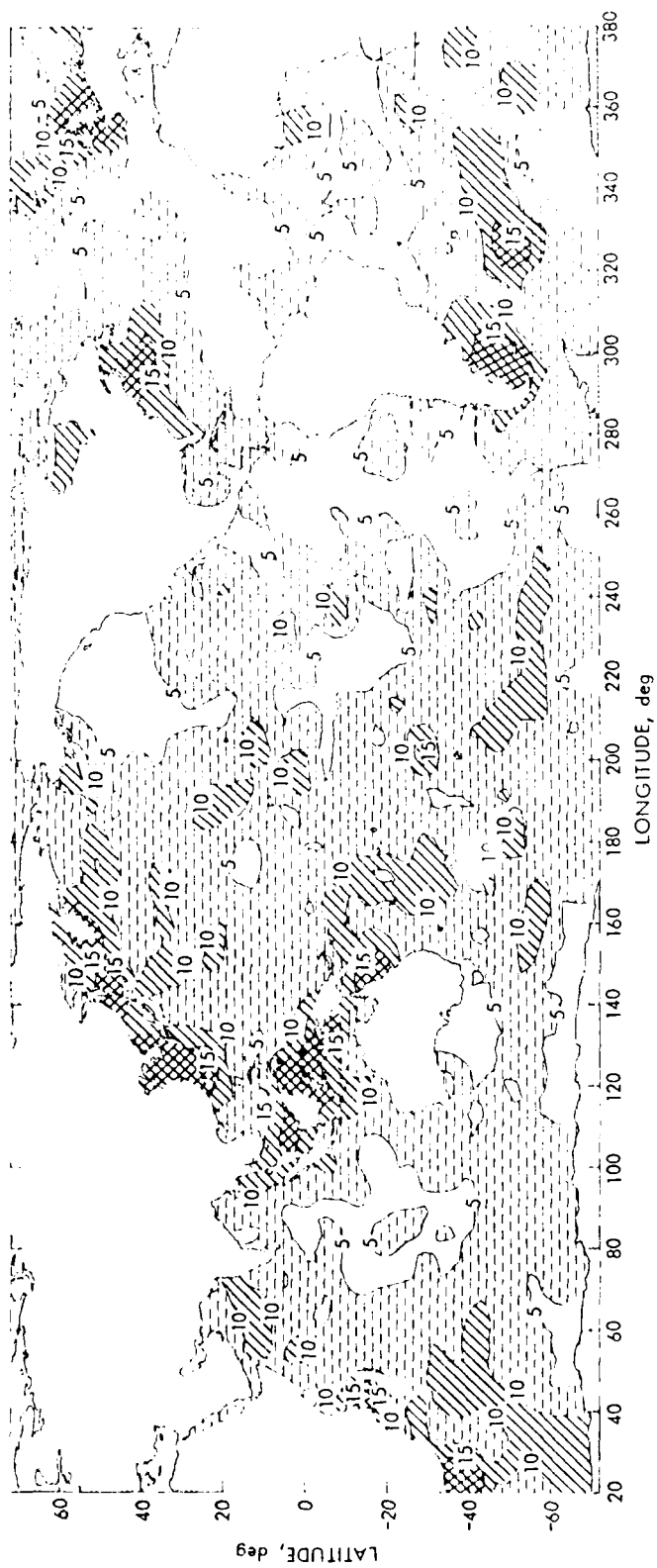
Fig. 5. Residual cross-over difference variability in cm, normalized by the square root of 2 (from Parke and Stavert, 1983).
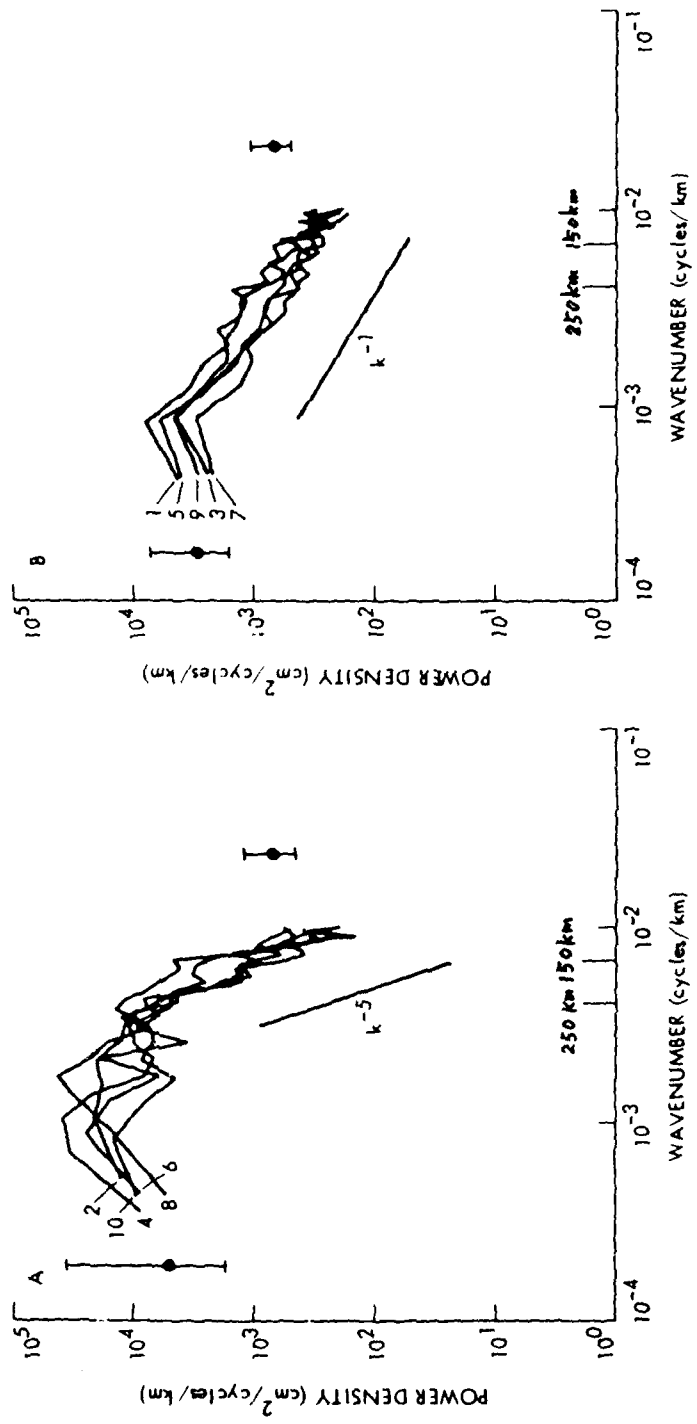
Fig. 6. Spectra of the sea-surface height variability in (a) the high-energy areas and (b) the low-energy areas. The ten labeled curves are from different areas in the world's oceans. The error bars are 95% confidence limits; the left one in each figure is for wavelengths greater than 250 km, and the right one is for wavelengths shorter than 250 km (from Fu, 1983).

In the low energy areas, the spectra follow roughly a -1 power dependence from 100 to 1000 km, implying a "blue" spectrum with +1 power dependence for the kinetic energy spectrum. This blue spectrum might sound striking; however, one has to keep in mind that the frequency content of the spectra in Figure 6 is limited by the transfer function expressed by (2). No theoretical results and in situ observations are available yet for interpreting wavenumber spectrum with this frequency content in the low-energy areas.

As revealed by the studies discussed above, the precision and coverage of the Seasat data are good enough to advance our knowledge of the global mesoscale variability. However, the utility of the data is limited severely by its short duration, as stated in the beginning of the section.

GENERAL CIRCULATION

To determine the general circulation (defined as the time-averaged circulation) of the oceans from satellite altimetry, an accurate, independently determined geoid is essential. The required geoid accuracy depends on the scales of the motion. For instance, to achieve a 10% accuracy in flow speed, a geoid accuracy of 10 cm over 100 km is required for western boundary currents, whereas an accuracy of 5 cm over 3000 km is required for subtropical gyres. Unfortunately, existing geoids do not satisfy either requirement. This is why there exists only a handful of studies attacking the problem of determining the general circulation from satellite altimetry.

The existence of high-resolution (5' x 5') gravimetric geoids in the western North Atlantic (Marsh and Chang, 1978; Mader, 1979) has generated a number of attempts at mapping the circulation in that region. Huang et al. (1978) and Robinson et al. (1983) presented maps of mean dynamic sea-surface topography constructed from the Geos-3 data and gravimetric geoid. Their results showed strong gradients at locations consistent with the mean Gulf Stream path. Using two weeks of the Seasat data, Cheney et al. (1982) obtained a quasi-instantaneous view of the Gulf Stream and geostrophic velocities that showed an error of about 50%. Mitchell (1983) constructed a one-month mean dynamic sea-surface topography from a combination of the Seasat and the Geos-3 data and obtained geostrophic velocities with similar errors (50%).

At basin-wide scales, gravimetric geoids are no longer available, but geoids based on satellite tracking have barely useful accuracies. These geoids are expressed commonly in terms of spherical harmonics. The error of each harmonic expansion coefficient increases with its degree and order. One such example is the geoid of GEM9 (Lerch et al., 1979) which is complete up to degree and order 20 (about 2000 km in wavelength). The error of GEM9 is about 1.9 m (root sum squares of all coefficient errors); the neglect of higher degree terms contributes another error of about 2.5 m, making a total error of abut 3.1 m.

Nevertheless, the error is only 16 cm for terms up to degree and order 4 (10,000 km in wavelength) and 30 cm for terms up to degree and order 6 (6700 km in wavelength).

GEM9 was applied first to the Geos-3 data by Mather et al (1979) to study the global general circulation. They found that the geoid error dominates the oceanic variability (based on hydrography) at degrees and orders greater than 4. Hence only the terms with degree and order up to 4 of the altimetric dynamic sea-surface topography can be used to improve the picture of the general circulation based on hydrography. A composite representation of the global dynamic sea-surface topography in terms of spherical harmonics up to degree and order 16 was then constructed, with the terms up to degree and order 4 from altimetry and the remaining terms from hydrography. This is the first dynamic sea-surface topography containing information from altimetry. Because the altimeter data used were not subject to cross-over adjustments, the altimetric dynamic sea-surface topography contained a substantial amount of orbital error in addition to geoid error.

Using cross-over adjusted Seasat data and GEM9, Tai and Wunsch (1983) and Tai (1983) constructed an altimetric dynamic sea-surface topography of the Pacific Ocean at a resolution of 20°. They made detailed comparisons of their results with the hydrography-derived dynamic sea-surface topography of Wyrtki (1975) at each degree of spherical harmonics up to degree 6. Examination of the quantitative differences at each degree (degree variance of the difference) between the two topographic maps (Tai, 1983, Table 1) indicates that the differences are greater than the estimated geoid error at degrees less than or equal to 3, and the differences are comparable to the estimated geoid error at degrees greater than 3. This implies that a real difference in addition to that caused by geoid error exists between the first three degrees of the spherical harmonic expansion of the two topographic maps. The three-degree expansion of the two maps (from Tai, 1983) are reproduced here in Figures 7a and 7b for the altimetric and the hydrographic maps, respectively. Despite the visual resemblance between the two maps, the altimetric map shows a circulation twice stronger than does the hydrographic map. This difference could still be attributed to the orbital error that has not been removed by the cross-over adjustments. On the other hand, it might just indicate that the large-scale circulation of the Pacific Ocean during the Seasat mission was somewhat stronger than the one shown on Wyrtki's map based on some 70 years hydrographic data and a "level of no motion" at 1000 db.

Douglas and Agreen (1983) developed a procedure to reduce satellite orbital error to a level better than that achieved by cross-over adjustment. They applied the procedure to three days of the Seasat data and used the corrected data with a geoid model called GEM-L2 to construct a global dynamic sea-surface topography at a resolution of 20°. In addition, Cheney and Marsh (1982) used a combination of the complete Seasat data and 1.5 years of the Geos-3 data (without corrections to orbital error though) with the GEM-L2 geoid model to construct a global dynamic
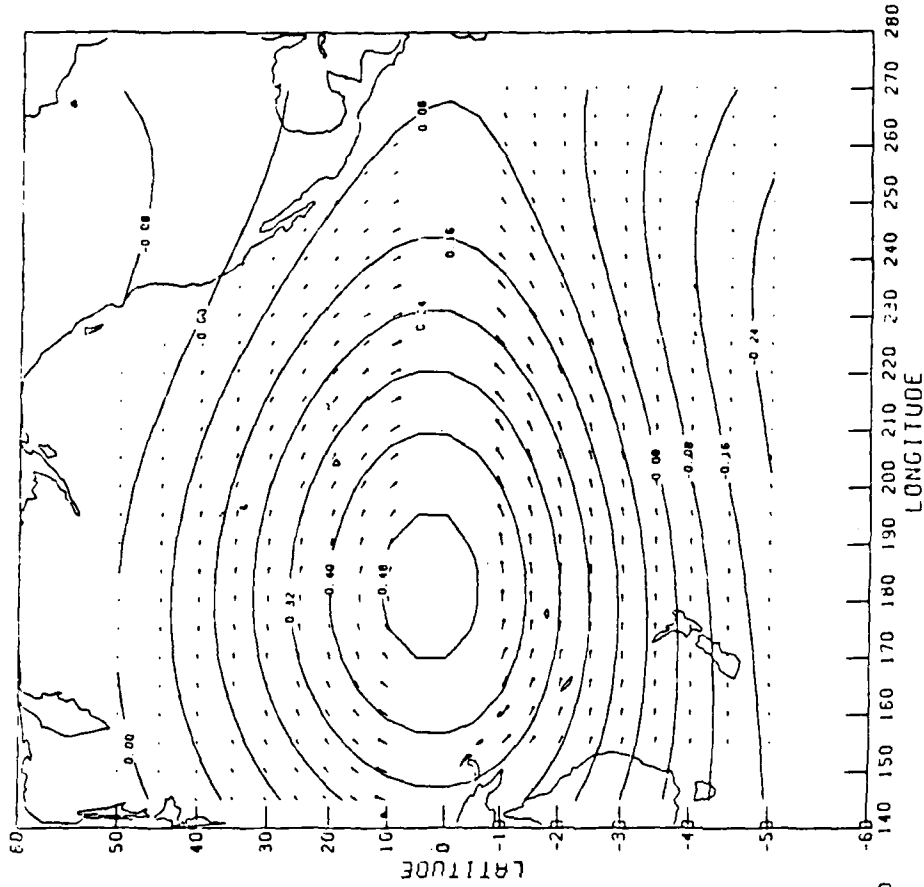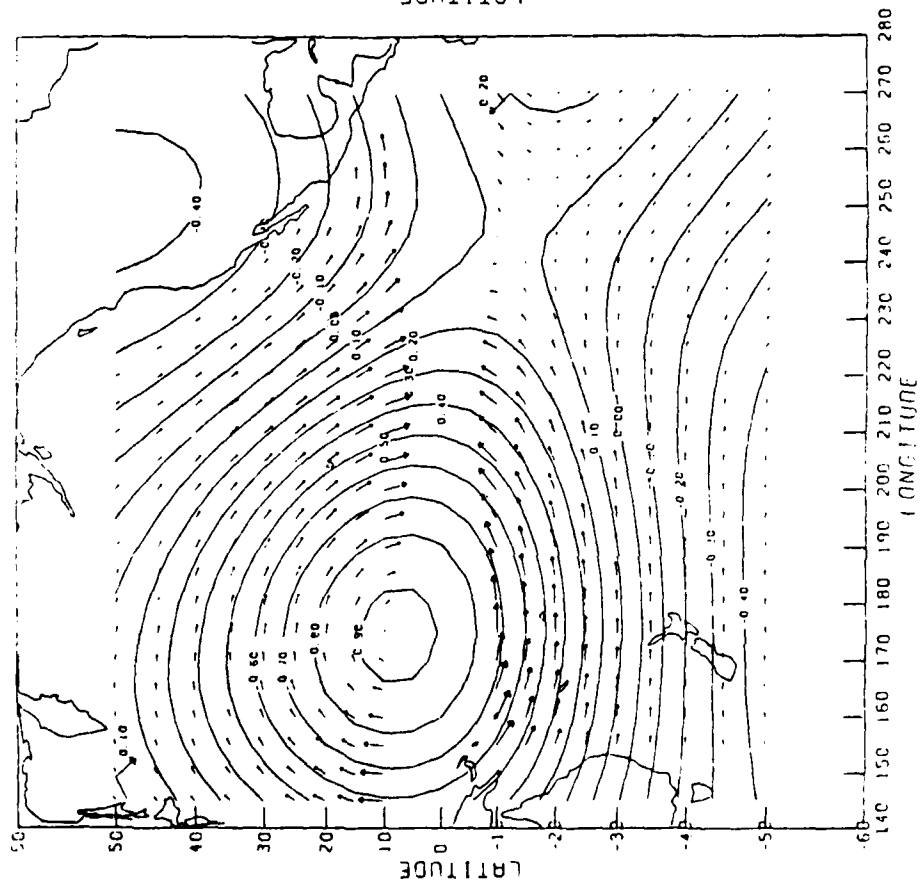
Fig. 7. Spherical harmonic expansion complete to degree and order 3 of the dynamic sea-surface topography based on (a) altimetry and (b) hydrography (from Tai, 1983). Contours are in meters. The arrows represent geostrophic velocities with a maximum speed of 8.2 cm/s in (a) and 3.9 cm/s in (b).

sea-surface topography at similar resolution. The results of these two studies revealed some common large-scale features, though somewhat distorted, of the global general circulation: the subtropical gyres of the North Pacific, the South Atlantic, and the South Indian Ocean, and the Antarctic Circumpolar Current, along with many significant regional differences. However, the results of Douglas and Agreen (1983) showed a better-defined gyre in the western North Atlantic. The GEM-L2 geoid presumably has less error than does the GEM9 geoid, but spherical harmonic analysis was not done in these two studies, so the contamination of geoid error in the results could not be rigorously assessed at various scales as in Tai (1983), making the differences between the altimetric and the hydrographic results difficult to interpret.

In summary, as one would expect, the accuracy of the presently available geoid models allows one to obtain only a rather crude picture of the general circulation that is hardly useful, except perhaps its largest components, in improving the picture obtained from hydrography.

CONCLUDING REMARKS

The major message from the various studies of the mesoscale variability from existing satellite altimeter data is the following: an optimally designed altimetric mission with a lifetime of several years will improve our knowledge of the global mesoscale variability to an extent unattainable by any other practical means.

Such a mission, called Topex (see Topex Science Working Group, 1981), has been proposed by NASA to the Congress for a FY-85 start with launch planned in the late 80's. The proposed altimeter has a precision level of 1.5 cm, extending the lower limit in wavelength of detectable oceanic variability from 100 km for Seasat to about 50 km. With a reduction of orbital error to the 10-cm level by new tracking methods, even the variability of basin-wide scales can be measured in addition to the mesoscale variability. The Topex orbit has a ten-day repeat cycle with equatorial separation of 300 km, a compromise between sampling requirements in space and time. The mission is planned to last three years with an option for a two-year extension. With the possibility of having five years of such data, one can begin to dream of viewing the global oceanic variability in such a wide range of periods and wavelengths: from 20 days to 5 years; from 50 to 10,000 km.

Before the advent of such a mission, effort should be made to design optimal schemes of utilizing altimeter data. Alan Robinson of Harvard University has initiated a program to study how to optimally assimilate altimeter data into numerical forecast models. Other areas of research include the study of the differences between the repeat-track method and the cross-over differences method in sampling oceanic variability, perhaps using numerically simulated data.

Determining the general circulation from altimetry is more

problematic, because a single altimetric mission will not solve the problem and a highly accurate geoid needs to be determined independently. The accuracies of the presently available geoid models are not adequate for determining the general circulation from altimetry. However, as discussed by Jekeli and Rapp (1980), the proposed Gravsat mission of tracking two satellites at a height of 160 km will provide a geoid with accuracies of ± 3.7 cm for $1° \times 1°$ averages and ± 1.5 cm for $2° \times 2°$ averages, which are good enough for determining the circulation down to a wavelength of 100 km. Therefore, the combination of Topex and Gravsat certainly will revolutionize the state of our knowledge of the general circulation.

Before the promise of Topex/Gravsat becomes a reality, there is more to learn from existing altimeter data and the best available geoid. As demonstrated by the results of Tai (1983), even GEM9 which is not the state-of-the-art geoid model is marginally useful in improving the picture of the general circulation at spherical harmonics of degree 3 or less. More useful information on the general circulation up to higher degrees must be obtainable from existing altimeter data and more up-to-date geoid models with complete error information (perhaps GEM-L2). A possible approach is conceived as follows. Starting with the best available Seasat orbit (perhaps the one constructed by J. G. Marsh of the Goddard Space Flight Center), one can then make further corrections to the orbit using the method of Douglas and Agreen (1983) or Parke and Stavert (1983). With the corrected orbit, one proceeds to construct an altimetric mean sea surface, from which the best available geoid is subtracted. The resulting altimetrically determined dynamic topography are then combined with existing hydrography (both with estimated errors) in an inverse procedure like the one outlined in Wunsch and Gaposchkin (1980) to improve optimally both the circulation and the geoid.

ACKNOWLEDGMENTS

REFERENCES

Bernstein, R. L., G. H. Born, and R. H. Whritner, Seasat altimeter determination of ocean current variability, J. Geophys. Res., 87, 3261-3268, 1982.

Born, G. H., J. A. Dunne, and D. B. Lame, Seasat mission overview, _Science_, _204_, 1405-1406, 1979.

Byrne, H. M. and P. E. Pullen, Western boundary current variability derived from Seasat altimetry data, in _Oceanography From Space_, edited by J.F.R. Gower, Plenum, New York, 1981.

Charney, J. G., Geostrophic turbulence, _J. Atmos. Sci._, _28_, 1087-1095, 1971.

Cheney, R. E., Comparison data for Seasat altimetry in the western North Atlantic, _J. Geophys. Res._, _87_, 3247-3253, 1982.

Cheney, R. E. and J. G. Marsh, Oceanic eddy variability measured by Geos-3 altimeter crossover differences, _EOS Trans. AGU_, _62_ (45), 743-752, 1981a.

Cheney, R. E. and J. G. Marsh, Seasat altimeter observations of dynamic topography in the western North Atlantic, _J. Geophys. Res._, _86_, 473-483, 1981b.

Cheney, R. E. and J. G. Marsh, Global ocean circulation from satellite altimetry, _EOS Trans. AGU_, _63_ (45), 997, 1982.

Cheney, R. E., J. G. Marsh, B. D. Beckley, Global mesoscale variability from repeat tracks of Seasat altimeter data, _J. Geophys. Res._, in press, 1983.

Cheney, R. E., J. G. Marsh, B. Beckley, and B. C. Douglas, Mesoscale features and variability from satellite altimetry, paper presented at the Seasat Altimeter Data Seminar, Jet Propulsion Lab., Pasadena, 1982.

Colton, M. T. and R.R.P. Chase, The interaction of the Antarctic Circumpolar Current with bottom topography: An investigation using satellite altimetry, _J. Geophys. Res._, in press, 1983.

Dantzler, H. L., Jr., Potential energy maxima in the tropical and subtropical North Atlantic, _J. Phys. Oceanogr._, _7_, 512-519, 1977.

Douglas, B. C. and R. W. Agreen, Observing global ocean circulation with Seasat altimeter data, submitted to _Marine Geodesy_, 1983.

Douglas, B. C. and R. E. Cheney, Ocean mesoscale variability from repeat tracks of Geos-3 altimeter data, _J. Geophys. Res._, _86_, 10931-10937, 1981.

Douglas, B. C. and P. D. Gaborski, Observations of sea surface topography with Geos-3 altimeter data, _J. Geophys. Res._, _84_, 3893-3896, 1979.

84

Douglas, B. C., R. W. Agreen and R. E. Cheney, Eddy energy of the northwest Atlantic determined from Geos-3 satellite altimeter data, submitted to J. Geophys. Res., 1983.

Fu, L.-L., On the wavenumber spectrum of oceanic mesoscale variability observed by the Seasat altimeter, J. Geophys. Res., in press, 1983.

Gordon, A. L. and T. N. Baker, Ocean transients as observed by Geos-3 coincident orbits, J. Geophys. Res., 85, 502-506, 1980.

Gordon, A. L., K. Horai, and M. Donn, Southern hemisphere western boundary current variability revealed by Geos-3 altimeter, J. Geophys. Res., 88, 755-762, 1983.

Huang, N. E., C. D. Leitao and C. G. Parra, Large-scale Gulf Stream frontal study using Geos-3 radar altimeter data, J. Geophys. Res., 83, 4673-4682, 1978.

Jekeli, C. and R. Rapp, Accuracy of the determination of mean anomalies and mean geoid undulation for a satellite gravity field mapping mission, Ohio State Univ. Geodetic Science Report No. 307, 1980.

Leitao, C. D., L. S. Miller and N. E. Huang, Detecting the Gulf Stream using satellite altimetry, Trans. Amer. Geophys. Union, 56, 1107, 1974.

Lerch, F., S. M. Klosko, R. E. Laubscher and C. A. Wagner, Gravity model improvement using Geos-3 (GEM9 and 10), J. Geophys. Res., 84, 3897-3916, 1979.

Mader, G. L., A revised 5' gravimetric geoid and associated errors for the North Atlantic calibration area, NASA Contract Rep., 156851, 32 pp., 1979.

Marsh, J. G. and E. S. Chang, 5' detailed gravimetric geoid in the northwestern Atlantic Ocean, Mar. Geod., 1, 253-261, 1978.

Mather, R. S., R. Coleman and B. Hirsh, Temporal variations in regional models of the Sargasso Sea from Geos-3 altimetry, J. Phys. Oceanogr., 10, 171-185, 1980.

Mather, R. S., C. Rizos and R. Coleman, Remote sensing of surface ocean circulation with satellite altimetry, Science, 205, No. 4401, 11-17, 1979.

McWilliams, J. C. and J.H.S. Chow, Equilibrium geostrophic turbulence I: a reference solution in a beta-plane channel, J. Phys. Oceanogr., 11, 921-949, 1981.

Menard, Y., Observation of the eddy field in the northwest Atlantic and northwest Pacific by Seasat altimeter data analysis, J. Geophys. Res., in press, 1983.

Mitchell, J., Synoptic mapping of the oceanic mesoscale with satellite altimetry, to be published, 1983.

Munk, W. and C. Wunsch, Observing the ocean in the 1990's, _Phil. Trans. Roy. Soc._, _A307_, 439-464, 1982.

Parke, M. E. and L. R. Stavert, Mean sea surface and variability from Seasat radar altimeter, _J. Geophys. Res._, in press, 1983.

Robinson, A., N. E. Huang, C. D. Leitao and C. G. Parra, A study of the variability of ocean currents in the northwestern Atlantic using satllite altimetry, _J. Phys. Oceanogr._, in press, 1983.

Stanley, H. R., The Geos-3 project, _J. Geophys. Res._, _84_, 3779-3783, 1979.

Stewart, R. H., _Methods of Satellite Oceanography_, Univ. of California Press, Berkeley, in press, 1983.

Tai, C. K., On determining the large-scale ocean circulation from satellite altimetry, submitted to _J. Geophys. Res._, 1983.

Tai, C. K. and C. Wunsch, Absolute measurement by satellite altimetry of dynamic topography of the Pacific Ocean, _Nature_, _301_, No. 5899, 408-410, 1983.

Tapley, B. D., G. H. Born and M. E. Parke, The Seasat altimeter data and its accuracy assessment, _J. Geophys. Res._, _87_, 3179-3188, 1982.

Topex Science Working Group, Satellite altimetric measurements of the ocean, JPL Doc. 400-111, Jet Propulsion Laboratory, Pasadena, CA, 1981.

Wunsch, C., _Low-frequency variability of the sea_, in _Evolution of Physical Oceanography: Scientific Surveys in Honor of Henry Stommel_, edited by B. A. Warren and C. Wunsch, MIT Press, Cambridge, MA, pp. 342-374, 1981.

Wunsch, C. and E. M. Gaposchkin, On using satellite altimetry to determine the general circulation of the oceans with application to geoid improvement, _Rev. Geophys. Space Phys._, _18_, 725-745, 1980.

Wyrtki, K., Fluctuations of the dynamic topography in the Pacific Ocean, _J. Phys. Oceanogr._, _5_, 450-459, 1975.

Wyrtki, K., L. Magaard and J. Hager, Eddy energy in the oceans, _J. Geophys. Res._, _81_, 2641-2646, 1976.

EDDY — MEAN FLOW INTERACTION DIAGNOSTICS

James R. Holton

Department of Atmospheric Sciences AK-40
University of Washington
Seattle, Washington 98195

ABSTRACT

Recent developments in the diagnosis of mean flow forcing by quasi-geostrophic eddies are reviewed. The so-called "Eliassen-Palm flux", which has been used to diagnose the forcing of the zonal mean wind by stationary waves, has recently been extended to three-dimensional eddy-mean flow interactions by Hoskins. This work may provide a framework for understanding the driving of mean flows by transient eddies in the atmosphere and the oceans.

INTRODUCTION

Much of the recent work on wave-mean zonal flow interaction in the atmosphere has been stimulated by observed features of the middle atmosphere such as the sudden warmings of the polar winter stratosphere, and the quasi-biennial oscillation of the equatorial stratosphere. These subjects are reviewed in Holton (1983). For these and other zonally symmetric circulations Andrews and McIntyre (1976) have shown that the net eddy forcing of the mean flow can be represented in terms of the divergence of a vector in the meridional plane which is now called the "Eliassen-Palm" (or "EP") flux in recognition of the classic work of Eliassen and Palm (1961). For quasi-geostrophic waves Edmon et al. (1980) showed that the EP flux $\underset{\sim}{F}$ appears in a conservation equation for "wave activity" of the form

$$\frac{\partial A}{\partial t} + \underset{\sim}{\nabla} \cdot \underset{\sim}{F} = D \qquad (1)$$

where A is the eddy potential enstrophy divided by the northward gradient of potential vorticity, and D is proportional to the dissipation of eddy enstrophy by thermal and mechanical damping. With the aid of (1) the eddy forcing of the mean flow, $\underset{\sim}{\nabla} \cdot \underset{\sim}{F}$, can be directly calculated in terms of eddy transience (time rate of change in amplitude) and eddy dissipation. Hence, for steady conservative waves the net eddy forcing of the mean flow vanishes, a result referred to as the "nonacceleration" theorem. Furthermore, it can be shown that when group velocity can be defined, $\underset{\sim}{F} = \underset{\sim}{c}_g A$, where $\underset{\sim}{c}_g$ is the group velocity vector in the meridional plane. Thus, for zonally symmetric

mean flows the EP flux vector provides an efficient diagnostic measure of the flow of wave activity in latitude and height and its net effect on the mean flow.

The utility of the EP flux vector as a diagnostic in both observational and theoretical studies of the atmosphere (e.g., Butchart et al., 1982) has stimulated searches for an equivalent three dimensional vector for diagnosis of the local interaction of transient eddies with the time mean circulation.

Andrews (1982) has derived a three dimensional version of the EP flux which satisfies an equation analogous to (1), but his flux contains time derivative terms and does not appear to be practical for diagnosis using real data. Hoskins et al. (1983) (hereafter referred to as HJW) have derived an "extended EP flux" which, while not satisfying a conservation law similar to (1), has the perhaps overwhelming advantage that it can be evaluated diagnostically from standard meteorological data.

Some of the concepts in HJW were previously developed in an oceanographic context by Rhines and Holland (1979) and Young and Rhines (1980). However, HJW have made an important contribution by showing how the mean equations can be transformed to provide a practical diagnostic for the local eddy forcing of the time mean circulation.

ZONAL MEAN DIAGNOSTICS

Before discussing the extended EP flux vector, it may be useful to review the EP theory for zonal mean circulations. To keep the development as simple as possible we will use the Boussinesq equations on an f-plane. The approximate zonally averaged dynamics equations scaled for quasi-geostrophic motions are then

$$\frac{\partial \bar{u}}{\partial t} = f \bar{v} - \frac{\partial}{\partial y} (\overline{u'v'}) \tag{2}$$

$$\frac{\partial \bar{\theta}}{\partial t} + \bar{w} N^2 = - \frac{\partial}{\partial y} \overline{v'\theta'} + \bar{Q} \tag{3}$$

$$\frac{\partial \bar{v}}{\partial y} + \frac{\partial \bar{w}}{\partial z} = 0 \tag{4}$$

where the buoyancy, $\bar{\theta}$, is related to $\bar{u}$ by the thermal wind equation

$$f \frac{\partial \bar{u}}{\partial z} = - \frac{\partial \bar{\theta}}{\partial y} \tag{5}$$

In the above, N is the buoyancy frequency, $\bar{Q}$ is the net zonal mean diabatic source, and overbars and primes stand for the zonal mean and eddy fields, respectively.

Although superficially it appears that (2)-(4) could be used to diagnose the eddy forcing of the mean circulation, it turns out in practice that a portion of the mean meridional circulation $(\bar{v}, \bar{w})$ described by (2)-(4) is an eddy-generated mean circulation which to a considerable extent cancels out the eddy flux terms so that the net driving by the eddies is usually much smaller than suggested by the mean equations (2)-(4). For example, in (4) the horizontal heat flux divergence tends to drive the $\bar{\theta}$ field out of thermal wind balance. As a result a secondary circulation is induced which restores the time mean flow to thermal wind balance and at the same time tends to compensate the eddy heat flux divergence through adiabatic cooling.

One approach to determining the net eddy drive is to use (4) to eliminate $\bar{v}$ and $\bar{w}$ between (2) and (3) to obtain the zonal mean potential vorticity equation

$$\frac{\partial \bar{q}}{\partial t} = - \frac{\partial}{\partial y} \overline{q'v'} - \bar{S} \tag{6}$$

where

$$\bar{q} \equiv f - \frac{\partial \bar{u}}{\partial y} + \frac{f}{N^2} \frac{\partial \bar{\theta}}{\partial z}$$

$$\overline{q'v'} = - \frac{\partial}{\partial y} \overline{u'v'} + \frac{f}{N^2} \frac{\partial}{\partial z} (\overline{v'\theta'}) = \nabla \cdot \underset{\sim}{F}$$

and

$$\bar{S} = - \frac{f}{N^2} \frac{\partial \bar{Q}}{\partial z}$$

Here $\underset{\sim}{F} \equiv (- \overline{u'v'}, \ f \overline{v'\theta'}/N^2)$ is the EP flux vector discussed in the introduction. Eq. (6) shows that the net eddy forcing of the mean flow can be expressed in terms of the poleward potential vorticity flux while the momentum flux $\overline{u'v'}$ and buoyancy flux $\overline{v'\theta'}$ alone may give very misleading impressions. Thus, (2) and (3) are not very useful in diagnosing eddy-mean flow interaction whereas (6), although providing a precise measure of the eddy forcing does not directly determine the momentum forcing.

Andrews and McIntyre (1976) have shown that a simple transformation of (2)-(4) can, however, provide momentum and buoyancy equations which do display the net eddy forcing in a convenient manner. They introduce a "residual" mean meridional circulation $(\bar{v}^*, \bar{w}^*)$ by letting

$$\bar{v}^* \equiv \bar{v} - \frac{\partial}{\partial z} \left(\frac{\overline{v'\theta'}}{N^2} \right); \qquad \bar{w}^* = \bar{w} + \frac{\partial}{\partial y} \left(\frac{\overline{v'\theta'}}{N^2} \right) \tag{7}$$

Substituting into (2)-(4) yields

$$\frac{\partial \overline{u}}{\partial t} = f\ \overline{v}* + \underset{\sim}{\nabla} \cdot \underset{\sim}{F} \tag{8}$$

$$\frac{\partial \overline{\theta}}{\partial t} = -\ \overline{w}*\ N^2 + \overline{Q} \tag{9}$$

$$\frac{\partial \overline{v}*}{\partial y} + \frac{\partial \overline{w}*}{\partial z} = 0 \tag{10}$$

From (9) it is clear that $\overline{w}*$ is just that part of the $\overline{w}$ field which is not cancelled by the eddy buoyancy fluxes, while from (8) we see that $\underset{\sim}{\nabla} \cdot \underset{\sim}{F}$ does indeed represent the eddy forcing of the zonal mean flow.

TIME MEAN DIAGNOSTICS AND THE EXTENDED EP FLUX

The time averaged Eulerian equations can be transformed in a manner closely analogous to that of the zonal mean equations discussed above. Following Hoskins (1983) we observe that for quasi-nondivergent eddies the momentum equations can be expressed in terms of the eddy vorticity flux as follows:

$$\overline{D}\ \overline{u} = f\ \overline{v} - (\overline{p} + K\ )\ + \overline{v'\zeta'} \tag{11}$$

$$\overline{D}\ \overline{v} = -\ f\ \overline{u} - (\overline{p} + K_e)_y - \overline{u'\zeta'} \tag{12}$$

where $\overline{D} \equiv \overline{u}\ \partial/\partial x + \overline{v}\ \partial/\partial y$, $K_e \equiv (\overline{u'^2} + \overline{v'^2})/2$, $\zeta' = v'_x - u'_y$ and $\overline{p}$ is the time mean pressure divided by a basic state density. The thermodynamic energy equation becomes

$$\overline{D}\ \overline{\theta} + \overline{w}\ N^2 = -\ (\overline{u'\theta'})_x - (\overline{v'\theta'})_y + \overline{Q} \tag{13}$$

while the continuity equation is

$$\frac{\partial \overline{u}}{\partial x} + \frac{\partial \overline{v}}{\partial y} + \frac{\partial \overline{w}}{\partial z} = 0 \tag{14}$$

As in the zonal mean equations (2) and (3), the eddy forcing here appears explicitly in both the momentum equations and the thermodynamic energy equation. To diagnose the net eddy forcing it is again useful to define a residual circulation by letting

$$\tilde{w} \equiv \overline{w} + \frac{\partial}{\partial x}\left[\frac{\overline{u'\theta'}}{N^2}\right] + \frac{\partial}{\partial y}\left[\frac{\overline{v'\theta'}}{N^2}\right] \tag{15}$$

$$\tilde{u} \equiv \bar{u} + \frac{1}{f} \frac{\partial}{\partial y} (\bar{p} + K_e) - \frac{\partial}{\partial z} \left[\overline{\frac{u'\theta'}{N^2}} \right] \qquad (16)$$

$$\tilde{v} \equiv \bar{v} - \frac{1}{f} \frac{\partial}{\partial x} (\bar{p} + K_e) - \frac{\partial}{\partial z} \left[\overline{\frac{v'\theta'}{N^2}} \right] \qquad (17)$$

Here in defining the horizontal residual circulation $(\tilde{u}, \tilde{v})$ we have subtracted from the time mean wind $(\bar{u}, \bar{v})$ not only the divergent portion associated with the vertical motion which compensates the eddy buoyancy flux, but also a nondivergent portion consisting of the geostrophic wind plus the ageostrophic circulation which balances the eddy contribution to the dynamic pressure (K_e).

Substituting from (15)-(17) into (11)-(13) and again using the fact that the eddies are quasi-nondivergent so that, for example

$$\overline{v'\zeta'} = \overline{v' \frac{\partial v'}{\partial x}} - \overline{v' \frac{\partial u'}{\partial y}}$$

$$= + \frac{1}{2} \frac{\partial}{\partial x} (\overline{v'^2}) - \frac{\partial}{\partial y} \overline{u'v'} + \overline{u' \frac{\partial v'}{\partial y}}$$

$$= - \frac{1}{2} \frac{\partial}{\partial x} (\overline{u'^2} - \overline{v'^2}) - \frac{\partial}{\partial y} \overline{u'v'}$$

we obtain the transformed equations

$$\bar{D} \bar{u} - f \tilde{v} = \nabla_3 \cdot \mathop{E}_{\sim u} \qquad (18)$$

$$\bar{D} \bar{v} + f \tilde{u} = \nabla_3 \cdot \mathop{E}_{\sim v} \qquad (19)$$

$$\bar{D} \bar{\theta} + \tilde{w} N^2 = \bar{Q} \qquad (20)$$

$$\tilde{u}_x + \tilde{v}_y + \tilde{w}_z = 0 \qquad (21)$$

where

$$\mathop{E}_{\sim u} \equiv \left[\overline{\frac{v'^2 - u'^2}{2}} , - \overline{u'v'} , \frac{f}{N^2} \overline{v'\theta'} \right]$$

$$\mathop{E}_{\sim v} \equiv \left(- \overline{u'v'} , - \overline{\frac{v'^2 - u'^2}{2}} , - \frac{f}{N^2} \overline{u'\theta'} \right) \qquad (22)$$

92

Thus, E_u and E_v can be interpreted as the net eddy momentum fluxes of zonal and meridional momentum, respectively. *Comparing (8) and (18) it is clear that the zonal mean of E_u is simply the EP flux F.* Thus, it is reasonable to call E_u the __extended__ EP flux.

HJW chose to work with the time mean potential vorticity equation rather than the momentum and thermodynamic energy equations. Their expression can be obtained by combining (18)-(21) in the usual manner to obtain for quasi-geostrophic motions:

$$\overline{D}\, \overline{q} = \nabla_3 \cdot \left(\frac{\partial E_v}{\partial x} - \frac{\partial E_u}{\partial y} \right) + \frac{f}{N^2} \frac{\partial \overline{Q}}{\partial z} \tag{23}$$

where

$$\overline{q} \equiv \frac{\partial \overline{v}}{\partial x} - \frac{\partial \overline{u}}{\partial y} + f + \frac{f}{N^2} \frac{\partial \overline{\theta}}{\partial z}$$

HJW show that in the atmosphere (23) can be approximated with reasonable accuracy as

$$\overline{D}\, \overline{q} = -\frac{\partial}{\partial y} \nabla_3 \cdot E + \frac{f}{N^2} \frac{\partial \overline{Q}}{\partial z}$$

where

$$E \equiv E_u + \left(\frac{\overline{v'^2 - u'^2}}{2},\ 0,\ 0 \right)$$

is the vector which HJW call the extended EP flux. Although HJW find that this approximation is quite accurate in the atmosphere where the zonal scale on which the components of E_u and E_v vary is much longer than the meridional scale, it is not clear that there is any reason to utilize the approximate form E when the objective is to diagnose the momentum forcing of the zonal flow.

HJW present statistics of E in the Northern Hemisphere winter for both high-pass and low-pass eddies with periods less than and greater than 10 days, respectively. The high-pass and low-pass __eddies are__ distinguished by generally having positive and negative values of $\overline{v'^2 - u'^2}$, respectively. Thus, the horizontal components of the high-pass and low-pass E have eastward and westward orientations, respectively. Their patterns in relation to the $\overline{u}$ field are shown in Figs. 1 and 2 taken from HJW. For the high-pass eddies E is divergent at low levels at the start of the "storm tracks" so that the eddies tend to strengthen the barotropic wind but weaken the vertical shear. Near the end of the storm track E is convergent at high levels so tends to weaken the barotropic flow. Further interpretations are given in HJW.
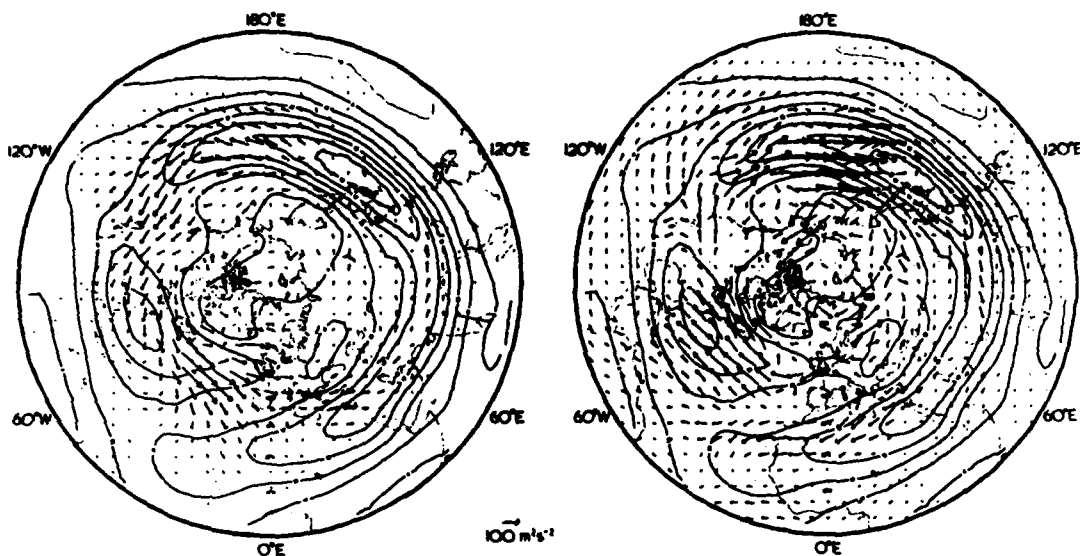
Fig. 1. The horizontal projection of $\underset{\sim}{E}$ at 250 mb for the Northern Hemisphere winter of 1979-1980. The solid contours are isolines of u with contour interval of 10 ms^{-1}. (a) High-pass transients; (b) low-pass transients. After Hoskins et al. (1983).
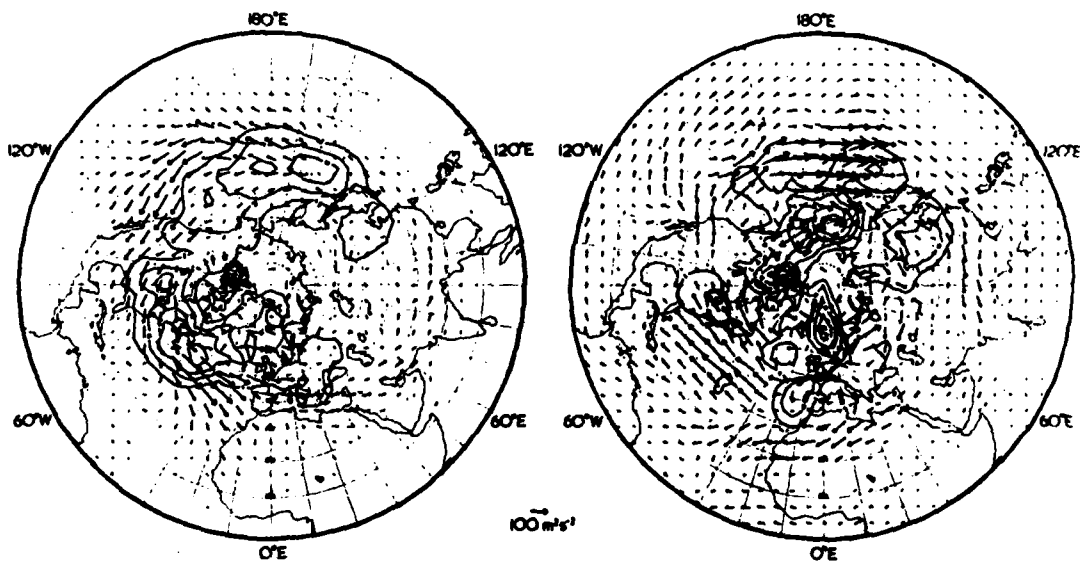
Fig. 2. The three-dimensional pattern of $\underset{\sim}{E}$. Horizontal projection shown as arrows as in Fig. 1. Distribution of vertical component shown by contours of $\overline{v'T'}$ (interval of 5 ms^{-1} K) at 700 mb, for the Northern Hemisphere winter of 1979-1980. (a) High-pass transients; (b) Low-pass transients. After Hoskins et al. (1983).

CONCLUSIONS

The zonal mean EP flux has already proved to be an invaluable tool for diagnosing wave-mean flow interaction in atmospheric observational studies as well as in numerical simulations. It seems likely that the extended EP flux discussed here will be equally useful for diagnosing the interaction of transient eddies and the time mean flow in the atmosphere, and perhaps eventually in the oceans as well.

ACKNOWLEDGMENT

REFERENCES

Andrews, D. G., 1982. A conservation law for small-amplitude quasi-geostrophic disurbances on a zonally symmetric basic flow. J. Atmos. Sci. (in press).

Andrews, D. G. and M. E. McIntyre, 1976. Planetary waves in horizontal and vertical shear: the generalized Eliassen-Palm relation and the mean zonal acceleration. J. Atmos. Sci., 33, 2031-2048.

Butchart, N., S. A. Clough, T. N. Palmer, and P. J. Trevelyan, 1982. Simulations of an observed stratospheric warming with quasi-geostrophic refractive index as a model diagnostic. Quart. J. Roy. Met. Soc., 108, 475.

Edmon, H. J., B. J. Hoskins and M. E. McIntyre, 1980. Eliassen-Palm cross sections for the troposphere. J. Atmos. Sci., 37, 2600-2616. (see also corrigendum, J. Atmos. Sci., 38, 1115).

Eliassen, A. and E. Palm, 1961. On the transfer of energy in mountain waves. Geophys. Publ., 22, No. 3, 1-23.

Holton, J. R., 1983. The stratosphere and its links to the troposphere. In Large-Scale Dynamical Processes in the Atmosphere, B. J. Hoskins and R. P. Pearce, Eds., Academic Press (in press).

Hoskins, B. J., 1983. Modelling of transient eddies and their feedback on the mean flow. In Large-Scale Dynamical Processes in the Atmosphere, B. J. Hoskins and R. P. Pearce, Eds., Academic Press (in press).

Hoskins, B. J., I. N. James, and G. H. White, 1983. The shape, propagation and mean-flow interaction of large-scale weather systems. J. Atmos. Sci., 40, 1595-1612.

Rhines, P. B., and W. R. Holland, 1979. A theoretical discussion of eddy-driven mean flows. Dyn. Atmos. Oceans, 3, 289-325.

Young, W. R., and P. B. Rhines, 1980. Rossby wave action, enstrophy and energy in forced mean flows. Geophys. Astrophys. Fluid Dynamics, 15, 39-52.

ADP002655

SIMULATION OF MIDLATITUDE VARIABILITY

William R. Holland

National Center for Atmospheric Research
Boulder, Colorado 80307

Models of eddy resolved ocean circulation have begun to aid in rational-
izing observations from midlatitude gyres. In particular, enhanced
transport of the western boundary current and its extension, patterns of
eddy energy, the structure of deep abyssal mean gyres, the nature of the
recirculation regime, and regions of homogenized potential vorticity in
observed gyres all have important analogues in models. Such models then
can be extremely useful in unraveling the underlying mechanism by which
large-scale midlatitude gyres reach a statistical equilibrium.

Regions of instability can be responsible for much of the mesoscale
transience found in ocean gyres. Models forced by steady winds produce
vigorous eddy fields due to important regions of eddy production and
radiation therefrom. These regions include the seaward extension of the
boundary current into the interior, the regions of recirculation (west-
ward flow) nearby and, indeed, the far flanks of the subtropical gyre
when the surface-intensified Sverdrup flow turns westward.

A second cause for transient oceans response is direct forcing by tran-
sient winds. The monthly mean wind stress curl (Hellerman and Rosen-
stein, 1983) shows considerable variance about the annual mean. Conse-
quently there is a liklihood that this transient forcing can be respon-
sible for a considerable proportion of the transient response in an
ocean that has both (interior) instabilities and (exterior) transient
wind forcing.

Recently, Schmitz and Holland (1982) made a first comprehensive attempt
to compare a number of simple steadily-forced, quasigeostrophic numeri-
cal experiments with observations. For the first time it became clear
that the first order problem was to be able to simulate the geographic
distributions of variability as measured, for example, by eddy kinetic
energy patterns and to associate these with the large-scale patterns of
mean flow. Moreover, it seemed necessary to do this from the near-Gulf
Stream region to the North Equatorial Current, from the ocean surface to
abyssal depths, and from the western boundary to the eastern basins.
While the data are and will continue to be very "broad brush" (i.e.,
sparse in space and time), the combination of analyses of older data,
the collection of new data from a few critical areas, and the develop-
ment and exploration of realistic numerical models should lead to a much
better synthesis of our understanding of the system.

Since the Schmitz and Holland study, EGCM development has proceeded in two ways: (i) simple, steadily forced, wind-driven oceans with rectangular domain and several layers in the vertical, and (ii) a model of the North Atlantic basin with realistic geometry and wind-forcing. A few results from both kinds of models are relevant to our topic.

Figures 1 and 2 show the mean (time averaged over five years) and instantaneous quasigeostrophic streamfunctions for a three-layer ocean in a 4000-km-square domain with a single wind gyre of forcing. The friction in the model is a combination of ordinary lateral friction with no-slip boundary conditions (A = 200 m^2/s) and bottom friction ϵ = 1x10^{-7} s^{-1}). See Holland (1978) for a full discussion of the two-layer version of this model.

Three important regions of eddy generation show up in this calculation: the Gulf Stream (a mixed barotropic/baroclinic instability), the recirculation regime (mainly a baroclinic instability), and the shallow Sverdrup flow on the southern flank of the subtropical gyre (completely a baroclinic instability). In all of these regions the eddy energy propagates mainly westward, filling out the ocean zonally from the region of origin. Figure 3 shows the eddy kinetic energy and eddy potential energy patterns associated with these multiple sources of eddy energy. As in earlier work (Holland, 1978) the deep sea is filled with eddy energy and deep mean gyres are forced by the eddy field.

Three layers allow a better sense of the vertical structure of the circulation and thermocline than earlier two-layer models. In particular, in the far reaches of the gyre (in the Sverdrup region) the flow is mostly confined to the upper layer; i.e., it is a shallow circulation. As one moves into the middle of the gyre, where eddy effects from the recirculation regime begin to be important, the circualtion deepens and the second layer begins to take part in the gyral circulation. The deep ocean, however, has important mean flows only very near to (and under) the Gulf Stream. Thus the depth of penetration of the gyre slopes poleward--shallow in the south, thermocline depth in mid-gyre, to the bottom at the Gulf Stream.

Two discoveries of potential importance were made with the development of these three-layer models: (i) the southern flank instability produces eddies near the latitudes of the North Equatorial Current (these eddies also drive deep weak mean flows that are like thin zonal jets with velocities of a cm/s or so; see Figure 1c); (ii) the potential vorticity of the interior of the subtropical gyre (i.e., in the middle layer) becomes homogenized over very large areas. Figure 4 shows maps of mean as well as instantaneous potential vorticity fields in the basin. Note the well-mixed region in the middle layer near the Gulf Stream region. This finding has led to new theories and observational analyses that suggest the importance of this effect.

Fig. 1. Mean quasigeostrophic streamfunctions at the three levels: 150 m, 650 m, and 3000 m.

Fig. 2. Instantaneous quasigeostrophic streamfunctions at the three levels.

Fig. 3. Mean eddy kinetic and eddy potential energies at the various levels in the model (K = 1, 150 m; K = 3, 650 m; K = 5, 3000 m; K = 2, 300 m; K = 4, 1000 m).
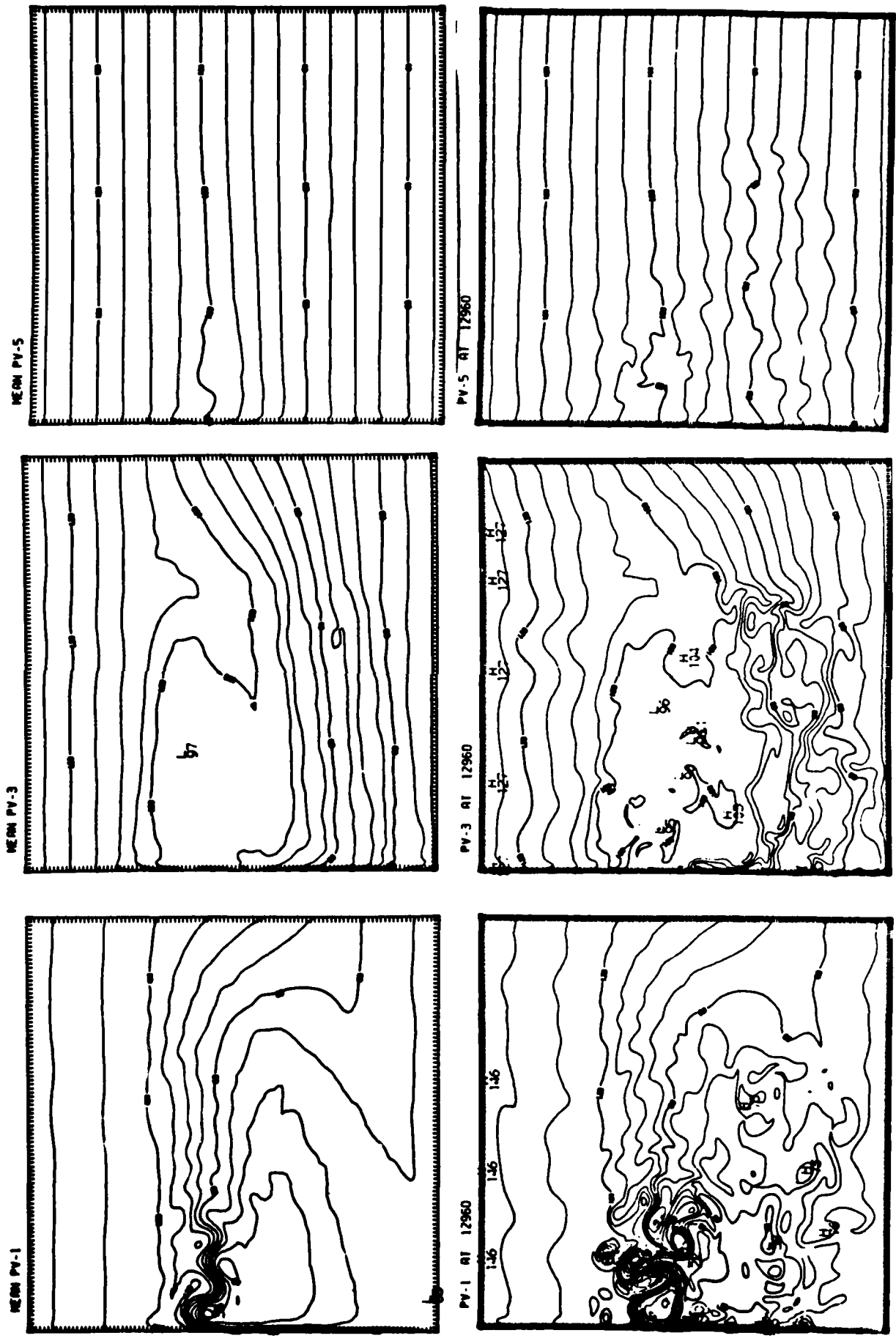
Fig. 4. Mean and instantaneous maps of potential vorticity at three levels in the model.

Recent efforts have turned toward the development of a realistic model of the North Atlantic basin. For the case shown, the horizontal resolution is 1/4° of latitude and longitude, the depth is constant, and the eastern boundary is simplified to a straight north-south coastline. Figure 5 shows the mean $\overline{\psi}_i$ for a three-layer model driven by the mean annual Bunker wind stress. Figure 6 shows the patterns of eddy kinetic energy; Figure 7 shows the patterns of eddy potential energy; and Figure 8 shows the time averaged potential vorticity in the middle layer. Finally, Figure 9 shows a time sequence of instantaneous upper layer streamfunction to show something of the time dependence.

These experiments have a realistic flavor to them. Gulf Stream meandering produces warm and cold core Rings; mesoscale eddy energy has about the right amplitude and structure; and the mean flows have about the right strength. Careful and thorough comparisons with observations have yet to be made but we are on the verge of having a true general circulation model of the North Atlantic basin in which we can test our ideas about realistic oceanic flows.

The experiments above have a major discrepancy associated with them; the regions far from the Gulf Stream and the Southern Flank of the gyre, particularly the eastern half of the basin, have too little eddy energy. The strong energy regions to the west do not seem to effectively radiate eastward to account for eastern basin energy levels. This suggests that transient forcing, not present in the above calculations, may be necessary.

Figures 10 and 11 show calculations in a new North Atlantic model (eastern boundary geometry and transient wind forcing now included). Here the model is forced only by the transient wind component; the mean forcing is omitted (temporarily) to clarify the nature of the transient response itself. Hellerman's monthly mean winds (annual average removed) are used for this purpose.

The results show a strong baroclinic response at the annual period (the forcing has one-to twelve-month periods). First baroclinic mode Rossby waves with an east-west wave length of about 500 km and a much longer north-south wave length, propagate westward from the eastern boundary. The main thermocline moves up and down (with nearly annual frequency) by about 5 to 10 meters and associated "eddy" currents are a few cm/sec. While these eddy signals are considerably less than the near Gulf Stream ones (when mean wind forcing is also included) they do constitute the major signal in the eastern regions.

At this point considerable effort is needed to understand these various competing energy sources as well as to examine more complex models with actual bottom topography and even more realistic wind forcing (actual storms with all their space/time structure). We are, however, well on our way toward simulations of the geographical structure of variability in midlatitude gyres and can hope that the models can then serve adequately as a testing ground for dynamical rationalization of the large-scale general circulation of the ocean.

MEAN PSI 1   CASE   6

MEAN PSI 3   CASE   6
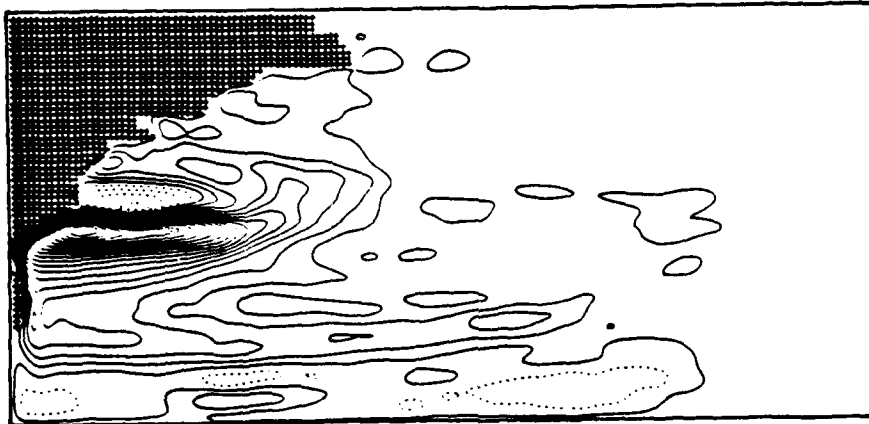
MEAN PSI 5   CASE   6

Fig. 5. Mean quasigeostrophic streamfunctions at the three
    levels in the North Atlantic Basin: 150 m, 650 m, and 3000 m.

MEAN EDDY KE 1 CASE 6

MEAN EDDY KE 3 CASE 6

MEAN EDDY KE 5 CASE 6

Fig. 6. Mean eddy kinetic energy at three levels in the
        North Atlantic basin: 150 m, 650 m, and 3000 m.

MEAN EDDY PE 2 CASE 6

MEAN EDDY PE 4 CASE 6

Fig. 7. Mean eddy potential energy at two levels in the
North Atlantic basin: 300 m and 1000 m.

MEAN Q 3 CASE 6
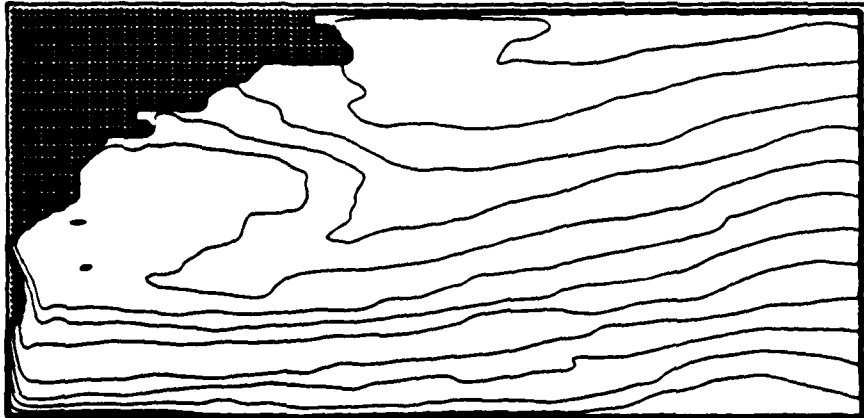
Fig. 8. Mean potential vorticity in the middle layer
(at 650 m) of the North Atlantic basin.

S-1 DAY=2680.0 CASE= 6
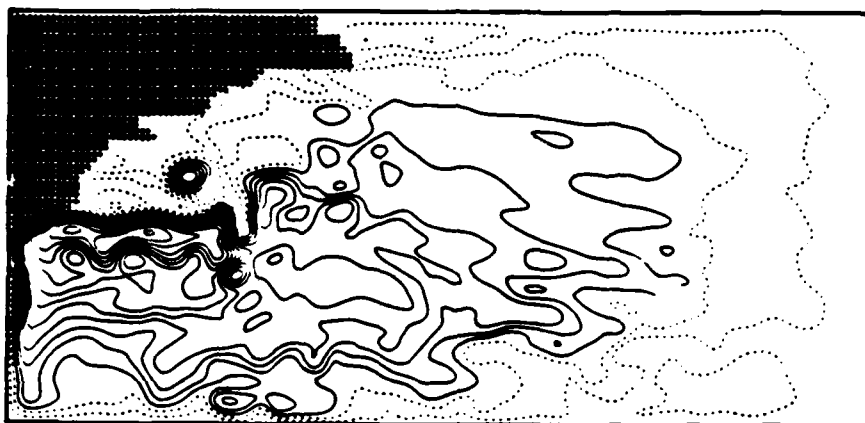
S-1 DAY=2720.0 CASE= 6

S-1 DAY=2760.0 CASE= 6

Fig. 9a. Instantaneous maps of upper layer quasigeostrophic
streamfunction at intervals of 40 days.

S-1 DAY=2800.0 CASE= 6

S-1 DAY=2840.0 CASE= 6

S-1 DAY=2880.0 CASE= 6

Fig. 9b. Instantaneous maps of upper layer quasigeostrophic
           streamfunction at intervals of 40 days.
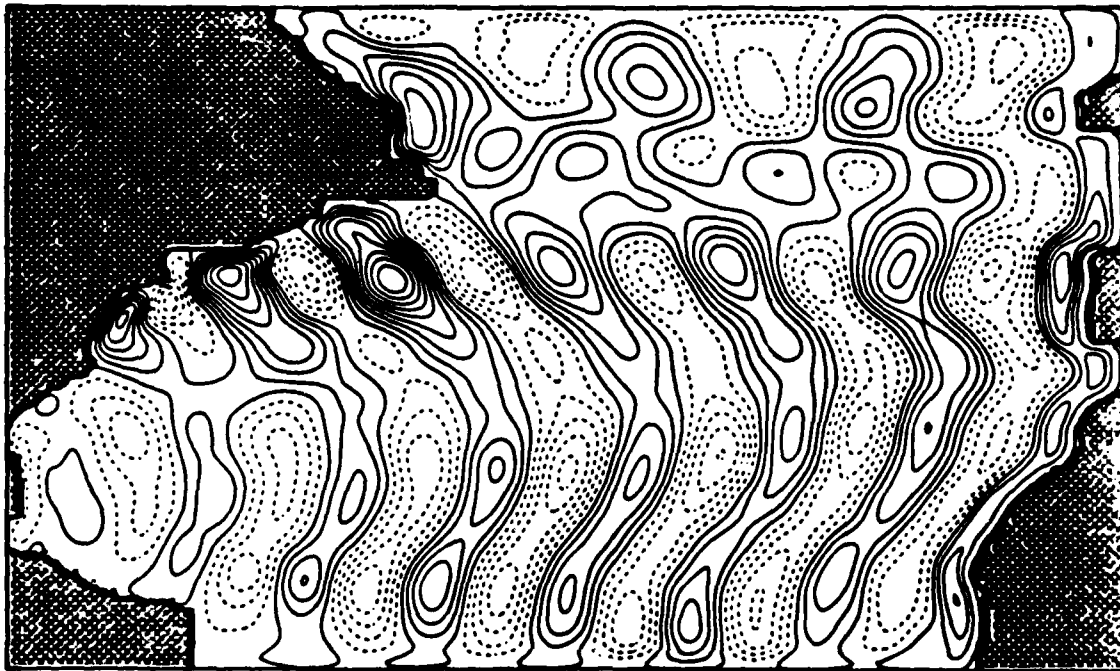
Fig. 10. An instantaneous map of the deviation in the depth of an isopycnal surface in the main thermocline (average depth 1000 m). The contour interval is 1.0 m.

RMS H-4 NA
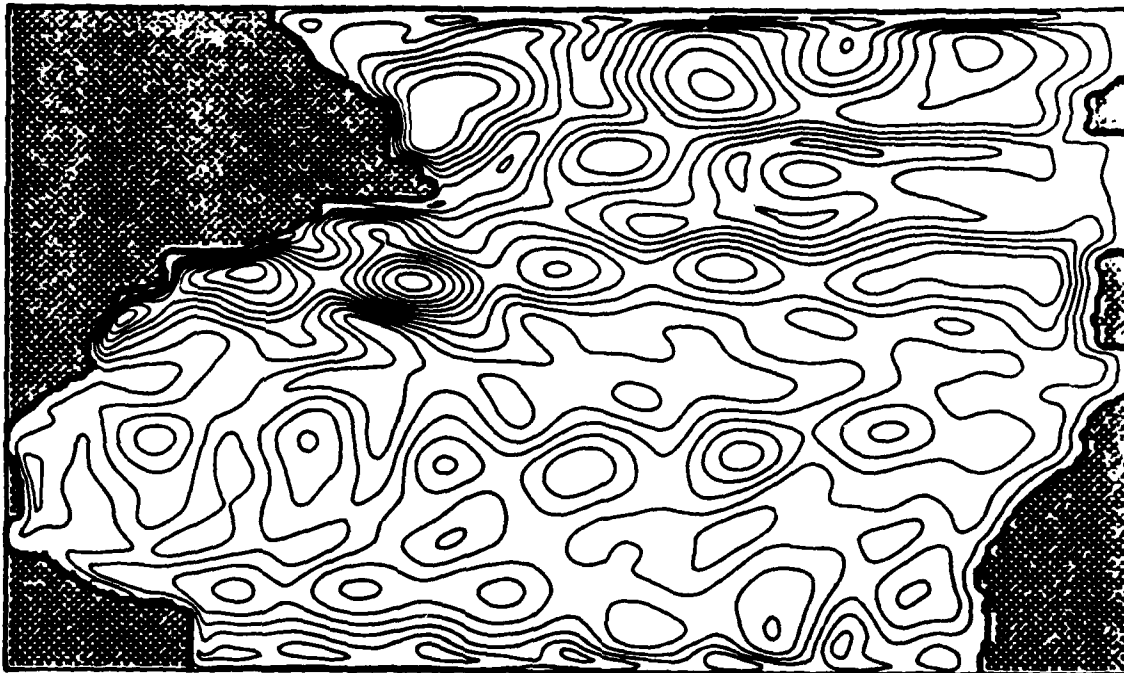
Fig. 11. A map of the RMS depth deviation of an isopycnal surface from its mean depth of 1000 m averaged over a one-year period. The contour interval is 0.5 m.

112

REFERENCES

Holland, William R., 1978: The role of mesoscale eddies in the general
circulation of the ocean--numerical experiments using a wind-driven
quasi-geostrphic model. J. Phys. Oceanogr., 8, 363-392.

Schmitz, William J., Jr. and William R. Holland, 1982: A preliminary
comparison of selected numerical eddy-resolving general circulation
experiments with observations. J. Mar. Res., 40, 75-117.

Hellerman, S., and M. Rosenstein, 1983: Normal monthly wind stress over
the World Ocean with error estimates. J. Phys. Oceanogr., in
press.
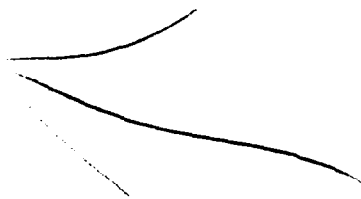
EVIDENCE FOR THE DIRECT ATMOSPHERIC FORCING OF MID-OCEAN EDDIES

Peter Muller

Department of Oceanography and Hawaii Institute of Geophysics,
University of Hawaii at Manoa, Honolulu, Hawaii 96822

ABSTRACT

Evidence for the direct atmospheric forcing of oceanic synoptic-scale motions is reviewed. The evidence comes from new insights into the structure of the atmospheric forcing fields, observations of the Ekman pumping velocity, model calculations, coherence observations, and seasonal modulation. The tentative conclusion is that a substantial part of the mid-ocean eddy field is directly forced by fluctuations in the atmospheric windstress. The oceanic synoptic-scale variability might hence be viewed as consisting of a random, low-level, homogeneous background field that is atmospherically forced, and on which are superimposed well-identifiable, energetic eddies, rings, and meanders that are caused by current instabilities.

INTRODUCTION

Oceanic synoptic-scale motions encompass a wide variety of phenomena and have widely varying energy levels. The most energetic motions are found near strong current systems and consist of eddies, current meanders, and rings spun off by meandering currents. Further away from the strong currents the synoptic-scale motions become the mid-ocean eddy field. This is less energetic and more homogeneous and covers a broad range of space and time scales. The energetic synoptic-scale motions around strong currents are generated by current instabilities. The generation mechanisms for the mid-ocean eddy field have not been identified yet. Here we review the evidence for generation by fluctuations in the atmospheric windstress.

The early studies of direct wind forcing calculated the oceanic response to simple deterministic forcing patterns and generally concluded

that wind forcing cannot explain the observed eddy amplitudes. The
mismatch of the dominant space-time scales and propagation directions of
atmospheric and oceanic fluctuations was offered as a plausible
explanation. The wind field over the ocean is, however, a broad banded
stochastic process with a large number of different wavenumber and
frequency components randomly superimposed. Detailed analyses by
Willebrand (1978) and Frankignoul and Muller (1979)(henceforth FM)
revealed that there is westward propagating variance in the wind field
that can resonantly, i.e. efficiently, excite oceanic Rossby waves. This
finding led Willebrand et al. (1980), Muller and Frankignoul (1981)
(henceforth MF) and others to reanalyze the atmospheric forcing problem
and to conclude that a substantial part of the mid-ocean eddy field is
directly forced by fluctuations in the atmospheric windstress. The
evidence for this conclusion comes from five areas: the structure of the
atmospheric forcing fields, observations of the Ekman pumping velocity,
model calculations, coherence observations, and seasonal modulation.
These five areas are briefly discussed below.

STRUCTURE OF THE ATMOSPHERIC FORCING FIELDS

    Variations in the wind field are generally ascribed to synoptic-scale
fluctuations, i.e. to eastward-propagating cyclones and anticyclones with
length scales of a few thousand kilometers and time scales of a few days.
Obviously, the time and space scales of these atmospheric fluctuations
does not match the scales of the eddy field in the ocean, nor does their
eastward phase propagation coincide with the general westward propagation
of oceanic eddies. Though it is true that most of the atmospheric variance
is at (atmospheric) synoptic scales (and micro scales) there is variance
at other scales. Willebrand (1978), FM and others analyzed in detail the
available information from weather maps, island stations, ocean weather
ships, and ship observations. They found that, at oceanic eddy scales, the
windstress spectrum is white in frequency space, is zonally symmetric, and
decays with a -2 power law in wavenumber space. These properties are
shown in Figures 1 to 3.

    Figure 1 shows the frequency spectrum of the east and north component
of the surface wind at Bermuda. The spectra show a broad banded process
with no lines or periodicities. The spectra are nearly white for
frequencies smaller than about $0.1d^{-1}$. Toward higher frequencies the
spectra fall off, slowly first and then with a -2 power law. Most of the
variance is at synoptic periods around five days. A variance conserving
plot would show a strong peak there. The white behavior at low
frequencies is typical for all atmospheric fields at mid-latitudes. It
can be interpreted as the white noise extension of the short (correlation)
time scale weather fluctuations.

    Figure 2 shows zonal wavenumber spectra of the meridional wind from
three different sources. The "weather-map" spectrum was constructed from
surface pressure maps by Pratt (1975). The spectrum has most of its
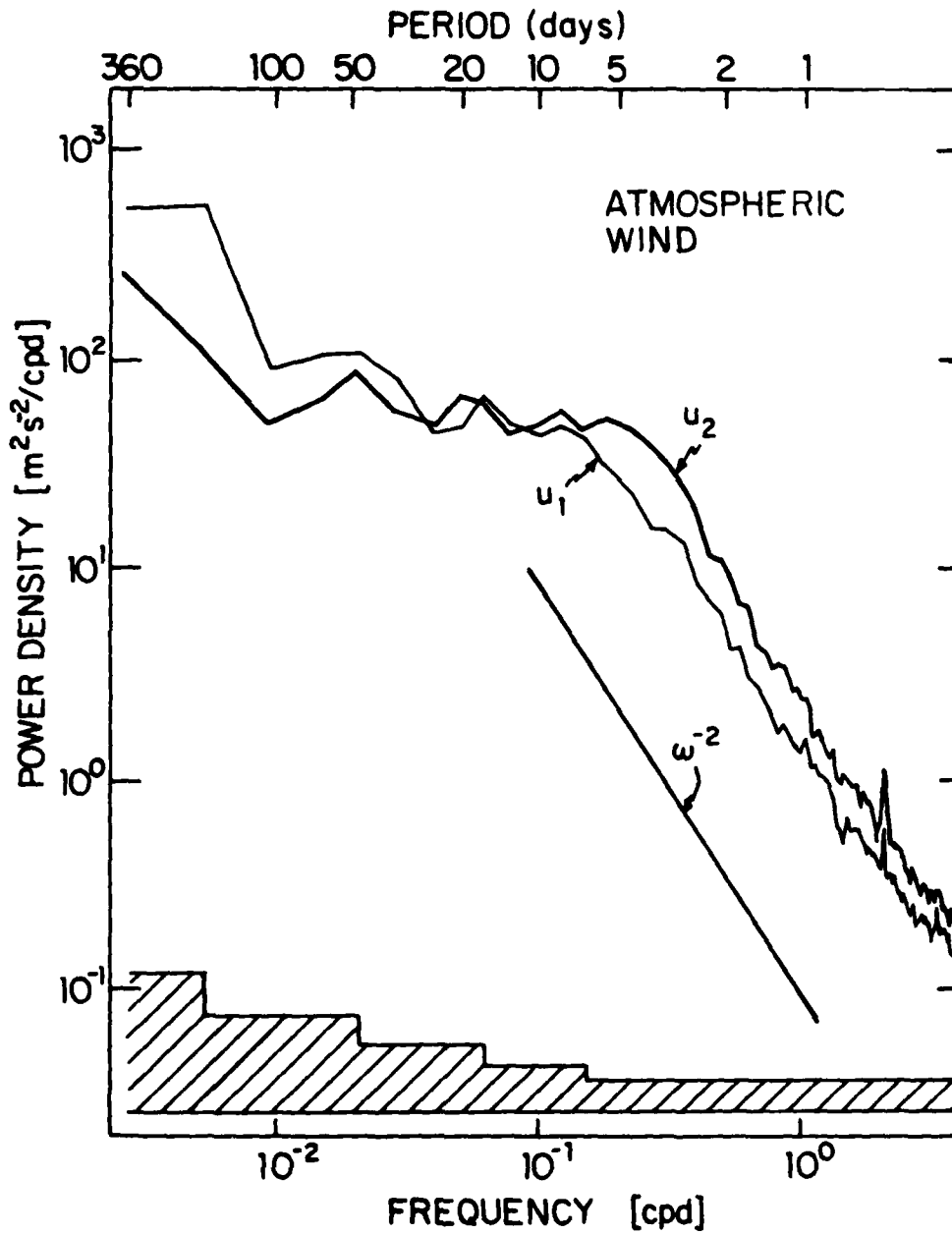
Fig. 1. Frequency spectrum of the east (u_1) and north component (u_2) of the surface wind at Bermuda for the period 1953-1960. The spectrum is estimated from eight one-year pieces. The error bars indicate the approximate 95% confidence limits (from Muller, 1982).
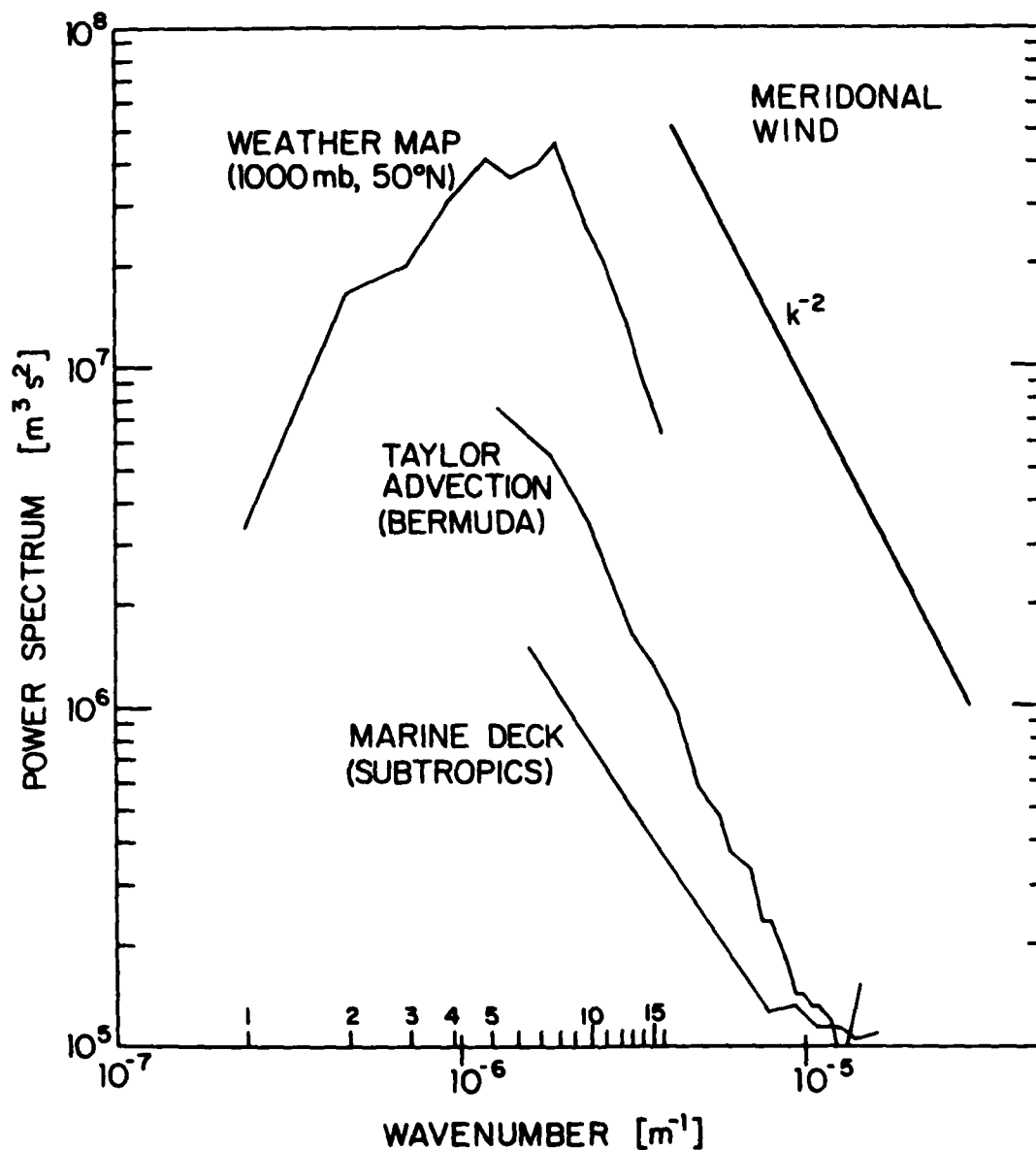
Fig. 2. Observed zonal wavenumber spectra of the meridonal wind. The "weather-map"-spectrum was constructed from four 132-day winters of NMC data by Pratt (1975). The "Taylor advection"-spectrum is constructed from the wind data shown in Fig. 1, using a $U_1 = 10$ ms^{-1} Taylor advection velocity in the frequency range from 0.2 cpd to 2 cpd. The "Marine Deck"-spectrum was computed by Gallegos-Garcia (1980) from ship weather observations (from Muller, 1982).

variance at synoptic scales around n ~ 6. Beyond n ~ 6 it decays up to n_{max} ~ 15, the limit set by the resolution of weather maps. The "Taylor-advection" spectrum was constructed from the wind data shown in Figure 1. The "Marine Deck" spectrum was computed by Gallegos-Garcia (1980) from ship weather observation. The spectra suggest a k^{-2} power law at oceanic eddy scales, i.e. at scales from about 1000 km down to about 100 km. This power law might reflect the random advection of small scale wind events like surface fronts. Note that in the troposphere data support a k^{-3} enstrophy cascading inertial range at the same wavenumbers.

Figure 3 shows the mean zonal wavenumber plus and minus one standard deviation as a function of frequency. The strong east-west asymmetry at synoptic frequencies is due to the eastward-travelling cyclones and anticyclones, but the asymmetry decays both toward higher and lower frequencies. At frequencies smaller than about 0.1 cpd there is no preferred propagation direction.

The figures show that there is variance in the wind field at the scales of oceanic eddies that can directly excite these motions in the ocean.

The diverse information about the atmospheric forcing fields was combined by FM into simple but realistic model spectra which are very useful for model calculation.

OBSERVATIONS OF EKMAN PUMPING VELOCITY

The atmospheric windstress forces oceanic eddies at the surface by an Ekman pumping velocity

$$w_{Ek} = \frac{1}{\rho_o f_o} (\partial_x \tau_y - \partial_y \tau_x)$$

where τ_x and τ_y denote the east and north component of the windstress. In regions of active forcing we hence expect that the near surface vertical velocity closely resembles the Ekman pumping velocity w_{Ek}. In mid-ocean regions this is indeed the case.

Figure 4 shows the observed frequency spectrum of the temperature at 300-m depth at the POLYMODE Array III, Cluster C (after Keffer et al., 1979) together with the prediction from Ekman pumping using FM's model windstress spectrum. For the prediction the spectrum of the Ekman pumping velocity was converted to a temperature spectrum by the relation $\partial_t T + w_{Ek} \partial_z \bar{T} = 0$ with a local mean vertical temperature gradient. The agreement between observation and prediction is good.

Similarly, Figure 5 shows the observed zonal wavenumber spectrum of the vertical displacement at 300 m depth in the Western and Central North Pacific (estimated from Bernstein and White, 1977) and the prediction from Ekman pumping, using the relation $\partial_t \zeta = w_{Ek}$ for conversion. The agreement is good for the Central North Pacific and poor for the Western North Pacific where the eddy field is dominated by the influence of the Kuroshio system.
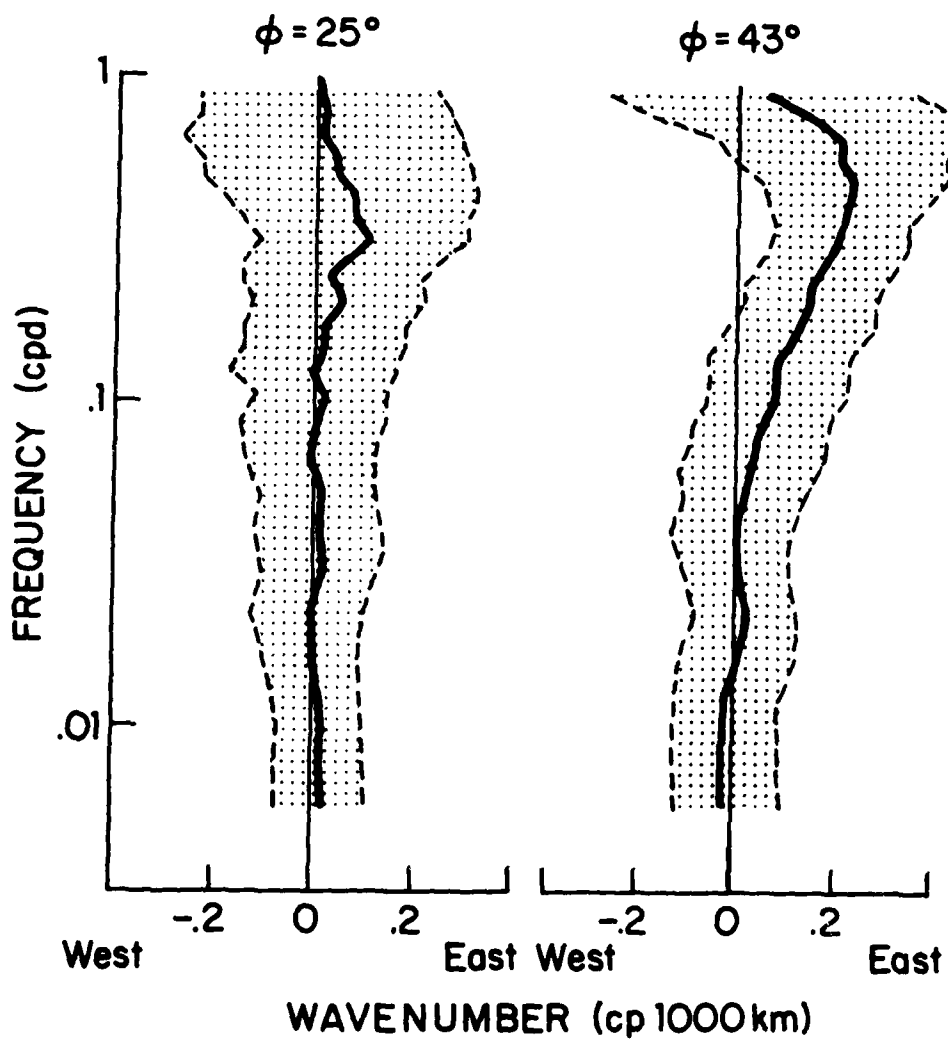
Fig. 3. Mean zonal wavenumber of the atmospheric pressure (solid line) plus and minus one standard deviation (dashed line) as a function of frequency for two latitudes (after Willebrand, 1978).

DAYS

(DEGREES C)**2/cpd

CPD

TEMPERATURE
Mooring 80
161 Meters

AUTOSPECTRUM
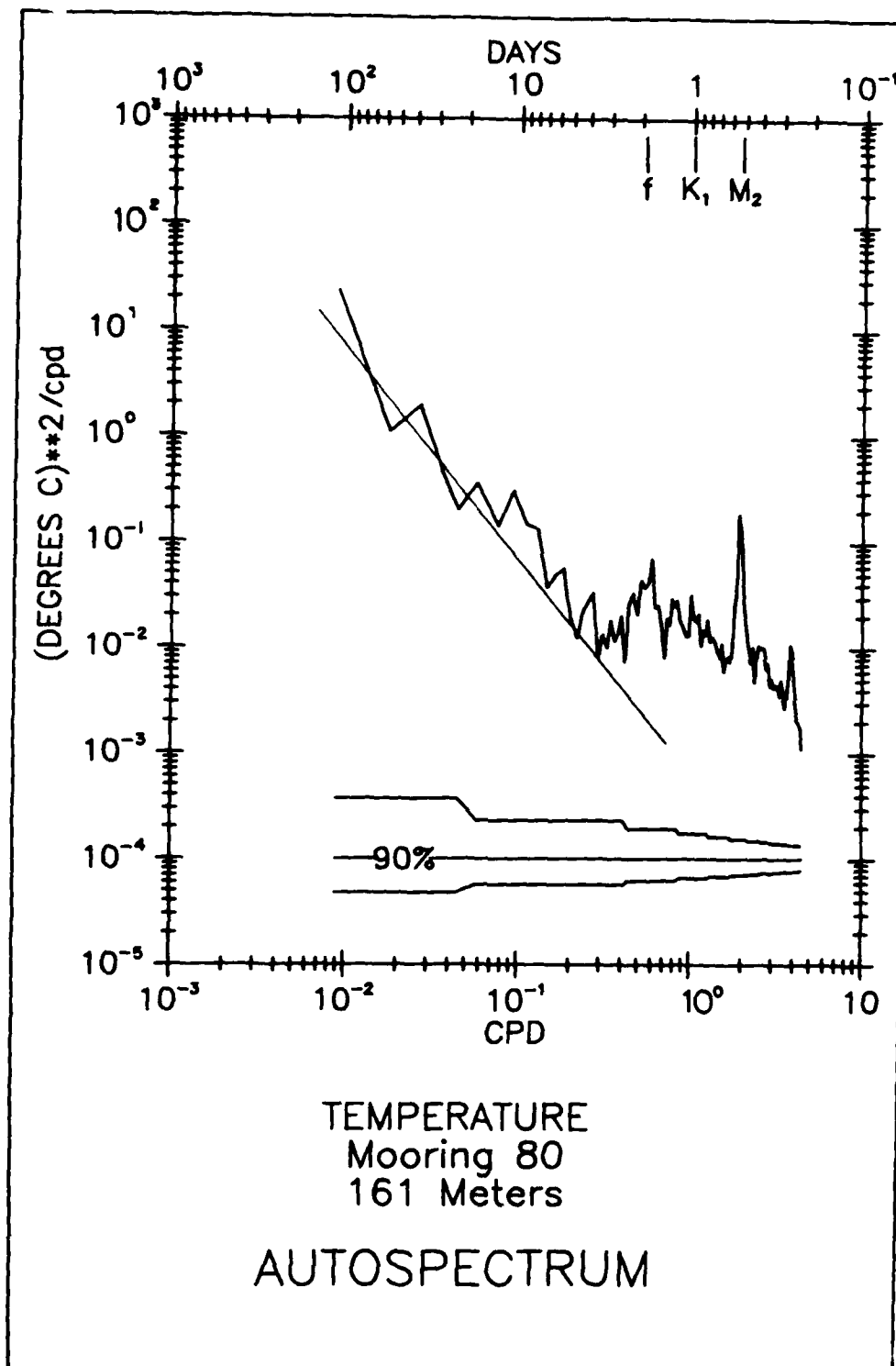
Fig. 4.   POLYMODE ARRAY III, Cluster C temperature spectrum at
   161-m depth (heavy line, after Keffer et al., 1979) and
   prediction from Ekman pumping using FM's model windstress
   spectrum (thin line)   (from MF).

120
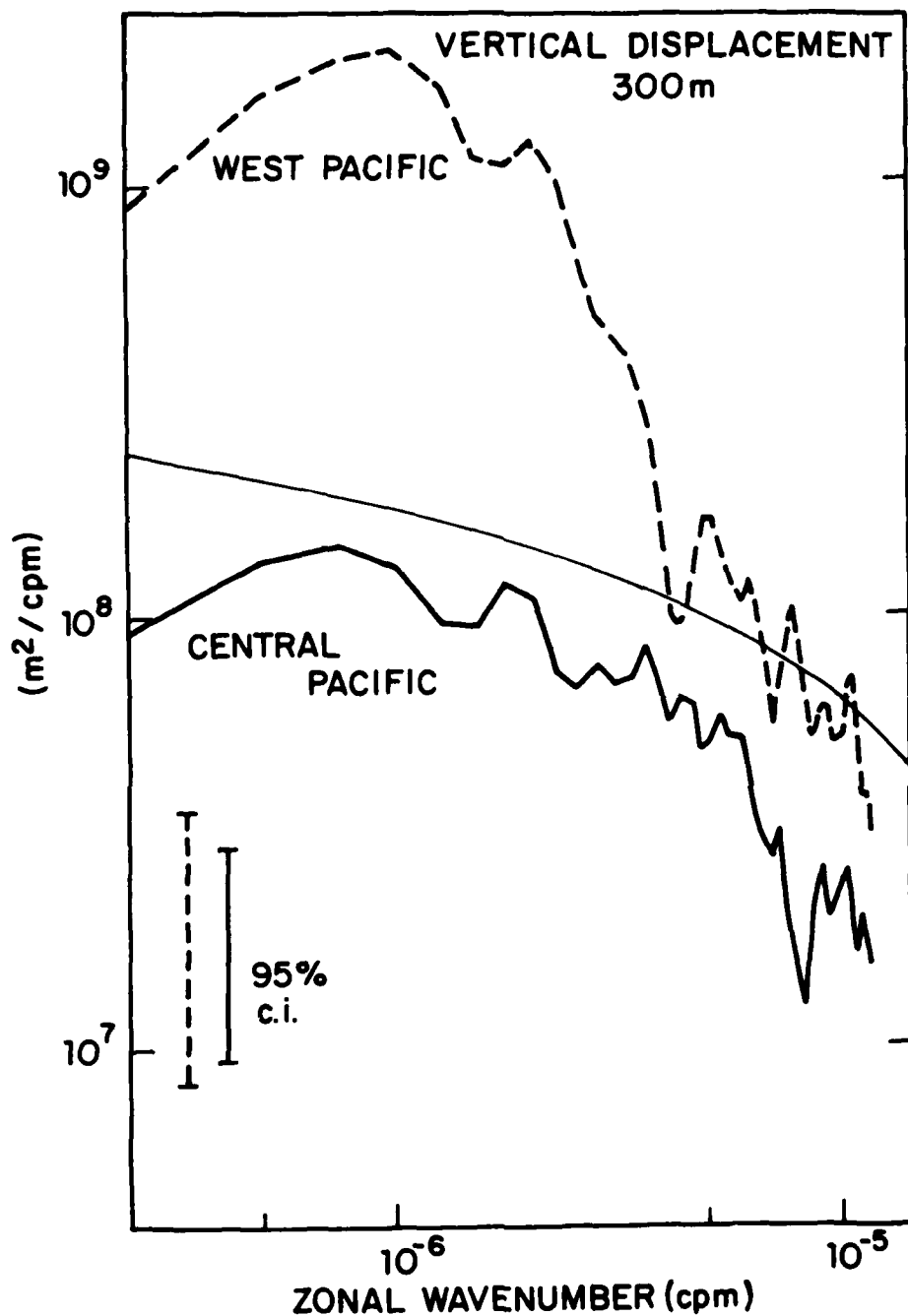
Fig. 5. Zonal wavenumber spectrum of the vertical displacement
at 300-m depth in the North Pacific, computed from zonal XBT
sections between 35°N and 40°N (after Bernstein and White,
1977). Heavy dashed line, Pacific west of 170°W; heavy
solid line, Central Pacific east of 170°W; thin line, pre-
diction from Ekman pumping using FM's model windstress
spectrum (from MF).

MODEL CALCULATIONS

Willebrand et al. (1980) calculated analytically and numerically the response of a homogeneous ocean to the fluctuating component of the windstress as calculated from twice-daily weather maps. The numerical model included nonlinear interactions, lateral boundaries, and bottom topography and dissipated energy by lateral friction. MF calculated analytically the barotropic and baroclinic response of a simple but stratified ocean model to their model windstress spectrum. The ocean model has linear quasi-geostrophic beta-plane dynamics, a flat bottom, no mean currents and no lateral boundaries, and dissipates energy by Rayleigh friction. The two studies agree where they overlap.

In both papers the model results are compared with available observations. The general conclusion of this comparison is that the models are able to reproduce the level and shape of observed spectra in mid-ocean regions far removed from strong currents, if the dissipation mechanism is appropriately chosen. The agreement becomes very good in regions of low eddy intensity.

A typical example of model-data comparison is given in Figure 6. It shows MF'S model prediction together with observations taken in the MODE area. The agreement is judged fair.

COHERENCE OBSERVATIONS

The most direct evidence of atmospheric forcing is expected from the determination of the coherence between atmospheric and oceanic fields. However, looking through the observational records one finds that only some of the oceanic fields are coherent with the atmospheric forcing fields. Most ocean fields do not show any significant coherence with the atmosphere. Furthermore, those fields which do show a significant coherence do so only at high frequencies.

This behavior is demonstrated in Figure 7. It shows the coherence between the subsurface pressure (which is proportional to the surface elevation corrected for the inverse barometer effect) and the atmospheric pressure at Bermuda and the coherence between the bottom and atmospheric pressure in the MODE area. The coherences are insignificant at low frequencies and significant at high frequencies.

The overall behavior of the observed coherences is expected even if the oceanic fluctuations are forced by the atmosphere. At low frequencies the oceanic response is dominated by propagating Rossby waves which are not related to the local atmospheric variability. At high frequencies, the response is locally forced and significant coherences become possible. The model coherence between atmospheric and oceanic pressure as calculated by MF is also shown in Figure 7 and agrees well with the observed coherences.
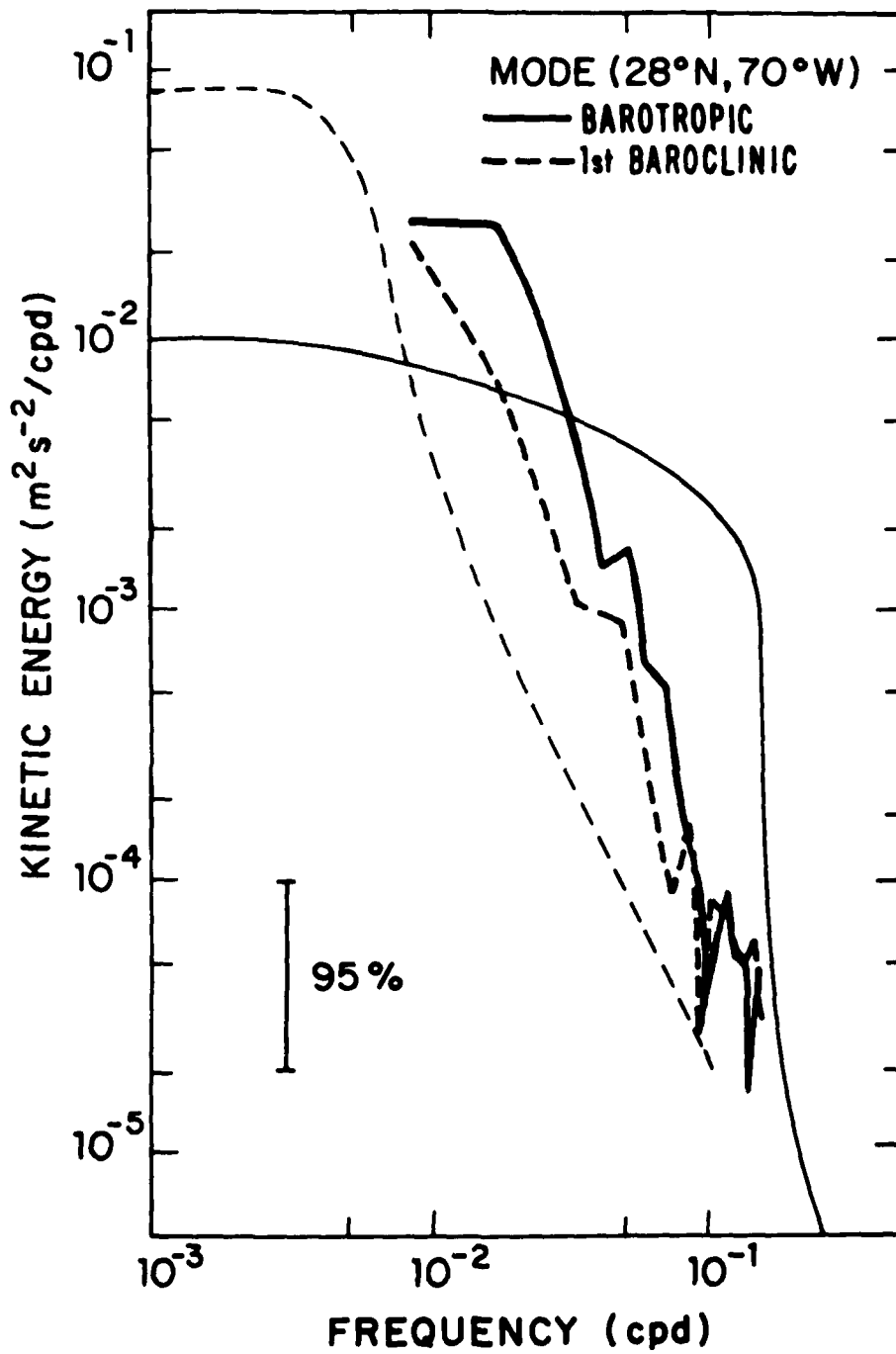
Fig. 6. Kinetic energy spectrum of the barotropic and first
baroclinic mode as observed in MODE and as predicted by MF's
model (from MF).

SUBSURFACE PRESSURE -ATMOSPHERIC PRESSURE
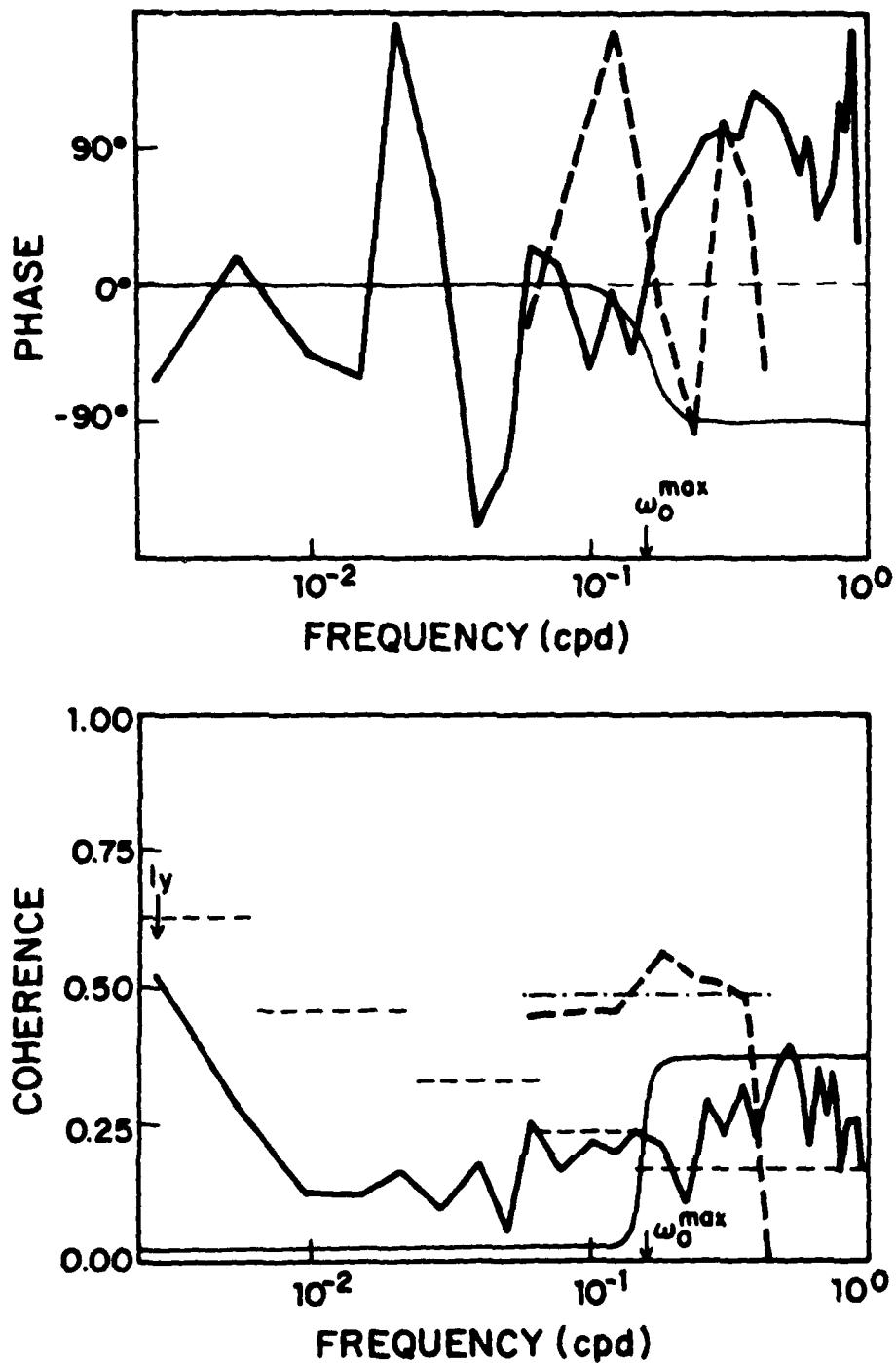
Fig. 7. Observed coherence and phase between subsurface and
atmospheric pressure at Bermuda (heavy solid line), between
bottom and atmospheric pressure in the MODE area (heavy dash-
ed line, after Brown et al., 1975) and MF's model prediction
(thin solid line). The 95% confidence limits of the observed
coherences are indicated by the broken thin line (from MF).
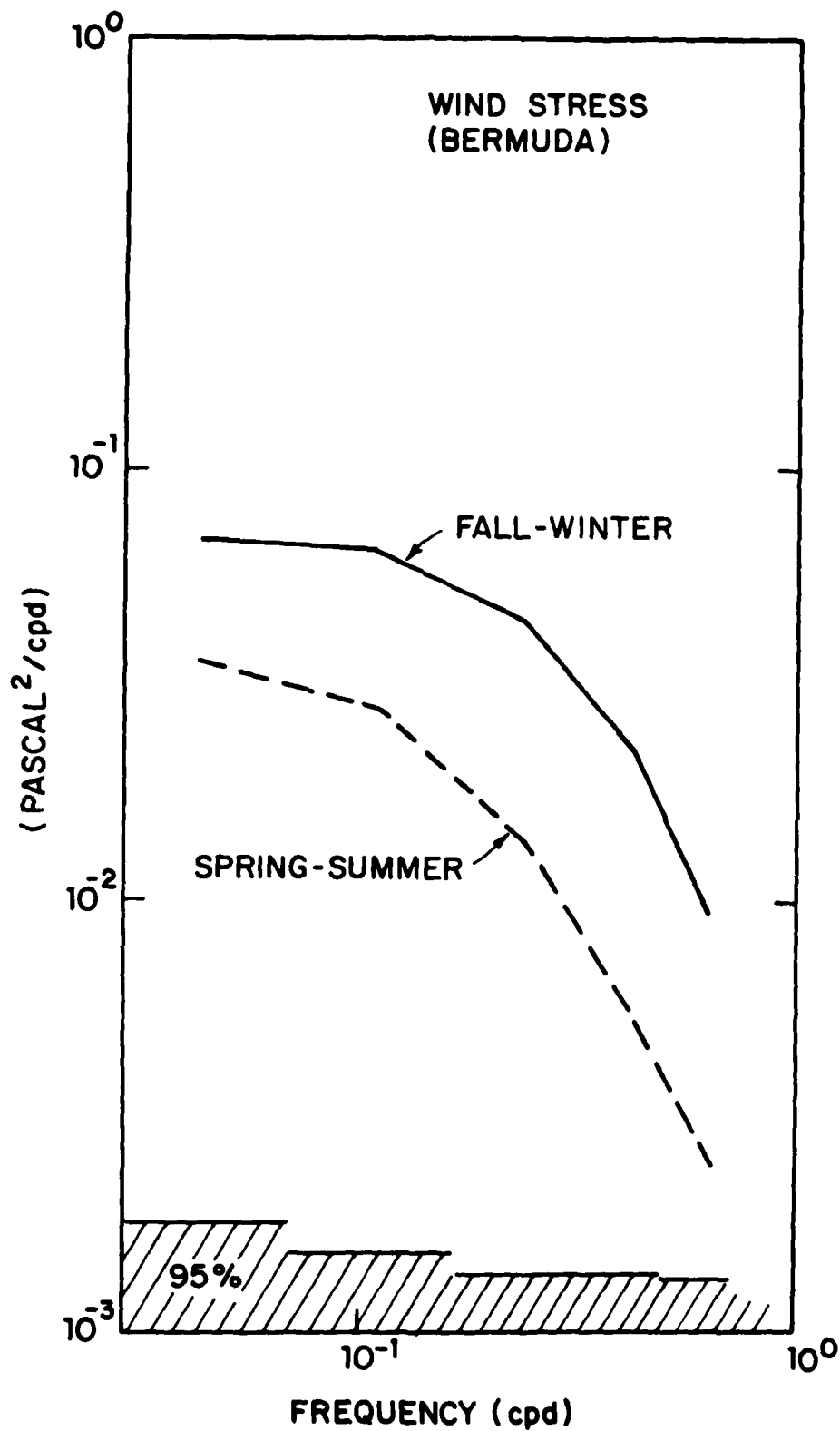
Fig. 8. Seasonal spectra of windstress and subsurface pressure at Bermuda. Spectra were estimated from three-month pieces (from MF).
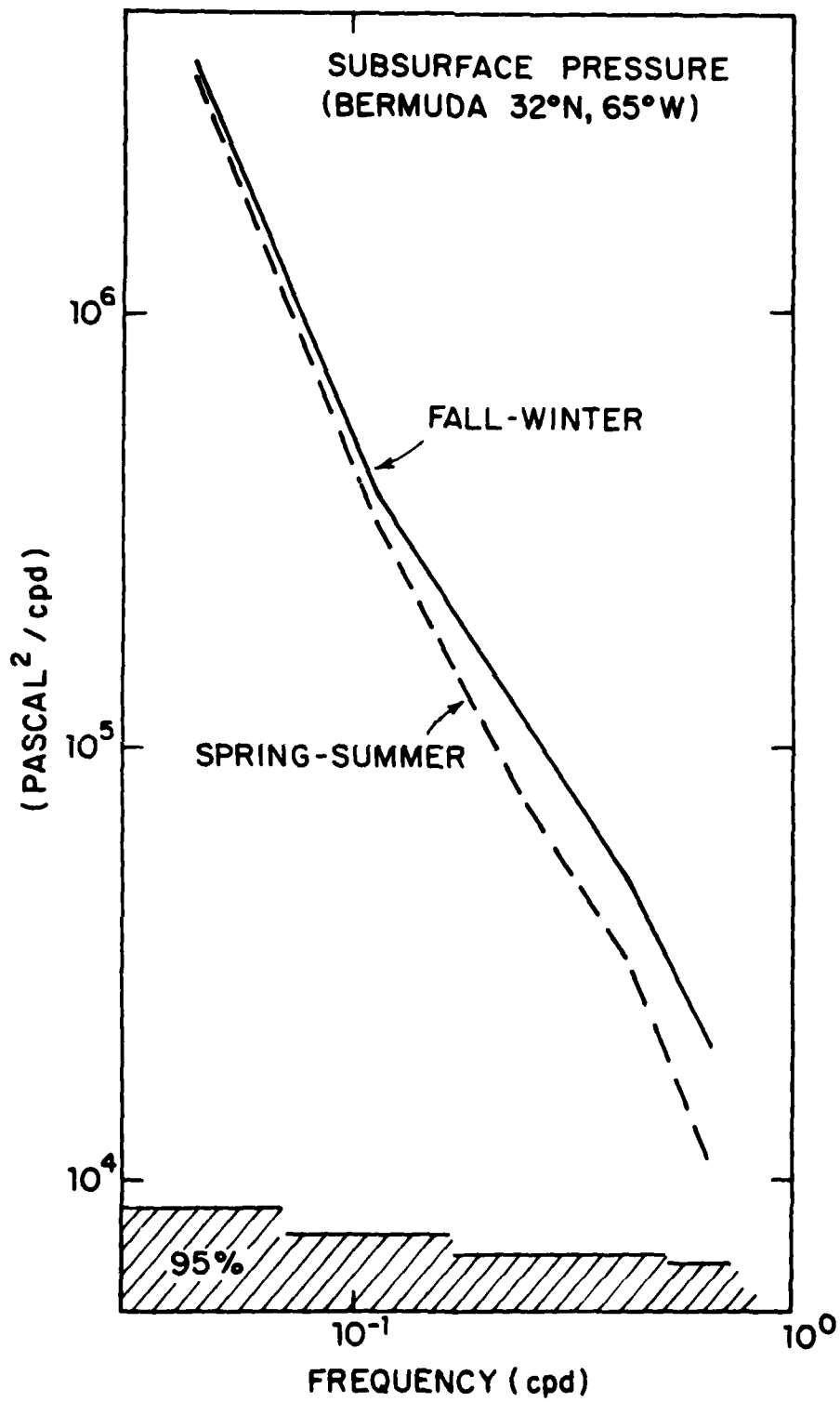
Fig. 8. (continued)

SEASONAL MODULATION

The windstress field over the ocean is more vigorous in fall and winter than it is in spring and summer. This behavior is usually evident when the high frequency part of the spectrum is calculated separately for the different seasons. An example is given in Figure 8a, which shows the fall-winter and spring-summer windstress spectrum at Bermuda. If the oceanic eddy field is directly forced by the windstress we expect a similar seasonal modulation of the high-frequency part of oceanic spectra. For the Bermuda subsurface pressure spectra, shown in Figure 8b, this is indeed the case. The fall- winter spectrum is slightly more energetic than the spring-summer spectrum. However, theory predicts a phase lag of about three months; such a lag is not observed.

Strong seasonal variations of deep oceanic motions have also been observed in the eastern North Atlantic and found to be associated with bottom topography (Dickson et al., 1982). Note that seasonal modulation only provides information about the high-frequency part of the spectrum.

CONCLUSIONS

We briefly reviewed some of the evidence for the direct forcing of mid-ocean eddies by fluctuations in the atmospheric windstress. Though the wind field has most of its variance at (atmospheric) synoptic scales there is variance at the scales of oceanic eddies that can directly force eddy motions in the ocean. Further evidence comes from the analysis of oceanic observations and from model studies. Observed coherences between some atmospheric and some oceanic fields provides direct evidence of atmospheric forcing. This evidence is, however, confined to the high off-resonant frequencies where there is little energy. At the lower resonant frequencies where most of the oceanic energy is, coherence is neither observed nor expected. The observed seasonal modulation of oceanic spectra also provides direct evidence for the atmospheric forcing of high-frequency motions. The model studies provide less direct evidence. The models are capable of correctly reproducing the level and shape of the eddy spectra in regions of low eddy intensity far removed from strong currents, but only by tuning the dissipation mechanism. The most convincing evidence comes from the observations of the vertical velocity field near the surface which is, in many places, consistent with Ekman pumping from the atmospheric windstress field.

All the evidence suggests that a substantial part of the mid-ocean eddy field is directly forced by fluctuations in the atmospheric windstress. The oceanic eddy field might hence be viewed as consisting of a random, low-level, homogeneous background field that is atmospherically forced. Superimposed on this background field are well indentifiable energetic, event-like structures like eddies, rings, and meanders that are generated by current instabilities.

REFERENCES

Bernstein, R. L. and W. B. White, 1977. Zonal variability of the distribution of eddy energy in the Mid-Latitude North Pacific Ocean. J. Phys. Oceanogr., v. 7, p. 123-126.

Brown, W., W. Munk, F. Snodgrass, H. Mofjeld, and B. Zetler, 1975. MODE bottom experiment. J. Phys. Oceanogr., v. 5, p. 75-85.

Dickson, R. R., W. J. Gould, P. A. Gurbutt, and P. D. Killworth, 1982. A season signal in ocean currents to abyssal depths. Nature, v. 295, p. 193-198.

Frankignoul, C. and P. Muller, 1979. Quasi-geostrophic response of an infinite beta-plane ocean to stochastic forcing by the atmosphere. J. Phys. Oceanogr., v. 9, p. 104-127.

Gallegos-Garcia, A., 1980. Frequency-wave number spectra of sea surface temperature and wind stress in the Eastern North Pacific and their relation to locally forced low frequency fluctuations in the ocean. Ph.D. dissertation, Texas A&M University, College Station.

Keffer, T., C. Koblinsky and P. P. Niiler, 1979. Polymode array III, Cluster C. Preliminary data report, Oregon State University.

Muller, P., 1982. The dynamics of synoptic-scale motions in the ocean. Mitteilungen des Instituts fuer Meereskunde der Universitaet Hamburg, v. 25, p.1-108.

Muller P. and C. Frankignoul, 1981. Direct atmospheric forcing of geostrophic eddies. J. Phys. Oceanogr., v. 11, p. 287-308.

Pratt, R. W., 1975. Space-time spectral analysis of large scale mid-latitude disturbances. Ph.D. dissertation, University of Washington, Seattle.

Willebrand, J. 1978. Temporal and spatial scales of the wind field over the North Pacific and North Atlantic. J. Phys. Oceanogr., v. 8, p. 1080-1094.

Willebrand, J., S. G. H. Philander, and R. C. Pacanowski, 1980. The oceanic response to large-scale atmospheric distubrances. J. Phys. Oceanogr., v. 10, p. 411-429.

VENTILATED AND UNVENTILATED MODELS OF THE WIND-DRIVEN CIRCULATION

W. R. Young

University of California, San Diego, Marine Physical Laboratory of the Scripps Institution of Oceanography, La Jolla, California 92093

Abstract

The quasigeostrophic theory of the wind-driven circulation given by Rhines and Young (1982a) is extended to take account of strong isopycnal displacements. Thus the quasigeostrophic approximation is abandoned. Instead exact solutions of the planetary geostrophic equations which satisfy both horizontal and vertical boundary conditions are presented.

It is shown that the planetary geostrophic equations have an infinite number of solutions, all of which satisfy identical boundary conditions. Other physical processes, not explicit in the planetary geostrophic equations themselves, must be considered to decide which solution is relevant to the real ocean.

To clearly illustrate this lack of uniqueness two solutions are discussed in detail. The first solution is a development of the model given by Luyten, Pedlosky and Stommel (1982). The second solution is a development of the model given by Rhines and Young (1982a). Both solutions satisfy the same boundary conditions but have qualitatively different flow patterns. It is argued that the latter solution (which is based on the assumption that potential vorticity is homogenized) is more realistic.

1. Introduction

The aim of this article is to compare two recently developed theories, both of which purport to model the wind-driven ocean circulation. In the process both theories will be slightly extended.

The first theory, which was originally developed using the quasigeostrophic approximation, is given by Rhines and Young (1982a) (RY hereafter) and Young and Rhines (1982) (YR hereafter). In the layered version of this theory only one layer is exposed to the surface, and is forced by the wind stress. If there is no dissipation at all (that is, no smaller scale processes such as mesoscale eddies) then there are an infinite number of solutions. In one particular solution all of the wind-driven flow is confined to the uppermost, directly forced layer. RY and YR argue that this solution is not stable in the presence of mesoscale eddies when the deformation of the isopycnals overpowers the β-effect and closes the geostrophic contours in the motionless subsurface layers.* This results in a vertical redistribution of the wind-driven

---

* Geostrophic contours are curves defined by the intersection of density surfaces with potential vorticity surfaces.

130

flow which was initially concentrated in the uppermost layer. Using the quasigeostrophic extension of the Prandtl-Batchelor theorem (Rhines and Young, 1982b) they argued that the wind-driven flow penetrates downward into the subsurface layers, until it reaches a state of equilibrium in which the potential vorticity is uniform within the closed subsurface geostrophic contours. Since eddy stresses are approximately proportional to the gradient of the mean potential vorticity (Rhines and Holland, 1979), these stresses vanish once the potential vorticity is homogenized. Perhaps the most striking confirmation of this theory is Holland's (1982) numerical simulation.

The second theory, which avoids quasigeostrophic approximation and explicit consideration of dissipative processes, is that of Luyten, Pedlosky and Stommel (1982) (LPS hereafter). This development is much closer in spirit to the classical thermocline theories (e.g., Needler, 1967 and Welander, 1971) than is that of Rhines and Young. It is, however, more successful than the thermocline theories because it manages to satisfy both vertical and horizontal boundary conditions in a convincing fashion. It is also more satisfactory than RY and YR because the quasigeostrophic approximation is not made. Indeed, one of the most interesting features of LPS is the way in which fluid injected at one latitude is ultimately overridden by less dense fluid injected at more southerly latitudes. The price paid for this success is that the density field must be approximated by a series of layers. It is not clear how one might extend the LPS solution to a continuously stratified fluid, although some tentative steps in this direction are made in the present note.

In this article, the isopycnals which outcrop (i.e., strike the base of the Ekman layer) in the subtropical gyre will be referred to as ventilated isopycnals or ventilated layers. The deeper layers which do not outcrop in the subtropical gyre will be called unventilated layers or unventilated isopycnals. Some of the uppermost unventilated layers come to the surface in the subpolar gyre where the Ekman velocity is positive.

Now, in the LPS model the uppermost unventilated layer is motionless in the subtropical gyre, even though some of its geostropic contours may be closed.* This is analogous to the quasigeostrophic solution discussed earlier, in which only the uppermost, directly forced layer is in motion. (In the analogy all the ventilated layers in the LPS model correspond to the one directly forced layer in the quasigeostrophic model.) This suggests that the LPS solution may not be stable in the face of very small vertical stresses produced by mesoscale form drag. Instead, following RY and YR, I shall construct a solution in which flow is established in the unventilated layers so as to homogenize the potential vorticity within all the available closed geostrophic contours. I shall argue that this hybrid model, which incorporates desirable features from both earlier theories, is more realistic than either of them. It supersedes the theory of RY and YR simply because the quasigeostrophic approximation is not made. I believe the hybrid model is also superior to the LPS model, because it explicitly considers the effects of mean flow

---

* The geostrophic contours in this layer will certainly close if one increases the vertical resolution of the model by decreasing the density jumps between the layers while simultaneously increasing the number of layers. This process ultimately ensures that vortex stretching, which is proportional to the fractional change in layer thickness, dominates the β-effect.

acceleration around closed geostrophic contours by eddy stresses. This process assumes overwhelming importance if one creates "more" closed geostrophic contours by incr:asing the vertical resolution of the model, either by adding more layers or using continuous stratification.

In any case, one important point which emerges unequivocally from the present study is that the planetary geostrophic equations do not have a unique solution. Rather it is possible to find alternative solutions of the ideal fluid equations which satisfy the same vertical and horizontal boundary conditions. As in the quasigeostrophic theory, one is then faced with the problem of deciding which solution is relevant. RY argued that weak dissipation selects a particular solution. Since different dissipative processes select different solutions, if one argues that a particular solution is more "realistic" one is asserting that a particular dissipative process is dominant in the "real" ocean. In this article, as in RY and YR, it is hypothesized that mesoscale form drag is the most important dissipative process.

2. Formulation

Throughout this article I use the planetary geostrophic equations (Phillips, 1963 or Pedlosky 1979 section 6.20) and the Boussinesq approximation. This approximation is appropriate when the Rossby number ($U/f_0 L$ in standard notation) is small and the horizontal length scale of the flow is comparable to the radius of the Earth (that is $\beta L/f_0 \leqslant 1$ but not $<< 1$). For simplicity I also use the β-plane approximation in which the vertical component of the Earth's rotation is approximated by:

$$f = f_0 + \beta y \tag{2.1}$$

and the coordinates are Cartesian (x,y,z). The vertical coordinate z is positive upward and z = 0 is the base of the mixed layer. The velocity is (u,v,w) and the fluid is forced by Ekman pumping or suction at the base of the mixed layer:

$$w(x,y,0) = w_E(x,y) \tag{2.2}$$

Strictly speaking, one should use spherical coordinates; however, these simply complicate the notation without introducing new physics.

The three components of the momentum equation are:

$$-fv = -p_x/\rho_0 \tag{2.3a}$$

$$fu = -p_y/\rho_0 \tag{2.3b}$$

$$0 = p_z + g\rho \tag{2.3c}$$

where p is the pressure, g is gravitational acceleration, ρ is the density and ρ_0 is the mean density of the fluid.

It is convenient to represent the density as:

$$\rho = \rho_0 [1 - g^{-1}B]$$

where B is the buoyancy. The Boussinesq approximation is made so the fluid is incompressible:

$$u_x + v_y + w_z = 0$$

By eliminating the pressure from (2.3) one obtains the three components of the vorticity equation:

$$fv_z = B_x \tag{2.4a}$$

$$fu_z = -B_y \tag{2.4b}$$

$$\beta v = fw_z \tag{2.4c}$$

Equations (2.4a, b) are the thermal wind equations while (2.4c) is the well known relationship connecting vortex stretching and north-south velocity. The vertical integral of (2.4c) is the Sverdrup relation. A result I shall use frequently is obtained by eliminating v between (2.4a) and (2.4c):

$$f^2 w_{zz} = \beta B_x \tag{2.5}$$

The final equation which closes the system is conservation of density:

$$uB_x + vB_y + wB_z = 0 \tag{2.6}$$

Differentiating (2.6) with respect to z and using (2.4) gives conservation of potential vorticity:

$$uq_x + vq_y + wq_z = 0 \tag{2.7a}$$

$$q \equiv fB_z \tag{2.7b}$$

Finally, in a layer model, in which the density changes are localized at surfaces, (2.4a and b) are:

$$f(\delta v) = (\delta B)h_x \tag{2.8a}$$

$$f(\delta u) = -(\delta B)h_y \tag{2.8b}$$

where $(\delta u, \delta v)$ is the jump in velocity at the surface, δB is the jump in buoyancy and $z = -h(x,y)$ is the position of the surface separating the two layers.

3. A Ventilated Theory of the Wind-Driven Circulation

In this section the consequences of increasing the vertical resolution of the unventilated isopycnals within the context of the LPS model are investigated. In this model, as in LPS, the unventilated isopycnals are motionless in the subtropical gyre where $w_E < 0$ and rise to the surface in the subpolar gyre where $w_E > 0$. I emphasize from the outset that the solutions obtained in this section are not physically reasonable and moreover the calculated density field is particularly unrealistic and does not resemble the observed density field. However, as in LPS the model does provide exact solutions to the thermocline equations of section 2 in which both horizontal and vertical boundary conditions are satisfied. Furthermore, this model is the logical generalization of the LPS model if one takes the unventilated layers to be continuously stratified.

The basic idea behind the model in this section is to consider a continuously stratified ocean which in the absence of Ekman pumping at $z = 0$ would be motionless with flat isopycnals. In the subtropical gyre the wind stress pumps fluid with uniform density down into the interior. This fluid lies above the motionless stratified fluid and assumes some equlibrium shape which must be calculated. In the subpolar gyre the stratified fluid is sucked out of the ocean interior into the mixed layer; each density layer is motionless until it is directly exposed to the Ekman pumping at $z = 0$.

The subtropical gyre

First consider the subtropical gyre where $w_E < 0$ so fluid is being pumped out of the base of the Ekman layer into the ocean interior; see Figure 1. It will be assumed for simplicity that the buoyancy of the unventlated layers (which are motionless in the subtropical gyre) is:

$$B = N^2 z \tag{3.1}$$

where N is the buoyancy frequency. The assumption (3.1) is purely for convenience; it will become apparent that it is straightforward to discuss an arbitrary continuous distribution of buoyancy in the unventilated region. Equation (3.1) is convenient because it allows one to present explicit solutions. Also assume that fluid of density ρ_0, or buoyancy 0, is pumped out of the base of the mixed layer at $z = 0$. This fluid lies above the unventilated fluid whose density is given by (3.1); see Figure 1. The surface $z = -D(x,y)$ separates the ventilated and unventilated regions. In this section I calculate the initially unknown $D(x,y)$ as well as (u,v,w) in the ventilated fluid.

The assumption (3.1), together with the assumption that there is only one density layer at the surface, can easily be relaxed. In fact, one can assume that the undisturbed stratification is an arbitrary continuous function of z and also, as in LPS, insert additional ventilated layers which surface at prescribed latitudes in the subtropical gyre.

Because the models discussed in this paper ignore the processes which determine these
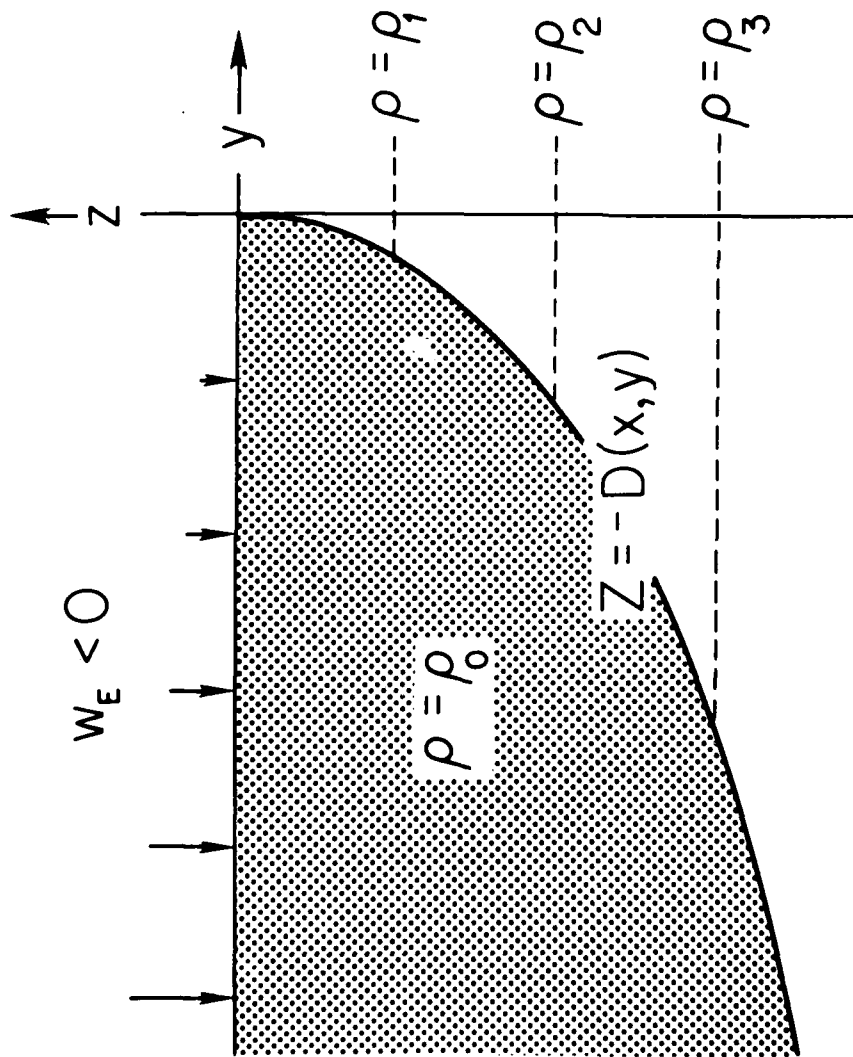
Figure 1: A schematic meridional density section of the subtropical gyre. The stippled area above $z = -D(x,y)$ represents fluid of uniform density injected from the Ekman layer at $z = 0$. Below $z = -D(x,y)$ the fluid is stratified and the dashed lines represent undisturbed isopycnals. Note how the strength of the density jump at $z = -D$ increases with depth.

important boundary conditions I have referred to them as investigations of the "planetary geostrophic equations". The more traditional nomenclature, "thermocline theory", is best reserved for more ambitious investigations which do not avoid the issue of what determines the underlying stratification.

Begin by observing that at $z = -D$ there is a buoyancy jump:

$$\delta B = N^2 D \qquad (3.2)$$

Now from (2.4a, b) the horizontal velocities are independent of z within the ventilated fluid. Vertically integrating (2.4c) from $z = 0$, where $w = w_E$, to $z = -D$, where $w = 0$ (because the unventilated layers are motionless) gives:

$$v = (f w_E / \beta D) \qquad (3.3)$$

Now at $z = -D$ the density is discontinuous and (2.8a) is:

$$f v = N^2 D \, D_x$$

where (3.2) was used. Eliminating v using (3.3) determines D:

$$D^2 D_x = f^2 w_E / N^2 \beta \qquad (3.4)$$

Integrating (3.4) from $x' = x$ to the eastern boundary $x' = a$ gives:

$$\frac{1}{3} D^3 = -(f^2/N^2 \beta) \int_x^a w_E(x', y) dx' \qquad (3.5)$$

From (2.5) the vertical velocity is given by:

$$w = w_E \left[1 + (z/D) \right] \qquad (3.6)$$

v by (3.3), and finally u is calculated from:

$$f u = \int_a^x \frac{\partial}{\partial y} (f v) dx'$$
$$= -N^2 D \, D_y$$

More general surface density distribution

It is worth remarking that, following LPS, it is straightforward to increase the vertical resolution of the ventilated region by adding additional layers which surface at prescribed latitudes in the subtropical gyre. The result is a model which is almost identical to LPS except that the unventilated region is continuously stratified. The unrealistic intersection of $z = -D(x,y)$ with the resting, stratified fluid below the wind gyre is still present.

The subpolar gyre

In the subpolar gyre, as in LPS, we look for a solution in which the unventilated isopycnals rise to the surface. In LPS each layer is motionless until the one above it outcrops (see Figure 2a).
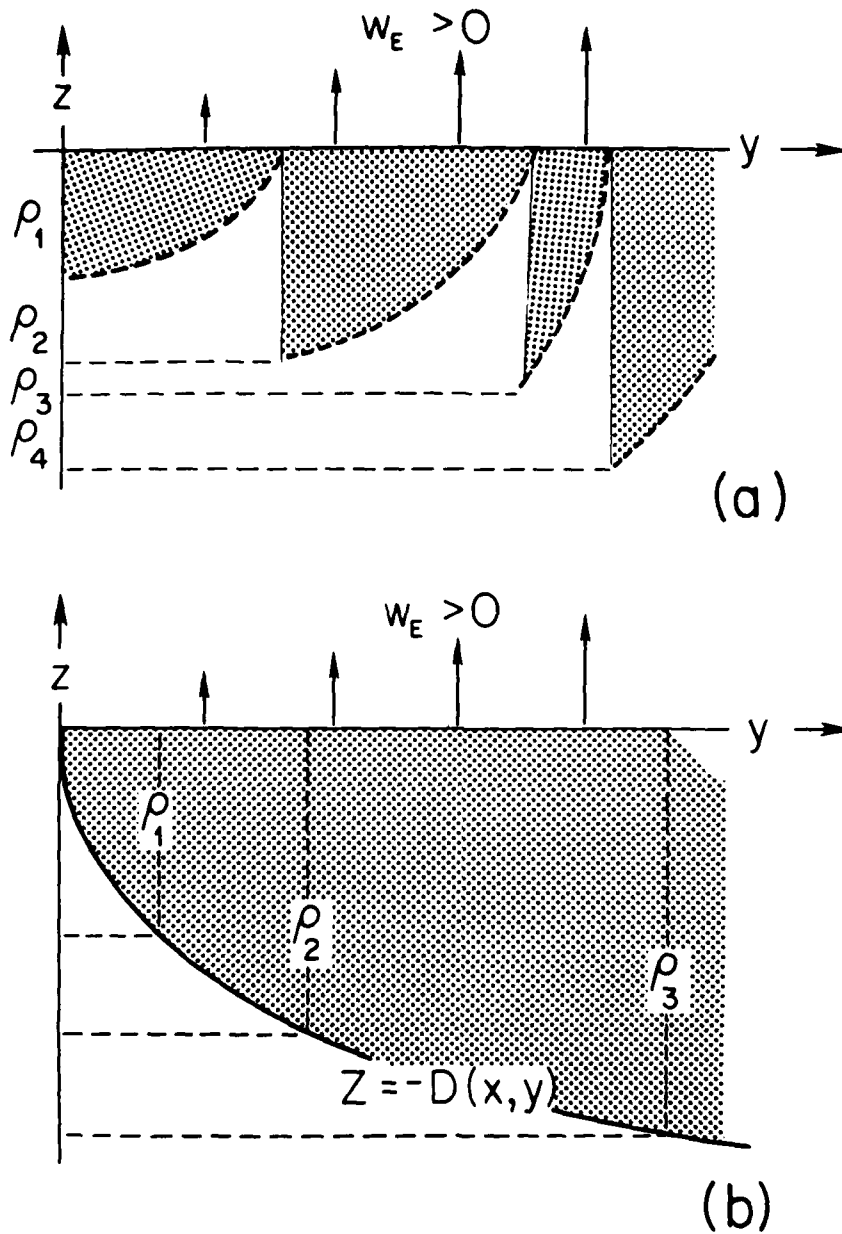
Figure 2: Schematic meridional density section of the subpolar gyre. (a) Layered stratification. Only the uppermost layer is in motion. All the Sverdrup transport is confined to the stippled area. (b) Continuous stratification. The dashed lines represent isopycnals. Below $z = -D(x,y)$ the fluid is motionless. All of the Sverdrup transport is in the stippled region abo $=$ $-D(x,y)$. As in case (a) only the uppermost density layer is in motion. Case (b) is the limit of case (a) as the number of layers is increased.

What is the continuously stratified analog of this solution? The appropriate generalization of the layered LPS solution is obtained by arguing that in the region where the fluid is in motion the density is uniform vertically. Thus suppose there is a surface $z = -D(x,y)$ below which the fluid is motionless with B given by (3.1) (see Figure 2b). Above $z = -D$ the fluid is being removed by Ekman suction at $z = 0$ and so $(u,v,w) \neq (0,0,0)$. In this region $B_z = 0$. Continuity of B at $z = -D$ implies:

$$B = -N^2D \quad \text{if } z > -D \tag{3.7a}$$

since

$$B = +N^2z \quad \text{if } z < -D. \tag{3.7b}$$

Now from (2.5):

$$f^2w_{zz} = -\beta N^2D_x \tag{3.8}$$

and integrating the above with respect to z gives:

$$w = -\frac{1}{2}(\beta N^2/f^2) D_x (z + D)^2 \tag{3.9}$$

where, in analogy with LPS, $w = v = 0$ at $z = -D$. Finally, D is determined by applying the boundary condition at $z = 0$:

$$w_E = -\frac{1}{2}(\beta N^2/f^2) D^2D_x \tag{3.10}$$

or integrating to the eastern boundary $x = a$:

$$\frac{1}{6}D^3 = (f^2/\beta N^2) \int_x^a w_E(x',y)dx' \tag{3.11}$$

(compare this with (3.5)).

Calculation of the pressure field

The pressure field can now be calculated by integrating the hydrostatic relation (2.3c) using:

$$p/\rho_0 = -gz + \frac{1}{2}N^2z^2 \quad \text{if } z < -D(x,y)$$

as the boundary condition. One finds:

$$p/\rho_0 = -gz + \frac{1}{2}N^2D^2 \quad \text{in the subtropical gyre}$$

and

$$p/\rho_0 = -gz + \frac{1}{2}N^2z^2 - \frac{1}{2}N^2(z + D)^2 \quad \text{in the subpolar gyre}$$

Conclusion

138

To summarize the solution, D has been calculated from (3.5) and (3.11) assuming that:

$$f^2 w_E = f_0^2 w_0 (\beta y / f_0) \tag{3.12}$$

Thus y = 0 is the boundary between the subpolar and subtropical gyres. A meridional density section at the western boundary x = 0 is shown in Figure 3. A sequence of zonal sections through the density field is shown in Figure 4. Below the surface z = -D the density field is undisturbed and is given by (3.1). Above this surface in the subtropical gyre the density is uniform and equal to the density pumped in at z = 0. Above the surface z = -D in the subpolar gyre the density is uniform in the vertical but varies in the horizontal. It is important to realize that fluid does not cross the surface z = -D in either the subtropical or subpolar gyre. In order to visualize the circulation in a complete double gyre, consider the forcing pattern:

$$w_E = (f_o / f)^2 w_0 \sin(\pi y / L) \tag{3.13}$$

where -L < y < L. When y < 0, w_E is negative while when y > 0, w_E is positive. Thus (3.13) models the Ekman pumping in a double gyre where y = 0 is the boundary between the gyres. In Figure 5 contours of constant pressure are plotted at two depths: z = 0 and z = 1/2 D_{max} where:

$$D_{max}^3 = 6 f_0^2 \ w_0 a / N^2 \beta$$

is the maximum depth of the gyre. These pressure contours are "streamlines" for the nondivergent vector field (fu,fv). In the subpolar gyre these curves are also isopycnals. Figure 6 shows a meridional density section through the double gyre. Note how the subtropical gyre is shallower than the subpolar gyre by a factor of $2^{1/3} \simeq 1.3$.

The principal weakness of the solution constructed in this section is the unrealistic density field. In the subtropical gyre the isopycnals intersect whereas in the subpolar gyre the isopycnals are vertical. It is obvious that, although these are exact solutions of the planetary geostrophic equations of section 2, other processes, which were neglected to obtain these simplified equations, must intervene and prevent the flow in Figures 3 and 4 from becoming established. The process favored by RY and YR is vertical stress transmission due to mesoscale eddies. This mechanism produces large mean flows when there are closed geostrophic contours. Now it is apparent from Figure 1 that the geostrophic contours in the motionless, stratified fluid immediately below z = -D(x,y) track the base of the gyre. Thus the region immediately below z = -D in Figure 1 is particularly susceptible to mean flow acceleration. This argument suggests a model in which there is a region of fluid, with density ρ_0, injected from the mixed layer, riding above a region where eddy stresses have removed all the closed geostrophic contours by homogenizing the potential vorticity. This alternative model is developed in the next section.

4. An Unventilated Theory of the Wind-Driven Circulation

The circulation in the previous model is ventilated in the sense that only the density layer directly forced by the Ekman pumping is in motion. This superficially plausible idea led to the
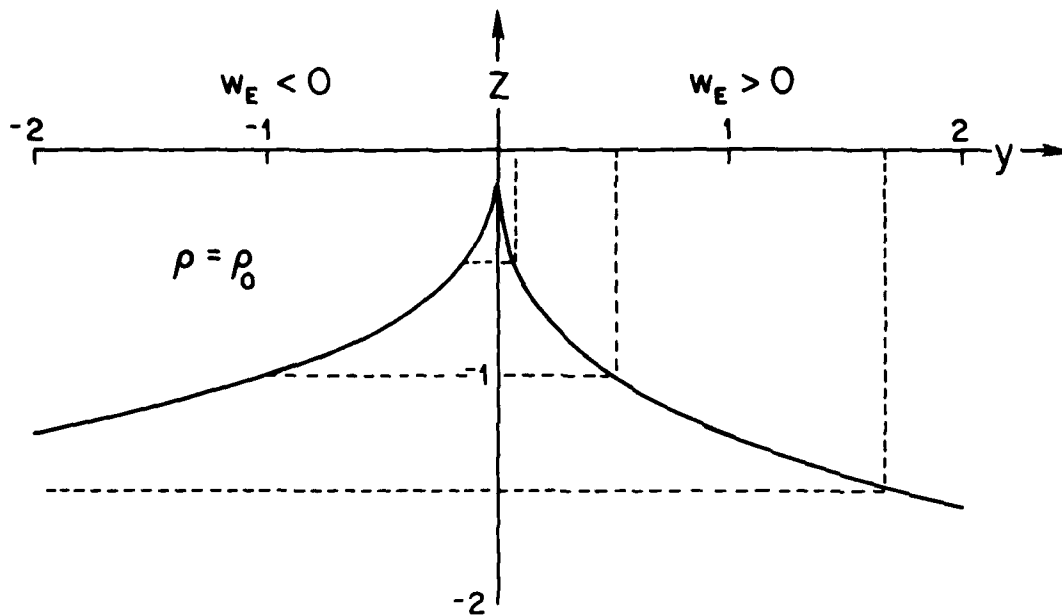
Figure 3.: A meridional section showing the density field (the dashed lines are isopycnals) in the vicinity of the latitude where $w_E = 0$. The surface $z = -D(x,y)$ is the solid curve. The section is at $x = 0$ and w_E is given by (3.12). The north-south distance is nondimensionalized by some arbitrary length scale L and the depth is nondimensionalized by $[f_0 aL \, w_0/3N^2]^{1/3}$.

x=0   x=a

$$\rho = \rho_0 \left[1 - N^2 g^{-1} Z \right]$$

(a) $y > 0$, $w_E > 0$

(b) $y = 0$, $w_E = 0$

$$\rho = \rho_0$$

(c) $y < 0$, $w_E < 0$
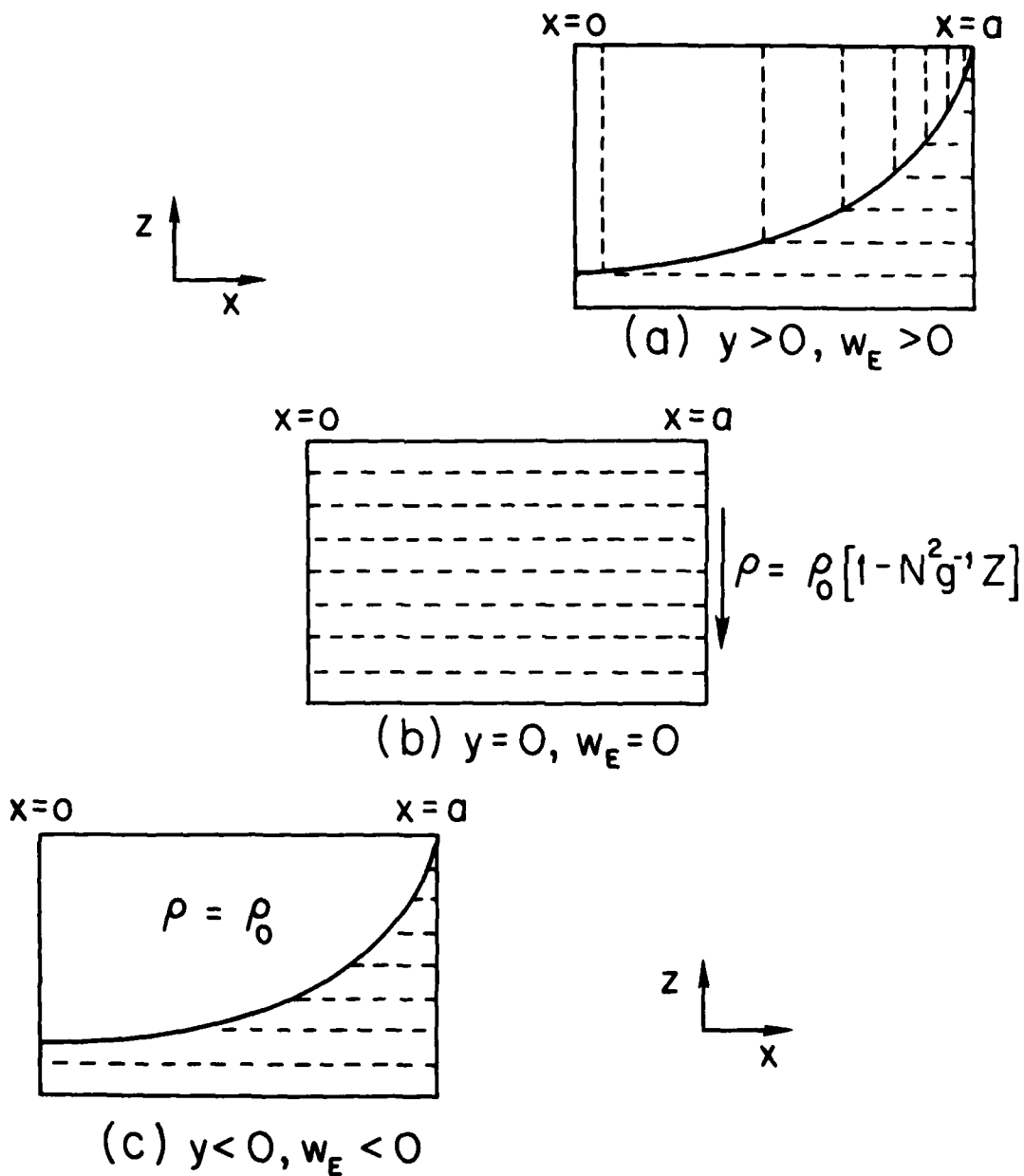
Figure 4: A sequence of zonal section through the gyre. The dashed curves are isopycnals while the solid curve is $z = -D$. It has been assumed that $\partial w_E / \partial x = 0$ so $D \alpha \ (a - x)^{1/3}$. (a) A zonal section in the subpolar gyre. (b) A zonal section at the boundary between the subpolar and subtropical gyres. The basic stratification is undisturbed since $D = 0$ at this latitude. (c) A zonal section in the subtropical gyre.
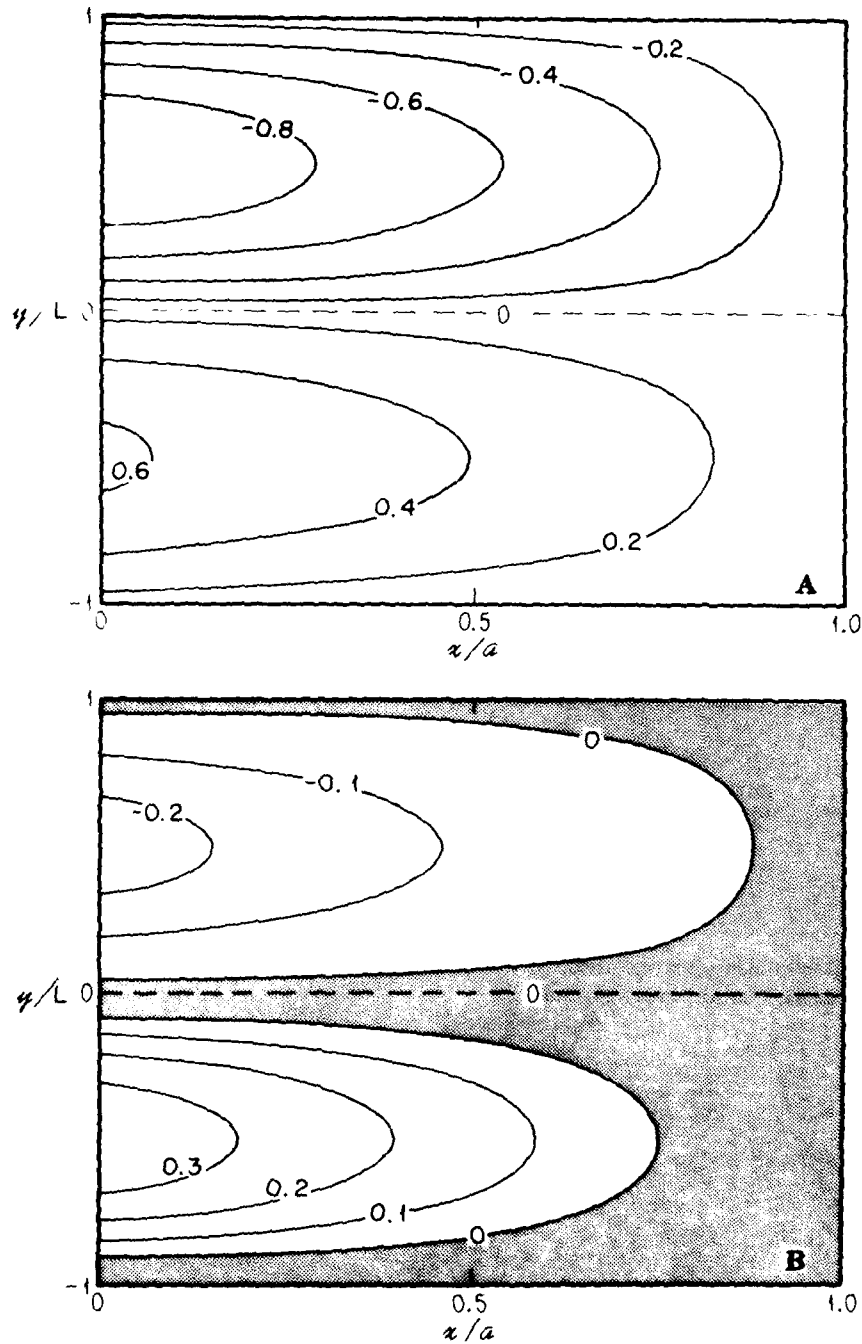
Figure 5: A plan view of the pressure field (actually $(p/\rho_0 + gz - 1/2\ N^2z^2)/(1/2\ N^2D_{max}^2))$ in a double gyre system at two depths. (a) $z = 0$. (b) $z = 1/2D_{max}$ where D_{max} is the maximum depth of the circulation defined in the text.
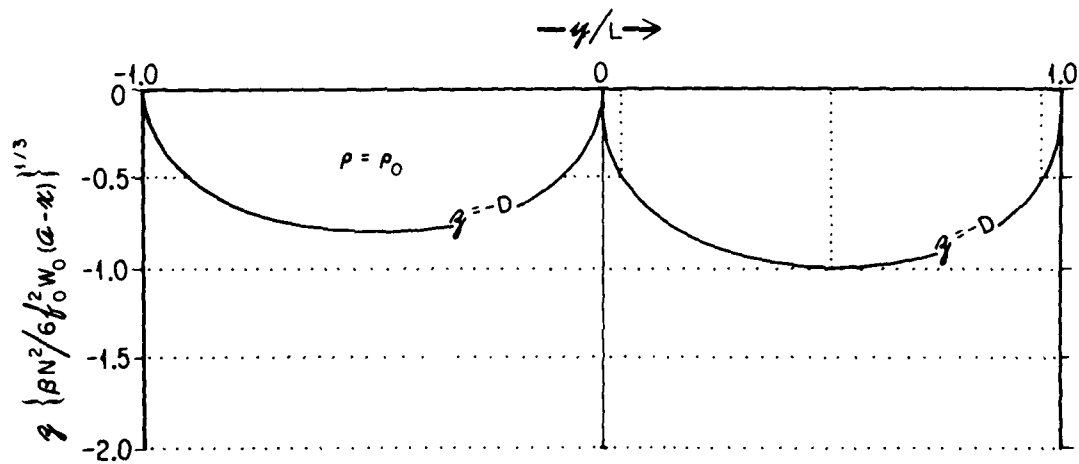
Figure 6: A meridional density section through the double gyre system. The solid curve is z = -D(x,y) while the dashed curves are isopycnals.

unrealistic circulation in Figures 3 and 4.

By contrast the model in this section is based on the more complicated idea that flow develops in the unventilated isopycnals so as to homogenize the potential vorticity within all the available closed geostrophic contours. This notion leads to more realistic density distributions than those of Figures 3 and 4.

The subtropical gyre

As in the previous section, fluid of density ρ_0 is pumped out of the Ekman layer. This fluid collects above a region in which the potential vorticity is uniform (see Figure 7). As in RY and YR the value of the constant potential vorticity in this region is determined by conditions at the boundary between the subtropical and subpolar gyres. As in the previous section this boundary is at $y = 0$ where $f = f_0$. Below the homogenized region lies motionless fluid in which the stratification is given by (3.1).

Thus the ocean is divided into three regions (Figure 7):

(i)   Region I where $0 > z > -D(x,y)$ and $\rho = \rho_0$ or equivalently $B = 0$.

(ii) Region II where $-D(x,y) > z > -H(x,y)$ and $q = fB_z = f_0N^2$. The potential vorticity is uniform on isopycnals and because of the special assumption (3.1), uniform across isopycnals.

(iii) Region III where $-H(x,y) > z > -\infty$ and $B = N^2z$ as in (3.1) while $(u,v,w) = (0,0,0)$.

I have assumed that the basic stratification is given by (3.1). In general the functional relationship between q and ρ in region II is obtained by eliminating z between B and fB_z at the northernmost point of the subtropical gyre (RY and YR). At this point the fluid is motionless at all depths and the basic stratification is undisturbed. It seems likely that one could construct a family of solutions by assuming different functional relations between q and B in region II. The choice of uniform q is motivated by the Prandtl-Batchelor theorem discussed by Rhines and Young (1982b).

In region II where $q = fB_z = f_0N^2$ it follows that:

$$B = (f_0N^2z/f) + b(x,y) \quad (-D > z > -H) \tag{4.1}$$

One now obtains two relations between the three unknowns. H, D and b by requiring the buoyancy to be continuous at $z = -D$ and $z = -H$.

At $z = -H$ one has:

$$-N^2H = -(f_0N^2H/f) + b \tag{4.2}$$

or

$$b = -(N^2H)(\beta y/f)$$

so that from (4.1):
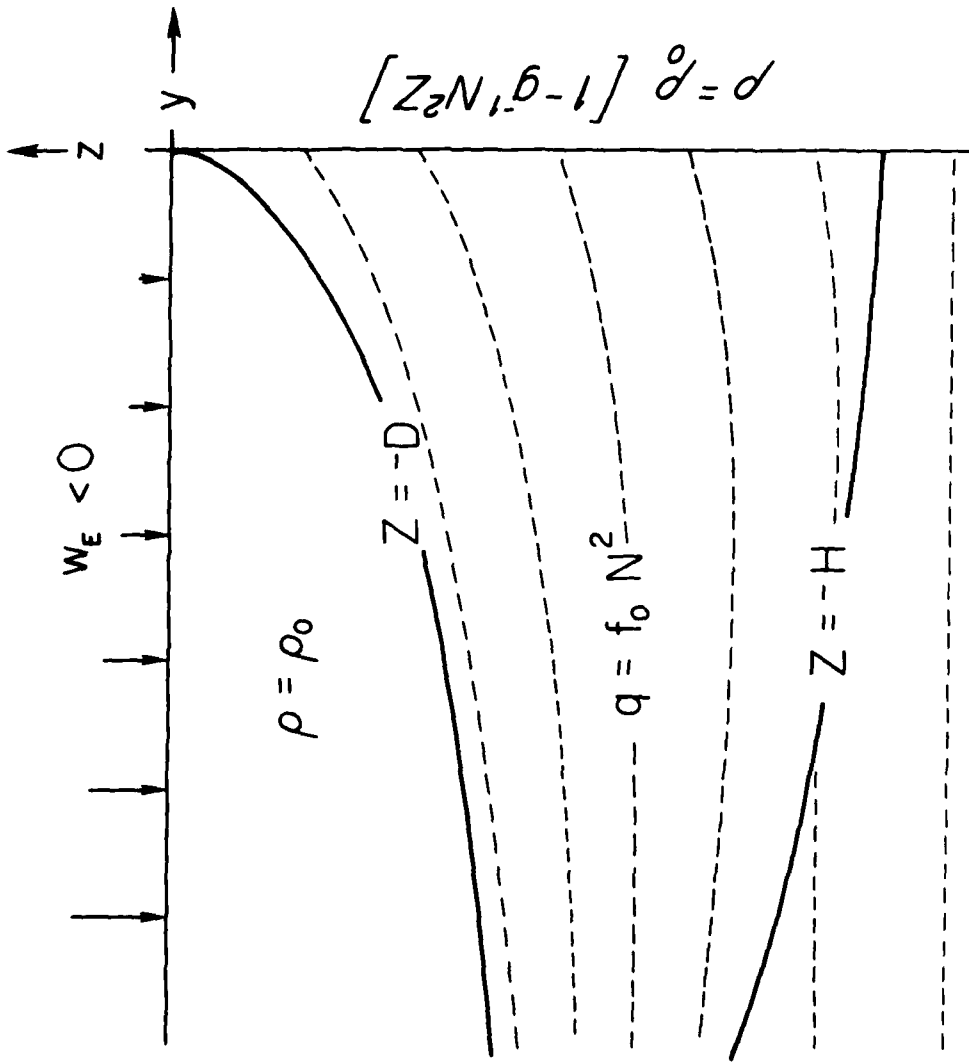
Figure 7: A schematic meridional density section of the subtropical gyre. The dashed curves represent isopycnals. Above $z = -D$ lies the fluid with density ρ_0 injected from the mixed layer. Between $z = -D$ and $z = -H$ the potential vorticity is uniform. Below $z = -H$ the fluid is motionless. At $y = 0$, where $w_E = 0$, the stratification is undisturbed.

$$B = (f_0 N^2/f)[z - (\beta y/f_0)H] \quad (-D > z > -H) \tag{4.3}$$

At $z = $ -D continuity of B gives:

$$D = -(\beta y/f_0)H \tag{4.4}$$

since from (4.3) this ensures that $B = 0$ at $z = $ -D.

To complete the solution we note that (4.3) and (2.5) imply:

$$w_{zz} = -(\beta^2 N^2 y/f^3)H_x \quad (-D > z > -H) \tag{4.5}$$

To make the transition to the motionless region below $z = $ -H as smooth as possible we integrate (4.5) with respect to z and choose the constants of integration so that v and w vanish at $z = $ -H:

$$w = -\frac{1}{2}(\beta N^2/f^2)(\beta y/f)(z+H)^2 H_x \tag{4.6a}$$

$$v = -(N^2/f)(\beta y/f)(z+H)H_x \tag{4.6b}$$

Now let v_* and w_* denote the values of v an w at $z = $ -D. In region I the fluid has uniform density, so $v = v_*$ throughout this region. Integrating (2.4c) from $z = 0$ to $z = $ -D gives:

$$\beta v_* D = f(w_E - w_*) \tag{4.7}$$

Using (4.6) and (4.4) one can eliminate v_*, w_* and D from (4.7) and obtain an equation which determines H:

$$\frac{1}{2}\left[\frac{\beta N^2}{f^2}\right]\left[1 - \frac{\beta y}{f_0}\right]\left[\frac{\beta y}{f_0}\right] H^2 H_x = -w_E$$

Integrating the above expression from $x' = x$ to the eastern boundary $x' = a$ gives:

$$\frac{1}{6}\left[\frac{\beta N^2}{f^2}\right]\left[1 - \frac{\beta y}{f_0}\right]\left[\frac{\beta y}{f_0}\right] H^3 = \int_x^a w_E(x',y)dx' \tag{4.8}$$

The above equation determines H and then D is obtained from (4.4).

Calculation of the pressure field

Now, the buoyancy field is:

$$B = \begin{cases} 0 & \text{if } z > -D \\ (Nf_0/f)[z-(\beta y/f_0)H] & \text{if } -D > z > -H \\ +N^2 z & \text{if } -H > z, \end{cases}$$

and so from (2.3c) one can calculate the pressure field:

$$p/\rho_0 = \begin{cases} -gz - \dfrac{1}{2}N^2(\beta y/f_0)H^2 & \text{if } > z > -D \\[2mm] -gz + \dfrac{1}{2}N^2z^2 - \dfrac{1}{2}N^2(\beta y/f)(z+H)^2 & \text{if } -D > z > -H \\[2mm] -gz + \dfrac{1}{2}N^2z^2 & \text{if } -H\ z \end{cases}$$

Note that below the gyre, $z < $ -H, the pressure is equal to the pressure in a resting ocean with $B = N^2z$; this provided the boundary condition for the integration of the hydrostatic relation. Given p one can now calculate and verify by direct substitution that (2.6) is satisfied.

Local analysis of (4.8) near y = 0

It is informative to investigate (4.8) near the boundary between the subtropical and subpolar gyres. Suppose that:

$$w_E = w_0(\beta y/f_0)$$

locally describes the forcing in this region and:

$$f = f_0$$

Equation (4.8) implies:

$$H^3 = 6\left(\frac{f_0^2}{\beta N^2}\right) w_0\,(a-x)$$

Thus in this second model the depth of the subtropical gyre is not zero at its northern boundary. This is also apparent in the meridional density section in Figure 8. The dotted curve in Figure 8 indicates the depth of the circulation ($z = $ -D) according to the earlier theory. This figure should be compared with Figure 3. The two theories predict very different flow patterns at the boundary between the two gyres. In the earlier theory the depth of the gyre goes to zero as $y \to 0$ whereas in the theory presented in this section the circulation is deepest at the northern boundary. Unfortunately, direct comparison of the two theories with observations is clouded by the presence of the separated western boundary current which lies along the boundary between the two gyres. This feature is absent from both theories. However, a deep northern boundary to the subtropical gyre is more consistent with traditional descriptive ideas (e.g., Montgomery, 1938).

Relative importance of vertically integrated transport in regions I and II

It is interesting to calculate the fraction of the Sverdrup transport which is in region I. This calculation provides some intuition about the relative strengths of the circulation in the ventilated and unventilated regions.
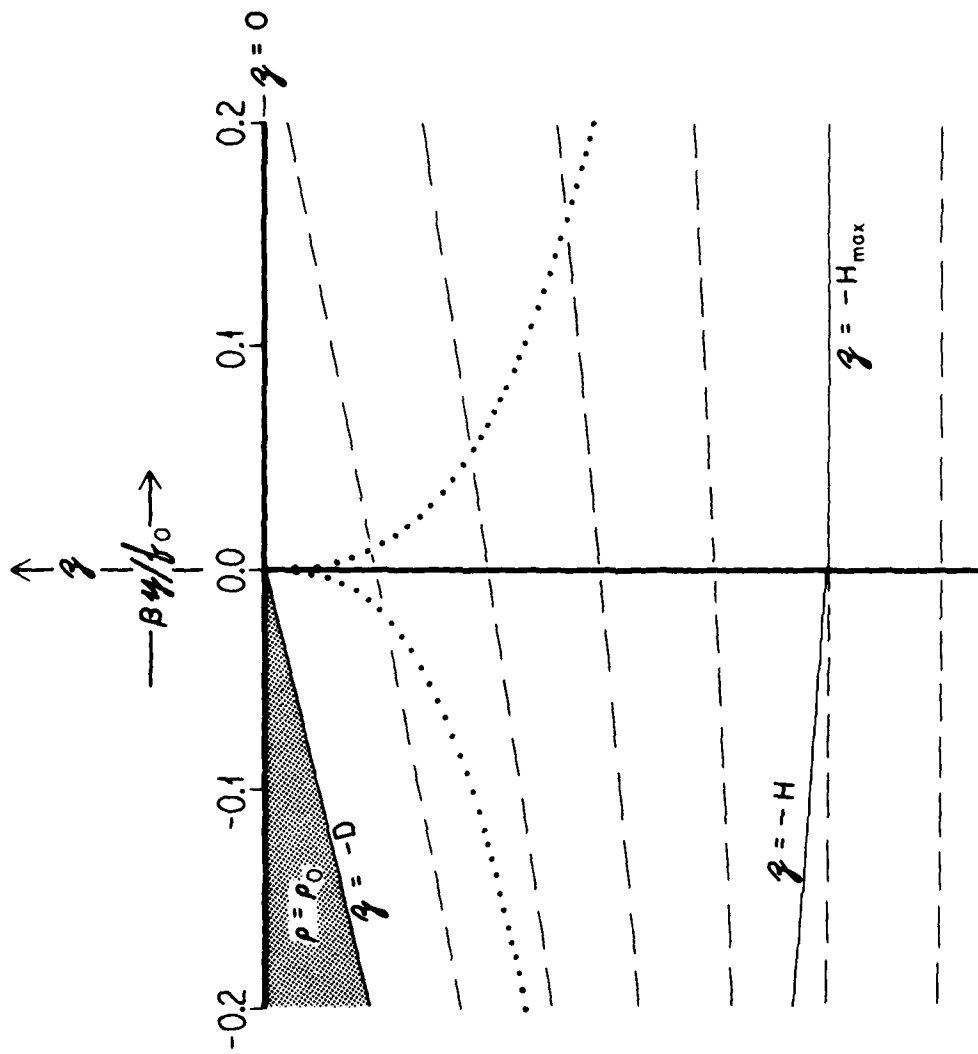
Figure 8: A meridional section (x=0) through the density field in the neighborhood of the boundary between the subtropical and subpolar gyres. The isopycnals are dashed. The boundaries z = -D and z = -H are solid. For comparison z = -D from (3.5) and (3.11) is shown as a dotted curve.

One has:

$$\int_{-D}^{0} v dz = v \cdot D$$

$$= 2y \left[\frac{f_0 + \beta y}{f_0 - \beta y} \right] w_E$$

so that the fraction of the total Sverdrup transport in the ventilated layer is:

$$\int_{-D}^{0} v dz / \int_{-H}^{0} v dz = \left[\frac{2\beta y}{f_0 - \beta y} \right]$$

Thus at the boundary between the gyres all of the Sverdrup transport is in the unventilated layer. As one moves south the ventilated layer becomes more important.

More general surface density distributions

It is possible to introduce additional ventilated layers which surface at prescribed latitudes in the subtropical gyre. Thus, as in LPS, one can satisfy more general density boundary conditions at $z = 0$.

Comparison with the quasigeostrophic model of RY and YR

In the continuously stratified quasigeostrophic calculations in R ' and YR the thickness of the ventilated region was taken to be negligible. From (4.4) we see that this is an acceptable approximation when:

$$\frac{\beta y}{f_0} \ll 1 \qquad (4.9)$$

Indeed it is easily seen that when (4.9) is satisfied, (4.8) reduces to the expression RY and YR give for H. Thus the quasigeostrophic models correspond to a local analysis of the planetary geostrophic equations about $y = 0$ (i.e., the latitude at which the Ekman pumping changes sign).

The subpolar gyre

Once again I construct a solution in which the ocean is divided into three regions (see Figure 9):

(i)   Region I where $0 > z > -D(x,y)$ and $B_z = 0$.

(ii) Region II where $-D(x,y) > z > -H(x,y)$ and $q = fB_z = f_0 N^2$.

(iii) Region III where $-H(x,y) > z > -\infty$ and $B = N^2 z$ as in (3.1) while $(u,v,w) = (0,0,0)$.

The dynamics of region I are similar to those of the subpolar gyre in section 3. Region II on the other hand has uniform potential vorticity.
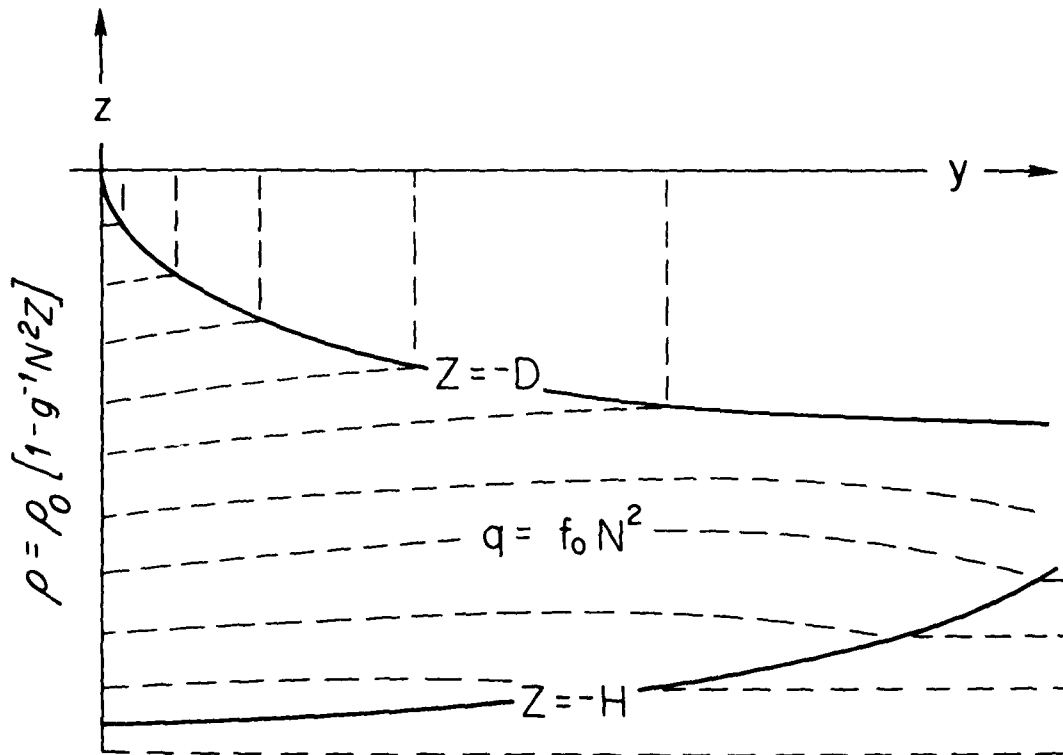
Figure 9: A schematic meridional density section of the subpolar gyre. The dashed curves represent isopycnals. Above z = -D the isopycnals are vertical. Between z = -D and z = -H the potential vorticity is uniform. Below z = -H the fluid is motionless. At y = 0, where w_E = 0, the stratification is undisturbed.

Begin by observing that in region II:

$$B = (N^2 f_0 z / f) + b(x,y) \quad \text{if } -H < z < -D \qquad (4.10)$$

Continuity of B at $z = -H$ gives:

$$B = (N^2 f_0 / f) [z - (\beta y / f_0) H] \quad \text{if } -H < z < -D \qquad (4.11)$$

Continuity of B at $z = -D$ gives B everywhere in region I:

$$B = -(N^2 f_0 / f) [D + (\beta y / f_0) H] \quad \text{if } -D < z < 0 \qquad (4.12)$$

One can now calculate w from (2.5). As in the previous examples one integrates upward, starting at $z = -H$ where:

$$w = w_z = 0$$

Thus in region II:

$$w = -\frac{1}{2} \left[\frac{\beta N^2}{f^2} \right] \left[\frac{\beta y}{f} \right] (z + H)^2 H_x \qquad (4.13a)$$

$$v = -\left[\frac{N^2}{f} \right] \left[\frac{\beta y}{f} \right] (z + H) H_x \qquad (4.13b)$$

In region I we again obtain v and w from (2.5) and (4.12). Since the density is continuous, v and w are continuous at $z = -D$. One finds:

$$w = -\frac{1}{2} \left[\frac{\beta N^2}{f^2} \right] \left[\frac{\beta y}{f} \right] (z+H)^2 H_x - \frac{1}{2} \left[\frac{\beta N^2}{f^2} \right] \left[\frac{f_0}{f} \right] (z+D)^2 D_x \qquad (4.14)$$

if $0 > z > -D(x,y)$.

Finally, since $w = w_E$ at $z = 0$ one has:

$$w_E = -\frac{1}{2} \left[\frac{\beta N^2}{f^2} \right] \left[\left[\frac{\beta y}{f} \right] H^2 H_x + \left[\frac{f_0}{f} \right] D^2 D_x \right] \qquad (4.15)$$

The above equation is only one relation between the two unknowns H and D. Thus there are an infinite number of solutions since one is free to specify an additional arbitrary relationship between H and D.

One choice is $H = D$ in which case (4.15) reduces to (3.11). In this case there is no region II and the isopycnals are vertical in the subpolar gyre. This is just the model from section 3.

An *alternative (and more plausible)* choice is $D = 0$. In this case there are no vertical

isopycnals and the potential vorticity is uniform everywhere in the subpolar gyre. This is essentially the solution given by RY and YR.

This particular set of solutions illustrates one of the principal conclusions of this article: there are an infinite number of solutions of the planetary geostrophic equations, all of which satisfy the same boundary conditions. Other physical processes, not explicit in the equations themselves, must be invoked to pick a solution. For example, a priori it seems unlikely that isopycnals are vertical in the subpolar gyre so $D = 0$ in (4.15). On the other hand, one might argue that there is very strong thermally driven vertical mixing in the subpolar gyre which vertically homogenizes the density field to some depth D. One could probably construct a simple model in which D is determined by the heat flux from the ocean to the atmosphere. This interesting possibility reinforces the original conclusion: additional physics is required to obtain a unique solution.

Calculation of the pressure field

With $D = 0$ the buoyancy field is:

$$B = \begin{cases} (N^2 f_0/f)[z - (\beta y/f_0)H] & \text{if } 0 > z > -H \\ N^2 z & \text{if } z < -H \end{cases}$$

and so from (2.3c) one can calculate the pressure field:

$$p/\rho_0 = \begin{cases} -gz + \frac{1}{2} N^2 z^2 - \frac{1}{2} N^2 (\beta y/f)(z+H)^2 & \text{if } -H < z < 0 \\ -gz + \frac{1}{2} N^2 z^2 & \text{if } z < -H \end{cases}$$

Once again one can now verify by direct substitution that (2.6) is satisfied.

Summary

The solution given in this section is summarized in the meridional density section shown in Figure 8. It is assumed that:

$$w_E = (f_0/f)^2 w_0 (\beta y/f_0)$$

so this figure displays the density field near the boundary between the two gyres. In order to visualize the circulation in a double gyre system we will again assume that w_E is given by (3.13). Two zonal density sections, one in the subpolar and the other in the subtropical gyre, are shown in Figure 10. At $y = 0$, where $w_E = 0$, $H = D = 0$ the stratification is undisturbed. Since $H, D \to 0$ as $x \to$ a the stratification is also undisturbed everywhere along the Eastern boundary (e.g., Figure 10). Figure 11 shows a meridional section through the double gyre system. Note how the isopycnal spacing increases poleward to ensure that the potential vorticity is uniform. Note also how the isopycnal displacements increase as $\beta L/f_o$ increases. Figure 12 shows plan views of the pressure and density fields at two depths in the
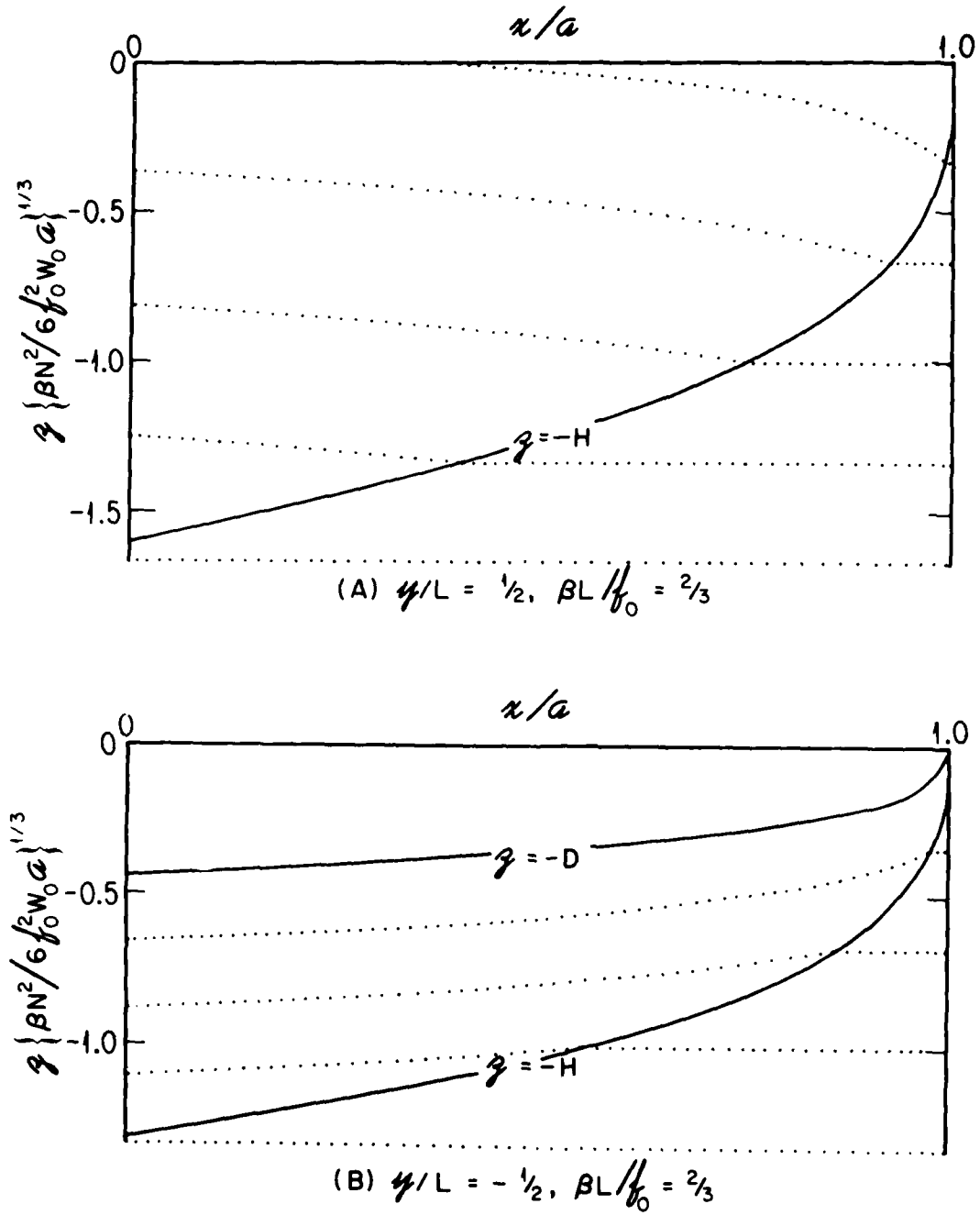
Figure 10: Two zonal density sections in a double gyre system where w_E is given by (3.13). The dotted curves are isopycnals. (a) A zonal section through the subpolar gyre. The surface $z = -H(x,y)$ is the solid curve. (b) A zonal section through the subtropical gyre. The solid curves are $z = -D(x,y)$ and $z = -H(x,y)$.
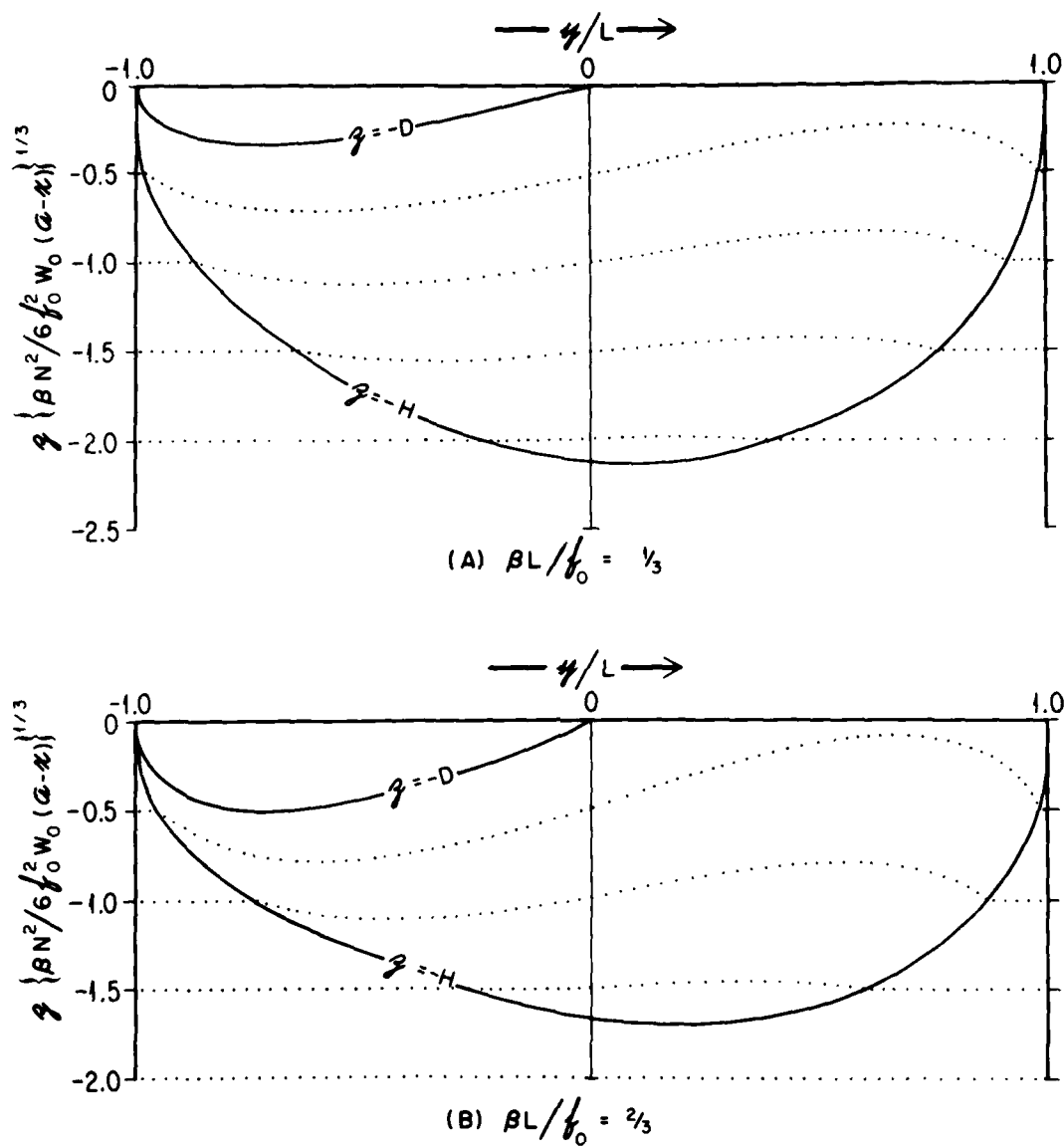
Figure 11: Meridional density sections in a double gyre system. The dotted curves are isopycnals. (a) $\beta L/f_o = 1/3$. (b) $\beta L/f_o = 2/3$ (c.f. Fig. 6).
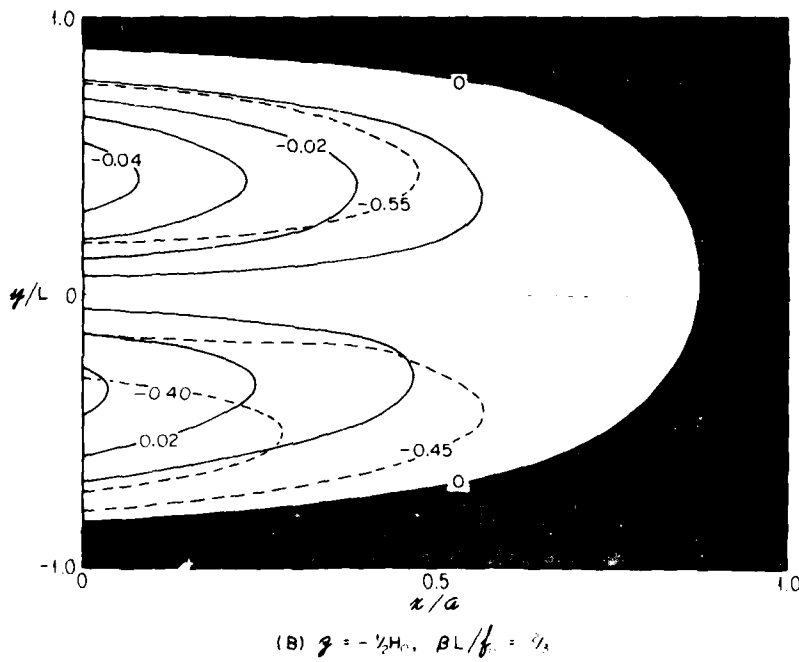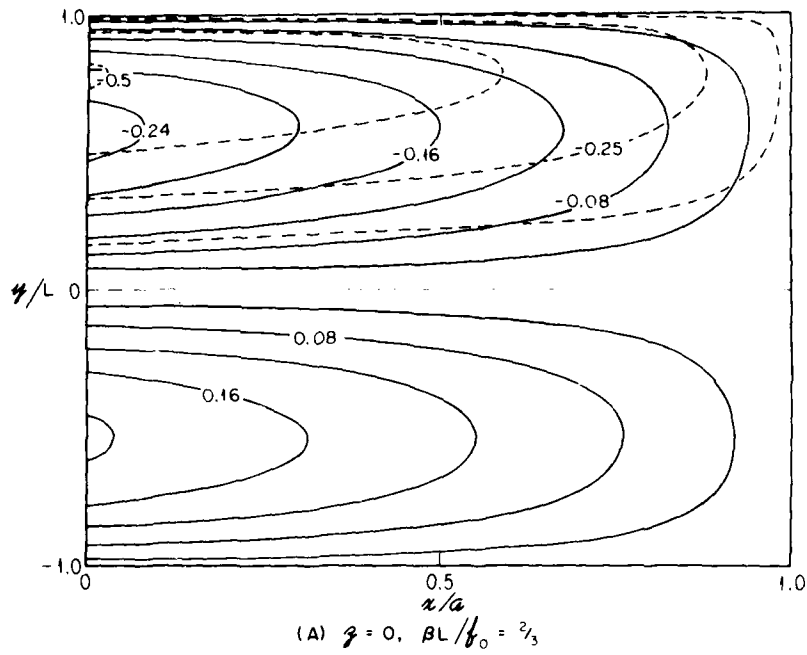
Figure 12: Plan views of the pressure field (actually $(p/\rho + gz - 1/2N^2z^2)/(1/2\ N^2H_0^2)$) and the density field (actually B/N^2H_0) at two depths in a double gyre system. The isopycnals are dotted while the isobars are solid (a) $z = 0$. The fluid in the subtropical gyre has uniform density at this depth. (b) $z = -1/2\ H(0,0)$. Note the change in the contour interval between (a) and (b). The stippled region represents motionless fluid.

double gyre system Figure (12a) is $z = 0$ while Figure (12b) is $z = -1/2 H_0$ where $H_0 = H(0,0)$. The stippled fluid in Figure (12b) has uniform density $(B = -1/2 N^2 H_o)$ and is motionless. Most of the qualitative features of the circulation patterns above are already present in the simpler quasigeostrophic model of YR.

5. Conclusions

It is ironic that after twenty years of contriving similarity "solutions", which are unable to satisfy both horizontal and vertical boundary conditions, it is now a simple matter to construct a variety of solutions all of which satisfy the same physically reasonable boundary conditions. Admittedly these solutions have weak singularities (e.g., w_{zz} is discontinuous at $z = -H$) but without introducing some explicit dissipation it is impossible to argue that these singularities are unphysical. In the ocean, dissipation is present and this study emphasizes its importance in selecting a unique solution.

Acknowledgements

REFERENCES

Holland, W. R., 1982. Regions of uniform potential vorticity in circulation models with mesoscale resolution. In preparation.

Luyten, J. R., Pedlosky, J., and H. Stommel, 1983. The ventilated thermocline. Accepted by Journal of Physical Oceanography, v. 13, p. 292-309.

Montgomery, R. B., 1938. Circulation in upper layers of southern North Atlantic deduced with use of isentropic analysis. Paper Physical Oceanography Meterology, v. 6(2), 55 pp.

Needler, G., 1967. A model for the thermohaline circulating in an ocean of finite depth. Journal of Marine Research, v. 25, p. 329-342.

Pedlosky, J., 1979. Geophysical Fluid Dynamics, Springer-Verlag, New York, Inc.

156

Phillips, N. A., 1963. Geostrophic motion. Review of Geophysics, v. 1, p. 123-176.

Rhines, P. B. and W. R. Holland, 1979. A theoretical discussion of eddy driven mean flows. Dynamics and Atmosphere in the Oceans, v. 3, p. 289-325.

Rhines, P. B. and W. R. Young, 1982(a). A theory of the wind-driven circulation I. Mid-Ocean Gyres. Journal of Marine Research, v. 40, Supplement, p. 559-596.

Rhines, P. B. and W. R. Young, 1982(b). Homogenization of potential vorticity in planetary gyres. Journal of Fluid Mechanics, v. 122, p. 347-367.

Welander, P., 1971. Some exact solutions to the equations describing an ideal fluid thermocline. Journal of Marine Research, v. 29, p. 60-68.

Young, W. R. and P. B. Rhines, 1982. A theory of the wind-driven circulation II. Circulation models and western boundary layer. Journal of Marine Research, v. 40, p. 849-872.
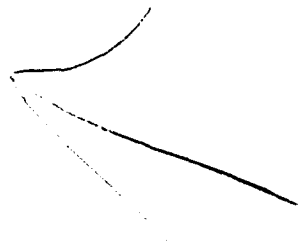
HAMILTON'S PRINCIPLE AS THE BASIS FOR OCEAN CIRCULATION MODELS

Rick Salmon

Scripps Institution of Oceanography A-025
La Jolla, California, 92093

Hamilton's principle of mechanics governs the motion of the geophysical fluids. As a statement of dynamical law, it has the following practical advantages over the more conventional Eulerian formulation of fluid dynamics:

1. It is extremely succinct. This means, for example, that once the exact Hamiltonian has been replaced by a discrete numerical analogue, then the numerical analyst has no further opportunity to exercise his bias. The principle of least action dictates the evolution equations for the discrete dependent variables.

2. Hamiltonian methods easily accomodate moving, disconnecting fluid boundaries. I believe, for example, that separated boundary currents are unrealistically unstable in models which prohibit the main thermocline from outcropping. However, Eulerian numerical methods cannot cope well with the outcrop.

3. There exists a well-known connection between the symmetry properties of the Hamiltonian and the conservation laws of the dynamical system. Analytical and numerical approximations which maintain these symmetries will automatically preserve the analogues of exact constants of the motion.

This talk will demonstrate how Hamilton's principle permits useful numerical approximations to the equations governing the motion of a shallow rotating fluid blob. Salmon (1982) used a similar model system for a numerical study of the ocean's main thermocline. However, the methods described here are distinctly superior to those of the earlier paper. The new methods generalize easily to continuously stratified and multi-layer flows.

A more complete description of the numerical experiments is given by Salmon (1983). That manuscript also illustrates the use of Hamilton's principle to derive a "balanced" approximation to the primitive equations of motion. The approximation closely resembles the well known "semi-geostrophic" equations, but, unlike the latter, it conserves proper analogues of the total energy and potential vorticity on fluid particles in the general case of nonconstant coriolis parameter. These conservation properties are guaranteed a-priori, because the approximation respects the time- and particle label symmetries of the exact Hamiltonian.

158

NUMERICAL EXAMPLE

The Hamiltonian for a rotating blob of homogeneous hydrostatic fluid is

$$(1) \qquad H = \frac{1}{2} \iint da\, db \left[u^2 + v^2 + y\, \frac{\partial(a,b)}{\partial(x,y)} \right].$$

The horizontal coordinates

$$(2) \qquad x(a,b,t)\ ,\quad y(a,b,t)$$

and velocity components

$$(3) \qquad u(a,b,t)\ ,\quad v(a,b,t)$$

of the fluid particles are considered to be functions of the labeling coordinates (a,b), which remain constant following particles, and the time t. The labels are assigned such that

$$(4) \qquad da\, db = d(mass)$$

and

$$(5) \qquad h = \frac{1}{\rho}\, \frac{\partial(a,b)}{\partial(x,y)}$$

is the fluid depth. The usual momentum equations

$$(6) \qquad \frac{D}{Dt} u - fv = -g\, \partial h/\partial x\ ,\quad \frac{D}{Dt} v + fu = -g\, \partial h/\partial y$$

result from Hamilton's principle in the form

$$(7) \qquad \delta \int dt \iint da\, db \left[(u-R)\partial x/\partial t + (v+P)\partial y/\partial t \right] - H = 0,$$

where δ stands for arbitrary independent variations $\delta x, \delta y, \delta u, \delta v(a,b,t)$ and $R(x,y)$ and $P(x,y)$ are any two functions satisfying

$$(8) \qquad \frac{\partial R}{\partial y} + \frac{\partial P}{\partial x} = f.$$

Suppose that the continuous fluid blob is replaced by a collection of N discrete particles, each with mass m. Let (x_i, y_i) and (u_i, v_i) be the position and velocity of the i-th particle. According to (5) the fluid depth is proportional to the mass per unit area. This motivates the replacement

$$(9) \qquad h(\underset{\sim}{x}) = \frac{m}{\rho}\, n(\underset{\sim}{x})$$

where

$$(10) \qquad n(\underset{\sim}{x}) = \sum_i S(|\underset{\sim}{x_i} - \underset{\sim}{x}|)$$

is a smooth estimator of the number of particles per unit area. For example,

(11)
$$S(r) = \frac{10}{3\pi r_c^2} \begin{cases} (1 - 3(r/r_c)^2 + 2(r/r_c)^3), & r < r_c \\ 0, & r > r_c \end{cases}$$

The parameter r_0 controls spatial resolution. Now replace the Lagrangian (7) by the discrete numerical analogue

(12)
$$L = \sum_i m \left[(u_i - R_i) \dot{x}_i + (v_i + P_i) \dot{y}_i - \frac{1}{2}(u_i^2 + v_i^2 + \frac{mg}{\rho}n(x_i)) \right]$$

and obtain the discrete equations of motion by the variations δx_i, δy_i, δu_i, $\delta v_i(t)$.

I illustrate the method by application to a problem of current interest. Griffiths, Killworth, and Stern (1982) recently described a new parallel flow instability for the same fluid system considered here. They suppose that the initial blob is a narrow fluid annulus in near-geostrophic balance. If the annulus width is comparable to the Rossbv deformation radius, then the annulus develops varicose meanders. The meanders grow, and the annulus eventually breaks up into a ring of anti-cyclonic eddies.

Figures 1 and 2 show the results of numerical experiments with the particle model described above. The two experiments have nearly the same number of particles per sampling area πr_0^2, but r_0 is twice as large in experiment 1 as in experiment 2. The end states are similar, and closely resemble the laboratory experiments of Griffiths et al.

REFERENCES

Griffiths, R.W., P.D. Killworth, and M.E. Stern, 1982. Ageostrophic instability of ocean currents. J. Fluid Mech. 117, 343-377.

Salmon, R. 1982. The shape of the main thermocline. J. Phys. Oceanog. 12(12), 1458-1479.

Salmon, R. 1983. Practical use of Hamilton's principle. (submitted).
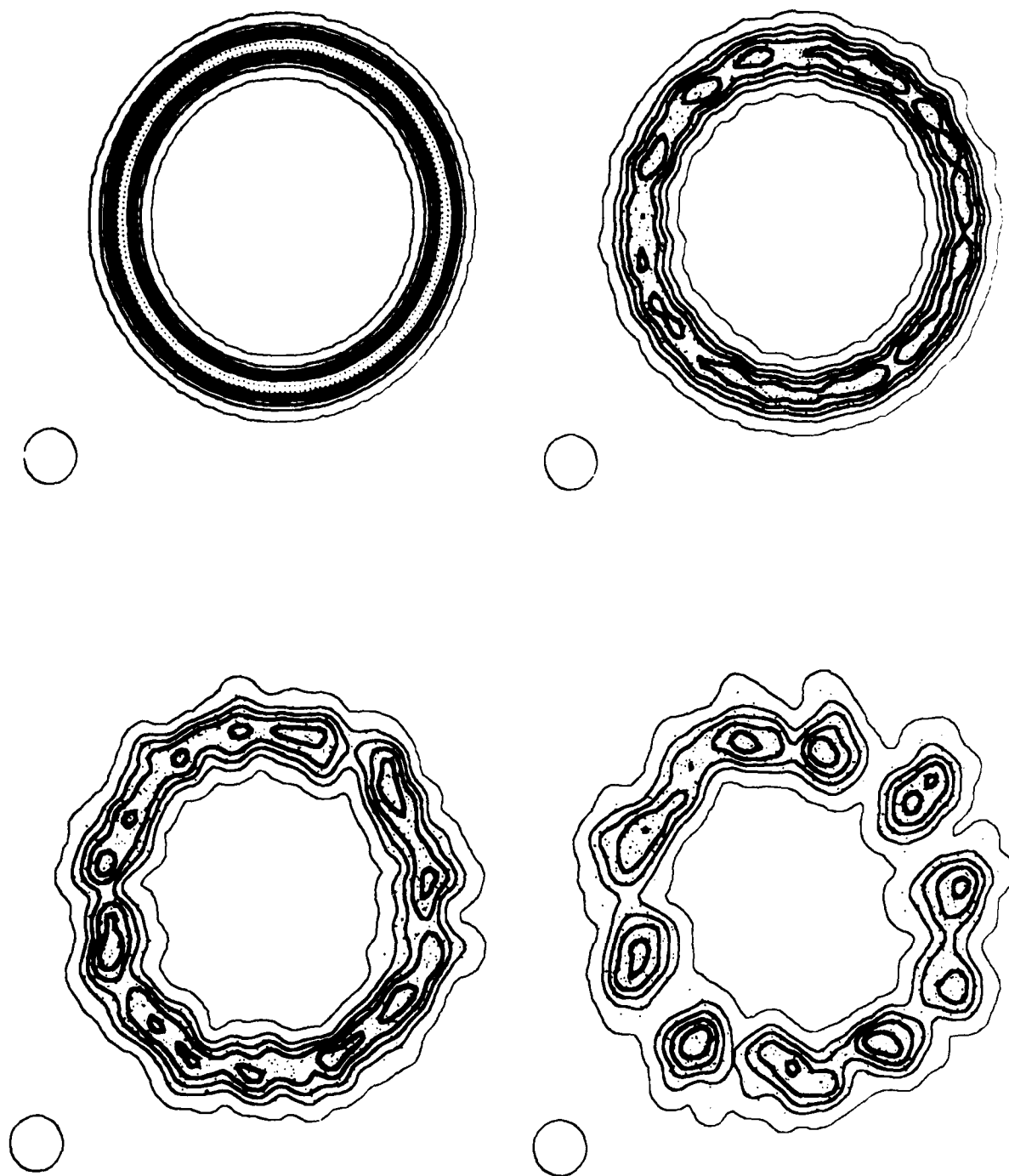
Fig. 1.   The fluid annulus after 0, 2.0, 3.6, and 6.4 rotation periods.   The
small dots are fluid particles.   Darker contours correspond to greater fluid
depth.   The circles at lower left have radius r_0.
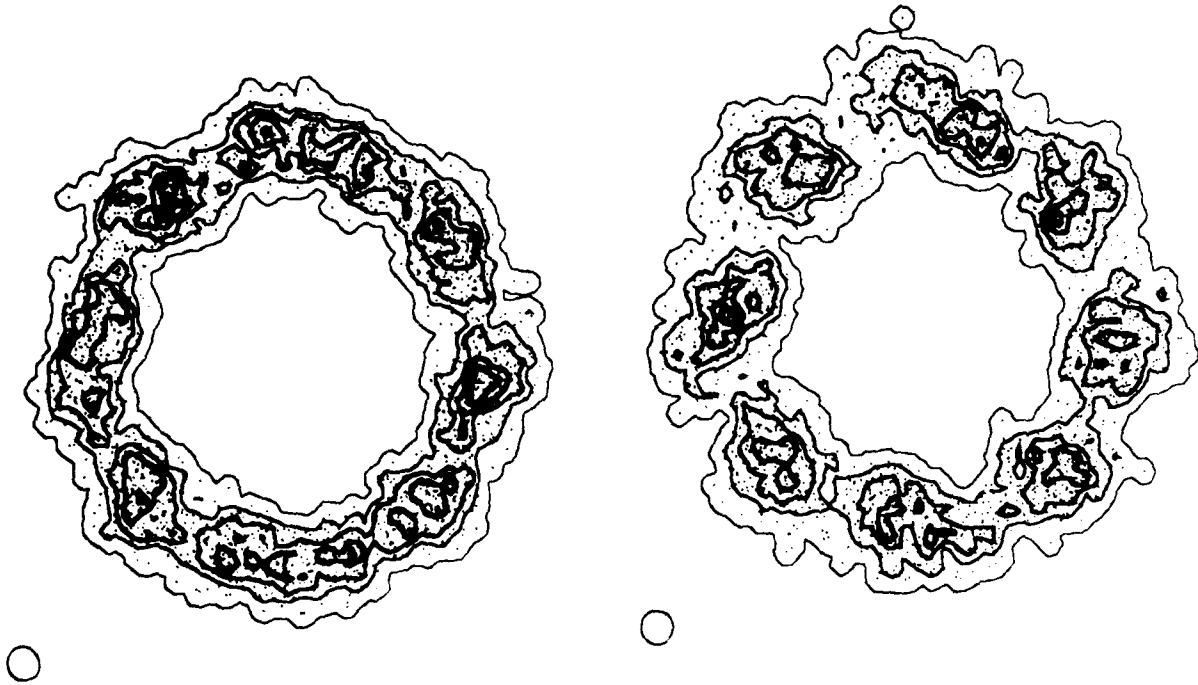
Fig. 2. The same experiment after 6.4 and 9.5 rotation periods with a finer resolution (smaller r_0).

ON THE DRIVING OF OCEAN CURRENTS BY ROSSBY WAVES

Lorenz Magaard

Department of Oceanography and Hawaii Institute of Geophysics,
University of Hawaii at Manoa, Honolulu, Hawaii 96822

For about the last seven years I have studied baroclinic Rossby waves
in various parts of the North Pacific. I have summarized some of the
results, concerning the potential energy of these waves, in a new paper
(Magaard, 1983). Two results of that work are presented here: Figure 1
shows a standard spectrum of baroclinic Rossby wave potential energy for a
5° square just east of the Hawaiian Archipelago($20-25^{\circ}$N, $160-165^{\circ}$W).
This spectrum shows a peak at 0.15 cpy (6.7 years) and a broad peak
ranging from about 0.5 to 1.4 cpy (2.0 to 0.7 years). Between 0.3 and 0.4
cpy I hypothesize a spectral gap. This spectrum will be an input function
to the study of the driving of ocean currents to be presented here.
Figure 2 shows the geographical distribution of the 6.7 year peak around
Hawaii. The peak disappears rapidly as one goes to the north; it has
practically disappeared north of 25°N. The remarkable east-west
sequence of this peak is as yet unexplained.

During my recent sabbatical year at the University of British
Columbia at Vancouver, Canada, Lawrence Mysak and I looked into the
possiblity of these observed waves driving mean ocean currents. This has
led to some results and a number of open questions that I would like to
present in this workshop.

In general, waves can drive currents by a divergence of their mean
momentum flux (radiation stress) leading to a Eulerian secondary flow and,
second, a Stokes drift can be associated with waves. By definition of our
wave models, the observed waves form a random wave field that is
stationary and horizontally homogeneous at least over 5° degree
squares. In an inviscid fluid such waves have a vanishing divergence of
their mean momentum flux and also have vanishing Stokes drift. Mysak and
I have studied the question of what happens when the Rossby waves observed
east and north-east of the Hawaiian Ridge impinge upon that ridge. For
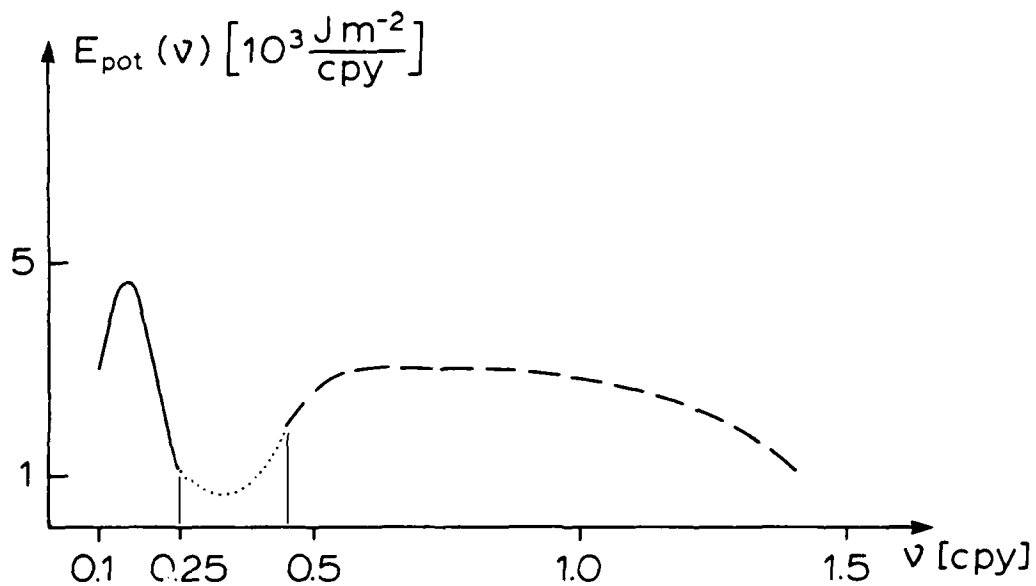
Fig. 1. Smoothed Rossby wave potential energy spectrum $E_{pot}(\nu)$ for the square 20-25°N, 160-155°W (from Magaard, 1983). Full line, after Price and Magaard (1980) and Price (1981); dashed line, after Price (1981) and Price and Magaard (1983); dotted line, hypothetical. Relative standard errors are 25 to 50%.
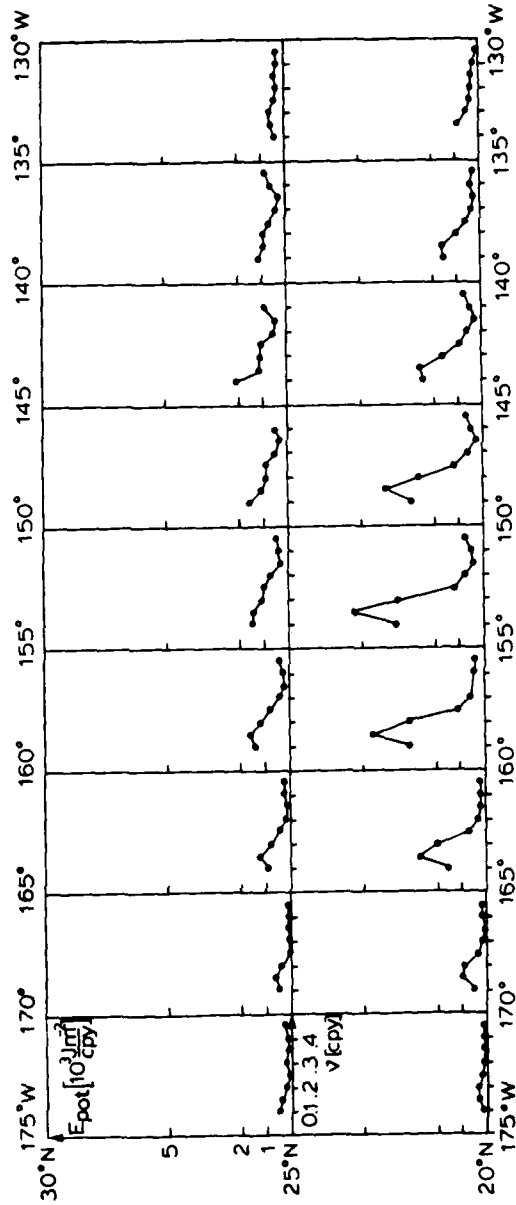
Fig. 2. Rossby wave potential energy spectra $E_{pot}(\nu)$ at 5° squares between 20 and 30°N, 175 and 130°W (from Magaard, 1983). These standardized results are derived from Price and Magaard (1980) and Price (1981). Relative standard errors are 25 to 50%.

this study we have taken the ridge as a vertical wall of infinite length making an angle $\alpha = 25°$ with the circles of latitude. The waves are reflected from that ridge, and for an inviscid ocean it is trivial to calculate the reflected wave field. We have calculated the Eulerian secondary flow produced by the total wave field consisting of the observed incoming and the calculated reflected waves. This total wave field is horizontally inhomogeneous with respect to the cross-ridge coordinate, and the divergence of its momentum flux turns out to be proportional to $\sin \alpha$. This is in accordance with the Eliassen-Palm theorem (Eliassen and Palm, 1961) according to which, in an inviscid fluid, the Reynolds stress of Rossby waves, which are stationary and homogeneous in the east-west direction, has a vanishing divergence. Hence, if the Hawaiian Ridge was zonal our waves would not lead to a Eulerian mean flow, but since $\sin \alpha \neq 0$ we get a Eulerian mean flow even in the inviscid case.

The general problem of Rossby wave mean flow interaction has been studied a great deal since 1961, and I would like to mention papers like Moore (1970), Holton (1974 and 1975), Boyd (1976), McWilliams (1976), Andrews and McIntyre (1976), McIntyre (1980), and Schoeberl (1981). These papers show that, for inviscid flow, there are very general non-acceleration theorems for Lagrangian mean flows such that the Eulerian mean flow produced by Rossby waves is exactly offset by the Stokes drifts of the waves. In viscous fluids, however, these non-acceleration theorems do not hold. We calculated the Stokes drift of our waves and indeed, it cancelled the Eulerian mean flow exactly. On the basis of his paper (Moore, 1970), Dennis Moore had predicted just that.

Now we had two reasons to introduce friction to our study: Our inviscid Eulerian flow assumed ridiculously large values (50 to 100 m s^{-1}), and we wanted to have a net Lagrangian effect. We decided to use Rayleigh damping because it is easiest to handle, and Muller and Frankignoul (1981) have shown that, for quasigeostrophic baroclinic motion, Rayleigh damping is more appropriate than bottom friction or horizontal diffusion. Also, they came up with a value of $R = 5 \times 10^{-8}$ s^{-1}, a value that we found appropriate for our work. We made the reflected waves subject to friction, i.e. we restudied the reflection of Rossby waves under friction. Figure 3 shows the resulting Eulerian flow at the surface, and Figure 4 shows its depth dependence.

From the very beginning of our study Mysak and I were in contact with Warren White (SIO) who informed us that he could see a current from historical temperature data north of the Hawaiian Ridge. Simultaneously with our theoretical study, White worked out the details of the current that he could infer from the historical temperature data. Figure 5 shows White's results of a temperature profile at a depth of 300 m running normal to the northeast coast of Hawaii at $20°N$. His figure further shows the vertical shear of the corresponding geostrophic current at 300 m
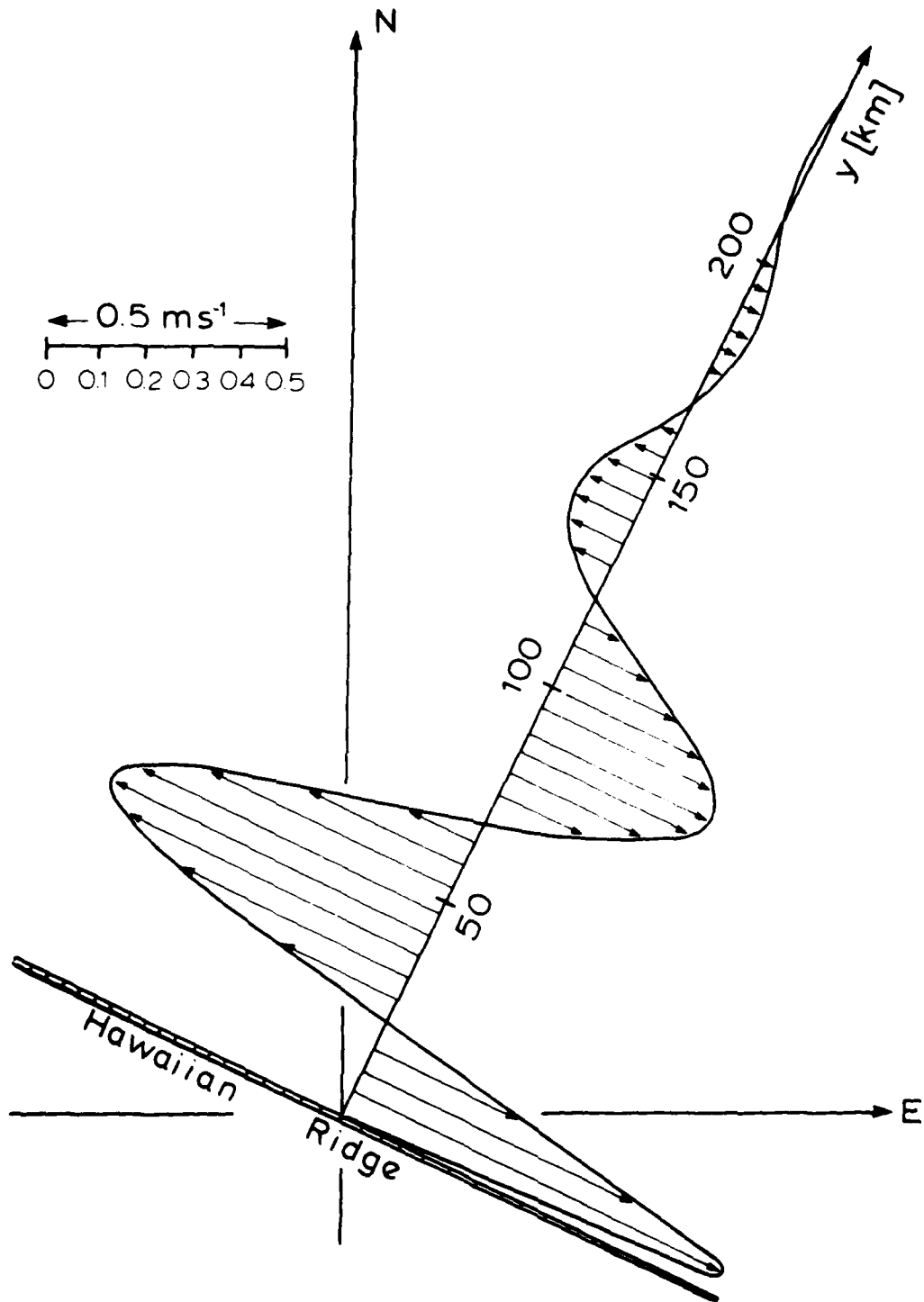
Fig. 3. The horizontal distribution of the Eulerian surface mean
flow along the north side of the Hawaiian Ridge (from Mysak and
Magaard, unpublished).

168
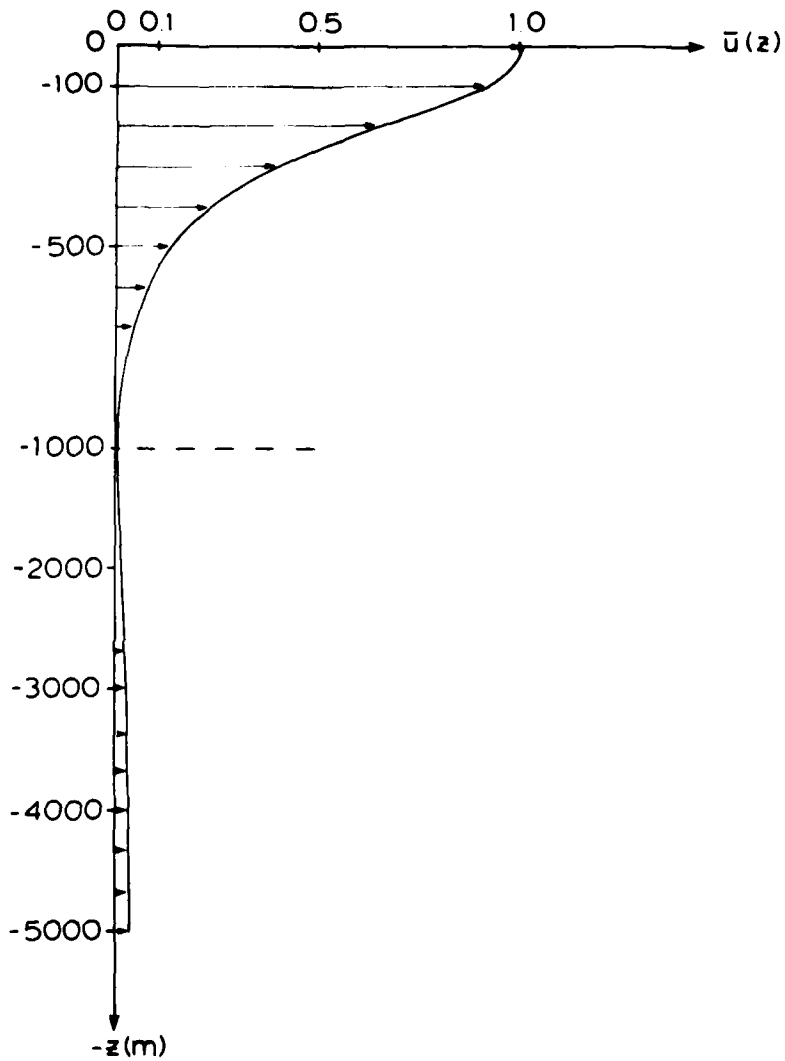
Fig. 4. Depth dependence of the Eulerian mean flow along the
   north side of the Hawaiian Ridge in relative units
   ($\bar{u}(z) = 1$ at the surface) (from Mysak and Magaard, un-
   published). Note the change in vertical scale at
   $z = 100$ m.
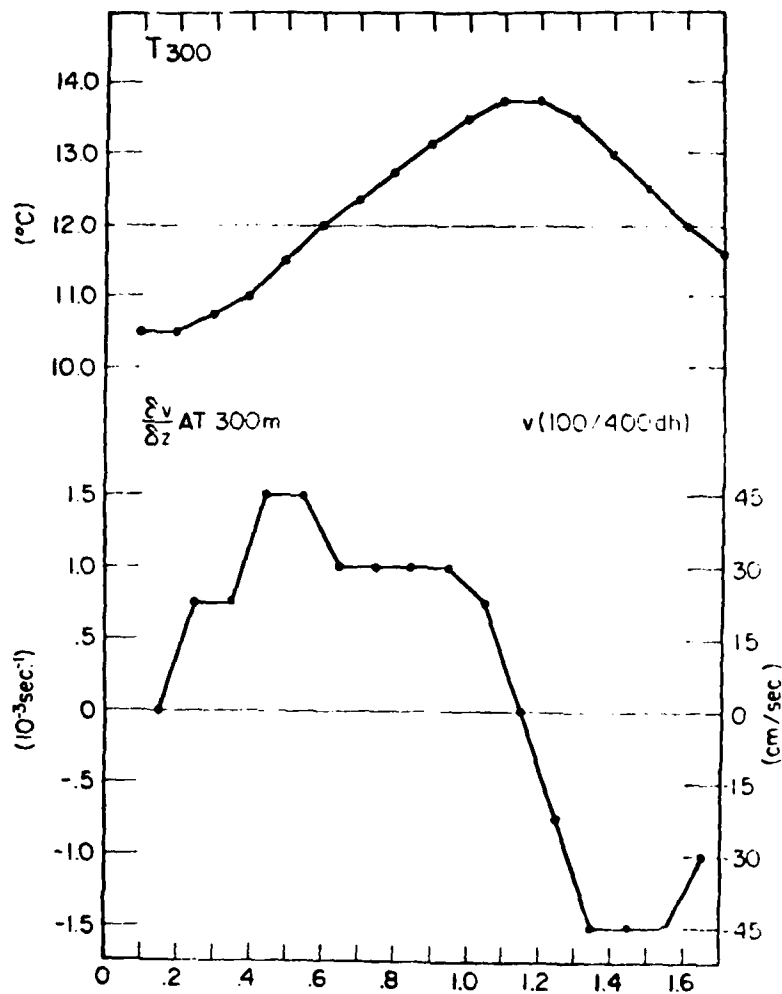
Fig. 5.   The cross-stream profile of temperature at 300 m,
the vertical shear flow, and the estimated relative geo-
strophic speed (100/400 db) normal to the profile, for
the North Hawaiian Ridge Current (from White, unpublished).

and an estimate of the resulting long-ridge current at 100 db versus
400 db (assuming constant vertical shear over the corresponding depth
range). Essential features of the Eulerian flow shown in Figure 3 and the
current shown in Figure 5 agree: a strong westward current band followed
by an eastward band of similar strength and width. If we extrapolate
White's results to a geostrophic current at the surface (versus 1000 db),
using the current profile displayed in Figure 4, we arrive at a maximum
surface current of 65 cm s^{-1}. This comes close to the maximum value
shown in figure Figure 3. Concerning the widths of the bands, White
obtains values between 70 and 100 km, whereas our values are closer to
50 km.

In addition to the Eulerian mean flow my colleague Im Sang Oh (UH)
and I calculated the Stokes drift and the Lagrangian flow resulting from
our wave field. Figure 6 shows the Eulerian flow (as in Fig. 3) and the
Lagrangian flow. I am convinced that the near-ridge part of the flow will
need a revision. We have not used a non-slip condition at the wall and we
have disregarded the influence of the mean flow on the incoming and, most
notably, on the reflected waves.

We checked further into the question of why the inviscid Eulerian
meanflow was so absurdly large. To that end we calculated the
characteristic

velocities U and the β - Rossby number $\epsilon = \dfrac{2Uk^2}{\beta}$, where k is the

wavenumber, of the incoming and reflected waves. For the incoming annual
waves we found ϵ - values between 0.1 and 1 and for the 6.7-year waves
ϵ = 3x10^{-2}. For the formally calculated inviscid reflected waves
ϵ = 4x10^1 for the annual and ϵ = 4x10^3 for the 6.7-year "waves".
Hence these reflected "waves", that have characteristic velocities of
U = 1.5x10^{1}cm s^{-1} and U = 5x10^{1}cm s^{-1}, respectively, cannot
propagate as free waves, and the answer to the question of what happens
when the incoming waves impinge upon the ridge, cannot be found by
studying a linear reflection process.

For R = 5x10^{-8}s^{-1} we have a relaxation time of 200 days. That
extinguishes the 6.7-year waves completely and clearly mutilates even the
annual waves. Hence, at this point, one can doubt whether the whole
process of wave relection applies to this case or not. We are planning to
repeat our study introducing a non-slip boundary condition at the wall.
If that does not lead to reasonable results the application of numerical
methods to study this nonlinear process might be the only viable way to
the solution of the problem.
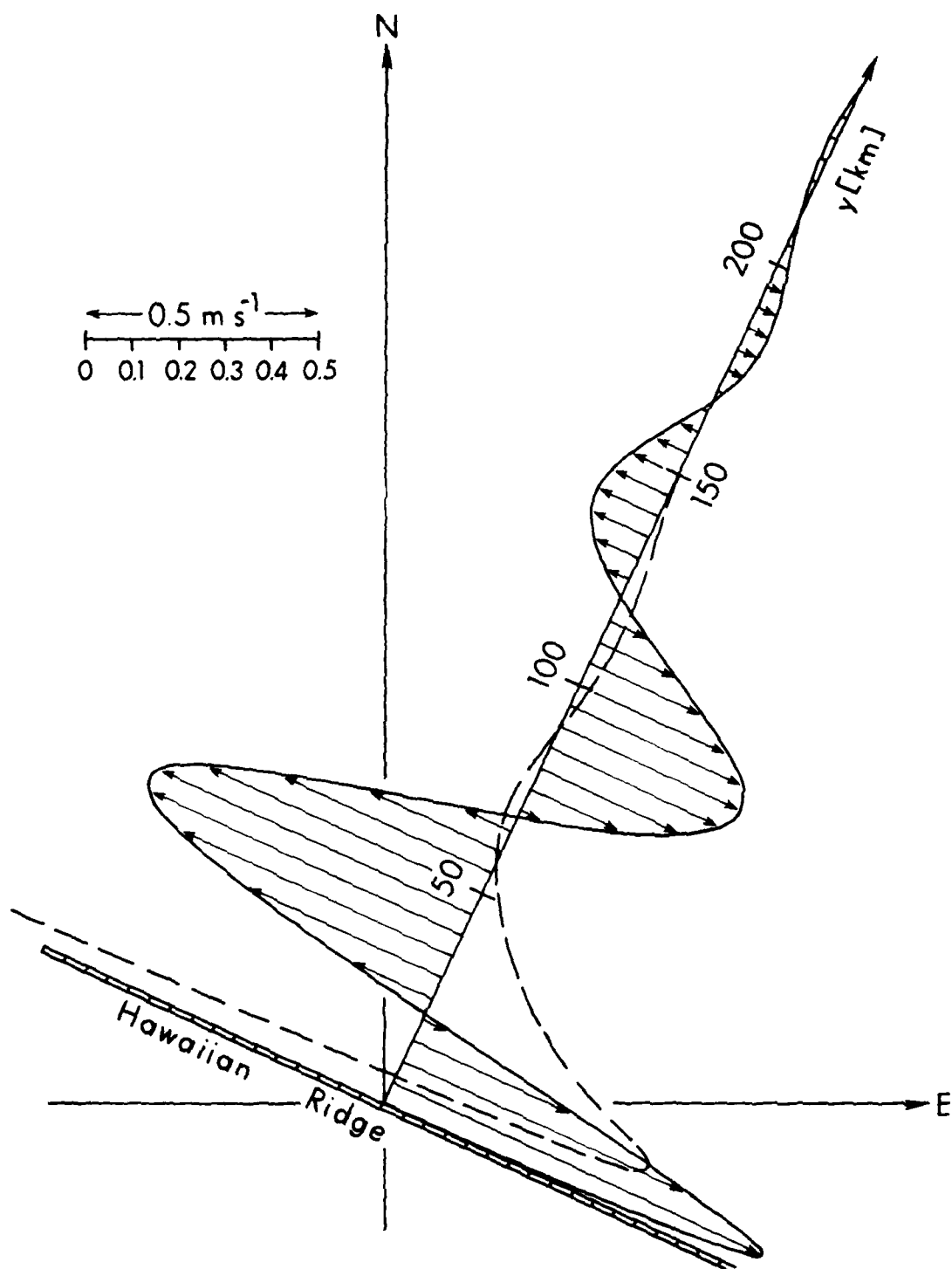
Fig. 6. The horizontal distribution of the surface mean flow
along the north side of the Hawaiian Ridge. Full line,
Eulerian mean flow (after Mysak and Magaard, unpublished);
dashed line, Langrangian mean flow (after Oh and Magaard,
unpublished).

172

In conclusion, we have calculated a Rossby-wave driven Eulerian mean flow along the Hawaiian Ridge which compares reasonably well with a current that was inferred from a weak historical temperature data base. Concerning this flow and the corresponding Lagrangian mean flow there are open theoretical questions that we are working on. In addition, we might go out and try to prove the existence of the hypothesized Eulerian mean flow by new observations.

REFERENCES

Andrews, D. G. and M. E. McIntyre, 1976. Planetary waves in horizontal and vertical shear: The generalized Eliassen-Palm relation and the mean zonal acceleration. J. Atmos. Sci., 33, 2031-2048.

Boyd, J. P., 1976. The noninteraction of waves with the zonally averaged flow on a spherical earth and the interrelationships of eddy fluxes of energy, heat and momentum. J. Atmos. Sci., 33, 2285-2291.

Eliassen, A. and E. Palm, 1961. On the transfer of energy in stationary mountain waves. Geofys. Publ., 22, 1-23.

Holton, J. R., 1974. Forcing of mean flows by stationary waves. J. Atmos. Sci., 31, 942-945.

Holton, J. R., 1975. The Dynamic Meteorology of the Stratosphere and Mesosphere. Am. Meterol. Soc., Boston, Massachusetts.

Magaard, L., 1983. On the potential energy of baroclinic Rossby waves in the North Pacific. J. Phys. Oceanogr., 13, 38-42.

McIntyre, M. E., 1980. An introduction to the generalized Lagrangian-mean description of wave, mean-flow interaction. Pure Appl. Geophys., 118, 152-176.

McWilliams, J. C., 1976. Large-scale inhomogeneities and mesocale ocean waves: a single stable wave field. J. Mar. Res., 34, 423-456.

Moore, D., 1970. The mass transport velocity induced by free oscillations at a single frequency. Geophys. Fluid Dyn., 1, 237-247.

Muller, P. and C. Frankignoul, 1981. Direct atmospheric forcing of geostrophic eddies. J. Phys. Oceanogr., 11, 287-308.

Mysak, L. A. and L. Magaard, 1983. Rossby wave driven mean flows along non-zonal barriers, with application to the Hawaiian Ridge. J. Phys. Oceanogr. (in press).

Oh, I. S. and L. Magaard. Unpublished figure.

Price, J. M., 1981. Baroclinic Rossby waves in the central and eastern Pacific. Ph.D. dissertation, University of Hawaii, Honolulu, 226 pp.

Price, J. M. and L. Magaard, 1980. Rossby wave analysis of the baroclinic potential energy in the upper 500 meters of the North Pacific. J. Mar. Res., 38, 249-264.

Price, J. M. and L. Magaard, 1983. Rossby wave analysis of subsurface temperature fluctations along the Honolulu-San Francisco great circle. J. Phys. Oceanogr., 13, (258-268).

Schoeberl, M. R., 1981. A simple model of the Lagrangian-mean flow produced by dissipating planetary waves. J. Atmos. Sci., 38, 1841-1855.

White, W. A., 1983. A western boundary current along the eastern side of the Hawaiian Ridge; the North Hawaiian Ridge Current. Submitted to J. Phys. Oceanogr.

OBSERVATIONAL EVIDENCE FOR AN EDDY-DRIVEN DEEP CIRCULATION IN THE NORTH
ATLANTIC

Nelson G. Hogg

Woods Hole Oceanographic Institution, Woods Hole MA   02543

ABSTRACT

Evidence from long-term moorings and water properties in the North West
Atlantic is presented which suggests that there are two components to the
deep, subthermocline circulation. Inshore of the 4000-m isobath is the
Deep Western Boundary Current, relatively rich in anthropogenically
derived material while offshore is a deep recirculating flow composed of
one or more gyres transporting perhaps 4 times as much water as the Deep
Western Boundary Current. The recirculating flows are similar in scale
to those described from numerical models by Holland and Rhines (1980)
although the flow under the Gulf Stream is in the opposite direction.

The thermocline heat flux in the Gulf Stream recirculation is southward
and down the mean temperature gradient. This causes a "thickness flux"
also toward the south which is of comparable magnitude to the relative
vorticity flux and, therefore, possibly the driving force for the deep
mean circulation. It appears that this "thickness flux" is driven by
spontaneous baroclinic instability of the mean flow.

INTRODUCTION

In the past decade a number of long-term moorings have been maintained in
the western North Atlantic for periods as long as 2 years. There is now
sufficient information to allow one to schematically outline parts of the
deep circulation in the region and discuss possible driving mechanisms.

The results presented in this paper are discussed more fully in two other
manuscripts: Hogg (1983) describes the mean circulation and relation to
the numerical models while Hogg (1984) gives evidence that the eddy-
driving stresses result from a baroclinic instability process.

During the 1970's mooring operations by the Woods Hole Oceanographic
Institution's (WHOI) Buoy Group expanded from short-term efforts
concentrated at Site "D" (70°W, 39°N) to large-scale arrays covering
large areas of the western North Atlantic with durations of a year or
more. (See summary in Tarbell, Chaffee, Williams and Payne, 1979).
Others have also developed mooring capabilities and extended their
interests toward the deep ocean. This study is concerned with the region

Table 1. Observational Data Base (mab = meters above bottom)

Source Label	Experiment	Number of Sites Used	Deployment Years	Nominal Duration (Days)	Nominal Instrument Depths (m)	Primary References
J	Site J	1	1970-1971	372	4000	Tarbell and Whitlatch (1977a, 1977b)
NSA	North-South Array	2	1970	130	4100-4200	Tarbell and Whitlatch (1977a)
GSA	Gulf Stream Array	3	1970	142-148	3300-4700 (200 mab)	Tarbell and Whitlatch (1977a)
L	Site L	1	1971	156	5270	Tarbell and Whitlatch (1977b)
KSA	Kelvin Seamount	7	1971	32	4600-5000 (200 mab)	Tarbell and Whitlatch (1977b)
GBA	Grand Banks	9	1972	55	3700-5500 (200 mab)	Chausse and Payne (1981)
RA	Rise Array	15	1974-1975	260	2000-4500 (200+800 mab)	Spencer (1979) Luyten (1977)
PM1	POLYMODE Array 1	2	1974-1975	254-307	4000	Spencer, Mills and Payne (1979)
BMA	Bermuda Microstructure	1	1975-1976	267	4000	McKee, Francis and Hogg (1981)
PM2	POLYMODE Array 2	15	1975-1977	235-780	4000	Tarbell, Spencer and Payne (1978)
RH		3	1975-1977	513	4000	Hendry (1982)
PR	Blake-Bahama	2	1977-1978	370	3800-5000 (200 mab)	Mills and Rhines (1979)
LDE	Local Dynamics	1	1978-1979	440	5250	Mills, Tarbell and Payne (1981) Owens, Luyten and Bryden (1982)
BWW	Bermuda Scarp	1	1978-1979	240	4260	Bird, Weatherly and Wimbush (1982)
HEBBLE	HEBBLE	6	1979-1982	170-360	4800	Weatherly (personal communcation)
GSE	Gulf Stream Extension	3	1979-1980	390	4000	Levy, Tarbell and Fofonoff (1982)
EL		1	1980-1982	622	4000	Pillsbury, Bottero, Still and Laine (1982; in prep.)
RISEX	Rise Experiment	5	1980-1981	100-270	2400-3500	Peter Smith (personal communication)

bounded by longitudes 45°W and 75°W and latitudes 30°N to 45°N. In Table
1 are listed experiments in this region since 1970 in which deep currents
were measured for at least 100 days. There are two exceptions to the
100-day rule: the Kelvin Seamount Array and the Gulf Stream Array. For
both, total number of data days is well in excess of 100 days and overall
means and mean trends have been calculated.

The mean current vectors from all the experiments in Table 1 are shown in
Figure 1. An estimate of the standard error in each of these vectors is
$(2\sigma^2 \tau/T)^{1/2}$ where σ^2 is the variance, τ the integral time
scale, and T the record length (Bendat and Piersol, 1966). Published
estimates of τ range from about 10 days in the LDE experiment (Owens et
al., 1982) to 5 days over the continental rise (Hendry, 1982; "RH" in
Figure 1). For simplicity 10 days has been used for measurements in
water depths greater than 5000 m and 5 days for shallower measurements.
The significant part of the velocity vector is the thicker portion in
Figure 1.

Also shown on Figure 1 are the historical limits of the Gulf Stream's
northern edge as indicated by the location of the 15° isotherm at 200 m
depth (from Fisher, 1977). The path has a spread of about 1° from 75°W
to 65°W and then broadens downstream of the New England Seamount Chain.

THE DEEP MEAN CIRCULATION

The flow near 70°W in Figure 1 can be seen to be well organized and
westward north of the 4000-m isobath, switching to a disorganized variable
flow with an easterly trend south before becoming westerly again at
Site L (34°N) and then easterly south of 33°N. Figure 2 shows a
meridional section of the mean zonal component of velocity at 70°W north
of 36°N. South of about 38° 40'N (the 3300 m isobath) westerly flow
intensifies toward the bottom and reaches a maximum of 5 cm/sec at
38° 40'N before decreasing under the Gulf Stream. This is the
thermohaline Deep Western Boundary Current (DWBC) first hypothesized to
exist by Stommel (1958).

Richardson (1977) has directly measured the strength of the DWBC for a
period of one to two months at Cape Hatteras where the Gulf Stream and
DWBC axes cross (74°W - 75°W). The DWBC has also been observed further
south at the Blake Bahama Outer Ridge by Jenkins and Rhines (1980) ("PR"
on Figure 1). Seaward at this latitude the mean flow is weaker and in
the opposite direction (north). Richardson (1977) has tabulated a number
of attempts to estimate the transport of the DWBC and shows them to vary
from as little as 4×10^6 m³/sec (Barrett, 1965) to as much as $50 \times
10^6$ m³/sec (Volkmann, 1962). Most were from short-duration
experiments combining neutrally buoyant float data with hydrographic
computations. An integration of the westerly flow below 1000-m depth in

Fig. 1. Deep mean current vectors in the western North Atlantic from experiments listed in Table 1. Thick portion of each vector indicates that portion that exceeds the estimated standard error in the mean. Also shown is the mean path of the north edge of the Gulf Stream and its root mean square displacement as calculated by Fisher (1977) from an analysis of the position of the 15°C isotherm at 200 m. Dashed vectors near 36°N on 55°W are 1500-m measurements.

Fig. 2. Mean zonal flow in a section down 70°W. Numbers at solid dots are the mean westerly component. Numbers at top are Buoy Group sequential mooring numbers. Speeds are in cm/sec.

the section down 70°W (Figure 2) gives about 12 x 10^6 m^3/sec westerly transport, all of it shallower than the 4000-m isobath.

The picture west of the New England Seamounts suggests a spatially coherent flow only inshore of the 4000-m isobath - the DWBC. Moving east a significant change occurs. Recent HEBBLE measurements, all within 300 m of the bottom (Richardson, Wimbush, and Mayer, 1981; Weatherly and Kelley, 1982 - "H" on Figure 1) have discovered a powerful westerly flow south of the 4000-m isobath at the foot of the Continental Rise. At the same time, measurements by the Bedford Institute of Oceanography (Peter Smith, personal communication, "RISEX" on Figure 1) show that the DWBC exists shoreward of the 4000-m isobath, has comparable strength to that at 70°W, and presumably transports a similar amount of water. The HEBBLE measurements indicate a continual decrease in current strength toward the north and suggest a decoupling between the two currents. If the deeper flow were to average 5 cm/sec over a depth of 4 km and span 2° of latitude, it would transport an additional 40 x 10^6 m^3/sec not seen at 70°W. There is no good information on the vertical structure of this flow except that it is virtually depth independent over the bottom 300 m (Weatherly and Kelley, 1982).

The longest duration and most extensive set of deep measurements in this region is the POLYMODE Array 2 ("PM2") with moorings at about 1° intervals along 55°W longitude. At the north end of this array the flow is westward at about 5 cm/sec. This is south of the 4000-m isobath and presumably not the DWBC but more logically connects to the deep HEBBLE flows at 63°W. Moving south of 39°N along 55°W the flow switches to eastward then again toward the west at 36°N before changing to an insignificant eastward flow south of 35°N.

With some exceptions the flows at 55°W are zonal. Near 36°N the presence of a small-amplitude seamount induces an anticyclonic tendency to the deep vectors (Owens and Hogg, 1980) -- those at 1500 m (dashed vectors in Figure 1) are more nearly zonal. The strong northerly flow to the west of the seamount at 36°N results from an instrument placed at 5000 m for just the last setting (9 months) when the mean flow was more northerly throughout this subarea. The weak easterly flow to the east of the seamount results from the full 2 years of data and remains an anomaly.

Schmitz (1977, 1980) has noted that the meridional distribution of zonal mean flow at 70°W is similar (in pattern, not magnitude) to that at 55°W if shifted 2°N, roughly the change in position of the mean Gulf Stream. This similarity would seem to be coincidental, for the strong westerly flows at the north end of PM2 do not result from the DWBC (not sampled by PM2) as they do at 70°W.

The excess 40 x 10^6 m^3/sec transport found in the HEBBLE area at 63°W must recirculate in some manner in order to conserve water. Superposed

on Figure 3 is sketched a circulation scheme for water with potential density greater than 37.08 (referenced to 2000 dbar) from Wunsch and Grant's (1982) inversion of hydrographic data in the area using an initial 2000-m level of no motion. A similar difficulty in rationalizing the flow east of the seamounts with that at 70°W arises. There are 10 x 10^6 m^3/sec of water flowing westerly all along the continental slope, but an additional 20 x 10^6 m^3/sec is found further offshore which does not reach 70°W but recirculates in a closed gyre.* There is, therefore, reasonable agreement in the northern half of the region where flow is mainly westward but the inverse scheme proposes flow directions in the south which are opposite to those directly measured. Wunsch's (1978) inversion of the same data set offers a similar scheme while Worthington's (1976) is similar in form but has the gyre circulating in the opposite sense.

The PM2 measurements along 55°W demand a tighter circulation, and in Figure 4 an alternative is proposed which, in place of the single recirculating gyre, has two which counter-rotate. The strong eastward zonal flow from 36° 30'N to 37° 30'N has been found by Schmitz (1977, 1980) to be only weakly depth-dependent up to 600 m and is quite capable of transporting the excess 40 x 10^6 m^3/sec observed at 63°W. The shorter term Kelvin Seamount (KSA) and Grand Banks (GBA) Arrays support this picture, and KSA, GBA and PM2 together indicate that the center of the cyclonic gyre is between 38°N and 39°N.

The southern, anticyclonic gyre has also been proposed by Schmitz (1980) and Richardson (1981) based on a map of temperature at 450 m (in the thermocline) averaged over 1° squares. Both authors suggest that this gyre is at least partially closed east of the Seamount Chain. There are two sites from PM1 and PM2 which indicate a continuation of the easterly flow at 55°. Based on the direct measurements alone, the more southern gyre's existence must be viewed with some caution. It is entirely possible that there are several, smaller-scale gyres. If the flows are dominantly depth independent (a good approximation at 55°W where there are vertical profiles available but clearly not reasonable under the Gulf Stream) then there would appear to be more water flowing east between 37°N and 38° 30'N than there is toward the west north of this point. This would demand some recirculation of the westward flow observed between 35°N and 36°N: hence a second gyre.

The other two gyres sketched in Figure 4 are somewhat weaker and even more uncertain. The very strong flow seen on the eastern escarpment of the Bermuda Rise ("BWW" on Figure 1) would seem to result from a local

---

* The 40 x 10^6 m^3/sec is assumed to be distributed uniformly below 1000 m. One-half to two-thirds of this would be below the 37.08 potential density surface giving comparable estimates to those of Wunsch and Grant (1982).

182
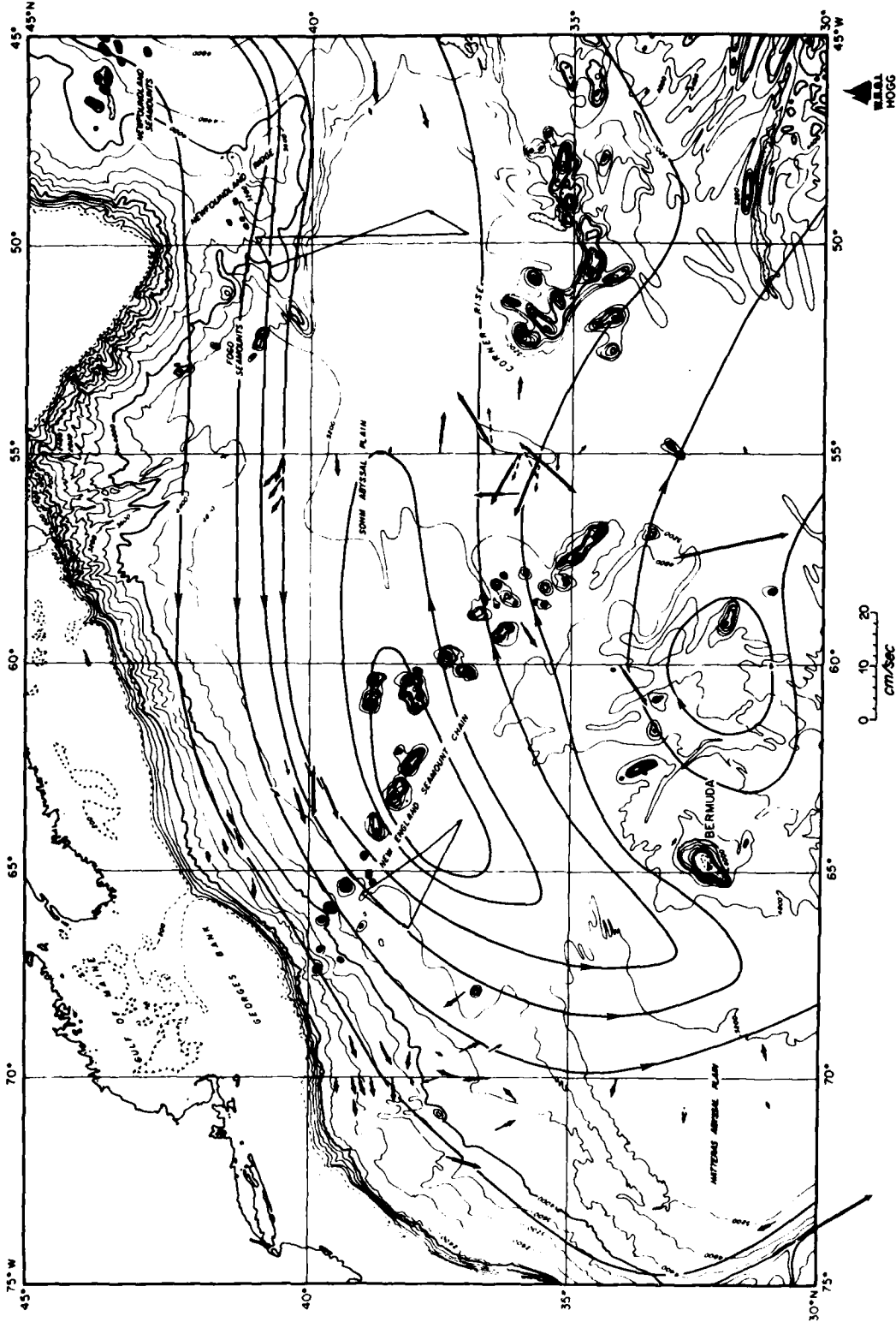
Fig. 3. A circulation scheme from Wunsch and Grant (1982) for water with potential density greater than 37.08 referenced to 2000 dbar. Each contour represents $5 \times 10^6 \mathrm{m}^3/\mathrm{sec}$. The 37.08 surface ranges in depth between 2000 m and 3000 m from the sea surface.
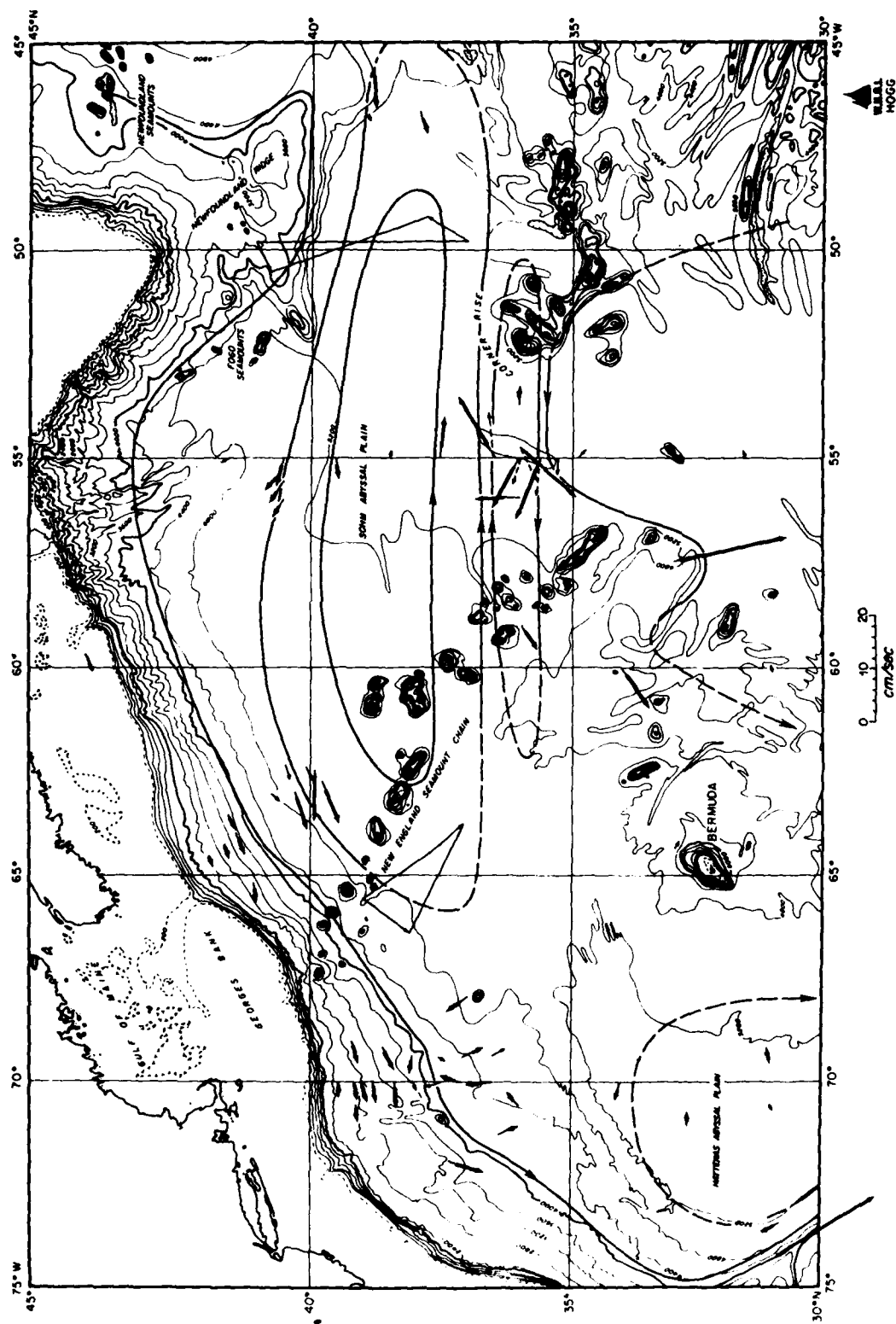
Fig. 4. A proposed circulation scheme for the deep water (sub-thermocline) based solely on the available long-term current meter data. Each contour is about 10 x 10⁶ m³/sec. Dashed portions are meant to indicate somewhat less certainty.

intensification of the circulation by the convergent isobaths, much as is the case in the DWBC at the Blake Bahama Outer Ridge.

One view of the hypothesized circulation in Figure 4 is that it is the largest pattern which is consistent with the directly measured currents. The fact that it is quite different from those schemes based solely on hydrography is, at least, partly because there is no level surface of nearly no motion. Under the axis of the surface Gulf Stream the deep flow is in the opposite direction, yielding an intermediate level of no motion. From 35°N to 37° 30'N along 55°W Schmitz (1977, 1980) finds the mean flow to be nearly depth independent. Of course, the hydrographic sections give inherently a different view of the circulation, each being quasi-synoptic but taken at different times over a period of several years. Viewed in this light the comparison between Wunsch and Grant's (1982) scheme (Figure 3) and Figure 4 is surprisingly good especially to the north where the intermediate reference level is appropriate.

Water property measurements also suggest that the recirculating flow regime is separate from the classical DWBC found shoreward of the 4000-m isobaths. The most graphic evidence that this water is of recent surface origin comes from measurements of anthropogenic tracers. Recent measurements of dissolved freon (from refrigerants, aerosol sprays) in the Transient Tracers in the Ocean (TTO) program have been made east of the New England Seamounts along about 57°W (R. Gammon and P. Hammer, personal communication). Here there is a prominent maximum concentration north of the 4000-m isobath and much lower values south much like the velocity section at 70°W in Figure 2 and very convincing evidence that the deep flows north and south of the 4000-m isobath have different sources.

DRIVING MECHANISMS

In the previous section, a proposal has been made to consider the deep circulation in the western North Atlantic as being composed of two distinct parts; a thermohaline current with origin at surface of the Norwegian Sea which hugs the Continental Rise above the 4000-m isobath and an additional circulation offshore composed of multiple recirculating gyres. Stommel (1958) has shown that the thermohaline flow is a natural consequence of bottom water formation processes on a rotating, spherical earth. Empirical evidence suggests that eddy Reynolds stresses are also important in maintaining this circulation.

Numerical experiments suggest that the vertical momentum flux, the so-called interfacial form drag, may be more important than the lateral flux (Rhines and Holland, 1979; Holland and Rhines, 1980). The mean streamfunction patterns for Holland's experiments (a symmetrically driven two-layer model), show broad upper-layer gyres with a Gulf Stream jet at

the zero wind stress curl latitude, but multiple counter-rotating gyres in the bottom layer with much smaller meridional scale forced by vertical eddy momentum transfer. Lateral Reynolds stresses, along with bottom friction, actually act to dissipate this input to the lower layer in the numerical model.

In the time-averaged mean vorticity equation the eddy vorticity flux $\overline{u'Q'}$ is composed of two terms, a relative vorticity flux $\overline{u'\zeta'}$ and a "thickness" flux $\frac{f_o}{H}\overrightarrow{u'\eta'}$. H is the lower layer thickness and η' the interface perturbation height. In the numerical model discussed by Holland and Rhines (1980, their Figure 7), the total eddy flux is everywhere down the gradient of Q ($\sim f$) and is dominated by the thickness flux.

Direct measurement of these vorticity flux divergences is exceedingly difficult in the ocean as they contain gradients of second order quantities. The components of the relative vorticity flux can be written:

$$\overline{u'\zeta'} = \frac{\partial}{\partial x}\overline{u'v'} - \frac{\partial}{\partial y}\left(\overline{\frac{u'^2 - v'^2}{2}}\right)$$

$$\overline{v'\zeta'} = -\frac{\partial}{\partial x}\overline{\frac{u'^2 - v'^2}{2}} - \frac{\partial}{\partial y}\overline{u'v'}$$

(1)

Separating the ocean crudely into two layers at the thermocline, a measure of the lower layer thickness perturbation is $-T'/T_z$, the temperature perturbation at a fixed level in the thermocline divided by the mean vertical temperature gradient. The thickness flux is in this approximation proportional to the heat flux:

$$-\frac{f_o}{H}\overline{u'\eta'} = \frac{f_o}{H\overline{T}_z}\overline{u'T'}$$

$$-\frac{f_o}{H}\overline{v'\eta'} = \frac{f_o}{H\overline{T}_z}\overline{v'T'}$$

(2)

The PM2 measurements along 55°W are the best long-term records available in the region for calculating these vorticity fluxes and even here there is little information available for computing the zonal derivatives needed in (1). In Figure 5 the heat fluxes for two levels, 600 m and 1000 m, are shown. Consistent with the numerical experiment, the flux is practically everywhere toward the south. Figure 6 gives a comparison of the meridional thickness flux at 600 m with the meridional vorticity flux at 4000 m as estimated from (2) neglecting the zonal derivative term: thickness flux is as large as relative vorticity flux and dominates north of 36°N.

If the flux divergence is estimated from the meridional slopes in Figure 6 both fluxes act to spin up the northernmost of the gyres postulated in Figure 3. Only the relative vorticity flux divergence has the correct sign to drive the more southern one although there is a small but insignificant change in slope of the 600-m thickness flux between 35° 30'N and 36°N.

These conclusions are speculative. The fluxes discussed above are likely to have large error bars and substantial zonal structure. However, it seems clear that the vertical stress transfer may be as large as the lateral.

RELATION TO BAROCLINIC INSTABILITY

The heat fluxes shown in Figure 6 are generally southward and down the mean meridional temperature gradient. Eddies are, therefore, releasing potential energy stored in the mean, large-scale circulation, a characteristic feature of the baroclinic instability process. In Figure 7 are shown spectra of meridional and zonal components of velocity at 600 m and 4000 m averaged over three moorings in the vicinity of 36°N, 55°W. There is a significant peak at 30-day periods of similar amplitude at both deep and shallow levels. Energy near this period is responsible for the energetic quasi barotropic motions reported by Schmitz (1980). Also noteworthy is a much weaker peak near 12 days which is only apparent at 600 m.

The time-averaged flow near 36°N is toward the west and also relatively independent of depth. This is plotted for three moorings in Figure 8. Also shown is an analytic profile used by Gill, Green and Simmons (1974) in their systematic study of baroclinic instability. The growth rate and phase speed of perturbations are plotted in Figure 9a as a function of wavenumber. Two maxima exist. The slower growing long wave peak has a wavenumber of $-.019$ km^{-1} and corresponds to periods of 42 days while the short wave peak at about $-.033$ km^{-1} has a period of 20 days, not too far from the observed 30-day and 12-day peaks.
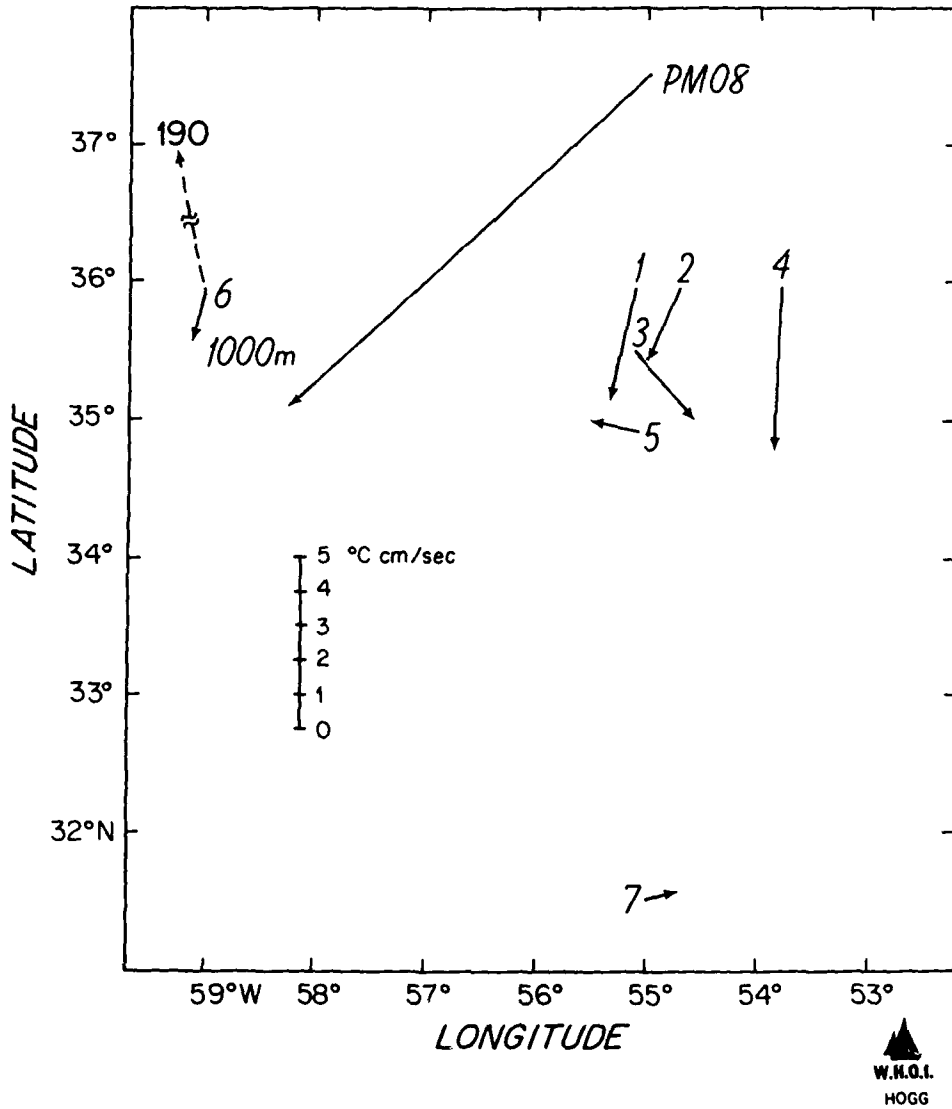
Fig. 5. Eddy heat flux from PM2 instruments. All vectors are
from 600 m with one additional vector on mooring PM06 at
1000 m. The 600-m value on this mooring is results from just
eight months of data (one setting) during which three Gulf
Stream rings passed by.

188
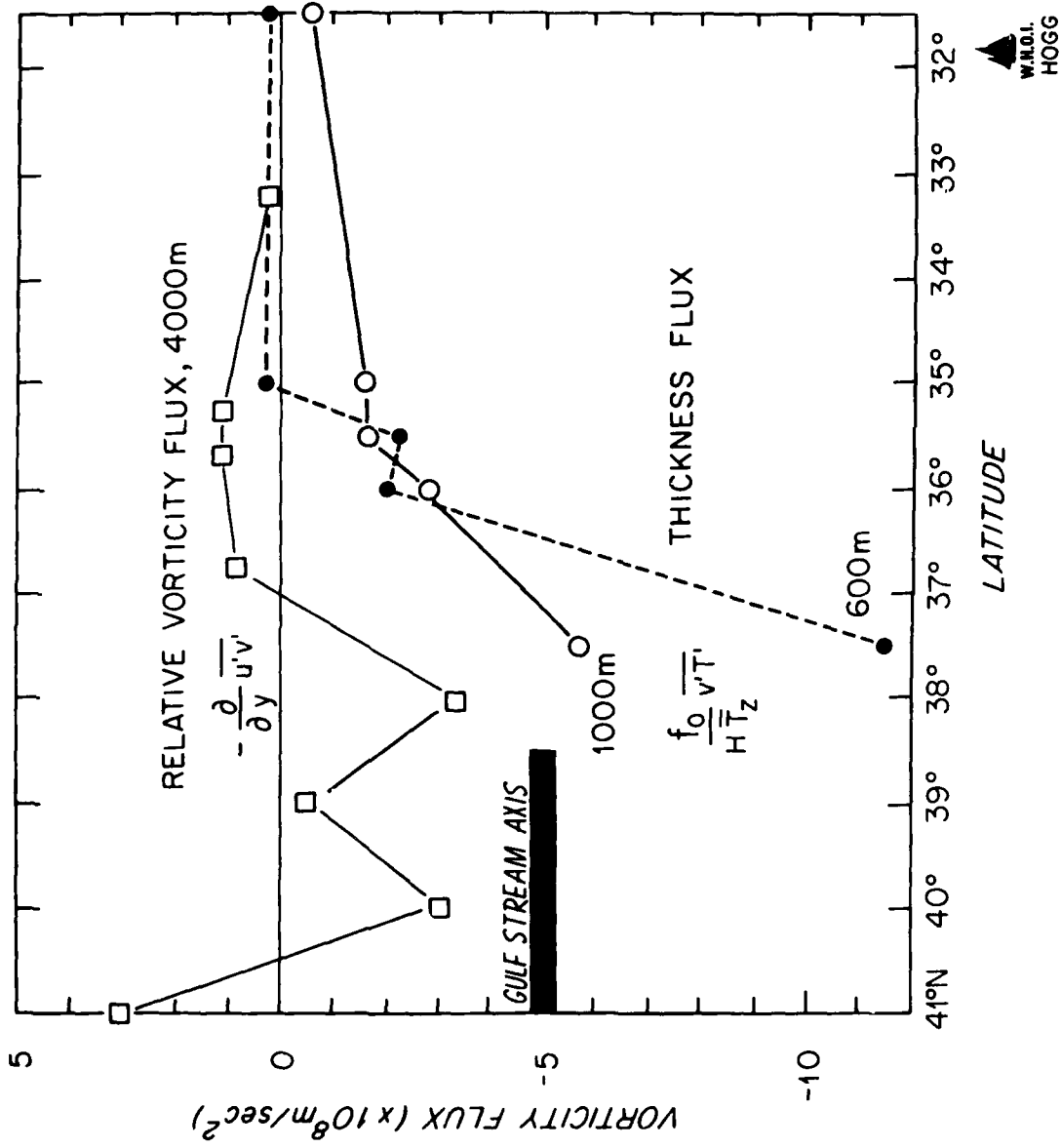
Fig. 6. Estimates of the meridional relative and thickness flux components of
the vorticity flux vector from POLYMODE Array 2 information. The solid bar
denotes the range in position of the Gulf Stream Axis from Fig. 1.
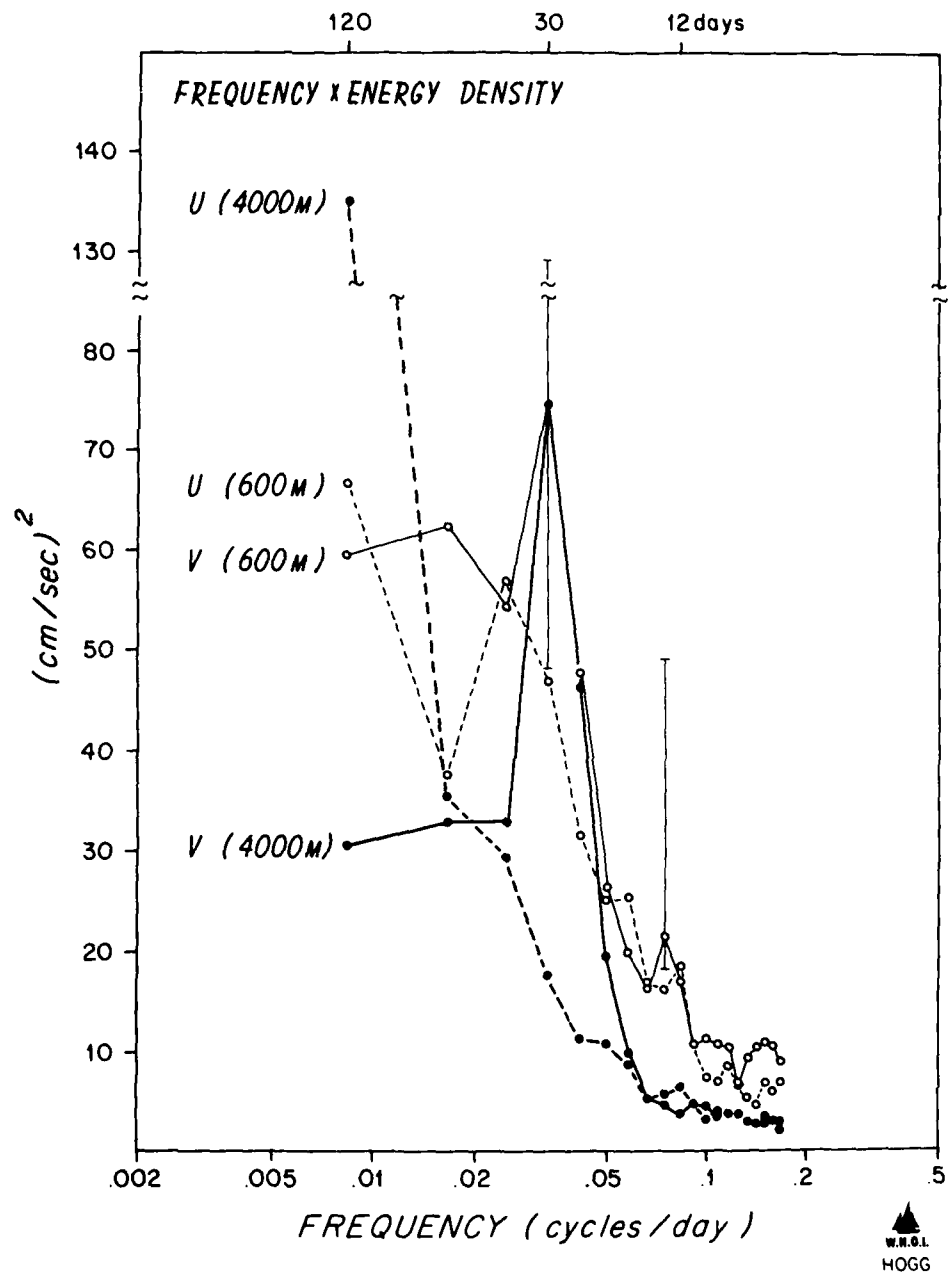
Fig. 7. A variance preserving plot of kinetic energy spectra from two depths, averaged over PM01, PM02, and P,03. The 95% confidence limits shown at 30 days and 12 days are determined from 72 degrees of freedom (3 moorings, 12 pieces, 2 degrees of freedom at each estimate).
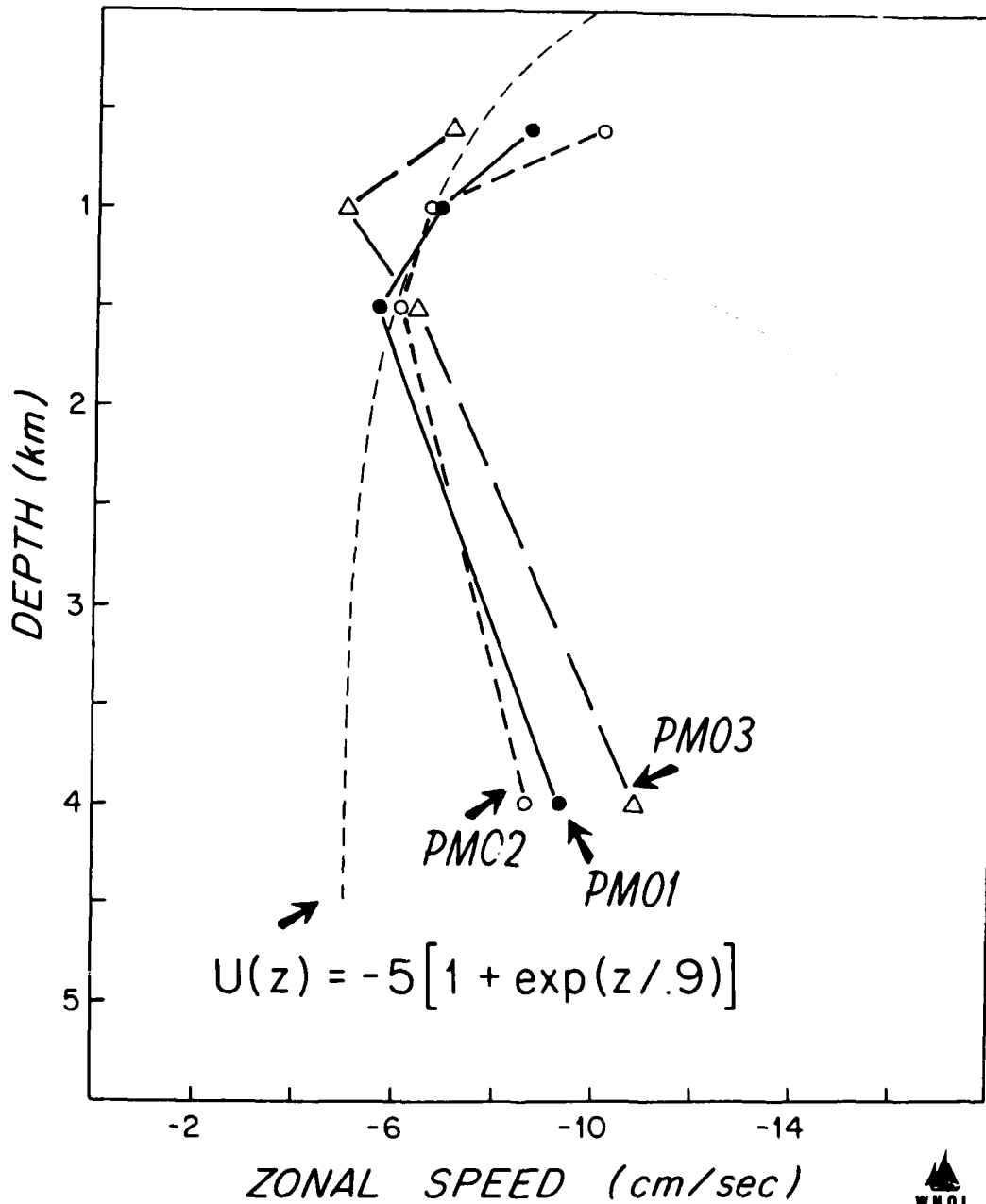
Fig. 8. Mean zonal velocity profiles at three moorings. Smooth curve is the distribution from Gill, Green, and Simmons (1974) adjusted by a uniform offset of -5 cm/sec.
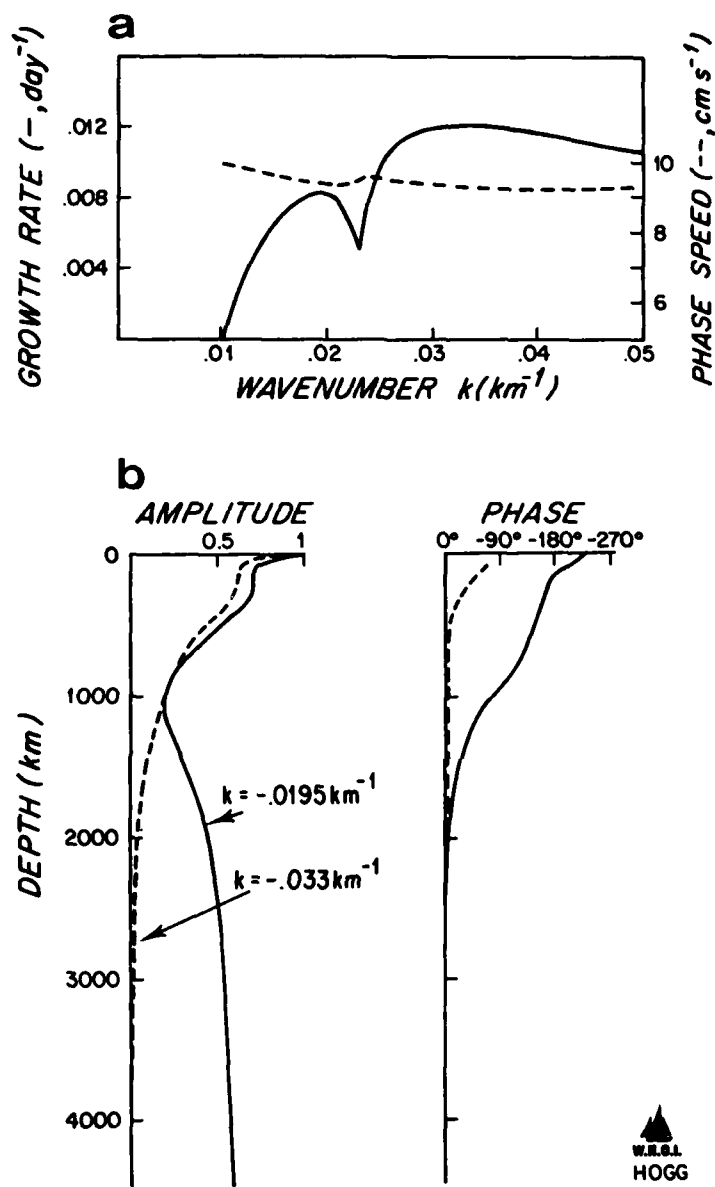
Fig. 9. (a) Calculated phase speed and growth rate as a
function of zonal wavenumber for the mean velocity
profile of Fig. 8. Adapted from Gill, Green, and
Simmons (1974).
(b) Vertical distributions of amplitude and
phase for velocity at the two growth rate peaks in (a).

The vertical structure of these unstable modes is quite revealing and is
displayed in Figure 9b. The long wave is relatively depth-independent
in amplitude but undergoes a 180° phase shift through the thermocline.
The short wave is very surface-intensified, decreasing in amplitude and
phase more or less exponentially with depth. As the top instrumented
level is at 600 m it should be no surprise that there is only weak
evidence for the most rapidly growing disturbance.

The secondary growth peak at longer wavelengths is only slightly less
rapidly growing than the primary peak and has a significant amplitude at
all depths. An empirical orthogonal function analysis in the frequency
domain of some of the time series from Polymode Array 2 has been made and
found to be a useful tool for describing the variance connected with
large-scale motions (see Hogg, 1984). For example, in Figure 10a is
shown the first EOF in a band centered at 30 days calculated from the
normalized cross-spectral matrix of all variables (east, north,
temperature) observed at four depths on 3 moorings along 36°N. Note that
phase progresses toward the west and yields a wavenumber of -.018
km^{-1}, close to that predicted by Gill, Green and Simmons (1974). Note
also that phase progresses upward for velocity but downward for
temperature, giving phase differences between meridional velocity and
temperature which concentrate the heat release in the thermocline. In
Figure 10b the westward phase propagation has been subtracted and the
residuals averaged. Also shown in the top panel are theoretical profiles
of phase and amplitude from Gill, Green and Simmons (1974). In the lower
panel the dashed lines show a prediction of the temperature profile from
the observed velocity profile of the upper panel assuming a monochromatic
disturbance that is hydrostatic. The strong resemblance between the
observed motion field and that calculated by Gill, Green and Simmons
(1974) strongly supports the notion that these motions result from
incipient baroclinic instability of the mean flows. There is weak
evidence that their amplitude is growing to the west. At this point the
perturbations do not appear to have reached a finite amplitude
equilibration.

CONCLUSION

1) There are, at least, two components to the deep circulation in the
western North Atlantic. One is inshore of the 4000-m isobath and is the
classical thermohaline Deep Western Boundary Current. The other is
further offshore and composed of one or more recirculating gyres each
transporting as much as 4 times the 10 Sverdrups carried by the Deep
Western Boundary Current.

2) The recirculating gyres are probably driven by eddy stresses. An
important component of this stress is the vertical "eddy form drag". In
the mean vorticity balance this appears as a "thickeness flux" which can

be related to a southward heat flux. Estimates from observations suggest that this thickness flux is at least as important as the relative vorticity flux.

3) The southward heat flux is derived from spontaneous baroclinic instability of the mean flow. The relatively depth-independent mesoscale eddy field observed in Polymode Array 2 closely resembles that predicted at the secondary long wave growth peak for a simple linear model. The fastest growing waves are much shorter and much more surface-trapped. It is probable that there exists a region of significant eddy heat transfer in the upper 500 m that has presently not been observed in moored experiments.

194
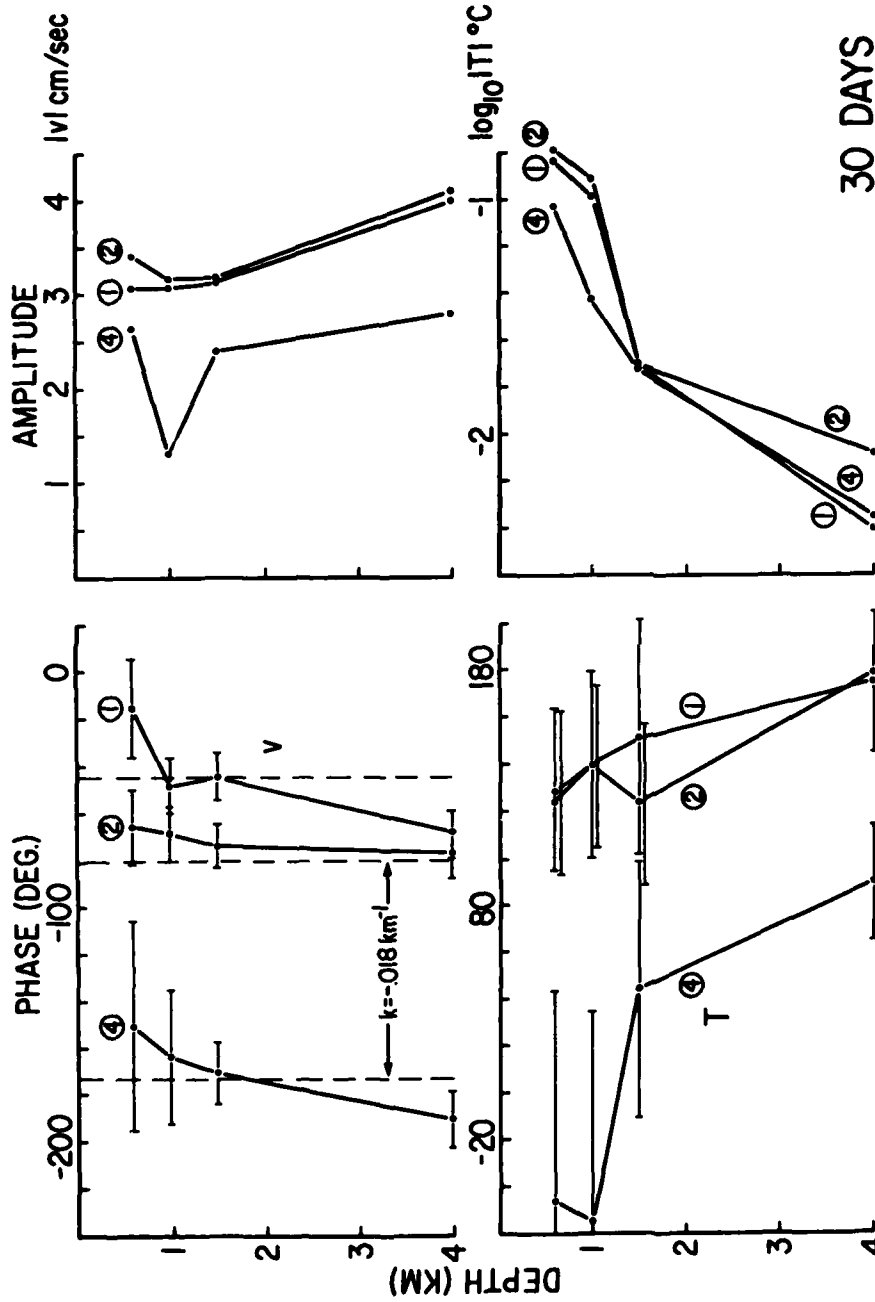
Fig. 10. (a) The first EOF for 30-day periods, amplitude and phase, calculated from all the information available at PM01, 02, and 04. Vertical dashed lines in the upper left panel give a best least squares fit of a uniform westward phase propagation to the meridional velocity component. Note that temperature phase is offset by 180° to emphasize the regions of southward heat flux.
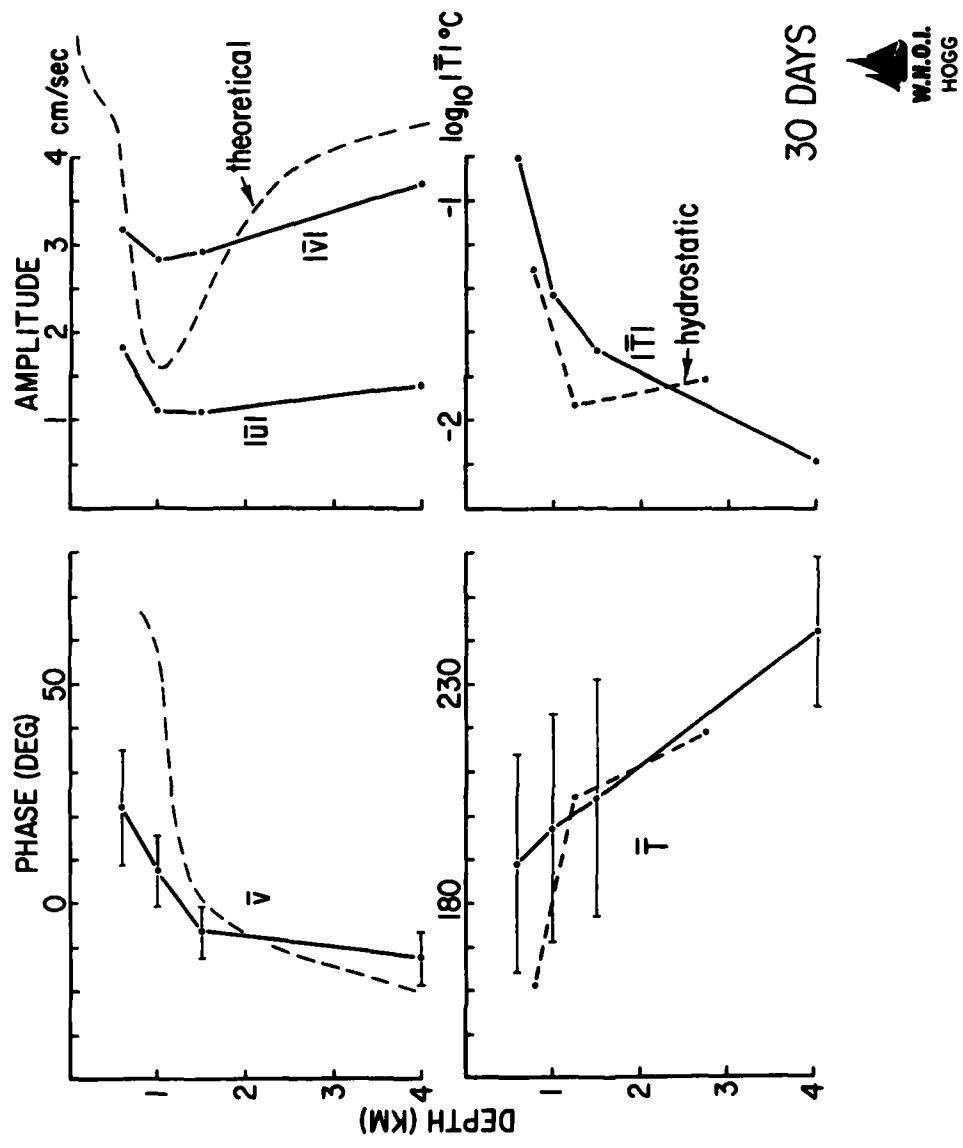
Fig. 10. (b) Average phase and amplitude distributions calculated after the uniform westward phase propagation has been removed. Dashed lines on the temperature plots are calculated from the velocity information with the geostrophic and hydrostatic assumptions. "Theoretical" curves at 30 days are those from the Gill, Green, and Simmons (1974) calculations (velocity only).

REFERENCES

Barrett, J. R., 1965. Subsurface currents off Cape Hatteras. Deep-Sea
Research, 12, 173-184.

Bendat, J. S., and A. G. Piersol, 1966. Measurements and Analysis of
Random Data. J. Wiley and Sons, New York, 390 pp

Bird, A. A., G. L. Weatherly and M. Wimbush, 1982. A study of the bottom
boundary layer over the eastward scarp of the Bermuda Rise.
Journal of Geophysical Research, 87, 7941-7954.

Chausse, D., and R. Payne, 1981. A compilation of moored current meter
and wind recorder observations, Volume XXVI (1972 measurements).
Woods Hole Oceanographic Institution Technical Report No. 81-45.

Fisher, A., Jr., 1977. Historical limits of the northern edge of the
Gulf Stream. Gulfstream, 3, 6-7.

Gill, A. E., J. S. A. Green and A. J. Simmons, 1974. Energy partition
in the large-scale ocean circulation and the production of
mid-ocean eddies. Deep-Sea Research, 21, 499-528.

Hendry, R. M., 1982. On the structure of the deep Gulf Stream. Journal
of Marine Research, 40, 119-142.

Hogg, N. G., 1983. A note on the deep circulation of the western North
Atlantic: its nature and causes. Deep-Sea Research, in press.

Hogg, N. G., 1984. Evidence for baroclinic instability in the Gulf
Stream recirculation. Progress in Oceanography, submitted.

Holland, W. R., and P. B. Rhines, 1980. An example of eddy-induced ocean
circulation. Journal of Physical Oceanography, 10, 1010-1031.

Jenkins, W. J., and P. B. Rhines, 1980. Tritium in the deep North
Atlantic Ocean. Nature, 286, 877-880.

Levy, E., S. A. Tarbell, and N. P. Fofonoff, 1982. A compilation of
moored instrument data and associated oceanographic observations,
Vol. XXX (Gulf Stream Extension and Norwegian Sea Overflow
intrusion experiments). 1979-1980. Woods Hole Oceanographic
Institution Technical Report No. 82-43.

Luyten, J., 1977. Scales of motion in the deep Gulf Stream and across
the continental rise. Journal of Marine Research , 35 (1), 49-74.

Luyten, J., and H. Stommel, 1982. Recirculation reconsidered. Journal
of Marine Research, Supplement to 40, 407-426.

McKee, T. K., E. A. Francis, and N. G. Hogg, 1981. A compilation of moored current-meter data from three topographic experiments: the Bermuda Microstructure Array, the Island Trapped Waves Array and the Gibbs Fracture Zone Array. Vol. XXVII. Woods Hole Oceanographic Institution Technical Report No. 81-68.

Mills, C. A., and P. Rhines, 1979. The Deep Western Boundary Current at the Blake-Bahama Outer Ridge: current-meter and temperature observations, 1977-78. Woods Hole Oceanographic Institution Technical Report No. 79-85.

Mills, C. A., S. A. Tarbell, and R. E. Payne, 1981. A compilation of moored instrument data and associated hydrographic observations, Volume XXVIII (Polymode Local Dynamics Experiment, 1978-1979). Woods Hole Oceanographic Institution Technical Report No. 81-73.

Owens, W. B., and N. G. Hogg, 1980. Oceanic observations of stratified Taylor columns near a bump. Deep-Sea Research, 27, 1029-1045.

Owens, W. B., J. R. Luyten, and H. L. Bryden, 1982. Moored velocity measurements on the edge of the Gulf Stream recirculation. Journal of Marine Research, Supplement to 40, 509-524.

Pillsbury, R. D., J. Bottero, R. E. Still, and E. P. Laine, 1982. Data report for current meters on mooring CMME-1, 1980-81; Atlantic Study Area E-N3. Oregon State University report OSU-15.

Pillsbury, R. D., J. Bottero, R. E. Still, and E. P. Laine, 1983. Data report for current meters on mooring CMME-2, 1981-82; Atlantic Study Area E-N3. Oregon state University report, in preparation.

Rhines, P. B., and W. R. Holland, 1979. A theoretical discussion of eddy-driven mean flows. Dynamics of Atmospheres and Oceans, 3, 289-325.

Richardson, M. J., M. Wimbush, and L. Mayer, 1981. An exceptionally strong near-bottom current on the Continental Rise of Nova Scotia. Science, 213, 887-888.

Richardson, P. L., 1977. On the crossover between Gulf Stream and western boundary undercurrent. Deep-Sea Research, 14, 139-159.

Richardson, P. L., 1981. Gulf Stream trajectories measured with free-drifting buoys. Journal of Physical Oceanography, 11, 999-1010.

Schmitz, W. J., Jr., 1977. On the deep general circulation in the western North Atlantic. Journal of Marine Research, 35, 21-28.

Schmitz, W. J., Jr., 1980. Weakly depth-dependent segments of the North
    Atlantic circulation. Journal of Marine Research, 38, 111-133.

Spencer, A., 1979. A compilation of moored current meter data,
    Whitehorse profiles and associated oceanographic observations,
    Volume XX (Rise Array, 1974). Woods Hole Oceanographic Institution
    Technical Report No. 79-45.

Spencer, A., C. Mills, and R. Payne, 1979. A compilation of moored
    current meter and associated oceanographic observations, Volume XIX
    (POLYMODE Array I data). Woods Hole Oceanographic Institution
    Technical Report No. 79-34.

Stommel, H., 1958. The circulation of the abyss. Scientific American,
    199, 85-90.

Tarbell, S., M. Chaffee, A. Williams, and R. Payne, 1979. The WHOI
    moored array project 1963-1978; Data directory and bibliography.
    Woods Hole Oceanographic Institution Technical Report No. 79-88.

Tarbell, S., A. Spencer, and R. Payne, 1978. A compilation of moored
    current meter data and associated oceanographic observations,
    Volume XVII (POLYMODE Array II data). Woods Hole Oceanographic
    Institution Technical Report No. 78-49.

Tarbell, S. A., and A. W. Whitlatch, 1977a. A compilation of moored
    current data and associated oceanographic observations, Volume
    XIII (1970 measurements). Woods Hole Oceanographic Institution
    Technical Report No. 77-18.

Tarbell, S. A., and A. W. Whitlatch, 1977b. A compilation of moored
    current data and associated oceanographi observations, Volume XV
    (1971 measurements). Woods Hole Oceanographic Institution
    Technical Report No. 77-56.

Volkmann, G., 1962. Deep current observations in the Western North
    Atlantic. Deep-Sea Research, 9, 493-500.

Weatherly, G. L., and E. A. Kelley, Jr., 1982. 'Too cold' bottom layers
    in the HEBBLE area. Journal of Marine Research, 40, 985-1012.

Worthington, L. V., 1976. On the North Atlantic circulation. The Johns
    Hopkins Oceanographic Studies, 6, 110 pp.

Wunsch, C., 1978. The general circulation of the North Atlantic west of
    50°W determined from inverse methods. Reviews of Geophysics and
    Space Physics, 16, 583-620.

Wunsch, C., and B. Grant, 1982. Towards the general circulation of the
    North Atlantic Ocean. Progress in Oceanography, 11, 1-59.

ON THE MEAN DYNAMICAL BALANCES OF THE GULF STREAM RECIRCULATION ZONE

James C. McWilliams
National Center for Atmospheric Research, Boulder, Colorado
80307

ABSTRACT

The time mean circulation is analyzed at a site on the southern edge
of the Gulf Stream Recirculation Zone (31°N, 70°W) from data taken in
the POLYMODE Local Dynamics Experiment. Additional mean quantities
are described from a combination of dynamical assertions and infer-
ences. The mean vorticity balance is examined to infer the mean ver-
tical velocity and eddy relative vorticity flux divergence. The ver-
tical velocity is found to be mostly upward and an order of magnitude
larger than the downward surface Ekman pumping. In the mean heat,
salt, density, and potential vorticity budgets, the mean advections of
these quantities are non-zero, and substantial eddy flux divergences
are again required for balance. These are inferred to be primarily
associated with mesoscale eddies. The corresponding horizontal eddy
diffusivities for these quantities are large ($\sim 10^8$ cm^2 s^{-1}) over an ex-
tensive depth range, from the surface to at least 4000 m. An assess-
ment is also made of the likelihood of a homogeneous potential vorti-
city layer in the Recirculaton Zone. From our estimates of the local
potential vorticity gradients, there is no clearly indicated zero gra-
dient layer, and the qualitative features of our local estimates are
consistent with the larger-scale analysis of McDowell et al. (1983).

INTRODUCTION

The purpose of this paper is to describe the local time mean state of
the ocean, commonly referred to as the general circulation, from data
taken over several years at 31°N, 70°W, the site of the POLYMODE Local
Dynamics Experiment (LDE).[*] Inferences of several aspects of the
general circulation which were not directly measured will be made from
the associated dynamical balance equations. The balances are assumed
to be geostrophic and hydrostatic, time derivatives are neglected in
the balance equations, and the time mean stretching vorticity is as-
sumed dominant over mean relative vorticity. The first two assump-
tions are traditional and reliable. The last two are plausible from
scale estimates. The upper surface boundary condition is an Ekman
velocity, and the lower one is no flow normal to the sloping bottom.
Several eddy flux divergences, associated with fluctuations in time
about the mean state, are inferred to be significant. Among these are
the horizontal eddy fluxes of heat, salt, momentum, and potential vor-
ticity. Inferences of eddy flux divergences in mean balance equations
are of considerable interest because direct observations of eddy
fluxes at the LDE site, and elsewhere, are too spatially limited at

---

[*] The LDE is described in McWilliams et al. (1982).

present to permit credible divergence calculations and to span the
ocean depth. The directly measured fluxes from the LDE are, however,
valuable as consistency checks upon the inferred flux divergences.

Diagnoses of the general circulation and its dynamical balances cannot
be made explicitly and completely with current oceanographic observ-
ing techniques. Too many relevant quantities are inaccessible: e.g.,
mean vertical velocity and diapycnal diffusivity. Hence, the diag-
noses must be inferential and significantly dependent upon the diag-
nostician's dynamical assumptions. Some recent examples of such diag-
noses, each with its own particular assumptions, are Stommel and
Schott (1977), Davis (1978), Wunsch (1978), and Keffer and Niiler
(1982).

The present study is akin to those above. It is, however, based upon
presumed knowledge of the vertical profiles of mean horizontal velo-
cities, as well as profiles of the mean hydrographic quantities: tem-
perature, salinity, and pressure. Most previous diagnoses have only
presumed knowledge of the latter, and hence have had to infer the
horizontal velocities, at least at one level, the reference level.
The LDE site is one of the few in the world where velocity measure-
ments of sufficient duration and vertical resolution have been made so
that a diagnostic method can be based upon them. We shall find, how-
ever, that even in such a well-measured location as this, the sampling
errors in determining the means are not comfortably small. That is,
even if our dynamical assumptions are correct, some of the inferred
properties of the general circulation are significantly uncertain.
This is a general defect of extant ocean observations and diagnoses,
and it must be accepted in our pursuit of the general circulation.

The LDE site is within the Gulf Stream Recirculation Zone, which is a
northwestern intensification of the circulation within the interior of
the North Atlantic Subtropical Gyre. This feature is shown schemati-
cally in Fig. 1a, with the site also marked. Note th~t the site ap-
pears to be on the southern edge of the zone. The LDE velocity mea-
surements confirm this (Section 2): the flow exhibits the Return Flow
character (i.e., flow with a component to the west) in the thermocline
but is reversed at greater depths. The mean wind stress in this loca-
tion produces a downward Ekman velocity at the upper surface (Fig.
1b), which is characteristic of the Subtropical Gyre. The bottom
topography is quite smooth, characteristic of the Hatteras abyssal
plain, with a gentle slope up towards the Bermuda rise (Fig. 1c).

The contents of this paper are as follows. The directly measured mean
horizontal velocities and hydrographic quantities are discussed in
Section 2. Subsequently, inferences are made of mean vertical velo-
city and the eddy flux of relative vorticity (Section 3), eddy fluxes
of heat, salt, and density (Sections 4 and 5), and mean potential vor-
ticity gradients (Section 6). Some remarks about the mean energy and
momentum balances are presented in Section 7, and Section 8 is a
summary.
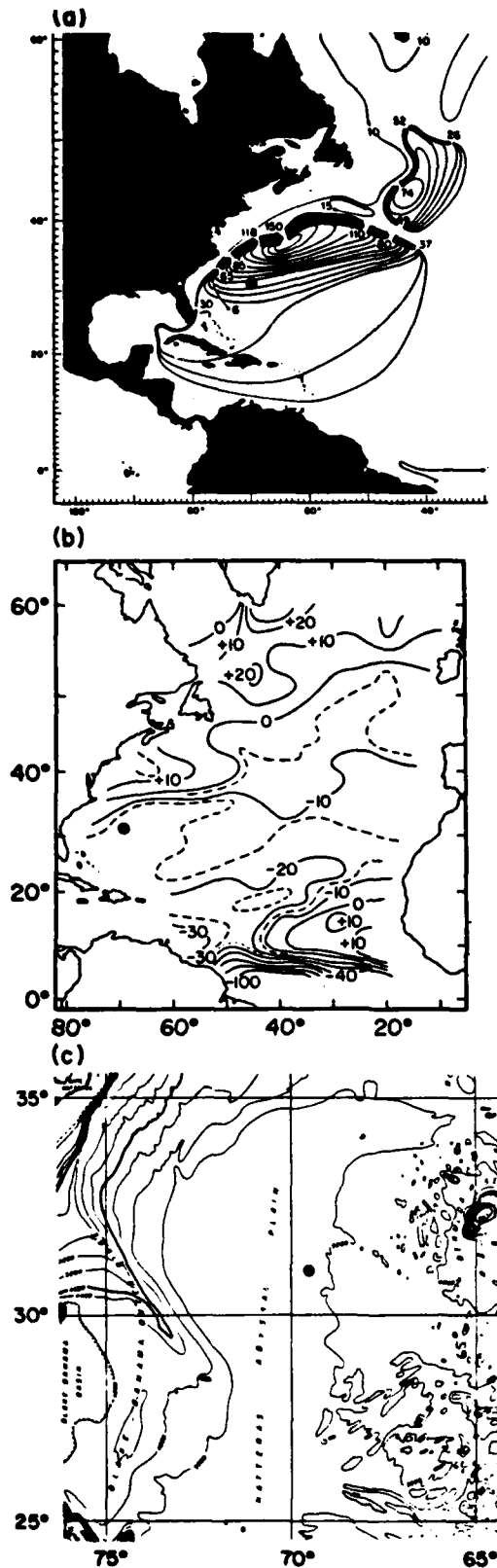
Fig. 1. The large-scale environment of the Gulf Stream recirculation
zone. The LDE site is marked with a dot. (a) A schematic of the
depth integrated mean circulation in Sv, with a contour interval
of 10 Sv (Worthington, 1976, Fig. 42). (b) The annual mean verti-
cal velocity at the base of the Ekman layer, in units of 10^{-5}cm s^{-1}
(Leetmaa and Bunker, 1978, Fig. 3. (c) Depth contours in meters
(Uchupi, 1971).

HORIZONTAL VELOCITIES AND HYDROGRAPHIC QUANTITIES

The LDE data we shall base our analyses on are of two types: tempera-
ture T, salinity, S, and pressure, P, from hydrographic profiling in-
struments and east and north velocity, u and v, from moored current
meters. The averaging and smoothing of each of these is discussed
below.

Hydrographic quantities

In each of the three years 1977-1979, a set of hydrographic profiles
was made, and for each set an average T(P) and S(P) has been calcu-
lated. In April 1977, a LDE site survey cruise was made (Bradley et
al., 1977; Ebbesmeyer et al., 1983). The 1977 average is taken over
the six profiles from that cruise which reached as deep as 5460 db,
within 100 km of the LDE center. Subsequent manipulations of the data
are made on a uniform P grid with spacing 20 db. In May-July 1978,
seven hydrographic surveys were made on an array with spacing 25 km
and radius 100 km (Taft et al., 1983). The average T and S profiles
span 0-3017.5 db with spacing 2.5 db. In July 1979, 10 profiles were
taken within 50 km of the LDE center (Bryden and Millard, 1980). The
average spans 0-5029 db with spacing 2 db.

The averaging among profiles within each data set is insufficient to
eliminate small-scale structure in the profiles. Since this structure
is implausibly present in the true mean, we shall smooth the profiles
until a subjectively satisfactory degree of smoothness is achieved,
with retained scales of 100 m and larger. We do this in stages. The
more highly differentiated quantities discussed in later sections will
require additional smoothing beyond that applied here. The smoothing
will be accomplished by repeated applications of a Gaussian 3-point
filter: for any quantity γ_i with a grid index i, the formula is

$$\gamma_i \leftarrow \frac{1}{4} \gamma_{i-1} + \frac{1}{2} \gamma_i + \frac{1}{4} \gamma_{i+1} , \tag{1}$$

with an endpoint formula of

$$\gamma_1 \leftarrow \frac{3}{4} \gamma_1 + \frac{1}{4} \gamma_2 \tag{2a}$$

or

$$\gamma_1 \leftarrow \frac{1}{2} \gamma_1 + \frac{1}{2} \gamma_2 , \tag{2b}$$

with analogous formulae at the other endpoint. The alternatives (2a)
and (2b) either tend to preserve the quantity value or diminish its
derivative at the endpoint, respectively. For most quantities we
shall apply (2a); (2b) will be applied only to horizontal velocities
and Brunt-Väisälä frequency at the top or bottom of the ocean.

First we smooth the P profiles of S and T. The formulae (1) and (2a)
are applied 10, 30, and 30 times, respectively, to each of the years'
data sets (n.b., fewer applications are required to achieve a given

degree of smoothness for a quantity on a grid with coarser spacing, in
this case the 1977 data). *The results are shown in Fig. 2a, a plot of*
potential temperature θ against S. Note that the three data sets
nearly coincide at depth (smaller θ and S values); more precisely,
they agree to within 0.005 0/00 in S at a given θ below 3°C. Near the
surface (above 18°C), they differ considerably due to their differing
phases in the seasonal cycle. Other locations of noticeable differ-
ences are the lower thermocline (7-11°C) and the Mediterranean water
(4-6°C), although these differences are likely sampling errors asso-
ciated with mesoscale variability [see Taft et al. (1983) for profiles
of S variance]. The slight change in slope below 2°C is associated
with Antarctic bottom water. It is of interest that here, and con-
tinuing in θ up to 3°C, all of our profiles are fresher, typically
by about 0.005 0/00, than measurements taken during the late 1950s
(Worthington and Wright, 1970). However, because of geographical in-
terpolation uncertainties, titration errors (Fofonoff, 1963), standard
water variations (Mantyla, 1980), and, possibly, mesoscale variations,
we cannot be completely confident this difference is a true decadal
scale change in the deep ocean, although it likely is because the
estimated uncertainty from the various sources is not larger than the
estimated signal. Additional evidence for decadal-scale freshening of
deep water in the North Atlantic has been reported in TTO (1981).

Another display of the hydrographic data sets is the plot of mean
Brunt-Vaisalla frequency in Fig. 2b. N^2 is here calculated from the
three set-averaged T and S profiles over pressure intervals of 40, 5,
and 16 db, respectively, and then smoothed using Eqs. (1) and (2) 30,
500, and 1000 times. In N(P) the data set differences are larger than
in S(θ), though still reasonably small. The local maximum near the
surface, of differing strengths in the different profiles, is in the
seasonal thermocline; the minimum near 300 db is in the 18°C thermo-
stad; the broad peak near 750 db is in the main thermocline; and the
small peak near the bottom is in the Antarctic bottom water. Some of
the differences in Fig. 2b are likely due to differing degrees of
smoothing: for example, the weaker extrema for the thermostad and main
thermocline in the more smoothed 1977 data.

We shall estimate mean hydrographic profiles as composites of the
three data set averages shown in Fig. 2. This is done as a linear
combination; for a quantity γ_i, we calculate the mean as

$$\gamma_i = \sum_j \alpha_i^j \gamma_i^j \qquad (3)$$

where the index j ranges over the data sets and i over pressure. The
coefficients are defined as follows:
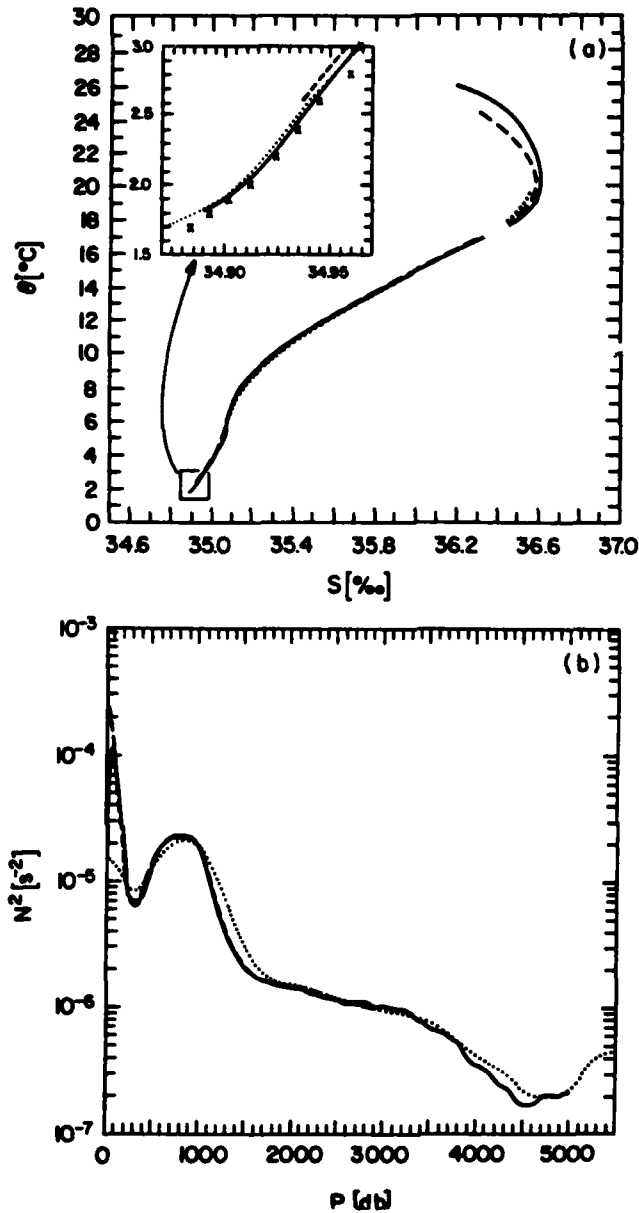
Fig. 2. Mean quantities from the three hydro-
graphic data sets: 1977, dotted line; 1978,
dashed line; 1979, solid line. (a
(a) Potential temperature (using the formula
of Bryden, 1973) and salinity; (b) the
square of the Brunt Vaisala frequency N.
Smoothing is as described in the text. The
crosses in the insert in panel (a) are taken
from the charts of Worthington and Wright
(1970).

P_i [db]	α_i^{77}	α_i^{78}	α_i^{79}
0-2500	0	1	0
2500-3010	(P-2500)/1020	(3010-P)/510	(P-2500)/1020
3010-4500	1/2	0	1/2
4500-5020	1/2 + (P-4500)/1040	0	(5020-P)/1040
5020-5460	1	0	0

$$\text{(4)}$$

The 1978 data are given greatest weight where they are available, because of their abundance, and the other two years are given equal weights. The formula (3) is applied to T, S, and N^2, and, from the first two of these, additional hydrographic quantities are calculated. Among these is density ρ. From density and the hydrostatic assumption, the depth is calculated as

$$z = - \int_0^P dP/g\rho \, , \qquad (5)$$

where g is the gravitational constant. We now transform all pressure profiles to depth profiles. The results are shown in Fig. 3: T, θ, S, N^2, and σ, where σ is the density anomaly,

$$\sigma = 10^3 (\rho - \rho_0) \qquad (6)$$

and ρ_0 is a reference density of 1 gm cm^{-3}. The mean ocean depth is 5350 m, as determined by local soundings in the LDE. The curves in Fig. 3 show the same hydrographic regimes identified in Fig. 2: the two thermoclines, the 18°C thermostad, the deep water layer, and Antarctic bottom water. These features in the density anomaly are, however, somewhat masked by the monotonic increase due to compressibility.

Obviously there is a degree of arbitrariness in the hydrographic data smoothing as just described. However, this arbitrariness is inconsequential for the qualitative character of the conclusions to be drawn below on vertical scales larger than about 100 m. Nor is the arbitrariness large compared to the sampling uncertainties in estimating the mean, as represented by the differences between the three profiles in Figs. 2a and 2b.

Horizontal velocities

Horizontal velocities were measured at 10 depths at the LDE center for intervals of up to 15 months between May 1978 and July 1979 (Owens et al., 1982). Two types of time averages are calculated at each depth, one over the full record interval, whatever its length, and the other over a particular, uniformly sampled, 290-day interval when all instruments were working. Both types of averages are plotted in Fig. 4, together in panel (a) and separately in panels (b) and (c). The sampling errors in these averages are not small. They vary with velo-
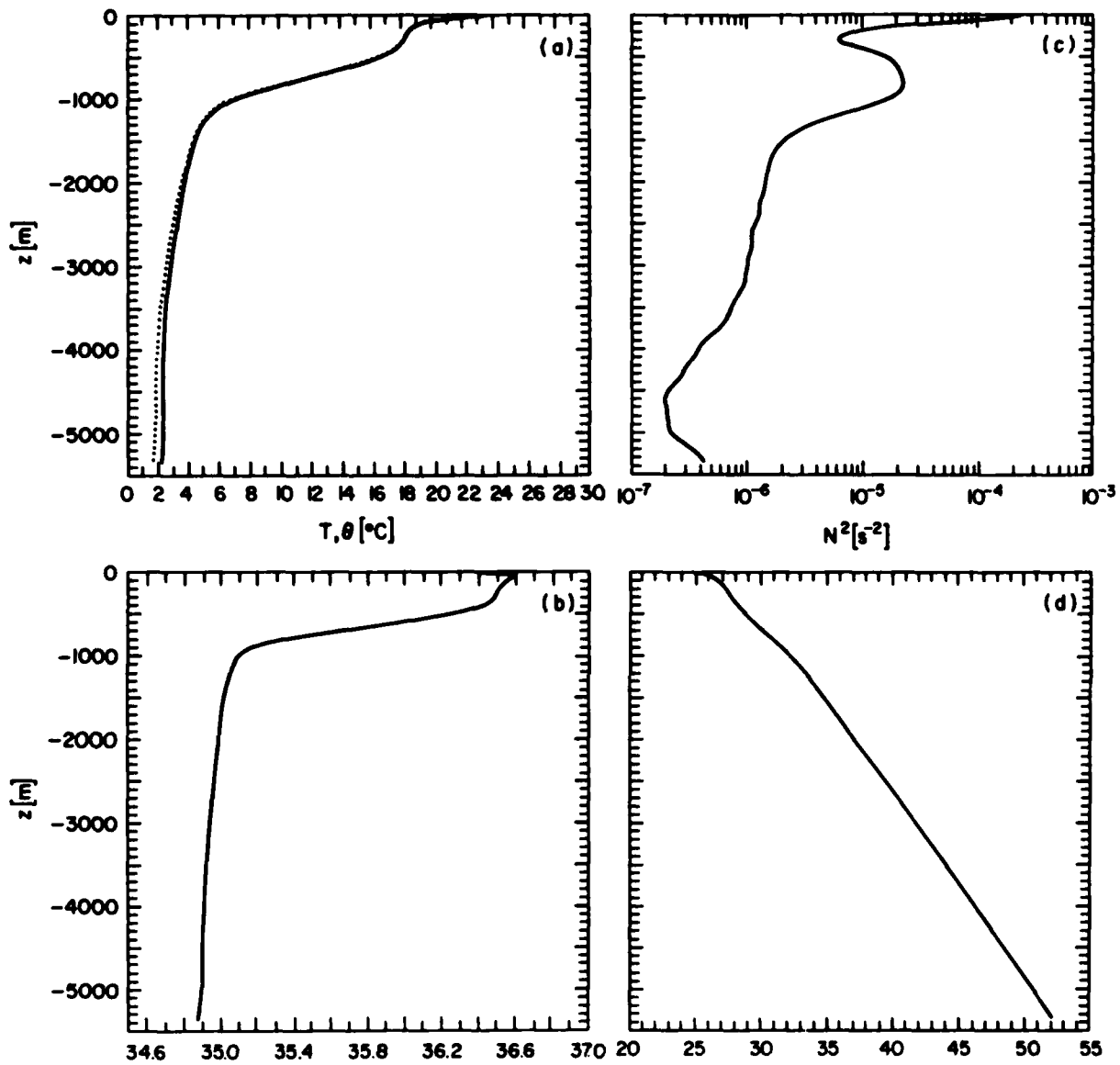
Fig. 3. Depth profiles of mean hydrographic quantities: (a) T and θ (solid and dashed lines, respectively); (b) S; (c) N^2; (d) σ.
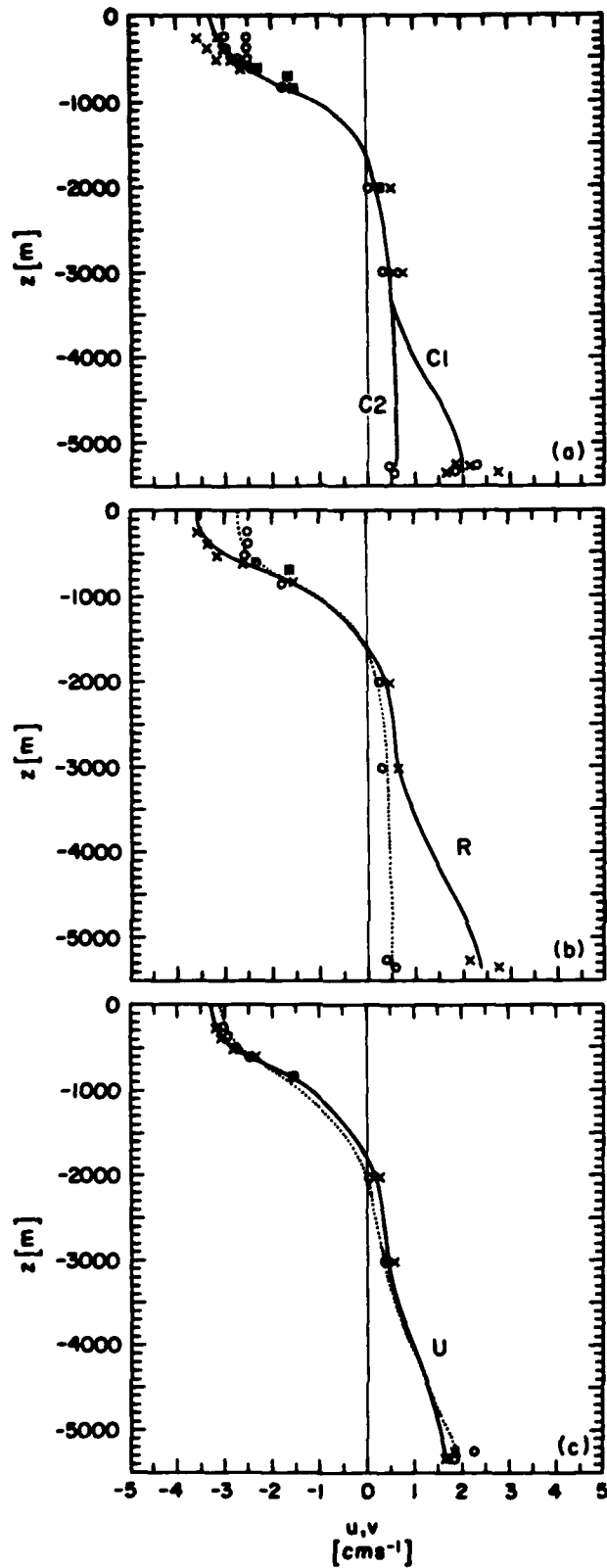
Fig. 4. Mean horizontal velocity measurements (x = u; 0 = v) and interpolated depth profiles: (a) both types of averages and composite profiles C1 and C2, assuming u = v; (b) full record averages and profile R with u ≠ v (u is plotted as a solid line and v as a dotted line); (c) 290-day, uniformly sampled averages and profile U with u ≠ v.

city component and depth, but are approximately 2 cm s^{-1} in and above the main thermocline and 1 below (ibid).

A particular form of samping error, of potential concern, is due to the episodic nature of the LDE site velocities: three times during the years 1977-1979, an intense, southwestward, thermocline jet occurred, lasting for about a month (McWilliams et al., 1982). Do such events seriously contaminate the mean velocity estimates? In my opinion, they do not. Owens et al. (1982, Fig. 4) computed mean velocities excluding the periods during which jets occurred and found qualitatively similar mean profiles to those in Fig. 4, albeit with smaller amplitude. On the other hand, one must be cautious in interpreting a mean obtained from a sample containing a few distinctive events, in addition to general eddy variability, particularly when the mean has some structural similarity with the events.

Within the sampling uncertainties there is considerable scope for estimating the true LDE mean. In particular, we cannot refute the hypothesis that u ≡ v at all z, which if true would have strong dynamical consequences (n.b., Sections 4-6). Because of these uncertainties, we shall work with several estimates of the mean, each of which is consistent with the sample averages, and only some of which assume u ≡ v. These alternatives do not span the full range of possibilities, but do expose the sensitivities of inferred quantities to the uncertainties. It is the uncertainties in the velocity profiles, rather than the hydrographic profiles, which most imperil our inferences. The uncertainty in velocity, as a fraction of the estimated mean, is much greater than that in potential temperature, for example.

The several estimates of the mean velocity profile are also plotted in Fig. 4. They are subjective interpolations of the point measurements from current meters, selected by the principle of incorporating greatest smoothness in z, while closely fitting the data values. Those in panel (a) are constrained by the condition u=v, and are fit to the composite data set, containing both components and both types of averages. Profile C1 includes a velocity enhancement near the bottom, as indicated by most of the data, while profile C2 has nearly uniform flow in the bottom 2 km, as indicated by the full-record-average v components near the bottom. In my opinion C2 is a less likely estimate of the mean than C1, although still within the samping uncertainties. Panels (b) and (c) (profiles R and U) are for the two different types of averages, with the u and v data fit separately.

We shall now discuss these LDE velocity profiles in the context of other estimated mean velocities from moorings in the Recirculation Zone, as well an idealization of the Recirculation Zone mean circulation within and beneath the thermocline (Fig. 5). This idealization represents a spatially smooth conception of the general circulation and is consistent with the available long-term average velocities from current meters located in topographically smooth regions, as well as certain gross characteristics of numerical model solutions (see be-
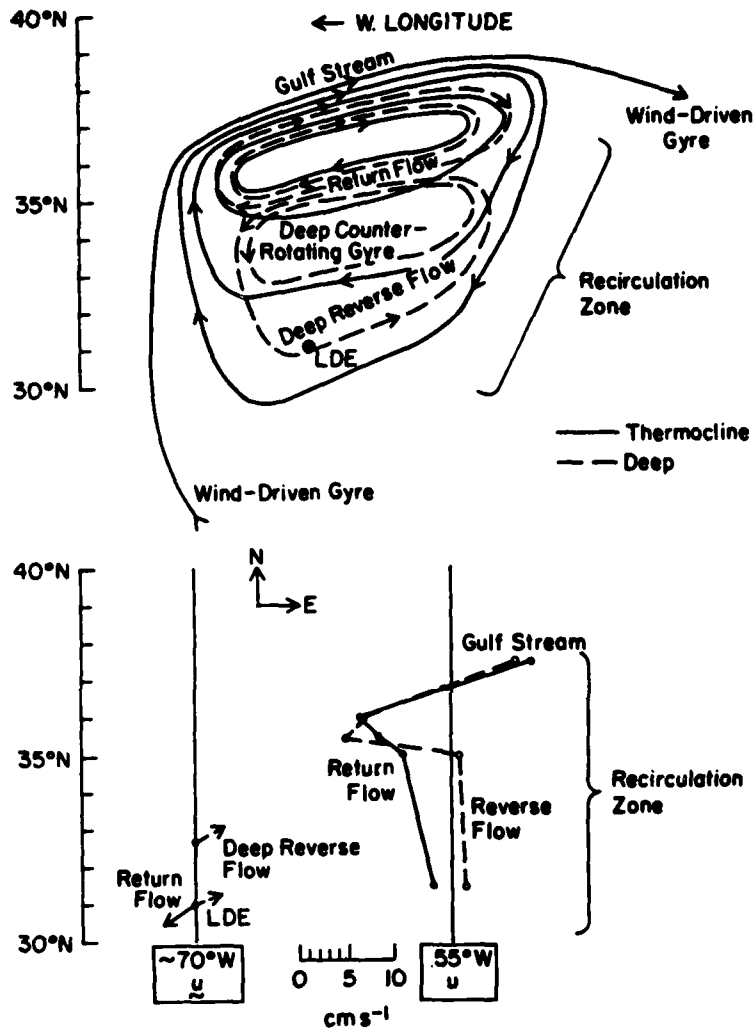
Fig. 5. A schematic drawing of mean circulation at two levels
for the northwest quadrant of the North Atlantic Subtropical
Gyre (top) and a depiction of observed mean velocities at
two longitudes from sources discussed in the text (bottom).

low). It is undoubtedly falsely simple in topographically rough regions (e.g., near Bermuda), and it certainly should not be given too much credence away from the indicated locations of available data.

The LDE velocity profiles show a Return Flow of several cm s^{-1} to the southwest in and above the thermocline. This is what we identify as the defining characteristic of the Recirculation Zone, as sketched in Fig. 1a. This is also consistent with the direct current measurements of a zone of westward flow at 600-m depth extending for about 400 km to the south of the Gulf Stream along 55°W (Schmitz, 1980); see Fig. 5. The vertical shear above z = -1800 m in Fig. 4 has the same shape as that calculated for this location from the historical archive of hydrographic profiles, but the historical magnitudes are only half as large (Lindstrom et al., 1980); this discrepancy can be attributed to the large horizontal smoothing interval (400 km) in the historical analysis. The LDE site is distinct from the MODE site 300 km to its south, outside the Recirculation Zone, where the thermocline mean flow is small and probably eastward (Tarbell and Spencer, 1978).

Below the thermocline the flow is oppositely directed to the northeast, which we call the Reverse Flow (Fig. 5). Its magnitude is a fraction of a cm s^{-1} at 2000- and 3000-m depth and several cm s^{-1} near the bottom. The mean flow is similarly directed to the northeast at a site 200 km closer to the Gulf Stream (32°40'N, 70°50'W). There the magnitude is a fraction of a cm s^{-1} at 1100 m depth and several cm s^{-1} from 3250 m to the bottom (Pillsbury et al., 1982). We therefore conclude that there is a reasonably large zone of deep mean flow opposite in sign to the thermocline Return Flow along 70°W. This is also seen along 55°W (Schmitz, 1980, and Fig. 5), although there the magnitude at 4000-m depth is only about 1 cm s^{-1}. Along 55°W, this Reverse Flow zone is to the south of a band of deep Return Flow of relatively narrow width (~200 km). Presumably a deep Return Flow occurs across 70°W as well, to the north of 33°N, although this is as yet undocumented. In the deep water as well, the MODE site mean velocity (Schmitz, 1977) is much smaller (and oppositely directed) compared to the Reverse Flow at the LDE site and farther north.

Modeling results exhibit somewhat analogous features in the mean circulation. Often a pair of gyres occurs in the deep ocean, one corotating, one counterrotating, relative to a broader-scale thermocline Recirculation Gyre (Holland, 1978; Schmitz and Holland, 1982); this structure is also drawn in Fig. 5. Across central meridians, this double gyre structure appears as a sequence of alternating currents: the Gulf Stream in the north, the Return Flow in the middle, and the Reverse Flow in the south.

Horizontal gradients

As a consequence of sampling errors, we cannot rely on direct estimates of horizontal gradients of mean hydrographic quantities and velocities, even though the LDE included arrays spanning either 200 km

(hydrography) or 50 km (moorings). With only one exception, the esti-
mated gradients are small compared to their standard errors,
$\ell(2\sigma^2/N)^{1/2}$, where σ^2 is the variance of the quantity in question, ℓ
is the horizontal span of the measurements, and N is the number of in-
dependent samples; values for these quantities are reported in Owens
et al. (1982) and Bryden (1982) for the mooring data. The one excep-
tion is the eastward derivative of northward velocity, $\partial v/\partial x$, whose
estimated value (i.e., $5\times10^{-7} s^{-1}$ at ~700 m depth; Bryden, 1982,
Table 4) is at least not much smaller than its standard error, and
which therefore has some credibility as to sign and order of magni-
tude. This estimate indicates a moderate southward turning of the
thermocline Return Flow as it passes through the LDE site. This fea-
ture, if real, is too much of a local detail to be seen in the highly
idealized Fig. 5. For the LDE hydrographic data, the sampling errors
are such that no significant horizontal gradients were resolved
beneath the surface boundary layer: the 1977 and 1979 measurements are
few in number and the two-month time interval in the 1978 data is too
brief. The historical archive of all hydrographic data, as analyzed
by Lindstrom et al. (1980), does show significant gradients (see Sec-
tion 2b above), but only after smoothing over a very large spatial
area. Perhaps a more local analysis of the archive, augmented by the
LDE hydrographic data, would yield a sufficiently accurate esimate of
horizontal gradients, but this has not been done, since in principle
it is redundant with $\underline{u}(z)$ (see Section 4).

Thus, sampling limitations in the data preclude extensive use of
direct estimates of local mean horizontal gradients and force us to
rely on inferrential estimates, such as using the thermal wind rela-
tion (23) to estimate $\nabla\theta$ in Section 4.

VERTICAL VELOCITY AND VORTICITY

Vertical velocity cannot be measured directly, at least not with suf-
ficient accuracy to obtain a credible mean. Hence it must be infer-
red. We shall do this from the mean vorticity equation (i.e., the
vertical component of the curl of the momentum equations), which we
write as

$$f\frac{\partial w}{\partial z} - \beta v - \nabla\cdot(\overline{\underline{u}'\zeta'}) = \underline{u}\cdot\nabla\zeta , \qquad (7)$$

with neglected terms of higher order in Rossby number, as is usual in
the quasigeostrophic approximation. In (7), w is the vertical velo-
city, f is the Coriolis frequency, β is its y derivative (i.e., north-
ward), the underwiggle denotes a horizontal vector, the prime denotes
a fluctuation about the mean, the overbar denotes a time mean (n.b.,
for simplicity the overbar is deleted from most mean quantities; e.g.,
we write w instead of $\overline{w}$), and ζ is the relative vorticity

$$\zeta = \frac{\partial v}{\partial x} - \frac{\partial u}{\partial y} . \qquad (8)$$

The mean vorticity equation (7) has, by definition, no time derivative term, $\partial\zeta/\partial t$. However, our estimated means from the LDE cannot be distinguished in practice from very low frequency components. This does not prevent our neglecting $\partial\zeta/\partial t$, as can be seen by the following scale estimate. The ratio of the relative importance of $\partial\zeta/\partial t$ in (7) is

$$\frac{\partial\zeta}{\partial t} \Big/ \beta v \sim (L\tau\beta)^{-1} \;,$$

where L and τ are, respectively, the horizontal and temporal scales for variations of the general circulation. From Figs. 1a and 5, we can estimate L as a few hundred km (200 km, say). τ is even less well known, but by the absence of obvious trends in the LDE time series, it is at least as long as a year. Thus,

$$(L\tau\beta)^{-1} \lesssim [(2\times10^{7}\,\text{cm})(3\times10^{7}\,\text{s})(2\times10^{-13}\,\text{cm}^{-1}\text{s}^{-1})]^{-1} = 0.01 \;,$$

which justifies our neglect of the tendency term. Even if we were to substitute for u/L the questionable, directly estimated ζ from Section 2c and (8), the preceding ratio would increase only to .05, still a small number. By a similar argument we can also neglect the mean advection of relative vorticity in (7); viz.,

$$\frac{\overline{u \cdot \nabla\zeta}}{\beta v} \sim \frac{\overline{u}}{\beta L^2}$$

$$\approx \frac{(2\ \text{cm s}^{-1})}{(2\times10^{-13}\text{cm}^{-1}\text{s}^{-1})(2\times10^{7}\text{cm})^2} = 0.03 \;,$$

which is small. This justifies the neglect of the final term in (7).

We therefore arrive at an equation for w:

$$w(z) = w_s(z) + \frac{1}{f} \int_z^0 dz'\, r(z') \;, \tag{9}$$

where w_s is the Sverdrup velocity,

$$w_s(z) = w_E - \frac{\beta}{f} \int_z^0 v(z')dz' \;, \tag{10}$$

w_E is the mean Ekman velocity (-1.5×10^{-4} cm s^{-1} in the LDE region; Fig. 1b), and r is the eddy relative vorticity flux divergence,

$$r(z) = -\nabla \cdot (\overline{u'\zeta'}) \;. \tag{11}$$

The Sverdrup velocities (10) are shown in Fig. 6 for the four different $\bar{u}$ profiles of Fig. 4. They are negative near the top surface, as forced by the Ekman layer, but only in a small depth range. They are positive throughout most of the water column. The mid-depth values are large compared to w_E, and hence not very sensitive to it. The bottom values are scattered about zero: the average for the four profiles is -0.1×10^{-4} cm s^{-1}, which is indistinguishable from zero within sampling errors. This implies that the meridional transport here is equal to the Sverdrup transport, fw_E/β ($= -0.5\times10^{5}$ cm^{2}s^{-1}). This result would be consistent with
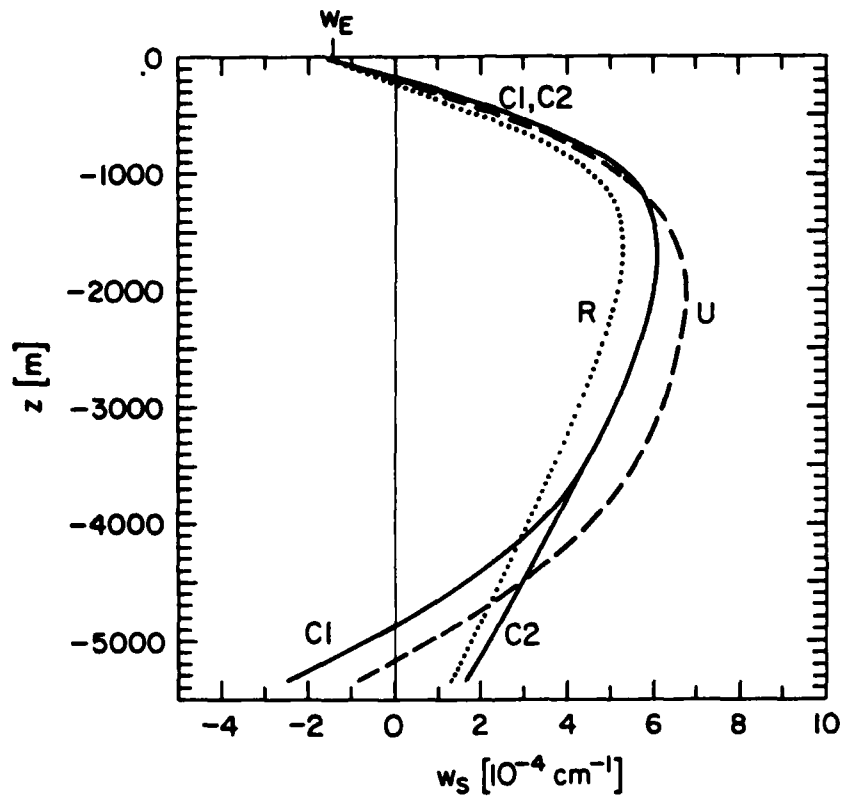
Fig. 6. The Sverdrup component of mean vertical velocity
from eq. (10), with w_E and $v(z)$ taken from Figs 1b and
4, respectively. The labels correspond to those of the
horizontal velocity profiles in Fig. 4: profiles Cl and
and C2 are drawn as solid lines, profile R as dotted, and
profile U as dashed.

$$r_0 = \frac{1}{H} \int_{-H}^{0} dz' r(z') \tag{12}$$

equal to zero in (9) and either a flat ocean bottom or zero horizontal velocity across topographic contours, so that w=0 at the bottom. However, we can show that this is not the correct bottom condition.

The bottom boundary condition of no flow normal to the ocean bottom can be expressed as

$$w(-H) = \underset{\sim}{u}(-H) \cdot \nabla \Delta H , \tag{13}$$

where the ocean bottom is the surface z = -H+ΔH($\underset{\sim}{x}$). From the topographic chart (Fig. 1c), we see that the local bottom slope is about 10^{-3} up to the east, if we assume a horizontal averaging scale of 100 km or so. A more precise value (Pratt, 1968) is

$$\underset{\sim}{\nabla}(\Delta H) = (1.5, -0.3) \times 10^{-3} . \tag{14}$$

This is the same slope value used by Price and Rossby (1982) in demonstrating that topography has an important influence on deep mesoscale variability in the LDE.

Table 1 lists the consequent bottom velocities from (13) and (14) along with the Sverdrup velocities (10) for comparison. w(-H) is very much larger than w_s(-H), and these two quantities cannot be made equal within our estimated uncertainties. Hence the eddy relative vorticity flux cannot be neglected. Its depth average, r_0, can be calculated from (9) evaluated at z=-H:

$$r_0 = f/H \left[w(-H) - w_s(-H) \right]. \tag{15}$$

Values for r_0 from (15) are also listed in Table 1.

Table 1
Vorticity Quantities

$\underset{\sim}{u}(z)$ Profile	w (-H) [10^{-4} cm s^{-1}]	w_s(-H) [10^{-4} cm s^{-1}]	r_o [10^{-13} s^{-2}]
C1	24	-2.5	3
C2	7	1.6	1
R	34	1.3	4
U	20	-0.9	2

These r_0 values can be compared with calculations of $\overline{u'\zeta'}$ from LDE moored velocity measurements in the thermocline (unfortunately, there is insufficient horizontal resolution to calculate r directly). E.

Brown and W.B. Owens (personal communication) obtain $\left|\overline{u'\zeta'}\right| = 0.4 \times 10^{-5}$ cm s^{-2}. A scale estimate for r is therefore

$$\left|\overline{u'\zeta'}\right|/L = 2 \times 10^{-13} \text{ s}^{-2} \text{ ,}$$

using the same L of 200 km as before. This is quite similar to the inferred, depth-average values r_0 in Table 1. Calculations of the empirical, orthogonal functions for the vertical structure of mesoscale eddies in the LDE also indicate that the most energetic mesoscale variability is only weakly depth-dependent (Owens, 1983). Together these results suggest that r(z) is also only weakly depth dependent. Consequently, we shall adopt a depth-independent model for it (i.e., r(z) = r_0). Hence, the inferential formula for total vertical velocity is

$$w(z) = w_s(z) - r_0 z/f \text{ .} \tag{16}$$

These profiles are plotted in Fig. 7. w is almost everywhere positive and tends to increase systematically with depth. Its magnitude is moderately sensitive to $\underline{u}(-H)$, as indicated, for example, by the much smaller w values for profile C2, which has a relatively small $\underline{u}(-H)$. If r(z) were moderately surface intensified, which is the most likely sense in which r ≡ r_0 is too crude, then the profiles in Fig. 7 would have the same end values but more outward bulge in between. Thus, the simple formula (16) is more likely to underestimate mid-depth w than overestimate it.

The magnitude of w_s is about 5×10^{-4} cm s^{-1} at the base of the thermocline, and the w value there is slightly larger due to r(z). If these values were typical of the Recirculation Zone, whose area can be estimated at 2×10^{16} cm^2 from Fig. 1a, then an upward transport through the thermocline of about 10^{13} cm^3 s^{-1} would be occurring. This latter figure is comparable to present estimates of sub-polar water mass sinking rates (Worthington, 1976). We note, however, that the large LDE w_s values result fom a substantial southward v in and above the thermocline; this may not be characteristic of the whole Recirculation Zone, and thus the total upwelling could be much less than the above estimate. In addition, for the reason discussed in the next paragraph, we do not expect $r_0 > 0$ everywhere in the Recirculation Zone, which provides a further caution about estimating total vertical transport from the LDE. Accompanying the w in Fig. 7 is a mean divergence of about 5×10^{-9} cm^{-1} s^{-1}, broadly distributed through the water column.

We can interpret r_0 crudely as an eddy diffusion process if we identify r with $\nu \nabla^2 \zeta$, where ν is a horizontal eddy viscosity. The previously described estimate of $\zeta \approx \partial v/\partial x$ in the thermocline indicates it is positive at the LDE. If we further assume that the Recirculation Zone spatial structure is more oscillatory than exponentially growing or decaying—as does seem to be true for the flow patterns in the schematic Fig. 5—then $\nabla^2 \zeta$ will most often have the opposite sign of ζ. $r_0 > 0$ and $\nabla^2 \zeta < 0$ imply $\nu < 0$; i.e., the relative vorticity flux would be counter-gradient. We shall return to this issue in Sections 6 and 7.
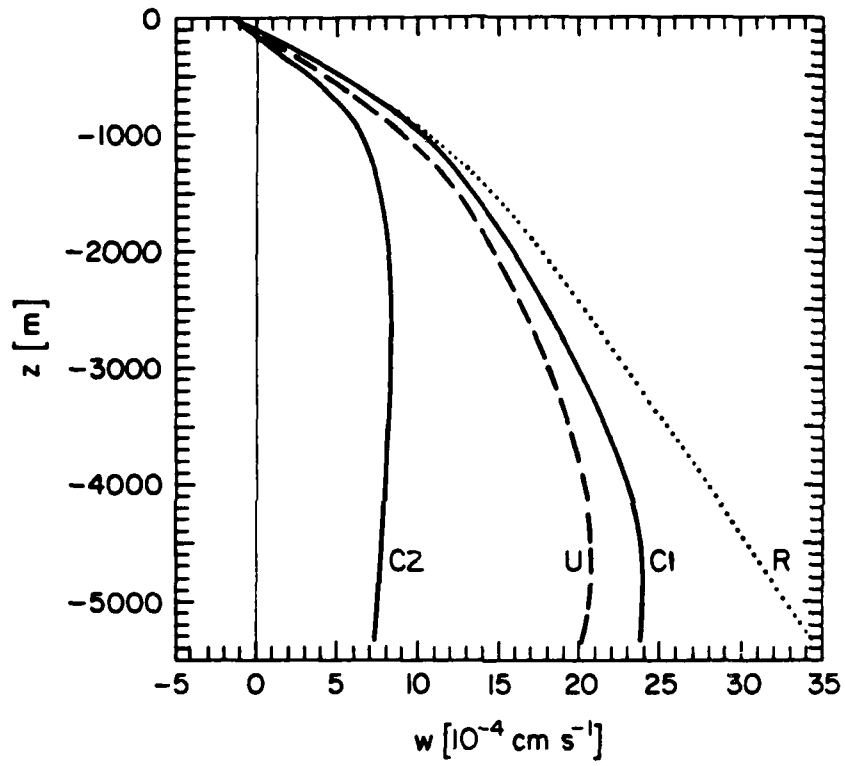
Fig. 7. Total mean vertical velocity from eq. (16). w_s is taken from Fig. 6 and r_0 from Table 1.

HEAT

The mean heat balance equation in the interior can be written

$$\underset{\sim}{u} \cdot \nabla\theta + w\,\frac{\partial\theta}{\partial z} = -\nabla\cdot\overline{(\underset{\sim}{u'}\theta')} - \frac{\partial}{\partial z}\,\overline{(w'\theta')} \ , \tag{17}$$

neglecting molecular conduction. This equation, as written, is not based upon a small Rossby number assumption.

From previous calculations, we know most of the quantities on the left side of (17); in particular, the vertical profiles of $\underset{\sim}{u}$, w, and $\partial\theta/\partial z$. We can calculate the remaining quantity $\nabla\theta(z)$ from a thermal wind relation based upon geostrophic, hydrostatic, and Boussinesq approximations, yielding

$$- \underset{z}{e}\times \frac{g}{f\rho_0}\,\nabla\,\rho = \frac{\partial u}{\partial z} \ , \tag{18}$$

a linearization of the equal of state for sea water,

$$\delta\rho = -\rho_0[\alpha_T(z)\delta\theta + \alpha_S(z)\delta S] \ , \tag{19}$$

and an assumption of local homogeneity of water masses, implying a strong correlation between θ and S variations,

$$\delta S = \mathcal{S}(z)\delta\theta \ . \tag{20}$$

In (18), e_z is a unit vertical vector. In (19), α_T and α_S are coefficients of thermal and saline expansion,

$$\alpha_T = -\frac{1}{\rho_0}\,\frac{\partial\rho}{\partial T} \ , \quad \alpha_S = -\frac{1}{\rho_0}\,\frac{\partial\rho}{\partial S} \ , \tag{21}$$

evaluated at each z with the mean T, S, and P values. Compressibility effects are neglected (e.g., an α_p in (19), or the difference between an α_θ and an α_T). The prefix δ in (19) and (20) denotes any infinitesimal variation of the indicated quantity. The quantity $\mathcal{S}(z)$ in (20) is calculated as

$$\mathcal{S}(z) = \frac{dS(z)}{d\theta(z)} \ , \tag{22}$$

the derivative of the composite $S(\theta)$ constructed from Fig. 2a. Combining (18)-(22), we obtain the desired expression for $\nabla\theta(z)$,

$$\underset{\sim}{\nabla}\theta = \frac{-f}{g[\alpha_T + \mathcal{S}\alpha_S]}\,\underset{z}{e}\times\frac{\partial}{\partial z}\,\underset{\sim}{u} \ . \tag{23}$$

Horizontal temperature advection can therefore be written as

$$\underset{\sim}{u}\cdot\nabla\theta = \frac{f}{g[\alpha_T + \mathcal{S}\alpha_S]}\left(u\,\frac{\partial v}{\partial z} - v\,\frac{\partial u}{\partial z}\right) \ . \tag{24}$$

A similar relation was derived by Bryden (1976). For the particular circumstance where $u(z) \equiv v(z)$, as in profiles C1 and C2 in Fig. 4, this advection vanishes. Even in profiles R and U, where $u \equiv v$, there is a considerable tendency for cancellation in (24).

Thus, all quantities on the left side of (17) are known. Unfor-

218

tunately, those on the right are not, except as residuals in this
equation. We shall make an interpretation of these residuals below.

The combined expansion coefficient, $\alpha_T + \beta \alpha_S$, and its components are
plotted in Fig. 8. Temperature effects are dominant throughout the
profile, although salt contributions are not negligible. The resulting
total mean advection,

$$A(z) = \underline{u} \cdot \nabla \theta + w \frac{\partial \theta}{\partial z} , \tag{25}$$

the left side of eq. (17), is plotted in Fig. 9. The largest values
are in the thermocline, and these imply a cooling tendency due to up-
welling of colder water. This effect persists throughout most of the
water column but is reversed near the upper surface, due to downward
Ekman pumping. The predominance of positive advection values is due
primarily to upward vertical advection, which itself has significant
positive contributions from both w_S and the eddy flux term in (16).
Even if the latter term were neglected (i.e., $r_0 = 0$), however, the
net advection would still be mostly positive, as seen in Fig. 5 by the
predominance of $w_S > 0$. Only in the bottom km would there be some
net warming (in profiles C1 and U). Mean horizontal advection
vanishes in profiles C1 and C2, for the reason given following (24).
For profiles R and U, it provides a warming tendency in the thermo-
cline, with a magnitude roughly 20% of the cooling due to upwelling.
Near the bottom, horizontal advection could also be important; profile
R produces a cooling and U a warming.

As in the previous vorticity equation, the time derivative term has
been neglected in (17). A scale estimate for this term can be
constucted from an upper bound on the changes in θ in the deep water
of 0.03°C (from comparing the different years' averages) and a lower
bound on the time scale of 1 year. Thus

$$\left| \frac{\partial \theta}{\partial t} \right| \lesssim 0.1 \times 10^{-8} \text{ °C s}^{-1} .$$

A comparison of this number with the mean advection profiles in Fig. 9
shows that the neglect of $\partial \theta / \partial t$ is a reasonable approximation for most
depths and profiles, although in a few circumstances (e.g., $z = -4800$
m and profile C2) the errors could be significant.

We shall interpret the residual from mean advection as eddy dif-
fusion. Thus, we formally make the following replacements for the
flux divergences in (17):

$$-\frac{\partial}{\partial z} \left(\overline{w'\theta'}\right) = \frac{\partial}{\partial z}\left(\kappa_v(z) \frac{\partial \theta}{\partial z}\right)$$
$$-\nabla \cdot \left(\overline{\underline{u'}\theta'}\right) = \nabla \cdot \left(\kappa_H(z) \nabla \theta\right) . \tag{26}$$

If only the sum of vertical and horizontal diffusion is known, as is
the case here, then the sum could be interpreted as either type. For
such alternative interpretations, the ratio of the associated diffu-
sivities would be approximately
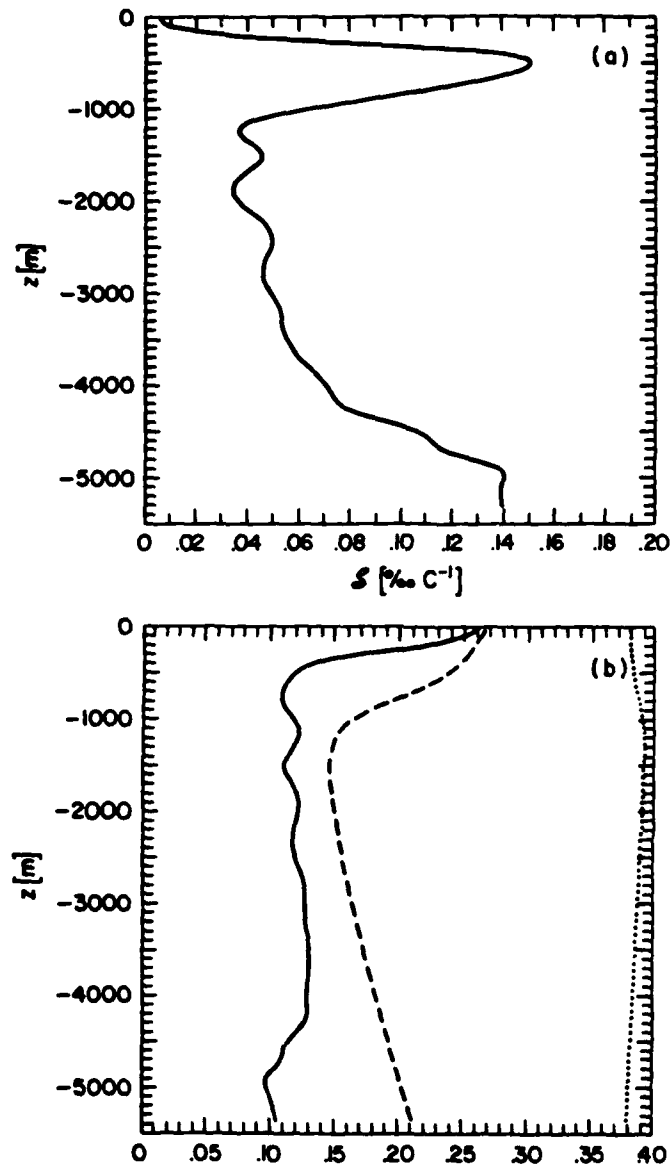
Fig. 8. (a) $\mathscr{S}(z)$ from eq. (16); (b) expansion
coefficients: $10^3 \, \alpha_T [C^{-1}]$, dashed line;
$-0.5 \times 10^3 \, \alpha_S \, [0/00^{-1}]$, dotted line;
$10^3 (\alpha_T + \mathscr{S}\alpha_S) \, [^{\circ}C^{-1}]$, solid line. These
quantities are computed from θ and S pro-
files smoothed with 400 applications of
eqs. (1) and (2a) to the profiles of Fig. 3
on a grid with $\Delta z = 10$ m.
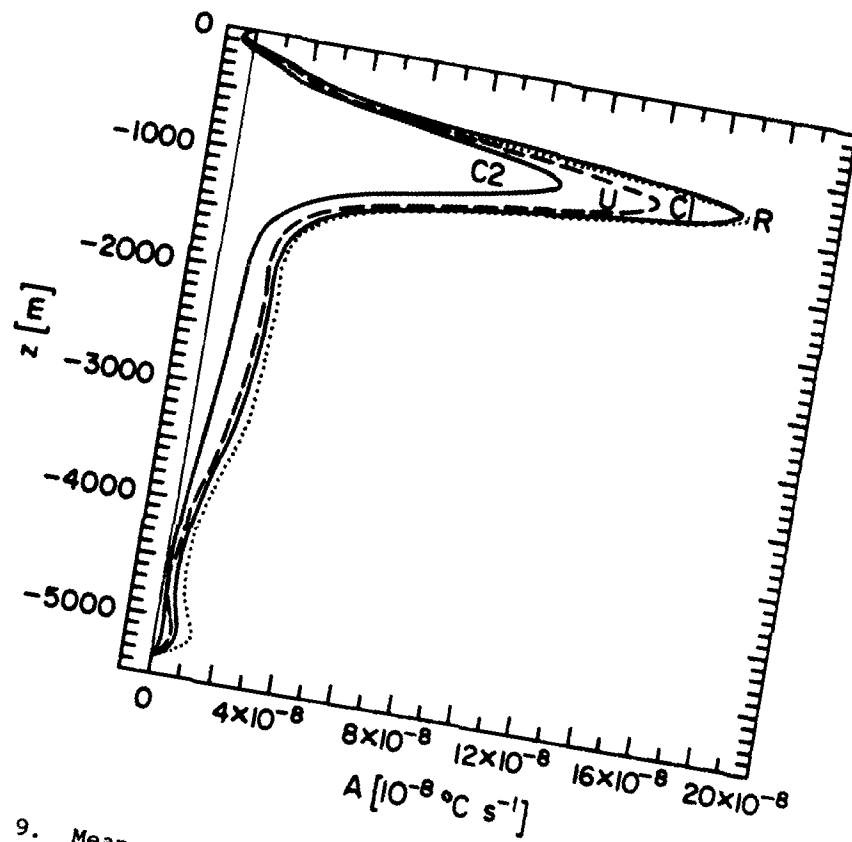
Fig. 9. Mean advection of potential temperature from eq. (25). Four hundred additional applications of the smoothing formulae (1) and (2) have been made to the profiles of Figs. 3-4 and 6-7. The labeling convention is as in Fig. 6.

$$\frac{\kappa_v}{\kappa_H} \sim \mu^2 \ ,$$

where μ is the slope of the mean isothermal surface relative to horizontal, in order that the total diffusion be the same for each alternative.

By quasigeostrophic scaling arguments, mesoscale eddy processes should have a ratio of heat flux divergences implying

$$\frac{\kappa_v}{\kappa_H} \sim \left(\frac{R}{B} \right)^2 \left(\frac{h}{\ell} \right)^2 \ ,$$

where R is a Rossby number ($=U/f\ell$) and B is a Burger number ($=N^2h^2/f^2\ell^2$) and h and ℓ are characteristic vertical and horizontal scales of the general circulation [see, for example, Stone's (1972) analysis of the baroclinic instability problem]. If μ and (h/ℓ) are approximately the same, then mesoscale eddies have a smaller ratio of diffusivities than the indistinguishable alternatives above since R/B $\ll$ 1. We shall therefore adopt the following interpretation for the eddy diffusion alternatives: if mesoscale diffusion processes were dominant, κ_H would be the dominant diffusivity; whereas, if κ_v were dominant, the processes could not be mesoscale or else an excessively large κ_H would be indicated, and hence we would associate κ_v with sub-mesoscale processes such as breaking internal waves.

First, we examine the possibility that the diffusion is wholly vertical; i.e., $\kappa_H = 0$. Then (17), (25), and (26) imply

$$\kappa_v(z) = \kappa_v(z_0) + \frac{1}{\partial\theta/\partial z} \int_{z_0}^{z} dz' \ A(z') \ , \tag{27}$$

We choose z_0 and the integration constant in (27) somewhat arbitrarily such that κ_v is a minimum at z_0 and its value there is 0.1 cm^2s^{-1}; for each of the four velocity profiles in Fig. 4, $z_0 = -H$. The result is shown in Fig. 10 for the C1 velocity profile (results from other profiles are similar). The inferred values are quite large throughout most of the water column, and, as such, are insensitive to the small value chosen for $\kappa_v(z_0)$. These values are in fact too large by several orders of magnitude compared to direct estimates of κ_v in the ocean and the laboratory (Gargett, 1982). Thus, we reject the hypothesis that the eddy diffusion is wholly vertical.

The extreme alternative is that the eddy diffusion is entirely horizontal ($\kappa_v = 0$). Hence, from (17) and (26),

$$\kappa_H(z) = \frac{\nabla\theta}{|\nabla\theta|^2} \cdot \int^{x} d\underset{\sim}{x}' \ A. \tag{28}$$

We cannot evaluate (28) because it requires knowledge we do not have about the horizontal variatiation of A(z). We are, therefore, forced to approximate (28) as

$$\kappa_H(z) \sim L \frac{|A(z)|}{|\nabla\theta(z)|}$$
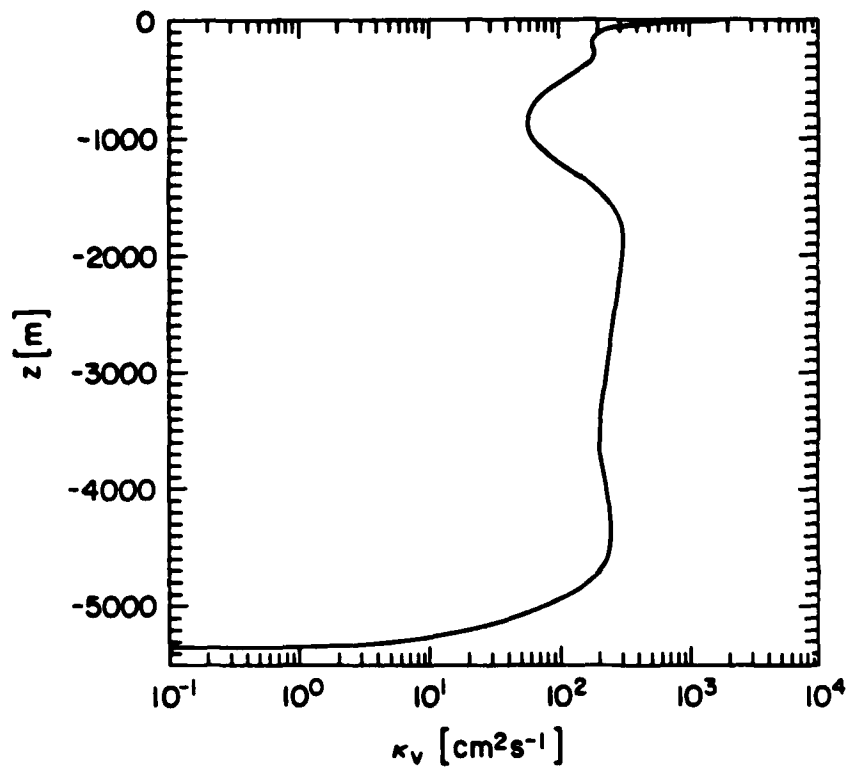
Fig. 10. Vertical diffusivity for heat from eq. (27), based
upon velocity profile C1. Incremental smoothing is as in
Figs. 8 and 9.

$$= \frac{Lg\,(\alpha_T + \beta\alpha_S)}{f\,|\partial \underline{u}/\partial z|} \; \left| \underline{u}\cdot\nabla\theta + w\,\frac{\partial\theta}{\partial z} \; \right| \; . \qquad (29)$$

In this final approximation, any depth dependence in the horizontal integral of (28) is lost, as is the directional information in the vector dot product.

The κ_H profiles from (29) are plotted in Fig. 11 for L = 200 km, as before. A change in L would simply shift the abscissa in Fig. 11. Also plotted are several more directly estimated diffusivities. Bryden (1982; Tables 1 and 3) lists thermocline values for both the numerator and denominator of

$$\kappa = -\; \overline{\underline{u}'T'}\cdot\nabla\overline{T}/\left|\nabla\overline{T}\right|^2 \; ,$$

based upon moored measurements; $\nabla\overline{T}$ is calculated from $\underline{u}_z$, as in (23). For two types of averages, essentially the same two as for the mean velocities in Fig. 4, one obtains values of 0.9 and 1.1×10^8 cm^2s^{-1} for κ; these are the circles in Fig. 11. Price (1983) has calculated single-particle Taylor diffusivities from the rate of spreading of clusters of SOFAR floats. Zonal and meridional diffusivities $\left(\kappa^{(x)},\; \kappa^{(y)}\right)$ at 700 m and 1300 m depths are respectively (0.8, 0.5) and (0.2, 0.2) x 10^8 cm^2s^{-1}. These are plotted as crosses in Fig. 10. There is, of course, no necessity for particles to be dispersed as heat is in situations where temperature is not dynamically passive; however, the two types of dispersion have been found to be similar in some relevant modeling studies (McWilliams and Chow, 1981), and we see that this is true for the LDE as well.

There is some indication that the particle diffusivities are slightly smaller than the thermal ones, but this feature is uncertain within the estimation errors quoted by the authors of the direct estimates. In any event, there is agreement to within half an order of magnitude between the inferred $\kappa_H(z)$ from (29) and the more directly estimated κ, $\kappa^{(x)}$, and $\kappa^{(y)}$ in the depth range where comparisons can be made. The worst agreement is with the 1300-m particle diffusivities, which are small relative to κ_H (1300 m). However, the former were estimated from a data set taken during a period dominated by Rossby wave motion (Price and Rossby, 1982) and are thus likely to underestimate the true mean diffusivity, which would also include contributions from other periods where the flow would be more turbulent and less wave-like.

This general agreement with directly estimated diffusivities gives credibility to the inferred values, which have the advantage of spanning the full depth of the ocean. Taking a broad view of the curves in Fig. 11, averaging over different profiles and small vertical scale structures [including the leftward cusps associated with the near-surface zero in A(z)], we can conclude the following: $\kappa_H(z)$ is large, of order 10^8 cm^2s^{-1}, and nearly uniform over a broad depth

224
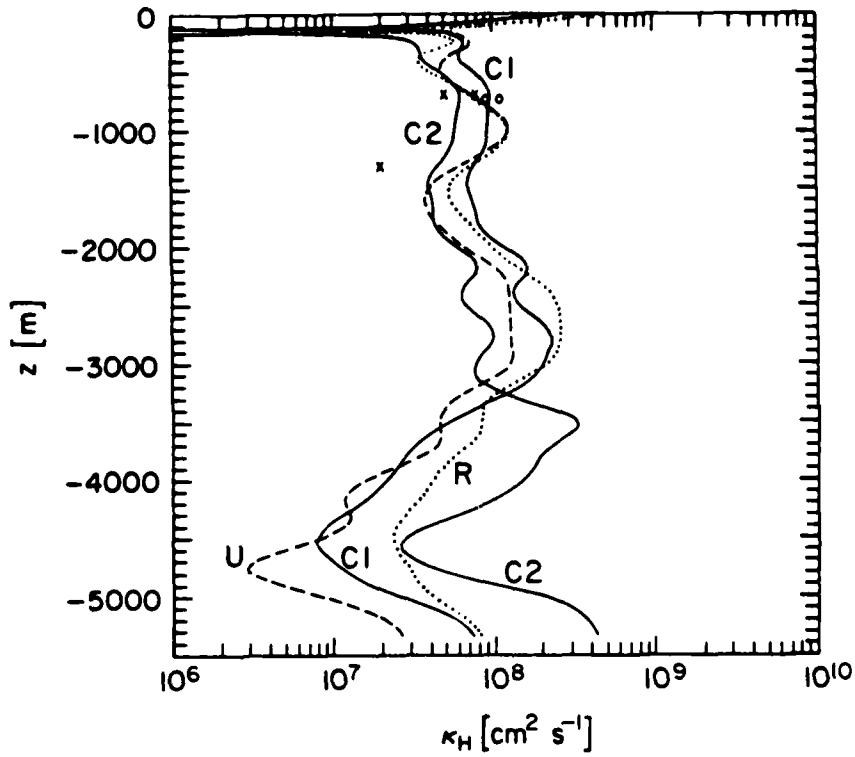
Fig. 11. Horizontal diffusivity for heat from eq. (29), based upon the four velocity profiles of Figs. 4 and 7, with incremental smoothing as in Figs. 8 and 9. Data points are directly measured diffusivities (0 = heat, x = particles) as described in the text.

range from near the surface to perhaps $z = -4000$ m. At greater depths the inference is more uncertain because of a sensitivity to uncertainties in the near-bottom velocity profile, but κ_H may be as large there as it is shallower.

Thus, on statistical grounds we cannot reject the hypothesis that the eddy heat diffusion is entirely horizontal. Of course, on physical grounds we would expect lesser, but non-zero vertical diffusion from both sub-mesoscale and mesoscale processes. We therefore conclude that thermal equilibrium in the Recirculation Zone is accomplished in the mean as a balance primarily between mean advection, mostly vertical, and mostly horizontal flux divergences associated with mesoscale eddies. These eddy heat fluxes are down-gradient ones, across mean isothermal surfaces, effecting a net warming in the Recirculation Zone by a diffusion of heat outwards from the warm core of the Gulf Stream Gyre.

The down-gradient characterization is correct at most depths since A is positive and the horizontal temperature gradient is in one quadrant (NW) because both velocity shear components are negative. Even near the surface, where $A < 0$, a down-gradient relation is possible if the temperature gradient reverses in sign as well. This is true at least at the surface where $\partial\theta/\partial y < 0$ (Oceanographic Atlas of the North Atlantic Ocean, 1967). We cannot assess accurately the sign of the mean temperature gradient in this depth interval from LDE measurements since there are too few available velocity measurements above 250 m depth.

SALT AND DENSITY

The mean balance equations for both salt and density have the same forms as that for heat, (17), with mean advection balancing eddy flux divergences. Furthermore, from (19) and (20), small variations in both quantities are linearly proportional to $\delta\theta$, with the proportionality constant only a moderately variable function of depth (n.b., Fig. 8). Therefore, when arguments analogous to those of Section 4 are made for S or ρ, the inferred $\kappa_v(z)$ will be similar to Fig. 10, the $\kappa_H(z)$ will be identical to Fig. 11, and the summary conclusion about a balance primarily between mean advection and mesoscale horizontal diffusion will be the same.

POTENTIAL VORTICITY

Mean potential vorticity variations δq are defined as

$$\delta q = \beta\delta y - \frac{fg}{\rho_0}\frac{\partial}{\partial z}\left(\frac{\delta\rho}{N^2}\right) + \delta\zeta \tag{30}$$

under quasigeostrophic assumptions. Thus, with (18), we write the mean horizontal gradients as

$$\frac{\partial q}{\partial x} = f^2 \frac{\partial}{\partial z} \left(N^{-2} \frac{\partial v}{\partial z} \right)$$

$$\frac{\partial q}{\partial y} = \beta - f^2 \frac{\partial}{\partial z} \left(N^{-2} \frac{\partial u}{\partial z} \right) ,$$

(31)

where $\underline{\nabla}\zeta$ is neglected, as in Section 3 [n.b., a scale estimate of its relative magnitude is the same as the ratio preceding eq. (9)]. The magnitude of $\underline{\nabla}q$ can be interpreted as a wave propagation strength, where, crudely, a phase speed is $|\underline{\nabla}q| \cdot k^{-2}$, with k a horizontal wavenumber. The sign reversal of $\underline{\nabla}q$ with depth is a necessary condition for baroclinic instability (Pedlosky, 1979). We see in Fig. 12 that the propagation tendency exceeds the Rossby wave measure (i.e., $\beta = 2 \times 10^{-13}$ cm^{-1}s^{-1}) in both components of $\underline{\nabla}q$ in some depth ranges. There are also multiple zero crossings, assuring that the necessary condition for instability is satisfied; Bryden (1982) and the discussion in Section 4 have shown that there are down-gradient eddy heat fluxes in the thermocline, which is a property associated with baroclinic instability. The vertical structure of $\underline{\nabla}q(z)$ is complicated, but qualitatively similar for the different velocity profiles considered. The largest amplitudes occur near the bottom. This is because $N^{-2}(z)$ is much larger at depth, even though velocity shears are somewhat smaller there than in the thermocline.

There have been recent predictions of potential vorticity homogenization from theory and modeling (Holland, 1983; McWilliams and Chow, 1981; Rhines and Young, 1982): $\underline{\nabla}q$ and q'^2 should be very small in the ocean interior if sub-mesoscale, non-conservative processes are sufficiently weak (i.e., their eddy diffusivities are sufficiently small). Furthermore, there is empirical evidence from the historical archive of hydrographic data that mean potential vorticity does not have large horizontal variations between perhaps 250-m and 850-m depth in the North Atlantic Subtropical Gyre, which contains the Recirculation Zone (McDowell et al., 1983). This feature is not obvious in our estimates of $\underline{\nabla}q$ (Fig. 12), which are not particularly small in this depth interval.

The data presented in McDowell et al. (1983) are estimates of

$$Q = - \frac{f}{\rho_0} \frac{\partial \rho_\theta}{\partial z} = \frac{f}{g} N^2 ,$$

(32)

where ρ_θ is potential density. This is a definition of potential vorticity based upon somewhat different assumptions than (30): δQ and δq are not equivalent, although they have the same dynamical inplications if we make the quasigeostrophic approximation and further neglect relative vorticity. We can compare our local estimate of Q with their data: it is simply f/g (= 7.4×10^{-8} s cm^{-1}) times $N^2(z)$, as plotted in Fig. 3d. The resulting profile matches well their nearest data at 31°N, 65°W), with small differences attributable to the degree of smoothing. Thus, the small range of horizontal variation of Q within the Subtropical Gyre, between the N^2 minimum in the 18°C thermostad
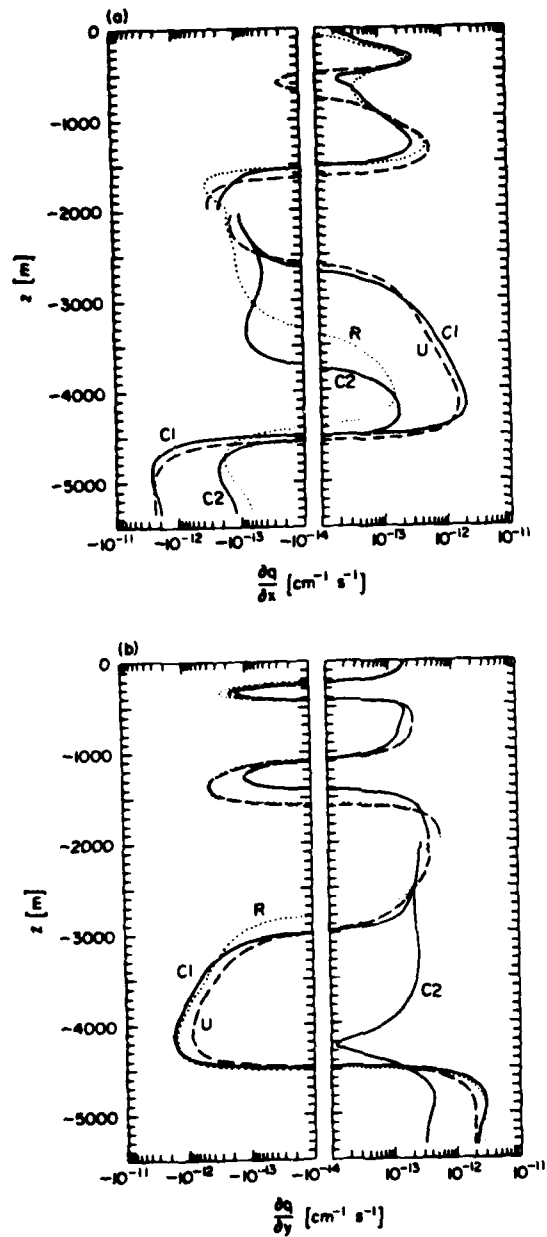
Fig. 12. Mean potential vorticity
gradients from eq. (31). Incre-
mental smoothing of $\underset{\sim}{u}$ and N^2,
starting from the profiles of
Figs. 3d and ¼, has been perform-
ed by NS applications of (1)-(2).
Above $z = -2000$ m, NS = 400, and
below that level, NS = 2000.

and the N^2 maximum in the main thermocline, is confirmed in the LDE data.

However, what is dynamically important is not the size of the absolute variations of Q; rather it is the size of the relative variations at a fixed depth (or on a fixed potential density surface—the quasigeostrophic approximation does not make a significant distinction between the two in this regard). This aspect of the Q distribution is best demonstrated in their Figs. 17-19, which are plots against latitude of Q averaged within three adjacent layers defined by particular surfaces of constant potential density. In each plot data are included from two sections (50°W and 65°W) which pass through the Recirculation Zone, as drawn in Fig. 1a, and for comparison the contribution to Q variations from β is also plotted. These Q plots are adapted slightly as our Fig. 13. The scatter in these plots is considerable, which makes interpretation difficult. However, our own estimates of ∇q from (31) are also of questionable accuracy since the indicated vertical scale is not large and a second vertical derivative of velocity is a difficult calculation to make from moderately uncertain mean velocity measurements. Nevertheless, a comparison of the two types of estimates indicates substantial agreement.

The shallowest of the three layers contains the N^2 minimum, and occurs between 200- and 400-m depth at the LDE site. The Q data show a northward decrease, opposite to the β-effect, until the approximate location of the Gulf Stream. In addition, the Q values along 50°W appear to be somewhat larger than those along 65°W in the Recirculation Zone. No substantial region of homogenization is indicated. The local estimates in Fig. 12 show

$$\frac{\partial q}{\partial y} < 0 \ , \quad \frac{\partial q}{\partial x} > 0$$

in this depth interval, with comparable magnitudes for each component, which is wholely consistent with the Q variations.

The middle layer extends from just below the N^2 minimum to just above the N^2 maximum, 400-700 m depth at the LDE site. The Q data show a very extensive region north of about 15°N where any large-scale variations are substantially less than the β-effect, and significant homogenization could be occurring. However, the northern edge of this region appears to coincide with the southern edge of the Recirculation Zone, near 30°N. Northward of this point, Q increases at approximately the rate due to β. The Q values appear to be somewhat smaller along 50°W than along 65°W, although this difference, if real, is smaller relative to the β-effect than the zonal difference in the upper layer. Again the comparison with our local estimates is very good. $\partial q/\partial y$ is positive with about the value of β, indicating that the homogeneous region, if it exists in this layer, does not extend into the Recirculation Zone. $\partial q/\partial x$ is locally diminished in this layer, and perhaps negative (profile U). The zonal gradient of mean potential vorticity does appear to be small in the upper thermocline of the Recirculation Zone.
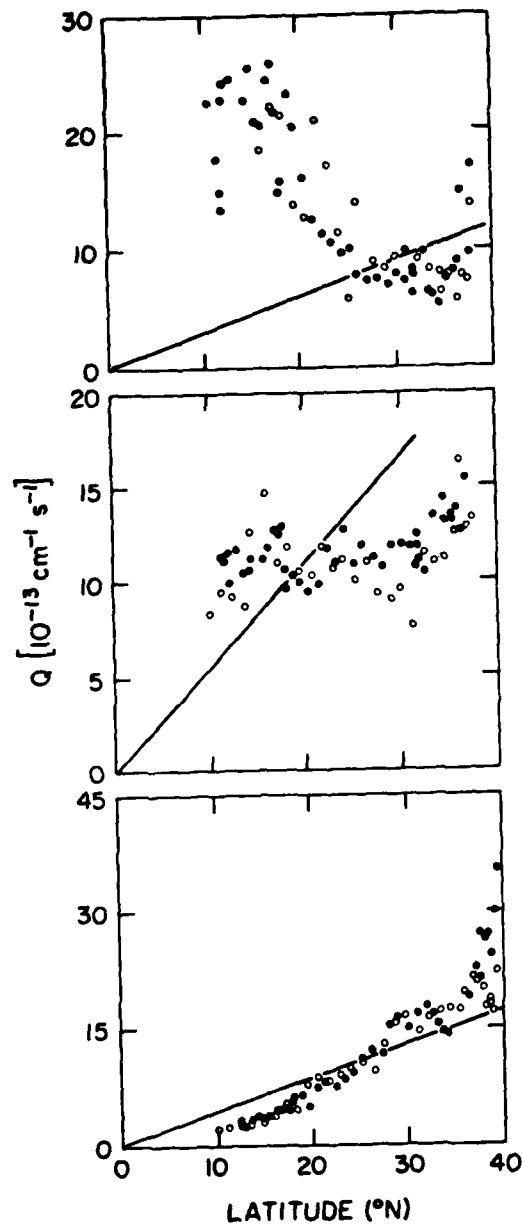
Fig. 13. Potential vorticity from eq. (32),
as calculated by McDowell et al. (1983),
from which this figure was adapted. The
data points are coded by longitude:
closed circles are from 65°W and open
circles are from 50°W. The plots are
form layers bounded by surfaces of con-
stant $\rho\theta$: the upper has bounds [1.0263,
1.0265], the middle [1, 0265, 1.0270],
and the lower [1.0270, 1.0273]. The
lines indicate the contributions to Q
variations from β alone.

The lowest of the three layers contains the N^2 maximum, 700-850 m depth locally. The Q data show a northward increase at about the rate due to β and a narrow region of eastward increase in the center of the Recirculation Zone, which decreases to a small, uncertain zonal trend on the southern edge. This is again in good agreement with the estimates in Fig. 12: $\partial q/\partial y \approx \beta$, and $\partial q/\partial x$ is more weakly positive.

In summary, therefore, the qualitative features of our local ∇q estimates are confirmed in the large-scale analysis of McDowell et al. (1983), and one can at least tentatively reject the occurrence of homogenization, at any level significantly below the contributions from β, in and above the thermocline in the Recirculation Zone. The theoretical predictions of homogenization assume vanishingly small values for sub-mesoscale eddy flux divergences. Perhaps homogenization does not occur in the ocean because these processes are not sufficiently weak. In support of this possibility, Brown and Owens (1981) have estimated a sub-mesoscale horizontal diffusivity for momentum of 3×10^6 cm^2s^{-1} in the thermocline in the LDE, and, above the thermocline in the 18°C thermostad, wintertime boundary layer turbulence is strong. It is unclear whether these are sufficient to obviate the $\nabla q \approx 0$ prediction in principle.

The mean balance equation for potential vorticity is

$$\underset{\sim}{u} \cdot \nabla q = -\nabla \cdot (\overline{u'q'}) \ , \tag{33}$$

again with a small Rossby number assumption. This is a reformulation of the vorticity equation (7), where the eddy fluxes of both relative and stretching vorticity explicitly enter on the right side [see (35) below]. From (31),

$$\underset{\sim}{u} \cdot \nabla q = \beta v + f^2 \left[u \frac{\partial}{\partial z} \left(N^{-2} \frac{\partial v}{\partial z} \right) - v \frac{\partial}{\partial z} \left(N^{-2} \frac{\partial u}{\partial z} \right) \right] \ . \tag{34}$$

Another aspect of the homogenization prediction discussed above is that the potential enstrophy $\overline{q'^2}$ should vanish. From (33), we see that this cannot happen unless the mean q advection vanishes (i.e., $\overline{q'^2}$ cannot vanish over a region while $\nabla \cdot \overline{u'q'}$ is required to remain nonzero). This mean advection is plotted in Fig. 14. In profiles C1 and C2, $u \equiv v$, and the advection is simply βv. In these profiles there is thus no indication of vanishing advection at other than a single depth. Profiles R and U show more complexity with depth, and, relevant to the prediction, they indicate a locally diminished advection in the 18°C thermostad. The true character of this feature is, unfortunately, hidden by the large uncertainties in our estimates, as indicated by the variations among the profiles. These uncertainties are so large below the thermocline as to make any interpretation doubtful.

The mean q balance in (33) and (34) is implicit in previous inferences of vorticity and heat balances. The eddy flux divergence can be decomposed as follows:
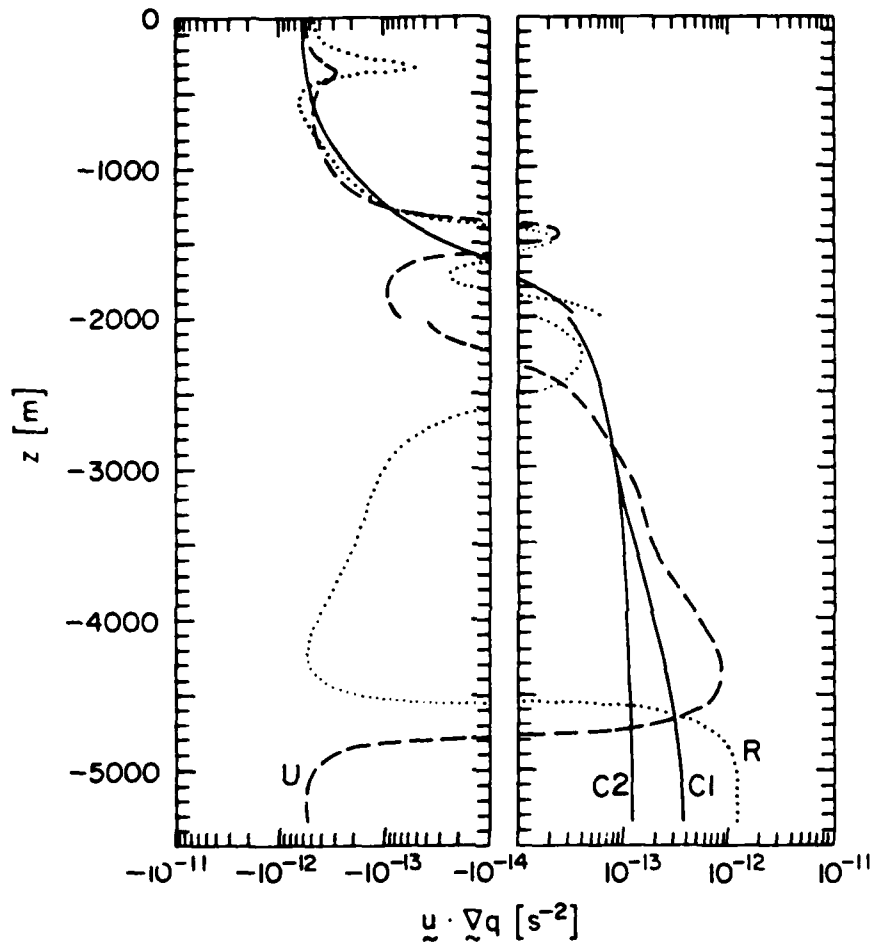
Fig. 14. Mean potential vorticity advection from eq. (34) and the profiles of Fig. 12.

$$-\underset{\sim}{\nabla}\cdot(\overline{\underset{\sim}{u}'q'}) = -\underset{\sim}{\nabla}\cdot(\overline{\underset{\sim}{u}'\zeta'}) - \underset{\sim}{\nabla}\cdot(\overline{\underset{\sim}{u}'\chi'}) , \tag{35}$$

where

$$\chi' = -\frac{fg}{\rho_0}\frac{\partial}{\partial z}\left(\frac{\rho'}{N^2}\right) \tag{36}$$

is the eddy stretching vorticity [analogous to the second term in (30)]. By the arguments of Section 3, we estimate the relative vorticity flux divergence as

$$-\nabla\cdot(\overline{\underset{\sim}{u}'\zeta'}) = r_0, \tag{37}$$

where values for r_0 are listed in Table 1. By previously presented arguments, we can also derive the following relations:

$$-\underset{\sim}{\nabla}\cdot(\overline{\underset{\sim}{u}'\chi'}) = \frac{fg}{\rho_0}\frac{\partial}{\partial z}\left(\frac{1}{N^2}\underset{\sim}{\nabla}\cdot(\overline{\rho'\underset{\sim}{u}'})\right)$$

$$= -f\frac{\partial}{\partial z}\left(\frac{1}{\partial\theta/\partial z}\underset{\sim}{\nabla}\cdot(\overline{\underset{\sim}{u}'\theta'})\right)$$

$$= f\frac{\partial}{\partial z}\left[w + (\underset{\sim}{u}\cdot\nabla\theta)/\frac{\partial\theta}{\partial z}\right]$$

$$= -r_0 + f\frac{\partial}{\partial z}\left[w_s + (\underset{\sim}{u}\cdot\nabla\theta)/\frac{\partial\theta}{\partial z}\right]$$

$$= -r_0 + \underset{\sim}{u}\cdot\nabla q . \tag{38}$$

The final relation in (38), of course, makes (33) an identity when combined with (35) and (37). The penultimate relation in (38) shows that the stretching vorticity flux divergence opposes the relative vorticity flux and contributes an additional term as well (which is equal to what is plotted in Fig. 14). This additional term is related to the mean heat advection without the enhanced vertical advection driven by r, and its balancing eddy heat flux is also predominantly down-gradient because $w_s\cdot\partial\theta/\partial z$ is predominantly positive (n.b., the discussion following (25) in Section 4). Brown and Owens (personal communication) have calculated the fluxes in (35) at 700-m depth from LDE moored measurements, although their divergences could not be calculated. They found, firstly, that $\overline{u'\chi'}$ was nearly an order of magnitude larger than $\overline{u'\zeta'}$ and, secondly, that $\overline{u'q'}$ had a magnitude of 2×10^{-5} cm s^{-2} directed toward 210° true. The ∇q at 700 m from Fig. 12 has a magnitude of about 2×10^{-13} cm^{-1}s^{-1} directed toward NNW. Thus, a potential vorticity diffusivity is 1×10^8 cm^{2}s^{-1}, acting almost directly downgradient.

The stretching vorticity flux is thus dominant and is associated with the down-gradient (i.e., positive diffusivity) heat flux described in Section 4. This suggests that the subordinate relative vorticity flux, acting in opposition, is a counter-gradient (i.e., negative horizontal eddy viscosity) process. This was also suggested from the signs of r and ζ in Section 3. Unfortunately, not enough is known of the spatial structure of the general circulation to confirm the sug-

gestion. In some modeling studies (e.g., McWilliams and Chow, 1981), these relations between the different fluxes have been demonstrated.

The ∇q profiles in Fig. 12, while not "homogeneous," do provide non-trivial constraints upon eddy potential vorticity q'. If a fluid parcel initially at rest traverses a horizontal distance while conserving q + q', then

$$q' = - \Delta x \cdot \nabla q . \tag{39}$$

Sufficiently intense, locally generated (i.e., $|\Delta x| \leq L$) eddy motions, if they occur, will have ζ' and χ' magnitudes much larger than q' . Consistency thus requires a degree of negative correlation between ζ' and χ', at a level set by (39) and the eddy intensity. Hua and Owens (1983) have demonstrated that this correlation exists in the LDE thermocline. This negative correlation also gives further support to the idea that the stretching and relative vorticity flux divergences in (35) are acting in opposition.

ENERGY AND MOMENTUM

In this section, some remarks are made about two mean dynamical balances which cannot be fully described from present observations.

A complete characterization of the mean energy balance is not feasible, because of unknown lateral fluxes, bottom boundary layer dissipation, and pressure work. However, Bryden (1982) has made estimates of some terms in the balance, the local rates of mean energy loss or gain in the LDE thermocline through interactions with mesoscale eddies. He has found that the loss of mean potential energy to the eddies through baroclinic conversion processes (e.g., baroclinic instability) is significant, while the loss or gain of mean kinetic energy due to correlations between the divergences of horizontal eddy Reynolds stresses and mean velocities is at least an order of magnitude smaller. On the other hand, the loss of eddy kinetic energy through correlations between horizontal Reynolds stresses and mean horizontal shear is positive, although smaller in magnitude than the baroclinic conversion process. Unfortunately, this estimate has substantial uncertainties due to its dependence upon ∇u (n.b., Section 2c). The imbalance between the two types of kinetic energy conversion, if real, would suggest the importance of lateral energy fluxes in the Recirculation Zone.

The baroclinic loss from the mean is consistent with down-gradient heat flux (Section 4) and stretching vorticity flux dominance (Section 6). From a counter-gradient momentum flux (Sections 3 and 6), one would expect a transfer of kinetic energy from the eddies to the mean at least in a volume average, whereas the preceeding evidence is ambiguous.

If there is a prevalent counter-gradient momentum flux in ... Recirculation Zone, then it would provide a force driving the northeastward

Reverse Flow below the thermocline, insofar as momentum is being transferred horizontally, with negative viscosity, from a hypothetical deep, southwestward Return Flow nearer to the Gulf Stream. Another force is associated with the down-gradient heat fluxes; it is often called isopycnal form drag, and it is characterized by a positive vertical eddy viscosity (McWilliams and Chow, 1981). Such a process would provide a local retarding force for the Reverse Flow, since this lies beneath an opposite Return Flow in the thermocline.

However, form drag may be a significant cause of the deep Reverse Flow, through action from a distance. In an analysis of the Deep Counter-rotating Gyre (see Fig. 5) in a numerical model solution, Holland and Rhines (1980) showed that form drag was the primary source of momentum for the gyre as a whole. Its accelerating effects, though, would occur in the northern branch, where Return Flow occurs in both the thermocline and deeper, and form drag can transfer westward momentum downwards. One can therefore imagine that the southern, Reverse Flow branch exists primarily to close the gyre mass budget for the more strongly driven deep Return Flow in the north. In this case, the local driving force in the Reverse Flow would be a weak, westward pressure gradient.

These two possibilities for Return Flow driving forces are not mutually exclusive; either or both may be occurring.

SUMMARY AND DISCUSSION

In this paper, an analysis has been made of the estimated mean hydrographic and horizontal velocity profiles in the southern part of the Recirculation Zone. The flow in and above the thermocline is to the southwest and is presumably part of the Return Flow for the Gulf Stream Gyre. Below the thermocline the flow is to the northeast, which is referred to as a deep Reverse Flow. In an analysis of the mean vorticity balance, an inference is made of a generally upward mean vertical velocity, balanced partly by a nearly depth-independent eddy relative vorticity flux divergence. These inferences follow from calculations of the planetary vorticity advection, which implies a mid-depth maximum in the Sverdrup velocity, and of the top (Ekman) and bottom (topographic) boundary conditions. The latter in particular implies a large upward w due to a horizontal velocity across topographic contour lines. In an analysis of the mean heat balance, an inference is made of a significant hortizontal eddy heat flux acting in opposition to a net cooling by mean advection through most of the water column. This heat flux can be characterized by a positive lateral eddy diffusivity on the order of $10^8 \mathrm{cm}^2 \mathrm{s}^{-1}$. Mean potential vorticity gradients exhibit moderately strong, though complex, possibilities for wave propagation and baroclinic instability. They do not, however, show a region of homogenization. In the mean potential vorticity balance, the eddy flux divergence balances the mean advection, with stretching vorticity dominating relative vorticity in the flux.

The two types of vorticity flux divergence provide opposing tendencies in the potential vorticity balance.

Many of the previous diagnoses of the general circulation have been concerned with inferring the horizontal velocity from the three-dimensional structure of density (this, of course, is not our present concern because velocity measurements are available from the LDE). The methods of Stommel and Schott (1977), Davis (1978), and Wunsch (1978) all assume conservation in the mean of density and/or potential vorticity. As we have seen in Sections 4-6, this appears to be incorrect for both quantities in the Recirculation Zone: the eddy flux divergences are not negligible in the mean balance equations. Thus, such methods are probably inapplicable in this region and others where mesoscale eddy energies, and presumably fluxes, are large. A similar conclusion was reached by Keffer and Niiler (1982) for other sites in the North Atlantic with even less mesoscale energy than the Recirculation Zone.

It is worth remarking that the inferential method of this paper requires measurements from only a single mooring, assuming that sufficient hydrographic data are available to estimate mean profiles. We have made some use of measurements from multiple moorings (e.g., for estimating $\underline{u}^+\zeta^+$ and ζ), but only to check the consistency of the single mooring inferences. The justification for this comes from sampling error considerations. In the LDE, the estimated vertical shear in $\underline{u}$ across the thermocline is clearly significant, while the horizontal shear is not (see Section 2c). It also seems preferable to base the inferences upon directly measured $\underline{u}(z)$ time series from moorings rather than $\nabla\rho(z)$ from shipboard hydrographic profiles, even though in theory their information content is largely redundant [n.b., equation (18)], simply because it is difficult to obtain enough independent samples of the latter where eddy variability is substantial. For estimates of very large-scale currents rather than local ones, however, the sampling advantage shifts to $\nabla\rho$ if somehow a large-scale reference level can be determined.

In any of the present diagnostic methods, however, sampling errors are significant contaminants of the inferences. Ours is no exception. Within the measurement uncertainties for horizontal velocity (Section 2), the true mean profiles could be such that mean advections of heat, salt, density, and potential vorticity could be zero in any small depth interval, so that our inferences of significant mesoscale eddy flux divergences could be nullified. Also, the mean potential vorticity gradients could be made zero locally. To do this, however, would require deforming the velocity profiles away from the estimated point means, as well as introducing unsubstantiated, small-scale vertical structure in the profiles. This would not be a straightforward or unprejudiced data analysis, though, nor would its result be consistent with the available point measurements of eddy fluxes (e.g., the data points in Fig. 11). Hence, we judge our inferences more plausible than the alternatives above, but they are far from being deductions.

236

REFERENCES

Bradley, A., C. Ebbesmeyer, J. McWilliams, T. Rossby, and B. Taft,
    1977. Preliminary report for POLYMODE Cruise: R/V Endeavor 7.
    POLYMODE News, No. 29.

Brown, E.D., and W.B. Owens, 1981. Observations of the horizontal in-
    teractions between the internal wave field and the mesoscale
    flow. J. Phys. Oceanogr., 11, 1474-1480.

Bryden, H.L., 1973. New polynomials for thermal expansion, adiabatic
    temperature gradient, and potential temperature of sea water.
    Deep-Sea Res., 20, 401-408.

Bryden, H.L., 1976. Horizontal advection of temperature for low-
    frequency motions. Deep-Sea Res., 23, 1165-1174.

Bryden, H.L., 1982. Sources of eddy energy in the gulf stream recir-
    culation region. J. Mar. Res., in press.

Bryden, H., and R. Millard, 1980. Spatially averaged Local Dynamics
    Experiment CTD stations. POLYMODE News, 77 (Woods Hole Oceano-
    graphic Institution).

Davis, R.E., 1978. On estimating velocity from hydrographic data.
    J. Geophys. Res., 83, 5507-5509.

Ebbesmeyer, C., B.A. Taft, J.C. McWilliams, C.Y. Shen, S.C. Riser,
    H.T. Rossby, P.E. Biscaye, and H.G. Ostlund, 1983. Variability
    of physical and chemical properties along a Northwestern Atlantic
    Oceanographic Section (23-33°N; 70°W), in preparation.

Fofonoff, N.P., 1963. Precision of oceanographic data for sound speed
    calculations. J. Acous. Soc. Am., 35, 830-836.

Gargett, A., 1982. A parameterization of the vertical eddy diffusiv-
    ity in the ocean interior. J. Mar. Res., submitted.

Holland, W.R., 1978. The role of mesoscale eddies in the general cir-
    culation of the ocean: Numerical experiments using a wind-driven
    quasi-geostrophic model. J. Phys. Oceanogr., 8, 363-392.

Holland, W.R., 1983. Well-mixed regions of potential vorticity in numerical models of midlatitude ocean circulation. In preparation.

Holland, W.R., and P.B. Rhines, 1980. An example of eddy-induced ocean circulation. J. Phys. Oceanogr., 10, 1010-1031.

Hua, B.-L., and W.B. Owens, 1983. Estimates of eddy potential vorticity and its balance in the POLYMODE Local Dynamics Experiment. In preparation.

Keffer, T., and P.P. Niiler, 1982. Eddy convergence of heat, salt, density, and vorticity in the sub-tropical North Atlantic. Deep-Sea Res., 29, 201-216.

Leetmaa, A., and A.F. Bunker, 1978. Updated charts of the mean annual wind stress, convergences in the Ekman layers, and Sverdrup transports in the North Atlantic. J. Mar. Res., 36, 311-322.

Lindstrom, E.J., D.W. Behringer, B.A. Taft, and C.C. Ebbesmeyer, 1980. Absolute velocity determination from historical hydrographic data in the western North Atlantic. J. Phys. Oceanogr., 10, 999-1009.

Mantyla, A.W., 1980. Electrical conductivity comparisons of standard seawater batches P29 to P84. Deep-Sea Res., 27, 837-846.

McDowell, S., P. Rhines, and T. Keffer, 1983. North Atlantic potential vorticity and its relation to the general circulation. Submitted.

McWilliams, J.C., and J.H.S. Chow, 1981. Equilibrium geostrophic turbulence: a reference solution in a β-plane channel. J. Phys. Oceanogr., 11, 921-949.

McWilliams, J.C., et al. (21 authors), 1982. The local dynamics of eddies in the western North Atlantic. Eddies in Marine Science, Ed.: A.R. Robinson, in press.

Oceanographic Atlas of the North Atlantic Ocean. Section II Physical Properties, 1967, 1967, U.S. Naval Oceanographic Office, Pub. No. 700, Washington, DC, 300 pp.

Owens, W.B., 1983. Empirical, orthogonal modes for the POLYMODE Local Dynamics Experiment. In preparation.

Owens, W.B., J.R. Luyten, and H.L. Bryden, 1982. Moored velocity measurements on the edge of the Gulf Stream recirculation. J. Mar. Res., 40, Supplement, 509-524.

Pedlosky, J., 1979. Geophysical Fluid Dynamics. Springer-Verlag, New York, 624 pp.

238

Pillsbury, R.D., J. Bottero, R.E. Still, and E.P. Laine, 1982. Data Report for Current Meters on Mooring CMME-1, 1980-81; Atlantic Study Area E-N3, Report OSU-15, School of Oceanography, Oregon State University, Corvallis, OR.

Pratt, R.M., 1968. Atlantic continental shelf and slope of the United States--physiography and sediments of the deep-sea basin. Geological Survey Professional Paper 529-B, U.S. Government Printing Office, Plate I.

Price, J.F., 1983. Particle Dispersion in the western North Atlantic. J. Geophys. Res., submitted.

Price, J., and H.T. Rossby, 1982. Observations of a planetary wave during the Local Dynamics Experiment. J. Mar. Res., Supplement, 543-558.

Rhines, P.B., and W. Young, 1982. Homogenization of potential vorticity in planetary gyres. J. Fluid Mech., 122, 347-368.

Schmitz, W.J., Jr., 1977. On the deep general circulation in the Western North Atlantic. J. Mar. Res., 35, 21-28.

Schmitz, W.J., Jr., 1980. Weakly depth-dependent segments of the North Atlantic circulation. J. Mar. Res., 38, 111-133.

Schmitz, W.J., Jr., and W.R. Holland, 1982. A preliminary comparison of selected numerical eddy-resolving general circulation experiments with observations. J. Mar. Res., 40, 75-117.

Stommel, H., and F. Schott, 1977. The beta-spiral and the determination of the absolute velocity field from hydrographic station data. Deep-Sea Res., 24, 325-329.

Stone, P.H., 1972. On non-geostrophic baroclinic instabilty: Part III. The momentum and heat transports. J. Atmos. Sci., 29, 419-426.

Taft, B.A., C.C. Ebbesmeyer, E.J. Lindstrom, J.C. McWilliams, and C.Y. Shen, 1983. Hydrographic property variability from the POLYMODE Local Dynamics Experiment. In preparation.

Tarbell, S., and A. Spencer, 1978. A compilation of moored current data and associated observations. Woods Hole Oceanographic Institution Technical Report 78-5, Woods Hole, MA.

TTO, 1981. North Atlantic Study, Preliminary Leg Reports, PACODF, Scripps Institution of Oceanography.

Uchupi, E., 1971. Bathymetric Atlas of the Atlantic Carribbean, and Gulf of Mexico. Woods Hole Oceanographic Institution Technical Report, WHOI, 71-72.

Worthington, L.V., 1976. On the North Atlantic Circulation. Johns Hopkins Oceanographic Studies, 6, 110 pp.

Worthington, L.V., and W.R. Wright, 1970. North Atlantic Ocean Atlas of Potential Temperature and Salinity in the Deep Water. Woods Hole Oceanographic Institution.

Wunsch, C., 1978. The general circulation of the North Atlantic west of 50°W determined from inverse methods. Rev. Geophys. and Space Phys., 16, 583-620.

THE IMPACT OF GULF STREAM RINGS UPON THE SLOPE WATER

Glenn R. Flierl

Department of Meteorology and Physical Oceanography
54-1422 M.I.T., Cambridge, MA 02139

INTRODUCTION

`Gulf Stream warm core rings are the dominant form of mesoscale
activity in the Slope Water region between the Gulf Stream and the
continental shelf. Simple scale arguments suggest that the
contributions of the 4-5 rings formed per year in this region could be
very important in the heat, salt, and vorticity balance in the Slope
Water. In this paper, we attempt to go beyond scale estimates and to
derive approximations which suggest the magnitude of ring-carried and
ring-influenced transport of a passive scalar in the Slope.

Rings contribute in two ways to the property distributions in the
Slope Water. First, in the formation process, water from the Sargasso
is transferred across the Gulf Stream into the core of the ring. As the
ring evolves, this material is slowly exchanged with the Slope Water.
The second process is less direct: as the ring moves through the Slope
Water, it swirls the surrounding waters around it. The associated
deformations of the fluid, especially on the north side of the ring,
lead to enhancement of the gradients and increased turbulent fluxes.
Essentially the presence of the ring increases the normal "background"
turbulent fluxes by a form of shear dispersion. We shall present simple
models of both these processes below.*

---

*We shall not treat the complexities of the structure and evolution of
the ring flow field in this manuscript, although it is of interest in
these problems. The talk at the conference did cover some issues

EXCHANGE PROCESSES

As a ring moves through the surrounding water, there is a substantial volume of fluid which is carried with the ring--the "trapped volume," estimated at about $10^{14} m^3$ by Flierl (1982). Dewar (1982) showed that the dynamic evolution of a quasigeostrophic ring was slow enough so that a trapped volume of comparable size still existed over long periods of the eddy's evolution. We will therefore model the exchange processes as weak diffusion occurring within a steadily translating but otherwise unchanging streamfunction field.

The evolution of the passive scalar will be modelled by an advective-diffusive equation

$$\frac{\partial}{\partial t} S + J(\psi, S) = K \nabla^2 S$$

with K being the "sub-grid scale" diffusivity. (We will use a value of 10^6 cm^2/sec from Brown & Owens'(1981) characterization of the internal gravity wave motions.) The steadily translating assumption gives $\psi = \psi(x + ct, y)$ where c is the westward speed of motion.

We can simplify this by transforming to a coordinate system x + ct, y where the ring becomes stationary. Nondimensionalizing S by the initial anomaly, x and y by the length scale W of the eddy, and t by the diffusive time W^2/K, we have

$$\delta \frac{\partial}{\partial t} S - J(\phi, S) = \delta \nabla^2 S$$

where

$$\phi = y - \epsilon \psi$$

---

concerning the modelling of warm core rings; these remarks reviewed and summarized material in:

Flierl, G. R.: The structure and motion of a warm core ring (to appear in *Aust. J. Mar. and Freshwater Research*).

Flierl, G. R., M. E. Stern, J. A. Whitehead, Jr.: The physical significance of modons: an integral theorem and laboratory experiment (to appear in *Dyn. At. & Oc.*).

Flierl, G. R.: Rossby wave radiation from a moving, nonlinear ring (to appear in *J. Phys. Oceanogr.*).

is the negative of the streamfunction for the flow relative to the ring (Figure 1). The two nondimensional parameters are

$$\epsilon = U/c \qquad (\sim 20)$$

$$\delta = K/cw \qquad (\sim .04)$$

where U is the typical particle speed in the ring.

For $\delta \ll 1$, the lowest-order approximation to (1) is

$$J(\phi, S^{(o)}) = 0$$

or

$$S^{(o)} = \mathcal{S}(\phi, t)$$

Rhines and Young (1983) have argued in some detail that this homogenization along streamlines occurs fairly rapidly due to shear-enhanced dispersion $(t \sim (\delta/\epsilon)^{1/3})$ unless the motion is uniform or in solid body rotation. In our case, too, the initial distribution of S is presumably not too variable along streamlines anyway.

The motion of the ring, however, continually brings it into water with zero anomaly: thus the open ϕ contours are pinned to value S = 0. The presence of this infinite sink has a strong impact upon the loss rates out of the trapped region. To see this, we consider the next order equation

$$\frac{\partial}{\partial t} S^{(o)} - \nabla^2 S^{(o)} = J(\phi, S^{(1)})$$

and integrate over an area bounded by a particular ϕ contour $\phi = \phi_o$. This gives

$$\frac{\partial}{\partial t} \iint \mathcal{S}(\phi, t) = \mathcal{S}'(\phi_o, t) \oint \nabla \phi \cdot \hat{n}\, d\ell$$

as an integral-differential equation governing the evolution of the scalar field. We can, following Rhines and Young (1983), transform this into a diffusion equation

$$\frac{\partial}{\partial t} \mathcal{S}(\phi_o, t) \oint_{\phi=\phi_o} \frac{d\ell}{|\nabla \phi|} = \frac{\partial}{\partial \phi_o} \bar{V}(\phi_o) \frac{\partial}{\partial \phi_o} \mathcal{S}$$

244
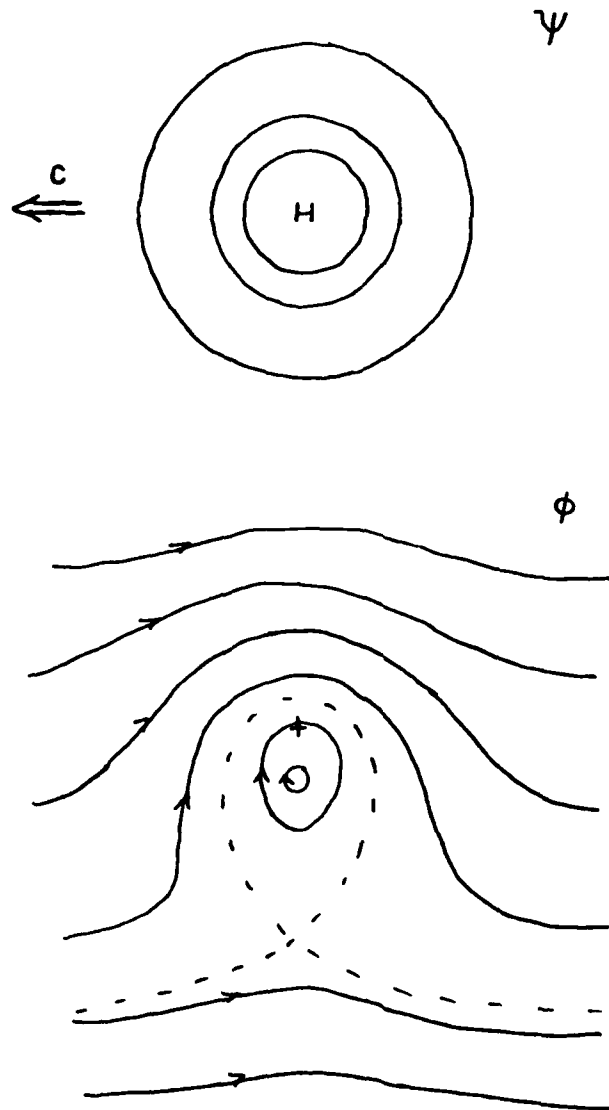
Fig. 1. Streamfunction ψ and "streakfunction" ϕ patterns for a westward-moving warm core ring. The + in the bottom figure represents the Eulerian center (marked by the H in the top view). The dashed line is the critical contour separating the trapped fluid from the exterior.

where
$$\bar{V}(\phi_o) = \oint_{\phi = \phi_o} |\nabla \phi| \, d\ell$$

is the integrated velocity around the streamline $\phi = \phi_o$. The only difficulty in applying this formula is the logarithmic singularity in the integral on the left-hand side as ϕ approaches the dividing streamline. This is the region in which this solution must be matched to the exterior $S = 0$ region. A boundary layer analysis near the stagnation point suggests that the dividing streamline should obtain the value $S = 0$ fairly quickly. It seems that the effects of the finite ring volume are to maintain S at 0 on the boundary and remove quickly all material which diffuses out. Therefore, the decay of the anomaly in the ring is more rapid, being exponential in time rather than algebraic (although the time <u>scale</u> is still L^2/K).

$$S \sim G(\phi) \, e^{-t}$$

The previous discussion suggests one way in which warm core rings may affect the distribution of passive scalar properties or dynamical quantities such as potential vorticity. Rings have substantial anomalies of salt, heat and potential vorticity on isopycnal surfaces. As the ring evolves, these are diffused into the surrounding fluid. If we use the formulae above, a small-scale diffusivity of $10^6 \, cm^2/sec$ and a six-month lifetime for a typical WCR (warm core ring), we find that

$$1 - e^{-Kt/w^2} \simeq .46$$

of the eddy anomaly is diffused into the surroundings. The total salt anomaly of a ring is about 3×10^{15} gms and roughly 5 rings undergo a full life cycle per year giving an annual flux of 7×10^{15} gms of salt into the Slope Water.

ADVECTION OF SURROUNDING WATERS

A second major influence comes from the mixing induced by the repeated passage of rings. One could consider the property distributions at the edges of the Slope Water as being fixed by Shelf Water or Gulf Stream conditions. In the absence of rings, the weaker, stochastic mixing processes would establish a mean distribution of properties within the Slope Water with particular values for the down-slope and cross-slope fluxes. The passage of a ring, however, will substantially distort the property distributions in both a short-term fashion as fluid parcels are swept around the ring and in a longer-term way due to the large net displacements parallel to the ring's track. Figure 2 shows schematically the behavior of a patch of ocean as a WCR passes. Notice the greatly enhanced gradients existing during ring passage, which remain afterwards until either another eddy passes or the field is smoothed out by the diffusive processes. The fluxes will, in general, be enhanced due to the increased gradients.

As a means for estimating the flux enhancements occurring because of the repeated passage of strong, deterministic rings, consider the following model problem. The fluid will be confined in a channel $y = 0$ to W, with the rings spaced an x distance LW apart and moving at speed c westward (Figure 3). The streamfunction for the ring will be taken as given

$$\psi = \psi(x + ct, y)$$

and the small-scale diffusion will be taken as isotropic and uniform (perhaps a questionable assumption, given the strong vertical and horizontal shears associated with the eddy). Nondimensionalizing using c, W and typical boundary variations of passive scalar but with $t \sim W/c$ gives

$$S_t + \epsilon J(\psi, S) = \delta \nabla^2 S$$

$$S = f_0(x, t) \quad y = 0$$

$$S = f_1(x, t) \quad y = 1$$

as the equation governing the distribution of the passive scalar S. We have solved this under the assumption that $\delta \ll 1$ for two cases: cross-channel gradients ($f_0 = 0$, $f_1 = 1$) and along-channel gradients ($f_0 = f_1 = x$). In addition to the distributions of S, we shall obtain the
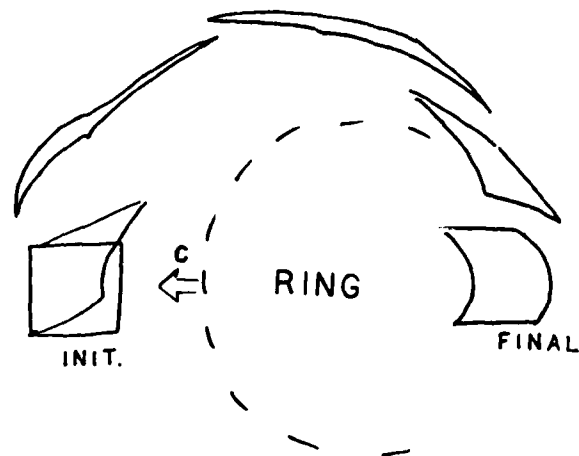
Fig. 2. Sketches of the changes in shape
and position of a patch of fluid struck
by a moving ring. Note the net east-west
(parallel to ring track) displacements
and the strong gradients existing as the
patch moves across the top of the ring.
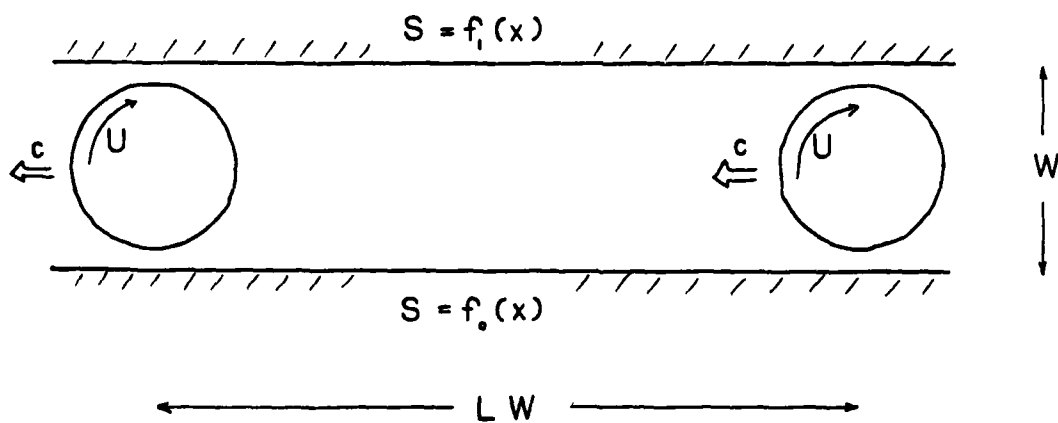
Fig. 3. Geometry for ring-induced flux enhancement calculations,
showing two rings and the edges of the domain with fixed values
of the passive scalar S.

nondimensional flux measure, Nu, which gives the enhancement of the flux over that which would exist without the rings.

When the S gradients are set cross-slope, we can again use the coordinate system moving with the rings. In this frame S, too, is time-independent so that

$$J(\phi, S) = -\delta \nabla^2 S$$

$$S = 0 \qquad y = 0$$
$$S = 1 \qquad y = 1$$

where

$$\phi = y - \epsilon \psi$$

At lowest order in δ we have

$$S^{(0)} = \mathcal{S}(\phi)$$

with $\mathcal{S}(\phi)$ being determined by solvability conditions on the next order equation

$$J(\phi, S^{(1)}) = -\nabla^2 S^{(0)}$$

If there are closed ϕ lines in the flow, we can integrate this equation over a region bounded by such a streamline to demonstrate

$$\mathcal{S}'(\phi) = 0 \qquad \text{closed } \phi \text{ lines}$$

For open streamlines ($0 < \phi < 1$), integrating over an area bounded by streamline ϕ_0 and the northern boundary (Figure 4) shows that

$$\mathcal{S}'(\phi_0) \int_{\phi_0} |\nabla \phi| \, d\ell = L \, Nu \qquad (2)$$

where the Nusselt number is

$$Nu = \frac{1}{L} \int_0^L dx \, (S_y - vS) \Big|_{y = \text{const}} = \frac{1}{L} \int_0^L dx \, S_y \Big|_{y=1}$$

This parameter, the ratio of the flux in the presence of the rings to that which would occur without rings, determines the impact of the rings. We can represent the effective diffusivity due to the ring plus mixing as
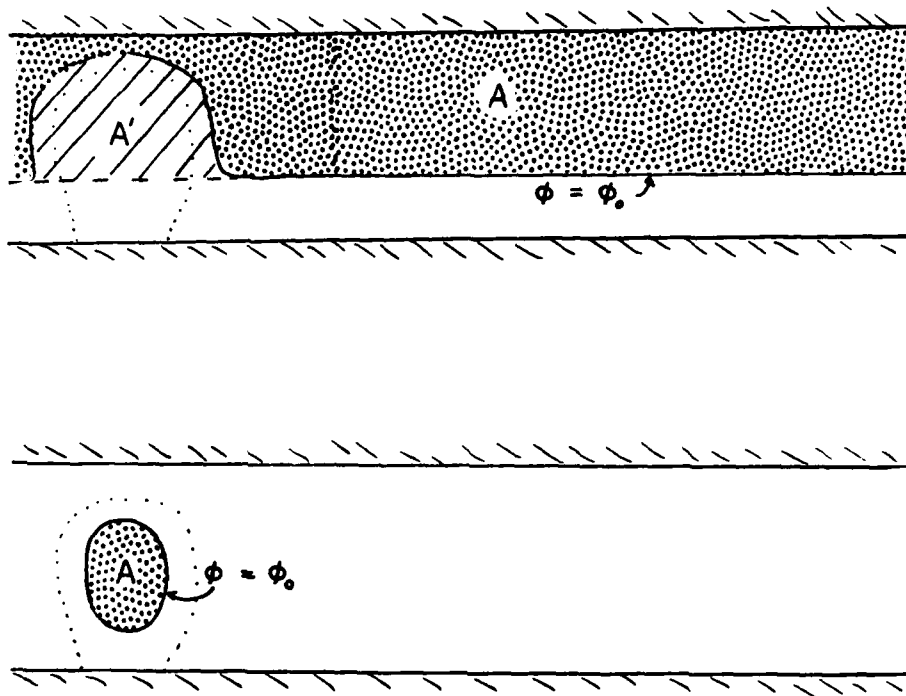
Fig. 4. Areas over which integrals are taken. The upper figure shows the case of an open ϕ contour $\phi = \phi_0$ with the areas A and A' appearing in the formulae marked. The lower figure shows the area A for a close contour.

$$K_{eff} = Nu \, K$$

so that the Nusselt number can also be viewed as the ratio of the diffusivities. Integrating equation (2) from $\phi = 0$, $S = 0$ to $\phi = 1$, $S = 1$ determines the value of Nu

$$Nu = \left\{ \int_0^1 d\phi_0 \; \frac{L}{\bar{V}(\phi_0)} \right\}^{-1}$$

Given the streamlines, then, we can find the ring-induced enhancement of the flux. The critical quantity is again the velocity integrated along the particle track,

$$\bar{V}(\phi_0) = \int_{\phi=\phi_0} |\nabla\phi| \, d\ell$$

which will be of order 5-10 L for typical rings moving at 5 cm/sec westward. The major conclusion, therefore, is that the cross-stream flux Nusselt number is not particularly large--order 1 to 10, depending upon the strength of the eddies.

The second case to be considered, where the boundary conditions establish an along-shelf gradient of S, gives a rather different result. When we take $f_0 = f_1 = x$, we also have to use a somewhat different solution technique: the passive scalar can be written in the form

$$S = x + \frac{1}{\delta} S(\phi) + S^{(1)}(x+t,y) + \cdots$$

with

$$S(0) = S(1) = 0$$

and

$$S_t^{(1)} + \epsilon J(\psi, S^{(1)}) - \epsilon \psi_y = \nabla^2 S$$

or

$$J(\phi, S^{(1)}) = -\epsilon \psi_y - \nabla \cdot S'(\phi)\nabla\phi$$

$$= \phi_y - 1 - \nabla \cdot S'(\phi)\nabla\phi$$

Integrating over closed regions shows that

$$\mathcal{f}'(\phi_0) = - \iint_{\substack{A \text{ within} \\ \phi_0}} dx\, dy \Bigg/ \bar{V}(\phi_0)$$

whereas for open regions, the integration yields

$$-\oint (\hat{x} + \epsilon \underset{\sim}{v}) \cdot \hat{n}\, S^{(1)} d\ell = \oint \phi\, \hat{y} \cdot \hat{n}\, d\ell - \iint_A dx\, dy - \oint \mathcal{f}'(\phi) \nabla\phi \cdot \hat{n}\, d\ell$$

(see Figure 4). The left-hand side vanishes since $S^{(1)}$ is periodic in x and the normal flow vanishes on the streamlines and on the north wall. The first term on the right simplifies to $L(1 - \phi)$, the second term is the area enclosed between $\phi_0 < \phi < 1$, and the third term becomes

$$\mathcal{f}'(1)\, \bar{V}(1) - \mathcal{f}'(\phi_0)\, \bar{V}(\phi_0)$$

so that
$$\mathcal{f}'(\phi_0) = \left[\mathcal{f}'(1)\bar{v}(1) + \iint_A dx\, dy - (1-\phi_0)L \right] \Bigg/ \bar{v}(\phi_0)$$

$$= \left[\mathcal{f}'(1)\bar{v}(1) - \iint_{A'} dx\, dy \right] \Bigg/ \bar{v}(\phi_0)$$

Again we choose $\mathcal{f}'(1)$ by requiring $\mathcal{f}$ to satisfy appropriate boundary conditions, giving

$$\int_0^1 d\phi_0\ \mathcal{f}'(\phi_0) = 0$$

The *flux down the channel* is given by

$$F = \int_0^1 dy\, \frac{1}{L} \int_0^L dt \left[-S S_x - \epsilon \psi_y S \right]$$

Using the form $S = x + \frac{1}{\delta}\mathcal{f} + S^{(1)}$ and $\epsilon \psi_y = 1 - \phi_y$, we find the leading contribution to the flux is

$$F \simeq -\frac{1}{\delta} \int_0^1 dy\, \frac{1}{L} \int_0^L dx\ (1 - \phi_y)\, \mathcal{f}(\phi)$$

(The x and t integrals can be used interchangeably because of the dependence of ϕ only upon $x + t$.) The Nusselt number, therefore, is given by

$$Nu \simeq \frac{1}{\delta^2} \int_0^1 dy\, \frac{1}{L} \int_0^L dx\ (1 - \phi_y)\, \mathcal{f}(\phi)$$

Clearly the down-slope transports are much larger than the cross-slope fluxes. The Nusselt number is now order ϵ/δ^2 rather than only order ϵ. In fact, the effective down-slope diffusivity

$$K_{eff} = K \, Nu \sim \frac{U W^3}{KT}$$

is order W^2/KT (typically 20) times larger than the typical eddy
diffusivity, UW.

It is useful to think of this result in the light of the
explanation given in Flierl (1982). This paper suggested that the
problem was analogous to diffusion in a pipe flow with the flow speed U_{eff}
(y) being produced by the repeated passage of the eddies which creates
a Stokes drift UStokes (y) for particles set outside the ring. The
resulting equation

$$U_{Stokes}(y) \, S_x = \delta \nabla^2 S$$

$$S = x \qquad y = 0, 1$$

can be solved easily given the Stokes' drift calculated from formulae
given in Flierl (1981). The S distribution

$$S = x - \int_0^y dy' \int_{y'}^1 \frac{1}{\delta} U_{Stokes}(y'') \, dy''$$

gives

$$Nu \simeq \frac{1}{\delta^2} \int_0^1 dy \, U_{Stokes}(y) \int_0^y dy' \int_{y'}^1 dy'' \, U_{Stokes}(y'')$$

When ϵ is small (weak currents), one can show that this reproduces the
results of the more accurate theory given above. In any case, this
model does give the proper scale for Nu and suggests the essential
mechanism: repeated passage of the rings induces strong up or downslope
drifts which also vary strongly across the slope. The contours of
constant S are advected long distances until large enough gradients
develop across the current so that the advection of S by drift down the
slope can be balanced by diffusion in the sides.

It should be noted, however, that there may be Eulerian currents
set up by the Reynolds' stresses of the rings which could counter the
down-shelf fluxes, at least in part (as in Andrews & McIntyre's, 1978,
theory). It may therefore be difficult to assess the impact of the rings
in isolation from the mean flows.

Specific examples are generally not analytically tractible since one must calculate the streamlines, integrate the tangential velocity along these lines and then integrate with respect to ϕ_o . As a rather artificial example, we can use a "square eddy" as sketched in Figure 5 to simulate rings with or without large currents near the edges of the domain, respectively. The contours become broken lines with $|\nabla\phi|$ being constant on each line segment. The resulting cross-slope Nu as functions of ϵ are shown in Figure 6 with typical S contours in Figure 7. Calculations are contained in the Appendix. Typical ring steepnesses of $\epsilon \sim 20$ indeed give a Nu of only about 6. The calculated "eddy diffusivity" is much smaller than the scale estimate of the eddy diffusivity UW $\sim 10^9$cm^2/sec. The down-slope Nu numbers are shown in Figure 8 with S contours sketched in Figure 9. For $S \sim 0.02$, typical Nu values are about 50 so that the down-channel flux is an order of magnitude stronger than the cross-channel value. The calculated eddy diffusivities for

$$
\begin{aligned}
&U = 100 \text{ cm/sec} \\
&W = 100 \text{ km} \\
&WL = 500 \text{ km} \qquad\qquad \epsilon = 20 \\
&c = 5 \text{ cm/sec} \qquad\qquad \xi = .02 \\
&K = 10^6 \text{ cm /sec} \qquad L = 7
\end{aligned}
$$

are

$$
\begin{aligned}
&K \,(_{xx})_{eff} = 3 \text{ to } 7 \quad 10^7 \text{ cm}^2/\text{sec} \\
&K \,(_{yy})_{eff} = 3 \text{ to } 6 \quad 10^6 \text{ cm}^2/\text{sec}
\end{aligned}
$$

implying fairly efficient mixing along the Slope Water due to the repeated passage of the warm core eddies.

ACKNOWLEDGEMENTS
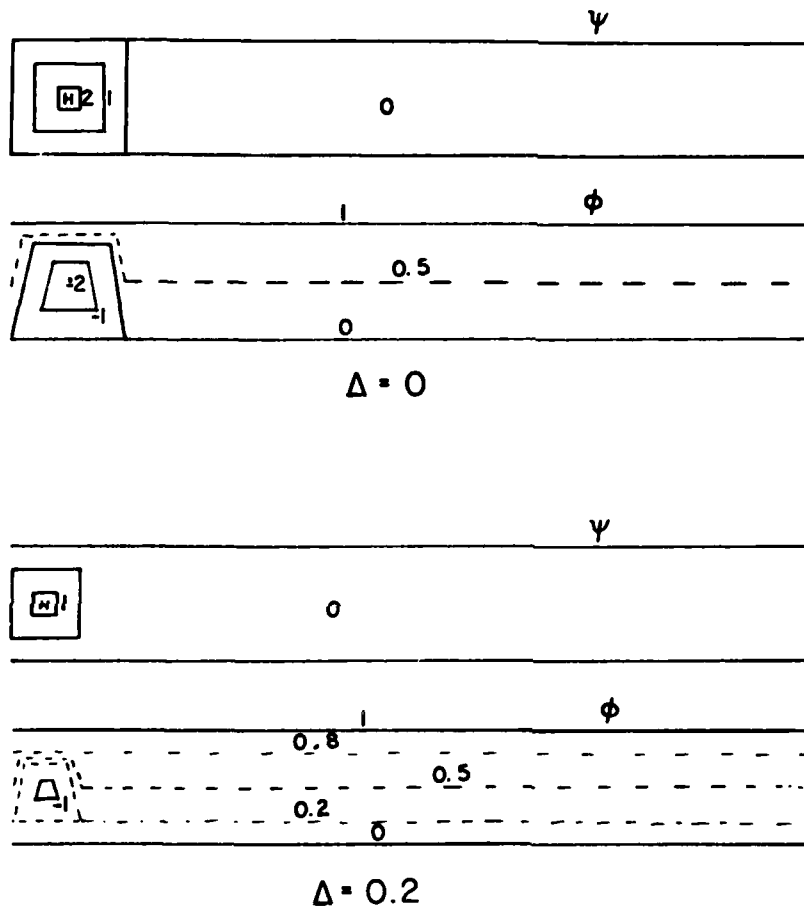
Fig. 5. Streamfunction ψ and "streakfunction" ϕ patterns
for square eddies in the case $\Delta = 0$ where the eddy has
strong currents at the walls of the domain and in the
case $\Delta = 0.2$ where the eddy has no flow at the walls.
The ϵ value is 5.
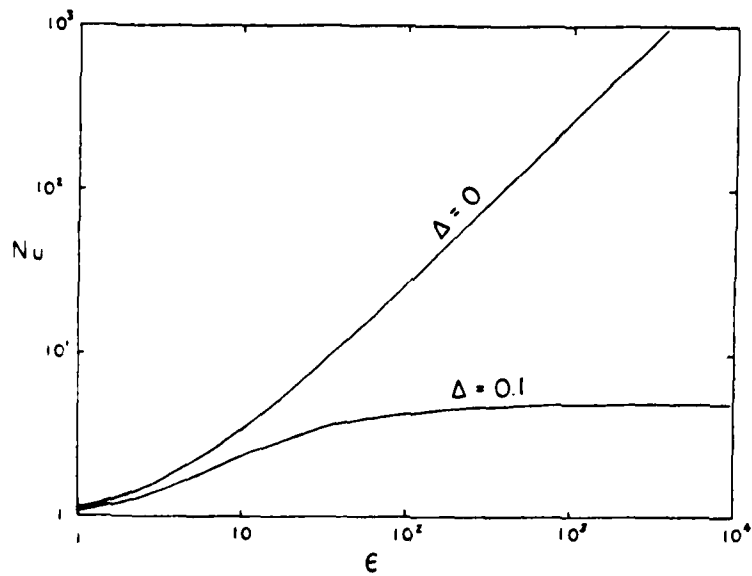
Fig. 6. Nusselt number as a function of eddy strength
ε for cross-channel fluxes. The two cases Δ = 0 and
Δ = 0.1 correspond to eddies with strong currents or
zero currents at the boundaries.
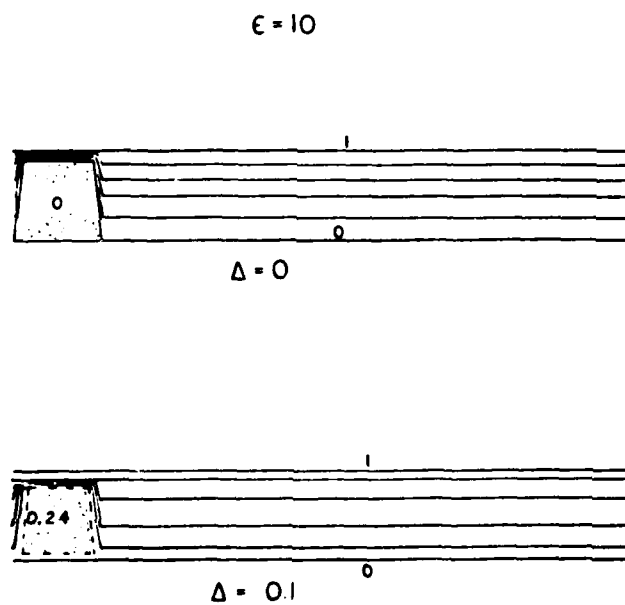
Fig. 7. Patterns of the passive scalar distribution
when the gradients are maintained across the channel.

256
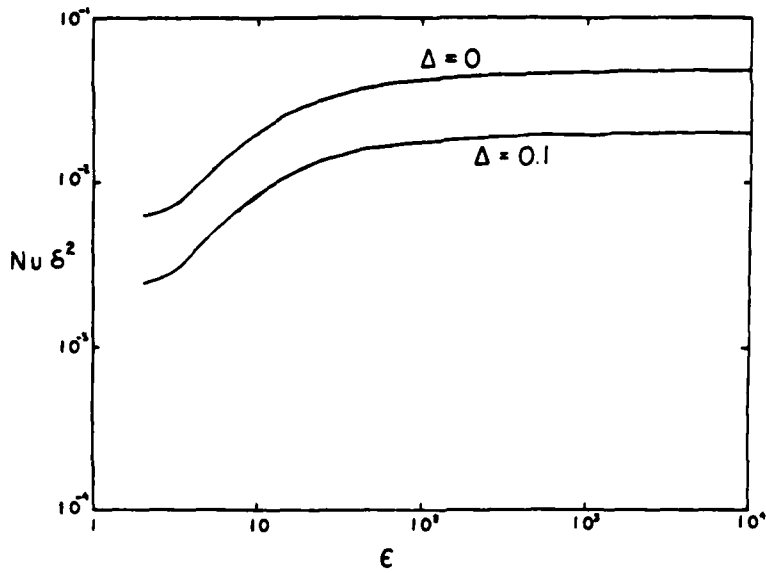
Fig. 8. Strength of eddy-induced down-channel
fluxes. The Nusselt numbers can be obtained
by dividing by δ_3^2 (which is typically on the
order of 4×10^{-3}).

$\epsilon = 10$

$\Delta = 0$

$\Delta = 0.1$
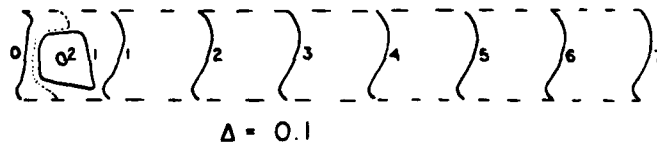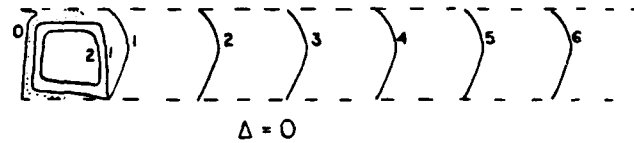
Fig. 9. Patterns of passive scalar distribution
when the gradients are maintained along the
channel.

APPENDIX

One simple case in which most of the algebraic complexities can be dealt with is that of "square" rings (Figure 5). The streamfunction is given by:

A) case with flow at wall

$$\psi = \begin{cases} x & x < y < 1-x \\ (1-y) & 1-y < x < y \\ (1-x) & 1-x < y < x \\ y & y < x < 1-y \\ 0 & 1 < x \end{cases}$$

B) case with no flow at wall

$$\psi = \begin{cases} x & x + \Delta < y < 1-x-\Delta \\ 1-\Delta-y & 1-\Delta-y < x < y-\Delta \\ 1-\Delta-x & 1-\Delta-x < y < x+\Delta \\ y-\Delta & y-\Delta < x < 1-\Delta-y \\ 0 & \begin{aligned} & 0 < y < \Delta \\ & 1-\Delta < y < 1 \\ & x > 1-2\Delta \end{aligned} \end{cases}$$

For these two cases, we can calculate the integrated velocity $\bar{V}(\phi_o)$ (to keep matters simple, we have considered only the case $\varepsilon > 1$, so that contours appear as shown in Figure 5). In all cases we find $\bar{V}$ is a linear function of ϕ_o

$$\bar{V}(\phi_o) = a + b\,\phi_o$$

with the coefficients listed in Table 1. (Case A can be obtained readily from Case B by taking $\triangle = 0$; therefore only the latter results are tabulated.)

For the case involving cross-channel fluxes, this data is sufficient to evaluate the tracer distribution and Nusselt number since Eq. (2) can be integrated with respect to ϕ_0. The results are listed in Table 2 and plotted in Figures 6 and 7. The computations for the case of down-channel fluxes are much more tedious. The areas are quadratic functions of ϕ_o

$$A \text{ or } A' = a_o + a_1\,\phi_o + a_2\,\phi_o^2$$

(Table 3). From this, we can find $\int(\phi)$ by integrating Eq. (3) or (4) as listed in Table 4. Finally, the flux integral (5) must be evaluated over the two triangles in which $y = 0$. This leads to the expressions in Table 5 for the Nusselt number; the results are also shown in Figure 8 and 9.

Table 1. Integrated velocities $\overline{V}(\phi_0) = a + b\phi_0$

ϕ_0 range	type of contour	a	b
$0 < \phi_0 < \Delta$	open	L	0
(1) $\Delta < \phi_0 < 1-\Delta$	open	$L + \epsilon(1-2\Delta) + \frac{2\epsilon(\epsilon-1)}{\epsilon+1}(1+\Delta)$	$-\frac{2\epsilon(\epsilon-1)}{\epsilon+1}$
$1-\Delta < \phi_0 < 1$	open	L	0
(2) $\phi_0 < \Delta$	closed	$4\epsilon^2\,\dfrac{\epsilon(1-2\Delta)-1}{\epsilon^2-1}$	$\dfrac{8\epsilon^2}{\epsilon^2-1}$

Table 2. Cross-channel case: tracer concentrations and Nu

ϕ_0 range	type of contour	$\mathcal{S}(\phi_0)$
$0 < \phi_0 < \Delta$	open	$Nu\,\phi_0$
$\Delta < \phi_0 < 1-\Delta$	open	$Nu\,\Delta + \dfrac{L\,Nu}{b}\ln\left(1+\dfrac{b}{a}(\phi_0-\Delta)\right)$ *
$1-\Delta < \phi_0 < 1$	open	$Nu\,\Delta + \dfrac{L\,Nu}{b}\ln\left(1+\dfrac{b}{a}(1-2\Delta)\right) + Nu(\phi_0-1+\Delta)$
$\phi_0 < \Delta$	closed	Δ

$$Nu = \frac{b}{2\Delta b + L\ln\left(1+\frac{b}{a}(1-2\Delta)\right)}$$

*a and b values from line (1), Table 1.

Table 3. Areas A or $A' = a_0 + a_1\phi_0 + a_2\phi_0^2$

	range	type of region	a_0	a_1	a_2
	$0 < \phi_0 < \Delta$	open, A'	0	0	0
(1)	$\Delta < \phi_0 < 1-\Delta$	open, A'	$\dfrac{-\epsilon\Delta + \epsilon^2(1-2\Delta)}{(1+\epsilon)^2}(1-\Delta)$	$\dfrac{\epsilon - \epsilon^2(1-2\Delta)}{(1+\epsilon)^2}$	$\dfrac{-\epsilon}{(1+\epsilon)^2}$
	$1-\Delta < \phi_0 < 1$	open, A'	0	0	0
(2)	$\phi_0 < \Delta$	closed, A	$\epsilon^2\dfrac{(\epsilon-1-2\Delta\epsilon)^2}{(\epsilon^2-1)^2}$	$\dfrac{4\epsilon^2(\epsilon-1-2\Delta\epsilon)}{(\epsilon^2-1)^2}$	$\dfrac{4\epsilon^2}{(\epsilon^2-1)^2}$

Table 4. Down Channel Flux Case S $\quad\quad f(\phi_0) = S_0 + S_1\phi_0 + S_2\phi_0^2 + S_L \ln \dfrac{a+b\phi_0}{a+b\Delta}$

ϕ_0 range type of region

$\quad\quad 0 < \phi_0 < \Delta \quad$ open $\qquad\qquad 0 \qquad\qquad \dfrac{q}{L} \qquad\quad 0 \qquad 0$

(1) $\Delta < \phi_0 < 1-\Delta \quad$ open $\quad \dfrac{q\Delta}{L} - \dfrac{a_2}{b}\left(\dfrac{\Delta a}{b} + \dfrac{\Delta^2}{2}\right) + \dfrac{a_1\Delta}{b} \quad \dfrac{a_2 a - a_1 b}{b^2} \quad -\dfrac{a_2}{2b} \quad \dfrac{q - a_0 + \frac{a_1 a}{b} - \frac{a_2 a^2}{b^2}}{b}$ *

$\quad\quad 1-\Delta < \phi_0 < 1 \quad$ open $\quad \begin{aligned} &S_0 + S_1(1-\Delta) + S_2(1-\Delta)^2 \\ &+ S_L \ln\dfrac{a+b(1-\Delta)}{a+b\Delta} - \dfrac{q}{L}(1-\Delta)\end{aligned} \quad \dfrac{q}{L} \qquad 0 \qquad 0$

(2) $\phi_0 < \Delta \quad$ closed $\quad \dfrac{q\Delta}{L} - \dfrac{a_2}{b}\left(\dfrac{\Delta a}{b} + \dfrac{\Delta^2}{2}\right) + \dfrac{a_1\Delta}{b} \quad \dfrac{a_2 a - a_1 b}{b^2} \quad -\dfrac{a_2}{2b} \quad \dfrac{q - a_0 + \frac{a_1 a}{b} - a_2\frac{a^2}{b^2}}{b}$ †

$$q = \dfrac{\dfrac{a_2}{b}\left(\dfrac{\Delta a}{b} + \dfrac{\Delta^2}{2}\right) - \dfrac{a_1\Delta}{b} - \dfrac{a_2 a - a_1 b}{b^2}(1-\Delta) + \dfrac{a_2}{2b}(1-\Delta)^2 + \dfrac{a_0 - \frac{a_1 a}{b} + a_2\frac{a^2}{b^2}}{b}\ln\dfrac{a+b(1-\Delta)}{a+b\Delta}}{\dfrac{2\Delta}{L} + \dfrac{1}{b}\ln\dfrac{a+b(1-\Delta)}{a+b\Delta}}$$

*uses lines (1) of Tables 1 and 3.

†uses lines (2) of Tables 1 and 3.

Table 5. Fluxes down-channel $\qquad Nu = \frac{1}{\delta^2 L}(I_1 + I_2)$

$$I_1 = \frac{4\epsilon^2(\epsilon-1-2\epsilon\Delta)}{(\epsilon^2-1)^2}\left[s_0\phi + s_1\frac{\phi^2}{2} + s_2\frac{\phi^3}{3} + s_L\phi\ln\frac{a+b\phi}{a+b\Delta} + s_L\frac{a}{b}\ln(a+b\phi) - s_L\phi\right]_{\epsilon\Delta-\frac{\epsilon-1}{2}}^{\Delta} \quad *$$

$$\frac{-8\epsilon^2}{(\epsilon^2-1)^2}\left[s_0\frac{\phi^2}{2} + s_1\frac{\phi^3}{3} + s_2\frac{\phi^4}{4} + s_L\left(\frac{\phi^2}{2}-\frac{a^2}{2b^2}\right)\ln\frac{a+b\phi}{a+b\Delta} - s_L\left(\frac{\phi^2}{4}-\frac{a\phi}{2b}\right)\right]_{\epsilon\Delta-\frac{\epsilon-1}{2}}^{\Delta}$$

$$I_2 = \frac{-\epsilon(\epsilon-1-2\epsilon\Delta)}{(\epsilon+1)^2}\left[s_0\phi + s_1\frac{\phi^2}{2} + s_2\frac{\phi^3}{3} + s_L\phi\ln\frac{a+b\phi}{a+b\Delta} + s_L\frac{a}{b}\ln(a+b\phi) - s_L\phi\right]_{\Delta}^{1-\Delta} \quad +$$

$$\frac{-2\epsilon}{(\epsilon+1)^2}\left[s_0\frac{\phi^2}{2} + s_1\frac{\phi^3}{3} + s_2\frac{\phi^4}{4} + s_L\left(\frac{\phi^2}{2}-\frac{a^2}{2b^2}\right)\ln\frac{a+b\phi}{a+b\Delta} - s_L\left(\frac{\phi^2}{4}-\frac{a\phi}{2b}\right)\right]_{\Delta}^{1-\Delta}$$

*uses s_0, s_1, s_2, s_L from line (2), Table 4 and a, b from line (2), Table 1.

+uses s_0, s_1, s_2, s_L from line (1), Table 4 and a, b from line (1), Table 1.

REFERENCES

Andrews, D. R. and M. E. McIntyre, 1978. An exact theory of nonlinear waves on a Langrangian mean flow. Journal of Fluid Mechanics, 89, 609-646.

Brown, E. and W. B. Owens, 1981. Observations of the horizontal interactions between the internal wave field and the mesoscale flow. Journal of Physical Oceanography, 11, 1474-1480.

Dewar, W. K., 1982. Atmospheric Effects on Gulf Stream Rings. Ph.D. Thesis, MIT-WHOI Joint Program in Physical Oceanography.

Flierl, G. R., 1981. Particle motions in large amplitude wave fields, Geophysical and Astrophysical Fluid Dynamics, 18, 39-74.

Flierl. G. R., 1982. Tracers in rings, in Notes of the 1982 Summer School in Geophysical Fluid Dynamics, WHOI-82-45.

Flierl, G. R. and W. K. Dewar, 1983. Motion and Dispersal of Dumped Material by Large Amplitude Eddies, Wastes in the Ocean, Vol. 5, edited by D. Kester, P. Park, B. Ketchum, and I. Duesdall, Wiley Interscience. in press.

Rhines, P. B. and W. R. Young, 1983. How rapidly is the passive scalar mixed within closed streamlines? Journal of Fluid Mechanics, 133, 133.

STUDIES OF THE VELOCITY STRUCTURE OF THE GULF STREAM
EAST OF CAPE HATTERAS

Thomas Rossby

Graduate School of Oceanography, University of Rhode Island,
Kingston, Rhode Island   02881

ABSTRACT

'Between September 1980 and May 1983 seventeen bimonthly sections of
velocity and temperature will have been obtained across the Gulf
Stream 200 km downstream from Cape Hatteras. Assuming the last
cruise goes well, we will have fourteen complete sections of high
quality, and several more from the central part of the Stream.
By summer 1983 the raw data will have been fully edited, calibrated
and organized for systematic analyses.

Preliminary analysis of the first eight transects gives a mean
transport of 78 ± 11 Sv between the surface and 2000 m. The
standard deviation is between sections. This mean appears to
be quite a bit smaller than the 91 Sv we estimate from Worthington's
book (1976) assuming a reference velocity of 4.5 cm/s at 2000 m.

BRIEF REVIEW

Since September 1980 we have, on a bimonthly basis, been taking a
series of transects of the temperature and absolute velocity fields
across the Gulf Stream about 200 km east of Cape Hatteras. The
program has been designed to provide quantitative estimates of the
total and partial mass transports by different strata of the water
column, their annual variability and shorter term fluctuations.
This information is important for the analysis and assessment of
theoretical and numerical concepts of the Gulf Stream, and its role
in the North Atlantic circulation. Detailed knowledge of the
velocity field is also sought so that(1) the structure of the

downstream and cross-stream velocity field can be examined,
including the distribution of vertical and horizontal shear,
2) the dynamical and statistical relationships between velocity
and density (via temperature and the mean T/S) can be developed,
3) Reynolds stresses can be estimated and their role as a
driving mechanism for the downstream increase in transport
assessed (Thompson, 1978), and 4) the distribution and variability
of potential vorticity on various density strata can be determined.

The ongoing program has established nine equidistant sites along a
line spanning the Gulf Stream near 36°N, 73°W, Figure 1. Vertical
profiles are obtained at each site from the surface to close to the
bottom. In Table 1 we summarize the data base to date.

Originally the field program was to have ended in November 1982.
Due to difficulties with weather, ship and instrumentation in early
1981, three additional transects have been scheduled for January,
March, and May 1983. In the end, we expect to have 14 essentially
complete transects, for many of which we have been able to repeat
the section twice. Further, we have four rapidly repeated sections
spanning the core of the Gulf Stream in October 1979. All of the
data have been obtained with the Pegasus instrument (Spain, Dorson,
and Rossby, 1981). Since July 1981 we have been working with a
new version, which can be operated at all depths (< 6000 m).
Standard T7 XBTs have been taken at all stations as well as at
the halfway points in between. In several cases, hydrographic
stations and/or CTD data are also available. For ma₁y of the
transects, spatial information on the path of the Gulf Stream is
available from the Inverted Echo Sounder array maintained by Prof.
R. Watts at URI.

What have we learned from the program thus far? Based on a very
preliminary analysis of eight sections (through May 1982), we can
make the following points:

1) The total transport by the Stream between the surface and
   2000 m is 78 ± 11 Sv (standard deviation between transects).
   We are not yet in a position to discuss the seasonal
   variability, but a major reason for maintaining this
   program for two years is so that we can determine -even
   if only roughly- the magnitude and phase of the annual
   cycle.

2) The vertically averaged transport per unit width between
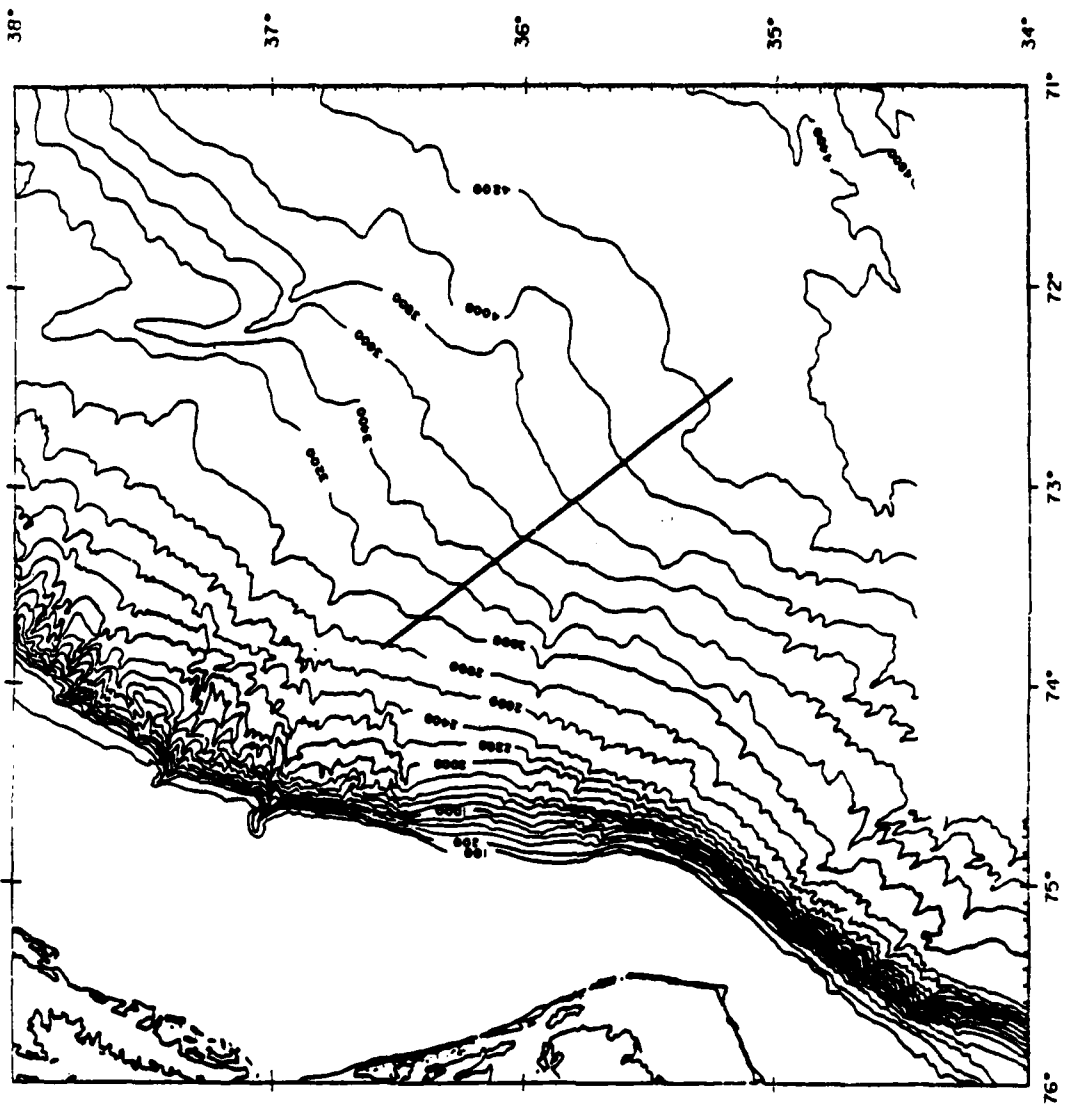
Fig. 1. Nine Pegasus profiling stations have been sited along the indicated line spanning the Gulf Stream about 200 km east of Cape Hatteras.

Table 1

1980	1981	1982	1983
	January (W,N)	January	January
	March (W,E,N)	March	March
	May (X)	May	May (S)
	July	July	
September	August	September	
November (W)	November (W)	November	

W = Weather problems
N = NOAA Vessel KELEZ, short cruise
E = Equipment failure
X = Cruise aborted due to ship
S = Scheduled

the surface and 2000 m shows a maximum of $\sim$50 cm/s about 30 km to the SE of the north wall, Figure 2. In this figure all transects have been registered so that 15°C at 200 m ("the north wall") is at 0 km. The downstream direction is defined by the direction of transport in the central part of the Stream. While the total width of the downstream transport is $\sim$130 km, two-thirds of the total occurs within a 70 km wide zone. Note the small standard deviations in mean velocity throughout the section.

3) The section is located in an area of evident entrainment from both the Sargasso Sea and the Slope Waters. On the northern side the inflow is $\geq$ 5 cm/s in the top 2000 m, Figure 3. The rate of inflow from both sides is equivalent to $\sim$ 20 Sverdrups/100 km with perhaps two-thirds of the total being supplied from the Slope Water region.

4) The cross-stream averaged downstream velocity at 2000 m is 4-5 cm/s. This is of great interest when comparing our directly computed transports with those estimated geostrophically using 2000 m as a level of no motion. If this reference velocity is added to Worthington's (1976) transports, his estimates increase from 78 to about 91 Sv. While the difference appears to be significant, its meaning is unclear. We return to this below.

5) The local velocity structure is quite variable. In Figure 4 and 5 we show preliminary plots of downstream (a) and cross-stream (b) isotachs from two transects, namely September 1980 and July 1981. One observes very strong cyclonic shear on the northern side (with relative vorticities of the order of 50% of f) and anticyclonic shear of somewhat smaller magnitude on the Sargasso Sea side. The cross-stream sections show inflow at all depths on the northern side.

The strong reversal of downstream motion in the deep waters in September 1980 is a bit of a mystery. It may be evidence of an eddy embedded in and advected by the Stream, but why, then, does it not appear in the cross-stream field (Figure 4b)?

The July 1981 section is fairly typical of a simple transect. Maximum surface velocities are about 200 cm/s. Speeds diminish to half that value by 500-600 m. Counterflow (to the SW) is almost always found on the Slope Water side.
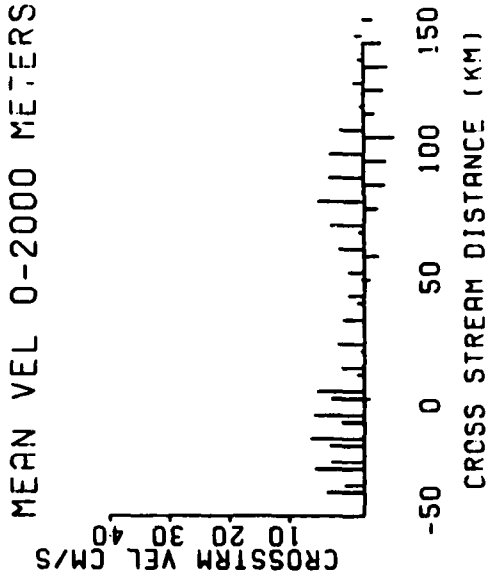
Fig. 3. Vertically averaged cross-stream velocity between the surface and 2000 m. The light line is the corresponding standard deviation.
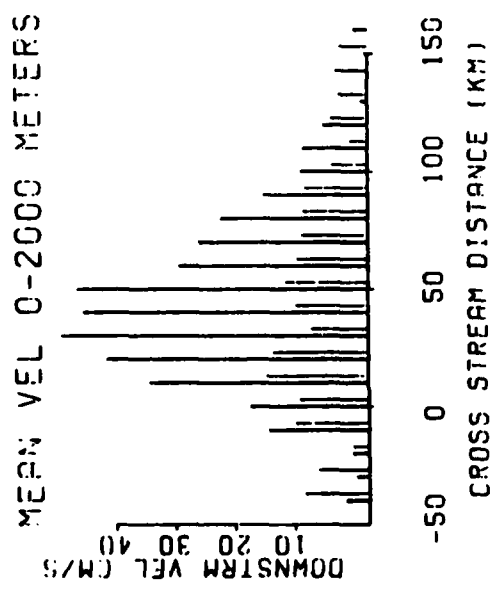
Fig. 2. Vertically averaged downstream velocity between the surface and 2000 m. The light line is the corresponding standard deviation.
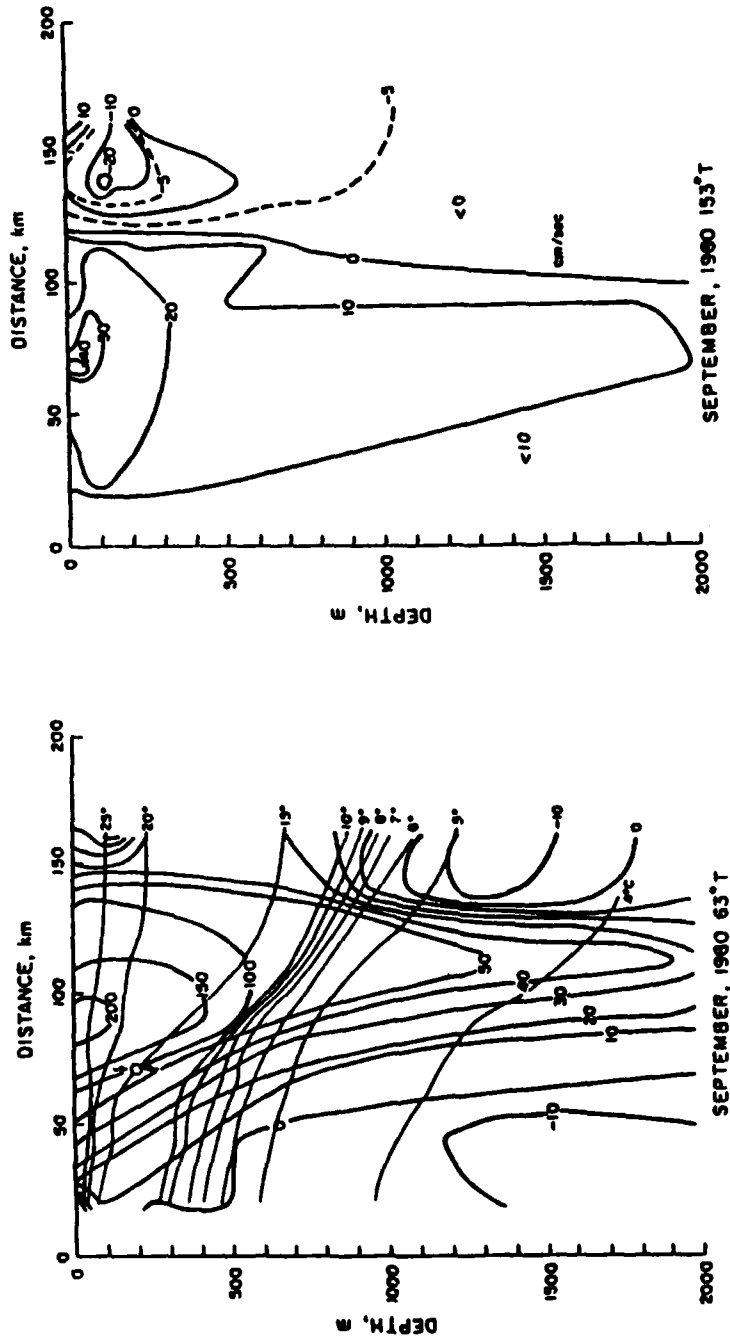
Fig. 4. Preliminary contour plots of velocity in the downstream (a) and cross-stream (b) directions for the transect in September 1980. The downstream direction is determined by the direction of flow of the central part of the Gulf Stream.
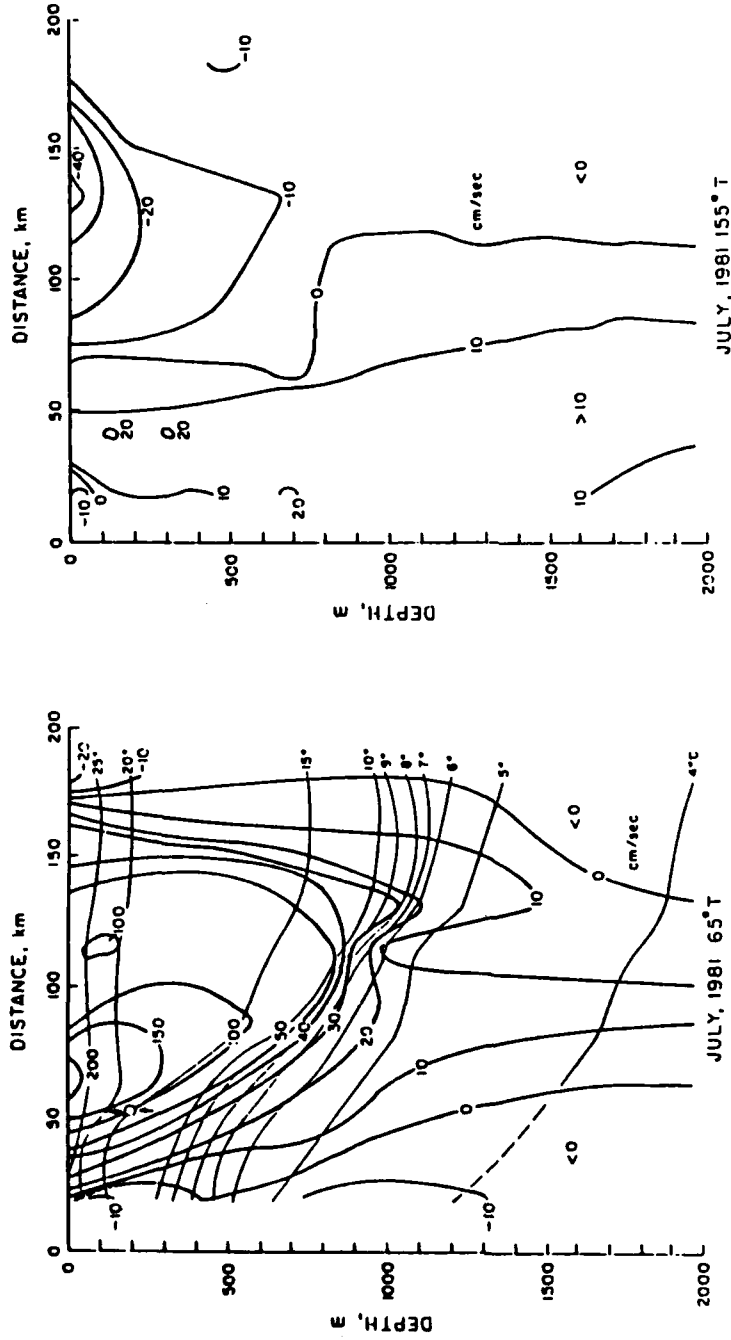
Fig. 5. Preliminary contour plots of velocity in the downstream (a) and cross-stream (b) directions for the transect in July 1981. The downstream direction is determined by the direction of flow of the central part of the Gulf Stream.

The rather large difference between Worthington's estimate
of mean transport and our results thus far has prompted us,
on several cruises, to take hydrostations at both ends of
the Pegasus section to obtain accurate measures of the total
dynamic height difference. In addition, in March 1982 we
attempted a detailed geostrophic test by taking hydrographic
casts to either side of a Pegasus profile. The result is
shown in Figure 6. Agreement is quite good except near the
surface where rapid time dependence or inertial effects may
come into play. Curiously, the geostrophically estimated
speed is larger, but it is not clear to us whether this
has any bearing on the above transport comparisons. In order
to pursue these questions further we have, in a two-ship
operation in July 1982, obtained two simultaneous Pegasus/CTD
sections. The density work was done by Prof. R. Watts and
his group on the R/V ENDEAVOR while the Pegasus profiling
was done from the R/V CAPE HATTERAS. The data are of high
quality and are presently being analyzed.

REFERENCES

Spain, P.F., D.L. Dorson and H.T. Rossby, 1981. Pegasus:
A simple, acoustically tracked velocity profiler. Deep-
Sea Res., 28A, pp. 1553-1567.

Thompson, R.O.R.Y., 1978. Reynolds stress and deep counter
currents near the Gulf Stream. J. Mar. Res., 36, pp. 611-615.

Worthington, L.V., 1976. On the North Atlantic Circulation.
Johns Hopkins Oceanographic Studies, Vol. VI. The Johns
Hopkins University press, Baltimore and London, 110 pp.

274
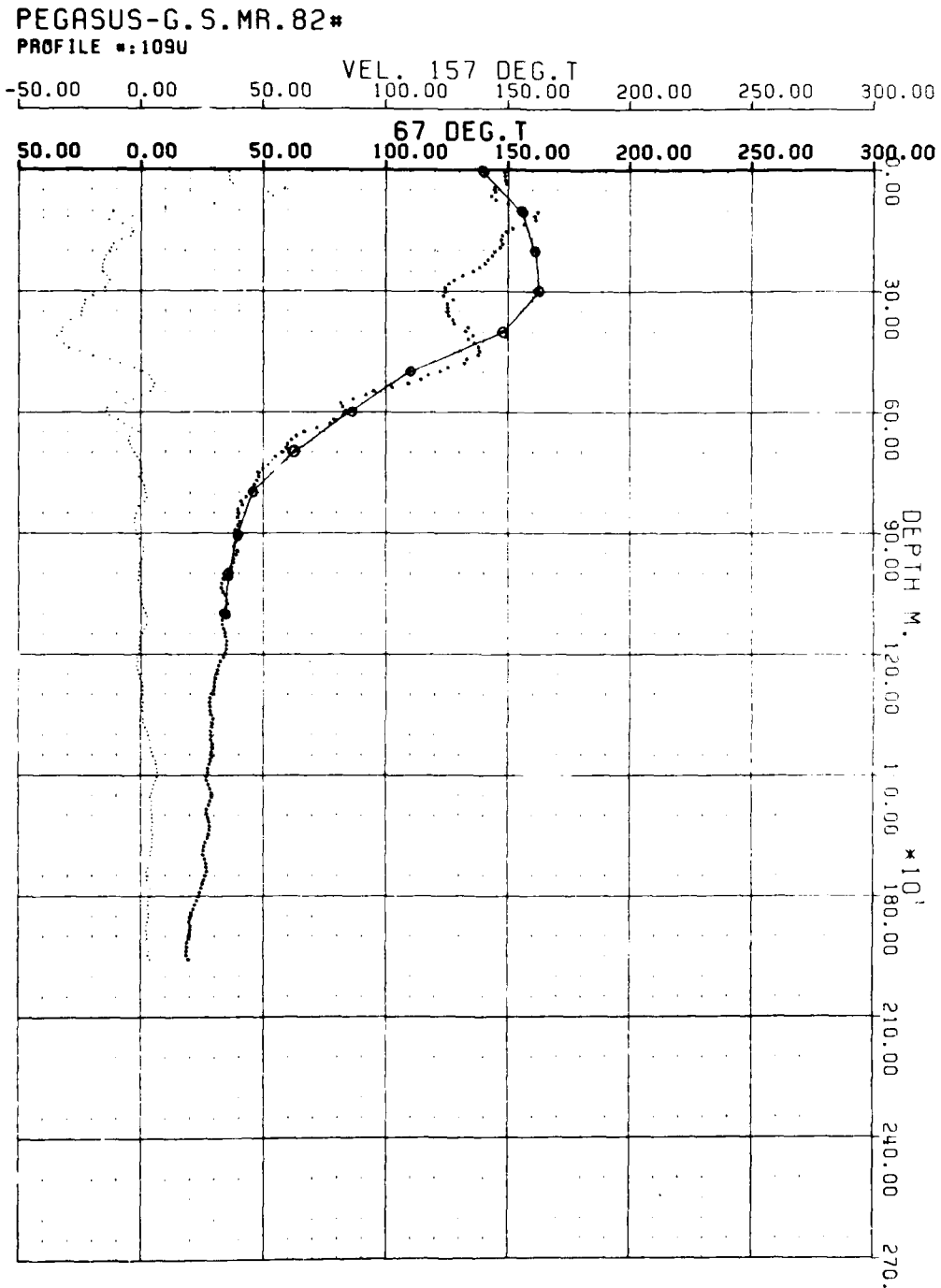
Fig. 6. A comparison of directly observed (......) and geostrophically
computed (o-o-o) profiles of downstream velocity. The latter is
adjusted to the Pegasus velocity at 1100 m.

ADP002664

THE EDDY FIELD OF THE CENTRAL NORTH ATLANTIC

Wolfgang Krauss

Institut fur Meereskunde an der Universitat Kiel
Dusternbrooker Weg 20, 23/Kiel, Germany

ABSTRACT

Sixty-eight satellite-tracked buoys were released in the western and central North Atlantic during 1981 and 1982. Mean velocity values and the variance about the mean were calculated for 20 selected areas. The mean velocities confirm the large-scale gyre circulation. The velocity variance decreases toward the east and south. East of the Mid-Atlantic Ridge the eddy kinetic energy reaches values of about 200 $cm^2 s^{-2}$ at 50°N, but only 50 $cm^2 s^{-2}$ at 30°N.

INTRODUCTION

The results of 110 satellite-tracked freely drifting buoys in the North Atlantic have been summarized by Richardson (1983). The buoys came from different sources and were released between 1971 and 1981. Richardson prepared a map of eddy kinetic energy on a 2 x 2 grid between latitudes 20° - 50°N. Maximum energy of about 3000 $cm^2 s^{-2}$ coincided with the Gulf Stream jet between Cape Hatteras and Newfoundland. In the area around the Grand Banks, values of 1000 $cm^2 s^{-2}$ were obtained. A weak tongue extends eastward across the Mid-Atlantic Ridge near 45°N. A second weaker extension is claimed to tend toward the southeast and to cross the ridge between 30° and 35°N. North and south of the Gulf Stream the energy diminishes rapidly to values of about 200 $cm^2 s^{-2}$ in the mid-gyre region and 100 $cm^2 s^{-2}$ in the Eastern North Atlantic and the North Equatorial Current. The number of buoys in the central and eastern North Atlantic, however, is very small. Most of the buoys released in the Gulf Stream area failed before they reached the Mid-Atlantic Ridge. Only a few experiments have been made in the eastern North Atlantic (e.g. Madelain and Kernt, 1978). Compared to ship drift data (Wyrtki, Magaard, and Hager, 1976) the results of Richardson are similar, but the buoy data lead to higher values of eddy kinetic energy in the Gulf Stream area and to lower values in the mid-gyre region.

PRESENT DATA BASE

Sixty-eight satellite-tracked buoys have been released by the Institute for Marine Research at Kiel during 1981 and 1982 in the North Atlantic. They are part of a long-term experiment to study the mean currents and the eddy field east of the Gulf Stream. Thirty of 68 buoys were deployed along the Mid-Atlantic Ridge north of the Azores, 18 in the North Atlantic Current east of Flemish Cape and 10 south of the Azores. Besides 10 buoys with drogues at 10-m depth (released east of Flemish Cape), all buoys were drogued by a window-shaped sail at 100-m depth. Simultaneous measurements of temperature and salinity in boxes of $5^\circ \times 5^\circ$ show that the trajectories are in close agreement with geostrophic currents derived from those data (Krauss and Meincke, 1982). Wind influence on buoys with shallow drogues (McNally, 1981), which can be considerable, seems to be of minor importance.

LARGE-SCALE CIRCULATION

The buoy tracks from May 1981 through August 1982 are shown in Figure 1. From these trajectories the zonal current $\bar{u}$ averaged over the entire North Atlantic between $8^\circ W$ and $50^\circ W$ and the meridional component $\bar{v}$ averaged between $25^\circ N$ and $55^\circ N$ have been computed. Figure 2 (top) displays $\bar{u}$ based on averages over 5° latitude and over 2.5° latitude. The number of buoy days available for these averages is indicated at the left. The figure shows the large-scale gyre with maximum zonal velocities of ± 10 cm s^{-1} at $50^\circ N$ and $25^\circ N$. The center of the gyre is at $35^\circ N$ and about $30^\circ W$. The latter follows from the meridional current component $\bar{v}$ which is depicted in Figure 2.

MEAN VELOCITIES AND VARIANCES

In order to study the spatial distribution of both mean currents and variations, the buoys were grouped into 20 boxes as shown in Figure 3. The size of these boxes depends on the geographic location and the number of buoy data available in that region. Fields 1, 2 and 3 follow the path of the North Atlantic Current; field 4 represents Flemish Cape; 6, 7, 11, 17, and 16 follow the Mid-Atlantic Ridge; 5, 9, and 10 are located in the western basins; and the remaining ones are in the eastern basins. Field 15 has been separated from 14 to allow for the Portugal current. Mean currents (arrows) and R.M.S. velocities (ellipses) for each box are shown in Figure 4 as averages of all buoys while they passed such a box. In general, the R.M.S velocities exceed the mean velocity by a factor of 2 to 3. The same holds for each platform separately (Fig. 5).

In order to relate the energy of inertial and tidal currents to the eddy kinetic energy and the mean kinetic energy, Figure 6 displays each part as separate column. Eddy kinetic energy is defined as energy
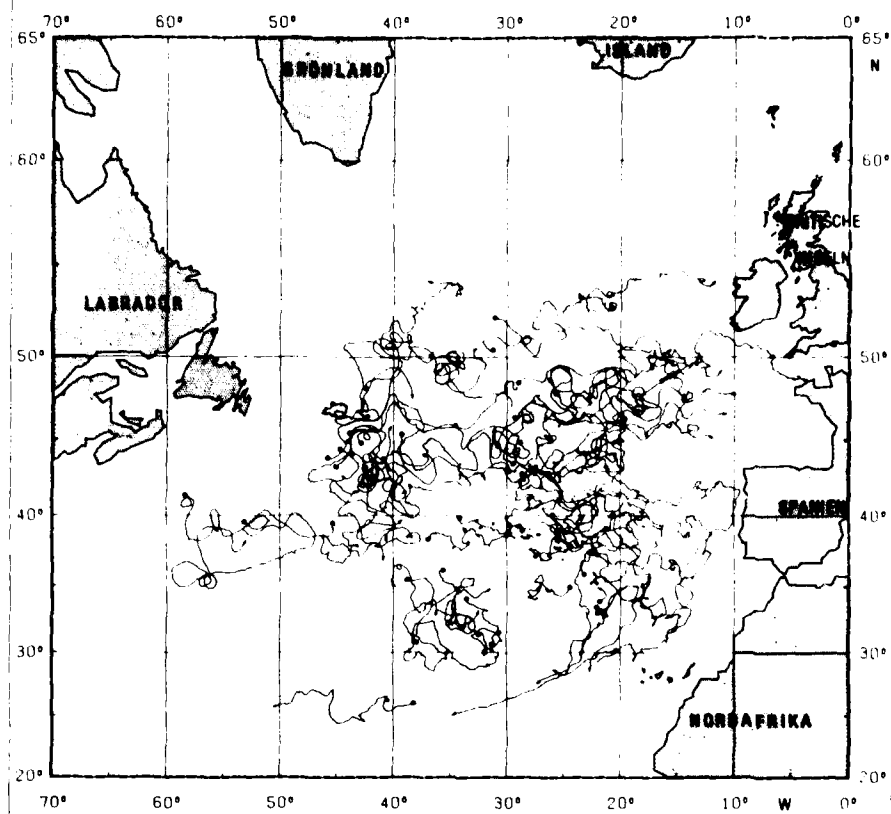
Fig. 1. Trajectories of satellite-tracked buoys released
between 1981 and 1982 in the North Atlantic by the *Institut
für Meereskunde*.
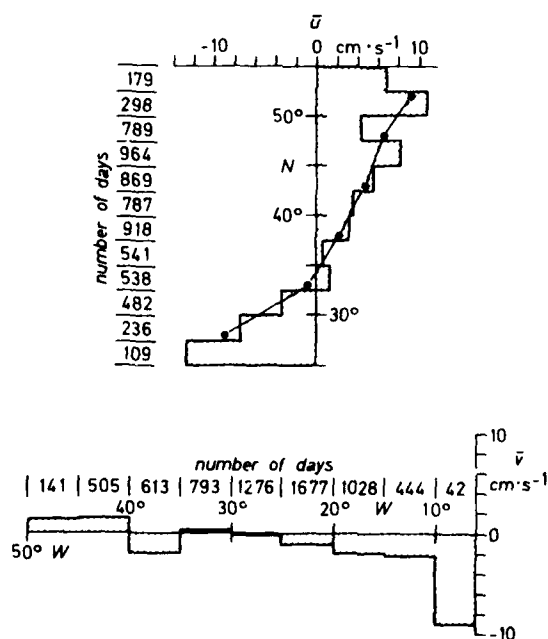
Fig. 2. Top: Zonal current $\bar{u}$ (ϕ) averaged between 8°W and
50°W (dots, averaged over 5° latitude; shaded area, averaged
over 2.5° latitude).   Bottom: Meridional current $\bar{v}$ (λ)
averaged between 25°N and 55°N (5° squares).
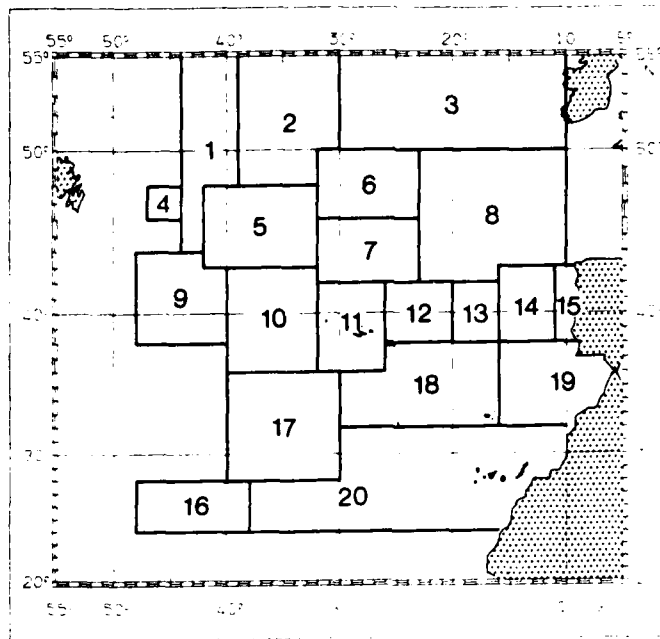
Fig. 3.   Distribution of fields used for statistical analysis
of drift data.
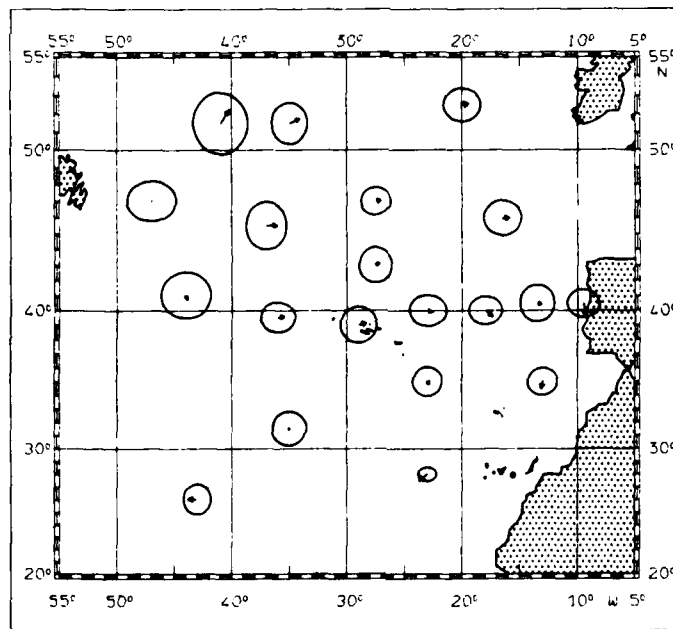
Fig. 4.   Mean current (arrow) and RMS velocity of current
fluctuations (ellipse) for twenty selected areas
according to Fig. 3.
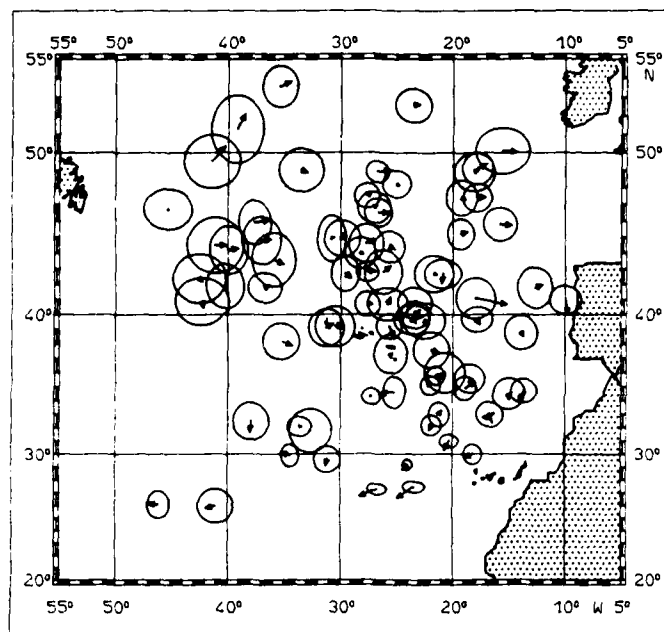
Fig. 5.   Same as Fig. 4, but for each drifter separately in
each field.
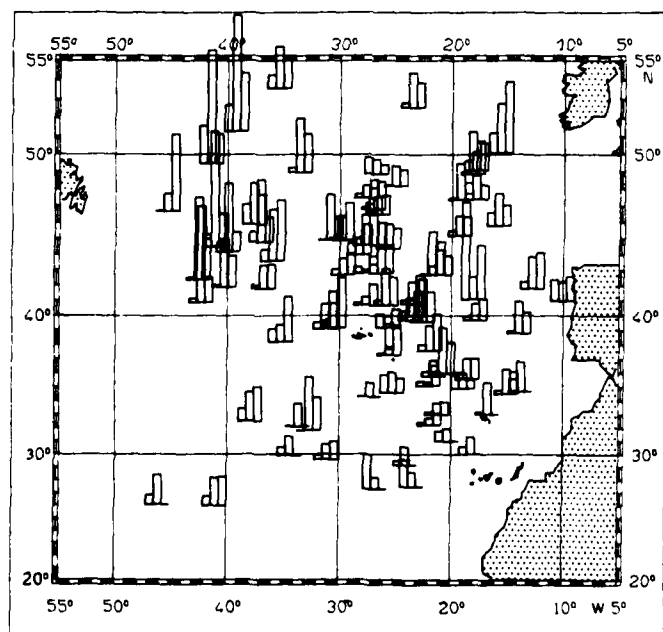
Fig. 6.   Mean kinetic energy (left column), eddy kinetic energy
(central column), and high-frequency part with periods less
than two days (right column) for the drifters shown in Fig. 5.

belonging to fluctuations with periods of more than two days; shorter periods are summarized as high-frequency part. In Figure 6 the left column refers to the mean, the central one to the eddy kinetic energy, and the right column to the high-frequency part. Eddy kinetic energy, in general, is much larger than the mean energy. But a considerable contribution to the variance is due to the high-frequency part which may also include variable wind influence.

Eddy kinetic energy east of 35°W (Mid-Atlantic Ridge) is shown in Figure 7. In addition to large scatters, a general increase of eddy kinetic energy from low latitudes ($50 \text{cm}^2\text{s}^{-2}$ at 30°N) toward the polar front ($200 \text{ cm}^2\text{s}^{-2}$) at 50°N is obvious.

CONCLUSIONS

Trajectories of satellite-tracked buoys obtained during 1981 and 1982 provide a large data set in addition to the existing data base. However, the number of drifting buoys is still too small for a statistical treatment. Eddy kinetic energy in the central and eastern North Atlantic is mainly due to eddies of 100- to 200-km diameter. Besides these, large meridional troughs and blocking highs have been observed (unpublished results of a Poseidon cruise in 1982) with associated meanders. It seems that they contribute considerably to the meridional heat exchange. An entirely open question is the source of this eddy kinetic energy. The increase of energy toward the north in the eastern North Atlantic may be due to either the polar front as possible source or the increasing variability of the wind field. It seems unlikely that the eddies stem from the Gulf Stream area, nor is the Mid-Atlantic Ridge visible in the distributions of eddy kinetic energy. Most likely the large-scale gyre itself may be the energy source for the eddies.
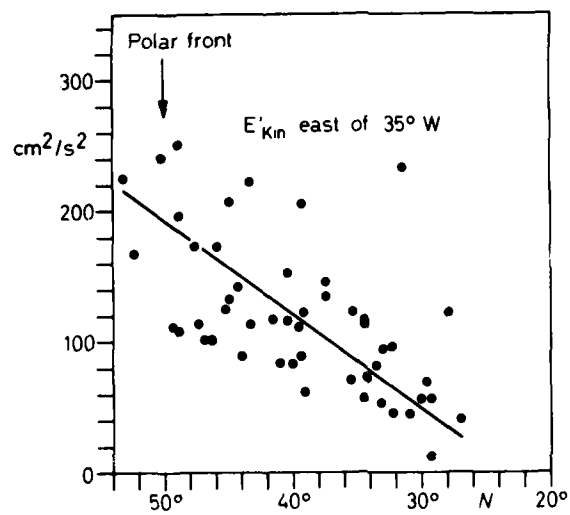
Fig. 7. Eddy kinetic energy of the drifters east of the Mid-Atlantic Mid-Atlantic Ridge as a function of latitude.

REFERENCES

Krauss, W. and J. Meincke, 1982. Drifting buoy trajectories in the North Atlantic Current. Nature, 296, 737-740.

Madelain, F. and E. G. Kernt, 1978. Evidence of mesoscale eddies in the Northeast Atlantic from a drifting buoy experiment. Oceanologica Acta, 1, 159-168.

McNally, G. J., 1981. Satellite tracked buoy observations of the near surface flow in the eastern mid-latitude North Pacific. Journal of Geophysical Research, 86, 8022-8030.

Richardson, P. L., 1983. Eddy kinetic energy in the North Atlantic from surface drifters. Journal of Geophysical Research, 88, 4355-4367.

Wyrtki, K., L. Magaard, and J. Hager, 1976. Eddy energy in the oceans. Journal of Geophysical Research, 81, 2641-2646.

ANNUAL AND INTERANNUAL VARIABILITY IN THE KUROSHIO CURRENT SYSTEM

Keisuke Mizuno
Tohoku Regional Fisheries Research Laboratory
Shiogama, Miyagi Prefect. Japan

Warren B. White
Scripps Institution of Oceanography
La Jolla, California 92037

ABSTRACT

Individual, seasonal, 300-m temperature maps were constructed over the Kuroshio Current System from 130°E to 170°W, for a four-year period from summer 1976 through spring 1980, by using TRANSPAC XBT data and JODC temperature/depth data. Quasi-stationary meanders in the Kuroshio Current System occurred at 137°E (i.e., Kuroshio Meander), at 144°E and 150°E (i.e., lee-wave meanders), and near 160°E (i.e., meander over the Shatsky Rise). A composite of the paths of the Kuroshio (i.e., the 12°C isotherm) from the individual seasonal maps, and the total variance map, finds nodes (i.e., minima) and anti-nodes (i.e., maxima) of variability to have existed along the mean Kuroshio path. The anti-nodes coincided with the location of the quasi-stationary meanders, the nodes in between. Zonal propagation of temperature anomalies accounted for 20-30% of the total interannual variance. These temperature anomalies propagated eastward at .5 -1.5 cm/sec in the region 140°-155°E, and westward at -1 to -2 cm/sec in the region 155°E-175°W. In the latter part of the four-year period (1979-80), the Kuroshio Meander became weak and the Kuroshio Extension was displaced southward, from 36-37°N during the first two years to 34°N during the latter two years. Associated with these large-scale changes, the quasi-stationary meander pattern in the Kuroshio Extension became unstable, associated with increased eddy activity and ring production. In fact, ring production doubled (i.e., from five to ten rings per year) from that of the previous three years.

INTRODUCTION

Past studies of time/space variability of the Kuroshio Current System (i.e., Kuroshio south of Japan and Kuroshio Extension east of Japan) have revealed the presence of both annual and interannual variability (Taft, 1972; Shoji, 1972). The Kuroshio south of Japan has been shown to exist in one of two stable paths, a zonal path and a meander path, each lasting for a period of years. Robinson and Taft (1972) attempted to explain this bimodality of the Kuroshio path through the influence of bottom bathymetry on the deep current of the Kuroshio, but with little success (Taft, 1978). White and McCreary (1976) attempted to explain the two paths in terms of stationary Rossby waves excited by the coastline topography of Japan; however, bimodality was not achieved. Recently, Chao

and McCreary (1982) showed three separate paths which arise from Rossby wave resonance with the coastline topography; two of these were similar to the observed paths.

The Kuroshio Extension east of Japan is known as a highly variable current, with cold and warm rings generated from unstable meander growth. Kawai (1972) showed the quasi-stationary existence of meanders near 144°E and 150°E. The first meander at 144°E displayed no annual variability but did exhibit significant interannual variability. The second meander at 150°E displayed no annual or interannual variability; however, data describing the time dependent nature of the second meander were sparse.

Bernstein and White (1977) first observed the eastward extension of intense meander and eddy activity in the Kuroshio Extension. It extended from the coast of Japan to at least 175°W, much farther to the east than had previously been realized. Wilson and Dugan (1978) produced a thermal map of the eddy activity in the Kuroshio Extension from 155°E-175°W, using XBTs from a single multiple-ship survey. Bernstein and White (1981) used XBTs deployed repeatedly from volunteer observing ships in sequential monthly construction of thermal maps over the region 140°E-180°E for two years (1976-1978). They showed westward propagation of meanders and eddies over this region.

Ring formation is one of the important processes of mesoscale activity in the Kuroshio Extension. Most of the previous work (Kawai, 1972; Hata, 1974; Kitano, 1975; Tomosada, 1978) concentrated on the warm rings in the Kuroshio Extension adjacent to Japan. More recently, Kawai (1979) studied the geographical distribution of cold rings, finding them to occupy the area southeast of Japan.

The effect of the bathymetric features of the Izu Ridge (Taft, 1972), the Shatsky Rise (Bernstein and White, 1981) and the Emperor Seamounts (Levine and White, 1983) upon the Kuroshio Current System has been studied. At each of these bathymetric ridge locations, the path of the Kuroshio has been observed to be deflected either northward over the ridge or through a channel in the ridge. In the North Atlantic, Richardson (1981) found Gulf Stream meander activity and ring generation to be intensified by the presence of the New England Seamounts. However, in the North Pacific, Bernstein and White (1981) found eddy activity in the Kuroshio Extension to be intensified over the abyssal plane between the Izu Ridge and the Shatsky Rise.

Past investigations into the variability of the Kuroshio Current System have been mostly local in nature and restricted in temporal coverage. The present study deals with annual and interannual variability over the entire Kuroshio Current System from 130°E to 175°W for a four-year period, 1976-1980. This was made possible by merging TRANSPAC XBT data (collected by volunteer observing ships) and JODC (Japan Oceanographic Data Center) temperature/depth data. Study is concentrated on temperature variability in the main thermocline of this current. Therefore, seasonal

maps of 300-m temperature were constructed for four years (i.e., summer 1976 through spring 1980), on a 1° latitude by 1° longitude grid. Bernstein and White (1981) demonstrated that 300-m temperature variability was correlated strongly with dynamic height (100/1000 db) variability in the western mid-latitude North Pacific. They also conducted time/space correlation studies, finding dominant variability to have a decorrelation space scale of about 250 km and a decorrelation time scale of about 3 months. This allows the present study to be conducted on a seasonal (3 month) basis over a 1° latitude/longitude grid.

The purpose of this study is to describe the space/time character of the annual and interannual variability over the entire Kuroshio Current System from south of Kyushu (130°E) to east of the Emperor Seamounts to 175°W. The long-term mean geostrophic flow (0/1000 db) and bottom bathymetry are shown in Figure 1, displaying the region of interest. here can be seen the basic structure of the Kuroshio Current System and the bottom bathymetry over which it flows.

DATA

Data on the depth distribution of temperature in the Kuroshio south of Japan were collected principally by Japanese research vessels using the deep MBT (mechanical bathythermograph), the XBT (expendable bathythermograph), and reversing thermometers. These data were archived at the Japanese Oceanographic Data Center (JODC). Temperature data in the Kuroshio Extension east of Japan were mainly collected by the TRANSPAC XBT field program and have been archived at Scripps Institution of Oceanography (SIO). Both of these data sets were then merged to provide the comprehensive data base for this study. From this data set, 300-m temperature values for each season were interpolated onto a 0.5° longitude by 0.5° latitude grid from the nearest eight raw observations, using a computer algorithm called Surface II (Sampson, 1973). A low-pass filter was then applied that suppressed two-grid variability. Therefore, spatial resolution was estimated to be 1° latitude and by 1° longitude, data permitting. The accuracy was determined to be ±.6°C by using the same conservative error estimation reported by White and Bernstein (1979). This range of error (i.e., 1.2°C) is slightly bigger than the contour interval (1.°C) used to delineate the oceanographic features in the seasonal maps.

Seasonal maps of 300-m temperature are displayed in Figure 2a,b for the period 1976-1980. By inspection, the average, nearest-neighbor, data separation in the vicinity of the Kuroshio Current System can be seen to have been less than 1° latitude/longitude. Away from the Kuroshio Current System the average, nearest-neighbor, data separation is seen to have been often larger than the 1° latitude/longitude grid spacing. In the latter case, the 1° grid spacing does not resolve 1° scale variability, but something larger. Also, a seasonal bias can be seen in these data distributions; data collected in summer are located farther north than in winter due to the seasonal, meridional migration of volunteer observing ships used to collect the TRANSPAC XBT data set.
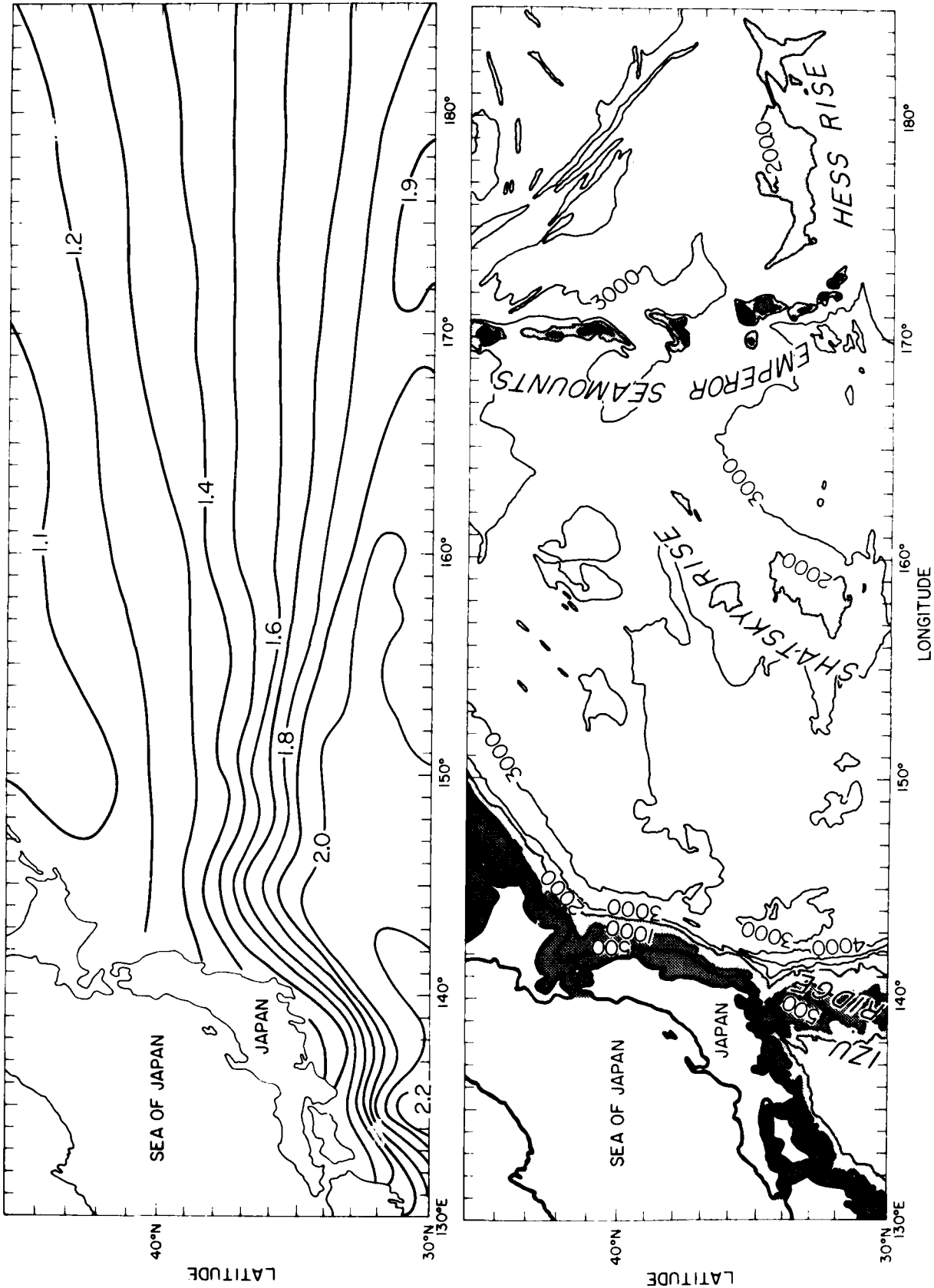
Fig. 1. Top: annual mean dynamic topography (dyn m) of the sea surface relative to 1000 db, after Wyrtki (1975). Bottom: bottom bathymetry (contours in fathoms) from Chase and Menard (1973).

Seasonal maps shown in Figure 2a,b were designed to observe annual and interannual variability in the Kuroshio Current System, with a decorrelation space scale no less than 100 km, with a decorrelation time scale no less than 3 months, and with an amplitude greater than .6°C. Variability with scales (magnitude) smaller than these is not resolved (detected) and is subsequently treated as ambient noise.

Justification for neglecting these smaller scales of variability derives from the following published works. Bernstein and White (1977) calculated the zonal wavenumber spectrum of 300-m temperature in the Kuroshio Extension for the range of wavelengths 100-1200 km, finding 90% of the variance to be located between wavelengths of 400-1200 km and less than 10% of the variance located at shorter wavelengths. Furthermore, the time decorrelation scale of monthly variability in 300-m temperature in the Kuroshio Extension was found by Bernstein and White (1981) to be 3 months, corresponding to a period scale of one year. Therefore, dominant spatial variability in the Kuroshio Current system is large compared to 1° latitude/longitude grid separation, but the temporal variability is barely resolved by the 3-month time grid.

Seasonal maps of 300-m temperature in Figure 2a,b show the Kuroshio Meander south of Japan to have existed all through the period. However, it was displaced east and west of its mean location; eg., westward in 1977 and eastward in 1980. Throughout most of the period the Kuroshio Meander was Type A (Nitani, 1969), with a big meander located to the west of the Izu Ridge. However, in 1980 the amplitude of the meander became smaller and in the last season (i.e., spring, 1980) it changed to a Type C meander (Nitani, 1969), with a small amplitude meander straddling the Izu Ridge.

The Kuroshio Extension east of Japan can be traced as a high-gradient frontal feature at least as far east as 170°E in each seasonal map. Adjacent to Japan (140°E-155°E), a quasi-stationary meander pattern in the Kuroshio Extension repeated itself in most maps prior to winter 1979, with two meanders located repeatedly at 144°E and 150°E, similar to that detected by Kawai (1972). After the winter of 1979, this pattern disappeared. In all maps, cold/warm rings can be found over the entire Kuroshio Current System, west of 170°E. The Kuroshio Extension can be observed to have bifurcated often between 160°-165°E; one of the branches, represented by the 7-8°C isotherm, consistently went northeastward along the Shatsky Rise as shown by Levine and White (1983), while the main branch extended eastward along 36°N, encountering the Emperor Seamounts. This bifurcation in the Kuroshio Extension was displaced westward to 150°E during winter/spring 1980, when the main path of the Kuroshio Extension shifted to the south. At that time, eddy activity in the Kuroshio Extension intensified and the Kuroshio Meander south of Japan became weaker. Also at that time, there seems to have been a change in the stability regime of the quasi-stationary meander pattern of Kuroshio Current System, from a relatively stable current to an unstable current. More on this regimal change is discussed in a later section.

Fig. 2a. Individual seasonal maps of temperature (°C) at 300 m over the region of interest, summer 1976 – spring 1978. Dots on the map indicate station locations. Contour interval is 1°C.

289
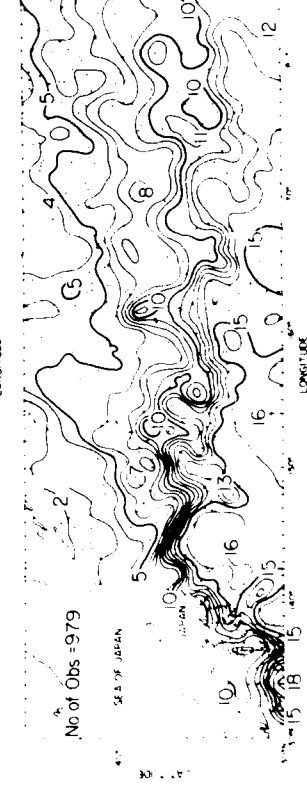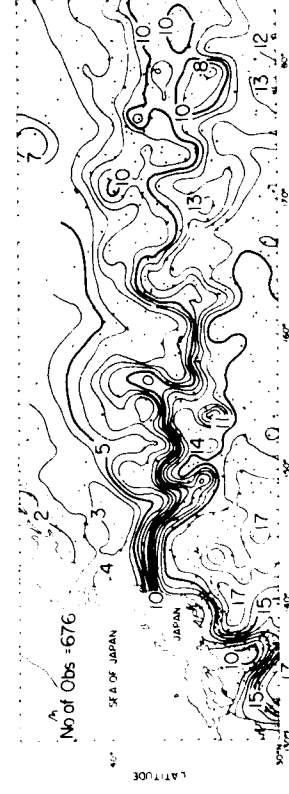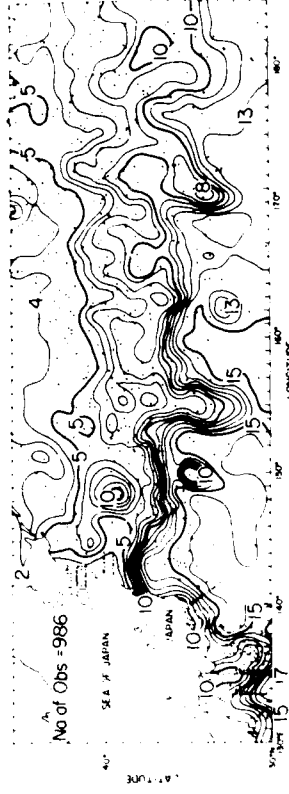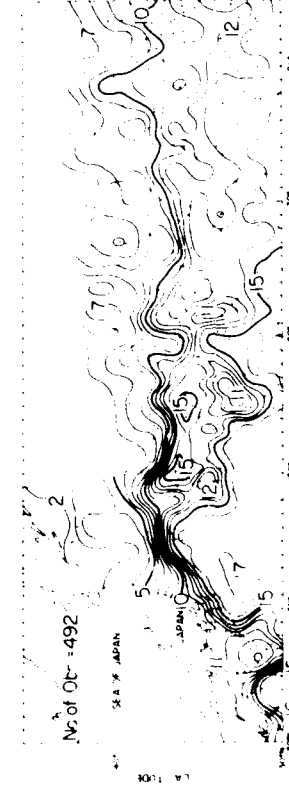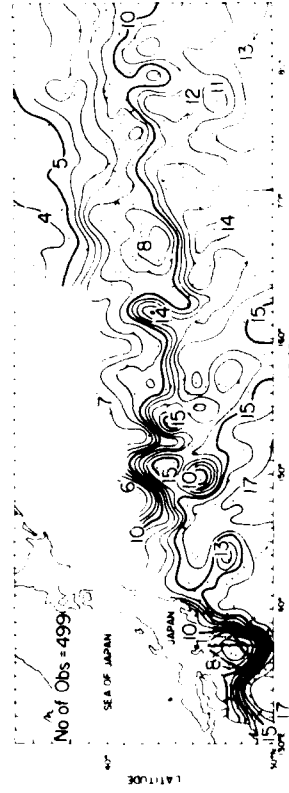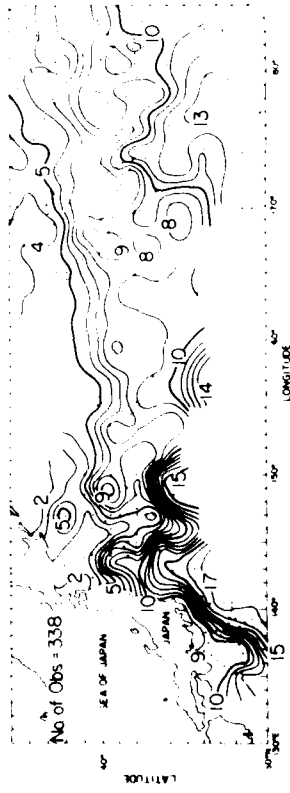
1979-80
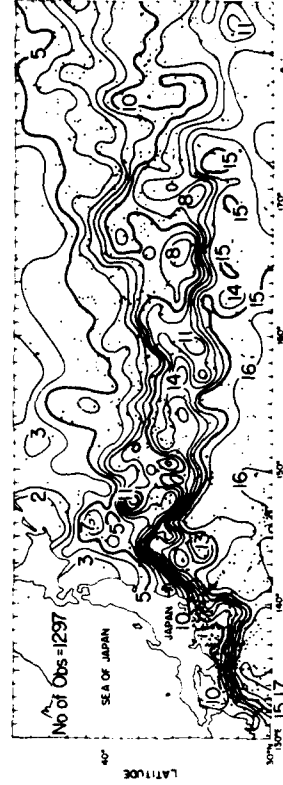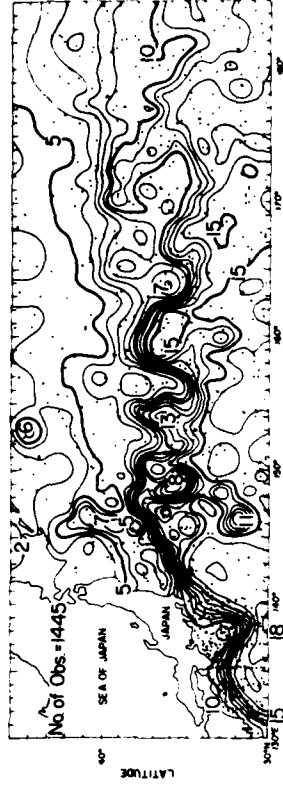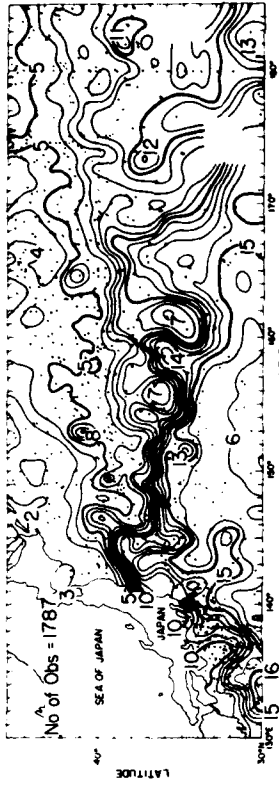
1978-79

SUMMER
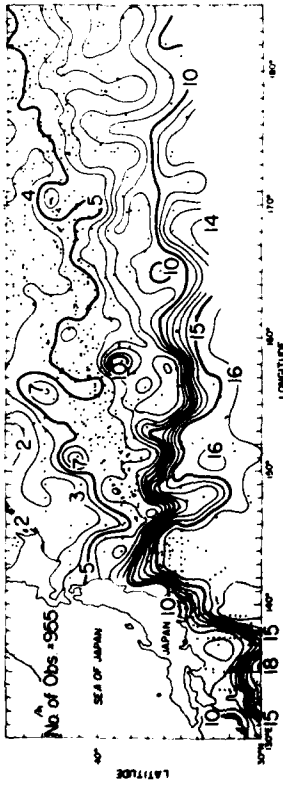
FALL
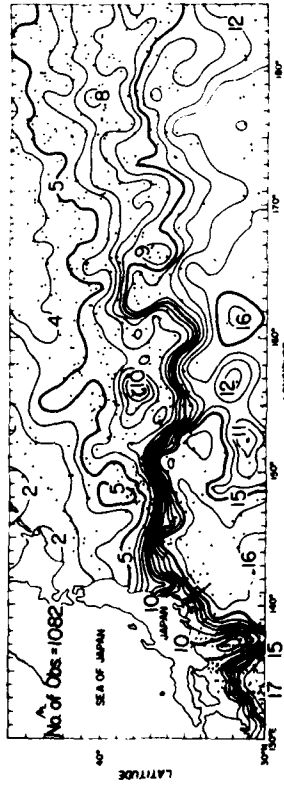
WINTER
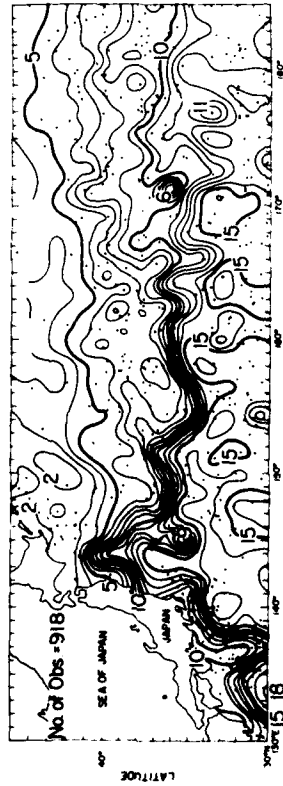
SPRING

Fig. 2b. Same as 2a, summer 1978 – spring 1980.

MEAN STATE AND VARIANCE

The long-term mean temperature distribution (Figure 3, top) shows a quasi-stationary meander pattern all along the length of the Kuroshio Current System. The Kuroshio Meander south of Japan at 138°E, the Kuroshio Extension meanders at 144°E and 150°E, and the meander over the Shatsky Rise near 160°E (Figure 1) display amplitudes of 1-3° latitude. East of the Shatsky Rise, meander activity is subdued except near the Emperor Seamounts (170°E) and immediately to the east of there. Comparing this map with that of Wyrtki (1975) shown in Figure 1 yields some similarity west of 155°E but none east of there because of the lack of hydrographic data in the region with which to construct reliable estimates of dynamic height (Wyrtki, 1975).

East of 160°E, the geostrophic shear flow of the Kuroshio Extension (i.e., related to the temperature gradient) bifurcated at 37°N, 163°E. This bifurcation actually divides the Kuroshio Extension into two branches: one proceeding along the Shatsky Rise to 40°N, where it turns east; the other extending directly east, where it impinges upon the Emperor Seamounts at 170°E. This bifurcation is consistent with that seen repeatedly in individual seasonal 300-m temperature maps shown in Figure 2a,b.

The total RMS difference of 300-m temperature (Figure 3, bottom) shows several secondary maxima along the mean geostrophic flow path of the Kuroshio Current System. One of these maxima was located in the Kuroshio Meander area; this is an expression of the east-west displacement of the Kuroshio Meander indicated in the discussion of Figure 2a,b. Other secondary maxima were located at the quasi-stationary meanders at 144°E and 150°E. It is determined that this variability was not due so much to an east-west displacement of the meanders but to a change in their amplitude. Another broad secondary maxima existed from 153°E-163°E at the same location as the meander over the Shatsky Rise (see Figure 1).

Comparing mean and RMS difference maps of 300-m temperature (Figure 3) with the map of bottom bathymetry (Figure 1) suggests a relationship among the quasi-stationary meander pattern, the distribution of RMS differences, and bottom bathymetry features. The mean path of the Kuroshio Meander passed along the west side of the Izu Ridge and crossed it adjacent to the Japanese coast, going through a channel in the deepest portion of the ridge. This caused the RMS differences to be small there. East of the Izu Ridge, two meanders appeared in the Kuroshio Extension at 144°E and 150°E, respectively. These meanders are thought to be lee-wave meanders induced by the flow of the Kuroshio over the Izu Ridge (see Appendix). In the vicinity of the Shatsky Rise, the mean path of the Kuroshio Extension (following the 12°C isotherm) formed a meander directly over the Shatsky Rise. There, the Kuroshio Extension bifurcated, with the northern branch paralleling the Shatsky Rise to 40°N. In the lee of the Shatsky Rise, evidence of lee-wave meander activity can be found in the branch of the Kuroshio Extension that extended eastward along 36°N. The strength of
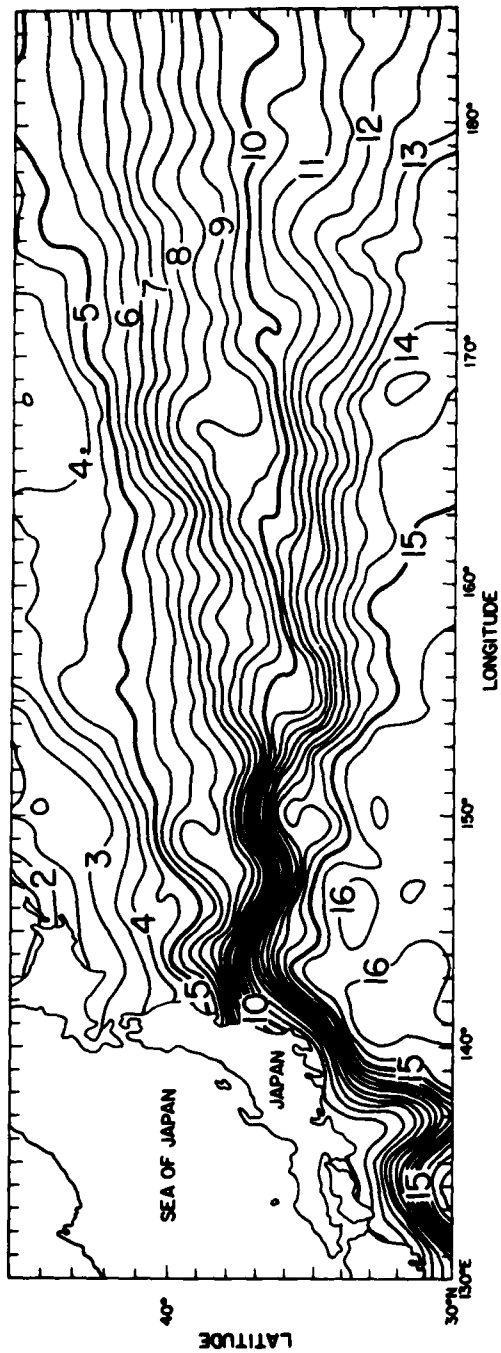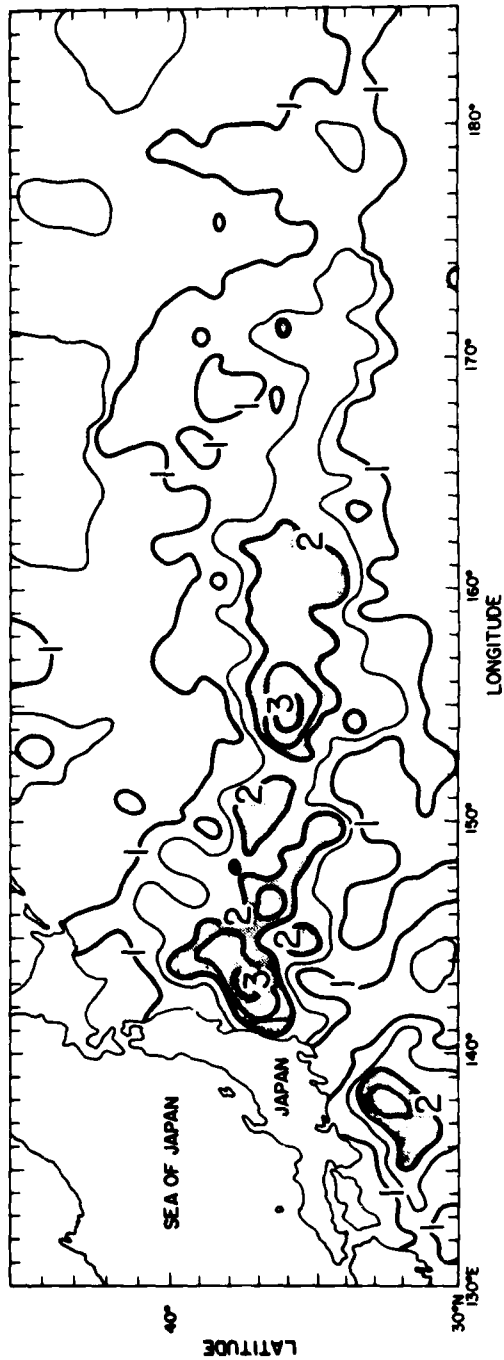
Fig. 3. Long-term annual mean (top) and total RMS differences (bottom) of temperature (°C) at 300 m estimated from maps in Fig. 2. Contour interval is 0.5°C on both maps. Regions where RMS differences exceed 2°C are shaded.

this latter branch remained constant to 170°E, where it decreased
significantly upon encountering the Emperor Seamounts. East of the
Emperor Seamounts, another quasi-stationary meander can be seen near
35°N, 175°E; however, the wavelength of this meander was too long, and
the shear flow too weak, for it to be considered as a lee-wave
phenomenon. Rather, it may have been related to the presence of the Hess
Rise at 177°E. A much more detailed discussion of the relationship
between bottom bathymetry and the path of the Kuroshio Extension east of
160°E is given by Levine and White (1983).

ANNUAL CYCLE

The long-term seasonal mean and interannual RMS differences in each season
for 300-m temperature are displayed in Figure 4. The mean position of the
Kuroshio Meander each season was the same but its wavelength changed, from
longest in winter to shortest in spring. Interannual RMS differences in
the vicinity of the Kuroshio Meander were maximum in winter and minimum in
summer. Two secondary maxima in RMS differences east and west of the
Kuroshio Meander occurred in fall through spring, indicating an east/west
displacement on an interannual basis. In summer, the Kuroshio Meander was
more stable, with a single RMS maximum in a comparatively narrow area
centered directly over the Kuroshio Meander.

In the Kuroshio Extension, the two lee-wave meanders observed in Figure 3
at 144°E and 150°E existed in summer, fall, and winter, but
practically disappeared in spring. From summer to winter, the wavelength
of these meanders became progressively larger, from approximately 450 km
in summer (the distance between the two wave crests at 145°E and
149°E), to 600 km in fall (144°E and 151°E), and to 700 km in winter
(145°E and 153°E). The second meander almost disappeared in spring,
when coincidentally the amplitude of the Kuroshio meander become weaker.
The magnitude of the interannual RMS differences changed seasonally over
the entire Kuroshio Extension, maximum in winter (i.e., ±4°C) and
minimum (i.e., not greater than 2°C) in spring/summer. In fall/winter,
secondary maxima in variance occurred at the location of the lee-wave
meanders at 144°E and 150°E, and at the meander situated over the
Shatsky Rise. Spatial minima occurred in between. The difference between
minima and maxima was significant at the 95% confidence level. However,
in spring/summer this spatial pattern of RMS differences was less clearly
defined, associated with a general overall weakness of the interannual
variability.

PATH OF THE KUROSHIO CURRENT SYSTEM

A composite of Kuroshio Current paths over the region of interest is shown
in Figure 5. The Kuroshio Current path is defined by the location at
300-m depth of the 12° isotherm, which was consistently located at or
near the center of the thermal front over most of the Kuroshio Current
System, in all seasons. This working definition allows the meander
pattern of the Kuroshio Current System in a particular season to be
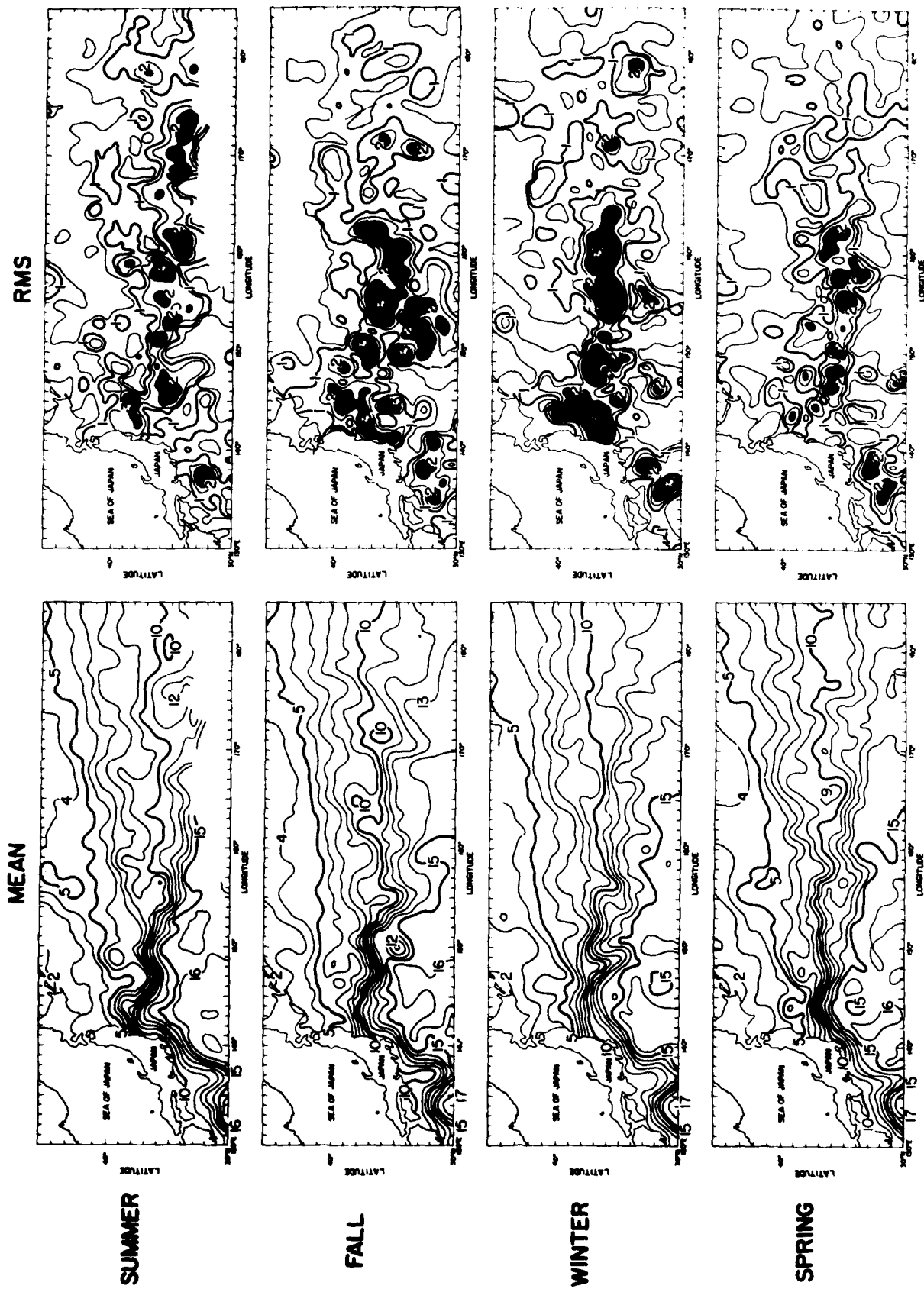
Fig. 4. Long-term seasonal mean and interannual RMS differences of temperature (°C) at 300 m. Regions where RMS differences exceed 2°C are shaded. The contour interval is 1°C on the mean maps and 0.5°C on the RMS differences maps.

1976 SUMMER – 1978 SPRING
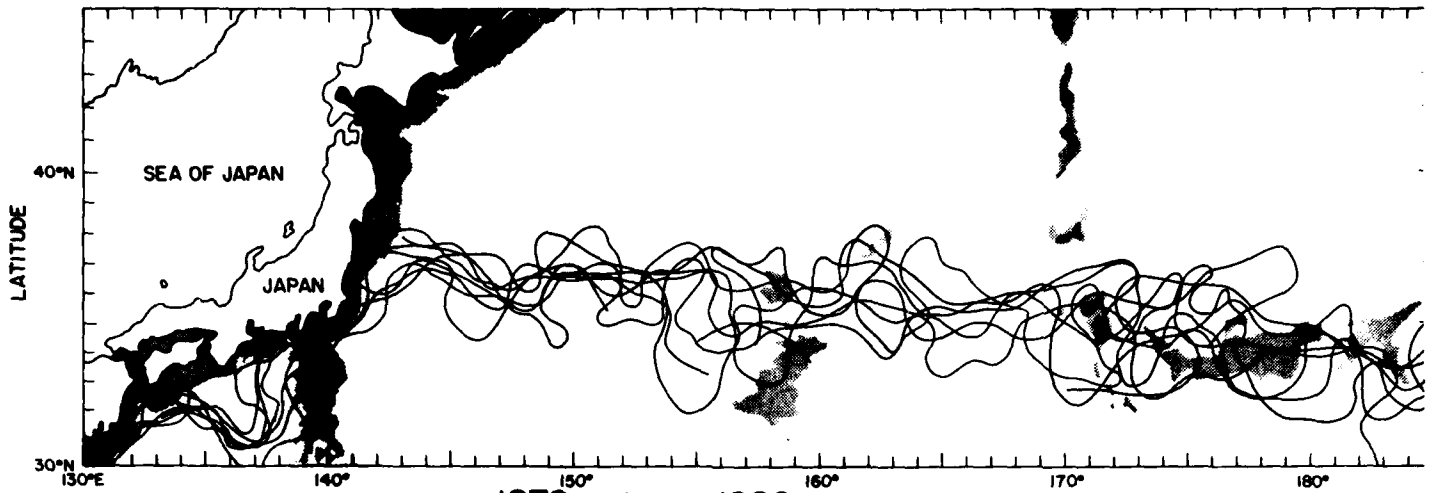
1978 SUMMER – 1980 SPRING
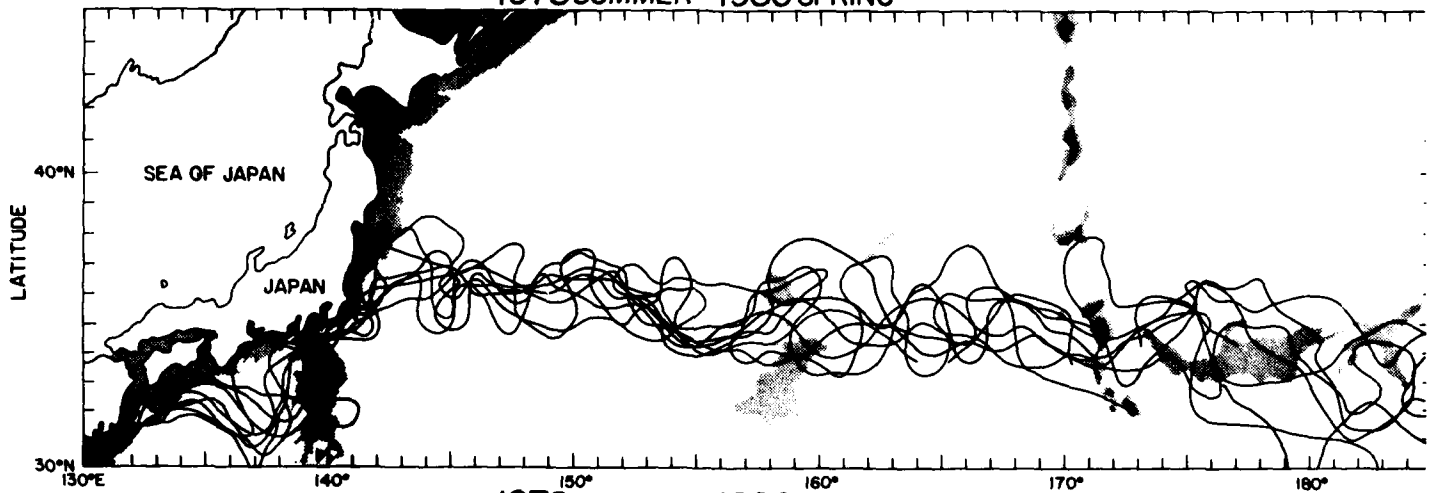
1976 SUMMER – 1980 SPRING
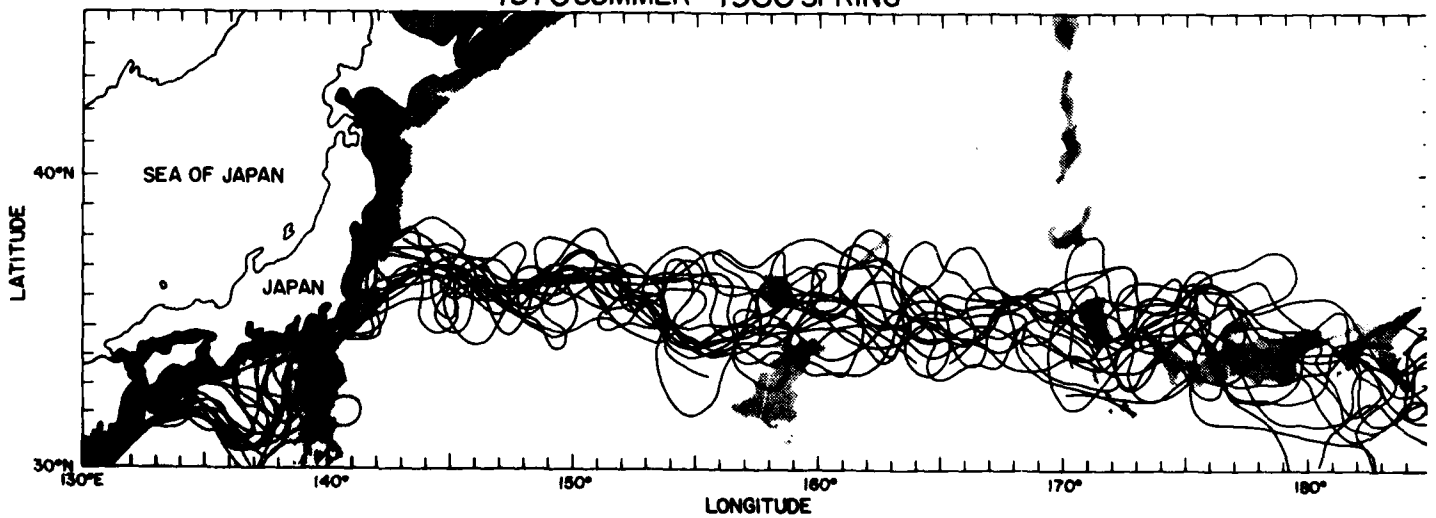
Fig. 5. Composite of the individual seasonal Kuroshio Current paths, superimposed upon prominent bottom bathymetry features (see Fig. 1). Top: summer 1976 – spring 1978. Middle: summer 1978 – spring 1980. Bottom: summer 1976 – spring 1980.

characterized by a single line, so that comparisons can be made between the meander pattern in different seasons and different years. Choosing a different 300-m isotherm (i.e., 11°C or 13°C), or taking the maximum temperature gradient, as an indicator of Kuroshio path does not alter the subsequent discussion on the annual and interannual changes that occur in the meander patterns of the Kuroshio Current System.

During the first two years (upper panel of Figure 5), the paths of flow in the Kuroshio Meander region changed little from one to the other, but during the second two years (lower panel) they changed dramatically. Greater season-to-season variability in the second two years also seems to have occurred in the Kuroshio Extension paths. During the first two years, the lee-wave meander at 144°E also changed little, but during the second two years it became more animated (i.e., its amplitude and wavelength changed by nearly a factor of two). On the western flank of Shatsky Rise, the seasonal paths of the Kuroshio Extension tend to have been located farther north near 37°N during the first two years, and farther south (near 34°N) during the second two years. In the vicinity of the Emperor Seamounts, the paths of the main branch of the Kuroshio Extension tend to have been located near 36°N during the first two years and 34°N during the second two years.

In the overall composite (bottom panel of Figure 5), the individual seasonal paths of the Kuroshio Current System can be seen to have occupied a kind of mean path west of 157°E, at least compared to east of there where none of the paths repeated themselves. Paths near 155°E seem to have been divided into two groups; i.e., a northern group at 37°N and a southern group at 34°N. This apparent bimodality of the path envelope in this region makes the temperature gradient in the mean (Figure 3) small and the RMS differences relatively large in this area. As such, the apparent bifurcation of the Kuroshio Extension that can be seen at 153°E in the mean picture in Figure 3 did not take place; rather, the current kept to the north path during the first two years and to the south path during the second two years. East of there, the envelope of paths spread, and no consistently repeated paths seem to have existed.

Over the Kuroshio Current System, paths were particularly focused at several locations. South of Kyushu at 32°N, 132°E and on the Izu Ridge at 34°N, 140°E, the paths coincided. At three other locations east of Japan (i.e., 37°N, 149°E; 36°N, 152°E; 35°N, 164°E) the paths also tend to have coincided. These five locations also display small total RMS differences (Figure 3), separating the secondary maxima in RMS differences. So, they behave as nodal locations in the quasi-stationary meander pattern of the Kuroshio Current System.

Inspection of the individual seasonal maps in Figure 2 indicates that a change took place in the stability regime of the quasi-stationary meander pattern in the Kuroshio Current System in 1979. To emphasize this change, the path composite for 1978-80 shown in Figure 5 is broken down into two one-year composites in Figure 6. This contrasts the comparatively stable meander pattern of 1978-79 with the relatively unstable meander
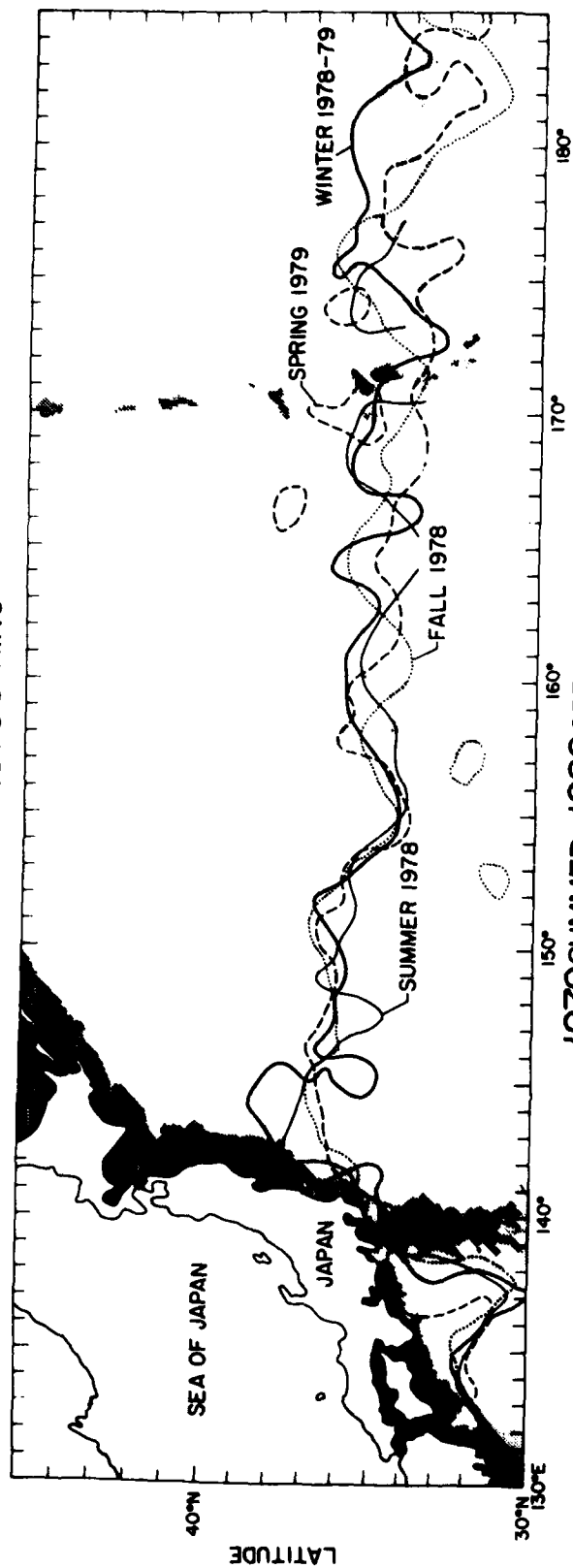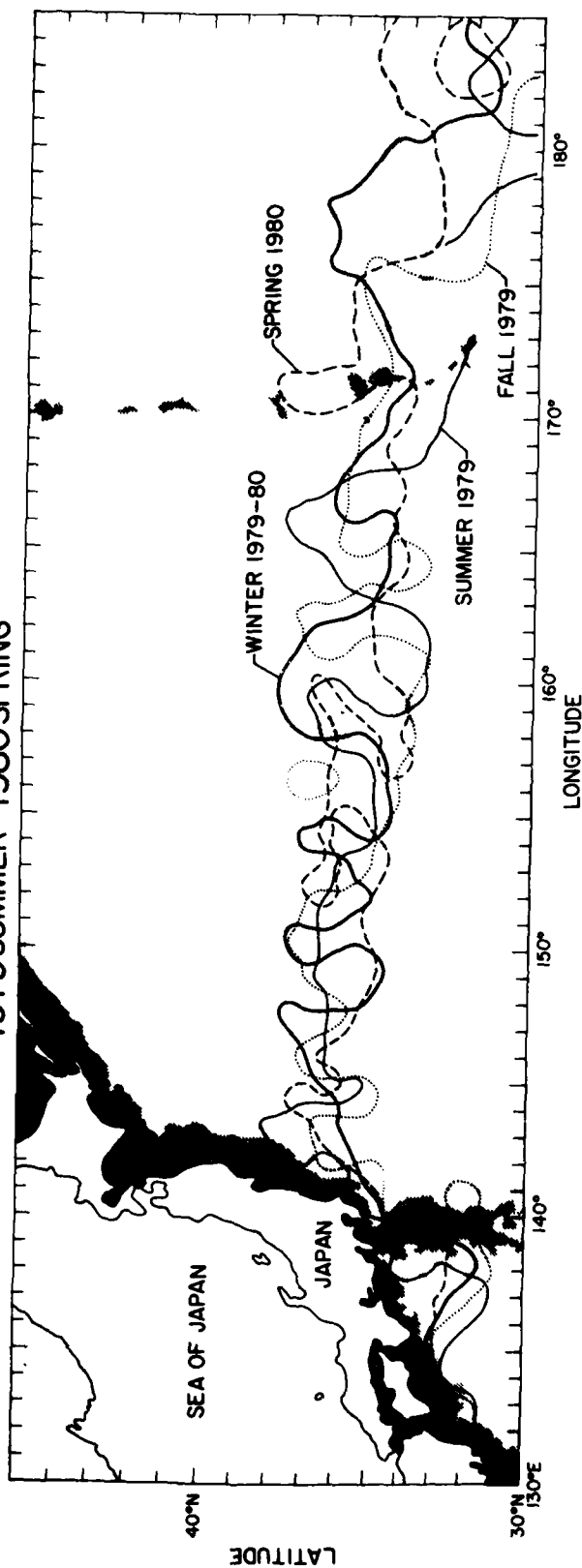
Fig. 6. Composite of the individual seasonal Kuroshio Current paths, from summer 1978 - spring 1979 (top) and from summer 1979 - spring 1980 (bottom). Prominent bottom bathymetric features are displayed (see Fig. 1).

pattern of 1979-1980. This is associated with the Kuroshio meander
changing from a Type A meander to a Type C meander (Nitani, 1969), as
observed in times past. In association with this, the Kuroshio Extension
began to exhibit intense meander and eddy growth, as can be seen.

RING DEVELOPMENT

Kawai (1979) defined cold rings in the North Pacific characteristically as
having water colder than 16°C at a depth of 200 m in the area south of
the Kuroshio Current. Lai and Richardson (1977) identified cold rings in
the North Atlantic characteristically as having greater than a 150-m
upward displacement in the thermocline isotherms. Both these studies
identified rings by the size of their temperature amplitude about the mean
background temperature field. In this study, rings were identified in the
following manner. First, in each individual seasonal map of temperature
at 300 m (Figure 2), rings were identified by a closed contour line of
greater than 0.5°C. Second, only those rings that could be traced
through three successive seasonal maps kept their designation. In this
way, 25 individual rings were defined. The location of these rings in
subsequent discussion is where they were first detected.

Kitano (1975) observed warm rings to move 50-250 km/season in the
northeast direction. Hata (1974) observed one warm ring almost
continuously for 21 months, moving also in the northeast direction at 110
km/season on average. Lai and Richardson (1977) investigated the movement
of the Gulf Stream Rings and obtained a mean speed of 250 km/season.
Therefore, it is expected that rings observed in this study would not
travel more than about 200 km/season (i.e., 2 km/day).

Ring formation is usually a fast process, taking two weeks to one month as
observed by Fuglister and Worthington (1951). But Kawai (1972) showed an
example of ring formation that took place more slowly over a six-month
period. So, the detection of ring formation by individual maps of 300-m
temperature in Figure 2a,b is difficult but not impossible. On the other
hand, the detection of ring movement is much easier due to their
relatively slow speed (i.e., < 2 km/day). The foregoing definition of
rings does not include a census of all rings, but it does allow an
investigation into their tendency, by observing the movement and
distribution of larger, more intense rings which have in the past, at
least, been observed to move slowly enough so that they could be detected
sequentially in the series of maps shown in Figure 2a,b.

The evolution of selected rings, taken from each year, is shown in Figure
7. In the upper panel (Example 1) a cold ring can be seen to have existed
in the same location south of the Kuroshio Current for up to three
seasons, diminishing in intensity abruptly in the last season. In the
second panel (Example 2), a cold ring was generated in Fall of 1977 near
150°W. Subsequently, through the next three seasons, it became detached
and reattached to the Kuroshio Extension repeatedly. In the third panel
(Example 3), a warm ring formed north of the Kuroshio Current, and like
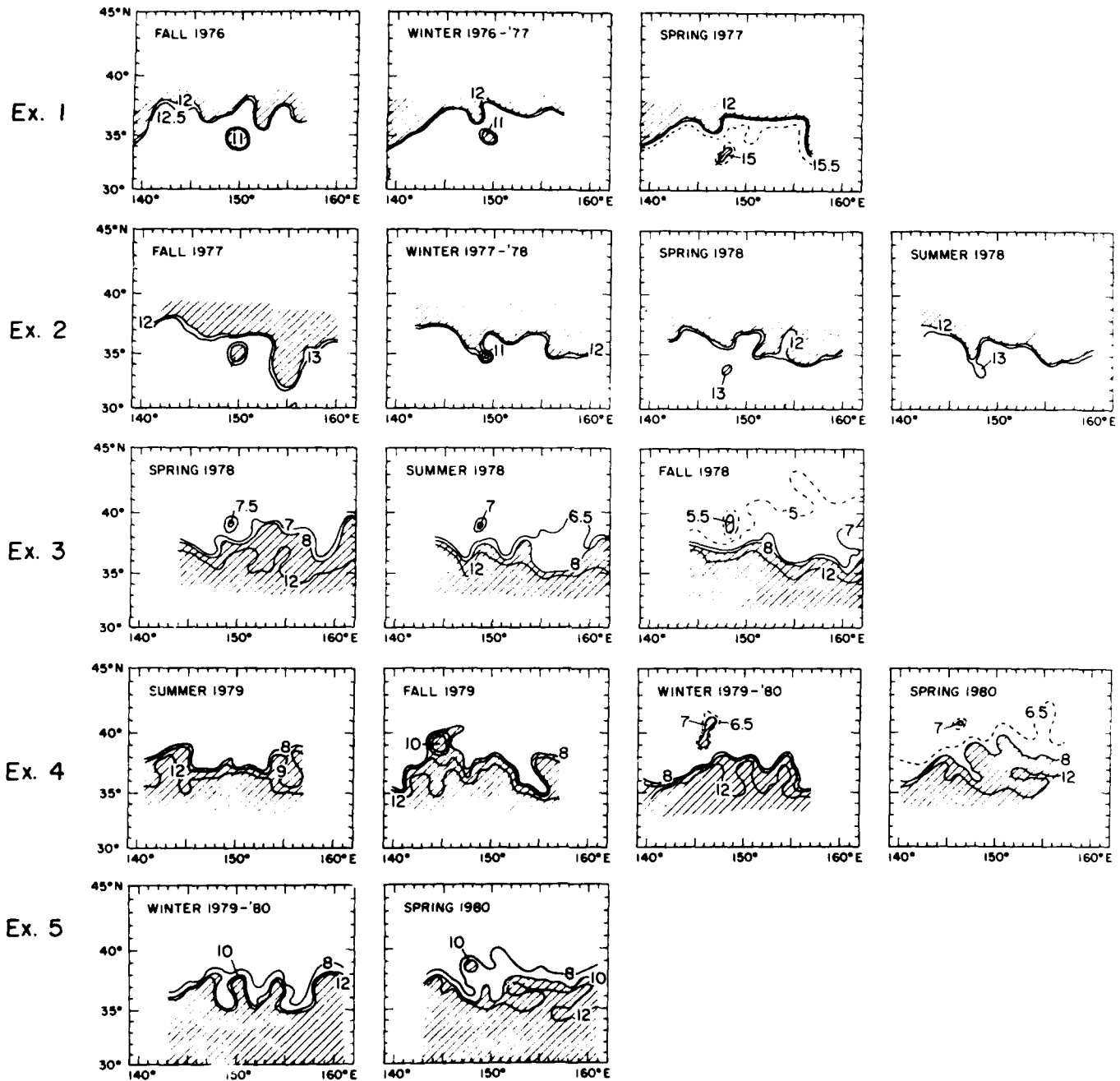
Fig. 7.   Evolution of rings of the Kuroshio Extension.   Five examples show the season-to-
season evolution of a ring found in each year.   In each example, the 12°C isotherm
indicates the Kuroshio Current path.   Shading is present to accentuate ring evolution.

that in the first panel, maintained its integrity in these maps for up to
three seasons. In the fourth panel (Example 4), a warm ring can be seen
to have formed from the season-to-season unstable growth of a meander.
Similarly, this occurred also in the fifth panel (Example 5).

The geographical distribution and the displacement of all 25 individual
rings are shown in Figure 8. Nine cold rings and sixteen warm rings were
observed over the four-year period. The difference in the number of cold
and warm rings may have been due to the sparseness of data south of 34°N
in summer (see Figure 2a,b). The location of maximum ring population
probably coincided with the location of maximum generation. Therefore,
warm rings were generated more uniformly along the Kuroshio Extension from
140°E-170°E, whereas cold ring generation was concentrated between
140°E-150°E. It is difficult to find a clear relation between bottom
bathymetry and the location of ring generation, as was shown by Richardson
(1981) for the North Atlantic. Rings of both types propagated to the west
at an average speed of 1 cm/sec. Cold rings were observed to have moved
consistently southward, at about .6 cm/sec, while warm rings moved
generally northward, at about .4 cm/sec, but less consistently. Some warm
rings even moved south, consistent with the observation of Mizuno and
Akiyama (1980) and with a model by McWilliam and Flierl (1979); such rings
were usually reabsorbed into the Kuroshio Extension and may have existed
in much larger numbers but may have been undetected because of their short
life-span.

When the numbers of both warm and cold rings are considered together as a
function of time (Figure 9), ring activity and generation is found to have
increased substantially from 1976-77 to 1979-80, resulting in a 2-3 fold
increase in ring activity per season over the four-year period. The
increase in ring activity during the first year may have been due to
sampling bias; i.e., relatively poor data coverage in the first year
compared to succeeding years (see Figure 2a,b). The increase in ring
activity during the last year is real and accompanied the regimal change
in the stability of the quasi-stationary meander pattern observed in the
current paths seen in Figures 2a,b and 6.

POLEWARD HEAT FLUX ESTIMATES DUE TO RING MIGRATION

The fact that warm rings tend to have moved poleward, whereas cold rings
tend to have moved equatorward in Figure 8 indicates that a net flux of
heat is being conducted poleward by the meridional movement of rings. The
question is whether this poleward transport of heat is significant in
relation to other processes important to the heat budget of the region.

Heat transport by warm and cold rings is estimated as follows. First, the
300-m temperature anomaly is computed by subtracting the annual mean
temperature from the temperature at the center of each ring in each
season. Second, this 300-m temperature anomaly (T') is multiplied by the
meridional speed of ring ($C'y$), which is considered a perturbation
quantity. Third, the individual products ($T'C'y$) were averaged over all
rings observed in all seasons, yielding the ensemble average ($\overline{T'C'y}$).
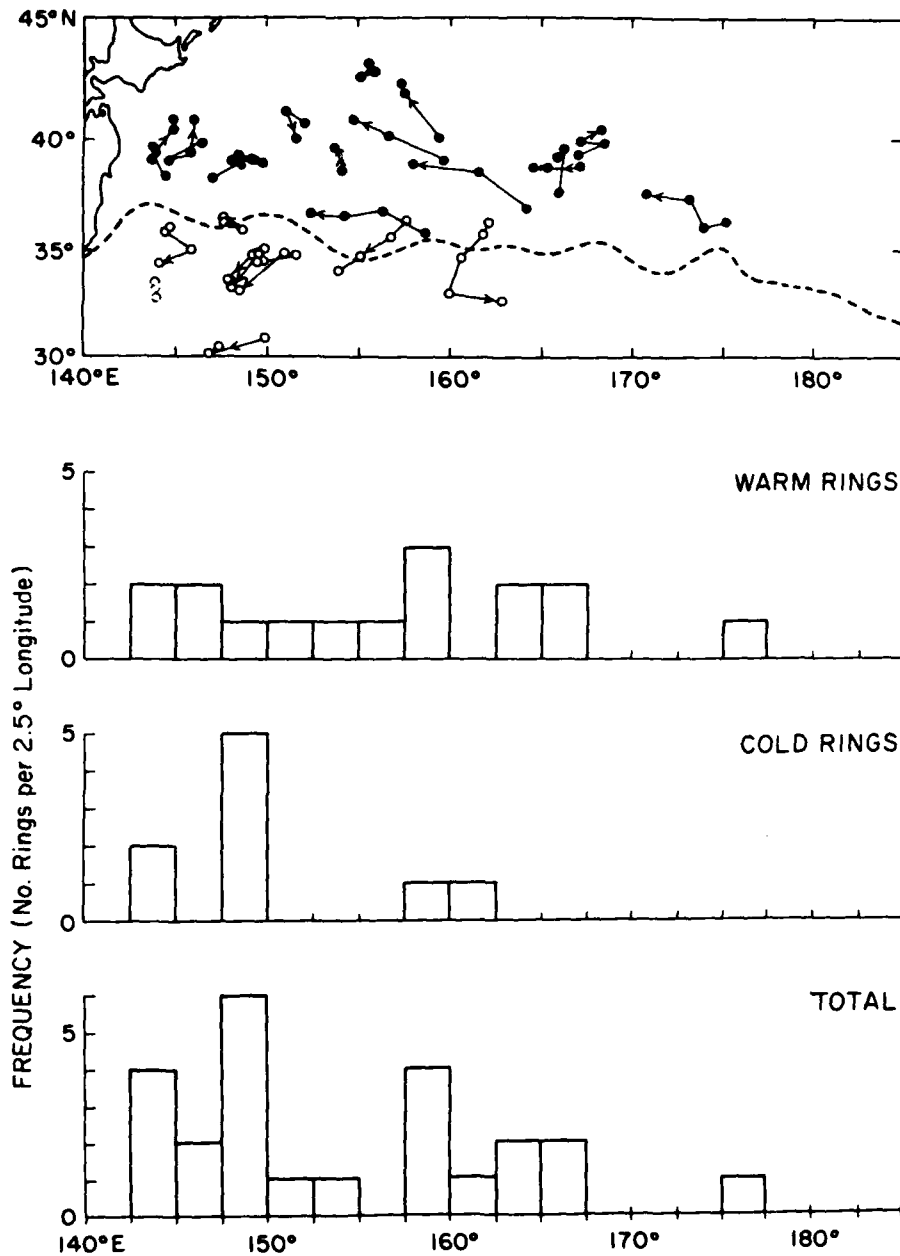
Fig. 8. Distribution and movement of rings. Top: season-to-season
location of the center of rings. Solid circles indicate warm rings;
open circles indicate cold rings. All rings identified during the
entire four-year period are shown together. Dashed line indicates
the mean Kuroshio path.   Bottom: frequency distribution of rings
as a function of longitude. Rings are contoured where first found,
not afterward.
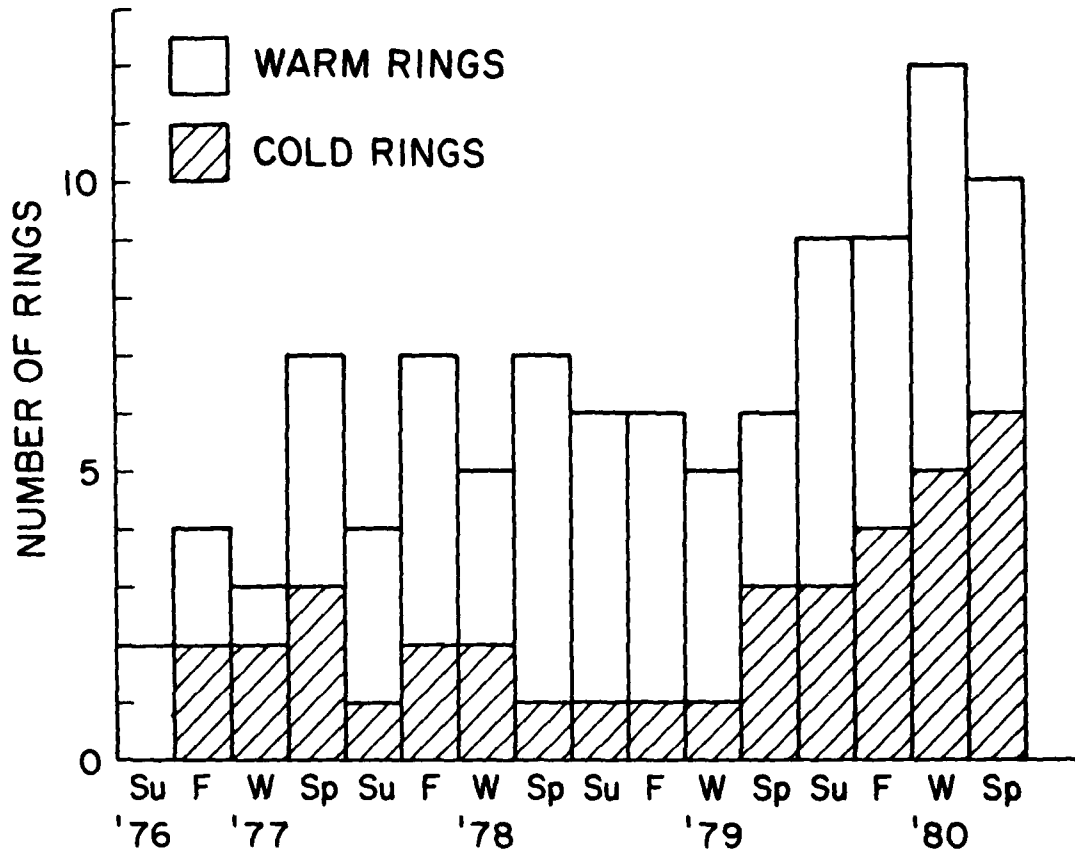
Fig. 9. Frequency distribution of total number of rings as a function of season from 1976 - 1980. The number of cold and warm rings is differentiated by hatched and unhatched regions, respectively.

With this in hand, the total meridional heat transport by rings (Tr) was estimated according to:

$$T_r = \rho C_p \overline{T'c_y'} D L \qquad (7.1)$$

where ρ is density of seawater; Cp is the specific heat of seawater; N is the average number of rings which existed simultaneously; D and L are the depth and zonal diameter of a typical ring, respectively. Some concern must be taken for estimating D and L in (7.1) from consideration of previous works. Hata (1974) observed the diameter and depth of a typical ring located north of the Kuroshio Extension. The diameter of the ring was from 100-200 km, extending to approximately 800-m depth. Tomosada (1978) also tracked two warm rings north of the Kuroshio Extension. These rings had diameters of approximately 200 km and extended to a depth of approximately 700-m depth. Wilson and Dugan (1978) observed cold rings south of the Kuroshio Extension, with diameters 200-300 km, extending deeper than 700-m depth. Kawai (1979) observed cold rings also to be 200-300 km in diameter, extending to approximately 1000 m. Therefore, representative values of 700 m (1000 m) and 200 km (300 km) for the depth and diameter, respectively, of warm (cold) rings are used in (7.1).

On average, two cold rings and four warm rings were found to have existed each season (see Figure 8). The heat transport by cold rings is estimated to have been 4×10^{13}W and that by warm rings 1×10^{3}W. In this estimation, cold rings carried more heat than warm rings despite their fewer numbers, not only because of the greater average intensity in cold rings of anomalous 300-m temperature observed in Figure 2a,b, but because it was assumed that the diameter and depth of cold rings were slightly larger than for warm rings. This latter assumption is based on only a few observations in the literature and may not be true under closer examination. Be this as it may, the total heat transport by observed rings was estimated to have been 5×10^{13}W. This value may have been too small because of underestimation in the total number of the rings, due to poor resolution of the observation network. Moreover, on the basis of numbers of rings alone (Figure 9), the value was surely less during the early portion of the period (by 25%) and greater during the later part of the period (by 25%). Still, this estimated average value (i.e., 5×10^{13}W) of the meridional heat transport is nearly an order of magnitude smaller than that (i.e., 3×10^{14}W) computed from the zonal tilt in the vertical orientation of the mesoscale eddy field by Bernstein and White (1982); the latter explained about 20% of total ocean meridional heat transport at 35°N over the entire Northern Hemisphere.

WAVE PROPAGATION

Bernstein and White (1981) observed mesoscale anomalies of 300-m temperature to have propagated westward near the vicinity (i.e., 33°-39°N) of the Kuroshio Extension. In our study, an analysis to

determine westward propagation is similarly conducted, but with a
four-year time sequence (1976-80), rather than two years (1976-78).
Anomalous 300-m temperature was calculated by subtracting the long-term,
seasonal, mean temperature from each individual seasonal value.
Time/longitude matrices of anomalous 300-m temperature are shown in Figure
10 from 30°N-44°N. In these matrices, a somewhat different result can
be seen in terms of westward propagation as compared with the study by
Bernstein and White (1981); i.e., eastward propagation seems to have
existed in the region adjacent to Japan eastward to 155°E.

To account for the possibility of oppositely directed propagation in the
regions east and west of 155°E, autocorrelation matrices were computed
(not shown) for each latitude in both eastern and western subregions. A
least squares estimation of possible traveling waves was then conducted.
At each point in the $(\Delta x, \Delta t)$ correlation matrix, the following difference
is made.

$$c(\Delta x, \Delta t) - A \cos\left(\frac{2\pi \Delta x}{L} - \frac{2\pi \Delta t}{T}\right) e^{-\frac{|\Delta x|}{L_e}} e^{-\frac{\Delta t}{T_e}} = \epsilon \quad (8.1)$$

Here C is the correlation, A is a constant amplitude, T is a constant wave
period, L is a constant wavelength, Le is the e-folding distance scale, Te
is the e-folding time scale, and ϵ is the difference. Parameters (A, L,
T, Le, Te) were computed so as to minimize the sum of squares of the
differences over the entire correlation matrix. This procedure was
conducted over correlation matrices from 32°-42°N for both eastern and
western subregions.

The estimated zonal wave speed (L/T) at each latitude for each subregion
was plotted in Figure 11, together with observed zonal wave speed computed
by Bernstein and White (1981) and the theoretical linear baroclinic long
wave speed. The theoretical linear wave speed is estimated as follows:

$$C_{\rho x} = -\frac{\beta g' H}{f^2} \quad (8.2)$$

where g' is reduced gravity, H is thickness of the upper layer of a
two-layer ocean model, f is the Coriolis parameter, and β is the
meridional derivative of f. The theoretical curve acts here as a
reference and is similar to that used by Bernstein and White (1981).

In the western subregion, at all latitudes, the waves that fit best, in a
least squares sense, with the correlation information are found to have
propagated eastward at 0.4-1.4 cm/sec. The portion of interannual
variance explained by these waves was, on average, 20%. In the eastern
subregion, wave propagation is found to have been westward over the entire
region, -1 to -2 cm/sec, nearly constant with latitude. This direction of
wave propagation was consistent with Bernstein and White (1981) but the
magnitude was not. Bernstein and White (1981) found consistently higher
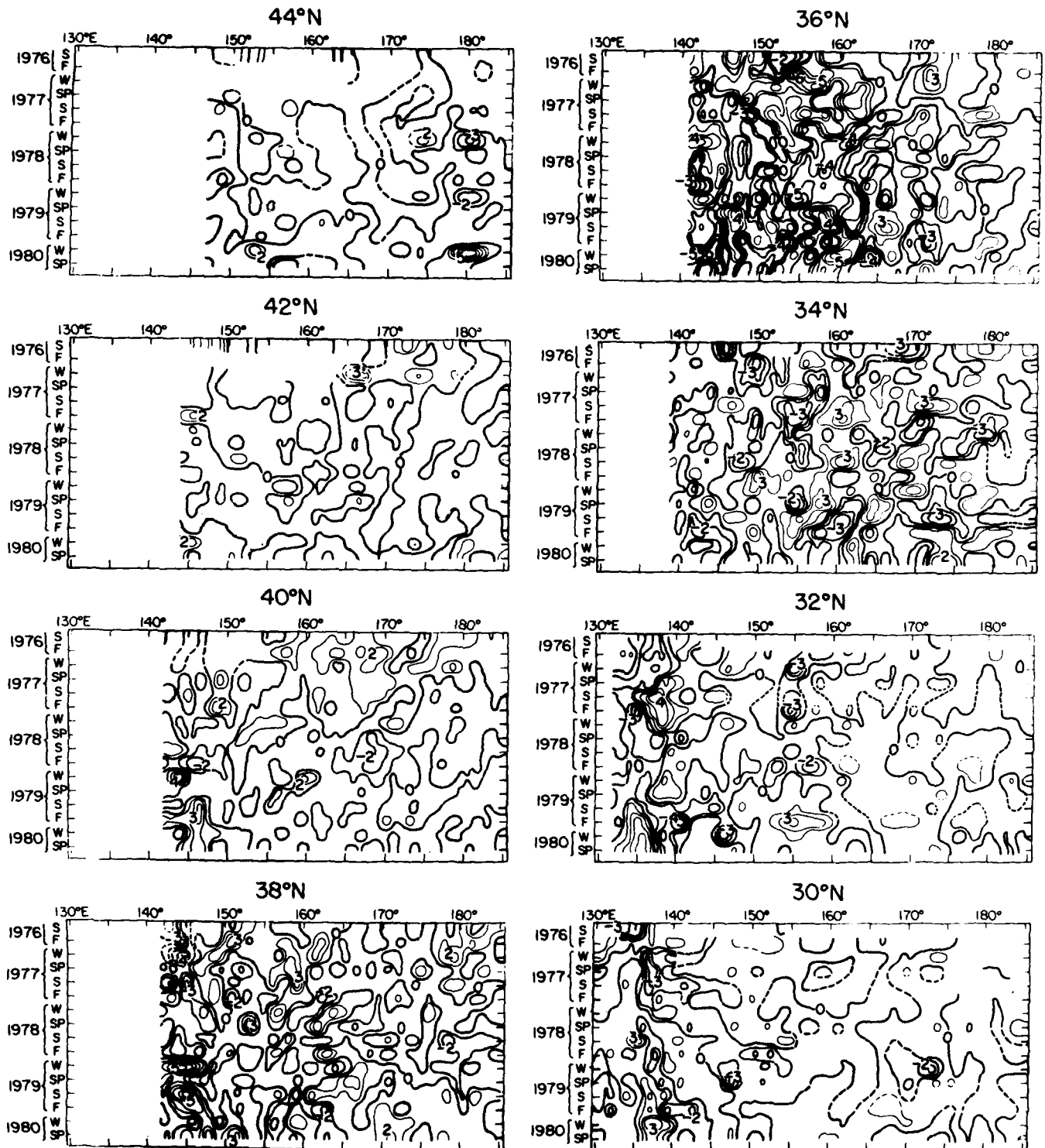
Fig. 10. Time-longitude matrices of anomalous 300-m temperature (°C) every 2° latitude from 30°N to 44°N. Contours are 1°C interval. Regions of negative anomalies are shaded.
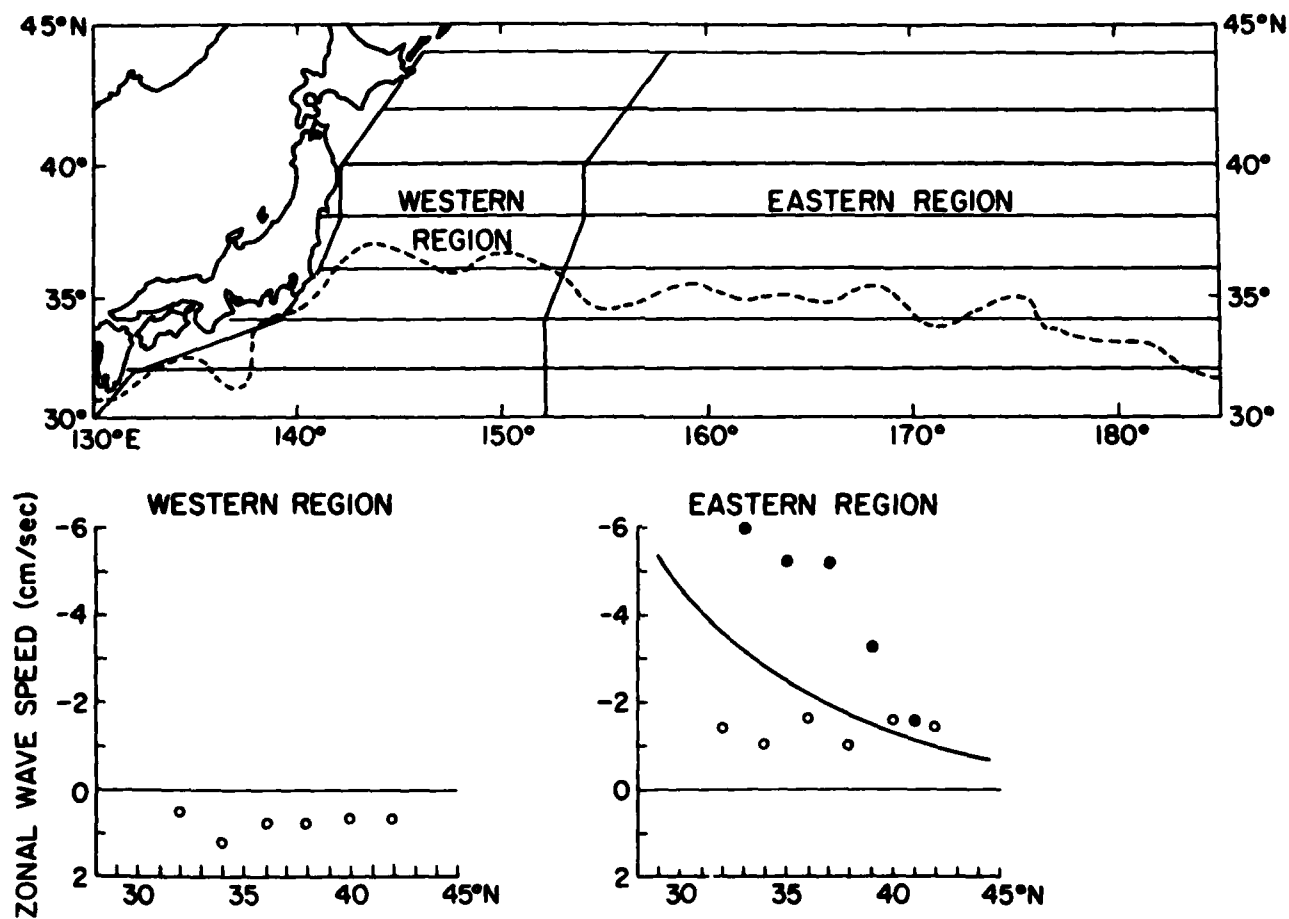
Fig. 11. Top: the direction of wave propagation is opposite, east and west of 155°E. Along each 2° latitude from 32°N to 42°N, the speed of wave propagation is estimated by the use of least squares estimation (LSE) analysis. Bottom: plot of zonal wave speed versus latitude. Open circles are zonal speed estimated from LSE analysis. Solid circles indicate speeds estimated by Bernstein and White (1981). Solid curve indicates linear baroclinic long wave speed. See text for further details.

values of westw i flow decreasing with latitude, as can be seen in Figure 11. The portion of interannual variance explained by these westward traveling waves in the present study was, on average, 30%.

SUMMARY AND CONCLUSION

In order to investigate annual and interannual variability over the entire Kuroshio Current System east of 130°E, 300-m temperature maps were constructed seasonally over the region 130°E-175°W, 30°N-45°N, from summer 1976 through spring 1980, using TRANSPAC XBT data and JODC temperature/depth data.

The results of this study are as follows:

1. In the mean Kuroshio Current System, a quasi-stationary meander pattern occurred, consisting of the Kuroshio Meander in the region south of Japan, lee-wave meanders at 144°E and 150°E in the Kuroshio Extension east of Japan, and a meander in the Kuroshio Extension over the Shatsky Rise near 160°E. East of there, the current bifurcated at 37°N, 163°E; a secondary branch extended north and eastward along 40°N and the main branch continued eastward along 36°N. This main branch is observed to have diverged at the Emperor Seamounts. Secondary maxima in RMS differences were observed in the regions of the Kuroshio Meander and of the quasi-stationary meanders in the Kuroshio Extension. In addition, a secondary maximum in RMS differences was located near the mean path of the Kuroshio Extension at the Emperor Seamounts.

2. The Kuroshio Current System displayed seasonal variability. The wavelength of two meanders at 144°E and 150°E in the Kuroshio Extension adjacent to the east coast of Japan became progressively larger from summer to winter, almost disappearing in spring, coincidentally, when the Kuroshio Meander became weak. Interannual RMS differences changed seasonally over the entire Kuroshio Extension, maximum in fall/winter and minimum in spring/summer.

3. A composite of the Kuroshio paths indicated standing mode variability, with nodes (locations of minimum path displacement) located at 32°N, 132°E south of Kyushu; at 34°N, 140°E on the Izu Ridge, and at three points (37°N, 149°E; 36°N, 152°E; 35°N, 164°E) in the Kuroshio Extension. Anti-nodes (locations of maximum path displacement) existed between these nodes. Paths near 155°E followed one of two tracks: a northern one (near 37°N) during the first two years and a southern one (near 34°N) during the last two years. When the amplitude of the Kuroshio Meander weakened in 1979/80, the path of the Kuroshio Extension became much more unstable than earlier, appearing to enter a different kind of stability regime with regard to the quasi-stationary meander pattern in the Kuroshio Current System.

4. The movement of cold and warm rings was westward and generally away from the Kuroshio Extension. The overall average rate of meridional

displacement was approximately 0.4-0.6 cm/sec, with a westward
displacement of approximately 1 cm/sec. Ring formation became intense in
1979-80, consistent with the development of an unstable meander pattern in
the Kuroshio Extension. Northward heat transport by these rings is
computed to have been 5×10^{13}W, which was nearly an order smaller than
the eddy transport of heat in the Kuroshio Extension computed by Bernstein
and White (1982).

5. Least squares estimation (LSE) analysis shows that in the region west
of 155°E waves occurred, propagating eastward with speeds of 0.5-1.5
cm/sec at all latitudes from 32°N-42°N. These waves accounted for
approximtely 20% of the interannual variance observed over the four-year
period. In the region east of 155°E waves occurred, propagating
westward with speeds of -1 to -2 cm/sec. These waves accounted for
approximately 30% of the interannual variance observed over the four-year
period.

ACKNOWLEDGEMENTS

APPENDIX

According to linear theory (e.g., White, 1971) the wavelength of a
stationary Rossby lee-wave in uniform eastward flow is

$$L = 2\pi \left(\frac{U_o}{\beta}\right)^{1/2}$$ (A1)

where L is the wavelength, Uo is the mean eastward current speed, and β
is the meridional derivative of the Coriolis parameter (1.9 x
$10^{-13} sec^{-1}$ at 36°N). White and McCreary (1976) showed that this
relationship is an adequate approximation for stationary lee-waves in an
eastward jet like the Kuroshio Extension. Therefore, using the value of
Uo computed by Nishida and White (1982) for the Kuroshio Extension east of
Japan (i.e., approx. 20 cm/sec), L is calculated to be approximately 600
km. This wavelength matches the mean distance from the meander at 144°E
and that at 150°E, shown in Figure 3. Therefore, the two meanders at
144°E and 150°E east of Japan in the Kuroshio Extension have a
wavelength that is consistent with Rossby lee-wave theory.

REFERENCES

Bernstein, R.L. and W.B. White, 1977. Zonal variability in the distribution of eddy energy in the mid-latitude North Pacific Ocean. Journal of Physical Oceanography, 7, 123-126.

Bernstein, R.L. and W.B. White, 1981. Stationary and traveling mesoscale perturbations in the Kuroshio Extension current. Journal of Physical Oceanography, 11, 692-704.

Bernstein, R.L. and W.B. White, 1982. Meridional eddy heat flux in the Kuroshio Extension current. Journal of Physical Oceanography, 12, 154-159.

Chao, S., and J.P. McCreary, 1982. A numerical study of the Kuroshio south of Japan. Journal of Physical Oceanography, 12, 679-693.

Chase, T.F., and H.W. Menard, 1973. Bathymetric atlas of the North Pacific Ocean. Publication No. 1301-2-3, U.S. Naval Oceanographic Office, Washington, D.C., 172 pp.

Fuglister, F.C., and L.V. Worthington, 1951. Some results of a multiple ship survey of the Gulf Stream. Tellus, 3, 1-14.

Hata, K., 1974. Behavior of a warm eddy detached from the Kuroshio. Journal of Meteorological Research, 7, 295-321.

Kawai, H., 1972. Hydrography of the Kuroshio Extension. Kuroshio, Its Physical Aspects, H. Stommel and K. Yoshida, Editors, University of Tokyo Press, 235-352.

Kawai, H., 1979. Rings south of the Kuroshio and their possible roles in transport of the intermediate salinity minimum and in formation of the skipjack and albacore fishing ground. Kuroshio IV. Proceedings of the fourth CSK Symposium, Tokyo, 250-273.

Kitano, K., 1975. Some properties of the warm eddies generated in the confluence zone of the Kuroshio and Oyashio Current. Journal of Physical Oceanography, 5, 670-683.

Lai, D.Y., and P.L. Richardson, 1977. Distribution and movement of Gulf Stream Rings. Journal of Physical Oceanography, 7, 670-683.

Levine, E.R., and W.B. White, 1983. Bathymetric influence upon the character of the North Pacific Current, 1976-1980. Journal of Geophysical Research, 88(C14), 9617.

McWilliams, J.C., and G.R. Flierl, 1979. On the evolution of isolated, non-linear vortices. Journal of Physical Oceanography, 9, 1155-1182.

310

Mizuno, K., and M. Akiyama, 1980. Hydrographic study of the Tohoku area using satellite IR imagery. Sora to Umi, 2, 47-55.

Nishida, H., and W.B. White, 1982. Horizontal eddy fluxes of momentum and kinetic energy in the near-surface of the Kuroshio Extension. Journal of Physical Oceanography, 12, 160-170.

Nitani, H., 1969. On the variation of the Kuroshio in recent several years. Bulletin of the Japanese Society of Fisheries and Oceanography, 14, 13-18.

Richardson, P.L., 1981. Gulf stream trajectories measured with free-drifting buoys. Journal of Physical Oceanography, 11, 999-1010.

Robinson, A.R. and B.A. Taft, 1972. A numerical experiment for the path of the Kuroshio. Journal of Marine Research, 30,65-101.

Sampson, R.J., 1973. User's manual for the Surface II Graphics System. Kansas Geological Survey, University of Kansas, 144 pp.

Shoji, D., 1972. Time variation of the Kuroshio south of Japan. Kuroshio, Its Physical Aspects, H. Stommel and K. Yoshida, Editors, University of Tokyo Press, 217-234.

Taft, B.A., 1972. Characteristics of the flow of the Kuroshio south of Japan. Kuroshio, Its Physical Aspects, H. Stommel and K. Yoshida, Editors, University of Tokyo Press, 165-216.

Taft, B.A., 1978. Structure of the Kuroshio south of Japan. Journal of Marine Research, 36, 77-117.

Tomosada, A., 1978. A large warm eddy detached from Kuroshio east of Japan. Bulletin of the Tokai Regional Laboratory, 94, 59-103.

White, W.B., 1971. A Rossby wave due to an island in an eastward current. Journal of Physical Oceanography, 1, 161-168.

White, W.B. and R.L. Bernstein, 1979. Design of an oceanographic network in the mid-latitude North Pacific. Journal of Physical Oceanography, 9, 592-606.

White, W.B. and J.P. McCreary, 1976. On the formation of the Kuroshio Meander and its relationship to the large-scale ocean circulation. Deep-Sea Research, 23, 33-47.

Wilson, W.S. and J.P. Kugan, 1978. Mesoscale thermal variability in the vicinity of the Kuroshio Extension. Journal of Physical Oceanography, 8, 537-540.

Wyrtki, K., 1975. Fluctuations of the dynamic topography in the Pacific Ocean, Journal of Physical Oceanograhy, 5, 450-459.

EDDY HEAT FLUX IN THE NORTH PACIFIC

Andrew Bennett

Institute of Ocean Sciences, Patricia Bay,
Sidney, British Columbia, Canada, V8L 4B2

ABSTRACT

Estimates of meridonal heat flux in the North Pacific are reviewed. The
1976-1980 TRANSPAC XBT data is used to estimate transient and standing
eddy heat fluxes above 400 dbar. The latter is marginally significant,
due to an offshore meander in the Kuroshio path.

INTRODUCTION

The only published direct estimate of meridonal heat flux in the North
Pacific is that of Bryan (1962), based on a NORPAC trans-Pacific section
along 32°N taken in August 1955. Bryan's estimate was -0.94 PW[*],
that is, a southward heat flux of magnitude comparable with atmospheric
meridional heat fluxes.

This result was surprising since the sign of the flux was opposite to
that inferred from surface heat budget studies. However, Bryan pointed
out that both estimates were suspect. The hydrographic stations in the
NORPAC section were mostly shallower than 2000 m, and had to be
supplemented with deep data from other sources. The surface budget
estimate was dubious since it was the difference between two much larger
terms.

In spite of the above-mentioned shortcoming of the hydrographic data, it
is instructive to examine the direct flux estimate in greater deatall.
It may be decomposed into five additive components: the flux through the
Sea of Japan (F_0 = +0.18 PW), the barotropic flux due to the
depth-averaged circulation and the depth-averaged heat content
(F_1 = + 0.04 PW), the large-scale baroclinic flux due to the meridi-
onally averaged circulation and heat content (F_2 = - 1.35 PW), the
small-scale baroclinic flux due to zonal fluctuations in the baroclinic

---

[*]1 PW = 10^{15}WATT

circulation and heat content (F_3 = + 0.11 PW), and finally the Ekman
or mixed-layer flux due to the wind-stress induced surface circulation
and heat content (F4 = + 0.08 PW).

The Sea of Japan Flux

Bryan estimated F_0 assuming a volume flux of 3-6 Sv[*]through the
Tsushima Straits, at a temperature 10°C warmer than the trans-Pacific
section average. Hasanuma (pers. comm.) reported contemporary data
indicating a slightly smaller volume transport (2-3 Sv), so Bryan's
estimate of F_0 should be revised downward to about + 0.10 PW.

The barotropic flux

Bryan estimated the barotropic transport using the Sverdrup integrated
vorticity balance, and wind-stress curl data due to Hikada (1958). These
all-ocean zonal mean data agree with the same statistics for the more
extensive data of Hellerman (1967) and are comparable with the detailed,
very extensive data of Kutsuwada (1982). This last data set leads to a
Sverdrup transport of - 40 Sv at 30°N (and hence a Kuroshio transport
of + 38 Sv at the same latitude). Taft (1972) estimated the Kuroshio
transport relative to 800 dbar to be about 40 Sv.

The point of all this is that the depth-averaged temperature of the
Kuroshio current in Bryan's section must have been only 0.5°C warmer
than the section average, since the heat flux F_1 was so small. This is
surprising since the Kuroshio crosses 32°N on a path over the contin-
ental slope near Cape Shionomisaki, where the depth is between 1000 and
2000 m. The depth-averaged temperature in such shallow water is at least
5°-10°C warmer than the section average. An explanation of this
disagreement may be found by inspecting the actual cruise track in the
NORPAC Atlas (NORPAC Committee, 1960): the section began at 35°N on the
east side, went south west to 32°N, proceeded due west to 143°W, then
went north west ending on the Japanese continental shelf at 35°N. Thus
the Kuroshio actually crossed the section near Cape Inobuzaki, on a path
in water between 4000 and 5000 m deep. It would not, in fact, be
surprising if the depth-averaged temperature on the path were <u>less</u> than
the section average, since the water column on the path was as deep as
the mid-ocean, and included relatively <u>cooler</u> Kuroshio waters
above 1000 m.

---

[*]1 Sv = 10^6 m^{3}s^{-1}

The large-scale baroclinic flux

This flux component depends on the meridionally averaged vertical temperature profile (which is a very stable statistic) and, by virtue of the thermal wind relation, only the dynamic heights at the ends of the section, at each depth. As already mentioned, both ends were actually at $35^\circ N$. The flux is clearly sensitive to conditions at the ends of the section, but at each depth the sign of the dynamic height difference is the same as the sign of the slope of a straight-line fit through the entire section. It may be noted that similar strong equatorward "Ferrel cell" circulations have been inferred from several sections in other oceans (Jung, 1952; Bennett, 1978; Bryden and Hall, 1980).

The small-scale baroclinic flux

It is conventional wisdom now to assume that estimates of this flux component made with standard hydrographic data are of no value since the mid-ocean synoptic scale eddy field is not resolved. The widely spaced stations record an apparent white noise field. Estimates of the sampling fluctuations, in this flux component, based on plausible values for energy RMS*velocities, indicate that quite large values for F_2 should be expected (Bennett, 1978). In fact, relative small values such as Bryan's + 0.11 PW are usually obtained (Bennett, 1978). One is led to conclude that the plausible values for the eddy intensities are, on average, rather excessive.

The Ekman flux

An examination of the modern wind data mentioned earlier indicates that Bryan's estimate of $F4 = + 0.08$ PW (in the North Pacific at $32^\circ N$ in August) is too large and its sign is in doubt.

Heat flux estimates based on atmospheric data

Indirect estimates of oceanic heat flux in the N Pacific around $30^\circ N$ vary greatly. Wyrtki (1965) and Hastenrath (1980) made surface budget calculations, yielding - 1.2 PW and + 1.1 PW, respectively. Oort (1980) and Burridge (unpublished) used planetary radiation data and atmospheric heat flux estimates based on (upper level) winds to arrive at +1.2 PW and -0.6 PW, respectively. Both methods have inherent difficulties and all investigators reported particular problems with their calculations.

---

*$v_{RMS} = 0.1$ ms^{-1}, with a length scale of 50 km.

Summary

Bryan's estimate of heat flux in the N Pacific at 32°N is dominated by a southward large-scale baroclinic flux. Its value is in error by at least some 3% or 0.04 PW due to the use of potential temperature and a mean specific heat in order to calculate potential enthalpy. Thus the values of the other flux components, which had been overestimated anyway, are individually insignificant. The estimate should be associated with 35°N, not 32°N.

The confusion amongst the indirect estimates gives no help in assessing the validity of Bryan's estimate. It may be a (roughly) correct estimate of the mean, or a (roughly) correct estimate of the flux in August 1955, or neither of these. That is, there may be significant seasonality in the heat flux, or broad band variability due to the unresolved eddy field.

EDDY HEAT FLUX

An attempt to shed some light on the eddy heat flux will be described here. A direct estimate of eddy heat flux was made using XBT data, obtained by the TRANSPAC observation program, and graciously made available to me by Dr. Warren White. The data had been interpolated onto a three-dimensional grid. The seven depths were 0 m, 50 m, 100 m, 150 m, 200 m, 300 m, and 400 m. The longitude range was 130°E to 120°W in 221 steps of 0.5°; the latitude range was 30°N to 50°N in 41 steps also of 0.5°. The half-degree spacing corresponds to about 50 km; the interpolation routine which produced the gridded data smoothed out scales below 200-300 km prior to sampling on the grid. The interior deformation radius in the mid-latitude N Pacific is about 40 km (Emery et al., 1982) corresponding to a wavelength of about 250 km. Thus synoptic scale eddies were not properly resolved by the XBT data. However, significant energy, and more importantly for heat flux, phase tilts in the vertical, have been found at wavelengths of 500 km (Bernstein and White, 1982). Hydrographic stations show that the significant phase tilts are found only in the upper 400 m, within the depth range of XBT casts (White, pers. comm.). Moreover, the gridded data were available in 24 bi-monthly average sets from June/July 1976 to April/May 1980, thus four well-resolved temporal cycles of the 500 km-wavelength eddies could be resolved, since such eddies have periods of about 1 year (White, 1982). In short, the TRANSPAC data set should shed light on the heat flux evidently associated with spatial and temporal fluctuations somewhat larger than the synoptic scale.

Computational method

Dynamic heights were calculated from the temperature data using the
climatological temperature-salinity look-up tables of Emery and Dewar
(1982). Meridional velocities relative to 400 dbar were calculated using
the thermal wind relation. The temporal and zonal correlations between
velocity and temperature were then calculated in the usual way (Lorenz,
1967) and integrated vertically from 400 to 0 dbar. Two eddy heat fluxes
were so derived. The first, the standing eddy heat flux (SEHF), is due
to zonal correlation between zonal fluctuations in the temporal mean
fields. The second, the transient eddy heat flux (TEHF), is due to zonal
and temporal correlations between zonal and temporal fluctuations in the
field.

Results

The two fluxes are graphed as functions of longitude in Figure 1. It is
clear that the transient eddy heat flux is negligible, being less than
0.02 PW in magnitude at all latitudes. The standing eddy heat flux
achieves marginally significant levels (+0.2 PW) at about 33°-34°N,
and is negligible elsewhere save possibly around 47°N (0.1 PW) where
the paucity of the raw XBT data casts doubt on the results. Inspection of
the zonal distribution of SEHF (not shown here) shows that by far the
dominant contribution at 33°-34°N is associated with a standing eddy
or steady meander in the Kuroshio path. The bimodality of the path
through the Shikoku basin is well documented (Taft, 1972). It may be
noted that in August 1955 the path was also in the offshore, meandering
mode (Shoji, 1972). As already mentioned the NORPAC section did not
cross the path in the Shikoku Basin so the meander could not have
contributed to Bryan's F_2 and F_3. The appreciable values of SEHF at
35°-36°N (+0.1 PW) are associated with further meandering in the
Kuroshio extension region. The fields of SEHF also show clearly the
influence of the Emperor Seamount chain. It should be emphasized that the
value of +0.2 PW for SEHF at 33°-34°N is tentative for two reasons.
First, there may be appreciable heat flux below 400 dbar in the Kuroshio
region, as opposed to the mid-ocean. Second, in light of the
predominance of the Shikoku Basin, the calculations need repeating with
more refined treatment of the coastal geometry and choice of look-up
table in the dynamic height calculation. However, it seems doubtful that
SEHF actually exceeds +0.5 PW at 33° -34°N, with smaller values at
35°N, and must be much less when the Kuroshio path is on-shore.

CONCLUSION

Of all the fluxes at all the scales which have been resolved so far, the
equatorward large-scale baroclinic flux is considerably the largest at
35°N. It should be possible to monitor at least the variability of
this flux component with hydrographic stations at only the ends of the
section.
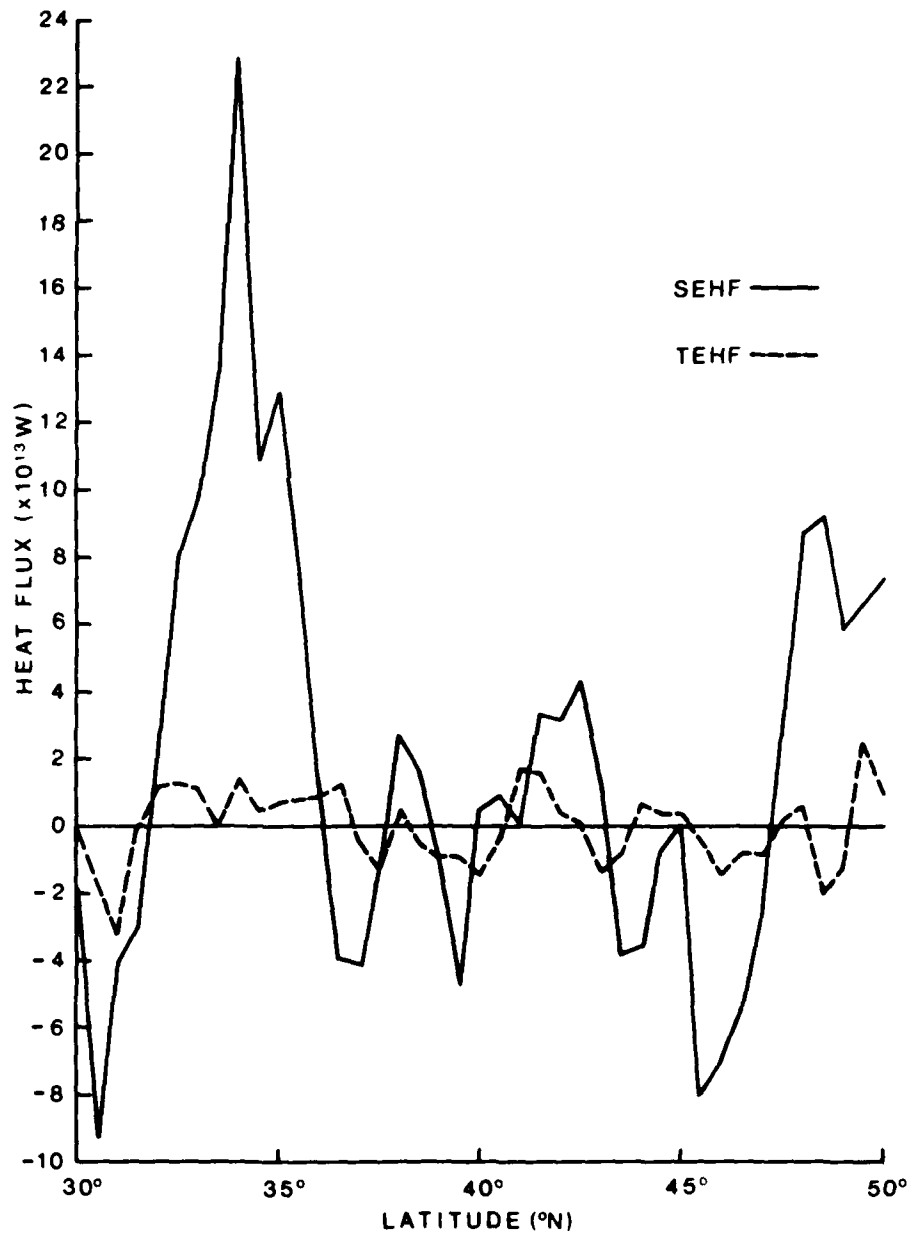
Fig. 1. Transient Eddy Heat Flux (TEHF) and Standing Eddy Heat Flux (SEHF) above 400 dbar in the North Pacific, versus latitude.

REFERENCES

Bennett, A. F., 1978. Poleward heat fluxes in Southern Hemisphere Oceans. Journal of Physical Oceanography, v. 8, p. 785-798.

Bernstein, R. L. and W. B. White, 1982. Meridional eddy heat flux in the Kuroshio Extension Current. Journal of Physical Oceanography, v. 12, p. 154-159.

Bryan, K., 1962. Measurements of meridional heat transports by ocean currents. Journal of Geophysical Research, v. 67, p. 3403-3414.

Bryden, H. L. and M. M. Hall, 1980. Heat transports by currents across 25°N latitude in the Atlantic Ocean. Science, v. 207, p. 884 886.

Emery, W. J. and J. S. Dewar, 1982. Mean temperature-salinity, salinity-depth and temperature-depth curves for the North Atlantic and the North Pacific. Progress in Oceanography, v. 11, p. 219-305.

Emery, W. J., W. G. Lee and L. Magaard, 1982. Geographic distribution of density, Brunt-Väisälä frequency and Rossby radii in the North Atlantic and North Pacific. (Unpublished report.)

Hastenrath, S., 1980. Heat budget of tropical ocean and atmosphere. Journal of Physical Oceanography, v. 10, p. 159-170.

Hellerman, S., 1967. An updated estimate of the wind stress over the world ocean. Monthly Weather Review, v. 95, p. 607-626; corrigendum, vol. 96, p. 62-74.

Hidaka, K., 1958. Computations of the wind-stress over the oceans. Geophysical Notes, Tokyo University, v. 11(1), 77-123.

Jung, G. H., 1952. Note on the meridional transport of heat by the oceans. Journal of Marine Research, v. 11, p. 139-146.

Kutsuwada, K., 1982. New computation of the wind stress over the North Pacific Ocean. Journal of the Oceanographical Society of Japan, v. 88, p. 159-171.

Lorenz, E. N., 1967. The Nature and Theory of the General Circulation of the Atmosphere. W.M.O., Geneva.

318

NORPAC Committee, 1960. Oceanic observations of the Pacific, The NORPAC Atlas. University of California Press and University of Tokyo Press, Berkeley and Tokyo.

Oort, A. H., 1981. Atmospheric circulation statistics, 1958-1973. NOAA Professional Paper.

Shoji, D., 1972. Time variation of the Kuroshio south of Japan. In: Kuroshio: Physical Aspects of the Japan Current. (See below.)

Taft, B. A., 1972. Characteristics of the flow of the Kuroshio south of Japan. In Kuroshio: Physical Aspects of the Japan Current. H. Stommel and K. Yoshida, Eds. University of Washington Press, Seattle and London.

White, W. B., 1982. Travelling wave-like mesoscale perturbations in the North Pacific Current. Journal of Physical Oceanography, v. 12, p. 231-243.

Wyrtki, K., 1965. The average annual heat balance of the North Pacific Ocean and its relation to ocean circulation. Journal of Geophysical Research, v. 70, p. 4547-4559.
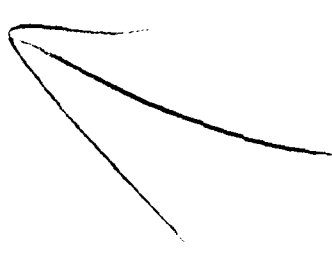
Round Table Discussions

Round Table Discussion Section 1
Lorenz Magaard, Chairman

Magaard: I have prepared a few questions I would like to ask you. I
hope that these will stimulate a discussion, which I will
then influence as little as possible. I will start with
something that I have thought up and then you take over as
you please.

My first question is this: In connection with mesoscale
motions, one often hears about the desire or the necessity
to parameterize the influence of these motions on the
general circulation. So far in this workshop we have heard
remarkably little about that. We have heard about
eddy-resolving models, but I don't think we've heard about
parameterization of the influences of the eddies on the
general circulation. I would have expected that we hear
more about that. I would like to know now, whether I have
an obsolete point of view and whether this problem is no
longer one of the most important problems. Then I would
like to see discussed the problem of where we stand on
these parameterization games, games that usually I've seen
related to the question of closing hydrodynamic equations
at a certain level.

My question is then reformulated: Where do we stand
concerning the parameterization of mesoscale eddies and the
related closure problems? I would like to direct this
question to Rick Salmon first because he has worked a lot
on geostrophic turbulence.

Salmon: I guess the answer would be that the ability now of
computers to resolve the eddies has taken a lot of the
thunder out of that issue. I do know that some work is
going ahead on interaction between eddies and mean flow,
usually based on the idea that there's a scale separation
between the eddies and the mean flow. We know that Greg
Holloway is working on this and there is a man at NCAR, Lin
Ho who's done some work, but I think these [studies] are
still at a quasi-homogeneous state; the mean flow is a
linear variation, usually, and there is assumed to be a
scale separation. It's not really clear whether the theory
that's been done on those, which is already quite
complicated, is the right way to approach things as
complicated as this counter-rotating gyre and so forth.
You might really learn more by just looking at the
eddy-resolving models.

I have a feeling that the turbulence closure business that I've been involved in has really two parts. There are the closure models which apply to disequilibrium phenomena. They are general and you have the faith that they really could close the problem if you wanted them to. But for statistically inhomogeneous situations they are so complicated that they don't seem like they would ever be practical for that purpose. On the other hand, there are little pieces of that theory which might be used, and one of them is this inviscid statistical mechanical equilibrium. I have dealt with that, too. Its virtue is that you can work it out, although with some difficulty, for even complicated situations where you wouldn't dare use these sophisticated closures. That's about all I can say in summary of what I think you mean by geostrophic turbulence and what it might contribute.

Perhaps just direct simulations right now are going to yield as much information as anything, particularly with Bill's [Holland] having considerable success, I would say. What's impressive to me about this meeting is that both Nelson [Hogg] and Jim [McWilliams] and were interpreting data in the light of some of the results of that numerical model and that's the first time that has been done, I think.

Magaard: You said several things I would like to come back to. You said we now have computers that can do the eddy-resolving models. Is that really true to a satisfactory extent and then, if that were true, would these models tell us everything we want to know? And as a third point concerning the applicability of closure models, I would dare to say that that depends a little bit on the closure models also, and the development of closure models might not be obsolete or superfluous. But let's see what the other participants would like to say on these problems.

Do we have computers that can handle eddy-resolving models to an adequate or satisfactory degree?

Robinson: The answer is yes and no. We have computers in which important eddy-resolved questions can be answered. On the other hand, because we do not have sufficient computing power, important questions that can be asked are not being asked. The direction of research itself is influenced by the computer ability. Do you agree with that?

Holland: Yes. I think that's exactly right.

McWilliams: The computer power issue has two sides at least: One is simply that if one were to contemplate global domain eddy-resolving calculation or even contemplate the North Atlantic right now, eddy-resolving calculations of many vertical level equations essentially are exceeding machine capacity. The other aspect is that even a lot of calculations that fit in machines aren't being done because those who own the computers aren't giving enough time to oceanographers. Power has those two aspects.

Robinson: There are two simple examples of problems that require more computer power. The question of topography and geometry and resolution and the qualitative structure of the general circulation, and the question of fluctuating wind forcing are problems which could be addressed and I believe would be addressed if adequate computing power were available. So there is more realistic forcing and geometry and better resolution of the existing type of interesting questions.

The second problem is the mixed thermodynamic and mixed thermohaline and wind-driven circulation of the eddy resolution. Even the GFD simple geometry version has not been done. Those are very important problems which are only two examples of things which can be done. We know how to do it. The intellectual ability is there, and the scientific feasibility is there. They are just not being done, and there are lots of other things that are being done which are not equally important but also very important.

Magaard: Are there any aspects of the eddy-resolving models including the economy that would make us pursue other approaches like the closure attempts, that could potentially make the whole thing cheaper? Or would you consider this basically a dead issue?

Robinson: It's not a dead issue. But one has to address aspects of the problem with the high eddy resolution, and when questions such as eddy mean field interactions have been clarified then one wants to parameterize those for longer time scales and global calculations and other kinds of things and questions. This may not be the right point but I think it would be interesting to ask Jim [McWilliams] and Tom [Rossby] to comment on these recent results on the diffusivity and the LDE and the floats and whether theoreticians should risk the parameterization attempts, a kind of energy level relationship.

Magaard: So that might even lead to the idea of no longer calling
these things "turbulence". That's of course an independent
issue, but at least it loses some of the characteristics of
turbulence studies, namely that we don't look at individual
fluctuations. Eddy-resolving models look at individual
fluctuations, don't they?

Rhines: In this subject area I think it helps a great deal to
imagine that parameterization is not a general procedure of
defining roles to write into a machine code which will give
you the correct mean fields but rather that it is a series
of very special dynamical questions; I don't think there's
any hope of a general formulation of eddy dynamics which
will apply to the entire domain of the oceans or
atmosphere. But it seems to me that in various special
areas progress certainly has been made and is possible and
this comes from asking very special questions about the
wind gyre. We (Bill [Holland] and I) have been pushing an
idea of a parameterization of eddies which suggests that
certain domains of the fluid are homogenized through the
spectral potential vorticity and tracers, and that's going
to be replaced eventually by something better, probably.
It's not an idea that applies everywhere; it can get you
into very wrong answers if you say it happens everywhere in
the ocean. I think the reason that it hasn't been done
very much before is that people would say that mixing by
eddies should uniformize tracers, perhaps, but they
wouldn't say where. And so it is defining the boundaries
of parameterization which helps make it work. Other areas
where parameterization from process models has begun to
interface with data involve things like the momentum and
vorticity fluxes in unstable jets (which were looked at by
Jim [McWilliams] and others in channel idealizations and
they do seem to carry over to the ocean). The vertical
structure of the energy level in eddies seems to accord
roughly with the models. So these are very special
questions and it means not saying, "Please give me a
general formula for momentum and vorticity flux."

Magaard: So as was known before and as is becoming increasingly
clear, an attempt to parameterize the influence of eddies
has to be process-oriented.

Rhines: Yes, exactly.

McWilliams: And I think it's fair to say that what many of us have been
doing for a long time is following the inherently

circuitous route to a parameterization. I want to be able
to distill, in simple particular situations, some useful
simple summary statements of what exactly the eddies do in
the dynamics of the flow field. We are, I think, years away
from having explicit right-hand-side mathematical
expressions, because we still are restricted to being able
to make essentially qualitative summaries of particular
calculations. Likely we will have to continue in this mode
for a long time because we certainly haven't calculated
anything like the greater part of realizable situations.

Muller: Is there the idea any more to go back to Kirk Bryan's type
of model parameterization, like global?

McWilliams: What a lovely idea. What parameterization do you want to
use?

Muller: I'm asking whether or not that's still the goal or whether
we say OK, we do those problems with eddy-resolving models.

McWilliams: My own guess is that Rick's [Salmon] view is the one we can
count on. We can build on the hope that we can calculate
eddy effects. Although it's expensive, although it's
laborious, we'll at least eventually get the answer that
way. If shortcuts were found we might escape having to
resolve the eddies directly, but that capability isn't
lurking right on the horizon.

Salmon: Because even if you find the shortcuts, you are going to
have to check them. No one does closure theory and then
believes it without checking. You should do the
computations anyway whether they are primary or secondary.

Magaard: You could check them, for example, in certain parameter
ranges against lab data.

Robinson: It seems partly clear that the Kirk Bryan-type models, even
though eddy-resolving, [unintelligible].

Magaard: That might lead us to my next question reasonably smoothly
because if the eddy-resolving models play such a role and
become increasingly important then how do we compare
results of eddy-resolving models with data?

Holland: Can I interrupt: It might be interesting if Jim [McWilliams] would tell us about the success or failures of parameterization schemes in the atmospheric context because they have been doing this much longer.

Magaard: OK. Maybe we should discuss that first.

Salmon: Their eddies are easier to resolve, too.

Magaard: Would you care to tell us about it, Jim?

Holton: Before I do, could I just say I am a bit discouraged by what I just heard because there is a large group of the atmospheric sciences community that is really enthusiastic about the prospects for coupled real climate models, coupled atmosphere-ocean GCM's , and what I seem to be hearing here is that first you have to do these eddy-resolving models and presumably it's going to take one hell of a computer to do a coupled atmosphere-ocean model if you want to resolve the ocean eddies. [laughter]

Harrison: Jim, I think that very much depends on what aspect of ocean-atmosphere coupling one is interested in and the time scales in particular involved. I think we can make a case that for some of the intermediate level time scales the effects of mesoscale eddies...

Holton: What do you mean by intermediate now?

Harrison: Monthly, seasonal-type time scales... the effects of the mesoscale are unlikely to be order one important in the coupled process, and so much simpler ocean models might let us gain a lot of insight into how the coupled system works.

Holton: To get back to Bill Holland's question: My own view is that in these attempts to parameterize the effect of the atmospheric eddies, emphasis has been on the heat transport. By and large, fancy methods have not been very successful, and it may be that the very simplest sort of adjustment to neutral baroclinic conditions may be as good as anything for the heat flux only. But then one asks, "Is the heat flux really the only question?' That's been what the people interested in climate have usually dealt with,

it's just the thermodynamics, the heat balance. Personally, I am not very interested in that.

The other aspect in which attempts to parameterize atmospheric eddies are going on now with renewed enthusiasm is the transport of chemical tracers, particularly in the middle atmosphere where there is a lot of photochemistry. Chemists now will write down 200 chemical equations and tell us that we have to include all of those if we really want to understand the global atmospheric chemical system. Well, then, the run of three-dimensional general circulation models to transport these things around and solve these will turn out, in many cases, to be extremely stiff. Systems of equations for the chemistry is an awesome task. There are people approaching the question in a way somewhat analogous to what I was speaking about in my own talk of rearranging; maybe this goes back to Allan Robinson's question, is it just the matter of efficiency diagnosis? Since maybe that is the primary thing but there is a thought at least among some people that if you transform the equations so that the net eddy forcing can be consolidated to a simplest possible form, then you may have a better chance of parameterizing in a reasonable way. This is the approach that K. K. Tang at MIT is taking at present to try to develop a two-dimensional latitude-height model for tracer transport in the stratosphere.

McWilliams: What successes have there been, though, with attempts to parameterize those tranposrts in that kind of a jump?

Holton: So far the successes have not been great, but I think because the attempts have been done in a very perverse manner; that is this old question of the fact that in the middle atmosphere and stratosphere the eddies are really mostly planetary waves, at least the eddies that transport stuff around. So it's not turbulence but a wave transport and so the non-transport theorems tend to be valid thus, for example, if you are thinking of trying to transport ozone, there will be strong meridional and vertical advection by the mean flow, but that may be almost exactly balanced by eddy flux divergences. Thus, you are trying to find a small difference between two very large numbers, each of which is ill-known, and the advantage of going to these transformed equations, or perhaps a Lagrangian mean if you can do it, is that you, to some extent at least, get around that problem.

McWilliams: As you remarked in your talks, today these transformed equations are purely diagnostic; there is no element yet being able to claim on theoretical grounds what those eddies in the transformed equations do.

Holton: For the zonally averaged case, that's not quite true;
                 that's the case I am speaking to now, and Tung and, well
                 actually, Ed Danielson somewhat earlier, have derived, for
                 these transformed equations, the various elements of the
                 diffusion tensor parameterization, but it has never been
                 actually tested yet.

Magaard: Maybe this next question is comparatively superficial, but
                 I still wonder how we compare results of eddy-resolving
                 models with data. In many cases we do not observe events
                 in the ocean because we are not able to do it or we are not
                 interested in doing it. Instead, we look at things on a
                 statistical basis. In that case would we have to apply the
                 same statistical techniques to the computer-simulated
                 data? In other words, for example, if Bill Holland would
                 produce an eddy-resolving model of the North Pacific and we
                 could see with our bare eyes Rossby waves running around
                 there, would I have to take these results and apply my same
                 model fittings to the computer-simulated data and then
                 compare it with what I see in the ocean to really compare
                 the computer-generated data with oceanic results? Or how
                 would I go about it? [silence] If nobody tells me I would
                 say, it's the only thing I could think of.

Robinson: I will say a couple of things and the other people will,
                 too. Much of what we heard in the last three days was
                 devoted to attempts to compare observations and models, if
                 there was a theme to the meeting, I think that would be it,
                 empirically; so there has been a lot said about it. The
                 comparison of data with models requires a hierarchy of
                 theories and models and requires using different data types
                 in different ways to establish the validity of processes
                 within models or to look at the overall statistics, have
                 another kind of model, etc.

                 Just let me make two or three specific points. My talk was
                 essentially on data simulation and it had to do with
                 bringing a large composite data set into conjunction with a
                 kind of dynamics which exhibits lots of processes which has
                 been shown by many workers over the past decade or so to
                 have a lot to do with mesoscale eddy-dynamics,
                 quasi-geostrophic model. I personally think that the
                 question of data simulation in models is one of the central
                 scientific technical questions in oceanography for the next
                 several years. And it will involve getting as much as we
                 can out of existing data sets and additional data and
                 extend all the way to the ability to utilize effectively,
                 remotely sensed data, tomography and other kinds of large

data sets which are being developed. So I think that the question that you raised here, too, is a serious one that will require a major scientific effort. I am not the only one who thinks this; there are other people who were saying the same thing. Now that is one remark.

The hierarchy of models and the different use of different data types is another remark. The comparison of models and experimental data, now, on the serious level that is required, takes a person who is expert on both the data sets and the models, such as [Jim] McWilliams, as an example. This is a rare kind of case. What is more likely is that we are going to have to develop real working relationships between experts on details of data analysis and experts on models, somewhat in the spirit of the Schmitz-Holland paper, which really requires a lot of thinking and the full spectrum of expertise. My final comment might be that maybe in oceanography the task is going to be made a little bit easier by the fact that we are data-limited. It is conceivable to me that in the next few years we can take all of the existing oceanographic data and put it in a form which is compatible for model comparison.

Salmon: Do you include satellite data?

Robinson: Yes, in doing this we would develop a methodology for comparison of the models with the data, which is essential, and also construct things like computer programs and data formatting, and so forth, so that the new data can flow into this at totally organized oceanographic data sets for model comparison.

Magaard: More on that?

McWilliams: Yes, I nominate Allan Robinson to do this. [Laughter]

Magaard: I second. Let me mention one particular example: Yesterday in his talk, Bill Holland showed a picture of buoy tracks as recorded by Phil Richardson, and you saw all these wiggles, and then he said that maybe one day your models will have been developed to an extent where they can allow a meaningful comparison between Richardson's buoy tracks and whatever you produced. What, in addition to what you already have, would have to be done to accomplish this? What steps are you thinking would be necessary to do a comparison?

Holland: We are already able to do that kind of calculation. There
              are any number of ways one can look into these models from
              long-term statistics and geographical variability, which
              seems to me to be the first easy thing to do, to much more
              phenomenological kinds of examinations focusing on certain
              pieces of the problems [such as] the eastern Atlantic or
              Pacific, of Gulf Stream ring formation and structure and
              propagation. These kinds of things can be done now. This
              is all in its infancy and what's needed is just manpower to
              look into the way in which these things work.

              A problem the modelers have is, when is a right time to
              take a model with all of its limitations and actually try
              to apply it to these problems? It's at that point that the
              observat..nalist has to get interested and say, "Yes, I
              think I see enough of interest in there from my particular
              focus to think that it is worhwhile doing the work, of
              doing that comparison." And I have to wait for Phil
              Richardson to look at my simulated floats and say, "Yes, I
              think there's enough interest to me that we should try to
              analyze side-by-side simulated dispersion characteristics
              of simulated floats and see how well the model reproduces
              those kinds of phenomena."

              Now if we did such a comparison you get two things out of
              it. It allows Phil Richardson and us as a community to try
              to understand what the physical underpinnings are for those
              observations. It also allows the modeler, primarily
              because of the discrepancies that he finds between
              observations and theoretical tracks, to decide what the
              next steps of improving the model are, where the
              deficiencies in the models are, and how we spend the time
              in the next year producing a better model of the phenomena
              that we are interested in. So this kind of very close
              cooperation of observationalists and modelers is absolutely
              essential at this point to drive the models to more
              realistic systems.

Magaard: Now, concerning wave fields, for example, I would feel on
              much safer ground to ask maybe not the complete set of
              meaningful questions but maybe at least a meaningful subset
              of meaningful questions. What should be compared? With
              respect to these eddy fields (or whatever you would call
              it) that you see in the buoys I would be less sure what to
              compare. You said, I think, "dispersion features". Would
              you elaborate a little bit on that?

Holland: Let me not speak specifically to the floats. I don't think
that the specific issue is of interest. It is more the
general question. If, for example, you were to look at a
Pacific version of my model and inquire whether there were
intersting Rossby waves in the eastern part of the basin,
and there were none, and your feeling is that this is a
primary piece of information about the general circulation
of the Pacific basin, then we have to inquire into the
physics of the model. What is left out if it doesn't
produce that phenomenon? In the calculations I have done
so far, for example, we've only done steady wind forcing;
certainly a part of the signal we see in the ocean is going
to be direct wind forcing. I have no doubts about that.
We don't know what amplitudes and form they will take, but
at some point we have to actually begin to look at that
aspect. And it is in that way - you coming to me and
saying this is an important phenomenon that I should have
in my model and why isn't it there? - that forces the
models in the direction that they should grow and develop.

Magaard: With respect to data, I mean buoy data was an example of
data, Ed Harrison in his talk made a rather provocative
statement; he said everything is secondary to obtaining
more data. Didn't you say that?

Harrison: I did say that. [Laughter]

Magaard: As one possible reaction to that, I would say that there
are a lot of existing data that have not really been
analyzed to any reasonable or sufficient degree, and I
think these buoy track data are an outstanding example.
For example, when I consider these pictures I have seen
from the FGGE buoys in the southern ocean, I feel that we
are far away from the goal of making optimal use of these
buoys. Is that a view that you would share or is there any
objection to a statement like that concerning the buoy data
in general? Have we really gotten out of these buoy data
the information that they contain?

Rhines: I think there has been sometimes a tendency to fall back
and use them as moving current meters; you don't get eddy
kinetic energy from them if you do not exploit their
Lagrangian or nearly Lagrangian nature. But, on the other
hand, there are examples counter to that. I think maybe in
the near future we will rather see some very important uses
of shallower drifter data because so many of us
now.....[pause in tape recording]

Round Table Discussion (cont'd)

Rhines:
the circulation, where does it come from? I hope we're about to see some more purely Lagrangian use of those.

Magaard:
So you're saying enough models have been developed now that can be checked against these data or the other way around. So to a certain degree you would agree with me, but you think the means are there to now make better use of these data. Is that what you're saying?

McWilliams:
I would like to add something here. I think most of the use of drifter data, subsurface data, has been primarily in the random walk current meter mode. And I think there's a very good reason for that, which is essentially that, one, in the absence of really being able to think of these as accurately Lagrangian over long times (which probably they're not, they're accurately Lagrangian over short times) and second, their sparseness, they've almost always been put out in small numbers (that's to a large extent economics). We haven't been able to make the kinds of calculations I think we're most comfortable with when we conceptually think Lagrangian, which is really a many-particle description expressed in such ways as: elongation of area elements defined by the particles and the boundary of that element - such things as dispersion statistics (one-particle dispersion statistics, two-particle dispersion statistics). We do some of these calculations and we do them in large error bars and we have done them in a few places. Potentially they would be an enormously more valuable, more informative piece of information if they could be deployed in an order of magnitude larger arrays (which is partly a technological problem of how you get them cheap enough to do that and partly a financial problem of how you pay for your inability of getting them cheap enough to do that).

Now speaking to a question Allan [Robinson] asked earlier and was passed over. If we could calculate with sufficient accuracy and sufficient spatial coverage the diffusivity, particle-from-particle separation rates, ther have one of the numbers that's potentially --- first of all it's calculable in models, so we have that direct comparison that we can make, and second, we have one of the potentially most directly applicable numbers to the hope of parameterization. Now whether that hope would work out or not, I don't know, whether the diffusivities of the ocean can be related to a few simple quantities -- such as distance from the boundary and energy level of the mean

flow or something like this -- I have no idea. And that
would be required for them to provide a universal
parameterization. But there are at least the <u>numbers</u> that
would be involved in such parameterization (if one would
work). So I would agree with you both in the statements
you made, but make a real pitch for a very high density,
very large number relative to the present experience
[regarding] Lagrangian deployment.

Magaard: Sounds like more data [are needed].

Salmon: I would just like to make a point. The atmosphere is the
best-sampled fluid in the universe. I think it's hard to
argue (and I may offend Jim [Holton] here) that the
fundamental theory of the general circulation of the
atmosphere is way ahead of that of the ocean. So it may be
that a great deal more data might not produce the
significant understanding breakthrough that you would
expect. Is that fair, Jim [Holton]? The meteorologists
have much more data than we can ever hope to have, and it
hasn't really blown the problem wide open for them, either.

Holton: In what sense do you mean? [Laughter]

McWilliams: Are you any closer to parameterizing the eddy effects on
the mean flow than we are -- things like that?

Holton: No.

McWilliams: But where you are is with working calculational tools that
are known to be essentially correct in their answers for
such things as the general circulation, while we're still
groping for that, and you have been guided substantially in
your observations in that process.

Holton: Sure, we know what the general circulation looks like and
we can do a pretty good job of simulating it.

Salmon: That's reason enought to collect data -- just to know
what's there -- just to know what reality is.

Holton: I'd like to make one point which might be helpful in your
thinking about how to use data in models, something that

Jerry Malmon has started to do with some of the GFDL models. Jerry realized these models, of course, can be used to produce beautiful time series of any parameter that's predicted in the model at given locations. So if you have a station making profiles or for some reason have a long time series at a given locality, you can check variances and so on from model output. That is one test of the models which can be done without having data assimilation schemes a la Robinson.

Magaard: Glenn.

Flierl: To make a couple of comments just cautioning on the use of floats and drifter data: I think that our tendency to regard them as Eulerian particles is perhaps deceiving, in that if you think of very simple models, such as a Rossby wave in a channel, and if you put a clump of particles in it and then ask for the mean flows, you'd find that on the eastward side of the channel the mean flows are larger than on the westward side of the channel — the mean eddy variance — just because the particles that have gone right have been caught in a high current and the ones that have gone left have been caught in the weaker currents. And that there's some serious problems with the way we've used float data in the past in that we tend to put them out in a clump rather than — and that's very different from doing an ensemble average. You can get diffusion in cases of spreading of clumps of particles, where there is no diffusion in reality. You can get errors in your estimates of variability as a function of space, and in means — in all of this. We really need more experience in using floats not just in general circulation models but even in very simple process models or analytical models.

McWilliams: That is a form of sampling error in float using.

Flierl: Well, it's not just sampling error. It's conceptually how do you use this data and how should you sample in such a way to be able to use the Lagrangian character of the data to your advantage and not to be deceived by it.

McWilliams: Fair enough, I agree with that. But I would argue an ensemble assumption.

Flierl: Perhaps, or else more uniform distribution of data.

Rossby: I've made this remark before, and maybe it's a little
           shopworn by now, but one of the things we've observed in
           the ocean are these baroclinic lenses...one that got us
           excited in the beginning was the Mediterranean eddy lens
           that was observed in the thermocline in the western North
           Atlantic, and that triggered some speculation that perhaps
           these eddies may be a mechanism by which the Mediterranean
           salt tongue penetrates across the Atlantic. We have since
           then picked some hydrographic sections and looked at others
           across the subtropical gyre and used current meters and
           floats as reference velocities... From this we have found
           with some degree of certainty that at least the southern
           half of the Mediterranean salt tongue has a mean flow to
           the east and not to the west. It points to the possibility
           that the "meddies", as we've come to call them, may be
           playing a rather explicit role in getting that salt to the
           west. The fact that the mean flow to the east is very weak
           implies that they don't have any difficulty in moving west
           against the mean flow. The lenses become a small-scale
           mechanism by which the salt can be transported to the west
           if they occur in sufficient quantities. Especially for
           those of you who are doing diagnostic calculations [this
           is] a potentially very dangerous situation of
           misinterpreting a scalar distribution as being the result
           of some kind of large-scale Eulerian mean flow and a fuzzy
           distribution diffusion on top of that. It has the
           properties of a large-scale flow but the mechanism by which
           it is being transported may, in fact, be a small-scale
           process.

Magaard: What is the lesson to the eddy-resolving model builder?
           That he still has to parametrize subscale things? You gave
           an example of a subscale process, is that what you meant to
           say?

Rossby: Yes, right, small-scale process that has the appearance of
           a large-scale mean flow balance.

McWilliams: I think there's another implication for the eddy
           calculations, which is that to date, although a number of
           these discrete, well-defined, long-lived, water-carrying
           circulations have been found in the ocean, none have yet
           been found in straightforward, unprejudiced, large-scale,
           forced, turbulence model -- eddy-resolving model. And
           whether it's insufficient resolution still, whether it's
           the lack of the formation processes, whether it's lack of
           vertical resolution, or perhaps incorrect forcing mechanism
           but to date no model has generated them except in very
           contrived situations.

Robinson: But you know how experimentalists threw out some of the small things because they thought it was noise; maybe some numerical modelers have thrown out runs that have noisy little spots.

Flierl: We also know from modon work that the resolution required to see a long-lived feature of that order is a factor of ten more than the current eddy-resolving models, if you're talking about something that is 20 kilometers in size.

McWilliams: Yes, there are a number of demonstrations now in various work on modons and other coherent vortices that recognize them as coherent vortices, as opposed to something that looks more like waves and turbulence, requires very high resolution. Now they are not always coherent vortices, that is, if you just go to high resolution everything just doesn't convert into coherent vortices. But it requires a great deal of resolution to recognize when you've got one of those in there that may be a lot of the present failure to do some of the modeling.

Magaard: Unfortunately, Ed Harrison had to leave early. So I cannot ask him what he has meant to measure when he said that it was so important to have more data -- more important than anything else.

McWilliams: He wants to know how to put out current meter moorings for ten years. He's already told us that.

Magaard: Everywhere forever. Now recognizing that we can't do that, let me ask you: What should we preferably measure to learn significantly more? I hope you do not find this question too trivial to answer it. At least it can have an answer in terms of what projects do you have on your mind, what measuring projects.

Robinson: One thing which the eddy dynamics community needs in the reasonably near future is more experimental work in the Gulf Stream system recirculation zone and extension region. This region has been identified as a major production region, has been implicated as such, but it has not been the site of as much experimental activity and modeling activity as is warranted. Every indication is

that a very substantial scientific advance could come from
scientific research in this generalized region. That's one
thing we have to measure.

I'd also like to make a general remark at some point, which
is obvious, but why not make it anyway. Science is a
wonderfully complicated human undertaking, and it requires
a balanced approach. We know that by taking new
observations with new instruments and new sampling
frequencies the last several years we've learned a lot of
new things: phenomenology, some quantitative information.
And we have to continue to make new kinds of measurements.
Because in the ocean in the next few years we're not simply
going to get better numbers for things, although we are
going to get better numbers, we're going to continue to
discover things. We do have to keep up our measurements.
But it has also evolved in oceanography in the last several
years -- a scientifically sounder and rather exciting and
productive interaction between theories, models, and
observations. We have to keep the modeling going; we have
to keep the feedback going. It's true that we have data
sets now that have more information in them than have been
analyzed, etc. There's lots to do. We're
manpower-limited. But we have to continue to advance with
balanced judgement between the different elements of the
research activity. It is essential that we do that.

Magaard: You emphasized the Gulf Stream area as a major production
area.

Robinson: I made two points. One, the Gulf Stream region as a site
of experimental modeling research, as being critical to
making our next step advance in our understanding of eddy
dynamics and relationship. [unintelligible] I made a
second remark, and that is that we have to have a balanced
approach to our scientific activity.

Magaard: Are there measuring projects coming up, in the planning
state or in any stage? Maybe the Gulf Stream is not the
only object of interest?

Hogg: Bill Schmitz is intending to follow up his work on the
Kuroshio with similar geographical exploration to the east
in the Kuroshio extension. And I myself am intending to
follow up this work that I showed you yesterday with a
program aimed both at filling in the holes in the deep
circulation, trying to better identify the extent of those
deep gyres and also for the first time getting some measure

of the heat flux and consequently this thickness flux through the Gulf Stream itself. So it's a double program with two goals; to better identify the deep circulation and also to give us more information on the forcing of the deep circulation.

McWilliams: I'd certainly agree with the sense of the last two remarks. I think the best combination of unknown and important in terms of the general circulation tendencies is the Gulf Stream right now. I would equally well say the Kuroshio except for the fact that we would have so many years of preparation to do to go through to get to the point of being able to interpret the answers as well as we probably could near the Gulf Stream.

Rhines: It really is the area. We all know and love the Gulf Stream, but there are many other important parts of the ocean. I'm sure it should be mentioned how much enthusiasm there is for high-latitude work in studying of formation of mode waters and chemical tracers. Maybe that doesn't qualify under eddy dynamics and the mean circulation but I think it's all one problem now. Many of us work in these different applications of eddy dynamics almost on our own, and problems like water mass formation are really full of questions involving eddies. So, that under-transient tracer program and others we certainly hope will go ahead in the future.

McWilliams: I would agree with that. But I would at least offer the opinion that we're in intellectually a better position, because of what we've done for the last ten years, to interpret an accurate description of the Gulf Stream than we are to interpret an accurate description of the water mass formation process. It's just as important in the long run to a complete theory of the general circulation. However, I think in some sense the Gulf Stream is "walking" and the water mass formation is "running."

Rhines: I sense that there is a growing feeling that we can now say something about the creation of the density stratification in the ocean and the creation of the water property fields that accompany it. Even though it's really the most challenging new domain for numerical models and probably the most difficult, to make the water wet instead of dry, "wet" meaning having solvent heat properties; "wet" meaning having chemical properties.

Rossby: I could add to your question about the Gulf Stream. We're hoping to start a program sometime this fall... essentially a path seeding or Gulf Stream monitoring-tracking experiment; essentially a SOFAR float experiment, where we plan to repeatedly seed the Stream right off Cape Hatteras. In the light of what we've learned now, we have good reason to believe that the floats will stay in the Stream at least as far as the New England Seamount. By repeatedly seeding on something like a weekly basis we hope to study in detail the space-time evolution of the path of the stream. Since the floats are planned to be isopycnal, we can also look at vertical motions in the Stream, such as subduction and upwelling.

McWilliams: Can you seed at several depths?

Rossby: Yes we can.

McWilliams: Down into the deep waters? ... Good.

Rossby: I have a funny feeling that this technology of isopycnal floats, or Lagrangian floats -- I realize this is said with a lot of bias -- is unextraordinarily cost effective. Although it has time and space wrapped up in it, it does go part of the way in answering questions of real interest, namely, what are the physical pathways of fluid particles. These are not Eulerian questions. But knowing how the water actually migrates is a question that is addressed naturally with this Lagrangian methodology.

McWilliams: But can you get at the deep circulation?

Rossby: Oh, yes. But one can only do so much in a year. At first we plan to work at only one level where the trapping in the Stream is efficient but eventually we hope to work at other depths and on other processes in the Gulf Stream system. For example, we would like to study the response of the Stream to various boundary conditions.

Hogg: I think one problem with the deep circulation would be that the eddy activity is so great compared to the mean that you would have to work a lot harder to uncover the circulation.

Rossby: One other remark about instrumentation in general. There is a very natural tendency to work with whatever equipment one can get off the shelf. But there is a lot happening in the area of instrumentation development. One of the instruments that I think is extremely exciting for certain classes of questions regarding Eulerian mean flows is the technology that's been developed for acoustic tomography. Acoustic tomography as a tool of for eddy resolving maps...that seems like a pretty tough one. But it can be used in reciprocal shooting for getting long line averages of mean flows in the sound channels and in the deep waters. That seems to me to offer a very real promise of getting large-scale averaging of Eulerian mean flows...

Magaard: You might remember, Tom, that about two and a half years ago, you and I were sitting in a review panel concerning acoustical tomography. Have you followed up on that? Does anyone here know what the state of the art is in acoustical tomography and what its inventors believe about it at this time?

Lukas: Walter Munk is very enthusiastic. [Laughter]
(Univ. of Hawaii)

Magaard: Nobody wants to say anything about that?

Lukas: Well, they've done one experiment in the Atlantic. They're just starting to crawl. They're just trying to find out what they're seeing -- it's kind of in the nature of what some of the satellite sensors are seeing -- we're just beginning to understand what it is that we're looking at. I think they're in the same position. It's going to be many years before basin-wide acoustical tomography is going to really come on line.

Spence: I can make perhaps a minor update. After that original
(ONR) deployment off of Florida (which they viewed as something of a limited success because they systematically began to have failures in the transponding network they had, and they also have the problem of matching their source of observations to baseline traditional oceanography), they attempted a reciprocal shooting experiment; I've learned in the last week or so that they had a very early failure and so at this point I suspect they're somewhat disappointed. The reciprocal shooting demonstration would have been one of the next steps they proposed. The next large-scale

effort that had been discussed was this large deployment in
the Pacific east of Hawaii, sort of a gyre-scale experiment
to get such things as vorticity and heat flux on what they
call thousand-kilometer scales. This point is still being
debated by funding agencies and by the PI's themselves as
to whether that is indeed the most profitable next step to
take. One view I have is that at least so far they have
not aimed the acoustic tomography tool at mesoscales in
particular. And I think it may indeed be a critical
component to assess eddy-mean scale interactions if in
addition to gyre-scale experiments it somehow has the
possibility of subsampling on the scales we've been talking
about in this meeting. One of their original experiments
was to try and do this in the Gulf Stream system, and they
turned their attentions away from that toward more of a
gyre-scale experiment. But I think the philosophical
feeling is that, "Hey, we've shown it to work at some level
of sophistication on a mesoscale issue, now let's show that
it has the potential for a gyre-scale experiment", and
indeed it may be one of the only sorts of instruments that
get large-scale integrated properties. Perhaps we should
have had a representative from the acoustical tomography
community here to speak to some of these issues because I
think we all have the gut feeling that it's potentially one
of the most important tools for us to use in the next 5- to
10-year time period.

Magaard: Well, thank you first of all; should I apologize for not
                having thought of that? [Laughter]

Spence: I think we certainly have identified a number of issues
                here on which their views would have been of value. By and
                large, we've covered the traditional view of mesoscale
                observations today. And they frankly have not made a
                contribution to oceanography per se except to demonstrate
                that tomography is a viable tool for probing on the
                mesoscale.

Magaard: I'd like to bring up one other issue, and that is the
                larger-scale monitoring programs in the Pacific. For
                example, the one organized by Warren White. Is that going
                to go on? We've seen that it has definitely a lot of
                relevance for mesoscale processes if we define them
                sufficiently large. What's the fate of that?

White: Well, right now it's an ongoing program, funded no longer
                by research money but by the Navy and by NOAA -- fleet
                Navy. As far as I know in the midlatitude Pacific, between

30° and 50° North, it's going to continue
indefinitely. There's a component program in the tropics
as well, to look at wave propagation in the
equatorial-tropical... But that is in possibly some
trouble, but it's been ongoing for three years now, funded
by NSF. And we're trying to get moneys to continue this
from the NOAA FGGE office during this TOGA program that
would be going on for the next few years. That's a
broad-scale program, that's about 10,000 BT's between
20°S and 20°N per year for X number of years. We'll
look at east-west wave propagation. We'll study El Nino
and the Southern Oscillation.

Magaard: So that will go on.

White: Well, hopefully, that'll go on. I expect it to. For the
last year and a half, there's been the development of an
XCTD that is scheduled to be completed, with on the first
test being done in June of this year. So that's going to
open up some possibilities for doing work, monitoring,
maybe for six months or a year, maybe in confined areas
where there are shipping lanes to deploy these things.
These will have 0.1 parts per thousand accuracy. And if
you have an alternate way of getting better surface
salinity data, it can do much better than that. It needs a
check sample. The drawback on that is that right now XBT
probes cost about 35 dollars a piece, and the XCTD's are
going to cost approximately $180.00, maybe more. But if
you're going to do a sampling program maybe one out of
three or four would be a CTD and the next one would be an
XBT, and you'd interpolate the salinity on density surfaces
or something like that. I think there's going to be a
possibility for doing some ventilation-type studies for
winter periods in areas where this kind of process occurs
[unintelligible] I suppose that if somebody really pushed
hard you can get these things down to 1500 meters, but I
don't think they're planning to do that right now. Do you
know that?

Unidentified: Eventually.

White: I know there's also a proposal for XBT work in the North
Atlantic. But I don't know much about it, since I haven't
really seen the propsal. There's certainly a lot of
opportunity for this kind of thing there.

Magaard: Does somebody want to say something about the measuring
activities in the eastern portion of the North Atlantic?
For example, the projects that are organized at Kiel.

Krauss: I mentioned already what's going on with respect to the
drifting buoys. In connection with this program there's a
lot of field work with moored stations; one half is in the
Central North Atlantic north of the Azores and the other is
in the Canary Basin. That's the main project from Kiel.
There are other projects in the Norwegian Sea mainly with
respect to generation of deep water. In the open Atlantic
Ocean the French start their program this summer, in
cooperation with our program. It's related to the heat
budget of the North Atlantic Ocean and it's concentrated on
the area of the mid-Atlantic Ridge. I don't know exactly
what the activity of the British institutions is, but I
think they're concentrating more now along their own
islands. The Norwegian program is in the Norwegian Sea
mainly along the continental slope, Norwegian current and
things like that. Most programs in the North Atlantic from
the European side now are more or less concerned with
climatological questions -- heat transports and things like
that.

Magaard: Our discussion has developed more in the direction of data
than I'd thought it would, but then, of course, I neither
cannot nor did I want to predetermine the discussion. I
would have thought there would be more discussion about
closure problems and so on. I understand now that it's not
the most fashionable thing at this time, even though it was
made clear to me that it is not dead either.

Rhines: It's just a question of who's here and who isn't here. We
only have 1-1/2 closure people here. [Laughter] And they
can't discuss with each other.

Magaard: Maybe with this remark we should conclude this part of the
round table discussion. Thank you very much.

Round Table Discussion Section 2
Peter Muller, Chairman

Muller: What evidence do we have that eddies actually play a role in the general circulation?

McWilliams: I challenge you to construct a general circulation model using only molecular diffusion.

Muller: What happened, for example, to Bill's [Holland] old ideas, that the increase in the Gulf Stream transport is due to bottom torque?

Holland: I think those kinds of physics are still working in the ocean. We're just finding that the physics are a lot more complicated than simple steady state theories predict.

Muller: What is the evidence from the observations? Isn't there evidence that . . .

Rhines: It's a little hard to tell. You define eddies and the general circulation first.

Muller: Do we agree on how to define the general circulation, and the eddy field?

Rhines: What is the general circulation? Is it where the salt flows or is it what a current meter shows after a long time?

Salmon: You have a viewpoint that the wind may be very important in eddy generation. But if you take the opposite viewpoint, that eddies come from larger scale motion instabilities or energy cascades, then the fact that they are there and they have so much energy means that the larger scales have lost a lot. So at the very least they're a big brake on the larger scales. To me that's evidence of their importance.

McWilliams: Which is the sense of the remark I was making. It's inconceivable to construct a model of the general circulation with molecular viscosity. You need the eddies, that's indisputable. Just how they do it . . . you can argue about.

Magaard:	Does somebody want to say something about the measuring activities in the eastern portion of the North Atlantic? For example, the projects that are organized at Kiel.

Krauss: I mentioned already what's going on with respect to the drifting buoys. In connection with this program there's a lot of field work with moored stations; one half is in the Central North Atlantic north of the Azores and the other is in the Canary Basin. That's the main project from Kiel. There are other projects in the Norwegian Sea mainly with respect to generation of deep water. In the open Atlantic Ocean the French start their program this summer, in cooperation with our program. It's related to the heat budget of the North Atlantic Ocean and it's concentrated on the area of the mid-Atlantic Ridge. I don't know exactly what the activity of the British institutions is, but I think they're concentrating more now along their own islands. The Norwegian program is in the Norwegian Sea mainly along the continental slope, Norwegian current and things like that. Most programs in the North Atlantic from the European side now are more or less concerned with climatological questions -- heat transports and things like that.

Magaard: Our discussion has developed more in the direction of data than I'd thought it would, but then, of course, I neither cannot nor did I want to predetermine the discussion. I would have thought there would be more discussion about closure problems and so on. I understand now that it's not the most fashionable thing at this time, even though it was made clear to me that it is not dead either.

Rhines: It's just a question of who's here and who isn't here. We only have 1-1/2 closure people here. [Laughter] And they can't discuss with each other.

Magaard: Maybe with this remark we should conclude this part of the round table discussion. Thank you very much.

Robinson: Nobody really wants to answer your question, Peter. It's
              not only the direct effects of the eddies but also the
              indirect effects. You remember the discussion two days ago
              on the heat current systems that are there only because of
              eddy effects. They may not locally be driven by eddy flux
              divergence.

Bennett: I'd like to make two or three points. First of all, I'd
              like to clear up a misconception I may have given people in
              the audience. Glenn [Flierl] had this misconception. Glenn
              just came up to me and said, "How can you possibly deny
              significance of transient eddy heat fluxes?" I don't deny
              it. All I can say is that I'm not going to be able to
              measure it with XBT's.

              Perhaps I should also elaborate some more on a couple of
              points which I didn't make in my talk. First of all, I'd
              like to think about the atmosphere very briefly which, of
              course, doesn't have coasts. As Jefferys pointed out, in
              the 20's, there necessarily must be eddies just to maintain
              the general circulation of the atmosphere. And the same
              sort of thing holds true for the annulus experiments. The
              cause there is no pressure gradient around the annulus. One
              finds that you have a turning cell which existed before the
              turntable was started up and is deflected into a geostrophic
              flow. This can't move heat very well. The only way to
              reach a steady state is to have a baroclinic eddy field.
              Now in the ocean, of course, that may not be necessary. It
              may be possible to meet all the mechanical and
              thermodynamical constraints without an eddy field. One of
              the attractions of looking at the heat flux measurements
              obtained by the meteorologists and what one can determine
              from oceanographic estimates which don't get the eddies is
              to ask, "Well, are the two reconciliable?" If they are not,
              then we must infer that eddies are important. So rather
              than measuring eddies directly we may also determine their
              significance by measuring everything else. [Laughter] To
              the extent that everything else is large scale, that may be
              a much more tractable problem. For example, why not pick a
              latitude, say 34° North? There are certain aspects of the
              circulation there that are particularly easy to measure,
              such as the barotropic heat flux; it's necessarily very
              small. We're not worried about Ekman flux because the
              Pacific is literally very pacific. We're not worried about
              the Sea of Japan flux and so forth, and we can get at the
              meridional circulation very easily with standard
              oceanographic techniques and climatological temperature
              atlases. Now if the meterologists can convince themselves

346

and us that they really do get the right answer from the
indirect assessments using the atmospheric meridional flux
then we have an indirect way of deciding whether eddies
matter or not.

Salmon: I'd like to add a comment. If the ocean were truly
barotropic, then there would be really no efficient
mechanism for getting energy in the large scales put in
there by the wind, into small scales — it would essentially
all be trapped there. You can show on quite general grounds
— you don't need a linear stability theory and its
limitations at all but just general budgeting — that
because the deformation radius is what it is, it is possible
to get energy out to that scale very, very efficiently. You
can get direct and very efficient energy from large, broad
scales to the deformation radius. One of the interesting
things is that scale spread in the atmosphere is about ten,
between the larger scales and the deformation radius. So in
the atmosphere things really are trapped in much larger
scales, but in the ocean it is about 25. That's a really
big difference in the two fluids. It means that large
scales in the ocean can lose their energy directly into much
smaller scales. The eddy viscosity, so to speak, could be
much greater in the ocean than in the atmosphere because
it's being taken down to a much smaller scale via baroclinic
instability directly.

Muller: Do we all agree on what the mean flow is and what the eddy
field is? Do we all apply the same algorithms to our
measurements to define these two things? All these
discrepancies we've heard about, are they physical
discrepancies or are they due to different algorithms or
definitions?

Magaard: If I may make a comment on that: about 2-1/2 years ago
(when I went to Europe in the summer) I stopped over at
Cambridge and asked Carl Wunsch what he thought the general
circulation was. And he said it's a five-year average of
everything. Concerning that statement, we've done our
Rossby wave analysis up to time scales of 10 years and find
that especially in that range I mentioned previously (6-7
years), we can explain a lot of the variability, say 50-80%,
by means of the wave model. That makes me wonder about the
general circulation being definable by a 5-year average.
Even 10 years, it would still be very problematic to say an
average over that time span results in finding the general
circulation. I have been very confused about the question,
"What is general circulation?" and I certainly still don't

know because there are fluctuations at all possible time scales, even if you take 100,000 years. Now where to say, "If we average over a time span T we have the general circulation," I don't know. But I don't think that it is 5 years.

Rhines: What about defining ᵣhe mean in terms of the equilibration rate of the various processes in the ocean? Clearly the mechanical energy, the momentum of upper circulation, is something that can get set up from rest or get changed to a new value reasonably quickly. The density field and water mass properties take much longer to adjust. At the farthest outside, the great overturning modes probably have a 100-year time scale to adjust. So you have different definitions of "mean" for each of these problems. I think this problem has been realized earlier in the Pacific than in the Atlantic. In the Atlantic there is a lot of interest in decadal climate fluctuations now, which is new for many of us. Our somewhat simplistic earlier feeling of a very well-defined mean, 5-years averaging, is something that's becoming much more interesting and sliding around on the decadal scale.

McWilliams: On the other hand, we do have lots of evidence that velocity spectra begin to lost power. I would defend Carl Wunsch's 5-year average, not on philosophical grounds (because I think we've had good discussions for the reasons why that is not philosophically defensible), but on practical grounds; it's a fairly useful time scale to talk about, just based on the spectral information we have to date.

Muller: Is the same true for temperature?

McWilliams: I think it's certainly true in many places. If you talk about the temperature in the main thermocline, Gulf Stream recirculation, yes, the spectra are turning over, but not as quickly as the velocities. If you're talking about the kind of thing Peter [Rhines] is talking about, which are changes in the T-S relationship in the deep water of the North Atlantic, I think 10 years is the beginning of the variability spectrum.

Hogg: I think I have to dispute what you said a little, Jim. There is certainly a peak in the velocity spectra in the mesoscale band, 30-100 days, but as far as I know, the spectra continue to rise at the longest time scales we've measured, which are a few years.

McWilliams: Outside the Gulf Stream; yes, in the MODE site for example, they were very red in the thermocline for as long as the measurements were taken. But the ARRAY II measurements which Bill Schmitz just published in his paper on the frequency content of the variability "show that the spectra within the recirculation zone have really turned over."

Hogg: There's a peak at the eddy band but Bill Schmitz has not resolved the secular scales, as he calls them.

McWilliams: The secular scale has a lot less energy, which is the point I was making.

Hogg: I guess my point is that the spectrum still is red at the longest time scales he can measure and you would have to go to 10 years to really make the next cut on this.

McWilliams: "Red" in my sense of the word means monotonically increasing as the frequency decreases. There is still energy at the lowest frequencies, on the secular scale; we haven't resolved the secular scale. And there are places outside the Gulf Stream in which the secular scale is dominant. That may even be true in the MODE thermocline, if I remember correctly.

Hogg: I'd say we don't have any real idea, Jim. There is certainly a peak at the mesoscale band, but the energy in the longer time scales has not been measured.

McWilliams: Agreed.

Magaard: How do the meteorologists define the general circulation of the atmosphere?

Holton: Well, it's embarassing to say, if you look in the glossary of meteorology, it states that the general circulation is the sum of all motions of the atmosphere. [Laughter]

McWilliams: Are you proud of that definition?

Holton: No, I'm not proud of that definition. Those who work on the
            general circulation of the atmosphere like my colleague,
            Wallace, are studying the time-average circulation in the
            largest scales. That is, on the planetary scale: monthly
            average, where you're looking at hemispheric scales of
            wavenumbers 0 out to 10 or so.

Robinson: We all know what we mean by the general circulation. There
            are some real problems that remain. For example, in EGCM's,
            the mean fields show quite rapid variations of some of the
            statistics, small-scale variations in the mean field. Now
            does the general circulation really have features like this
            in the ocean? Have those calculations been well enough
            converged? When we get at the description of the general
            circulation, are you going to have to deal with very short
            spatial scales in general circulation monitoring? Questions
            like this bear some discussion and thought, whether it's
            7-1/2 years or 4-1/2 years. When we have certain data
            records we can convince ourselves that this record is
            reasonably converged and what information content is among
            the frequencies. But there still are descriptive questions
            of the general circulation we don't have an answer to. Are
            we allowed to do mixed space-time averaging in the
            description of the general circulation and put our thought
            in those kinds of features or not? To me that's a very
            important question.

Muller: How could we resolve these questions? Do you have any idea?

McWilliams: Most easily in models, I would think. To what degree do
            models settle down with increasingly long time averages so
            that there is no other structure than the mean? And I would
            look at the calculations that Bill [Holland] has done, for
            example, and say that I'd be very interested in knowing what
            an average 10 times longer looked like for a lot of the
            statistical parameters.

Holland: Just a comment about that. It certainly is clear in almost
            all of the calculations we've done that there's a lot of
            energy out at the longest time scales we've averaged over,
            5- to 10-year time scales. If one tries to look at those
            (and these are steadily forced problems so that the
            transience is all coming from the instabilities of the
            system) and if you try to cleverly filter the faster time
            scales out to longer and longer periods, you find that you
            still have an ocean which is very slowly changing and -- I

don't know how to describe it — pulsing or whatever. That is, the Gulf Stream will move back and forth a bit over even 5- and 10-year time scales in this class of models that I've been looking at. So I still don't know where the limit of that is. We've not done averaging that's long enough really to show completely statistically steady results.

Muller: In the real ocean, what's the longest current meter record we have?

Hogg: Site D is probably the longest combined record we have — something on the order of 800 days, I think.

McWilliams: That really is a disgrace.

Muller: Would it be a good idea to put out a couple of current meters in some key locations for 10 or more years?

Magaard: But we have much longer time series for the temperature and the longest probably for the sea level record. I mean we have sea level records that are more than a hundred years long. That can give us some impression what happens on that time scale.

McWilliams: Well, but we like to think about velocity work.

Muller: What do the sea level records show, Klaus [Wyrtki], and how does the sea level spectra look like?

Wyrtki: A few years ago, we analyzed 100-year records from San
(Univ. of Hawaii) Francisco, Honolulu, and Sydney. They increase with one over frequency toward the low end. And that goes down to about a 25-year period. Of course, we don't know what the spectrum will do beyond that, because if you go much farther beyond that then you come to the ice ages.

Muller: What about temperature spectra?

White: Temperature spectra are red as far as you can take them out. We have 25- to 30-year records. The biggest signals, at least in the tropics, are El Nino type signals. In the

Western Pacific you can get 50 dynamic-cm disturbances for over about a 3- or 4-year period. These are very, very large disturbances especially for 20° North. It represents a large shift in mass from one side of the ocean to the other as part of the Southern Oscillation. There are some big signals.

Muller: Shifting to another topic. We as a community are mostly interested in understanding how the ocean functions, but what is required from an ocean model for atmospheric or climate purposes?

Holton: One is primarily interested in the heat budget at the surface, and the water budget. I don't think that from the climate point of view, we're worried directly about currents. I guess you have to get those right to get the heat budget right, I presume.

Muller: Can you add anything?

Huang:
(NOAA)
I would like to add a comment on that. I was optimistic when I came to this meeting. Eddy studies have been carried out for many years, and I hoped that with so many experts here we would be able to reach some kind of conclusion on eddy phenomena and the general circulation as well as their effect on atmosphere interactions. It seems to me, however, that we still have a long way to go before we can draw certain conclusions. The World Climate Research Program, after the first GARP Global Experiment, is now focusing on the study of climate. Some atmospheric and oceanic scientists are trying to develop climate models for climate prediction. The climate time scale they're talking about is a couple of weeks to decades. Climate modelers are looking for the essential parameters that will affect the atmosphere, mostly air-sea interaction parameters, for momentum and heat exchanges on the climate time scale. They couldn't obtain these kind of parameters from the meteorologists. They are turning to oceanography, hoping that oceanographers can provide the essential parameters they are looking for. From the oceanographer's point of view, this offers the opportunity to concentrate on certain oceanic studies that will solve one of the essential problems in ocean dynamics. The heat exchange and momentum exchange are essential in air-sea interactions. And the heat exchange and momentum exchange also affect other physical processes in the general circulation. How can we go about it? In climate studies, we have to consider large

spatial scales of a couple of hundred kilometers, and time
scales of a couple of weeks or longer. Whether or not the
eddy phenomena affect the exchange of heat and momentum on
these temporal and spatial scales, is the essential problem
to meteorologists in climate studies -- can oceanographers
provide answers now? It seems that at the present, we are
not able to provide the climate modelers with the conclusive
statements they're looking for.

I would like to take this opportunity to pass out some
information on oceanography in the World Climate Research
Program (WCRP). So far, the WCRP is pushing for the world
ocean circulation experiment, which as you know depends
mostly on the future satellite situation. And still
endorses the CAGE experiment, but, presently it is uncertain
about how the CAGE experiment should be carried out.
Therefore CAGE will be postponed for an indefinite time,
until certain precursor experiments come to a certain
conclusive state.

I think some of you might have participated in the previous
Princeton meeting on El Nino and Southern Oscillations
(ENSO). A lot of interest was generated among United States
scientists on this climate problem. The ENSO program is
referred to as the Tropical Ocean and Global Atmosphere
[TOGA] program in the WCRP. This program will provide
short-range climate predictions of anomalous situations.
Klaus Wyrtki knows much about the El Nino phenomenon. In
general, according to studies based on available data,
certain sequences of atmospheric and oceanic events happen
in a definite coherent order. When a typical situation
happens you can get predictions of the next event from its
precursors. However, last year was not typical. Under the
present budget constraint, it is very, very difficult to get
a large program funded. However, because of the scientific
evidence and climate applications, many scientists are
working very hard for it. We, in NOAA, have brought this
program to the attention of the administration. This is the
only program, the only new initiative to get funded in 1984,
although the funding level is not as high as we expected.
From 1984 on, the U. S. will have some effort concentrated
on the equatorial Pacific region. According to WCRP plan,
the TOGA program will include the Pacific, Atlantic, and
Indian oceans. However, the present funding level is not
adequate to work in all three oceans. So right now the
focal region is in the Pacific. In the Pacific, the NOAA
has some coordinated activities together with NSF, ONR, and
NASA. There are physical processes experiments -- the
Tropic Heat and EPOCS programs as parts of the coordinated
TOGA/Pacific program. For the next 4 to 5 years, at least,
the U. S. will carry out more activity in the tropical
region.

McWilliams: One understands the desires for oceanographic answers. I would ask this question, though rhetorically, or specifically if you prefer. What would we be doing different given our manpower than we're doing now to be responsible about working in a systematic way toward being able to provide the right heat fluxes at the ocean surface? Insofar as there's at least logically a connection between surface winds which drive currents which influence surface temperature which in turn influences the atmosphere. That's part of the price which is involved in getting the heat fluxes.

Huang: I was talking with some of the meteorologists -- they are
(NOAA) saying it's the oceanographers who hold up the climate study. Now that's just a comment, not a statement, but some of the meteorologist are seeing it that way. Understanding the ocean is the essential part of the climate problem right now.

Lukas: I would like to answer Jim's [McWilliams] question. Until
(Univ. of Hawaii) we can couple atmosphere and ocean eddy resolving models, the eddy scientists among us could tell the observationists how to most efficiently observe the ocean so as to specify the sea surface temperature in an efficient way to the meteorologist. Eddies are a significant sampling problem, as has been highlighted earlier.

McWilliams: But they are also part of why the sea surface temperature is what it is. It is not just a sampling problem. If you want simply the sea surface temperature, fly a radiometer.

Lukas: Of course. But how do we go about efficiently applying our limited resources to monitoring the ocean sea surface temperature?

McWilliams: Should we mortgage our future with perhaps being able to predict the sea surface temperature some day, or calculate it in order to pay the enormous price of monitoring it now?

Lukas: They can go hand in hand.

Wyrtki: I have another question. I can understand the importance of
                 the eddies for maintaining the general circulation, and
                 their role in the dynamics of the ocean. But, I'm
                 interested in the fluctuations of the general circulation
                 from year to year, from decade to decade. Now I ask the
                 question, is there a definite role of the eddies in the
                 fluctuations of the general circulation?

Magaard: Well, the eddies <u>are</u> the fluctuations. [Laughter]

Wyrtki: I'm not so sure in the way you define the eddies. I mean if
                 you go to the point of saying that the eddies are typically,
                 let's say, shorter than 500 km, then it is a field, like a
                 turbulent field that is there, and I cannot see much reason
                 that this field or the effect of this field substantially
                 changes with time. That means the dynamics of the ocean
                 doesn't change with time. The hydrodynamics remains the
                 same. The question is: Do eddies have anything to do with
                 the fluctuations of the circulation on the basin scale?

Robinson: There are various statistics of the eddy field. And the
                 scale of the statistics is not the eddy scale itself, it's
                 larger — subgyre and gyre — and you don't really know what
                 all the relevant scales are of the statistics of the various
                 eddy quantities. And these statistical quantities, which
                 are averages over eddy effects, do change in time. And they
                 change in time on scales which are mixed up with fluctuation
                 scales that you're interested in. I don't think cause and
                 effect is understood in these issues.

Wyrtki: Maybe you want to go as far as saying that cause and effect
                 may not be separable.

McWilliams: In our modeling and really in our observations insofar as we
                 define eddies and general circulation, we're really only
                 reaching down to low enough frequencies to be talking about
                 the fluctuations you're concerned with. So we really have
                 much better evidence for saying that the eddies are playing
                 an important role in the fluctuations, that is, 2-, 3-, 4-,
                 or a 5-year mean than we have for saying what role they play
                 in the infinite-year mean. We don't know anything about the
                 infinite-year mean either in the models or in the
                 observations.

Muller: We're not claiming that eddies are responsible for everything we see in the ocean or what happens in the ocean.

McWilliams: Undoubtedly, a lot of what Warren [White] showed in the Eastern Pacific has very little to do with eddies, it also may have very little to do with climatically important air-sea interactions, and it may be a rather self-contained phenomenon. But surely the fluctuations of the Kuroshio over a several-year time scale have a lot to do with the eddies which are providing dynamical balances for the Kuroshio.

White: Also in the tropical ocean Jim O'Brien's been running a realistic model that's had surprising success in specifying sea level for example in comparison with what Klaus (Wyrtki) has been getting.

McWilliams: But even that situation is not safe yet. What is fairly solidly demonstrated is that the equatorial thermocline responds to atmospheric wind changes in fairly simple ways that don't seem to involve eddies. How then the sea surface temperature is what it is to feed back on the atmosphere in order to change the winds isn't a connection which has been made. And so that has to be said to be open. One of the most recently interesting observations in that problem is the fact that in the EPOCS's moorings, there are big $V'T'$ values.

Muller: Are there any other points which one of you would like to have discussed here?

Robinson: An important topic which probably hasn't received as much airing as it deserves is the interaction of mesoscale eddies with higher frequencies, mostly the interaction of internal waves with fronts.

Muller: I agree. One of the major open problems is where does the eddy field dissipate its energy, where in physical space, whether in the interior or in the surface mixed layer or in the bottom boundary layer. We also don't know the dissipation rates. We don't know the processes. In the models you have to specify a dissipation mechanism. Another question is how sensitive are model results to the specification of the dissipation mechanism, given the fact

that we don't know the physics of the dissipation mechanism in the ocean. Can you comment on that?

Robinson: That's really why I brought this question up because sensitivity or dependence on dissipation mechanisms is continually plaguing eddy dynamicists, and that was something that came out a lot the first day or two of this meeting. So getting a better understanding of the processes is in fact a major question.

Muller: We have one estimate from the LDE experiment of the energy flux to the internal wavefield by horizontal stresses. That's a fairly large number, but it's at just one spot in the ocean, so it's a single estimate. I don't know of too many other experiments or observational results which really can pin down a number for the dissipation rate.

Fu: I'd like to point out a probably overlooked mechanism for eddy energy dissipation. Over rough topography, eddies generate internal waves. In Polymode array-3 a and b, which is over very rough topography in the Mid-Atlantic Ridge, the eddy kinetic energy at the 4,000 meters level is one order of magnitude smaller than in similar dynamic regions. The internal wave energy is about factor 2 or 3 larger than in other regions.

Muller: I'm looking at the dissipation of eddy energy which comes about by the interaction of the eddy field with the surface mixed layer. By lifting up the interface the eddies increase mixing, which in turn increases the potential energy. This potential energy increase has partly to be supplied by the interior eddy fields. This mechanism leads to an entrainment damping of the eddies. Rough estimates look as if this might be a relevant process. So I agree with Allan [Robinson] that we should do both theoretical and experimental studies of the possible dissipation mechanisms.

I would like to ask Bill [Holland] again: How sensitive are the modeling results? How urgently do we need a good dissipation model?

Holland: Well, it is the primary unknown in the models. It is one of the parameters or the parameter which does strongly alter results. That's why we're in a stage where we need to do many, many experiments. Most of the experiments that are done are trying to assess at least in simple ways the

sensitivity to the parameterization, that are in any given model. There is no doubt that it is a fairly important determinant to certain aspects of the solutions.

Muller: From an experimental point this implies that we have to go to even smaller scales to measure the subgrid motions of the eddy field.

Holland: Well, it's a little bit unclear to me. I don't have any answer, really. Certain of the large-scale features are importantly determined by the kind of friction and the strength of the friction that one uses. But also other aspects -- to some degree the eddy generation mechanisms and the basic way in which the gyre equilibrates -- is not too sensitive to it. So I think we're capturing part of the problem pretty well. We don't quite know where the limits of that lie.

Robinson: What about your own study on the frictional dependence of barotropic versus baroclinic instability processes. . .

Holland: That is exactly what I was referring to. It's easy to crank friction up until it is so big that eddies all disappear and one has a steady state circulation model like Kirk Bryan's. The question is what happens when you crank it down to as small a value as you can consistent with some grid size. There are a whole host of other questions that we don't have solid answers to. For example, if you choose a boundary condition which is a no-slip boundary condition, that fundamentally changes the nature of the vorticity transport by the western boundary current. That is an important parameter of the problem. We do the same calculation with the slip boundary condition; the western boundary current doesn't separate at Cape Hatteras but turns the corner and works its way up the boundary. That allows me to toss one boundary condition out of the problem. I am not particularly interested in that one anymore.

In terms of setting some amplitude for the size of the lateral friction in the models that we've been using, we found in fact, that the kind of eddy coefficient that you refer to, based upon interaction of mesoscale eddies with the internal wave field from the LDE data, is about what we need in the models to get realistic amplitudes at the end. If we make it much smaller than that, the ocean goes unrealistic in other ways; the Gulf Stream is very strongly unstable -- it tears itself apart immediately upon leaving

the western boundary. If we make it much bigger than other aspects, the amplitude and the structure of the eddy field are wrong. At this point we have to completely treat the viscosity of the problem as the one parameter that we have to search very carefully through parameter space to understand how the solutions depend upon it.

Young: How sensitive is the homogenization of salt?

Holland: You can alter it quite significantly, although I can't be very specific without getting out a bunch of pictures and looking at them carefully. But it changes; the area of homogenization is definitely dependent on size of viscosity.

Young: And having no-slip boundary conditions?

Holland: The whole shape of the gyre changes if you have slip boundary conditions; so yes, it changes quite dramatically. But whether the homogenization processes are fundamentally different, I don't know.

Salmon: Some of the ARRAY II data initially suggested that there was a strong barotropic component in the area. Is that also evident in the mean? You seem to find that the Gulf Stream changes direction in the mean?

Hogg: The problem is that the measurements in the thermocline go only as far north as 37° North; they only cover half of the array. Certainly in that band south of 37° North, both mean and the eddy are relatively depth independent.

Salmon: Is that also true in your model, Bill? Is the Gulf Stream extension region really pretty barotropic most of the time?

Holland: It certainly has a strong barotropic signal, although it's not entirely like the real data, by some measure. There's some real problems in getting the right vertical structure both in the mean and in the eddy energy in these models. The point that I hope I've made strongly enough, is that it's very nice to look at pretty pictures but these models involve enormous amounts of compromise. We're really at a very early stage at developing models of this kind. There are many different alternative physics that can be used,

that is, primitive equation physics with outcropping isotherms and so forth. And we don't really understand what the results are going to be as we improve the models and add these little pieces of the problem. In some ways it seems remarkable that we get as much realism with the simplicity of this model. But it is extremely simple and when one looks at it in detail there are very many ways in which we would like to alter and improve it.

Muller: Is there any problem in reconciling these large viscosity coefficients with the long lifetimes of these small lenses you saw in the LDE experiment?

McWilliams: Of course they don't apply . . . If one takes the simple-minded interpretation of a 10^6 cgs horizontal diffusivity due to transfer to the internal wave part of the spectrum, one gets decay times of several years . . . no difficulty with that . . . But if one blindly applied that diffusivity to a very small-scale lenses they would disappear in a few days, and they obviously live for years. So clearly such a submesoscale diffusivity is not a formally accurate one.

Muller: Are there any other questions which one of you might want to bring up?

Huang: Maybe I might make another comment. Based on Bill Holland's
(NOAA)   mesoscale general circulation models, all the experiments carried out seem very time-consuming, and are quite difficult to do. However, at the present stage, there are more atmospheric modelers than oceanographic modelers. Only small portions of computer time are available for oceanographers to do the work on the aliasing phenomena, that is so difficult to resolve and so hard to model. I think this is probably a very appropriate group to make some kind of recommendation, especially Jim [McWilliams] and Allan [Robinson], to the nation and I hope that sometime in the near future a dedicated computer can be donated to work on ocean problems, such as eddies. [Applause]

Muller: Perhaps this is a good point to stop. I would like to thank all the participants and all the speakers of this workshop, and the students for taping. Thank you.

REPORT DOCUMENTATION PAGE		READ INSTRUCTIONS BEFORE COMPLETING FORM
1 REPORT NUMBER	2. GOVT ACCESSION NO.	3. RECIPIENT'S CATALOG NUMBER
4 TITLE (and Subtitle) The Role of Eddies in the General Ocean Circulation		5. TYPE OF REPORT & PERIOD COVERED 6. PERFORMING ORG. REPORT NUMBER
7. AUTHOR(s) Lorenz Magaard, Peter Muller, Rita Pujalet (Eds.)		8. CONTRACT OR GRANT NUMBER(s) ONR N00014-83-G-0017
9. PERFORMING ORGANIZATION NAME AND ADDRESS Hawaii Institute of Geophysics 2525 Correa Road Honolulu, Hawaii 96822		10. PROGRAM ELEMENT. PROJECT, TASK AREA & WORK UNIT NUMBERS
11. CONTROLLING OFFICE NAME AND ADDRESS Office of Naval Research		12. REPORT DATE 1983
		13. NUMBER OF PAGES
14. MONITORING AGENCY NAME & ADDRESS(if different from Controlling Office) Office of Naval Research Department of the Navy University of California, San Diego La Jolla, California 92093		15. SECURITY CLASS. (of this report) Unclassified
		15a. DECLASSIFICATION/DOWNGRADING SCHEDULE

16. DISTRIBUTION STATEMENT (of this Report)

Approved for public release; distribution unlimited.

17. DISTRIBUTION STATEMENT (of the abstract entered in Block 20, If different from Report)

18. SUPPLEMENTARY NOTES

19. KEY WORDS (Continue on reverse side If necessary and Identify by block number)

Eddies; Rossby Waves; General Circulation; Gulf Stream Rings; Mesoscale
Variability; Eddy-Mean Flow Interaction; Atmospheric Forcing of Eddies;
Prediction of Oceanic Eddy Fields; Eddy-Resolving General Circulation Models;
Eddy Heat Flux; North Atlantic Deep Circulation; Gulf Stream Recirculation;
Kuroshio; Satellite Altimetry; North Atlantic; North Pacific

20. ABSTRACT (Continue on reverse side If necessary and Identify by block number)
These proceedings contain the lectures of 17 participants of the workshop and a
near-verbatim reproduction of round-table discussions held at the end of the
workshop. The lectures and discussions cover the major aspects of the state of
the art and plans for future directions concerning the role of eddies in the
general ocean circulation.

DD FORM 1473 EDITION OF 1 NOV 65 IS OBSOLETE
1 JAN 73
S/N 0102-014-6601 |